Springer
Tokyo
Berlin
Heidelberg
New York
Barcelona
Hong Kong
London
Milan
Paris
Singapore

K. Sato, Y. Iwasa (Eds.)

Groundwater Updates

With 338 Figures, Including 3 in Color

Springer

KUNIAKI SATO, Dr.
Professor
Hydroscience and Geotechnology Laboratory
Faculty of Engineering
Saitama University
255 Shimo-ohkubo, Urawa, Saitama 338-8570
Japan

YOSHIAKI IWASA, Dr.
Professor Emeritus, Kyoto University
Institute of Earth Science and Technology
3-5-22 Kitahama, Chuo-ku, Osaka 541-0041
Japan

ISBN-13: 978-4-431-70283-2 e-ISBN-13: 978-4-431-68442-8
DOI: 10.1007/978-4-431-68442-8

Springer-Verlag Tokyo Berlin Heidelberg New York

Typesetting: Camera-ready by authors/editors

Preface

Groundwater is a constituent element of the earth and maintains the water cycle on land. Groundwater resources today are threatened by excessive use, quality contamination, and environmental impacts resulting from industrial activities, agricultural practice, below-ground development, and waste disposal. Many researchers and engineers in the fields of hydrology and groundwater hydraulics have concentrated their efforts on these issues over the last decade.

Recent progress in research and analysis has rapidly altered the traditional approach of groundwater management and modeling as well as the dynamic methodology. Numerical simulation of groundwater and data processing using personal computers are the most rapidly developing fields of study. Furthermore, recent advances in subsurface hydrology require a broad knowledge of interaction between surface and subsurface water.

Given this background, the International Symposium 2000 on Groundwater is scheduled for May 8–10, 2000, at Sonic City, Omiya, in Saitama Prefecture under the sponsorship of the International Association for Hydraulic Engineering and Research (IAHR). The target of the international symposium, to create "new science and technology for a sustainable groundwater environment," is of interest not only for IAHR members but also for many researchers and practitioners in various fields of groundwater. Fortunately, many leading scientists and engineers in those fields graciously accepted our invitation and contributed excellent articles to this book, *Groundwater Updates*. We are very indebted to their efforts and full cooperation with our wish to publish the book in advance. We will be greatly pleased if new paradigms germinate from the book during and after the symposium.

We would like to acknowledge support for the symposium from the Ministry of Construction, the Environment Agency, and the National Land Agency of Japan, and from the Saitama Prefectural Government, Japan. We also extend our thanks to members of the Hydraulic Committee of the Japan Society of Civil Engineers (JSCE) for their well-coordinated support, and to Springer-Verlag Tokyo for help in preparation of this book.

KUNIAKI SATO
January 2000
Urawa, Saitama, Japan

YOSHIAKI IWASA
January 2000
Kyoto, Japan

Local Organizing Committee (LOC) & Steering Committee

Honorary chairman:	Dr. Y. IWASA, Prof. Emeritus, Kyoto Univ.	(Japan)
Chairman:	Prof. K. SATO, Saitama Univ.	(Japan)
Co-chairmen:	Prof. I. KONO, Okayama Univ.	(Japan)
	Prof. K. TAKAMURA, Rissho Univ.	(Japan)
	Prof. N. TAMAI. Univ. of Tokyo	(Japan)

Advisory Members

Prof. T. AKAGI, Toyo Univ.	(Japan)
Mr. Y. ENDO, Director-General, Environmental Agency	(Japan)
Mr. K. TAKADA, Director-General, Ministry of Construction	(Japan)
Mr. Y. ISHII, President, CTI Eng. Co., Ltd	(Japan)
Dr. M. KADOYU, Deputy Director, Central Res. Inst. of Electric Power Industry	(Japan)
Dr. Y. KAMIBAYASHI, Vice President, NEWJEC Inc.	(Japan)
Dr. H. KURIHARA, Vice Director, Tech. Res. Inst. Kajima Corp.	(Japan)
Prof. K. MURAOKA, Osaka Univ.	(Japan)
Mr. K. NAKANO, Executive Director, Saitama Pref. Government	(Japan)
Dr. K. MORI, President, Japan Geotechnical Consultant Association	(Japan)
Mr. T. SUZUKI, Director-General, Water Res. Dept. National Land Agency	(Japan)
Prof. Emeritus, H. SHIIGAI, President, Yamanashi Univ.	(Japan)
Prof. F. TAKAGI, Nagoya Univ.	(Japan)
Prof. R. YOSHINAKA, Saitama Univ.	(Japan)
Prof. A. WADA, Nihon Univ.	(Japan)

Scientific Members

Prof. R. ABABOU, INP CNRS IMFT.	(France)
Prof. V. CVETKOVIC, RIT, Stockholm	(Sweden)
Prof. A. DAS GUPTA, AIT.	(Thailand)
Prof. DI SILVIO, Univ. degli Studi di Padova	(Italy)
Prof. T. FUKUHARA, Fukui Univ.	(Japan)
Prof. R. HELMIG, TU Braunschweig	(Germany)
Prof. K. JINNO, Kyushu Univ.	(Japan)
Prof. T. KAWATANI, Kobe Univ.	(Japan)
Prof. W. KINZELBACH, ETH. Zürich	(Switzerland)
Prof. H. KOBUS, Inst. Was., Univ. Stuttgart	(Germany)
Prof. E. A. KONTAR, P.P.Shirshov Inst. of Oceanology	(Russia)
Prof. K. KOVAR, RIVM	(The Netherlands)
Prof. K. MUSHIAKE, Univ. of Tokyo	(Japan)
Prof. K. OGIWARA, Toyo Univ.	(Japan)
Prof. M. OJIMA, Fukuyama Univ.	(Japan)
Prof. H. J. OVERBEEK, Secretary General IAHR	(The Netherlands)
Prof. Y. RUBIN, UC. Berkeley	(USA)
Prof. Emeritus S. SHINDO, Chiba Univ.	(Japan)
Dr. F. STAUFFER, ETH. Zürich	(Switzerland)

Prof. S. SUGIO, Miyazaki Univ. (Japan)
Prof. K. SUNADA, Yamanashi Univ. (Japan)
Prof. K. TAKARA, Kyoto Univ. (Japan)
Prof. WANG BINGCHEN, CIGIS (China)

Steering Committee Members

Mr. M. IWATA, Environment Agency (Japan)
Mr. Y. FUJISHIRO, Japan Geotechnical Consultant Association (Japan)
Dr. A.M. GAD Ali., Saitama University (Japan)
Mr. M. HIRAYAMA, Taisei-kiso Sekkei Co. Ltd. (Japan)
Dr. S. IMAMURA, Taisei Corp. (Japan)
Dr. T. KITAGAWA, Nishimatsu Co. Ltd. (Japan)
Mr. T. MAEKAWA, Kokusai Kogyo Co. Ltd. (Japan)
Mr. H. MINOURA, Ministry of Construction (Japan)
Dr. N. MIYAKE, Inst. of Tech., Shimizu Corp. (Japan)
Prof. M. MORITA, Shibaura Inst. of Tech. (Japan)
Mr. S. NISHINA, Ebara Co. (Japan)
Mr. Y. OCHIAI, Saitama Univ. (Japan)
Prof. Y. SAKURA, Chiba Univ. (Japan)
Prof. Y. TANAKA, Toyo Univ. (Japan)
Mr. T. UENO, Tech. Res. Inst., Obayashi Corp. (Japan)
Dr. T.C. VU, Saitama University (Japan)
Mr. M. YAMAKAWA, National Land Agency (Japan)
Mr. K. YASUI, Saitama Pref. Government (Japan)

Sponsor

International Association of Hydraulic Engineering and Research *(IAHR)*
Committee on Groundwater Hydraulics

Co-sponsors

American Society of Civil Engineers (ASCE)
International Association for Hydrological Science
The Japan Society of Civil Engineers (JSCE)
The Japanese Geotechnical Society
Japanese Association of Groundwater Hydrology
Japan Society of Hydrology & Water Resources
The Japan Groundwater Technology Association
Japan Research Institute of Groundwater Physico-chemistry

Supporting Organizations

Ministry of Construction, Government of Japan
Environment Agency, Government of Japan
National Land Agency, Government of Japan
Saitama Prefectural Government, Japan

Reviewing and Editing

More than 140 papers and short communications were received in answer to the call for papers in our second announcement. The number was much greater than could be accommodated within the Symposium timetable. All submissions were reviewed by two experts in the field in terms of their relevance to the chosen themes and their quality. In screening the number of accepted papers for the symposium down to a manageable total of about 80, the editors were able to keep to an international standard in spite of some tough decisions.

As chief editor, I would like to thank all the members of the editorial board and reviewers for their expertise and enthusiasm in completing a difficult task in a very short time. Their efforts and skills have ensured a high technical standard as well as progress for this symposium.

K. SATO and Y. IWASA
Chief Editors

Contents

Groundwater Pollution and Remediation Technologies

Underground Development and Groundwater Technologies

Interaction Between Surface and Subsurface Water

Reliability of Numerical Methods and Scaling in Geohydraulics

Short Papers

Optimization of Groundwater Resources in Basins

Groundwater Pollution and Remediation Technologies

Invited and Special Lectures

Soil and Groundwater Contamination and Remediation Technology in Europe

Prof. Dr. h. c. Helmut Kobus, Ph. D.

Institut für Wasserbau, Universität Stuttgart, Pfaffenwaldring 61, D-70550 Stuttgart, Germany

ABSTRACT: Groundwater is the major drinking water resource in Europe. However, serious deterioration of soil and groundwater quality has been observed due to pollution from urbanization, industry and intensive agriculture. The lecture will provide a survey of the observed impacts and of the considerable efforts that have been made to develop strategies and tools

- for cost- and time effective local remediation technologies for contaminated sites (including examples from the technical-scale research facility VEGAS),
- for prediction methods and urban development strategies including derelict land,
- for groundwater-compatible subsurface construction,
- for groundwater protection policies and preventive strategies,
- for reducing impacts of agriculture on groundwater quality.

An important consequence of these developments is the integration of subsurface issues, groundwater awareness and sustainability considerations into engineering education and professional development.

KEY WORDS: Groundwater pollution, remediation strategies, in-situ technologies, brownfield redevelopment, groundwater management.

INTRODUCTION: GROUNDWATER - THE ENDANGERED RESOURCE

Groundwater is a strategic resource due to its natural quality and availability, which is used in most European countries as the major source for public drinking water supply. Percolation of water through the subsurface has a good effect due to the combined action of filtration, sorption, chemical reactions and micobiological processes. The percentage of groundwater used for drinking water supply is 65% for France, 72% for Germany, 84% for Switzerland and over 90% for Austria. However, soil and groundwater systems are highly vulnerable to pollution. The increasing density of settlements, subsurface structures and traffic systems, the heritage of a century of industrialization, the storage and transport of hazardous substances, as well as intensive agriculture have had drastic impacts causing serious deterioration of groundwater quality. These impacts cause long-term effects, are sometimes irreversible and in any case very difficult and expensive to recover. Hence groundwater pollution is a major environmental problem [1].

A sustainable use of the groundwater resources implies a balanced water budget (no over-exploitation), only moderate changes in the residence times within the system, and limitation of groundwater pollution to the conditions of the natural self-purification capacity of the subsurface system.

Groundwater contaminations have developed into one of the key environmental issues in most industrialized countries. Regional-scale contaminations from industrial sources include waste sites, leakages, accidental spills, abandoned industrial sites, storage and transport of hazardous substances, etc. Nuclear and/or chemical contaminations may result from nuclear and fossil power plants and

gasification plants. Pipelines and traffic systems, roads and railroads serving the transport of hazardous substances also possess a groundwater contamination potential. The same holds for septic tanks. Agricultural contamination sources include animal farming as well as fertilizer applications (nitrates) and the use of herbicides and pesticides. Finally, air pollution contributes by deposition, etc. Virtually any kind of human activity or land use is connected with a potential danger of contamination of the regional groundwater resources.

A major issue common to all European countries is the increasing level of nitrates and pesticides in the groundwater and in surface waters, mainly due to intensive agriculture, with nitrate concentrations approaching or exceeding the level of 50 mg/l which is the upper allowable limit for drinking water according to EC-standards. This gives rise to a strong controversy between agricultural production and water supply. It has been shown that the nitrate input to the groundwater can be reduced substantially by appropriate agricultural technology, although with a certain loss in production efficiency. This has led in some countries to a legislation requiring the user of water to pay for making use of the natural public good, and to use the income from this regulation in order to recompensate farmers for the economic production losses provided that they use environmentally compatible farming techniques. This regulation reverses the polluter-pays-principle, but with a noteably positive result for the groundwater quality [2].

The use of groundwater leads also to various conflicts with the competing demands of ecology, such as the issue of groundwater withdrawal versus biotope preservation and the controversy of wetland restoration, the effects of groundwater withdrawal on surface waters, issues of flood protection schemes, flood plain ecology and groundwater withdrawal for water supply. Further conflicts are connected with the controversy of land use restrictions in groundwater protection areas, issues of competing uses of water resource systems, the socio-economic aspects of regional separation of drinking water "production" (groundwater withdrawal) and water consumption (beneficiaries), including interbasin water transfer and the potential conflicts in the use of international river systems [2].

A sustainable water resources management has to account for all these needs and demands on the groundwater resources, minimizing the local and regional impacts upon the groundwater, terrestrial and aquatic ecosystems involved. At the same time, our most important natural water resource has to be safeguarded against a broad range of competing and sometimes overwhelming interests on land uses for settlement and industry [3].

URBAN AND INDUSTRIAL GROUNDWATER CONTAMINATION

Our groundwater resources in urban areas experience manifold hazards and contaminations due to settlements incuding sewage systems, traffic, industry and trade, agriculture, air pollution, waste deposits and old contaminated sites. This is a natural consequence of the fact that aquifers are open systems with exchange of water, substances and energy across the system boundaries. The main inputs of substances into the groundwater occur through the soil zone by infiltration. Because the natural residence times in aquifers are very large, groundwater damages are always long term damages, and this becomes explicitly visible from the problem of old contaminated industrial sites and deposits.

Intensive measurements, observations and surveys have made clear the enormous potential danger due to contaminated sites for soil and groundwater and hence for man, animals and plants. A substantial part of these old contaminated sites has to be classified as in need of remediation. However, groundwater and contaminated-sites-restoration measures can be extremely expensive in terms of time and money needed [4]. For Germany alone, the total estimates of the costs for

remediation measues to be expected range in the order of magnitude of 100 to 300 billion DM: this makes obvious that due to financial constraints not every contaminated site can be remediated, and hence priorities for remediation needs and goals have to be formulated. In this process, also the limitation and constraints of the technical possibilities to achieve a remediation goal have to be considered in a realistic manner together with the limits due to the available financial means.

The challenge of subsurface remediation is a case in point illustrating the necessity to consider water-related issues in a broad and encompassing manner, where the various hydraulic engineering tasks in water resources management have to be seen in their interactions with ecology, land use and society [5].

Proactive pollution control and preventive schemes for avoiding contaminant inputs are priority needs. The delineation of wellhead protection areas with priority for water supply and with corresponding restrictions on land uses, restrictions on applications of water-hazardous substances, regulations for handling and transport of water-relevant hazardous substances (industry, storage tanks, roads, railroads, etc.) or even a ban and prohibition of the production and use of certain persistent chemicals are elements of a proactive pollution control. Rainwater runoff from sealed surfaces in urban areas such as roads or runways is affected by virtually unavoidable pollutants, such as oil residues, fuel residues, de-icing agents, cleaning agents and tire wear residues, which have to be collected and treated in a suitable way. Furthermore, provisions for immediate actions in cases of accidental spills have to be made, such as e.g. soil removal and treatment in order to minimize the contaminant input into the groundwater.

In all engineering construction activities, precaution must be taken to ensure that the groundwater balance and quality are not impaired by the construction and operation of industry, airports, roads or deposits. During major constructions, it is necessary to monitor the groundwater quantity and quality regularly.

Of particular relevance are all subsurface construction activities which interfere directly with the local groundwater system. Prominent examples are tunnel constructions and construction pits below the groundwater table. In these cases, the interference with the groundwater system and the temporary as well as lasting effects upon the groundwater system have to be considered carefully (barrier or drainage function of constructions, contamination sources, regional effects on water levels and water quality, etc.). Several examples to illustrate such effects will be presented, including the planning for a subsurface railroad system both in a metropolitan area and in a nature preserve, describing the various conflicts arising and the corresponding structural and hydraulic options for sustainable solutions (Schnellbahntrasse Stuttgart - München and Stuttgart 21).

REMEDIATION CONCEPTS AND TECHNOLOGY DEVELOPMENT

A contaminant plume originating from an industrial pollution source can spread with time (often many years) with the natural groundwater flow over large distances of many kilometers and thus poses a long-term danger for water supply plants located in the same aquifer, even if their location is quite distant from the contamination source. There are numerous examples in the literature [6] which illustrate these long-term large-scale effects. Such regional effects have been investigated by the Deutsche Forschungsgemeinschaft (DFG) in the 1980's in a special research program at the universities of Stuttgart, Hohenheim and Karlsruhe [7].

These research efforts, among others, have made clear that an effective clean up cannot be limited to the catchment and cleaning of the contaminant plume, but must be directed at the removal or immobi-

lization of the contamination source. Only in this manner, the long-term and large-scale negative effects upon the aquifer - and hence finally also endangering of the drinking water supply - can be avoided or reduced. With this demand, research is faced with a very complex, interdisciplinary task.

Obviously, first priority should be given to preventive schemes rather than repair actions, and to short-term actions on the spot in accidental spills. Restauration efforts essentially depend upon remediation schemes at the pollution source (this is the focus of the VEGAS research) by elimination or extraction of the contaminants or by immobilization. Frequently, this has to be complemented by remediation of the contaminant plume.

In view of the big uncertainties and the inefficient performance of the standard source remediation technologies, the big need has been recognized for the development and application of new and better remediation technologies. In order to pursue this goal systematically, the facility VEGAS (acronym for "Versuchseinrichtung zur Grundwasser- und Altlastensanierung") has been conceived and constructed.

VEGAS is a research facility for remediation experiments under controlled laboratory conditions but at technical scale. The facility bridges the gap between conventional small-scale laboratory experiments and field applications. The main features of the facility and typical ongoing research and development activities are described in [8].

Generally, the methods of subsurface remediation at the contamination source can be classified into methods without soil removal and methods with excavation. The latter group, which has already reached a high degree of development, is limited in its range of applications (limited depth of excavation, limited areal extent, not applicable under buildings, etc.). On the other hand, in-situ methods and containment methods are of particular relevance, because they may offer, depending on the circumstances, more cost effective and more flexible possibilities, covering not only the soil zone but also the groundwater zone, which may be more compatible with the environment. The VEGAS research program therefore is directed exclusively towards remediation technologies without soil removal.

Several VEGAS research projects are devoted to the elimination or reduction of the risk-potential of contaminations in the subsurface, particulary through in-situ procedures at the spill site, e.g. by injections of solubilizing and mobilizing agents, such as surfactants or alcohol, in order to enhance chemically the extraction of harmful contaminations. The main aim is the rapid remediation of hot spots. Another VEGAS project on in-situ bioremediation investigates stimulation and regulation of biodegradation, where the production of toxic metabolites must be controlled or avoided. Also, new procedures and strategies for field exploration and appraisal are necessary to handle the multitude of large and heterogeneous contaminated sites. In contrast to field investigations, VEGAS offers controllable and reproducible conditions, and hence lends itself to control measurements as well as for validation of numerical models. Further topics of VEGAS research include the artificial modification of permeabilities as well as the creation of in-situ remediation containments or in-situ reaction cells, such as reactive walls or absorption barriers in aquifers.

A highly successful new technology developed in VEGAS is the thermally enhanced soil vapour extraction (TUBA). The widely used soil vapour extraction method for removal of volatile non-aqueous phase liquids from the unsaturated zone usually needs extended remediation times. A considerable reduction of remediation times and increase in recovery rates is achieved by thermal enhancement using steam and hot air injections. The new technology has been applied in several case studies with good success, as will be shown in the presentation [9].

The times and costs involved in remediation technologies play a central role in land use development

in urban areas. The reuse of old industrial sites is of high interest in view of the pressing needs for land development in densely populated countries. In Germany, the daily consumption of land for settlement, traffic and industrial activitites amounts to 120 hectares, of which 50% will be sealed by an impervious cover. Thus, the need to reduce land consumption by reusing abandoned industrial sites in cities is evident, and an interdisciplinary research group "Figura" is developing procedures and methods for "brownfield redevelopment" as an important contribution to reducing land consumption taking into account both the technological aspects as well as socio-economic and land use planning considerations [10].

With increasing concentration in urban centers and increasing value of land, the intensity and scale of subsurface constructions affecting the groundwater system increases and often results in considerable changes in the natural groundwater regime, drawdown and changes in the flow system with all consequences for buildings, for flora and fauna in the region, for surface waters and for the local water supply. Because of the intricate interactions, a comprehensive groundwater management including a monitoring system, a simulation model and appropriate structural and hydraulic compensation possibilities will be needed.

OUTLOOK: TOWARDS SUSTAINABLE GROUNDWATER RESOURCES MANAGEMENT

Groundwater research can contribute to improve groundwater protection, to make remediation techniques more effective, to improve groundwater management techniques and protection concepts, and finally to lead to a sustainable development of groundwater uses [6]. Criteria for the planning of groundwater remediation schemes and for assessing the need for and chances of remediation are:

- prognosis of the expected spreading and transport of the contaminants in the groundwater system,
- effects upon environmental goods (drinking water / plants / surface water, etc.),
- definition of remediation goals: environmental standards to be achieved,
- efficiency and limitations of remediation technology to be applied.

In the effort to contribute to the improvement of groundwater management and pollution control, the general goals of the large-scale experiments in VEGAS have to be seen in the broader framework of scientific-technological research and engineering application [8]. The general goal is to contribute to a sustainable management of our natural resources groundwater and soil and to support the efforts of environmental politics for an improved environmental protection and in particular for an improved groundwater protection, both in a preventive and also in a restaurative manner. The large-scale experiments are intended to provide technical and planning contributions aimed at remediation technologies. Beyond the technical aspects, also the economical, the ecological and sociological aspects of remediation efforts and their significance for human health (drinking water) and land use planning have to be considered.

Research must also lead the way in the education of engineers who have to face the world's water problems of tomorrow. Here, the multifacetted groundwater research provides an important contribution for education and training of scientific talents by the fact that the basic university education in the various disciplines is complemented and enlarged by training the capabilities for interdisciplinary cooperation - a property which is of central significance for creative research and for innovative economical development. International graduate programs with mobility of students - such as e.g. the program "Water Resources Engineering and Management" (WAREM) at the Universität Stuttgart, enhance technology transfer and preparation for the future global water problems.

Groundwater protection carries high stakes and can be taken as the proof for our society on its efforts for sustainable development. However, it is not an easy task to create awareness for the high priority of groundwater protection as an ecological issue, because - unlike rivers or lakes - groundwater can not be seen, heard or felt. It can only be observed through the narrow keyhole of boreholes and geophaphical logs or through the quality of the water drawn from it.

Our efforts today are geared towards maintaining groundwater systems as the most valuable drinking water resource and the undeniable supporter of terrestrial ecosystems. It may still be a long way towards a global sustainable groundwater resources management, but the concepts are visible and the needs for mankind undeniable. To pursue these goals in teaching, research and engineering practice is therefore a major responsibility of our society for future generations.

REFERENCES

1. International Association of Hydraulic Research (IAHR): "Hydraulics and the Environment, Partnership in Sustainable Development". IAHR-Journal, extra issue, Vol. 29, 1991.

2. Kobus, H.: "Water supply from groundwater resources and ecology: issues and controversies", NATO Advanced Research Workshop 'Controversies between Water Resources Development and Protection of Environment', Visegrád, Hungary, May 1996

3. Kobus, H., Cederwall, K.: "Groundwater - The Policy and Management Perspectives"; Proceedings of the 8th Stockholm Water Symposium, Stockholm, 10-13.8.1998, SIWI-REPORT 3, 1998

4. Der Rat von Sachverständigen für Umweltfragen: "Altlasten II - Sondergutachten Februar 1995", Bonner Universitäts-Buchdruckerei, Bonn, Germany, 1995

5. Kobus, H., de Haar, U. (editors): "Perspektiven der Wasserforschung", Mitteilung 14 der Deutschen Forschungsgemeinschaft (DFG), VCH Verlagsgesellschaft, Weinheim, 1995

6. Kobus, H.: "Groundwater pollution control - a challenge to hydraulic research", Proceedings of the XXV. IAHR-Congress, August 23-27, Tokyo, Japan, pp 109-116, 1993

7. Kobus, H; Kinzelbach W. (editors): "Contaminant Transport in Groundwater", IAHR Proceedings 3, International Symposium Stuttgart, April 1989, Balkema-Publishers, Rotterdam NL, 1989

8. Kobus, H., Barczewski, B., Koschitzky, H.-P.: "Groundwater and Subsurface Remediation - Research Strategies for In-situ Technologies", Springer Verlag, Berlin, Heidelberg, 1996

9. Betz, C., Färber, A., Green, C.M., Koschitzky, H.-P., Schmidt, R.: Removing Volatile and Semi-Volatile Contaminants from the Unsaturated Zone by Injection of a Steam/Air-Mixture, In: Conference Proceedings Contaminated Soil '98, ISBN 0 7277 2675 7, 6th International FZK/-TNO Conference, pp 575-584, May 17-21, Edinburgh, UK, 1998

10. Juckenack, Ch. C., Barczewski, B. & Schrenk, V.: "Flächenrecycling und Flächenmanagement in Ballungsräumen. Ein Ansatz zur Strukturierung: der Projektverbund 'FIGURA' in Baden-Württemberg". TerraTech 5, S. 50-53, 1999

Current Trends in Groundwater Hydraulics

Fritz Stauffer[1]

[1]Institute of Hydromechanics and Water Resources Management, ETH Zurich, CH-8093 Zurich / Switzerland

ABSTRACT. Research and technical activities in the field of groundwater are characterized by their multidisciplinary aspects. Current topics of interest concern the use of aquifers, specifically their management, protection and remediation. These tasks involve an adequate assessment of the risk and potential impact caused by human activities which can alter natural conditions. This requires a good knowledge of the relevant processes involved. Moreover, conceptual and mathematical models on various levels and scales need to be formulated in order to forecast or assess physical, chemical and biological processes. These formulations require an adequate consideration of the usually heterogeneous structure of aquifers, which often results in complex flow and transport processes.

KEY WORDS: Groundwater resources, aquifers, flow, transport processes, modeling, remediation, protection

INTRODUCTION

Engineering and research in groundwater is strongly related to the development, management, protection and remediation of aquifers. Both quantitative and qualitative aspects in general characterize the impact on groundwater resources. What are main problems of concern?

From a quantitative point of view, unfavorable alterations of the storage capacity of aquifers, of the flow rates, of the natural recharge, and of the level of the water table or the piezometric surface are relevant. Of primary concern is the overexploitation of natural groundwater resources, mainly due to the long time scales of recovery involved. In such cases the sustainability of the utilization of water resources is jeopardized. The water table or piezometric surface has fallen dramatically particularly in arid regions. Moreover, over-pumping can cause severe land subsidence. In other regions, however, a rise of the water levels due to the abandonment of wells and/or an increase of the infiltration can represent a threat to urban areas and the environment. Finally, unfavorable alterations of the groundwater flow conditions caused by technical interventions should be mentioned. Examples are alterations of flow by underground constructions, or the clogging of the ground surface which may cause a reduction of the recharge rates.

Qualitative aspects mainly concern the chemical and microbial composition of the groundwater and its alteration. When groundwater is used for drinking water supplies, it must fulfill the quality requirements for food. A deterioration of groundwater quality can, for example, be caused by the following reasons:

- Infiltration of surface water which is polluted by various constituents.
- Infiltration of sewage from sewers or other sanitary systems.
- Inappropriate use of fertilizers and pesticides in agriculture. An example is the widespread groundwater pollution by nitrates.

- Leachate from polluted sites. Examples are waste landfills with inappropriate liners.
- Inappropriate transportation, storage, and application of substances which potentially endanger groundwater. Examples are spillage from traffic accidents or the leakage of storage facilities of mineral oil or chlorinated hydrocarbons, or accidents occurring in storage sites of radioactive waste.
- Deposition of air-borne pollutants on the ground surface and their subsequent infiltration.
- Salt water intrusion in coastal aquifers caused by an over-exploitation of groundwater.
- Thermal influences on groundwater and subsequent alteration of its physical, chemical and biological properties.
- Mixing of groundwater of different origins which may alter the physical, chemical and biological properties.
- Impact of technical constructions on groundwater quality.

In general, the main concerns are overexploitation and the long term release of pollutants. Consequently, the groundwater systems often play a prominent role in environmental impact studies. The protection of groundwater resources is a necessary measure to enable its sustainable use. Therefore, the flow of groundwater and the migration and fate of dissolved substances, of non-aqueous-phase liquids, and of colloidal particles in the subsurface are problems of primary importance. It should be kept in mind that aspects of water quality and flow are strongly interrelated, since the advective motion is the main process for the migration of dissolved substances and of energy. Therefore an adequate understanding of the flow conditions is a general prerequisite for other investigations.

CURRENT RESEARCH TOPICS

Based on recent conferences and publications on groundwater [1,2,3] a few selected current topics are listed below. They provide some insight into the wide spectrum of recent engineering and research activities in groundwater and represent at the same time an indication of current trends in groundwater. Nevertheless, they should mainly be considered as examples.

Measurement techniques in groundwater

- In situ detection of dense non-aqueous phase liquids in aquifers using laser induced fluorescence. How can this method be used to assess a contamination? [2].
- Measurement of groundwater velocity using CCD camera observations in boreholes [2].
- Estimates of soil moisture and temperature from remote sensing observations. Development of a methodology [3].

Processes in aquifers

- Measurement of the seepage rates from rivers to aquifers and of the related water quality changes by means of monitoring stations and tracers. Estimates of regional seepage rates based on such local measurements. Modeling of surface water – groundwater interaction, and incorporation of complex clogging mechanisms [1,2,3].
- Modeling of density driven flow in aquifers using numerical techniques. How accurate are these methods? How can they be improved? [3].
- Fingering effects in saturated porous media containing trapped residual fluid, which are caused by dissolution processes [2].
- Improved determination of the retention and relative permeability relations for immiscible fluids in porous media based of pressure cell data [2].

- Investigation of the mass transfer process between residual non-aqueous phase liquids and the water phase. Validity of various concepts [3].
- Influence of a reduction in the interfacial tension on the migration of organic liquids in groundwater. How does it affect remediation? [3].
- Investigation of the impact of the injection of treated wastewater in aquifers. What are the relevant processes? [3].
- Modeling of coupled chemical and biological transformations. How good are these models and how can they be calibrated? [3].
- Numerical modeling of the influence of phase change on moisture content and temperature during a bioventing of the vadose zone of contaminated sites. Assessment of the influence on the biological decay of contaminants [2].
- Heat transport in the unsaturated zone. Investigation of vapor transport in soils using radon-222 measurements [1,3].

Numerical techniques for groundwater models

- Improvement of numerical schemes for groundwater models with respect to numerical accuracy and computational efficiency [3].
- Use of neural networks and of genetic algorithms in optimization problems. Do they represent valuable alternatives to more conventional techniques? [2,3].

Modeling the effect of spatial variability of parameters

- Solute transport in heterogeneous formations. What are the methods? [1,3].
- Use of hydrogeological and geophysical data to condition the stochastic generation of permeability fields [3].
- Calculation of block effective macrodispersivities to represent the effect of sub grid scale variability on the mixing of solutes in numerical models [3].
- Inference of geostatistical hydrogeological parameters from tracer breakthrough curves [3].
- Modeling of solute transport with random contaminant sources [3].
- Evaluation of the uncertainty of the extent of well capture zones. Methods and techniques [3].
- Modeling of multiphase flow in heterogeneous formations [3].
- Development of techniques to estimate the uncertainty of groundwater models [3].

Determination of input parameters for groundwater models

- Parameter estimation and model calibration in a stochastic framework [3].
- Combined use of different types of field data for improved coupled parameter estimation [3].

Management of groundwater resources

- Groundwater management under uncertainty. Development of methods and techniques [3].
- Management of groundwater resources. Objectives and techniques [3].

Groundwater remediation

- Stochastic evaluation of flow and transport for the design of groundwater remediation schemes [2].
- Pilot tests for air sparging of contaminated sites coupled with vapor extraction in order to examine the effectiveness of the method [2].
- Management of groundwater remediation and risks. Methods and techniques [3].

Fractured rock and karst aquifers

- Numerical modeling of flow in fractured aquifers. Use of the heat balance in such models. Investigation of fracture-matrix interactions on flow and transport. Concept and methods [1,2,3].
- Use of the method of characteristics for transport in fracture networks. Evaluation of the effectiveness and accuracy [1,3].
- Estimation of mean water residence times for karstic springs by using stable isotopes [2].
- Deterministic and stochastic modeling of flow processes in karst aquifers. Use of wavelet transforms. Applicability and parameter estimation [2,3].
- Use of geostatistical tools to map groundwater flow behavior in karstic systems. Development of methods and techniques [2].

Underground constructions

- Experimental and numerical investigation of tunneling technique under compressed air [2].
- Investigation of flow in heterogeneous rock formations. Flow around storage caverns [1,3].

CONCLUSIONS

Many current topics of interest concern the development and the use of aquifers, specifically their exploration, their management, protection and remediation. A series of more basic investigations concern relevant physical, chemical and biological processes involved in these activities. Numerous studies of complex coupled flow and transport processes are mentioned. An increasing number of contributions concern engineering applications in groundwater. For the above mentioned purposes conceptual, mathematical and numerical methods and models on various levels and scales are further developed and improved in order to forecast or assess physical, chemical and biological processes. It is not surprising that many studies incorporate an adequate consideration of the usually heterogeneous structure of aquifers, which is of concern for both flow and transport processes.

Current trends in groundwater research seem to proceed in similar directions. An immense task still lies ahead to adequately assess and model the influence of spatial variability of the physical, chemical/biological properties on the various processes under consideration. Furthermore, improved methods for the estimation of parameters and boundary conditions are needed for solving regional groundwater problems. This includes the investigation of surface water – groundwater interaction as well as natural recharge in order to enable a sustainable management of water resources.

REFERENCES

1. Special Volume on Groundwater Hydraulics, Section on Groundwater Hydraulics, J. Hydraulic Research, IAHR, Vol. 36, (6), 1998.
2. Proceedings XXVIII IAHR Congress "Hydraulic Engineering for Sustainable Water Resources Management at the Turn of the Millennium", Theme A: "Sub-Surface Hydraulics and Engineering", Eds. D. Gutknecht and F. Stauffer, Graz, Austria, 22-27 August 1999, Proceedings on CD.
3. Proceedings ModelCARE'99, International Conference on "Calibration and Reliability in Groundwater Modelling, Coping with uncertainty", IAHS/IAHR, ETH Zürich, Switzerland, 20-23 September 1999, Eds. F. Stauffer, W. Kinzelbach, K. Kovar, and E. Hoehn.

A New Control System of Groundwater Resource

Kuniaki Sato

Hydroscience and Geotechnology Laboratory, Faculty of Engineering, Saitama University, 255 Shimo-ohkubo, Urawa, Saitama 338-8570, Japan.

ABSTRACT. The suppression of land subsidence has enforced as to keep a constant challenge in control and management of groundwater resource during the last few decades. The Northern part of the Kanto basin has been one of the most seriously affected areas by land subsidence in Japan. The continuously increasing trend of subsidence in this region has disclosed the inadequacy of traditional monitoring and management procedures. This paper proposes a new performance of recently introduced telemeter data and its application technique to realize real time active measures against heavy land subsidence due to abnormal groundwater pumping during drought season. A methodology to determine management criterion for localized sub-basin through analyzing observed data over the past 7 years and a new management procedure for sustainable utilization of groundwater resource are suggested.

KEY WORDS: groundwater resource, telemeter system, land subsidence, drought season

INTRODUCTION

Various problems related to groundwater resource use have arisen in many areas in Japan since the late of 1930's [1]. Land subsidence can be considered as one of the most important groundwater problems that cause unacceptably serious damages, especially, to infrastructures and environment. An accelerated trend of land subsidence in industrialization and urbanization became the social topic in 1950-1965 after the World War II, obviously due to the increased demand of groundwater with economic restoration. This trend later calmed down at some designated areas by virtue of new rules of groundwater pumping restriction and development of new surface water resources [2].

Recently, the increased frequency of weather fluctuation has resulted in serious period of shortage in surface water resources. This has initiated an extra demand for groundwater and brought about an unexpected impact on subsidence, accordingly. Traditionally, the accustomed procedure for managing groundwater resource has been based on a set of groundwater and land subsidence data produced by mechanical plotters and manual processing at an interval of few months to feed the results back to the field of concern.

The incessantly increasing trend of land subsidence in Northern Kanto basin has consequently pointed out several problems such a traditional procedure to control the subsidence phenomenon appearing in a relatively short period during drought season. The Environmental Agency, Japan has recently introduced new real time telemeter systems into five monitoring stations in Saitama basin to collect groundwater level and land subsidence data. The objective of the paper is to present a new concept and its operational procedure by telemeter systems, and to propose the feasibility of this system to mitigate heavy land subsidence caused by abnormal pumpage during drought season.

OBSERVATION METHODS AND TELEMETER SYSTEM

At present, many traditional observation wells are being utilized to monitor groundwater level and land subsidence in Saitama basin. Five observation wells are equipped with telemeter systems to cover most rigorously affected areas in the basin. Fig. 1 gives the location map of observation wells with and without telemeter system which also keep groundwater level and land subsidence records using mechanical plotters. Fig. 2 shows a schematic diagram and system hardware of an observation well equipped with a telemeter system.

A traditional observation well constitutes a mechanical float in the inner pipe of bored well, a displacement meter mounted on the inner pipe separated from the movement of the bored well and mechanical plotters. In the case of an observation well equipped with a telemeter system, the groundwater level and land subsidence data sensed by the float and vertical displacement meter, respectively, are first directed to an A/D converter and temporarily stored in a digital data logger in each well. These data in binary format are periodically sent by a MODEM through

Fig. 1. Map of Japan and locations of monitoring wells in Saitama basin

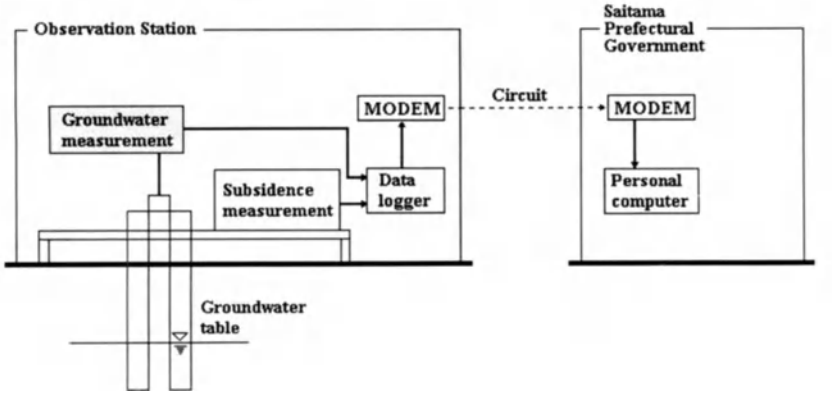

Fig. 2. Telemeter system : Schematic diagram of data collection

telecommunication line to a personal computer in the Atmosphere and Water Quality Protection Section, Saitama Prefectural Government. These data are necessarily modified by several software prepared for data processing. The present behavior of groundwater level and land subsidence in each locality is detected on line and then fed for the decision making on necessary management, such as pumping volume reduction, redistribution of local pumping rates etc. Official message for self-control of groundwater use will be distributed to all well operators and other related organizations through Internet via a data server at the Prefectural Government (Fig. 3.). A facsimile system is also available.

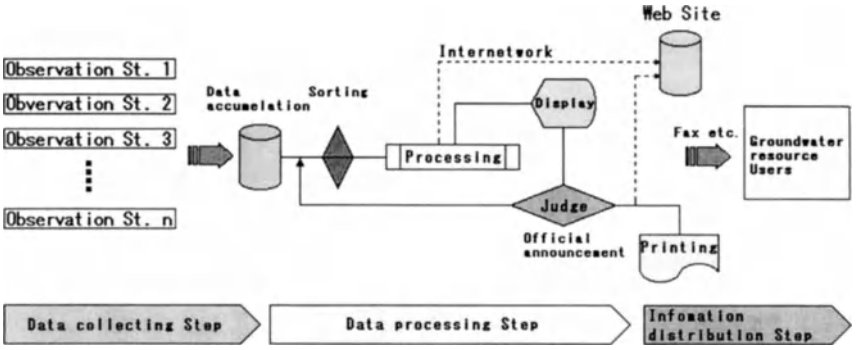

Fig. 3 Concept of management procedure

PRACTICE AND PROCEDURE OF GROUNDWATER CONTROL

During the last few decades, the groundwater management practice in Japan, in general, and in Kanto basin specifically, has been based on a long-term management policy in aiming at the development of new surface water resource in place of reduction of excessive groundwater use. The policy, however, has not always been adequate for settling land subsidence, because strong and abrupt land subsidence during drought season occurred due to much groundwater use in a short time. The groundwater control by telemeter system is available for minimizing severe land subsidence in drought season. A new control system of groundwater resource in Saitama Basin, Japan is worth special mention.

The project area has been divided into four control areas (sub-basins), each covering an approximately equal land area of similar hydrologic characteristics. An observation well equipped with telemeter system and centrally located in each control area is representatively designated to identify present characteristics of groundwater level fluctuation and land subsidence as shown in Fig. 4. Past records of groundwater level and land subsidence are extensively analyzed to ascertain the correlation and interdependency between two phenomena [3].

Control and management during drought season is achieved by a higher groundwater depth (h_i) than a critical one (h_{ci}) through imposing pumping restriction. An operational manual is drafted to establish the following stages of water management in response to different groundwater conditions in different control areas. The less restricted stage imposes a slight reduction of pumping rate. More strong restriction will be applied to regions where groundwater level and

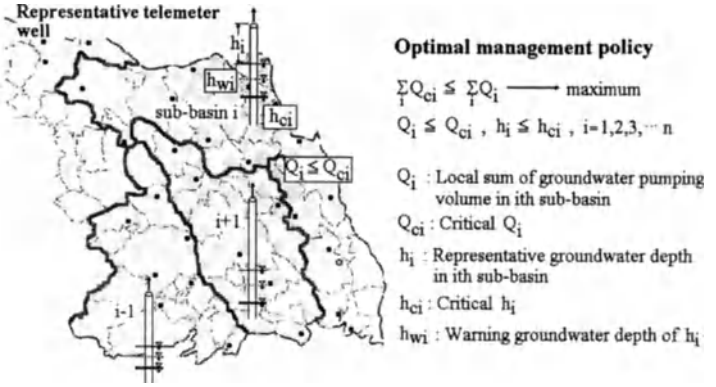

Fig. 4. Demarcation of control area

land subsidence trends are unacceptable. Management criteria in terms of depth of groundwater table for each control area have been determined by referring to data observed over the past 7 years.

The forecast of future trend of groundwater level is of the utmost concern to us when sending warning message to all groundwater users. The distribution of warning message and related information to all groundwater users will be carried out through Internet, e-mail, and facsimile etc. Groundwater management practice through telemeter data requires a consistent cooperative participation of groundwater users, and popularization of the system will be also needed.

CONCLUDING REMARKS

An approach based on telemetry to manage groundwater resource and to mitigate land subsidence during drought season is discussed. The real time operation through telemeter system in Saitama basin will attain a positive measure to optimize groundwater resource in future. Management criteria in terms of depth to groundwater table have been determined for each control area by referring to past data. The approach ensures a stable groundwater use not only for short-term groundwater management but also for long term one to develop a sustainable groundwater use policy.

The authors would like to express their sincere gratitude to Saitama Prefectural Government for the support and generosity extended to materialize this study.

REFERENCES

1. Shibasaki, T., and Research, Group for Water Balance, Environmental Management of Groundwater Basins, Tokai University Press, Tokyo, pp. 24-53, 1995.
2. Sato, K., and Hoang, N. V., Recent Countermeasures for Land Subsidence and Groundwater Resources in Japan, Proceedings of the Fifth International Symposium on Land Subsidence, Hague, pp. 471-479, 1995.
3.Gibson, R. D., Statistical Methods for Groundwater Monitoring, John-Wiley and Sons, Inc., New York, 1994.
4. Brockwel, P. J., and Davis, R. A., Introduction to Time Series and Forecasting, Springer-Verlag, New York, pp. 136-213, 1996.

Optimization of Groundwater Resources in Basins

Groundwater Sources and the Urban Development–a Possible Coexistence

Rasula Goran

Jaroslav Cerni Institute for the Development of Water Resources, 11223 Beli Potok, P.O. Box 33-54, Belgrade, Yugoslavia, E-mail: rasula@beotel.yu Web page: www.geocities.com/mgirasula

ABSTRACT Groundwater protection becomes a matter of current interest mostly when a polluting incident occurs. Recently, different approaches to define groundwater preventive measures have been developed in the domain of hydrogeological investigations. They mainly serve to evidence compliance with the legal regulations, while quality protection is undertaken only when a polluted area or endangered groundwater bodies have to be treated (e.g. accidental contamination of: the groundwater in the Pozega railway station area, of the Belgrade water source from the direction of the Makis marshalling yard, of the "Mediana" water source from the direction of the "Electronic industry" in the town of Nis, etc). This paper helps to identify possibilities for a quality hydrogeological approach to design a modern groundwater protection system, which is particularly important in the zones of transport infrastructure (railways, highways), dump areas, landfills with adequate sanitary measures and disposal areas for industrial wastes, etc., and particularly in the urban areas communicating with, or adjacent to existing, or potential, groundwater source zones.

KEY WORDS: groundwater protection, hydrogeology, sources, urban development

INTRODUCTION

Since 1984, when an incidental spillage of a great quantity of xylene happened in "Makis - Belgrade" marshalling yard (Fig. 1), Geotechnics Division of Institute of Transportation, Belgrade, has been continually performing certain research/study hydrogeological investigations, synchronized with extensive remedial measures in order to define groundwater and surface water pollution in the wide zone of the marshalling yard, transform pollutants and physically migrate them. In the last Phase V investigations (1995/96) a pilot monitoring system was established to periodically monitor the groundwater and surface water regime and quality, and after this, an active groundwater quality monitoring system was proposed on the basis of a Work Resumption Programme. According to these results since 1997, Jaroslav Cerni Institute for Development of Water Resources, Belgrade, Yugoslavia has been speeding the possibility of developing a new modern methodology of specific detailed hydrogeological investigations for establishing groundwater monitoring stations around all 'dirty' structures in the urban zones of Belgrade, especially Makis alluvial area between Belgrade-Obrenovac highway and the main zone of Belgrade source on the right hand bank of Sava river. This paper presents an example from our experience, a part of the results and scope of performed hydrogeological investigations needed to place and test the first pilot monitoring stations for the groundwater quality regime in the background of the part of Belgrade water resource.

THE CONCEPT AND SCOPE OF PERFORMED INVESTIGATIONS

Groundwater protection is generally presented by a set of prevention and treatment procedures and measures, which should primarily prevent pollution from occurring, particularly in water source

zones and on the ground containing considerable groundwater accumulation. Complex and comprehensive methods for solving concrete problems directly depend on the geological structure, i.e. the hydrogeological properties of rock; namely, it is necessary to investigate the terrain thoroughly. This calls for development of appropriate and concrete methodology for hydrogeological investigations in full accordance with the local conditions. The investigations themselves were reliably and in a modern way designed to enable a determination of the main hydrogeological parameters for the investigated area, definition of the nature and optimum number and technical characteristics of the groundwater monitoring system and structures, finding the way to achieve the rational operation by testing of the first pilot model of monitoring system and give a quality forecast of the system operation in the future.

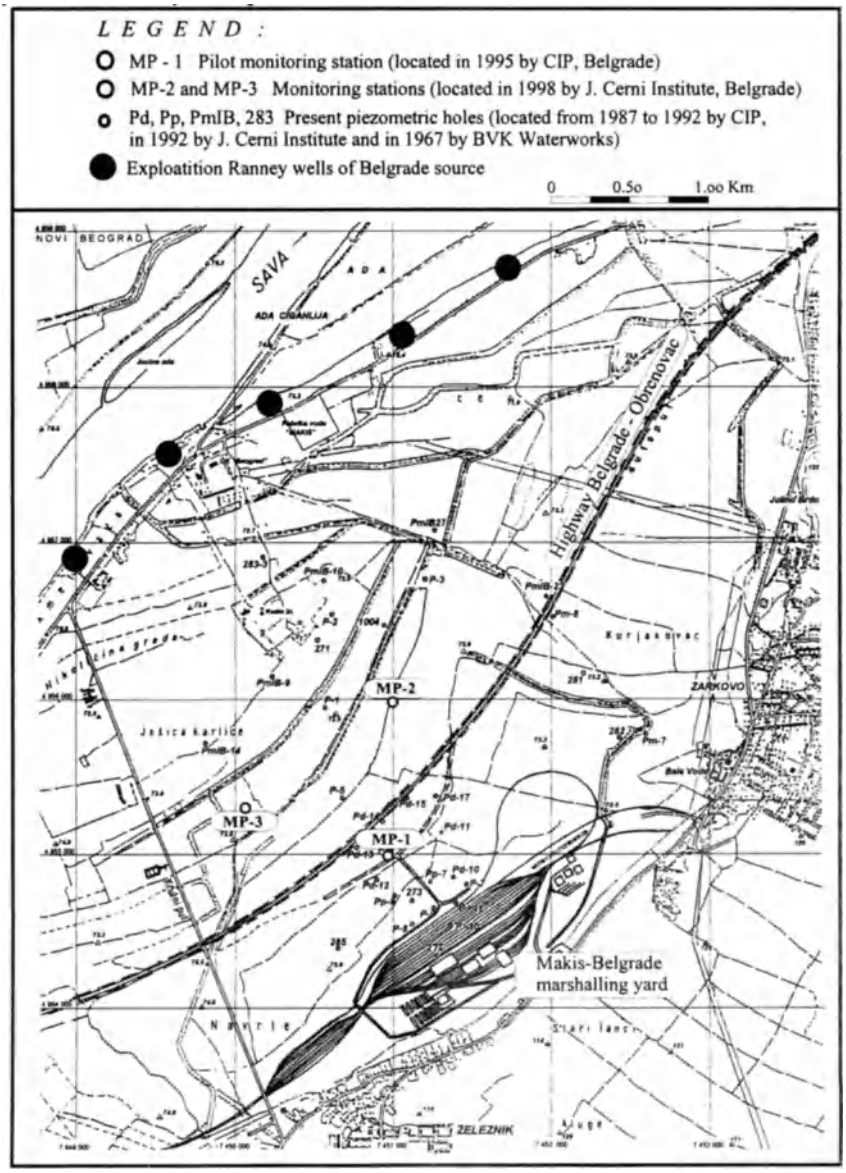

Fig. 1. Situation map with all hydrogeological structures in the wide investigated area

The investigation programme comprised the following:

* A detailed reconnaissance of the site in a wider area of investigation, hydrogeological mapping and registration of all the existing water structures, their stage, output and other characteristics;
* Boring of ten new piezometric holes (Fig.1.) down to the impervious strata (approximately 25 m per one structure) in order to define all local hydrogeological characteristics of the ground and the key hydrogeological parameters of the analyzed aquifer;
* Recording and land registering of all active and potential pollutants, which are in indirect or direct connection with the water source zone, especially the present facilities in marshalling yard and surrounds, frequency and quantity of toxic materials transport on the highway and the like, and to understand the way in which the structures and people function and might, for some reasons, cause any other groundwater quality degradation.
* Determination of detailed hydrogeological characteristics in the zone of extensive and immediate protection:
    - The aquifer type and its potential,
    - The infiltration characteristics and geometry of the aquifer complex, and the capacity of the present water intake structures and the water source in the zone of Makis,
    - Conditions of groundwater recharge, migration and outflow,
    - Detailed infiltration characteristics and position of the roof/surface complex, in the zone of impact of the water source, particularly at the highway belt and at the contact of marshalling yard and base alluvial complex,
    - The groundwater table regime, and hydrodynamic relations between surface and ground waters,
    - In the field and laboratory, the transporting velocity of several expected pollutants through the protective, roof humus-clay soil complex and aquifer complex, were analyzed and also the sorption, dispersion and other parameters, and pollutant transformation,
    - "Zero state" of hydrochemical groundwater parameters were analyzed to determine four parameters, which should be continually monitored over one year period.

The results of the investigations, designed and performed as described above offered a basis for scheduling the best possible conditions for placing the 'pilot model' of groundwater monitoring station. In the first step, the results of previous field investigations and laboratory tests were systematized. Then hydrogeological, hydrochemical, hydrodynamical and other basic data were interpreted as well as the results of earlier hydrogeological investigations preceding the opening of the Belgrade source in the zone of Makis. Finally, a complex analysis and synthesis of the collected data was done and the best technical solutions for groundwater monitoring were defined.

BASE HYDROGEOLOGICAL CHARACTERISTICS OF THE TERRAIN

The alluvial region on the right hand bank of the Sava river, in the south part of Belgrade (Fig. 1), covers an area of about 10 km^2. With regard to geomorphology the said region is in the form of a gentle plateau, average altitude 73 m above sea level. In some parts, the terrain is marshy or contains traces of the old meliorate channels or meanders of the Zeleznicka river, which flows through the central part of the terrain. From the Sava river basin to the east, the terrain gently rises towards the marshalling yard 78 m above sea level and further eastwards passes into steep hilly background of Zarkovo and Zeleznik with their highest crests rising to altitude 130-171 m above sea level. A distinctive characteristic of the region is its moderate continental climate. Mean precipitation according to the records of the hydrometeorologic station in Belgrade for the period 1965-1994 amounted to 781 mm. The hydrographic network consists of the Sava river stream and several minor permanent surface streams of which the most significant ones are Zeleznicka and Topciderska rivers. Alluvial sediments occur everywhere in the region varying in depth between 10 and 25 m. They are represented by sandy gravel and sands in which the main water-bearing environment is formed, while the roof ground complex, conditionally of low permeability is made

of humified sands - clays and silts of different thickness. The confined aquifer is replenished with atmospheric and surface water percolating through the diluvial and proluvial sediments on the eastern flanks of Zarkovo and from the Sava river in the southern part of terrain.

The natural direction of groundwater flowout is towards the southwest sections of the Sava river, with variation that depends on the exploitation in Ranney wells of Belgrade source. The confined aquifer regime in the sand-gravel complex on one part and the small depth (less than 3 m) and filtering properties of the roof protective complex on the other part may have a direct effect on the quality of groundwater.

GROUNDWATER MONITORING STATIONS

Initial steps in the hydrogeological investigations of the Sava river alluvium, in the zone of Belgrade-Obrenovac highway and Makis marshalling yard, were to compose a register of all the existing water intake structures (wells, piezometers) and a register of active and potential contaminants from the highway transport and within the railway facilities that may directly or indirectly cause degradation of groundwater quality in the future, and to have the above actions systematically monitored. Subsequent hydrogeological activities were focused on the identification of general hydrogeological and hydrochemical parameters, geometry and percolating properties of the roof complex and groundwater quality in the aquifer.

When all the piezometer boreholes from the earlier investigation phases (1982-1994) were prospected and their functional properties were determined, work started to make ten new piezometers and form a network of a total of 40 observation stations. Afterwards the hydrochemical zero quality of groundwater was to be determined. Several physical chemical parameters were selected and successively monitored over time. These were temperature, conductivity, pH, xylene concentrations, Fe ions, Mn ions, phenol and ammonia. Some of these parameters were monitored by digital measurements at each 0.50 m of the water column in the network of observation stations - piezometers while the others were monitored by taking water samples and performing dedicated chemical analysis. To monitor xylene concentrations, beside laboratory analysis a special probe was constructed to measure variations in specific electrical resistivity of groundwater. There were ten series of measurements in the course of one year.

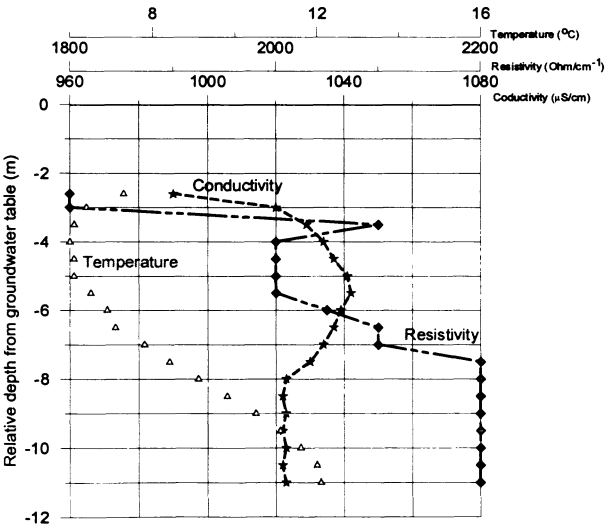

Fig. 2. Diagrams of groundwater conductivity, specific electric resistivity and temperature at the MP-1 monitoring station on December 17, 1996

Results, selected for this presentation are from one serie of conductivity, resistivity and temperature monitoring on a pilot monitoring station MP-1, shown in Fig. 2 & 3. By continual monitoring of groundwater temperature regimes in plan and profile, it was stated that there were zones and localities where surface water from the existing meliorate channel network directly infiltrated into the underground. All the results obtained indicate that in the process of a pilot monitor station installation it was justified to carry out detailed hydrogeological investigations that enabled rational selection of appropriate modern measuring equipment and technology for continuous monitoring of the selected parameters of groundwater quality. To this end, a specific stations were designed and put into operation, enabling start-up of observations in 1998 (MP-2 and MP-3 shown on Fig. 1).

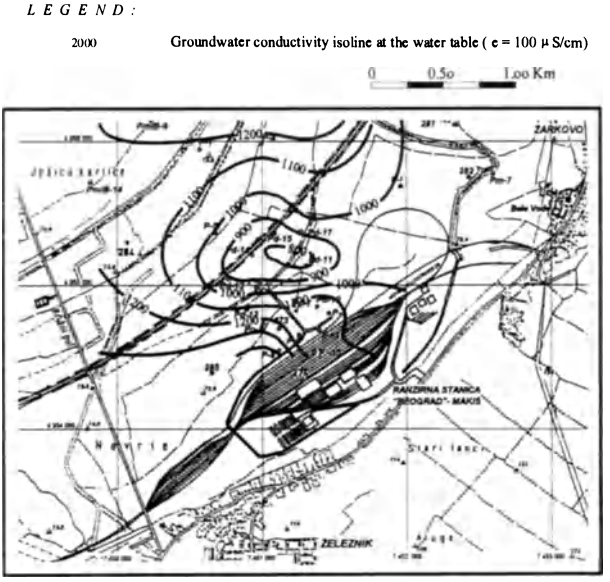

Fig. 3. Map of groundwater conductivity isolines at the water table measured on Dec.17, 1996

GROUNDWATER MONITORING SYSTEM - BASIC FEATURES AND FUNCTIONS

The essence of a groundwater quality monitoring system in road belts is a modern, rational, effective and permanent water quality control, a way to direct all activities in the domain of preventive protection against degradation and pollution, to find, in incidental cases, effective and adequate remedial measures, and to monitor and control the aftermath of incidents. With regard to the zones of large important water supply or perspective systems and regional water sources, which are tangent by highways, the Monitoring System would unite functions of a large number of services and institutions that are responsible for the monitoring and guidance of the system, while with regard to minor water sources or prospective regions, only the basic segment of a hydro-ecological station and control module would suffice.

The basic parts of the Monitoring System are:

1) Hydro-ecological gauging stations (MP-2 and MP-3, Fig. 1), hydrogeological investigation team, authorized control chemical laboratory and a technical service for work coordination,
2) Module to control and manage the Monitoring System,
3) Authorities and a network of interrelated users and participants in the system operation.

A hydro-ecological monitoring station or a cluster of them depending on the area to be protected must be located between the risk zone of contamination and the water structures in use (wells,

galleries, intake structures, terrain to protect, etc). That is, in fact, a standard investigation piezometer ϕ 146/110 mm borehole. The equipment and type of piezometer depend primarily on the lithology and type of water intake structures in the zone of water sources. After placing the piezometer construction, special waterproofing and heat insulating material are inserted in the manhole at the top. A digital instrument or logger for measuring the temperature, pH values, O_2 concentration, turbidity, conductivity, specific electrical resistivity, and a device for automatic continual groundwater table gauging are inserted, and lowered to the piezometer level through special measuring tips. The gauging device are fed with power via conductor or from a generator set suitable for continuous operation of minimum six months. An A/D converter (analog-digital) for signal conversion, and an independent modem device for direct, wireless connection to standard phone or GSM link are integral parts of this device. Authorized chemical laboratory for monitoring the hydro-ecological station in operation serves for permanent surveillance and identification of irregularities, if any, then for groundwater sampling, detailed laboratory analysis and indications to the control module of the type of measures to be undertaken with regard to quality. A PC server with a wide network of computer terminals will be incorporated in the control module to serve for a complete control of the Monitoring system. They will have a constant modem connection with a network of interrelated users. For the operation of the system it will be necessary to prepare control-information software containing an active analytical and graphic database on all the parameters of the system functioning, and a processing control module for controlling, managing the system and automatic signaling of even minor incidents or changes in the groundwater quality.

An additional part of the system will be a network of interrelated users, that will be able to have at any moment precise information about the groundwater quality, about any adequate protection measures undertaken, and in incidental cases about other effective measures undertaken to solve the problem. This network will be available to all educational and scientific institutions, professional and other teams, allowing them to further their developments in the environmental field, and use their experience wherever needed. This system will also be open and available to the media, that will accurately and timely inform the public. The system is getting preventive and educational character, then.

CONCLUSIVE REMARKS

Specific hydrogeological investigations in the process of groundwater protection should be essential for the establishment of an active groundwater quality monitoring system in the urban zones, especially industrial areas, which will be a base for defining conditions for preventive groundwater protection, prospective expansion of the existing water sources and opening of new ones. In the present water supply systems this should become the framework, for global environmental protection in the future. If opposite, with further traffic and local industrial development, and new economic trends a situation may arise, that, after 2000, many important and potential groundwater sources may not be adequately exploited in spite of their considerable capacity.

REFERENCES

1. Rasula G., (1996) Importance of systematic groundwater quality measurement by establishing an active monitoring system", Proceedings of 17th Yugoslav Symposium 'Waterworks and Canalization', Edited by DIT, pp.111-115, Sabac, Yugoslavia
2. Rasula G., Rasula M., (1998) Groundwater monitoring in the road belts, Proceedings of Yugoslav Experts Symposium 'Road and environment', pp. 239-245, Zabljak, Montenegro
3. Rasula M., Rasula G., (1998) Groundwater quality monitoring as a base parameter in existence of the alluvial aquifers", Proceedings of the International Conference on the World Water Resources at the beginning of the 21st Century :"Water-a looming crisis?" Edited by H. Zebidi, pp.205-211, HP-V, No.18, UNESCO, Paris, France

Modeling Density-Driven Groundwater Flow in Vertical Cross-Sections

Ekkehard Holzbecher

Inst. of Freshwater Ecology and Inland Fisheries (IGB), Rudower Chaussee 30, 12489 Berlin, Germany

Abstract: Density gradients in fluid systems can induce complex flow patterns that are different from the constant density situation. These effects are increasingly studied using numerical models. In order not to be additionally affected by complex three dimensional phenomena, it is recommended to focus on two-dimensional models in vertical cross-sections. In order to set up successful field models codes need to be tested first on established benchmarks. Results for the Elder test case are presented in detail. Other test-cases are mentioned.

Key Words: Density-driven flow, Buoyancy effects, Groundwater, Modeling, Saltwater, Convection, Heat flux

INTRODUCTION

Usually, when groundwater flow is investigated, density effects can be ignored. The main reason is that density gradients are very low. In constant density fluids flow is not influenced by density. But density-driven flow patterns can emerge in natural systems under certainly not rare conditions. A necessary condition is that there are gradients in salinity or temperature. In the following I list some typical circumstances in which those gradients are present:

- in coastal regions, where continental fresh water comes into contact with saline sea-water
- in the vicinity of salt-lakes or other saline ground surface bodies, like salt-marches or salt-crusts
- in regions with sub-surface salt-formations, like salt-layers, salt-domes, embedded salt
- in regions with salinization at the ground surface, for example due to irrigation
- in regions with appearance of hot subsurface water, like in hot-spring reserves
- in the contact between (almost) constant temperature groundwater and seasonally heated/cooled surface water
- when water of different temperature is discharged into the subsurface, like in cold/hot-water storage
- when heat is extracted from the subsurface, as in heat-pumps

The list is probably not complete. Sometimes a combination of reasons is found that cause density differences and may lead to density-driven flow patterns. Thermohaline phenomena emerge when both salinity and temperature gradients are present in a system.

Looking back at groundwater modeling and code development in the last decade, it is obvious that density-driven flow has attracted the attention of most advanced modelers. The irritating feature is that expectations on a density-driven flow model are sometimes higher than expectations on usual flow models.

ANALYSIS

The situation in variable density flow patterns is characterized by an interaction between flow and transport processes. In usual situations with constant density flow and transport can be treated separately.

Flow in porous media can be described by a single differential equation:

$$\frac{\partial}{\partial t}(\varphi\rho) = \nabla\cdot(\rho\frac{\mathbf{k}}{\mu}(\nabla p - \rho\mathbf{g}))$$

with porosity φ, density ρ, dynamic viscosity μ, permeability tensor $\mathbf{k}$, pressure p and gravity vector $\mathbf{g}$. The equation can be derived from the principle of fluid mass conservation and from Darcy's Law. Salt transport can as well be described by a single differential equation:

$$\frac{\partial}{\partial t}(\varphi\rho c) = \nabla\cdot\left(\rho\left(-\mathbf{v}c + \varphi\mathbf{D}\nabla c\right)\right)$$

with salinity c, (Darcy-) velocity vector $\mathbf{v}$ and dispersion tensor $\mathbf{D}$. The transport equation results from the principle of salt mass conservation and from a generalized Fick's Law. In the generalization the diffusivity is replaced by the so-called dispersion tensor

$$\mathbf{D} = \left(D_{ij}\right) = \left((D + \alpha_T u)\delta_{ij} + (\alpha_L - \alpha_T)\frac{u_i u_j}{u}\right)$$

with diffusivity D, longitudinal dispersivity α_L, transversal dispersivity α_T, amount of velocity u and velocity components u_i, u_j. In order to account for effects from temperature gradients the energy equation has to be considered additionally:

$$\frac{\partial}{\partial t}\left((\rho C)^* T\right) = \nabla\cdot\left(-\rho C\mathbf{v}T + \lambda\nabla T\right)$$

with temperature T, specific heat capacity of porous medium $(\rho C)^*$, specific heat capacity of water ρC and thermal conductivity λ. The equation is derived from Fourier's Law and the principle of energy conservation. More details on the derivation of the equations, on simplifications and alternative formulations can be found in Holzbecher (1998). One example: as alternative to the pressure formulation given above the flow equation can be stated in terms of generalized hydraulic head or in terms of streamfunction. The latter alternative is preferred when flow is described in vertical cross-sections and variables are transformed into dimensionless form. For genuine saline or thermal problems the set of differential equations then becomes:

$$\nabla^2\Psi = \pm Ra\cdot\frac{\partial\theta}{\partial x}$$

$$\nabla^2\theta - \frac{\partial\Psi}{\partial x}\frac{\partial\theta}{\partial z} + \frac{\partial\Psi}{\partial z}\frac{\partial\theta}{\partial x} = \frac{\partial\theta}{\partial t}$$

with streamfunction Ψ and normalized salinity or temperature. As only input parameter the dimensionless Rayleigh number $Ra = \frac{g\cdot k\cdot\Delta\rho\cdot H}{\mu\cdot D}$ remains.

Several boundary conditions are required on the boundaries. One of flow conditions has to be stated at all locations along the boundary; one transport condition concerns salinity, another temperature.

Depending on the application different types of boundary conditions have to be specified. Most common are Dirichlet- (1st type) and Neumann (2nd type) boundary conditions. Note that the type of boundary condition is different for the different alternative formulations.

Together with the equations of state in which density and viscosity are given as functions of salinity, and boundary conditions the three differential equations form a nonlinear mathematical problem.

MODELING

As solutions for the problems can hardly be given in an analytical form, these have to be tackled on a computer with use of numerical methods.

Several codes are available which help users to set up their own models of density-driven flow. The FAST-C(2D) code was developed by the author and is described in detail in [1]. The code is based on the streamfunction formulation mentioned above. Some features of the FAST-C(2D) code can be found in references from the author cited below. Modelers use the GeoShell graphical user interfaces to provide input and control data for the simulation code [2,3].

A list of codes other than FAST-C(2D) that can be used to set up models for variable density flow can be found in the internet at address: *http://www.igb-berlin.de/www/abt1/book2/book2.htm*

EXPERIMENTS

Several laboratory experiments have been set up in order to investigate density-driven flow. It is only one aspect that real situations can be represented in an idealized form in experiments in a handy scale and under controlled conditions. Another aspect is that numerical models can be validated easier on experimental set-ups.

A classical experiment for density-driven flow is the Elder experiment, in which a Hele-Shaw cell is partially heated from below [4]. Boundary conditions are discussed in [5].

Fig. **1** shows isotherms and streamfunction contours in a half system. Two eddies emerge from the initial no-flow isothermal situation gradually gaining strength. In the original publication [4] in the final state, representing 20 s after turning on the heater, graphical output shows only one eddy in the half system. Results presented here were obtained with refined grid and improved numerical methods. Figures show flow development in a vertical cross-section, partially heated from below. Six different times are represented in the lines starting form the top. The right figure in each line depicts isotherms. The left figure shows streamfunction contours. Unbroken lines represent positive values and anti-clockwise rotation, solid lines represent negative values and clockwise rotation. Bold zero valued contour is the borderline between the two eddies which emerge with proceeding time.

Several numerical experiments for density-driven flow are reported in scientific publications. Aside from the aim to gain insight into an application case, these experiments are test-cases for developers of new codes for density-driven flow and transport. Some of these are:

- Free steady convection in porous media [1, 7, 8, 9]
- Oscillating convection in porous media [1, 10]
- Horizontal heat and mass transfer [1]
- Henry's problem of saltwater intrusion [1, 11]
- Saltwater upconing [1, 12, 13]
- Salt-dome problem [1, 14, 15, 16, 17]
- Salt-lake problem [1, 18, 19, 20]
- Geothermal flow [1, 21]

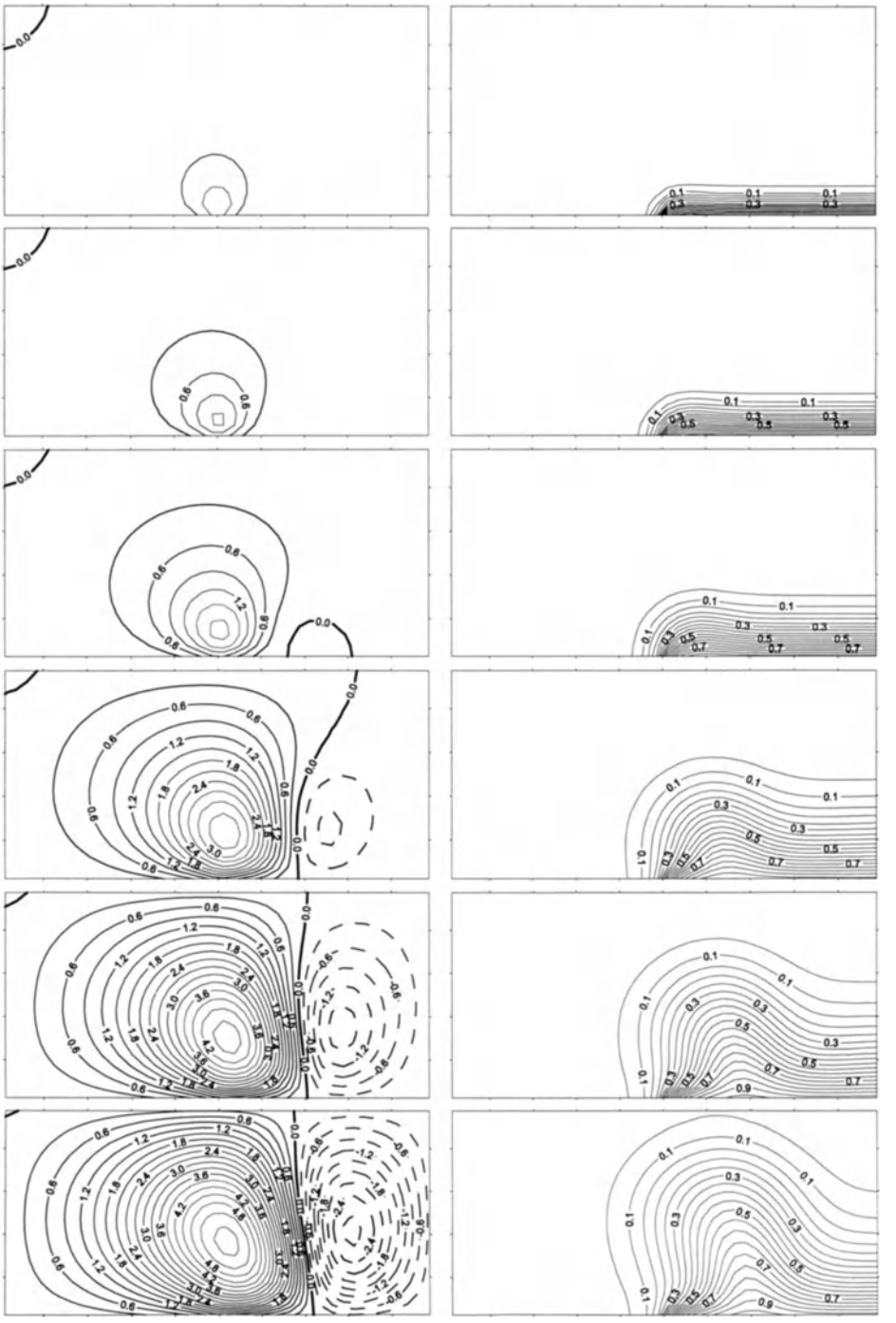

Fig. 1: Model of the Elder heat experiment, set-up and calculated with FAST-C(2D) code

APPLICATIONS

Models for density-driven flow in porous media have been used in application cases. One of the main fields in which such models are applied, is seawater intrusion [22]. In the Henry problem a salt-water wedge enters from the seaside at the bottom of an aquifer (see [1,11]). Driving force for that phenomenon well known from coastal shorelines all over the world is increased density of seawater in relation to fresh water.

With a simple set-up, similar to the one used in the Henry problem, Holzbecher and Kitaoka were able to estimate land subsidence that occurred during an earthquake from increased penetration of the salt-water wedge after the event [23]. As an early example for a field situation the model was quite successful. For the simulation the FAST-C(2D) code was applied.

A more complex model, using FAST-C(2D) was constructed in order to model salt-water intrusion from the Mediterranean into the Nile-delta aquifer [24, 25]. The center cross-section through the middle of the delta from Cairo in the south to the Mediterranean in the north was modeled. It could be shown that saltwater intrusion in it's current state is not problematic, but could become a problem when groundwater pumping rates in the delta will be increased in the future.

The current situation shows that modeling obviously becomes increasingly accepted even for relatively complex phenomena as density-driven flow. Nevertheless the success of the models depends very much on the accuracy and quality of the codes. The codes in turn have to be benchmarked on well established test cases. It is a task of the scientific/technical community to set-up and work-out convenient test-cases. In order to enhance the success of models it is a need that scientists and funding agencies become more aware of this task.

REFERENCES

1. Holzbecher E (1998) Modeling density-driven flow in porous media. Springer Publ., New York: 286p
2. Holzbecher E, Holzbecher H (1993) Input-Shell für verteilte Parameter zur Verwendung in Grundwassermodellen, Forum Bauinformatik, München, in: Mackert , Stark (eds) Fortschrittsberichte VDI, Reihe 20, Nr. 99: 102-108
3. Holzbecher E (1995) Modeling software for groundwater flow, in: Pahl PJ, Werner H (eds) 6.th Intern. Conf. Computing in Civil and Building Engineering, Proc.: 1225-1232
4. Elder JW (1967) Transient Convection in a porous medium. J. Fluid Mech. 27: 609-623
5. Heredia L, Holzbecher E (1986) Model for variable-density-flow, Proposal for test problem HYDROCOIN level 2 case 2, Int. HYDROCOIN project
6. Holzbecher E (1986) Supplement to specification of HYDROCOIN level 2 case 2, internal HYDROCOIN paper: 2p
7. Holzbecher E (1996) Convective heat and mass flow in porous media, 6. V.M. Goldschmidt Conference, Journal of Abstracts, Cambridge Publications, Cambridge: 271
8. Holzbecher E (1997) Numerical studies on thermal convection in cold groundwater. Int. J. Heat Mass Transfer, Vol. 40, No. 3: 605-612
9. Holzbecher E (1998) The influence of variable viscosity on thermal convection in porous media, Heat Transfer 98, Proc.
10. Holzbecher E (1999) On the relevance of oscillatory regimes for convection in porous media, submitted to: Computers & Fluids

11. Holzbecher E, Borisov V, Yakirevich A, Sorek S (1999) Spectral Fourier Methods for Solving Henry's Saltwater Intrusion Problem, submitted to: Computer Methods in Applied Mechanics and Engineering,

12. Holzbecher E (1995) Modeling of saltwater upconing, in: Wang S. (ed.) II. Int. Conf. Hydro-Science and Hydro-Engin., Proc. Vol. 2, Part A: 858-865

13. Holzbecher E, Heinl M (1995) Anisotropy and dispersivity effects on saltwater upconing, Comp. Methods and Water Ressources, Beirut: 117-126

14. Holzbecher E (1990) Modeling saline convection in subsurface water, International Workshop on the Application of Mathematical Models for Assessment of Changes in Water Quality, Tunis

15. Holzbecher E (1991) Zur Modellierung von Dichteströmungen in porösen Medien, in: Holzbecher E, Nützmann G (eds) Modellierung von Strömung und Grundwasser im Grundwasser. TU Berlin, Inst. Wasserbau TU Berlin, Mitteilung Nr.120

16. Konikow LF, Sanford WE, Campbell PJ (1997) Constant-Concentration Boundary Condition: Lesson learned from the HYDROCOIN Variable-Density Groundwater Benchmark Problem. Water Res. Res.h, Vol. 33, No. 10: 2253-2261

17. Holzbecher E (1998) Comments on 'Constant-Concentration Boundary Condition: Lesson learned from the HYDROCOIN Variable-Density Groundwater Benchmark Problem' by L.F. Konikow, W.E. Sanford, and P.J. Campbell, Water Res. Res., Vol. 34, No. 10: 2775-2778

18. Simmons CT, Narayan KA (1997) Mixed convection processes below a saline disposal basin', J. of Hydrology, Vol. 194: 263-285

19. Holzbecher E (1999) Comment on 'Mixed convection processes below a saline disposal basin' by Simmons C.T. and Narayan K.A. (Journal of Hydrology Vol. 194 (1997) 263-285), submitted to: J. of Hydrology

20. Holzbecher E (1999) Salinization of Groundwater from Salt Lakes - Conceptual and Numerical models, 8th Int. Conf. on Conservation and Management of Lakes, LAKE99, Proc.: S4B-2

21. Holzbecher E, Yusa Y (1995) Numerical experiments on free and forced convection in porous media, Int. J. Heat Mass Transfer, Vol. 38, No. 11: 2109-2115

22. Bear J, Cheng AHD, Sorek S, Herrera I, Ouazar D (eds) (1999) Seawater intrusion in coastal aquifers - concepts, methods and practices, Kluwer Acad. Publ.

23. Holzbecher E, Kitaoka K (1993) Saline disasters and modeling approach, XXV. Gen. Ass. IAHR, Tokyo, Proc.

24. Baumann R (1995) Untersuchungen zum anthropogenen Einfluß auf die Salzwasserinvasion im Nildelta. TU Berlin, Inst. für Wasserbau und Wasserwirtschaft, Mitteilung 129: 113p

25. Holzbecher E, Baumann R (1994) Numerical simulations of saltwater intrusion into the Nile Delta Aquifer. in: Peters A, Wittum G, Herrling B, Meissner U, Brebbia CA, Gray WG, Pinder GF (eds), Comp. Meth. in Water Res. X, Proc. Vol. 2, Kluwer Publ., Dordrecht: 1011-1018

Macroscopic Monitoring of Deep Underground Fluid Flow by Repeat Gravity Measurements

J. Nishijima[1], S. Ehara[1], Y. Fujimitsu[1], T. Motoyama[1], N. Shimosako[1], Y. Nakano[1] and K. Yoneshige[1]

[1]Laboratory of Geothermics, Department of Earth Resources Engineering, Graduate School of Engineering, Kyushu University, 6-10-1, Hakozaki, Fukuoka, 812-8581, Japan

ABSTRACT. Repeat gravity measurements have been conducted at four geothermal fields (Takigami, Hatchobaru, Oguni and Yamagawa geothermal fields) and an erupting volcano (Kuju volcano) in Kyushu, Japan for recent several years, in order to monitor the movement of the deep underground geothermal fluid. Common features of gravity changes were detected at both geothermal fields and an erupting volcano. In the production zones or near the active crater, gravity decreased rapidly just after production of geothermal fluid or the phreatic eruption and then rather rapidly increased. After that, gravity decreased gradually and finally became stable. In the reinjection zones, gravity increased a little just after the reinjection of wasted geothermal fluid and after that did not change so much. Such a pattern of gravity change shows that the deep underground fluid flow may rebuild a new hydrological equilibrium state after the commencement of production and reinjection of geothermal fluid or the phreatic eruption. The repeat gravity measurement is concluded one of an effective method to monitor the deep underground hydrological system macroscopically.

Key word. Gravity change, Repeat gravity measurements, Fluid flow monitoring, Multivariate regression model

INTRODUCTION

The production and reinjection of geothermal fluid cause mass fluid movement. These mass redistributions reveal measurable gravity changes at the surface of the earth. Repeat gravity measurements have been carried out in some geothermal fields. Gravity gave its decrement about 1000μgal after 30 years in the Wairakei geothermal field, New Zealand [1].

A strong qualitative correlation has been observed both in the pressure change and gravity change at the Hatchobaru geothermal field, Oita, Japan [2], but quantitative correlation are poor. The observed gravity change depends significantly on changes in shallow groundwater level change [3]. It is necessary to eliminate such effects before applying repeat gravity measurements for the monitoring of the deep underground geothermal fluid movement.

The authors started the repeat gravity measurements at the Takigami geothermal field before the geothermal exploitation. We estimated the gravity changes caused by the seasonal changes of the shallow groundwater level using a multivariate regression model and eliminated this effect in order to extract the gravity changes associated with the production and reinjection of deep underground geothermal fluid

REPEAT GRAVITY MEASUREMENTS

We have been regularly making repeat gravity measurements at four geothermal fields and an erupted volcano: Takigami, Hatchobaru, Oguni and Kuju volcano (central Kyushu) and Yamagawa (southern Kyushu)(Fig. 1). We used Scintrex CG-3 and CG-3M gravimeters to measure precise gravity change. At each geothermal field, repeat gravity measurements were made at intervals of a few weeks to several months. The two-way measurement method was used to evaluate the instrumental drift and precision; we estimated the errors of observation as ± 10 μgal at each study field.

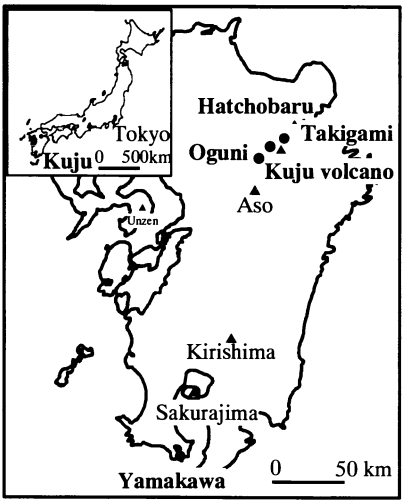

Fig. 1. Study fields for repeat gravity measurements in Kyushu, Japan

GRAVITY CHANGES and DISCUSSIONS

Takigami Geothermal Field. Takigami geothermal field is located in the southwestern part of Oita Prefecture, central Kyushu, Japan (Fig. 1). The Takigami geothermal power station (25MW) was completed in November 1996. We started repeat gravity measurements in May 1991, at 26 observation stations.

We determined the gravity changes caused by the seasonal changes of the shallow groundwater level using a multivariate regression model [4]. This enabled us to eliminate the effects of shallow groundwater level changes and so extract the gravity changes associated with the production and reinjection of geothermal fluid (Fig. 2).

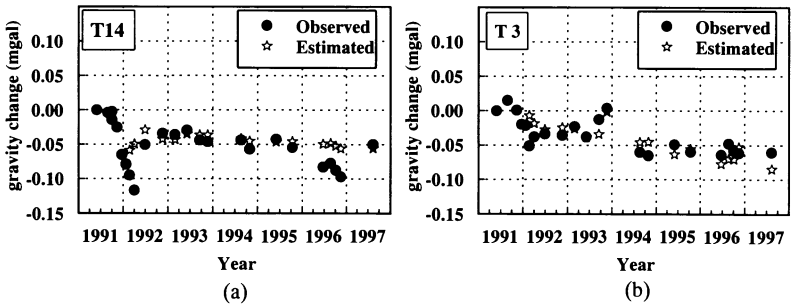

Fig. 2. Comparison between the observed and estimated gravity changes at the Takigami geothermal field. (a): in the production zone, (b):in the reinjection zone.

The residual gravity (due to production and reinjection effects), taken as the difference between the observed and the calculated gravity effect of groundwater level changes at each observation station, can be subdivided into four types of response. The data suggest there were decreases of residual gravity (up to 40 μgal) in the production zone and increases of residual gravity (up to 10 μgal) in the reinjection zone just after the production and reinjection started [4] (Fig. 3).

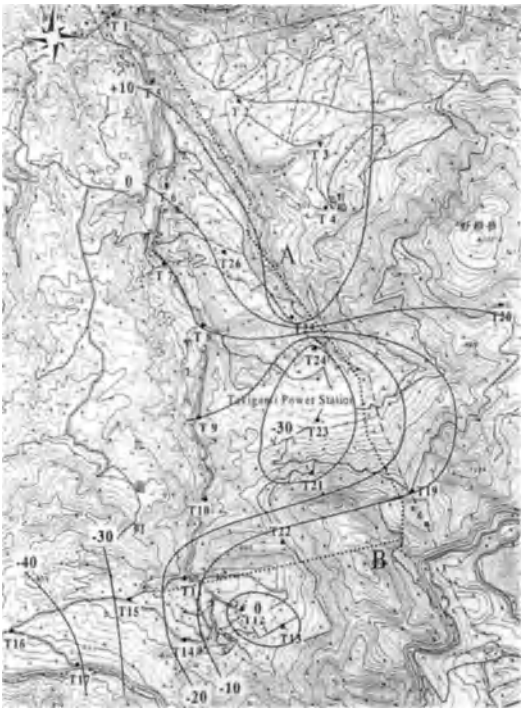

Fig. 3. Contour map of the gravity changes, for which the effect of precipitation has been eliminated, at the Takigami

Hatchobaru Geothermal Field. Hatchobaru geothermal field is located 5km northwest of Kuju volcano, central Kyushu. At this site, Hatchobaru No. 1 unit (55MW) was completed in June 1977, and Hatchobaru No. 2 unit (55MW) was completed June 1990. We started repeat gravity measurements in May 1990 just before the commencement of operation of the No. 2 unit. There are 44 observation stations for repeat gravity measurements.

Increases in gravity were observed in the reinjection zone and part of the production zone just after the commencement of No. 2 unit. After that, a rapid decrease of gravity (up to 200 μgal) was observed in production area (Fig. 4).

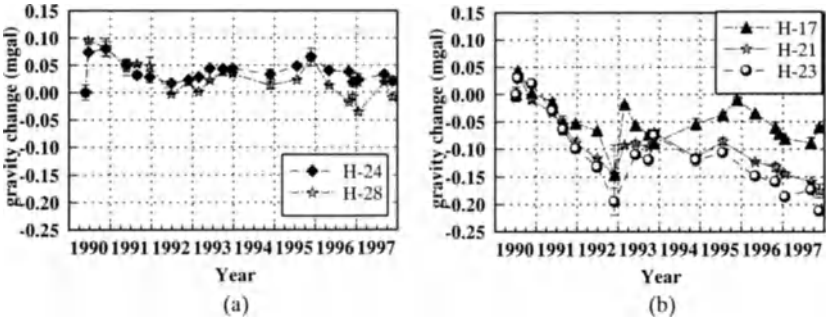

Fig. 4. Example of gravity change at the Hatchobaru geothermal field. (a): in the reinjection zone, (b):in the production zone.

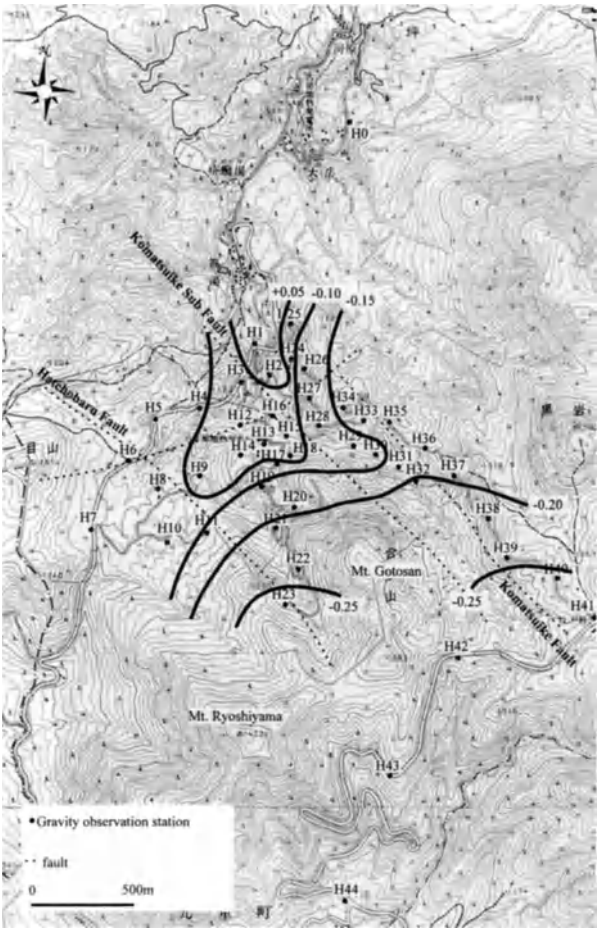

Fig. 5. Contour map of the gravity changes at the Hatchobaru geothermal Field from June 1990 to November 1992.

A contour map of gravity change (from June 1990 to November 1992)(Fig. 5) shows there is the zone of gravity decrease around the production zone, especially towards to southern part of production zone.

Leveling surveys showed that vertical ground movements ranged from –15mm to +35mm from August 1990 to March 1996. Assuming a free-air gradient of -308.6μgal/m, this ground movement caused about –10 to +5μgal of gravity change [2]. Therefore, the effect of vertical ground movement on observed gravity is negligible.

The pattern of gravity change in the production zone is very similar to that of reservoir pressure, and there is good correlation (>0.8) between gravity change and reservoir pressure [2]. This result shows that the decrease of gravity in the production zone reflects the net mass loss in the reservoir.

Application of Gauss's Potential Theorem [5] to gravity changes gives quantitative estimate of the mass changes. Based on the produced and reinjected mass and the values of the net mass change, we calculate there has been a natural mass recharge of 16.3Mt (Fig. 6).

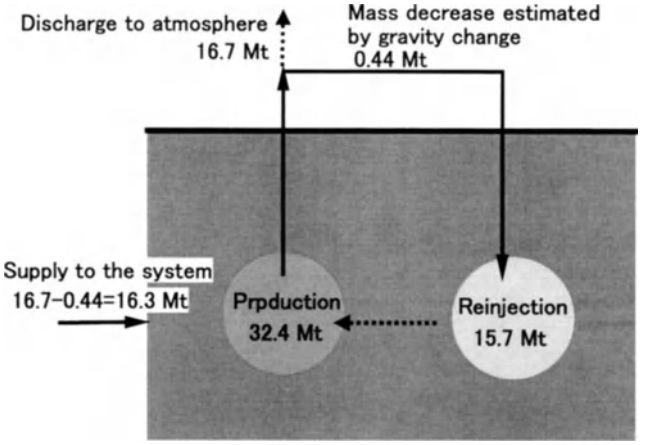

Fig. 6. Mass balance in the production and reinjection zones at the Hatchobaru geothermal field.

Oguni geothermal field. Oguni geothermal field is located in the northeast part of Kumamoto Prefecture. We started repeat gravity measurements in September 1993, at 28 observation stations. In this field, we try to grasp the background gravity changes before development to estimate the background gravity change by applying a statistical technique.

Gravity changes (up to 170μgal) were observed from September 1993 to August 1997. Examination of the data shows there is a good correlation of gravity with precipitation, with a phase lag of about 6 months exists. As a result, these gravity changes are attributed to changes of shallow ground water level.

Yamagawa geothermal field. Yamagawa geothermal field is located southern Kyushu. The Yamagawa power station (30MW) was completed in March 1995.We started repeat gravity measurements in June 1996, at 22 observation stations, and we have repeated gravity measurements at an interval of about three months.

These gravity changes can be subdivided into two types of response. On one hand, the gravity changes seasonally, and there is good correlation between the gravity changes and shallow ground water level changes. This type is located in the southern part of the field. This type is attributed to changes of the shallow ground water level change.

On the other hand, the stations that are located in the northern part of the field, show increases of gravity from June 1996 to August 1997 and decreases from August 1997 to December 1997. There is poor correlation between gravity changes and ground water level changes.

Kuju volcano. Kuju volcano, central Kyushu, began to erupt on 11 October 1995. And the second eruptions occurred in December 1995. After that, no eruptions occurred, but crater activities still continue. Precisely repeated gravity survey began from 14 October 1995, every two weeks to clarify gravity changes caused by eruption.

Gravity decreases up to 90 μgal, were detected in the gravity stations around the new craters in the period from 19 October 1995 to 13 January 1996 (Fig. 7). After that, the rate of gravity decrease became smaller. This rapid gravity decreases may be attributed to changes of the shallow ground water level by the vaporization of ground water heated by the magmatic fluid. Recent gravity changes about three years after the eruption may be attributed to seasonal variation of ground water level.

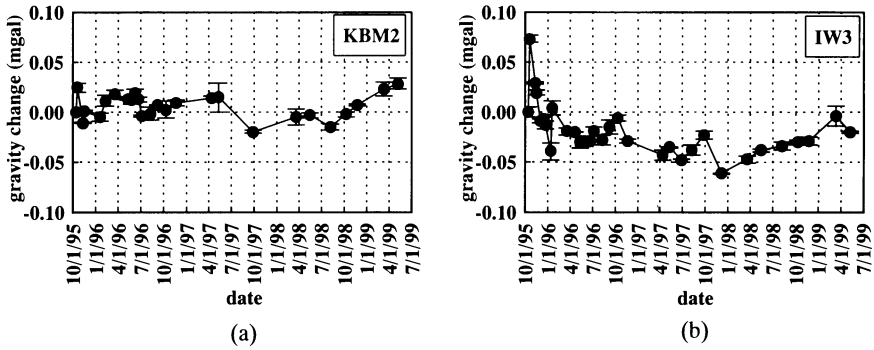

Fig. 7. Example of gravity change at the Hatchobaru geothermal field. (a): distant from the new craters, (b):near the new craters.

Estimation of underground mass balance that is mainly water, based on Gauss's theorem shows that the ground water recharge from the region around new craters is increasing after the eruption and about three months after, the underground water flow is gradually reaching to the equilibrium state.

CONCLUSIONS

We have conducted repeat gravity measurements at four geothermal fields and an erupting volcano. Especially, in the Takigami geothermal field, we estimated the background gravity change that is caused by seasonal changes of shallow ground water level by using the multivariate regression model relating gravity to precipitation. As a result, we were able to estimate the back ground gravity change with an accuracy of $\pm 20\mu$gal. We can use the correlation to eliminate the effect of the background gravity change. Residual gravity increases of up to 10 μgal were detected in the reinjection zone, and residual gravity decreases of up to 40 μgal were detected in the production zone. These residual gravity changes are consistent with the changes in mass balance in the geothermal reservoir. Thus, the effects of field operations can be isolated, even for fields with relating low production rates like Takigami. These estimation and the results of repeat gravity measurements show that repeat gravity measurements is an effective method to monitor the underground hydrological systems.

REFERENCES

1.Allis, R. G. and Hunt, T. M., 1986, Analysis of exploitation induced gravity changes at Wairakei geothermal field. Geophysics, Vol. 51, pp.1647-1660.
2.Tagomori, K., Ehara, S., Nagano, H and Oishi, K., 1996, Study on reservoir behavior based on gravity changes in the Hatchobaru geothermal field, Jour. Geothermal Research Society of Japan, vol. 18, pp. 91-105.
3.Ehara, S., Fujimitsu, Y., Motoyama, T., Akasaka, C., Furuya, S., Gotoh, H. and Motomatsu, T., 1995, Gravity monitoring of geothermal reservoirs – A case study of the production and reinjection test at the Takigami geothermal field, central Kyushu, Japan, Proc. World Geothermal Congress, 1995, pp. 1955-1958.
4.Nishijima, J., Fujimitsu, Y., Ehara, S., Motoyama, T., Shimosako, N., 1999, Reservoir monitoring by observation of gravity changes at the Takigami Geothermal Field, Central Kyushu, Japan, Geothermal Resources Council Transactions, Vol. 23, pp. 425-431.
5.La Fehr, T. R., 1965, The estimation of the total amount of anomalous mass by Gauss's Theorem, Jour. Geophys. Res., vol. 70, pp. 1911-1919.

Investigation and Analysis on Changes of Discharge and Saline Concentration of Groundwater in an Alluvial Plain

Masaru OJIMA
Member of IAHR, Civil and Environmental Eng., Faculty of Eng., Fukuyama Univ.
Gakuencho-ichibanchi Sanzo, Fukuyama 729-0292, Japan

ABSTRACT
The regions of this research, in Tokushima Prefecture, have been blessed with abundant groundwater since ancient times. Therefore, until quite recently the amount of groundwater available for use was substantial. Now, however, groundwater levels are declining and water quality is worsening in several zones.
Therefore, it was recognized that a comprehensive investigation of groundwater activity was a most urgent subject. And secondly, the future predictions of negative effects of water use must be accelerated.
It was collected as much as possible through field investigation, data of precipitation, discharge of river flows, water levels at observation wells and pumping volumes.
Several hydraulic analyses were carried out based on the survey data in order to clarify the characteristics of groundwater hydraulics in this area.

KEY WORDS: field investigation, fluctuation of water level
saline concentration, correlation analysis

INTRODUCTION

From the National Land Agency, the amount of water use in 1994 in Japan, was estimated at about 90.8 billion m^3, and judging from the origins of the water resources, river water accounted for about 77.8 billion m^3 (85.7% of the national total), whilst groundwater accounted for about 13.0 billion m^3 (14.3%). In addition, other groundwater was pumped for fishery purposes and for buildings cooling. The volumes used were 1.8 billion m^3 and 0.98 billion m^3, respectively. Therefore, the total volume of groundwater use amounts to about 15.77 billion m^3, with the following breakdown; municipal use 25.7%, industrial use 32.1% agricultural use 24.6%, fishery use 11.4% and building cooling use 6.2%.
In the alluvial plain of the eastern part of Tokushima Prefecture, the region studied in this investigation, there was always sufficient groundwater and riverbed water and so rates of pumping have been quite large since early times. But, recently, the decline in groundwater level and the worsening of water quality are appearing in some regions of this prefecture. It seems that the above-mentioned phenomena are caused by a change in groundwater runoff in facts such as the change in hydrological and meteorological conditions, the transition of water usage, and the progress of river improvements. Therefore, it has been recognized as an urgent subject to estimate an accurate existence of groundwater, to forecast a highly precise future impact, and to propose prevention or reduction means against groundwater obstacles.

GENERAL CONDITIONS OF THE REGION INVESTIGATED

Geographical and Geological Condition of Tokushima Plain

In this region, both the Yoshino River and the Naka River flow eastward into and the Seto-Inland Sea. The Tokushima Alluvial Plain was formed by the accumulation of earth and sand transported by river runoff.
These river systems are especially important from the viewpoint of national land conservation and the national economy, so each has been designated as a Class A river by the Ministry of Construction.
The drainage area of the Yoshino River is about 3750km^2; its main length is 194km and its total length is about 1600km. It ranks in 18-th order of drainage scale in Japan. On the other hand, the Naka River falls within the middle scale range with a drainage area of 874km^2, a main length of 125km and total length of about 360km.
The sub-surface geological strata are as follows: overlying basement rock which consists mainly of Izumi-sand stone and Sanpagawa-crystal schist, there is alluvial gravel, termed the D-layer. Above the D-layer, exists the so-called C-layer gravel which was formed about 18,000 years ago,

and then above the C-layer, lies the B-layer consisting of silt and clay, which was formed about 6,000 years ago. The top stratum is the so-called A-layer formed by river sediments of mainly sand and sandy-gravel. In the characteristics of hydrogeology of this region, the A-layer is an unconfined aquifer, its-thickness is about 10～20m, the B-layer is an aquitard its thickness increases toward the coast, and its maximum thickness is about 30m near the coast. These aquitards are, however, exhausted both at about 22km upstream of the Yoshino River and about 8km upstream of the Naka River. Both the C-layer and D-layer are good aquifers. The thickness of the C-layer is about 30～50m, and that of the D-layer is generally larger than the C-layer.
The groundwater existing in both the C-layer and D-layer is confined to the downstream regions where the aquitard B-layer is located. The values of permeability coefficients obtained by past pumping tests, vary widely and are as follows. A-layer: 9.8×10^{-4}～2.64×10^{0}cm/sec, B-layer: 3.7×10^{-6}～5.0×10^{-5}cm/sec, and C-layer: 1.0×10^{-2}～4.75×10^{0}cm/sec.

Precipitation and Discharge Conditions
Topographically, the steep Shikoku Mountains run east to west in the central part of Shikoku Island. The climate is mild, and the yearly mean temperature is 15 to 17 °C. However, Shikoku is frequently visited by baiu fronts and typhoons and is one of the most pluvial districts in Japan. Annual precipitation reaches 2500 to 3500mm in the southern zone of the Shikoku Mountains and 1200 to 1500mm in the northern zone. Because the drainage area of the Naka River lies in the southern part of the Shikoku Mountains, the amount of precipitation exceeds 3000mm in the upstream zone, and reaches 2000 to 2500mm in the downstream zone.
The discharge duration conditions of both rivers are shown in Table 1.

Table 1 Discharge duration conditions

	Normal discharge (185-day discharge)	Low discharge (275-day discharge)	Drought discharge (355-day discharge)	Annual mean discharge	Annual total runoff	
Yoshino River (Chuo-Bashi)	65.53	44.19	29.55	123.01 (m^3/s)	4172×10^6 (m^3)	(1976～1995)
Naka River (Furusho)	28.55	14.48	7.49	66.63 (m^3/s)	2104×10^6 (m^3)	(1956～1991)

The flood runoff of these rivers is generally sharp with high peak discharge within a short duration. Though the annual precipitation is relatively large due to occasional torrents during the typhoon season, the discharge of rivers is normally small in other seasons. Namely, drought discharges of the Naka and Yoshino rivers are 7.49m^3/sec, and 29.55m^3/sec, respectively. And the low discharges (275-day discharge) are 14.48m^3/sec and 44.19m^3/sec, respectively. As shown in this table, the discharge conditions of the Yoshino River are relatively 3 or 4 times more stable in comparison with those of the Naka River. The facts in the above-mentioned are shown as the difference in coefficient values of each rivers regime, namely 900 and 256, respectively.

GROUNDWATER INVESTIGATION AND CONSIDERATION

Investigated regions
The extensive area chosen as the object of the first study is shown in Fig. 1. It is a lowland about 40km^2 stretching from the Yoshino River Bridge (4.6km upstream from the river-mouth) to the Nada Bridge (10.4km upstream) along the course of the Yoshino River. The 32 new observation wells were chosen as an arrangement throughout this area in 1983. At seven observation wells, A～G in Fig. 3, a daily monitoring of the groundwater level has been conducted by the Ministry of Construction. [1]
The second extensive area covering the whole downstream basin of the Naka River is shown in Fig. 2. It is also a lowland about 50km^2 stretching from the river-mouth to the Mochii Bridge (11.2km upstream). This objective area was divided into three zones. Namely, the first is a triangle zone lying between the Naka River and the Kuwano River, in which a great volume of pumping is carried on, the second is the left bank side of the Naka River and the third is in the southern part of the Kuwano River. As shown in Fig. 2, about 40 observation wells were chosen to make an arrangement crosswise in this area. Furthermore, data of ten observation wells A～K, in Fig. 2 were investigated by the public agencies of this district from 1981 to 1998 [2].

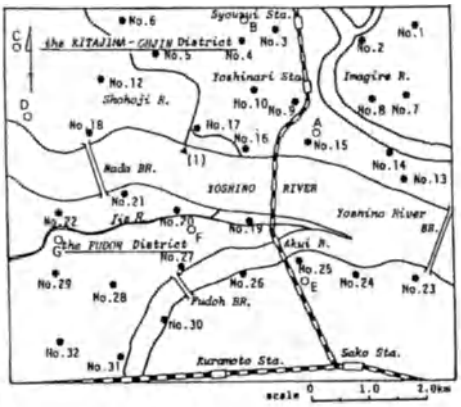

Fig. 1 Investigated region of the Yoshino River basin and observation wells

Fig. 2 Investigated region of the Naka River basin and observation wells

Fluctuation in groundwater level

(1) Characteristics in the Yoshino River basin

Using data obtained for the 11-year period from 1974 to 1984, long term variation characteristics of the unconfined groundwater in the A-layer of this basin were determined. In Fig. 3, fluctuations in the monthly maximum groundwater level are shown by solid lines and those of the monthly minimum by dotted lines together with monthly rainfall recorded at the Tokushima Meteorological Observatory. Long term variations tendencies are shown graphically in Fig. 4.

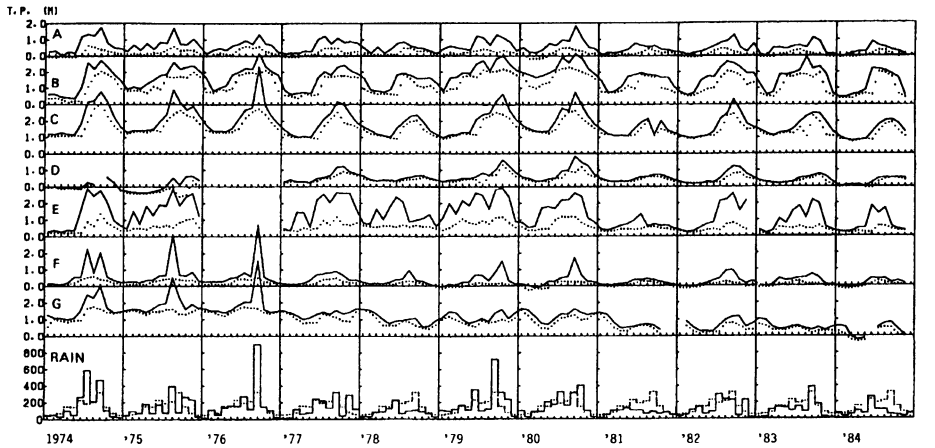

Fig. 3 Monthly fluctuations in groundwater level and rainfall

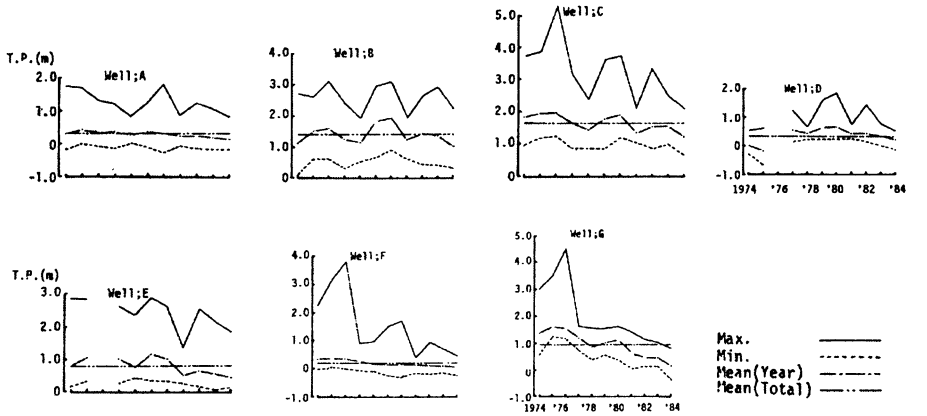

Fig. 4 Long term variations in water level in each well

Fluctuation characteristics based on these diagrams are as follows:

i) The mean value for the total annual rainfall during 11 years, from 1974 to 1984, 1620mm, is somewhat small in comparison to, the average for the 30 years from 1941 to 1970 (1800mm). Therefore, the long term trend seems to be gradually decreasing.

ii) Fluctuations in the groundwater level in the left side zone of the Yoshino River, show that an increase in the water level takes place in summer and a decrease in winter, the fluctuations agreeing with the varied pattern of rainfall. Because the most prominent fluctuations are shown for wells B and C in Fig. 4 and the minimum groundwater level for each well increases during the irrigation season, it seems that the groundwater supply is in excess of its consumption, namely the amount used in groundwater pumping in this area.

iii) As shown by the fluctuations for wells E, F and G, there is a marked difference in comparison with fluctuations at wells in the left-side zone. Because the minimum water level during the irrigation season shows only a slight rise, the groundwater supply is estimated as being less than the amount of water consumed. At well G in particular, from 1977 to 1984, the highest water level appears in winter and the lowest in summer, as evidence that the groundwater supply is not sufficient to meet the demands of pumping in summer. These phenomena are called over-pumping of groundwater.

(2) Characteristics in the Naka River basin

Using data obtained for the 15-year period from 1981 to 1995, the long term and middle term variation characteristics of the groundwater are discussed. In Fig. 5, fluctuations of the monthly mean groundwater level of each observation well (A-layer) and the monthly mean river water level are shown curves with symbol numbers together with monthly rainfall.

And those in the monthly mean value of each confined well (C-layer) are discussed similarly.

Fluctuation characteristics based on these diagrams are as follows;

i) The mean value for the total annual rainfall during 15 years, from 1981 to 1995, is 1971mm. The value of a drought year of this period, 1984, is 1327mm and that of the wettest year, 1990, is 3003mm. Therefore, it is evident that the range of fluctuations in rainfall is fairly large.

ii) The fluctuation pattern in the groundwater level at shallow wells (A, B) in the right side zone agrees approximately with the varied pattern of rainfall. But, judging from the coefficient of simple correlation between groundwater and rainfall, it is not so large such as 0.68 for well A, and 0.40 for well B. On the other hand, the coefficients of correlation for river water, are 0.80 for A, and 0.53 for B, respectively, which seem better responses than the former.

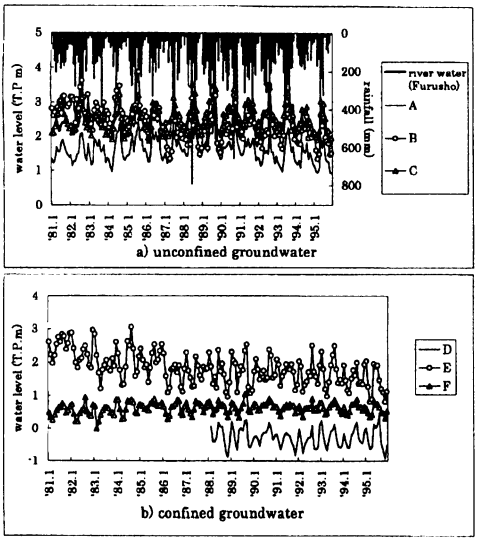

Fig. 5 Monthly fluctuation patterns for observation data

iii) As for the fluctuation in the groundwater level at well C in the left side zone, the coefficient values for rainfall or river water are 0.72 or 0.75, respectively. And the coefficient values for shallow wells A, B are 0.91 and 0.61. Good responses are indicated between mutual groundwater wells in this area.

iv) There is a clear tendency of a draw-down in groundwater level (water head) during the long-term in the right side zone of the Naka River. On the other hand, in the left side zone, there is rather a clear tendency for the groundwater level (head) to increase.

Salinity behavior in aquifers of the second objective region [3]

In the estuary basin of the Naka River, since about 1961 the intrusion of seawater into the confined aquifers is gradually actualized along the coast, and then in the early 1970's, the distributing zone of the self-spouting wells has been intruded by excess saline concentration of seawater for the permissible criteria of drinking water (200mg/ ℓ). These causes are estimated whereby the amount of pumping increased more than in proportion to the spread of aquaculture such as eel or ayu, and that the total amount of intake for industrial water or city water increased much more than in proportion to the urbanization of this area.

The change of Cl-concentration in the confined aquifer, for example, is shown in Fig. 6.

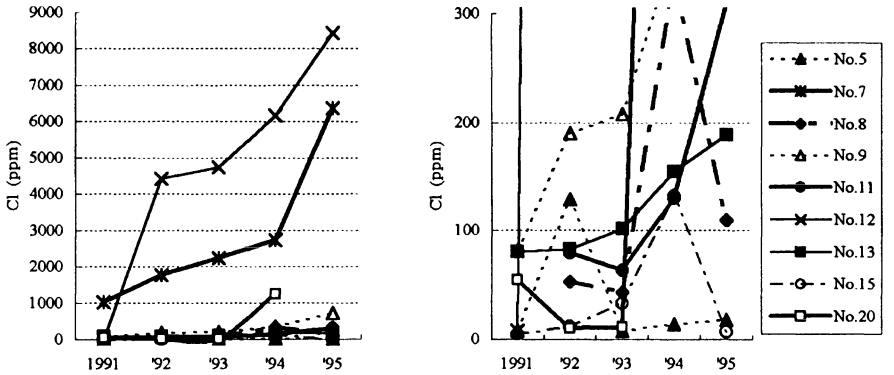

Fig. 6 Yearly changes of saline concentration in each well

There were at least six saline-intruded wells, namely, No. 7, No. 8, No. 9, No. 11, No. 12 and No. 20. It was found that the intrusion of salinity had made scarce progress since 1990. The concentration values at No. 12 and No. 7 wells, however, are increasing sharply and reach a high value of 6000～8000mg/ℓ.

POSTSCRIPT

In this study, monthly observations were made of groundwater level and vertical distribution of saline concentration, and several hydraulic analyses based on the survey data obtained were made.

The main discussions are as follows;

1) Using the observation data for the groundwater level at each of the 7 wells during the 11-year period from 1974 to 1984, the long term variation characteristics of the unconfined groundwater level in the estuary basin of the Yoshino River were determined by auto-correlation coefficients, cross correlation coefficients and power spectrum.
2) Using the data obtained for the groundwater level at each of the 11 wells during the 15 years from 1981 to 1995, the long term and middle term variation characteristics of the groundwater in the estuary basin of the Naka River were estimated.
3) Using the Cl-concentration values for the confined observation wells, the activity of the saline intrusion into the confined aquifers in the estuary basin of the Naka River were made clear.

REFERENCES

1. Ojima, M. (1986), Natural Disaster Science, Vol. 8. No.2 pp.29～48.
2. Office Reports (1999), Observation Data, the Ministry of Construction.
3. Ojima, M. (1998), Proc. of the 5th China-Japan Groundwater Seminar,

Land-use Intensity as a Key Factor towards Unsustainability of Groundwater Resources: the case of Israel's Coastal Aquifer

Abraham J. Melloul[1] and Martin L. Collin[2],

1. Hydrological Service, Water Commission, P.O.Box 6381, IL-91 603 Jerusalem, ISRAEL
2. Hydrological Service, Water Commission, P.O.Box 57081, IL-61 570 Tel-Aviv, ISRAEL

ABSTRACT. Sustainable groundwater management guidelines must highlight various factors which can, in parallel, lead to unsustainability. These include environment and land-use. Both can lower groundwater quality and availability, and ambient environmental quality. Environmental factors which characterize the sensitivity of the media to percolation and recharge from the ground surface into the aquifer are natural factors which are difficult to alter. In contrast, such land-use factors as excessive demand for agricultural irrigation, population pressure, resource demands, market structures, and other anthropogenic activities can more easily be handled and remedied. The objective of this paper is to highlight land-use factors leading to unsustainability, taking into consideration environmental factors which enhance these adverse effects and impede sustainable groundwater management. Two areas of Israel's Coastal aquifer have been considered in this paper, each representing different hydro-ecological and demographic situations. Environmental sensitivity of the two areas is considered, and land-use concentrations are recommended, to respond to the desired groundwater resource needs of these areas. Such an approach is can tie land-use planning guidelines to sustainable groundwater management.

KEYWORDS: land-use alteration, environmental factors, sustainable groundwater management, planning, anthropogenic pollution,

INTRODUCTION

Coastal regions are generally characterized by high levels of population and intensive land-use and urbanization [1]. Urbanization of coastal phreatic aquifers is most often accompanied by a rise in anthropogenic pollution percolating to the water tables [2, 3, 4, 5,], along with a rise in salinity from sea water intrusion owing to a drop of inland hydraulic head following excessive pumpage [6]. In the United States, in Boston, Staton Island, and Philadelphia [1]; Chicago [7]; and Baltimore [8,9] land-use levels have been harmonized with natural terrain restrictions and attempts have been made to assess the relative degree of intolerance of the terrain with regard to given land-use alterations by relocating port and industrial centers and replaced these with parkland and open-space, accessible to the public.

In Israel, innovative suggestions have been advanced regarding development of the Mediterranean coast near Tel Aviv and Haifa. These involve patterns similar to those embarked upon in Chicago and Baltimore, with public parkland and marinas along the seafront, and even the building of islands off the coast for further residential and commercial development [10]. Long-term land-use planning and integrated ecological perspectives are thus increasingly becoming the norm for land-use alteration. Regrettably, urbanization in stressed coastal aquifers has amplified unsustainability factors [11, 12], and resulted in a malaise, limiting the human spirit, sharply reducing quality of life, degrading the quality and lowering the quantity of resources available to users, and impeding sustainable groundwater development [13]. It is

therefore urgent to determine and control these unsustainability factors in order to mitigate their adverse effects upon sustainable groundwater management [14, 15].

ENVIRONMENTAL AND LAND-USE UNSUSTAINABILITY FACTORS

Floods, high winds, etc, along with low natural vegetative groundcover, can lead to rampant erosion, which can cut into steep slopes denuded of vegetation, sedimentation may clog streams. High levels of natural recharge are desirable in a clean environment. In an unclean environment, recharge can lead pollute groundwater resources. Above highly permeable soils, inappropriate placement of industrial or commercial sites, or high-intensity residential areas can significantly degrade groundwater quality. Intensive irrigation with minimally treated effluents, excessive administration of fertilizers or pesticides can have a serious impact upon groundwater in below permeable soil. Excessive pumpage can clearly have a severely detrimental effect upon available resource reservoirs, lowering water tables and altering groundwater flow-directions. In coastal aquifers, this enables intrusion of saline sea water into fresh inland reservoirs, making salinisation almost irreversible.

Unsustainability factors can also be social, economic, and ecological. Socio-economic norms affect population growth. The degree to which a society's population succeed in getting used to "dirty their own nest" and wasting without thinking of tomorrow is a social illness. These tendencies can be mitigated and impeded by appropriate education, and by altering market structures. For instance, potential pollutants can be recycled as raw materials for on-going manufacture. The planning process should control these unsustainable factors as regard their environmental context and society's needs .

In this paper, certain guidelines are proposed to control these unsustainability factors and mitigate their adverse proclivities for groundwater. The ultimate objective is to arrive at optimal and sustainable development

METHODOLOGY

This paper focuses upon guidelines for sustainable groundwater management, involving the combination of two factors: environmental potential for water recharge (PWR) and land-usage potential of groundwater pollution potential (GPP). Together, these factors can characterize an area of study and yield to guidelines for sustainable groundwater resource management. Key unsustainability factors which could impede sustainable development can be pinpointed. Numerical evaluation of PWR and GPP values can be obtained by averaging weights of specific environmental sensitivity and land-use categories intensities.

Table 1 presents environmental factors along with land-use categories and concentrations, enabling characterization of a study area. Four environmental categories are considered: hydrology, physiography, soils, and ambient vegetation. To assess sensitivity, each factor is subdivided by ranking criteria. For each environmental factor, five land-use types are considered: conservation, recreation, agriculture, residences, commerce and industry. Certain land-use categories have varying intensities. Agriculture use can involve field crops which tolerate and therefore receive high levels of pesticide and fertilizer applications, or orchards which are so sensitive to salinity that they restrict use of pesticides and fertilizers to minimal application levels. Each category can vary from low to high intensity usage.

Combining environmental and land-use categories and concentrations, this table delineates "scenarios". A set of scenarios can characterize a specific area. For each, appropriate groundwater water management is required. To numerically assess these conditions, PWR and GPP must be numerically evaluated and weighted. Table 1 presents four levels of sensitivity with regard to environmental factors as well as land–use impact. Highly sensitive environmental factors and significant land-use impact upon groundwater quality are represented by "H" = 4; moderately high by h = 3; moderately low by l = 2; and low by L = 1. Combined weightings characterize an area.

Table 1. Combined Influence of Potential of Water Recharge for Environmental Factors (PWR) and Groundwater Pollution Potential from Various Land-usages (GPP)

Environmental Factors				Land-usage Categories and Intensities								
Categories	Components	Conditions		Conser-vation	Recreation		Agriculture		Residential		Industry and Commercial	
					Low	High	Orchards	Field Crops	Low	High	Low	High
			Potential Impact ⇨ / Rechargibility ⇩	L / E	L / E	h / R	l / R	h / R	l / E	h / R	h / R	H
Hydrology	Water Table	Shallow	H / E	HL	HL	Hh	Hl	Hh	Hl	Hh	Hh	HH
		Deep	l / R	lL	lL	lh	ll	lh	ll	lh	lh	lH
	Recharge	High	H / E	HL	HL	Hh	Hl	Hh	Hl	Hh	Hh	HH
		Low	l / R	lL	lL	lh	ll	lh	ll	lh	lh	lH
	Hydraulic Conductivity	High	h / E	HL	HL	Hh	Hl	Hh	Hl	Hh	Hh	HH
		Low	l / R	lL	lL	lh	ll	lh	ll	lh	lh	lH
Physio-graphy	Slope	< 20%	h / E,R	hL	hL	hh	hl	hh	hl	hh	hh	hH
		> 20%	L / -	lL	lL	lh	ll	lh	ll	ll	lh	lH
Soils	Permea-bility	Perme-able	H / E	HL	HL	Hh	Hl	Hh	Hl	Hl	Hh	HH
		Imper-meable	L / R	LL	LL	Lh	Ll	Lh	Ll	Ll	Lh	LH
Tree and Other Vegetation Cover		Low	h / E,R	hL	hL	hh	hl	hh	hl	hl	hh	hH
		High	l / -	lL	lL	lh	ll	lh	ll	ll	lh	lH

Key symbols: H = high; h = moderately high; l = moderately low; L = low
In the darker cells: Names of the study areas: E for Erez –Shikma; R - for Raannana area

PWR and GPP are the perpendicular axes in Table 2. Average PWR and GPP values from Table 1 yield coordinates delineating the position of the study area as regards these factors. This table delineates four "extreme situations", a, b, c, and d. Each requires particular groundwater management measures.

For a = HL, the area has the highest PWR and lowest GPP. Groundwater recharge from the surface with fresh water would have highest priority.

For b = HH, the area has the highest PWR and highest GPP. Highest priority for pollution prevention must be given to this situation.

For c = LL, the area has lowest PWR and lowest GPP. Groundwater recharge into wells with fresh water would have highest priority.

For d = LH, the area has the lowest PWR and highest GPP. In situ remediation of groundwater would have highest priority.

In a given study area, situations would likely fall between these extremities, such that differing appropriate operational measures would apply.

Table 2. Characterization of Study Areas as regards Environmental Factors and Land-usage Concentrations

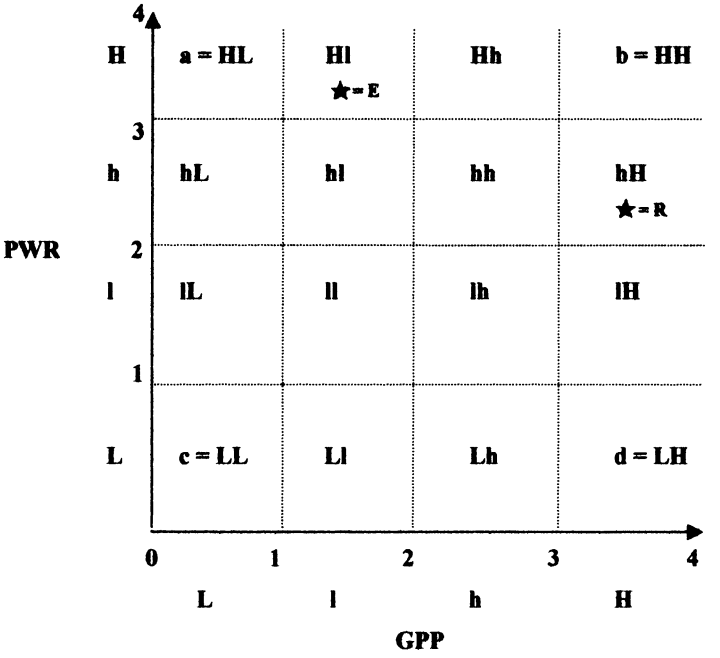

where a = highest PWR and lowest PGP, b = highest PWR and GPP, c = lowest PWR and GPP, d= lowest PWR and highest GPP

Key: Weighting Values: H = 4, h = 3, l = 2, L = 1; Area Symbols: R = Ra'anana, E = Erez Shiqma

APPLICATION TO THE ISRAEL COASTAL AQUIFER

Israel's coastal plain extends from Mt. Carmel in the north to the Gaza Strip in the south, from the seashore on the west to the limestone aquifer on the east . The aquifer is composed of layers of dune sand, sandstone, calcareous sandstone, silt, loams and clay lenses [16].

Two study areas were selected for this paper. The first is the urban Ra'anana vicinity (R), northeast of Tel Aviv. The second is Erez-Shiqma (E), a low-density dune area characterized by low anthropogenic activity, extending between Ashqelon and the Gaza Strip, south of Tel Aviv. Specifications characterizing these areas are presented on the shaded cells by the symbols E and R. Each shaded cell corresponds to a numerical level, enabling evaluation of average PWR and GPP values for the study areas. Thus, the arithmetic mean for rechargability (shaded column) for the more developed Ra'anana area is 2.2, whilst that for the Erez-Shiqma area is 3.5. The arithmetic mean for potential impact of land-usage (shaded row) for the Ra'anana area is 3.0, whilst that for the Erez-Shiqma area is 1.3. The combined PWR/GPP for the Ra'anana area

places it within the hH cell of Table 2, whilst the combined PWR/GPP for the Erez-Shiqma area places it within the Hl cell of the table. These values closely relate to the eco-hydrological situation of the study areas [17]. Potential pollution site density (Pollsite) of the Ra'anana area clearly exceeds that of Erez-Shiqma [12].

DISCUSSION AND CONCLUSIONS

Table 2 indicates that the Ra'anana area differs substantially from the Erez-Shiqma area as regards land-use planning and recharge of the aquifer. In the Erez-Shiqma area, pollution remains at a relatively low level, such that land-use siting guidelines must be enforced to maintain groundwater availability and quality. This is a coastal area, where the waterfront could be properly developed for low-intensity recreation [7, 8, 9] while maintaining the open, sandy ground for maximal natural surface recharge from seasonal rainfall and artificial recharge with fresh water, as from a planned desalinization plant. Groundwater management should involve appropriate measures to combat sea water intrusion. By way of contrast, Table 2 shows the Ra'anana area to be more polluted, so that land-use guidelines must aim at mitigating potential pollution. Recharge is still possible in this area, but only by means of injecting treated water into wells. Table 1 shows that the Ra'anana area, in contrasted to Erez-Shiqma, is characterized by deeper water tables, lower levels of recharge potential, hydraulic conductivity, and permeability, low slope and low amounts of vegetative cover on the land. Environmental factors themselves clearly mitigate potential pollution of groundwater in the area. Nonetheless, improved long-term land-use planning in the area should be tied to these natural characteristics.

The environmentally stressed Ra'anana area should incorporate renovation of urbanized land and stringent ecological guidelines. These should maximize tree cover and ground vegetation, public access to natural amenities within urban environs, and effectively zone industrial, residential, agricultural, and natural areas so as to promote optimal efficiency and life quality for each land-use involved.

In more pristine areas, as in the Erez-Shiqma area, new land-use alteration can still be conducted in accordance with constructive environmental guidelines to produce results which will maintain its well area's ecological character while providing for the economic and residential needs of the population.. Remediation methods should include recharging water and use of the area for groundwater recharge and as a multi-annual groundwater reservoir.

The approach taken in building "new towns" should enable decision-makers to proceed in a comprehensive and ecologically sound manner. Where land has already been significantly altered, comprehensive renovation can relieve the stress and raise the quality of life of the region. Utilizing these guidelines for delineating the ideal land-use for any area requires employing land types for the purpose for which they are most suited.

Such unsustainability factors as a significant decline of groundwater quality and quantity can result from inappropriate patterns of land-use. A rational approach to land-use planning should take into account the complex ecological, hydrological, social, educational, and economic parameters which characterize every region, and should result in a healthy and appropriate "fit" to present and future society, and to groundwater sustainability.

REFERENCES

1. McHarg I L (1969) Design with Nature. Doubleday, N.Y. 198 pp.
2. Muszkat L, Rosenthal E, Ronen D, Margaritz M (1989) Organic contaminants in the Israeli Coastal aquifer. Environmental Quality and Ecosystem Stability, Proceedings of the 4th International Conference of the Israel Society for Ecology and Environmental Quality Sciences. Jerusalem. . IV-A:471-477.
3. Melloul AJ, Goldenberg LC (1994) Groundwater pollution by airborne toxic contaminants: a factor to be considered in groundwater management. GQM 93, Ed. Kovar and Soveri, IAHS Publication, 220:95-105.
4. Zoller U, Goldenberg LC, Melloul AJ (1998) Shortcut-enhanced contamination of the Gaza Strip Coastal aquifer. Water Research Journal, 32:1779-1788
5. Mitchell JG (1996) Our polluted runoff. National Geographic. 189(2):106-125.
6. Melloul AJ, Zeitoun L (1999) A Semi - Empirical Approach to Seawater Intrusion Monitoring in Israel Coastal aquifer. . In the book of " Seawater Intrusion in Coastal Aquifers: Concepts, Methods and Practices" Ed. Bear J, Cheng AHD. Sorek S, Ouazar D, Herrera I Chapter 16:543-557.
7. Burnham DH, Bennett EH (1909) Plan of Chicago. Da Capo, N.Y. Reprint, 1970. 164 pp.
8. Collin ML (1973) An Evaluation of Baltimore Harbor Land Use Potentials. Baltimore Regional Planning Council, Baltimore, MD. 239 pp.
9. Collin ML (1975) The Baltimore Harbor Plan. Baltimore Regional Planning Council, Baltimore, MD. 134 pp.
10. Lewy-Yanswitz I (1999) Islands off the Coast. HaAretz Newspaper Magazine, July 1999
11. Melloul, AJ, Goldenberg LC (1993) The rainy winter of 1991/92 and its influence on the Groundwater quality in the Coastal plain aquifer of Israel. Water and Irrigation Journal, 319:51-54. (Hebrew).
12. Collin ML, Eitan G (1999) The POLLISTE Land-use Register. Israel Hydrological Service, Hydro-Report 1/99, Jerusalem. 159 pp.
13. Melloul AJ, Collin M (1994) The hydrological malaise of the Gaza strip. Israel Journal of Earth Sciences, 43(2):105-116.
14. Pretty JN (1996) Sustainability works. UNEP. Our Planet. 8(4):19-22
15. Wingo L (1975) Cities and Space: the Future Use of Urban Land. Johns Hopkins
16. Tolmach Y (1979) Hydrological Atlas of Israel. Hydrological Service, Jerusalem 30pp
17. Hydrological Service (1996) Hydrological Situation Report. Israel Hydrological Service, Jerusalem. 242 pp. (in Hebrew)

The Water Resources System and Water Utilization in the Arid Northwest of China

Wang Bingchen[1] Qiu Hanxue[2]

[1]Comprehensive Institute of Geotechnical Investigation & Survey, 177 Dongzhimen Nei Street, Beijing, 100007, China
[2]Dept. Of Environmental Engineering, Ocean University of Qingdao, 5 Yushan Road, Qingdao, China, 266003)

ABSTRACT Water resources exploitation and sustaining development of arid and semi-arid area are among the most important global environment problems. One third of the total earth surface is arid or semi-arid, and in China, this area amounts to 47.5%. Water system in arid area has the following characters: total water resources shortage, poor recharges, distribution unbalance, evaporation playing a key role in water cycle, river and connected aquifers forming a uniform system, shallow groundwater having certain present recharge but deep groundwater usually having no recharge with the evidence of very low tritium detected. A series of environment deterioration problems, such as desertification, salinization of soil and groundwater, have risen during water resources exploitation because the ecosystem is rather weak. To realize the reasonable utilization of water resources in the arid area, we need to manage water resources in a scope of catchment, to control the oasis scale according to the water capacity of systems, to keep reasonable ecosystem water level, and to construct water saving society.

KEY WORDS: Arid area, River-aquifer system, Oasis scale control, Ecosystem water table, Water saving society

INTRODUCTION

The UNEP report in 1996 pointed out that the main crisis that human being will face in 21st century is water shortage rather than energy crisis. The water resources sustainable development will be the key obstacle to the development of society, especially for the arid and semiarid area. The water resources shortage, limited environment capacity and weak ecosystem are the main problems of arid area.

Arid and semiarid area occupies one third of the total earth surface, having the area of about $4.88\times10^7 km^2$. And besides, there is an area of $9.1\times10^6 km^2$ "human times" desert formed because of over exploitation. Water resources is the main constraint factors to the development of these regions. Statistics from UNEP shows that the distribution of arid area is rather unbalance [1] (Tab.1), more than 1/3 of Asia is arid and semiarid.

In China, arid and semiarid areas distribute in the Northwest. Using arid index and water balance factor comprehensive method, The area of arid index greater than 3 occupy 47.5% of the total area of China and the arid area with precipitation less than 200mm is 26 % of the total area [2].

THE DISTRIBUTION AND CHARACTERS OF WATER RESOURCES SYSTEM IN ARID AREA

The scarce of precipitation, shortage and distributing unbalance of all kinds of water resources are the main characters of arid area of China. There is an area of $1.6\times10^6km^2$ area with no runoff at all and five inland catchment formed in Northwest of China. In this area, the annual water resources of $3.61\times10^4m^3/km^2$ is only 12.25% of the country's mean value. In some region, the figure is even smaller. For example, the west part of Inner Mongolia and Hexi Corridor, the value is only 5.2~5.6%.

Another character of arid area is the intensive evaporation. The water surface evaporation is usually at the order of 1500~3000mm/a. But the land evaporation is often limited by a low water content of the surface soil. So the actual evaporation is not so high. However, the evaporation coefficient (land evaporation/precipitation) goes rather high, reaching 0.79 in Northwest and 0.77 in North of China respectively. The intensive evaporation has great influence to the local water cycle, since it is difficult to produce effective recharge.

The precipitation and snow melt in the middle and high mountainous area is the main water resource for the arid area. The surface water and groundwater in riverbed from mountainous river usually occupy about 80% of the total water resources in arid plain or basin. Other resources like lateral recharge of groundwater, precipitation in plain area and flood occupy a little ratio in the total water resources of a basin plain. It was found that in the Northwest of China, the lateral recharge is only 5% of the groundwater and less than 3% of the total resources[3,4] (Tab.2).

Table .1 Arid land area (10^6km^2)

Continent	Extremely arid(p<50mm)	Arid (P=50-150mm)	Semi arid (P=150-250mm)	Total	Percent of continent (%)
Australia	---	3.9	2.5	6.4	83
Africa	4.50	7.3	6.0	17.9	59
Asia	1.00	7.9	7.5	16.5	38
North and Middle America	0.03	1.3	2.6	4.0	10
South America	0.20	1.2	1.6	3.0	8
Europe	---	0.2	0.8	1.0	1
Total	5.73	21.8	21.0	48.13	36.3

Table .2 Groundwater recharge resources in inland plain area in northwest China ($10^8m^3/a$)

System or region		Hexi Corridor and Alashan	Zhungeer Basin	Talimu Basin	Chaidamu Basin	Total
Runoff of Mountain river		66.3	332.5	381.5	67.9	838.2
The ground water recharge	River water infiltration	24.1	51.4	69.7	21.5	166.7
	Channel & land infiltration	24.3	55.1	157.5	2.7	239.6
	Lateral recharge from mountain area	3.5	9.5	5.6	6.2	24.5
	precipitation	8.5	23.6	1.9	2.7	38.7
	Total	60.4	139.3	236.7	33.1	469.5
Total water resources of the system		78.3	355.3	391.0	76.8	901.4
Mountain river water change to ground water (%)		73.0	32.0	59.6	35.6	48.5
The Mountain river water/ Total aquifer-river system water (%)		84.7	93.6	97.6	88.4	93.0

THE RIVER-AQUIFER SYSTEM IN ARID AREA

The exchange between groundwater and surface water is very common. However, in arid area, this exchange is quite intensive and frequent. No matter under the artificial or natural conditions the fluctuation and balance of river and groundwater will intensively influenced each other and formed a uniform system.

Under the natural conditions, the runoff formed by rain, snow/ice melting in the mountain area intensively recharge to groundwater at the quite thick pluvial and alluvial fan. In the Northwest China, 20% river water seepage to groundwater flows directly through riverbed and 28% through the channel system. Totally 48.5% of river water changes to groundwater within this area (see Tab.2). The groundwater in coarse gravel aquifer of the alluvial fan moves quickly because of the high conductivity and discharges out in the frontier of the alluvial fan forming the down stream Spring-recharge rivers. Usually, the plain river disappears because of seepage and evaporation in the running procedure and finishes the 3rd change to the groundwater. Some large river may pour into terminal lake in basin and the groundwater also discharges into the terminal lake.

It is clear that rivers and groundwater in an arid area form a uniform system. From the alluvial fan to the center of the basin, the water change from surface water to groundwater and then change back 3-4 times in the natural conditions. The subsystems keep tight relation and it is impossible to evaluate the groundwater or surface water individually. So, the water utilization, no mater groundwater or surface water will unavoidably cause regional hydrological effect that involves the whole catchment (system), and the transforming condition between groundwater and surface water may change in large scope.

THE WATER RECYCLE OF DEEPER CONFINED AQUIFER

Some researchers hope to explore the deep confined aquifers to alleviate the water shortage in arid areas. Even some experts in the operation of 9th 5 year-plan of China consider the deep fresh water as a hopeful source for the arid land. However, a regional investigation proved that the deep groundwater circulate rather slowly.

According to the investigation of environmental isotope of water in all subsystems in Northwest China, the phreatic and confined groundwater are all originated from precipitation, the stable isotope $\delta D‰ \sim \delta {}^{18}O‰$ spots are all on the Crig Line. However, the shallow water (mainly the unconfined) subject to evaporation. The deeper (confined) groundwater with scarcer D and ^{18}O proved the influence of continent effect, long cycling journey and limited recharge.

The groundwater in Northwest China is usually affected by nuclear test since 50's and precipitation usually contain high tritium. Shallow groundwater (0-20m) has tritium of 7-254 TU for its fast circulating. Middle deep aquifer(20～80m) have low tritium of 7～2TU and the deep groundwater (>80m, usually confined) affected little by the nuclear test with the tritium less than 2TU. According to the site sampling [5] on the vadose zone in Northwest of China, the precipitation in 1963 infiltrated only 6m and nuclear tritium containing rain in 1953 penetrated only 10m. So we can conclude that the deeper confined aquifer is not affected by nuclear test and the low tritium illustrates that the deep water formed in 40 years ago.

The different parts of a river-aquifer system also present the different cycling condition with the tritium content in groundwater as evidence. In the north alluvial plain to basin plain of Tianshan Mountain, the upstream phreatic water circulate fast and the tritium is 22～254TU, and in the middle stream, the tritium is 5-46TU in the shallow confined aquifer. In the deeper confined aquifer in the down stream the tritium is less than 2TU[6,7].

From the above discussion it can be concluded that the deeper aquifer have very limited recharge and the idea of seeking deep fresh water to alleviate the water shortage in Northwest of China is very dangerous.

THE UTILIZATION OF WATER RESOURCES IN ARID AREA

In the arid aquifer-river system, from the foot of mountain to the terminal lake, surface water and groundwater change each other 3～4 times naturally. This easily transforming condition makes the reuse of water resources possible. In some systems, the reusing rate is 40%～50% (see Tab.3). For example, the water was reused at least 3 times in the Shiyanhe aquifer-river system. This means that the usable water resources is greater than the total resources of the system.

Table.3 The rate of water reuse in Northwest China ($10^8m^3/a$)

System or region	Hexi Corridor & Alashan	North foot of Tianshan	Talimu Basin	Chaidamu Basin	Total inland area
Total water resources	78.3	97.3	391.0	76.8	901.4
Water entering cannel system	62.1	60.2	266.4	9.4	466.1
Reinfiltation	34.0	28.0	157.5	2.7	239.6
The most great reuse rate (%)	0.43	0.29	0.40	0.04	0.26

THE ENVIRONMENTAL PROBLEMS CAUSED BY WATER RESOURCES UTILIZATION

The shortage of water resources in the arid area causes over exploitation in Northwest of China, the over exploitation results in a series of environmental problems.

Desertification of land

The utilization of groundwater reduces the groundwater recharge and draws the groundwater level down regionally. The vadose zone thickening and water content in soil lessening cause the land extremely arid and the desert ecosystem deterioration. And as a result, the desert enlarges and intrudes to agricultural land and pasture.

The Heihe River can be a typical example of water resources over exploitation. The reservoirs and well irrigation upperstream reduce water resources entering Ejina oasis greatly (Tab.4) and the forest withered and river-along oasis narrow the range. Sacsaoul forest reduced from 1.13×10^6ha in 1950's to 2.0×10^5ha in 1980's in Ejina Qasis. The sandstorm disaster happens frequently may mainly be attributed to the desertification of land.

Table.4 The runoff at Zhengyixia station of Heihe River and the amount of entering Ejina Oasis

Time	1940-1949	1950-1959	1960-1969	1970-1979	1980-1989	1990	1991	1992
Runoff at Zhengyixia Station	13.3	12.25	10.65	10.55	10.44	8.52	6.98	5.0
Runoff entering Ejina Oasis	-	9.925	3.84	4.03	-	3.10	2.54	1.82

Soil salinization

The artificial factors play important role in soil salinization and the direct cause is unreasonable water use.

The waste land rapidly become saline because of no irrigation water to wash the accumulating salt in soil and no cultivating measures to cut the evaporation capillary. The strong evaporation accumulates lots of salt in soil after cultivated land be wasted. For instance, the Cl^- and Na^+ content in 1m soil of waste land in Minqin Basin are respectively 16 and 9.55 times higher than those in cultivated land.

Unreasonable irrigation (excessive irrigation or impeded drainage) makes the groundwater level raised and salt accumulated in soil. This kind of problems exist in large-scale irrigation area, Hetao, Yinchun and Talimu in Northwest of China.

The downstream area often suffers from the lack of runoff so wells are used for irrigation, however, the salty groundwater makes the soil saline immediately.

Groundwater salinization

The arid climate has the condition of making the groundwater salinization, but the water use (irrigation) and reuse (use, reinfitration, and use in the downstream again), cause more evaporation and increase the salt content in water. The groundwater TDS in 2/3 area of Yaoba Oasis in Inner Mongolia has rise from less than 1 g/l to 3-4 g/l during the running of well irrigation oasis in latest 20 years.

THE REASONABLE WATER USE IN ARID AREA

The control of oasis scale

The amount of water resources determines the scale of oasis. That is, the scale of oasis should be reasonably controlled. Over enlargement of Minqin oasis make the land desertfication and the Badanjilin desert and Tenggli Desert have connected together in some places.

Keep reasonable ecosystem-water table

The plants in arid area usually live in a condition of definite groundwater table. We can call the definite water table as **ecosystem water table.** To control the well depression we can avoid the withering of plant and protect the ecosystem.

Livestock feeding in fold and village gathering

The over herding causes the deterioration of pasture and the water resources reduce. So the village gathering and a suitable scale land cultivating may provide forage for livestock fold feeding. And the adjacent pasture may regain its sustainment. Luanjing Tan irrigation region with an area of 1.3×10^4ha started in 1994 in Inner Mongolia can attract 1/3 of the local herdsman in Alashan district to live in the irrigation area and some of them may be engaged in land cultivation and fold-livestock feeding. As a result, the adjacent desert pasture are hoped to recovered in the future.

Set up water saving society

The Oasis center town in arid area should be water saving society and the agriculture should use water saving irrigation technology. The soil ameliorating and water keeping technologies is the life of arid agriculture.

CONCLUSION

The population increase and economic development show an increase tendency of water demand. However, the water environment and ecosystem deteriorate in recent years because of water resources excessive exploitation. Counter-measures like water saving, oasis scale control, keeping reasonable ecosystem water table and fold-livestock feeding will improve the pasture and arid ecosystem.

REFERENCE

1. Qiu Hanxue, Wang Bingchen, Adams B., (1998) Water Resources Exploitation and Sustaining Development in Arid Area, Marine Geology & Quaternary Geology, (4):97-108
2. Hydrology Bureau of Water Conservancy Ministry of China,1989, Evaluation of water resources in China, Water Conservancy Press, pp64-65
3. Fan. X. P, (1990) The characters of groundwater resources and environmental problems caused by water exploitation in Northwest China (I), Hydrogeology & Engineering Geology (in Chinese), (1): 3-7.
4. Fan. X. P (1990) The characters of groundwater resources and environmental problems caused by water exploitation in Northwest China (II), (2): 12-16.
5. Zhang. Z. G., (1990) The water movement and recharge amount investigation using environmental tritium, Hydrogeology & Engineering Geology (in Chinese), (3):5-8.
6. Yuan. Z. M., (1988) Isotope hydrogeology in Erlintu water supply field, Hydrogeology & Engineering Geology (in Chinese), (5): 30-33.
7. Bin, L, (1992) Isotopic studies for the rational use of water resources in the front plain of Tianshan Mountain. Environmental Geology, 24(3):217-212

GIS Application for Monitoring Groundwater Arsenic Contamination in Bangladesh

Md. Rowshon Kamal[1], Md. Masud Karim[2] and Kwok Chee Yan[1]

[1]Department of Biological and Agricultural Engineering, Faculty of Engineering, University Putra Malaysia, 43400 UPM Serdang, Selangor DE, Malaysia.
[2]Dainichi Consultant Inc., 3-1-21 Yabuta Minami, Gifu 500-8384, Japan.

ABSTRACT. Bangladesh is a nation of over 125 million population with a geographical area of 1,48,393 km^2 and located on the Ganges, Brahmaputra, and Meghna Delta. The major part of the country is now severely affected by mass poisoning from arsenic in groundwater. The latest statistics on the arsenic contamination in groundwater indicates that 59 out of 64 districts, about 80% of the total area of Bangladesh and about 40 million people are at risk. Presently about 116 million people depend on water from tube-wells for drinking, cooking, washing and bathing and about 60 million people are drinking and using arsenic contaminated groundwater. Arsenic level now ranges from 0 ppm to 0.98 ppm and the maximum permissible level of arsenic in Bangladesh drinking water is 0.05 ppm. Average values of different tubewells data on thana census blocks have been used in this study. A spatial and temporal distribution of Groundwater Arsenic Contamination Intensity (GACI) has been developed using Geographical Information System (GIS) in order to assist decision making process in some critical areas, particularly to protect human health. The digitized thana boundary maps with longitude-latitude coordinates storing information in the form of metadata has also been developed to visualize GACI information in thana census blocks of Bangladesh. The MapBasic Professional 4.5 has used for developing user-interface design and MapInfo Professional 4.5 for the visualization of spatial information. The user-interface GIS approach can help policy makers deciding proper groundwater utilization and taking necessary steps to supplying safe drinking water to the domestic and industrial areas.
KEY WORDS: groundwater, arsenic contamination, monitoring, Bangladesh and GIS.

INTRODUCTION

Natural resources are not only the basis for economic activities and human welfare, but also make up essential components of our natural environment. They are subject to ever increasing demands and exploitation by growing populations and per-capita requirements. Government regulations and international agreements, market mechanisms, cultural traditions and individual preferences affect and control these resources, but rarely do these mechanisms suffice to ensure a sustainable management of resources, and in particular, the commons [1]. Groundwater provides safe drinking water to over 86 percent of the rural population in Bangladesh [2]. This extensive coverage is indicative of the country's successful attempt to provide safe drinking water to its general people. This respectable public health effort was overshadowed when in 1993 an alarming discovery confirmed of arsenic contamination in groundwater. The arsenic contamination discovery was first made in the northeastern part of the country. Groundwater contamination of arsenic has already affected 59 out of 64 districts of Bangladesh. It is estimated that around 1.12 million tubewells are contaminated by arsenic of the whole country [3].

Now a days, advanced technology has become emerging management tool to various environmental agencies to provide spatial and temporal updated information in their environmental problems. The powerful GIS software tools in problem oriented systems provides direct and easy access to large volumes of data. It supports their interactive analysis and helps to display and interpret results in a format directly understandable and useful for decision-making processes. An organized collection of computer hardware, software, geographic data, and

personnel designed to efficiently capture, store, update, manipulate, analyze, and display all forms of geographically referenced information. GIS provides a valuable tool for information analysis, automated mapping and data integration. Mark et al. [4] gives a useful definition that encompasses its functionality. It is defined as a computerized system for the storage, retrieval, manipulation, analysis and display of geographically referenced data, where include physical, biological, cultural, demographic or economic information and provide valuable tools in the natural resources, social, medical and engineering sciences, as well as in business and planning.

Information technology in particular, GIS provide powerful tool for effective decision support in natural resources management. A GIS can automate existing as well as provide enhanced capability to analyze geographic information for decision-making purposes. This study has been conducted on the arsenic databases of all thanas in Bangladesh. These basic databases are utilized for visualizing geographically located arsenic contamination level by User-interface GIS Tool. It will help to provide temporal and spatial GACI information to policy personnel about current situation and take necessary steps for supplying safe drinking water to the domestic and industrial areas and to mitigate the groundwater arsenic contamination.

DATA REQUIREMENTS AND SOURCES

Various information are stored in the GIS in the form of geographic data sets or layers. The digitized thana census blocks map provided the geographical framework. In studies using GIS the first requirement is the availability of a map which is the backbone of the system. MapInfo Professional 4.5 used for digitizing the study area. The accuracy of manual digitizing merely depends on how accurate the hardcopy map is duplicated on a computer by hand. Geographically referenced arsenic data were collected on a number of tubewells in the different locations for the individual thana census block and after then average values were taken in this study. Data on some thanas was not available. To perform the monitoring of GACI, geographically referenced data were typically obtained from the Dainichi Consultant, Incorporated, in Japan working with the Arsenic Mitigation Project in Bangladesh. The lack of information is the major bottleneck for the study.

DATA STRUCTURES

The database is a core of GIS. The MapInfo Professional software used to generate inputs of Groundwater Arsenic Contamination Intensity in the Thana census block (3rd largest area). GIS software provides flexibility in developing and tailoring output formats to meet individual requirements. Its database allows storage, retrieval, and analysis of data in formats that are interchangeable between different computer based application packages and helps to develop the user-interfaces. Database is facilitated by structured format defining fields (Columns) and records (Rows) data repository. The completeness and accuracy of database give the quality of analysis and final products of the system. This database helps to portray geographical locations and monitor changes of the GACI in both spatial and temporal dimensions. Secondary data may be generated from that in the database. MapBasic provides powerful Database-access tools. The structure of the database is customized to the needs of the user. Linking database with the User-interface helps to understand about the overall pictures of country's GACI for the policy makers.

DESIGN AND OPERATIONS OF USER-INTERFACE GIS TOOL

Description of Main Menu

The MapBasic programming language has used to develop user-interface tool for monitoring Groundwater Arsenic Contamination Intensity. The main menu of Arsenic Monitoring appears

directly in the Menu bar of MapInfo. It comprises eight menu items and its sub menu items named by district, as detailed in Figures 2 and 3. This tool is devoted to the monitoring of the present situation of GACI for the thana census blocks of whole of the country, individual divisions and districts, respectively. The dialog window is activated in the MapInfo window when user clicks on Sub-menu item Arsenic Intensity shows in the Figure 4. It proposes the display of maps, browses and charts to visualize the GACI level when user clicks on a particular CheckBox dialog and/or any number of dialogs. These CheckBox dialogs are directly linked with programming modules and instantly display output within the MapInfo window when dialog window is terminated. OKButton and CancelButton dialogs control the dialog window. By clicking on the Menu item Exit, then instant message appears to inform the user that the application is terminated. It gives dialog message during operation period and user will be able to know how to get information for specific query from dialog window.

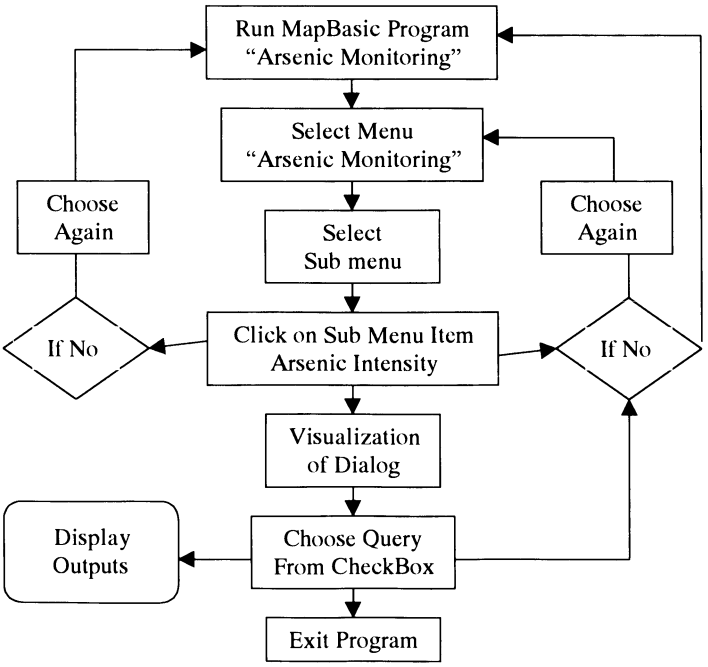

Fig. 1. Flowchart Showing Operational Systems to Arsenic Monitoring Program

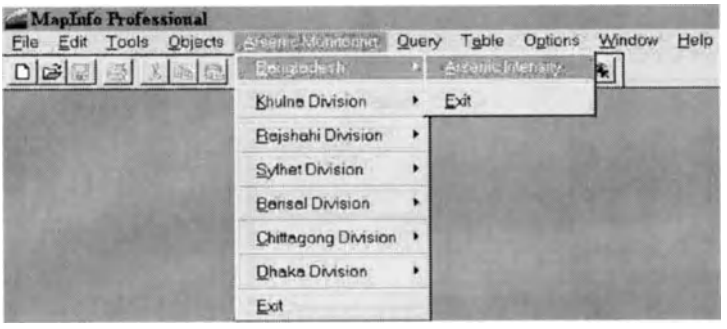

Fig. 2. Main Menu and Menu Items of Customized Window for Arsenic Monitoring.

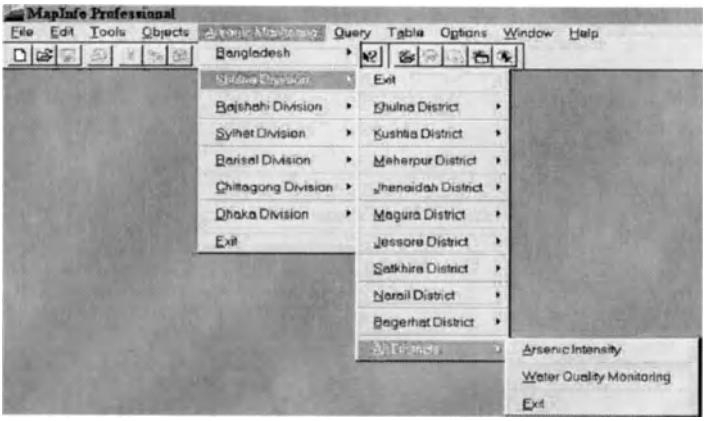

Fig. 3. Showing Customized Window for Monitoring of Individual District

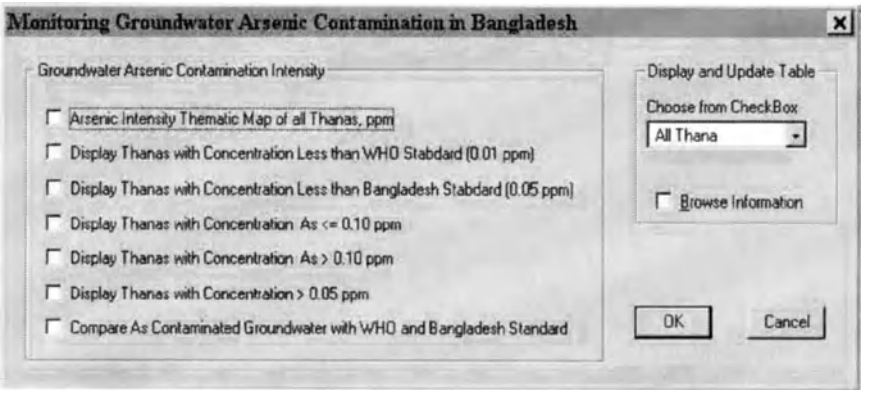

Fig. 4. Showing Dialog Window and Queries by CheckBox Dialogs for Arsenic Monitoring.

RESULTS AND DISCUSSIONS

At present several groups of the government (British and Swiss) with financial and technical assistance from international donor agencies (World Bank), NGOs and Universities are working on the arsenic problems and exchange of information among themselves. Groundwater concentration below 0.01 mg/l is considered safe according to World Health Organization (WHO) Drinking Water Guidelines. However, in Bangladesh, the maximum permissible limit of arsenic in drinking water is 0.05 mg/l. In many different ways (i.e. map, graphs and tabular form), the user-interface GIS could provide rapid information on the present status of arsenic contaminated groundwater of the thana census blocks. Figures 5 and 6 explain the present arsenic concentration by graph and color-coded map of the whole country. The first two light colors show arsenic concentration under permissible limit for drinking and rests are above the limit in the Figure 5. Arsenic concentration of 163 thanas has exceeded the permissible level 0.05-ppm out of 460 shows in Figure 5. The arsenic concentration of some thanas is several times higher than of permissible limit of 0.05, shows in Figures 7 and 8. The user can get also

affected thana name by using label button or by keeping the cursor on the particular thana. Figure 9 shows spatial distribution of arsenic concentration > 0.05 ppm with labeling of thanas in Khulna division. Table 1 also presents average and maximum arsenic concentrations of affected thanas in Khulna.

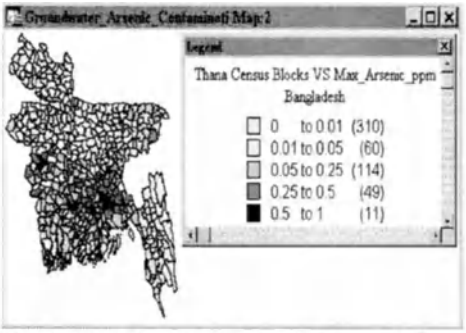

Fig. 5. Thematic Map of Arsenic Concentration on Thana Census Blocks of the Country.

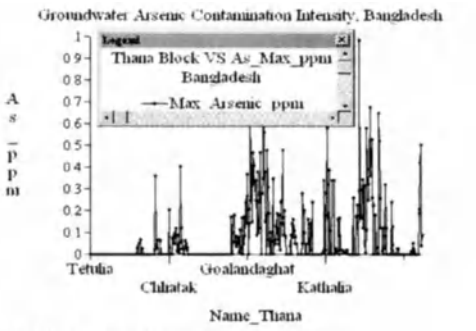

Fig. 6. Arsenic Concentration of Thana Census Blocks of the Country.

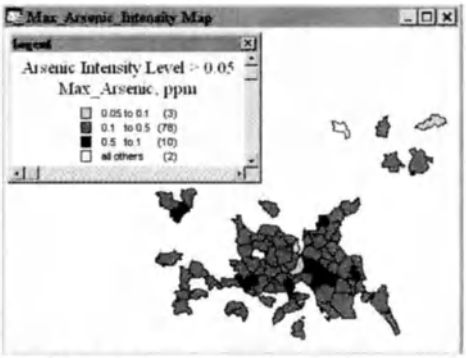

Fig. 7. Thematic map on affected Thana Census Blocks of arsenic concentration > 0.05 ppm.

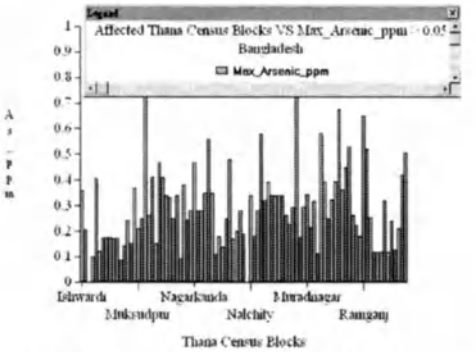

Fig. 8. Arsenic Concentration > 0.05 ppm of Thana Census Blocks of the Country.

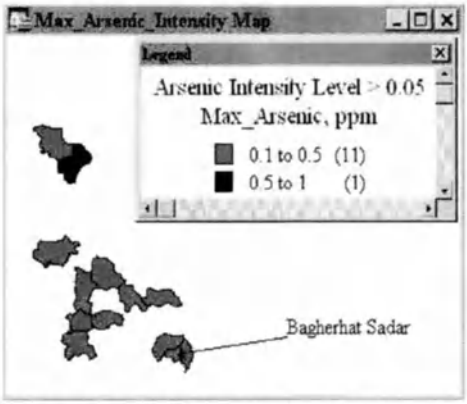

Fig. 9. Thematic Map of Khulna Division where Arsenic Concentration > 0.05 ppm.

Table 1. Arsenic Concentration of Thana Census Blocks of Khulna Division.

Max_Arsenic_Intensity Browser

Name_Thana	Name_District	Avg_Arsenic_ppm	Max_Arsenic_ppm
Daulatpur	Kushtia	0.0738	0.3500
Mirpur	Kushtia	0.2100	0.5600
Mohespur	Jhenaidah	0.1078	0.3500
Kalia	Narail	0.0560	0.1100
Jessore Sadar	Jessore	0.0725	0.1800
Jhikargachha	Jessore	0.0513	0.1400
Keshabpur	Jessore	0.0613	0.2500
Abhaynagar	Jessore	0.1214	0.4800
Kaliroa	Satkhira	0.0613	0.1700
Satkhira	Satkhira	0.0660	0.2000
Bagherhat Sadar	Bagerhat	0.0540	0.2800
Fakirhat	Bagerhat	0.0771	0.1900

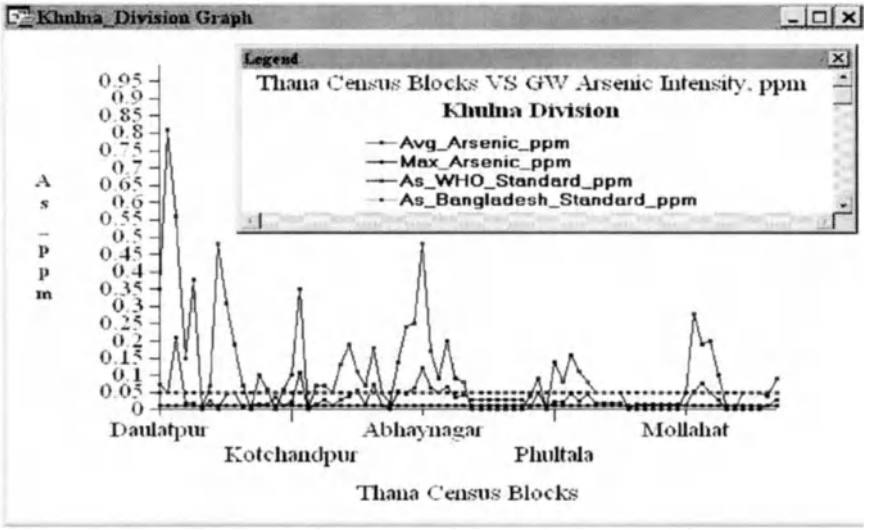

Fig. 10. Comparison of Average and Maximum Values of Arsenic Concentration on Thana Census Blocks along with WHO and Bangladesh Standard of the Khulna Division.

Average and maximum arsenic concentration of all thana census blocks have also presented along with the values of WHO and Bangladesh standard in Figure 10. The two straight lines represent arsenic safe level by WHO and Bangladesh Standard 0.01 and 0.05, respectively. Dot line shows maximum values of all thana census blocks in Khulna division and other straight line for the average values. Dialog window would be able to give information by clicking the CheckBox dialogs for different queries for all divisions and districts accordingly.

CONCLUSION

The discovery of arsenic in groundwater in several areas of Bangladesh has aroused widespread concerns. We need to conduct the assessment rapidly, compiling existing information and integrating these data with GIS. The user-interface GIS can be used successfully for monitoring groundwater arsenic contamination intensity on the basis of thana census data. The information can be explored to enable monitoring arsenic contamination evolve towards decision making using GIS user-interface tool. This program can be used for monitoring of GACI in different scales after updating of database in the future. This study would be helpful for building up monitoring technique for different depths with geographically referenced tubewell locations for individual thana census block. This comprehensive study will give detail picture of GACI throughout the country and can be helpful to coordinating among the different working groups on arsenic mitigation projects in Bangladesh.

REFERENCES

1. Hardin, G. (1968) The tragedy of the commons. Science 162:1243-1248.
2. BBS, Statistical Year Book of Bangladesh, Bangladesh Bureau of Statistics, 1997.
3. Karim M. M. and Z. R. Begum (1999) Groundwater Arsenic Contamination Inventories and Risk Assessment using GIS: Case Studies Kishoreganj and Netrokona Districts of Bangladesh. 92nd Annual Meeting of A & WMA, San Diego, St. Louis, USA.
4. Mark. D M. Et al (1996) The GIS History Project. www.spatial.edu/ucgis/mark/chgis.html

Multivariate Classification Method in Groundwater Research

A.I.Gavrishin[1], L.I.Bondareva[1], A.Coradini[2], M. Fulchignoni[3]

[1]Novocherkassk State Technical University, Russia
[2]Istituto Astrofisica Spaziale, Rome, Italy
[3]Paris University, France

ABSTRACT: This paper presents the results of development and application to a multivariate statistical technique for the detection of populations groupings in data arrays. The classification procedure referred to as the G-method is based on a new Z^2 criterion. This method allows an automatic classification in terms of homogeneous taxonomic units, without any a priori knowledge of the taxonomic structure of the natural observations; it provides information on the different levels of classification present in the data set under study, on the level of information residing in each variable, on the level of similarity among homogeneous classes. G-method used to investigate taxonomic structure of multivariate observations on hydrogeological, engineering geological, ecological and other types of data. The results obtained analyzing chemical composition of groundwater on territory of Novocherkassk are described in paper.

KEY WORDS: multivariate classification, groundwater chemistry, regime, urban environment, monitoring, waterlogging

INTRODUCTION

Anthropogenic activities are causing widespread deterioration of the geological environment. The waterlogging, land subsidence, pollution of geological environment are the most important processes of environment quality degradation for Steppe Zone of Russia. Monitoring is a major mean for the investigation and the quality assessment of urban geological environment; such monitoring was made in Novocherkassk town.

Multivariate classification methods are important for the investigation and prediction of natural-object transformation. The problem of the classification of observations is a general problem, common to the fields of geological sciences, as well hydrogeology, engineering geology and the environment. The problem consists of the definition of the taxonomic structure of the statistical universe under study. In general we deal with multivariate observations: thus, the above mentioned problem, from the statistic-mathematical point of view, consists of the identification of homogeneous taxonomic units in the multivariate space of the observations. Several multivariate methods exist and are widely used in geology; they are based on different statistical and heuristic principles, and each of them presents advantages and disadvantages. We would like to describe here the G-method, particularly suitable when geological observations are concerned, and to give examples of the environmental applications.

It should be stressed that the G-method can be used without a priori knowledge of the taxonomic structure of the observations; thus, an automatic classification in terms of homogeneous taxonomic units can be performed. The main characteristics of this method can be summarized as follows:

- the independence of variables and observations is not needed;
- any relationship between the number of variables (M) and number of observations (N) can be present in the considered universe;

- the presence of various levels of classification can be recognized, such as classes and subclasses;
- the classification is performed using the average, the dispersion and the correlation of the set of variables;
- the level of information residing in each variable is evaluated;
- the level of similarity and/or differences among homogeneous classes is measured;
- the classification of new observations, not previously considered in the classification is possible.

THE Z^2 CRITERION AND G-METHOD

The classification procedure is based on the Z^2 criterion having quasi-χ^2 distribution [2]:

$$Z^2 = \frac{M}{\sum_{sk} r_{sk}^2} \sum_{i=1}^{M} \left(\frac{N}{\sum_{ph} {}_i r_{ph}^2} \sum_{j=1}^{N} Z_{ij}^2 \right) = K \sum_{i=1}^{M} \left(K_i \sum_{j=1}^{N} Z_{ij}^2 \right) \tag{1}$$

$$Z_{ij} = \frac{x_{ij} - \mu_i}{\sigma_i} \tag{2}$$

$$K = \frac{M}{\sum_{sk} r_{sk}^2} \tag{3}$$

$$K_i = \frac{N}{\sum_{ph} {}_i r_{ph}^2} \tag{4}$$

where x_{ij} is the value of variable i ($i=1,2,...,M$) for observation j ($j=1,2,...,N$); μ_i and σ_i are mean and the standard deviation of variable i in a homogeneous taxon of observations; and r_{sk} and r_{ph} are coefficients of correlation between variables s and k and observations p and h.

The null hypothesis is that one or several observations belong to a given homogeneous taxon. The hypothesis is rejected if $Z^2 \geq \chi^2_{q,f}$ where $\chi^2_{q,f}$ is the critical value of χ^2 at the confidence level q and f degrees of freedom:

$$f = N \times K \times \sum_i K_i \tag{5}$$

For the sake of simplicity it is possible to transform the original Z^2, following a χ^2 distribution, into a normal distribution havin the first moment equal to those of the χ^2 distribution. The normal distribution is expressed as

$$G = \sqrt{2Z^2} - \sqrt{2f - 1} \tag{6}$$

In most cases, for independent observations, criterion (1) takes the following form:

$$Z^2 = \frac{M}{\sum_{sk} r_{sk}^2} \sum_{ij}^{MN} Z_{ij}^2 = K \sum_{ij}^{MN} Z_{ij}^2 \tag{7}$$

$$f = N \times M \times K \tag{8}$$

The classification procedure, referred to here as the G-method, is as follows:

(1) select a coordinate system in which multivariate space is transformed to the Z^2 distribution;

(2) find the centre of the first homogeneous taxon;

(3) convert the coordinate system and identify all observations that belong to the first homogeneous taxon;
(4) repeat steps (1) through (3) for all observations that were not included in previous homogenous taxon;
(5) estimate the similarities and/or differences among the taxons for each variable and collectively for all variables;
(6) estimate the information content of the variables that were included in the taxonomic structure;
(7) repeat steps from (3) to (6) for the various levels of the individual taxon that were reliably isolated.

Among possible different methods to determine the baricenter of a homogeneous taxon, the Central Method of Closed Points has been found to be the most effective. For this method, the centre was represented by observations that were closest to it in the multivariate space and a minimum value of

$$Z^2_{phr} = \sum_i \left[\left(Z_{ip} - Z_{ih}\right)^2 + \left(Z_{ip} - Z_{ir}\right)^2 + \left(Z_{ih} - Z_{ir}\right)^2 \right] \qquad (9)$$

where Z_{ip}, Z_{ih} and Z_{ir} were normalized variable i for observations p, h and r, respectively.
All observations that belong to given homogeneous taxon were identified from the G radius (6).The classification was obtained for various level of detail and degrees of taxon homogeneity by changing the critical value of the homogeneous taxon G radius. Taxon homogeneity and detail of the classification increase as the G radius decreases, and differences among taxons became less pronounced and detectable. Similarities and/or differences among homogeneous taxon was also evaluated dispersion for each individual variable and all variables collectively. The G-method was coded in FORTRAN [1, 2, 3].

G-METHOD APPLICATION

The G-method was used to construct the taxonomic structure of hydrogeological, engineering geological, geoecological, cosmochemical, and other types of data. Some results obtained by the application of the method in research field from urban environment will be given here.
Geoecological monitoring was made on the territory of Novocherkassk city. The monitoring has the network of observation wells and subsystem of information. Soils, rocks and waters are major observation objects of geoecological monitoring. Repeating control carry out for the investigation of alteration of structure, properties and chemical composition of the objects; it allows to fix environment damage, to analyze factors and processes of the formation of ecological situation, to make the ecological forecast and the decisions for rehabilitation of the environment.
The monitoring data show that the waterlogging, land subsidence and pollution of soils, rocks and waters are the leading processes of environment transformations. The rise of groundwater reaches 15 m during 40 years; the waterlogging of territory is 70-80%; the contamination of geological environment exceeds the critical level.
The G-method was used to map and investigate the natural and urban effects on groundwater chemistry, regime, circulation and so on. Some of the most interesting results obtained by the application of the method to groundwater chemistry are given here.
The average major ion and total dissolved solids (TDS) concentrations in groundwater are listed in Table 1. Waters were dominated by high concentrations of SO_4 and Na. The group of "TDS – SO_4 – Na – Mg" has the high coefficients of correlation.
The classification G-method was applied to investigate the chemical composition of water samples collected on territory of Novocherkassk town. The groundwater chemistry is a complex and dynamic system that is spatially and temporally very heterogeneous. An

analysis of the water classification results (Table 2) and the corresponding hydrogeo chemical

Table 1. Average major ion and TDS (salinity) concentrations, in $mg \cdot dm^{-3}$ and %-mol, of groundwaters.

Date	Number of observation	TDS	HCO_3	SO_4	Cl	Ca	Mg	Na
1994	21	4400	500	2200	410	290	190	690
			13	69	18	29	25	46
1995	22	3550	470	1680	360	250	140	660
			14	67	19	24	22	54
1996	21	3450	490	1640	330	270	150	580
			16	66	18	26	24	50
1997	25	3400	480	1480	400	270	130	600
			10	61	23	27	21	52

map (Figure 1) indicated that hydromorphology, relief, intensity of water circulation and anthropogenic activities are the primary factors controlling the groundwater chemical composition. The classification shown that three main hydrogeochemical zones could be isolated (A, B, C). The average major ion concentration in groundwaters of each zone and differences among homogeneous zones are listed in Table 2. Minimum of differences among zones are differences among C_1 and C_2, A and B zones. Of the chemical constituents in groundwater, variations in Cl, SO_4, Na concentration and total dissolved solids (TDS) are the most informative (the most discriminant variables).

Table 2. Average chemical composition ($mg \cdot dm^{-3}$ and %-mol) of groundwaters in homogeneous hydrogeochemical zones (samples collected in 1995).

Zone	TDS	HCO_3	SO_4	Cl	Ca	Mg	Na
A	7000	540	3100	1100	480	280	1360
		8	62	30	23	21	56
B	3800	450	2100	260	340	170	630
		12	75	13	29	24	47
C_1	2100	590	900	78	105	56	490
		30	64	6	17	15	68
C_2	1300	340	520	140	150	65	130
		28	52	25	37	26	37

Waters of A zone have more high water salinity (TDS - 7 $g \cdot dm^{-3}$). Water freshering takes place from A zone to C zone; the water salinity decreases as the water level increases. In the initial period, water were dominated by high concentrations of SO_4, Cl and Na, when the groundwater table rose, concentrations decreased by a factor of 5 – 10 and the water was dominated by SO_4, HCO_3, Na and Ca (Table 2). The main reason of water freshering is the flow of water from urban communications. The similar changes of composition of groundwater are found out at classification of results of approbation in 1996 and 1997 (tables 3 and 4). Thus, the important regulation of groundwater composition transformations on the background random heterogeneous area was detected the G-method classification.

Table 3. Average chemical composition (mg dm-3 and %-mol) of groundwater on homogeneous hydrogeochemical zones (samples collected in 1996).

Zone	TDS	HCO_3	SO_4	Cl	Ca	Mg	Na
A	5400	630	2400	690	390	200	1000
		13	63	24	24	21	55
B	3300	380	1700	190	400	200	240
		13	75	12	43	35	22
C_1	2400	580	970	270	130	88	530
		26	54	20	18	20	62
C_2	1100	380	430	69	120	55	170
		34	50	16	32	27	41

Table 4. Average chemical composition (mg dm-3 and %-mol) of groundwater on homogeneous hydrogeochemical zones (samples collected in 1997).

Zone	TDS	HCO_3	SO_4	Cl	Ca	Mg	Na
A	5900	540	2600	540	380	180	1000
		11	69	20	24	19	57
B	3200	500	1300	330	270	120	480
		18	61	21	31	23	46
C_1	1200	430	340	110	150	52	130
		41	41	18	42	25	33
C_2	570	250	150	61	84	30	53
		46	35	19	46	28	26

ACKNOWLEDGEMENT

A classification method, G-method, was developed and applied to environmental investigations. The method is based on the Z^2 criterion of quasi - χ^2 distribution, and allows classification of data without any a priori knowledge of the taxonomic structure of observations. The G-method provides a basis for environmental mapping, because it provides a means to isolate homogeneous taxonomic units, define their boundaries and compare them. The method was used to map and investigate the patterns of environment composition under natural conditions and anthropogenic impacts.
The practical application of the classification method has demonstrated its potentially extensive capabilities for the solution of various problems arising in process-level investigations.

REFERENCES

1. Coradini, A., Fulchignoni M., Fanucci O. & A.I. Gavrishin 1977. A FORTRAN Program for a new classification Techniques: the G-mode Central Method. Comput. Geosci. 3:85-105.
2. Gavrishin, A.I. 1978. The procedure of geological objects classification with the help of multivariate criterion Z^2. In: Mathematical Methods of Research in Geology, vol. 1: 1-12, Moscow.
3. Gavrishin, A.I., Coradini A. & M. Fulchignoni 1980, Some Regularities in chemical composition of Lunar Rocks and Glasses. Geochemistry 3: 353-371. Moscow.

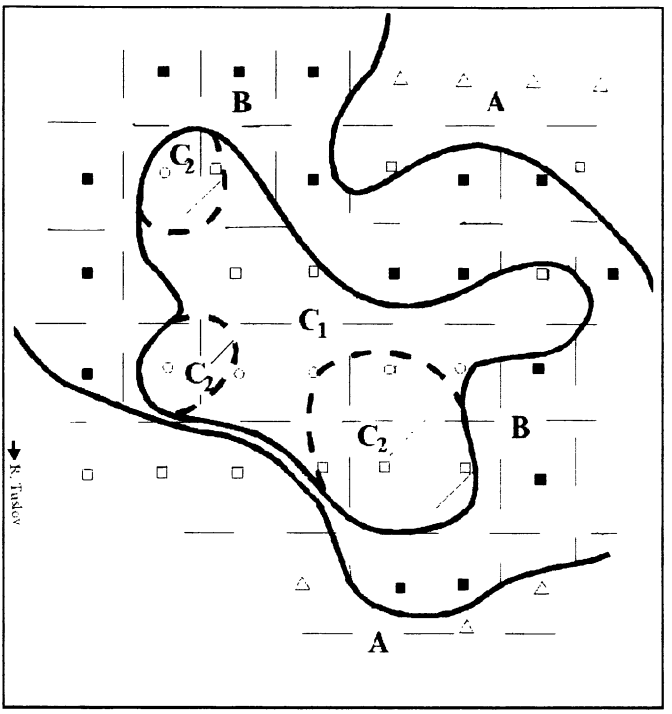

Name of component	HCO_3	SO_4	Cl	Ca	Mg	Na
Predominant 25 - 75 %-mol	○ ○ ○	□ □ □	△ △ △			
Dominant > 75 %-mol	● ● ●	■ ■ ■	▲ ▲ ▲			

— Zone boundary — Subzone boundary A — Name of zone

Figure 1. Hydrogeohemical map.

Challenges, Monitoring and Development of Groundwater in North India

R.B. Singh

Department of Geography, University of Delhi, Delhi - 110 007, INDIA.

ABSTRACT. In order to fulfil the requirements for agricultural, domestic and industrial purposes, the dependency on groundwater in North India is rapidly increasing. Agriculture being the main source of livelihood of the rural population, heavy dependence on groundwater is evident from the fact that 95 % of the total irrigated area receives groundwater irrigation. A few prominent questions which the planners and decision makers are confronted with relate to the quantity and quality of groundwater. Other factors include location of recharge in intake areas, temporal and spatial variability of recharge, inter-linkage between groundwater and surface water, existing hydraulic gradients and water table situation, groundwater flow between different formations, etc. Groundwater has experienced major problems resulting from indiscriminate exploitation as well as combination of imprudent irrigation, different pollution sources such as urban runoff, nitrogenous fertilisers used in agriculture, seepage from contaminated industrial sites and industrial discharges. Enhancement in water availability and safe water supply should always be guided by the effective public policies, plans and local technologies, in addition to political, socio-economic and other factors.

KEY WORDS: groundwater monitoring, quality assessment, groundwater depletion, impact study, socio-economic dimensions

INTRODUCTION

About 75 - 80 % of human requirements are fulfilled by groundwater. In recent studies it was observed that there is an accumulation of inorganic fertilizers, as a result the groundwater has shown increasing nitrates. Subsequently, water supply in India is being threatened due to the degradation in quality of water. An uncontrolled disposal of urban waste into water bodies, open dumps and poorly designed landfills causes ground water contamination. The issues of groundwater pollution have become one of the most important toxicological and geoenvironmental issues in India. In January 1994, the Central Pollution Control Board (CPCB), Delhi, had undertaken the first major groundwater quality monitoring exercise. The report published in December 1995 identified 22 places in 16 states of India as 'critical' sites of groundwater pollution, CPCB found industrial effluents to be the primary reason for groundwater pollution [1,2,3]. Many critical regions have to depend on ground water resources for various needs due to scarcity of surface water. In Industrial and urban fringe zones of Delhi, the subsoil water in the area has already been polluted due to industrial effluents. Industries are releasing high concentration of toxic substances. The wells in many residential areas are contaminated with nitrate, and detergents. The high content of fluoride in groundwater resources posses negative effects and is subject to severe health hazard in surrounding region [4].

GROUNDWATER PROBLEMS IN GREEN REVOLUTION STATES

The green revolution in Punjab and Haryana states brought prosperity to the region, but the problem of soil and water degradation came into existence. Recently it acquired a greater importance because these states make a significant contribution to national food security.

Gross irrigated area in these states has more than doubled during 1965-95. Consequently, the major crops-rice, wheat and cotton-are totally irrigated in the region. The number of tubewells has increased tremendously during the last three decades in the region. This has resulted in over-exploitation of groundwater in many blocks leading to decline in groundwater table up to 2 m in last 20 years depending on the region (Table 1). This decline forces farmers to lower the pumps further deeper in the wells, increasing the costs of pumping and energy use and thus decreasing profitability and efficiency of agriculture. Government policy of highly subsidised power supply to rural areas further aggravates the problem. The deep groundwater aquifers in most parts of Haryana are marginal and highly saline. Pumping water from greater depths could, therefore, result in the use of irrigation with saline water. Precaution in the use of groundwater is thus essential for a long-term sustainable agriculture [5].

Table 1. Groundwater development in Punjab and Haryana

States	Name Of the District	Total replenishable G.W. resources MCM/Yr	Utilisation G.W. Resources for Irrig. MCM/Yr	Net Draft MCM/Yr	Balance G.W Potential available for Explotation MCM/Yr	Present of G. W. Development (%)
Punjab	Amirtsar	1918.8	1630.9	1647.3	-16.3	101.0
	Firozpur	3588.3	3050.0	1509.8	1540.2	49.5
	Gurudaspur	1620.8	1377.7	832.5	545.2	60.6
	Jalandhar	827.2	703.1	1491.7	-788.6	212.3
	Kapurthala	392.7	333.8	668.4	-334.6	200.3
	Ludhiana	1686.5	1263.5	1953.6	-690.1	154.6
	Patiala	1365.9	1161.0	2376.7	-1215.6	204.7
	Sangrur	1511.9	1285.1	2190.0	-904.9	170.4
Haryana	Ambala	1057.5	898.8	585.2	313.7	65.1
	Karnal	1281.9	1089.6	1411.6	-322.0	129.9
	Kurukshtra	774.1	658.0	1253.3	-595.3	190.5

Source: Various Reports

GROUNDWATER QUALITY IN NORTH INDIA: CHALLENGES AND RESPONSES

Disposal of untreated mercury-contaminated effluent from caustic manufacturers has heavily contaminated groundwater. Reckless dumping of effluent and hazardous waste is as common here as in other industrial areas. Industries and factories used to release untreated effluents directly into the ground, contaminating underground aquifers. In one of the sample mercury had more than 268 times than it is considered safe. Groundwater in the industrial areas of North India is unfit even for agriculture. A tubewell sunk to a depth of about 200 feet (61 metres) by Suruchi Dyeing Udyog, a factory south of the G.T. Road in Ghaziabad, Uttar Pradesh, was yielding yellow-coloured water. The Central Ground Water Authority (CGWA) found para-nitrophenol, an organic compound, in the water in a concentration of 0.54 milligrammes per litre (mg/1). The permissible limit of the compound is 0.001 mg/1. Obviously, some factory in that area was pumping untreated effluent into the groundwater. Considering the 80 per cent of the country's drinking water needs are met by groundwater, the Facility for Ecological and Analytical Testing (FEAT) of the Indian Institute of Technology (IIT), Kanpur conducted survey of the groundwater. There were traces of heavy metals like iron and zinc in all the sample, cadmium in five samples and lead in three. But all the samples had one striking similarity: the levels of mercury were very high. High levels of

mercury in drinking water can severely impair the nervous system, causing neuropathy. Moreover, it has severe health hazards [6].

The concentration of mercury in the sample taken from a tubewell near an industrial area in Panipat was 0.2683 mg/1, contained more than 268 times the permissible limit of 0.001 milligrammes per litre (mg/1) set by the World Health Organisation for drinking water. The chemical oxygen demand (COD, which is the amount of oxygen required by chemicals in the water to oxidise and stabilise themeslves) of the water was 360 mg/1. The maximum permissible COD level even for industrial effluents is 250 mg/1. The groundwater is as bad or worse than untreated industrial effluents. The presence of chemicals was found to be more than what is permitted for industrial effluents. According to the findings, effluent with COD levels as high as 2,400 mg/1 were pumped into the aquifer. In order to provide assured water supply, the municipal corporation is exploiting groundwater resources through 80 extraction points. Besides most residents and industrial units also extract groundwater. The responsible units are 1,311 thriving industries which are engaged in producing cycles and textiles, among other things, and include foundries. According to a Central Ground Water Board (CGWB) report, the units are discharging about 50,000 cum of industrial effluents - mostly of toxic contents - each day into the Budha Nala, a stream that recharges the groundwater of the city. CGWB's report on Ludhiana's groundwater status affirms that many industrial units are deliberately pumping effluents into the aquifers. The groundwater board found that levels of heavy metals such as cadmium, cyanide, lead and chromium were all above permissible limits in the shallow aquifers, while traces of arsenic were within the permissible limit. Small quantities of these heavy metals were also traced in the deeper aquifers. In the absence of suitable modes of disposal, indiscriminate discharge of effluents has caused serious pollution of groundwater. The indiscriminate discharge of mercury along with industrial pollutants may result into significant build-up of the metal in the aquatic environment.

IMPACTS OF URBANISATION ON GROUNDWATER QUALITY: CASE OF DELHI

The industrial growth in Delhi got intensified only after India's Independence. From a small number of about 8,000 industrial establishments in 1950-51 the number increased to 90,000 in 1995. Government policies helped this rapid establishment of industries by providing facilities and incentives. This resulted in a mixed and even conflicting land use and causing deterioration in the quality of land and water. The prime cause of critical insanitary conditions is due to the lack of facilities to collect wastewater and to dispose off after treatment. Data on wastewater generation and collection is less when compared to information on water supply. Owing to this, it is difficult to assess the total pollution potential. The municipalities dispose off their treated or partly treated or untreated wastewater into natural drains joining rivers or used on land for irrigation or fodder cultivation or into the groundwater. A higher value of residual sodium carbonate (RSC) in irrigation water causes increase of sodium adsorption and thus the value greater than 5 meq/l shows detrimental effect on crop growth because of sodium hazard. In case of anions, the concentration of chloride and sulphate to some extent are increased. The levels of nitrate in all the groundwater samples are within the permissible limit set for drinking water purposes. The RSC values in some places such as Mundka, Bawana and Qutabgarh are more than 5 meq/l. This indicates that those areas are affected by sodium hazard [7]. Like Alipur block, the predominant caution in Kanjhawala is sodium where a considerable number of stations contain chloride ion as dominant anion. The areas below the Rohtak road have high conductivity values. The ground water from Kanjhawala block and upper Rohtak road may be considered as the enclosure of sodium hazard and high salinity.

The trace elements surveyed in all those stations are lead, zinc, copper, nickel and cadmium. Other metals except lead in few well waters, were within the permissible level of drinking water. Data revealed that out of 30 locations in Alipur and Kanjhawala block (fifteen each), 3 locations in Alipur and 2 locations in Kanjhawala block were contaminated with calcium (Table 2). None of the well water monitored in Alipur block indicated concentration of calcium exceeding drinking water standard ranges between 11 and 25 ug/l. The calcium concentration of the well, which exceeded drinking water standard, is 17 and 11 ug/l, respectively. Other metals except lead in few well waters, were within the permissible level of drinking water. Out of 42 wells in both the blocks, the survey revealed that the level of lead in 6 wells, 3 in each blocks, exceeded the drinking water standard. The lead contamination in the well water of Chandpur were recorded as 110 and 204 ug/l respectively in both the layers. The values of nitrate never exceeded the permissible limit (50 mg/l as No3). On the basis of detailed analysis of groundwater quality, Central Ground Water Authority (1998), New Delhi recently informed public that groundwater from shallow water bearing zones up to 30 meters of National Capital Territory of Delhi has high concentration of Fluoride and Nitrate and is not fit for drinking purposes. It is advised that groundwater of the areas given in Table 3 should not be used for drinking purposes without proper treatment [8].

Table 2. Groundwater condition in rural Delhi

Parameters	Maximum Permissible Limits for drinking Water (ug/1)	Frequency distribution of actual observed values			
		No. of samples Out of 42 samples		Concentration (ug/1)	
		Alipur Block	Kanjhawala Block	Alipur Block	Kanjhawala Block
Cadmium	10	21	17 4	0-5 -	0-6 11-25
Lead	100	18 3	18 3	0-58 142-428	0-96 102-204
Chromium	50	20 1	21	0-34 50	0-27 -
Zinc	15,000	21	21	0-34	0-78
Copper	1,500	21	21	0-38	0-31

Source: Central Board for the Prevention and Control of Water Pollution (1985)

PEOPLE'S PERCEPTION AND POLICY ISSUES

Residents of the surrounding areas were unaware of the danger in groundwater, though they could see that something was wrong. The pollution control boards are either unwilling to deal with the offenders or are simply ineffective at implementing the anti-pollution laws. On December 10, 1996, the Supreme Court directed the Union ministry of environment and forests (MEF) to empower the Central Ground Water Board (CGWB) under the Environment Protection Act, 1986, against overexploitation of groundwater. This led to the creation of Central Ground Water Authority (CGWA). Pollution control authorities are not capable of dealing with the groundwater crisis. It is very important to involve the local people and civil society in checking further pollution of our groundwater as they are the most important stakeholders of the country's natural resources and are the worst affected by pollution. Utilization of groundwater resources should be so regulated as not to exceed the recharging possibility. Groundwater recharge projects should be initiated for augmenting the available supply. A phased programme should be implemented for improvement in water quality.

Urban development and related activities should be planned with due regard to the constraints imposed by the configuration of water availability. There is a need for water zoning in metropolitan region and the economic activities should be regulated in accordance with such zoning.

CONCLUDING REMARKS

In order to address issue of long-term policy on water-use, the following strategies are important; 1.) Technologies or strategies are needed or are available for bringing water-table to 1970 levels; 2.) Water supply in the areas having a falling water-table trend needs to be replenished through artificial groundwater recharge. The surplus water during rainy season as surface run-off or escape from canals needs to be made use of for this purpose; 3.) On-farm irrigation water management should be given top priority to have maximum productivity per unit of water and to avoid the development of water-logging and soil salinity. This will require scientific utilization of surface water in conjunction with groundwater. Between April and June, the recommended cropping pattern should include only such crops which are less water-consuming, particularly in those agro-climatic irrigation zones where there is already a negative water balance. Groundwater resources may be planned to meet the mega city needs for the next fifty years. Aquifers may be recharged by harnessing rain water. There is promising scope of remote sensing technique in pollution detection through a close and continuous monitoring.

REFERENCES

1. Central Pollution Control Board (1998) Report on groundwater pollution in NCT of Delhi, New Delhi
2. Central Pollution Control Board (1995) Status of water supply wastewater generation, collection, treatment and disposal in Metro cities (1994-95), Control of urban pollution series CUPS/42, New Delhi, 1-38
3. Central Pollution Control Board (1979) Industrial survey, UT of Delhi control of urban pollution series, New Delhi, 1-10
4. Singh RB (1999) Urban impacts on groundwater quality in the Delhi region.. in Impacts of Urban Growth on Surface Water and Groundwater Quality, Ed. Bryan Ellis, IAHS Pub. No 259:227-236
5. Indian Council of Agricultural Research (1998) Decline in crop productivity in Haryana and Punjab: myth and reality?. New Delhi
6. Down To Earth (1999) Analysis on groundwater. August 31: 30-41
7. Central Board for the Prevention and Control of Water Pollution (1985) Groundwater quality in the Union of Delhi- Abridged report and programme objectives series, New Delhi
8. Central Ground Water Board (1998) Report on groundwater resources, it depletion and contamination in Najafgarh Block of NCT Delhi, New Delhi

Table 1. High concentration of flouride and nitrate in Delhi

Areas	Fluoride (mg/l)	Nitrate (mg/l)	Areas	Fluoride (mg/l)	Nitrate (mg/l)
BLOCK-KANJHAWALA	(Maximum Permissible Limit of Fluoride: 1.5 mg/l; Nitrate: 100 mg/l)				
Bawana	3.18	–	Shahbad Dairy	3.03	–
Gherva	2.21	–	Tikri Kalan	5.47	–
Garhi Ringhala	2.59	-	Kanjhawala	10.00	140
Sultapur Dabas	2.6	–	Korala	1.53	–
Mohammad Pur Mairi	1.92	161	Agar Nagar	2.43	–
Mundka	2.29	119	Kirari	4.21	184
Sultanpuri	4.9	208	Mangol Pur Khurd	6.1	114
Mangol Pur Kalan	4.06	652	Rajiv Nagar	4.78	–
Rithala	5.1	–	Punjab Khor	3.48	–
Qutabgarh	5.26	–	Katewra	4.07	–
Mungeshpur	6.43	–	Auchandi Border	3.73	–
Nijampur	–	106	Mangolpuri	–	180
Bhagey Vihar	–	115	Jat Khor	–	390
Kirshna Vihar	–	141			
BLOCK - NAJAFGARH					
Palam Gaon	3.3	105	Pappan Kalan	3.65	–
Bamnauli	3.65	–	Chawala	1.8	130
Kangan Hari	1.9	300	Daulatpur	2.05	–
Shikarpur	2.55	–	Goela Khurd	7.25	–
Kharkhari Nahar	1.6	203	Nangloi	3.8	–
Ugersain Park	2.4	–	Kakrola	3.05	379
Mitraon	5.47	–	Pindawala Kalan	2.21	361
Dhansa	3.84	377	Ujwa	2.14	508
Jharoda Kalan	7.3	208	Dichaun	3.69	178
Neejwal	5.08	117	Jafarpur	6.9	–
Qazipur	11.0	389	Kair	–	264
Isapur	–	106			
BLOCK - ALIPUR					
Shahbad	2.14	–	Puthkhurd	3.48	266
Pehladpur	5.42	–	Palla	–	277
Bokali	–	113	Tikri Khurd	3.2	–
Mamurpur	–	236			
BLOCK - CITY					
Munirka D.D.A. Flats	2.2	–	Sant Nagar	4.4	–
India Gate Nursary	2.54	121	Delhi zoo	2.97	1589
Nizamuddin	4.83	–	Jamia Millia	2.46	194
Ashram Chock	2.3	–	UPSC	1.75	–
Vikas Puri	1.85	–	Rajouri Garden	4.25	–
Meera Bagh	2.05	–	Vasant Enclave	2.43	133
Hastal	1.85	171	ParsiDharamShala	2.03	100
Majnu Ka Tilla	2.28	–	Timarpur	2.73	–
Shalimar Village	3.69	–	Naharpur	7.46	108
Rohini Sec-2	2.4	–	Maharani Bagh Bazar	3.99	–
Zakhira	2.63	–	Rana Pratap Nagar	2.28	–
Inderpuri	1.67	–	Lakshmi Bai Nagar	3.65	–
Pragti Vihar	6.43	–	Jeevan Nagar	3.23	232
Panchkuian Road	2.38	–	Kishan Ganj	–	190
Kotla Mubrakpur	–	328	Sanjay Camp	–	240
Sudershan Puri	–	202	Shanti Van	–	144
Okhla Ind. Phase I	–	110	Sarita Vihar	–	149
New Friends Colony	–	102	Naraina	–	600
Begampur	–	240	Moti Bagh Part I	2.11	–
BLOCK - SHAHDARA					
Ghazipur	–	139	East Vinode Vihar	–	180
Durga Puri Chowk	–	141			
BLOCK - MEHRAULI					
Dera Gaon	–	690	Rajokari Road	–	262
Gadaipur	–	743	Jaunapur	–	124

Source: Central Ground Water Authority (1998), New Delhi

Qanat as an Iranian Ancient Method for Using Groundwater

Mohammad J. Pouraghniaei, Mohammad Mahdavi, and Shahram Khalighi

Division of Watershed Management, Department of Reclamation of Arid Zone and Mountain Regions, Faculty of Natural Resources, Tehran University, IRAN.

ABSTRACT. Qanat is one of the most interesting human's inundation for getting at, one of the most important needs of human being , water .
Qanat is a technique which brings up the water on the ground and make it available to be used. It consists underground channel where groundwater infiltrates in to them and finally in this outlet (Mazhar of Qanat), comes up on the surface of land. Qanat inundation is resulted of modification in the techniques, which were used by ancient miners in order to discharge accumulated water in the mines.
Climatic, hydrogeologic and topographic conditions of area should be considered before establishment . In order to establish a Qanat, selecting a suitable area is the main step. First step is finding a reach aquifer, then after, they dig the main well (madar chah). Digging under ground channel is the next step.

Key Words: Qanat, Groundwater, Iran, Well, Ecologically Balance

INTRODUCTION

Iran is located between 25 to 40 North latitude and from 44 to 64 East longitude .It lies at the east of Arabian peninsula and comprises the western and larger part of the Iranian plateau ,extending from the Persian gulf to the Caspian sea .The majority of the country is semi-arid except on the northern Alborz mountain range , where the rainfall varies from 1000 mm to 2000 mm (40 in-80in)annually; On the plateau ,the average annual rainfall of over 200 mm (8 in)in the north , decreases to less than 100 mm (4 in)in the south and south east .

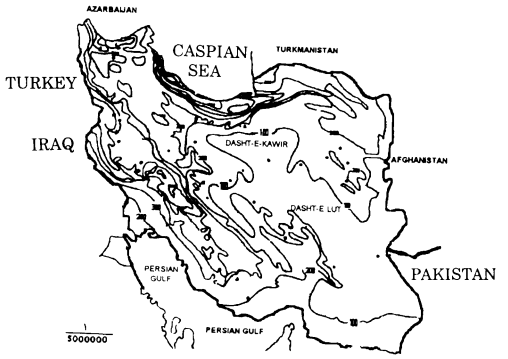

Fig. 1. Mean annual amount of precipitation of Iran

In Iran ,the climate and rainfall conditions make irrigation essential for raising crops in the most parts of the country .Under these circumstances , the hill foot fans offer plentiful supplies of ground water of suitable quality to be used by men,crops, and animals .

The main aquifer in the Iranian plateau consist of alluvium of the Pleistocene age which may locally reach a thickness of 400 meters (440 yd) .The alluvial fans offer the opportunity to convert seasonal runoffs into a form of semiperennial source at water .

The graduation from coarse to fine materials from the apex of the fan to the periphery is common to all tectonically undisturbed alluvial fans, and encourages the seasonal rainfall and flood to sink into the upper area .Recharge of the ground water is therefore high at the fan heads which are composed of most permeable materials .

Fig. 2. Place of main Qanats in Iran

Qanat is a subterranean aqueduct -or subsurface canal - engineered to collect ground water and direct it through a gently sloping underground conduit to surface canal which provide water to agriculture fields .

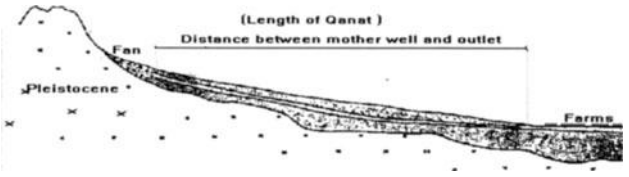

Fig 3 : Longitudinal Profile of Qanat

The system is unique and one of the most common means of underground exploitation in Iran and other arid countries .These system is variously known as Qanat, ghanat , kanat , kariz , fogaras , khetart etc. .

Qanat is not an irrigation method , but produced water can be used for irrigation crops .

Qanat system includes four main parts:
1- Upper most shaft or mother well (madar chah)
2- Vertical shafts for aeration or access (mileh)
3- Tunnels as a path for water transportation or diverting water toward the out let (koreh)
4- Outlet and open part on conveyance canal (mazhar & haranj).

In a quick glance each Qanat divides in two parts :
1- Wet part or the drainage wells and tunnel (tar kar)
2- Dry part or conveyance tunnel (khoshke kar)

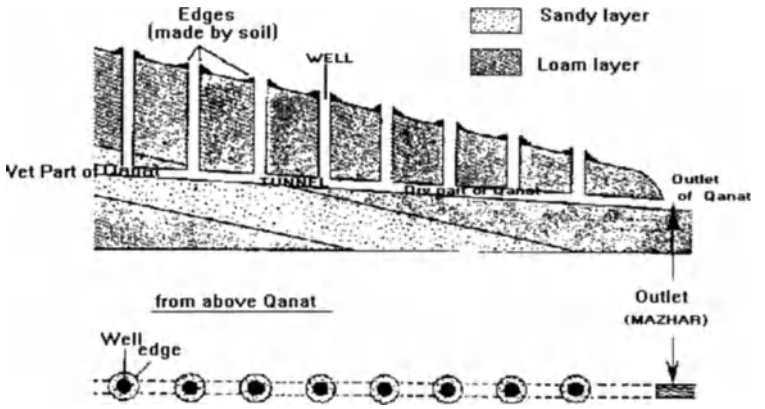

Fig.4: Side and Above Landscape of Qanat

Water seeps through the walls of mother well, which is dug into an aquifer up slope from the fields being irrigated (this is true for the other wells in the chain that penetrate into the water table-tarkar),and then is carried by natural gravity flow through the tunnel to a point hundreds of meters to tens of kilometers away.

When a single tunnel fails to yield an adequate flow of water , branch infiltration galleries that feed into the main tunnel may be added upslope , or the mother well maybe extended deeper into the water-bearing strata.

HISTORY OF QANAT

Qanat craters are seldom out of the sight of people who travel across or fly over the persian plain .
About 3000 years ago , the persians learned how to dig underground aqueducts that would bring ground water to arid plains surface .But the precise dating of Qanat is virtually impossible unless their construction was accompanied by documentation or occasionally, by inscription .

The most ancient evidence which regarding to Qanat is in the description of the eight war of Sargon II (705-722 BC) against Urato empire in 714 BC. Sargon regions were from Oromiea lake in Western Azarbaijan Province in northwest of Iran and continued in the Zagross mountain range (Northwest of Iran).The description of this war was in cuneiform writing in a great inscription which is kept in Louver museum . Qanat extended from Urato's empire toward east, south and to all of Iran's plateau .[4]

Without Qanat some great cities as Ray (near Tehran) , Neishabor , Yazd and ... couldn't exist or survive .If Qanat were not created many of cities around desert of Iran Arabia and Africa ,probably wouldn't exist anymore.

In early first millennium (BC) Qanat was created and after this extended in the world ,with a high speed .Then during centuries from the origin and because historical events , extended to the east and west of the world .

Iranian transferred this system to Egypt in about 500BC ,and about 750AC it was transferred to Spain by Muslims .[1]

Now Qanat can be found in about 34 countries in the world :
In Asia : Syria , Pakistan , Turkey ,China ,Iraq ,India , Palestine , man ,etc. .
In Africa : Egypt , Algeria , Tunisia , Libya , Sahara , etc. .
In Europe : Spain , cyprus , etc. .
In America : Peru , Chile , Mexico , etc. .

Karaji , a famous persian scholar of 11th century AD , compiled a comprehensive treatise on " Exploration for hidden water "in which he elaborated on different aspects of ground-water flow and the means of its exploitation .In this book many chapters are devoted to Qanat , presenting different cases and pertinent practical solutions .The most important discovery of Karaji , was that he attributed the flow of water to gravity and sloping water table .

SUITABLE NATURAL CONDITION FOR QANAT

Climatic , topographic and hydrogeologic conditions which are needed for a Qanat are :

Climatic : most of Qanats constructed in regions which have temporary surface water resources (either because of shortage of water or unsuitable distribution of water in yearly cycle) , then Qanat almost belongs to low water climates .

Hydrogeologic Condition : Because of shortage water , it must be compensated by ground water and these aquifers are useable where they feed continuously and in adequate quantity, then exist of a chain of high mountains is essential which could change cloud's to rain .

Topographic Condition : Qanat is normally limited to sloping lands , almost whatever slope of land is less ,length of Qanat will be more .

METHOD OF CONSTRUCTION

Qanats are normally limited to gently sloping lands, usually alluvial fans or gravel outwash at foot of mountain. It is obvious that any seepage from the alluvial fans or the presence of springs suggest the possible presence of ground water is ascertained. It can be utilized, by digging either a vertical shaft or a horizontal tunnel, where the slope of tunnel ensures a steady flow due to the gravity .

To dig an underground tunnel with a length of even 1 km is not an easy task, particularly when everything is done through manual labor. The evacuation of excavated materials, the alignment of tunnels, and fresh air required by Moghannies (diggers) are among the serious handicaps .To overcome such difficulties, the ancient Iranians sunk a line of shafts, spaced 30 m- 100 m apart (33 yd- 110 yd).These shafts facilitated the digging of the tunnel and the evacuation of the excavated materials , as well as supplying fresh air for the labors .

To dig a Qanat , the Moghannies first locate some points on the upper slope of an alluvial fan where they sink one or two shafts to assess the depth of the water -bearing strata and their approximate discharges .This is usually done by the leather buckets which are dipped periodically into the shafts to measure their rate of water accumulation .If the initial observation wells prove satisfactory in locating water at the elevation high enough to provide the necessary head required to reach the area of utilization ; then a survey of the proposed alignment of the qanat is made. After the outlet point is determined ,the digging of the shafts and the dry tunnel commence from this point.

The Qanat usually start from the lower slope in the form of a shallow ditch , which eventually develops into a tunnel as the depth increases upslope .From each of the shafts the tunnel is extended in both directions . When the dry tunnel intersects the water table , it continues through the aquifer acting as a drain . The slope of the tunnels is usually very gentle, ranging from less than 1m to several per kilometer, depending on the physical properties of the soil .

The tunnel is usually enough for the worker to crawl through, and the cross section of the tunnel is generally elliptical, with a height of at least 1.2m(47in.) and width of 0.8 m (32 in.). The shafts are usually 30m -100m(33yd-110yd)apart .The initial diameter of the shafts varies from 0.75m-1.0m(30in-40in).the spacing of the shafts is a function of the type of terrain and the depth of the tunnel, but is always greater for the drainage tunnel than for conveyance tunnel .

Qanat varies in length from several hundred meters to tens kilometers. The most common length is approx. 5km -9km (3miles-5miles).The depth of mother well may range from few meters to 400m(440yd) with the most common depth being 30m-50m(33yd-55yd).A Qanat is in Gonabad (northeast of Iran)with depth of mother well about 370m. The discharge of Qanat varies from a few liters over 400L/S (107gal/sec).

The total discharge of Qanats is estimated at about $500m^3/S$ (0.4 acre-ft/sec) .[2]

The number of Qanat in Iran, often estimated but not substantiated , is reported to amount to 50,000 ; it is said by ministry of agriculture that these Qanats provide from one-third of all irrigation water in country .

CONCLUSION

Qanat is one of the most ecologically balanced water recovery methods available for arid regions . There is a natural law which has allowed Qanat to flow continuously for many centuries that shouldn't be ignored by modern water engineers and farmers: the natural supply of water in a Qanat can never exceed ground-water recharge. Mechanically-pumped wells allowe this natural law to be exceeded for the time to be-pumping more water out of aquifers than to be recharged. However, without coordinated state-level monitoring and management of water resources, to include spatial and temporal limits on ground-water withdrawal ,aquifers will not be capable of sustaining ambitious irrigation schemes, and modern pumping devices could follow the fate of Qanats.

Qanat system is a way for water recovery in arid regions, which provide the best ecological balance .

Qanat digging cost lot of money and is very time consuming ,However they are being distroyed and left useless, which is a significant harm to the national resources.

So, maintanance and rehabitation of present Qanat could be a considerable step toward sustainable development of ground water resources especially in arid and semi-arid regions.

REFERENCES

1. Behnia A.K (1989) Make and Manage of Qanat Book, pages:16-22 .

2. Bybordi M (1974):Ghanat of Iran (drainage of Sloping Aquifer).J of Irrigation &Dinage,10785,P:245-255 .

3. lightfoot (1996) Syrian Qanat Romani . J of Arid Environment .

4. Goblot Henry (1991) Translation to Persian by Papoli-Yazdi M.H , Sarvqad Moqadam A.H published by astan-e-qodserazavi.

Land Subsidence Prediction and Its Visualization Using Geographical Information System (GIS)

S. Murakami[1], K. Yasuhara[1] and F. Murata[2]

[1]Department of Urban and Civil Engineering, Ibaraki University, Nakanarusawa 4-12-1,Hitachi, Ibaraki, 316-8511, Japan
[2]Japan Regional Development Corporation, Kasumigaseki 3-8-1,Chiyoda,Tokyo, Japan

ABSTRACT: Nearly 80% of land subsidence due to groundwater pumping in Japan takes place in the Northern Kanto region. It is important to estimate potential damage caused by land subsidence and to visualize this on a map over a wide area such as the Northern Kanto Plain, Japan. This paper describes the present situation and future prediction of land subsidence in this area and the evaluation of damage potential caused by land subsidence using a Geographical Information System (GIS). A simplified method for predicting future trends using observed settlements has been proposed and the applicability of the model has been verified by comparing the predicted and measured results at 1,282 points over the area. Using GIS, the present and future land subsidence has been visualized on a map. In addition, the occurrence of damage caused by land subsidence for each site can be assessed by means of a map based on a database consisting of a combination of predicted land subsidence and existing regional information.

KEY WORDS : land subsidence, groundwater pumping, visualization, geographical information system (GIS), Northern Kanto Plain.

INTRODUCTION

Nearly 80% of land subsidence due to groundwater pumping in Japan takes place in the Northern Kanto Plain whose bordered area covers the five prefectures as shown in Fig. 1, Saitama, Gunma, Tochigi, Ibaraki and Chiba. According to recent subsidence records, the average amount of subsidence in this area due to groundwater pumping for agricultural, industrial, and drinking purposes has been approximately 5cm every year although the situation is different depending on the prefecture. The amount of land subsidence and its variation with time are normally evaluated by adopting one-dimensional consolidation theory which is modified to take into account the variation in live loads due to seasonal changes in groundwater level. To achieve this and in particular, to prevent disasters to the infrastructure and to regulate groundwater pumping, we need a great deal of information on geotechnical properties from field and laboratory investigations over the whole area under consideration. However, this is not practical from the viewpoint of expense and time. To overcome this difficulty, a simplified method is proposed which is capable of forecasting the future time-settlement relations based upon the information presently available, regarding settlements due to groundwater pumping. This method can be used even where the soil profiles are unknown although the soil parameters are necessary for conventional settlement calculations.

Fig.1 Objective area for land subsidence

A SIMPLIFIED PROCEDURE

Strictly speaking, the solution of one-dimensional consolidation theory cannot be directly applied to land subsidence due to groundwater pumping. However, as a first approximation, it is here assumed that using the solution of Terzaghi's theory for one-dimensional consolidation of clayey soils, settlements due to groundwater pumping can be simply expressed as (see Appendix):

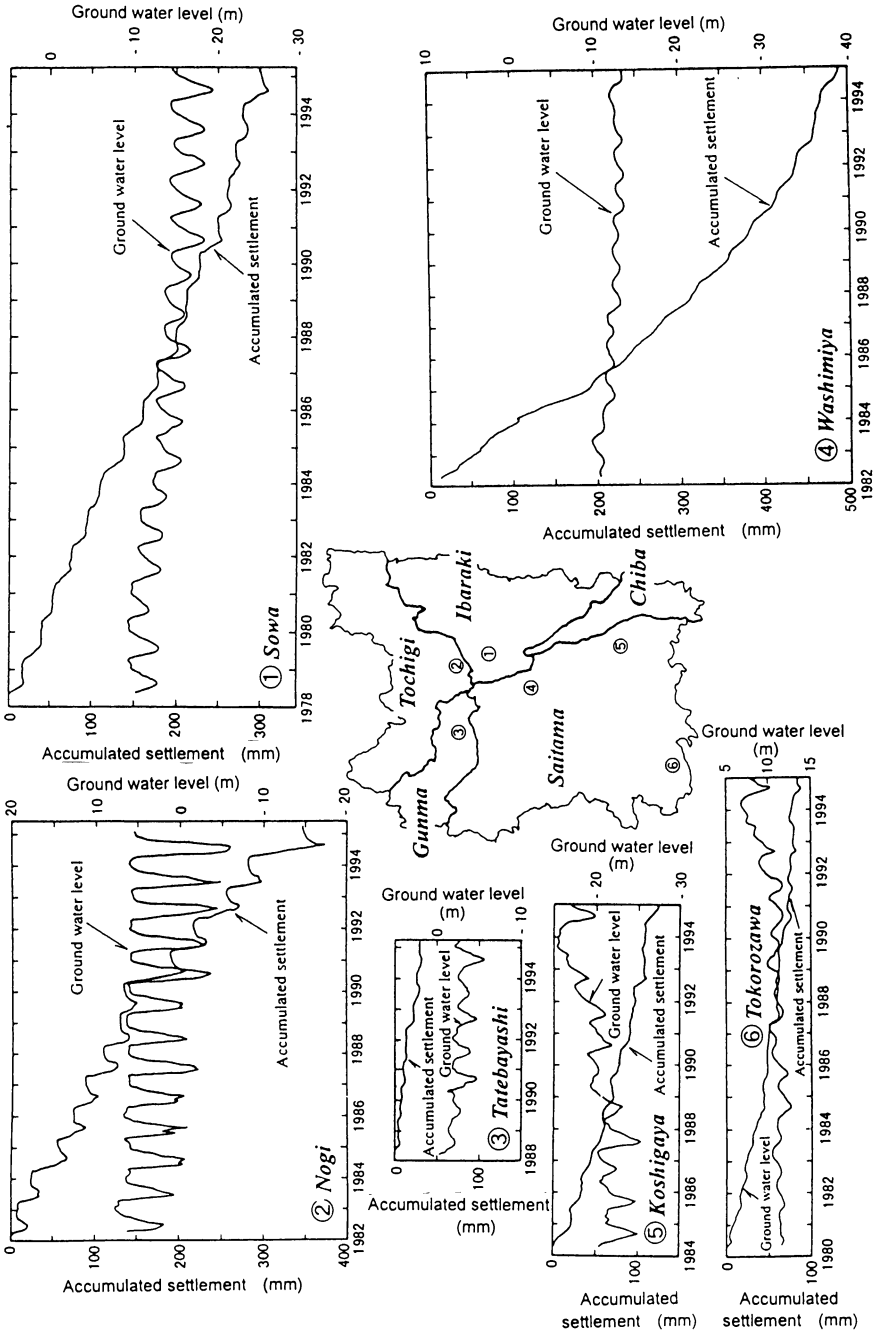

Fig.2 Variations of settlement and ground water level with elapsed time

$$S = S_{po}[1 - \exp(-C_R t)] \quad (1)$$

where S_{po} is the residual settlement expected from the present time until the termination of subsidence under the assumption that the groundwater variation is kept the same as observed at the present time, and C_R is a parameter corresponding to settlement strain rate. These are given by:

$$S_{po} = S_{r,f} = (8/\pi^2) \exp(-T_{vo}/4) \quad (2a)$$

$$C_R = T_{vi}/t_i = 4c_v/H_d^2 \quad (2b)$$

where $S_{r,f}$ is total residual settlement, T_{vo}, T_{vi} are time factors at the starting time to measure settlement and the arbitrary time during subsidence, t_i is an arbitrary time during subsidence, c_v is coefficient of consolidation, and H_d is the maximum length of drainage path for the clay layer.

If instead of such soil parameters as c_v, H and T_v two parameters, S_{po} and C_R, denoted by Eqs. (2a) and (2b) can be determined by using a statistical analysis of previously observed settlement records, the amount of settlement and settlement versus elapsed time relations can be obtained using the "non-linear least squares method".

APPLICATION OF THE METHOD PROPOSED

Applicability of the method proposed above is illustrated by comparing the calculated settlements with those observed. The two parameters $S_{p,o}$ and C_R were determined by a statistical analysis of land subsidence settlement-time records from 1970 until 1990 at 1,282 locations in the Northern Kanto plain in Japan covering the five prefectures: Tochigi, Gunma, Saitama, Chiba and Ibaraki. Typical variations of settlements and groundwater level with time for several locations are shown in Fig. 2. It was found that the variation of groundwater level and amount of settlements with elapsed time depends on each location. One of the characteristic features in Fig. 2 is that observed fluctuations in settlements followed seasonal changes in groundwater level except for one case in Washinomiya, Saitama Prefecture where the settlements were small in comparison to the change in modifying one-dimensional consolidation theory conventionally used for settlements under sustained or static loads.

The above-mentioned procedure was applied to the previously observed settlements versus time records accumulated in the Northern Kanto district for approximately the last twenty years. The typical examples of observed and calculated settlement versus time relations for records from 1970 to 1995 are shown in Fig. 3. The relations of total observed and predicted settlements are given in Fig. 4 corresponding to the same period as used in Fig. 3. The comparisons in Fig. 3 and Fig. 4 are in fairly good agreement with each other.

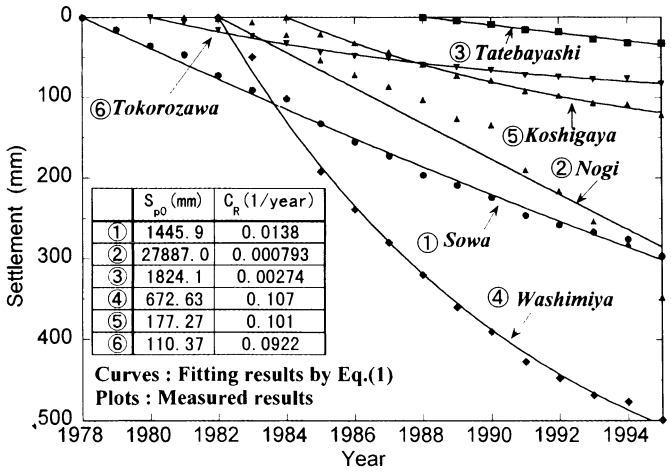

	S_{p0} (mm)	C_R (1/year)
①	1445. 9	0. 0138
②	27887. 0	0. 000793
③	1824. 1	0. 00274
④	672. 63	0. 107
⑤	177. 27	0. 101
⑥	110. 37	0. 0922

Fig.3 Comparison for observed and calculated settlement versus time relations

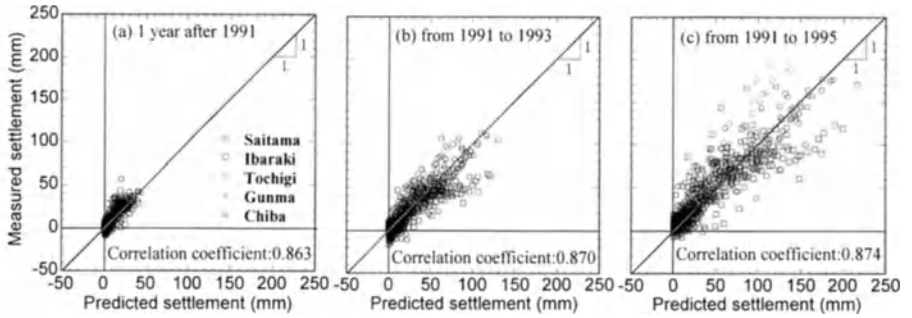

Fig.4 Comparison between predicted and measured settlements

FUTURE SETTLEMENT PREDICTION AND ITS REPRESENTATION USING GIS

Following the above-mentioned procedure for predicting land subsidence settlements using the previously observed field records at total of 1,282 locations, the future prediction of settlements was conducted for the next 5 years from 1998 to 2002. The results are represented and illustrated in Fig.5 as a hazard map of land subsidence in the Northern Kanto plain using a Geographical Information System (GIS). It is predicted that severe settlements will probably accumulate in some areas if the groundwater is pumped with continuous variations in groundwater level, although there is a tendency for gradually decreasing settlements in most areas in the Northern Kanto plain. Considering that there is possibility of big earthquakes occurring in this area, it is also suggested that through further investigation the potential for disastrous land subsidence from anticipated earthquakes could be demonstrated using a hazard map developed using GIS.

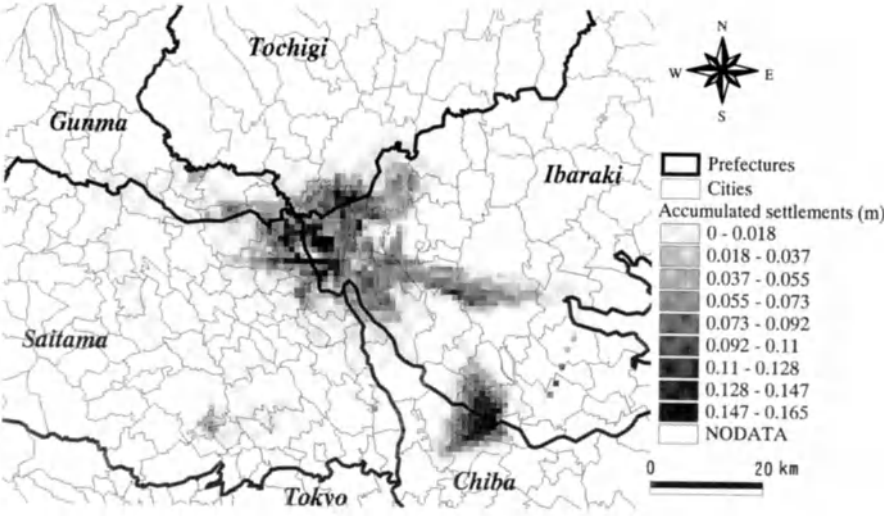

Fig.5 Map of land subsidence in the Northern Kanto Plain using GIS (1998-2002)

ESTIMATION OF DAMAGE POTENTIAL CAUSED BY LAND SUBSIDENCE

Damage caused by land subsidence is different for each site in the objective area because the characteristics of the sites are different. For example, water supply for irrigation deteriorates in agricultural areas. Bearing capacity of structures on piled foundations declines and underground lifelines are broken in industrial and business areas. Therefore, it is necessary to consider the characteristics of the sites for estimating the possible damage caused by land subsidence.

Damage potential D_p at a site expresses the summation of the products of the degree of damage D_i and the weighting w_i as is given by:

$$D_p = \Sigma\, w_i D_i \qquad (3)$$

For simplicity, D_i is assumed to be given by the following equations:

$$D_i = d_i / d_{max} \qquad (4a)$$

where d_i and d_{max} are:

$$d_i = A_i S \qquad (4b)$$

$$d_{max} = \max \{ d_i \} \qquad (4c)$$

In Eq. (4b) A_i is the damage area and S is the future settlement in a site, and d_{max} is the maximum value of d_i in the objective area.

Using the above, we have tried to draw a damage potential map. The built up areas and rice fields obtained from a database of existing regional information were used as the damage area A_i and the predicted settlements, from Fig.5, were used as the future settlement S. The weighting w_i was assumed to be 1.0. The results are presented in Fig.6. The occurrence of damage caused by land subsidence for each site can be specified by means of this map rather than a mere future settlement map.

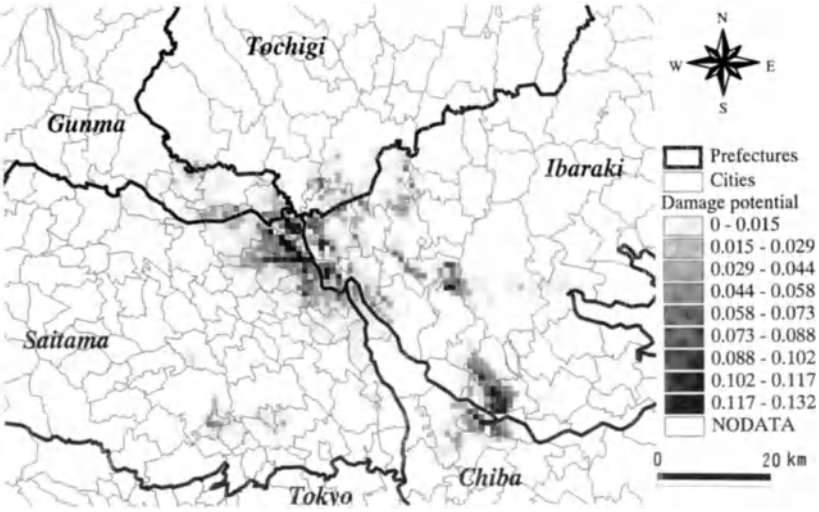

Fig.6 Damage potential map by land subsidence in the Northern Kanto Plain

CONCLUSIONS

The results in this study are summarized as follows :

1) It is recognized that the land subsidence in the Northern Kanto Plain is caused by seasonal

changes in the groundwater level due to the groundwater pumping.
2) A simplified method for predicting future trends using observed settlements has been proposed and the applicability of the model has been verified by comparing the predicted and measured results at 1,282 points over the area. Using GIS, future land subsidence has been visualized on a hazard map.
3) In addition, the occurrence of damage caused by land subsidence for each site can be assessed by means of a hazard map based on a database consisting of a combination of predicted land subsidence and existing regional information.

REFERENCES

1. Murakami, S., K. Yasuhara, K., Noguchi, N. and Hinoki, Y. (1997): Journal of the Faculty of Engineering, Ibaraki University, Vol.45, pp.65-72, 1997. (in Japanese)
2. S. Murakami, S., and K. Yasuhara, and F. Murata (1998): Proc. Intn'l Symp. Lowland Technology, Vol. 1, pp.507 - 512, 1998.

Appendix : Derivation of Eq. (1)

If land subsidence would approximately be governed by the one dimensional consolidation theory, the general solution for the both drainage ends is given by:

$$U = 1 - \frac{4}{\pi^2}\sum_{n=0}^{\infty}\frac{1}{a_n^{\,2}}\exp(-a_n^{\,2}T_V) \qquad \cdots(A.1)$$

When we consider the interval in two time factors of T_{vo} and T_{vi}, as shown in Fig. A1(a), the difference, δU, in degree of consolidation yields:

$$\delta U_t = U_t - U_0 = \sum_{n=0}^{\infty}\{\frac{2}{a_n^{\,2}}\exp(-a_n^{\,2}T_{V0}) - \frac{2}{a_n^{\,2}}\exp(-a_n^{\,2}T_{vt})\} \quad \cdots \quad (A.2)$$

In the above equation, by replacing $T_{vt} - T_{vo}$ as δT_v and then neglecting the difference in inherent values after the second order of the solution of the consolidation theory, Eq. (A.2) leads to:

$$\delta U_t = \frac{8}{\pi^2}\exp(-\frac{T_{v0}}{4})\{1-\exp(-\frac{\delta T_{vt}}{4})\} \qquad \cdots (A.3)$$

By referring to Fig. A1(b), Eq. (A3) can be rewritten as:

$$\delta Si = S_{P0}\{1-\exp(-C_R\delta t_t)\} \qquad \cdots(A.4)$$

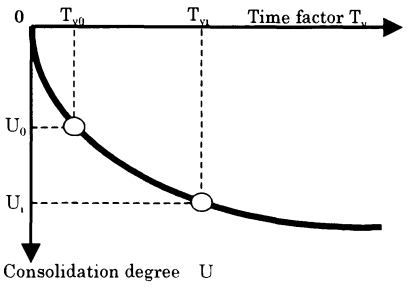

Fig.A1(a)

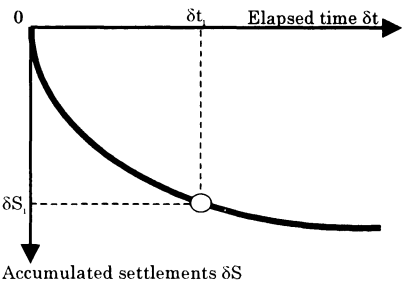

Fig.A1(b)

Artificial Recharge for Sustainable Groundwater Development in Jinhe Water Source Field of Zaozhuang City, Shandong Province, CHINA

Wen Zhonghui[1], Shu Longcang[1], Liu Xianglong[2], and Wu Xianfeng[2]

[1] Department of Hydrology and Water Resources, Hohai University, Nanjing, Jiangsu 210098 P. R. China
[2] Commission of Water Resources Management of Zaozhuang City, Zaozhuang, Shandong 277000 P. R. China

Abstract. The Jinhe water source field is one of two water source fields of Zaozhuang City, Shandong Province. It plays an important role in the social and economic development of Zaozhuang City. Since the late 1980's, groundwater has been heavily pumped from the Jinhe water source field with the result that a large groundwater level depression cone has formed and groundwater levels have declined continuously. In order to control the spread of these environmental problems, artificial recharge of groundwater was carried out in 1993 within this water source field.

A previously established mathematical model was run for three different recharge strategies. The results show that the artificial recharge of groundwater can substantially control the development of the groundwater level depression cone. It can also increase the assured supply of irrigation water for cultivated lands along the recharge ditches and has obvious social and economic benefits.

Key words. artificial recharge, sustainable groundwater development, water source field, Zaozhuang City

INTRODUCTION OF STUDY AREA

Jinhe water source field is located to the west of Zaozhuang City and is one of two water source fields of Zaozhuang City, Shandong Province. The long-term average precipitation of the study area is 772.5mm (from 1963 to 1997). The maximum was 1340.4mm in 1971 and the minimum was only 492.6mm in 1966 (Figure 1). The precipitation from June to September accounts for 70% of the total annual precipitation. This characteristic of the precipitation distribution is not beneficial for recharge of groundwater. Dashahe river flows through the east side of the study area. The area of this river basin is 260km^2, its length is about 8km in the study area, and its average flow rate is 5962×10^4m^3/a. The seasonal variation of river flow rate is great. In dry seasons (or years), the flow rate is very small and river may even become dry. But, in rainy seasons (or years), the flow rate is very big. The maximum flow rate was 2.12×10^8m^3/a while the minimum was only 0.03×10^8m^3/a.

There are two different kinds of aquifers in this area. One is a loose porous aquifer; the other is a karst aquifer. The average thickness of the porous aquifer is greater than 9m. It consists of medium, coarse sands and gravel. The karst aquifer is covered by the porous aquifer. The depth of karst development is from 35 to 212m. The hydraulic connection between these two aquifers is close. Their recharge and discharge conditions are the same.

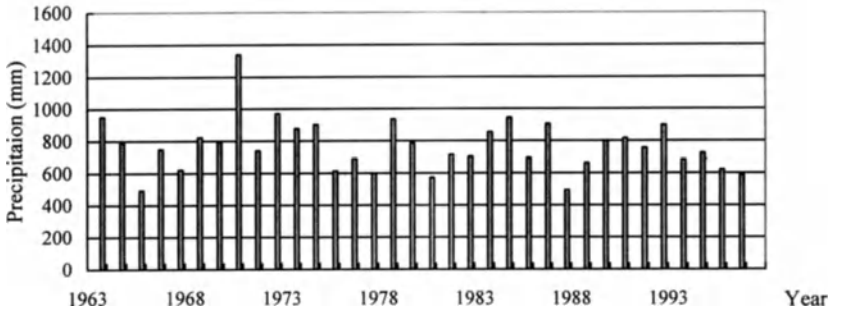

Fig. 1. Variation of precipitation in the study area

In this water source field, there are 320 wells for irrigation and 20 wells for industrial users. In recent times, groundwater pumping has increased greatly. It was only $768\times10^4m^3$ and $871\times10^4m^3$ in 1985 and 1990 respectively, but by 1997, it has risen to $3092\times10^4m^3$ (Figure 2).

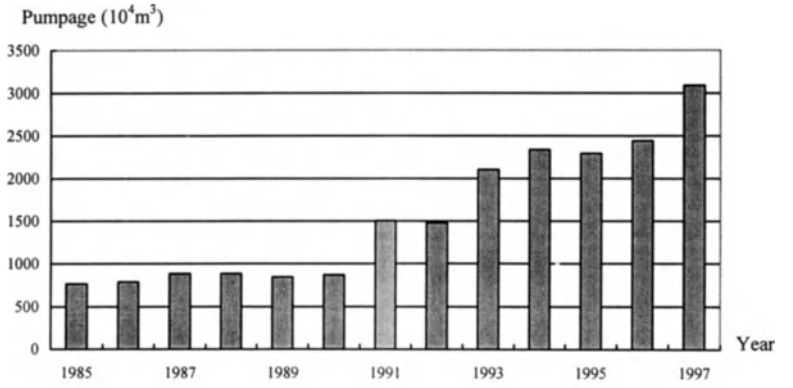

Fig. 2. Variation of groundwater pumpage in the study area

Groundwater overdraft caused a groundwater level depression cone to form over a large area and the regional groundwater level continuously declined. The area of the groundwater level depression cone is about $15km^2$ and the maximum depth of the groundwater level is about 32m. In order to control the spread of these environmental problems, artificial recharge of groundwater was carried out in 1993 within this water source field.

ARTIFICIAL RECHARGE OF GROUNDWATER

In order to retain the Dashahe river water, a rubber dam was built in the lower reaches of the river in 1991. The length and width of the dam are 88m and 9m respectively. Artificial recharge

ditches were excavated within the water source field in 1992. The length of the main ditches is 1110m, and the lengths of the south and north branch ditches are 2250m and 5100m respectively. The main ditches and branch ditches are connected to the Dashahe river. The design flow rates of the main and the branch ditches are 1.8 m^3/s and 0.5m^3/s respectively. In order to monitor changes of groundwater quantity and quality after carrying out artificial recharge, a monitoring network was established.

For the purpose of evaluating the influence of artificial recharge on groundwater quantity, a groundwater balance equation was established and the hydrogeological parameters (i.e. specific yield and coefficient of precipitation infiltration) in the equation were optimized using a genetic algorithm. Based on the observation data, the optimal values of these two parameters are obtained. The specific yield and coefficient of precipitation infiltration are 0.028 and 0.30 respectively. The components of the water balance were calculated for 1997 and the values are shown in Table 1.

Table 1. The values of items in water balance equation in 1997. unit: 10^4m^3

Items of water balance		Values	Total
Recharge	precipitation infiltration	411.66	2844.93
	infiltration from river	234.0	
	infiltration from irrigation	39.4	
	artificial recharge	302.0	
	lateral recharge	1857.87	
Discharge	industrial pumpage	2424	3092.4
	agricultural pumpage	615	
	domestic pumpage	53.4	
Recharge – Discharge = -247.47			

According to Table 1, the variation of groundwater storage was $-247.47\times10^4m^3$ in 1997, which means that groundwater declined 3.79m. The observed average value of groundwater level variation was –3.55m. These two values are close, which indicates that the water balance equation established is correct and the parameters in the equation were correctly determined. Artificial recharge accounts for 10.62% of the total recharge of groundwater.

From the analysis of variation of precipitation (Figure 1), after 1990, the minimum precipitation was 587.7mm in 1997. But the groundwater pumping was at a maximum and was $3092\times10^4m^3$ in 1997 (Figure 2). So, the variation of groundwater level was analyzed by choosing the groundwater balance equation in 1997 under three different conditions.

Plan 1. Groundwater pumping is assumed to increase from $3092\times10^4m^3$ (1997) to $3749.4\times10^4m^3/a$, the gross increase of $657.4\times10^4m^3/a$ being supplied for Shandong Huazhong Paper Manufacturer. In this case, the total discharge is $3749.4\times10^4m^3/a$, the total recharge remains at the same value, i.e. $2844.93\times10^4m^3/a$, so the total deficit equals $-904.47\times10^4m^3$, which implies that groundwater level will decline by 13.83m.

Plan 2. Groundwater pumping is assumed to be the same as Plan 1. Artificial recharge is assumed to increase from $302\times10^4m^3$ (1997) to $800\times10^4m^3/a$, this value being the long-term maximum allowable rate of withdrawal from Dashahe river. So the total recharge minus total discharge equals $-406.47\times10^4m^3$, which implies that groundwater will decline 6.21m.

Plan 3. Groundwater pumping is taken to be the same as at present and this was $3092 \times 10^4 m^3$ in 1997. Artificial recharge is assumed to increase from $302 \times 10^4 m^3$ (1997) to $800 \times 10^4 m^3/a$ the same as Plan 2. In this case the total recharge minus total discharge equal $250.53 \times 10^4 m^3$, which implies that groundwater level will rise 3.83m.

Comparing the results of Plan 1 and Plan 2, with increased pumping, if artificial recharge is increased, the decrease of groundwater level will be 6.21m, instead of 13.83m that will occur if there is no increase in artificial recharge. Following Plan 3, on the other hand, the groundwater level will rise 3.83m from the situation of 1997. So, increasing the artificial recharge is very important to control declining groundwater levels.

The close relationship between river water quality and groundwater quality also indicates that the groundwater is recharged by river water. The groundwater quality is better than that of the river water and they have the same variation tendency (Figure 3). The correlation coefficient between hardness of No. 5 monitoring well, Y (mg/l) and hardness of river water, X, is 0.91 and their linear regressive model is as follows:

$$Y = 0.9099X - 81.8216$$

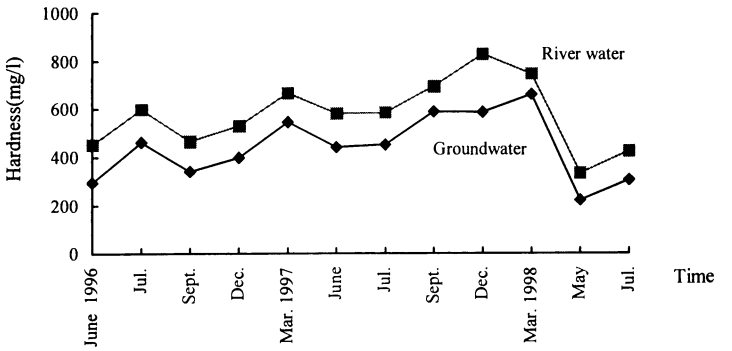

Fig. 3. Variation of hardness of No. 5 well and river water

Groundwater quality in the recharge area is also obviously affected by surface water quality.

CONCLUSIONS AND SUGGESTIONS

The study area is an important water source field where groundwater is being overdrawn. A groundwater level depression cone has formed covering a large area and groundwater level has declined continuously. The results obtained from the artificial recharge experiment indicate that artificial recharge has increased groundwater allowable withdrawal. This has provided significant social and economic benefits and the direct economic benefit is about US$ 1.25M.

In order to protect groundwater quality, wastewater discharged by industries should be treated before discharging to the river. Groundwater quality monitoring should also be emphasized in the future. Finally, sustainable groundwater development must be implemented in the study area.

REFERENCES

1. A. K. Biswas (1991) Water for sustainable Development in the 21st century: a global perspective. Water International. 16: 219-224
2. A.K. Biswas (1994) Sustainable water resources development: Some personal thoughts. Water Resources Development. 2: 109-116
3. S. P. Simonovic (1996) Decision support systems for sustainable management of water resources: 1. General Principles. Water International. 21: 223-232
4. S. P. Simonovic (1996) Decision support systems for sustainable management of water resources: 2. Case Studies. Water International. 21: 233-244

The Use of Long-term Tritium Concentration Records to Estimate Recharge to Confined Aquifers in Metropolitan Tokyo

Masayuki IMAIZUMI[1], Hiromasa HAMADA[1], Satoshi NIHIRA[1], Shin-ichi KAWASHIMA[2] and Masafumi KAWAI[2]

[1] National Research Institute of Agricultural Engineering, 2-1-1, Kannnondai, Tsukuba, Ibaraki 305-8609, Japan
[2] Institute of Civil Engineering of Tokyo Metropolitan Government, 1-9-15, Shinsuna, Koutou -ku, Tokyo, 136, Japan

Abstract. Long-term tritium concentration records for 1969 to 1997 were used to estimate the recharge of a confined aquifer in Metropolitan Tokyo. The fluctuation patterns of tritium concentration are classified into the following four types: (1) Gently-sloping peak type (GP type), (2) Sharp peak type (SP type), (3) Decreasing type, (4) Irregularly changing type. The GP type and SP type are considered to correspond to the diffusion flow model and the piston flow model, respectively. The GP type has a broad peak of tritium concentration. The SP type has a sharp peak of tritium concentration. These peaks may correspond to the maximum tritium concentration of bomb tritium in 1963. The depth of penetration of bomb tritium into a confined aquifer was used to calculate the rate of recharge to the confined aquifer. The rate of recharge to a confined aquifer was found to range from 493 to 1,752 mm/yr assuming that the only downward groundwater flow through the flow path in an aquiclude was a result of the potential difference caused by pumping. However, the time variations of tritium concentration at the Higashi-yama and Higashi-kurume observation sites indicates that some silt beds function as an aquiclude that restricts groundwater flow. Lateral groundwater flow as well as the downward groundwater flow is dominate in the confined aquifer in Tokyo. Therefore it should be concluded that the calculated rate of recharge assuming the only downward groundwater flow is not the real rate of recharge.

Key words. tritium concentration, bomb tritium, confined groundwater, recharge

INTRODUCTION

Recently, isotope-hydrology using environmental tritium as a natural tracer in an unsaturated zone and in an unconfined aquifer with a simple geological structure, such as a dune, has revealed the recharge mechanism[1]. However, there is little research on the recharge mechanism in a confined aquifer using tritium. The real state of the recharge mechanism in confined aquifers is poorly understood. Because there are many geological data and monitoring data concerning the groundwater level in Metropolitan Tokyo, confined groundwater in Tokyo is suitable for research on the recharge mechanism from the perspective of human activity. In this report, the recharge mechanism of confined groundwater is discussed based on long-term tritium concentration data.

HYDROGEOLOGY IN TOKYO METROPOLIS

1. Hydrogeology

The topography of Metropolitan Tokyo (hereafter, Tokyo) consists of 3 areas: from west to east with decreasing altitude - hilly area, Musashino upland, and Shitamachi lowland (Fig. 1). Thick Quaternary strata underlie the hill, upland and lowland areas. The Stratigraphy in Fig.2 shows that the Kazusa Group is overlain by the Tokyo Group. Terrace deposits and Kanto loam are distributed over the Tokyo Group in the uplands. The Terrace deposits and Kanto loam are buried in the eastern part of the lowland area. Soft silt beds, such as the Nanagochi formation and Yuraku-cho formation, are distributed over these beds in the lowland zone [2]. The Kazusa Group is subdivided into 4 formations. The Tokyo Group is also subdivided into 4 formations. The strike of the Kazusa and Tokyo formations is mainly northwest - southeast. They dip 1 to 2 degrees in the northeast [3].

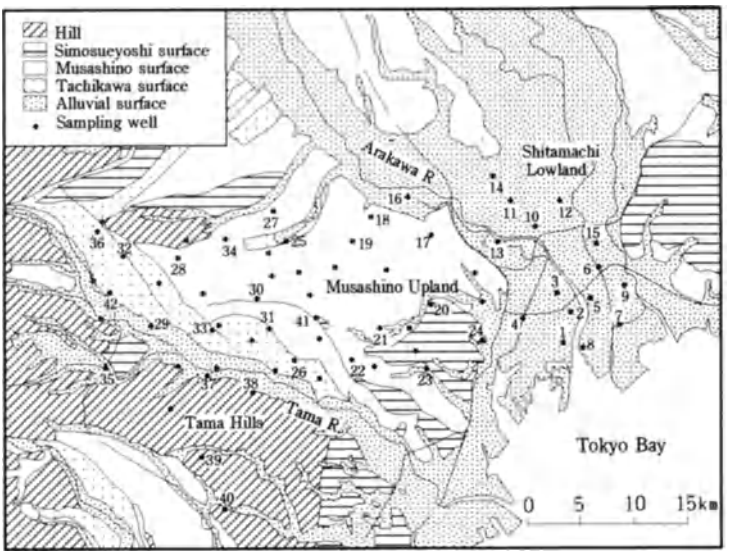

Fig. 1 Topography of Tokyo Metropolis

Table 1 Sampling well

District Lowland	No.	Name of sampling site	District Upland	No.	Name of sampling site
Koto	1	Minamisuna-machi 1, 2	Higashi-kurume	25	Higashi-kurume 1, 2, 3
	2	Kameido 1, 2	Chofu	26	Chofu 1, 2, 3, 4
Sumida	3	Agatsuma A, B	Kiyose	27	Kiyose 1, 2, 3
	4	Ryogoku 1, 2	Higashi-yamato	28	Higashi-yamato 1, 2, 3
Edogawa	5	Shin-edogawa 1, 2, 3	Tachikawa	29	Tachikawa 1, 2
	6	Koiwa	Koganei	30	Koganei 1, 2, 3
	7	Edogawa-Toubu 1, 2, 3		31	Koganei-minami 1, 2
	8	Kojima 1, 2, 3, 4		32	Musashimurayama 1, 2,
	9	Shinozaki 1, 2, 3	Musashi-murayama	33	3Fucyu 1, 2, 3
Adachi	10	Shin-adachi	Fucyu	34	Higashimurayama 1, 2,
	11	Ioki	Higashi-murayama	35	3Hachiouji 1, 2
	12	Shinmei-minami 1, 2, 3	Hachiouji	36	Mizuho 1, 2
	13	Kodai 1, 2, 3	Mizuho Town	37	Tama
	14	Toneri 1, 2, 3	Tama City	38	Inashiro
Katsushika	15	Takasago	Ibashiro City	39	Machida 1, 2
Itabashi	16	Todabashi 1, 2, 3	Machida City	40	Machida-minami 1, 2
	17	Itabashi	Mitaka City	41	Mitaka 1, 2
	18	Kami-akatsuka 1, 2, 3	Akishima City	42	Akishima 1, 2
Nerima	19	Nerima 1, 2			
Shinjyuku	20	Shinjyuku			
Suginami	21	Suginami			
Setagaya	22	Setagaya			
Meguro	23	Meguro			
Chiyoda	24	Chiyoda 1, 2			

The confined aquifers are sand and gravel beds of the Kazusa and Tokyo Groups. The Kitatama formation consists mainly of a hard silt bed. The upper surface depth of the Kitatama formation is regarded as an upper limit depth for the basement of the confined aquifer. The upper surface depth is near the ground surface in the south-western part of Tokyo [2]. It gradually increases in depth towards the north and the east. It is below about 500 m from the ground surface in the northern part of Adachi Ward and the eastern part of Edogawa Ward. The hydraulic conductivity of these aquifers ranges from 10^{-4} to 10^{-6} m/sec in the sand bed and 10^{-4} m/sec in gravel beds. The effective porosity of the entire confined aquifer, including its silt beds, sand beds, and gravel beds, ranges from 0.1 to 0.3. The average value is 0.15 [4]. In the lowland area of Tokyo, serious subsidence occurred between 1955 and the late 1960s. Moreover, even in the Tama District, which corresponds to the Musashino upland,

serious subsidence occurred in the late 1960s. The government gradually introduced various restrictions on pumping, beginning in 1961. As a result, the groundwater level has tended to rise in recent decades. For example, the groundwater level (GWL) increased by 57 m between 1971(GWL- 45 m) and 1994(GWL. 12 m). The amount of subsidence has simultaneously decreased throughout Tokyo [5].

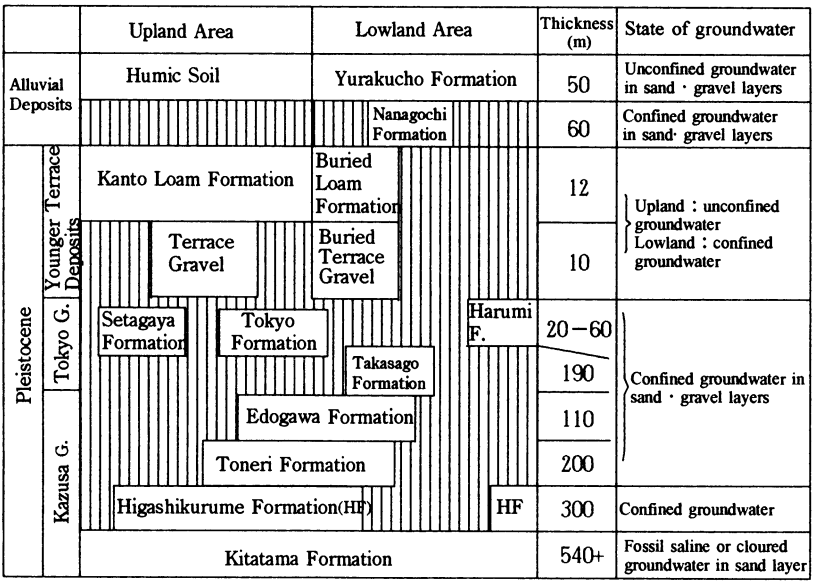

Fig.2 Stratigraphy of Tokyo [2]

METHODOLOGY

The tritium concentration at the well points shown in Fig. 1 and Table 1 has been measured once a year during the period from 1969 to 1997. The sampling wells are mainly subsidence and groundwater level observation wells used to set up screens at specific depths in the aquifer. Water supply pumping wells, and those used to supply public baths, were also used. All these wells are equipped with screens. The sampling was carried out from December to November every year. Study of the data began in 1969 with the analysis of 21 samples from low land. Afterwards, the number of analyses points was gradually increased. Since 1981, more than 100 points have been used. A total of 2,608 samples have been analysed. The tritium concentration was estimated using Kimura's method [6]. Tritium is reported in tritium units (TU). A precision of ± 5% to 10% of estimated value was obtained by routine analysis.

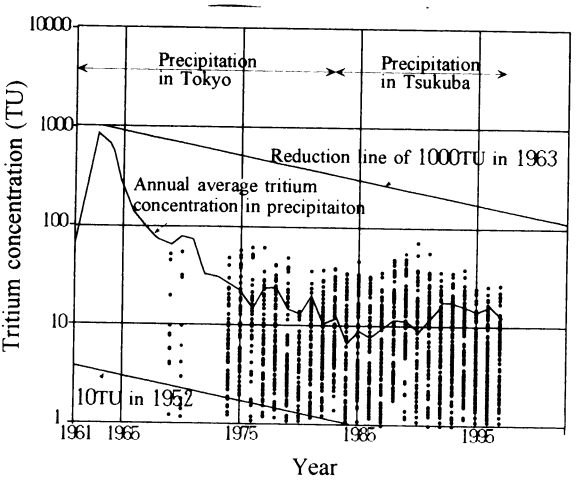

Fig. 3 Temporal variation of tritium concentration in confined groundwater in Tokyo

INVESTIGATION RESULTS

The results of the analysis are shown in Fig. 3. The broken line in Fig. 3 shows the annual average tritium concentration in precipitaiton ; data from Tokyo between 1961 and 1983 by the IAEA, data from Tsukuba between 1984 and 1997 by authors. The tritium in precipitation trends are now fairly well known; the natural tritium concentration in the precipitation was presumed to be about 10 TU. After nuclear testing in 1952, the tritium concentration abruptly increased. The maximum value of tritium concentration in precipitation was observed in 1963 (hereafter refer to bomb tritium). Afterwards, the tritium concentration continually decreased. It has now almost returned to its natural level. Two straight lines show the reduction lines of the precipitation of 10 TU in 1952 and 1,000 TU in 1963 calculated using the half life for the radioactive decay of the tritium: 12.35 years.

Points of tritium concentration values in confined groundwater in Fig. 3 are distributed from 70 TU to 1 TU of the detection limit. The names of the wells with a tritium concentration of 50 TU or more and the year it was recorded, are: 50 TU at New Edogawa in 1969, 56 TU at Higashi-murayama in 1975, 60 TU at Koiwa in 1976, 53 TU at Hagino-yu public bath in 1989, and 68 TU at Machida in 1990. There are no observation wells where a high concentration of 100 TU or more was recorded. If a mixing of precipitation (new water) with groundwater (old water) did not occur, the points should be distributed near the reduction line of 1,000 TU in 1963. Therefore, the conclusion that can be drawn from the above observations are that the mixing of new water with old water occurred during the period from the infiltration of the precipitation to the sampling.

CONSIDERATION

1. Classification of fluctuation pattern of tritium concentration

Three different models can be used for the circulation and mixing of precipitation with groundwater of different ages in an aquifer: the diffusion flow model, the piston flow model, and the well-mixed model [1]. Because the well-mixed model is a model that is applied to an unconfined aquifer with high groundwater velocity and abundant recharge [1], the only models which should be considered for a confined aquifer are the diffusion flow model (DF model) and the piston flow model (PF model). These models should preserve the peak of bomb tritium.

The tritium concentration fluctuation patterns in the confined groundwater of Tokyo can be classified into the following four types (Fig. 4): (1) gently-sloping peak (GP type), (2) sharp peak (SP type), (3) decreasing type, and (4) irregularly changing type. The GP type and SP type are considered to correspond to the DF model and the PF model, respectively. The decreasing type appears to correspond to stagnant groundwater because the tritium concentration values are distributed around the line of the radioactive decay. The irregularly changing types consist of an irregular fluctuation of tritium concentration and an unknown type whose pattern cannot be classified because the observation period is too short.

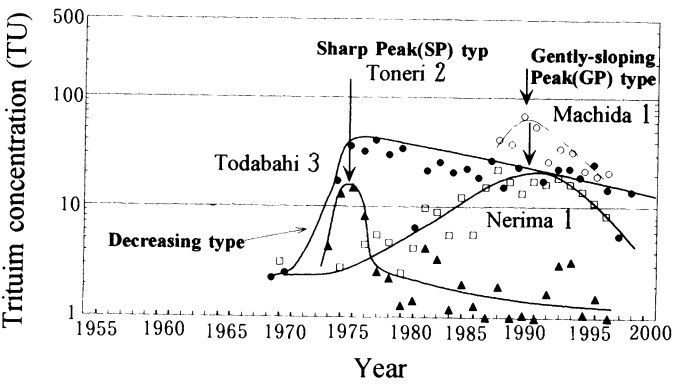

Fig.4 Fluctuation patterns of the tritium concentration in the confined groundwater of Tokyo

The groundwater residence time can be

accurately estimated from the time of the peak corresponded to the bomb tritium in 1963. This idea may be applied to determine the residence time of the GP and SP types. However, even taking account of the radioactive decay and diffusion, the SP type concentration peak is too low. The concentration of bomb tritium of this type is about 15 TU, as represented by the concentration at Toneri 2 well. The concentration after the peak amounts to several TU. Such a phenomenon cannot be explained without assuming the occurrence of mixing with an old groundwater mass having an extremely low tritium concentration, such as groundwater squeezed from a silt bed. Therefore, the sharp peak type is not a piston flow model that follows the the rigorous scientific definition.

2. Estimation of rate of recharge to the confined aquifer

The tritium concentration profile in an upland dunes having a simple hydrological structure usually preserves trace of the bomb tritium in unconfined aquifer because the only downward groundwater flow occurs. The rate of groundwater recharge in an unconfined aquifer is estimated by the following equation [7].

$$R = (PD)/T \quad (1)$$

Where:R=Rate of recharge, P=Effective porosity, D=Depth of bomb tritium, T=Residence time.

The rate of recharge to the confined aquifer in Tokyo was estimated using equation (1) assuming that the only downward groundwater flow through the flow path in the aquiclude occurred as a result of the potential difference caused by pumping. For the effective porosity (P), the average value of the entire stratum of 0.15 was adopted. The residence time (T) was estimated from the difference between the year the bomb tritium arrived and year when the highest tritium concentration was observed in precipitation. The central depth of the screen was adopted as (D). The calculated rates of recharge ranged from 488 to 1,752 mm/yr. These values are almost the same as rates of recharge obtained in the unsaturated zone in the uplands of Tokyo[1]. The rate of recharge in the lowland tends to be higher than that of the upland. This is thought to be a result of the fact that the potential difference caused by pumping in the lowland is higher than in the uplands.

It is necessary to verify the validity of the assumptions made in order to estimate the rate of recharge. Fig. 5 shows the time dependence of tritium concentration at the Higashi-yamato and Higashi-kurume observation sites in Musashino upland, where four wells with different depths were installed. Each aquifer and central depth of screen is also shown in Fig. 5. Geological structure indicates that the recharge area of the confined groundwater is on the western side of the Higashi-yamato site. The depth and aquifer of wells where the bomb tritium was detected are different at these sites: the 10 m (Musashino terrace deposit), 79 m (Toneri formation) and 159.5 m (Upper Higashi-kurume formation) at Higashi-yamato site. 4.5 m well (Musashino terrace deposit) at Higashi-kurume site. The bomb tritium reached simultaneously the 10 m well and 79 m well at the Higashi-yamato site. The bomb tritium reached 159.5 m well in several years later than 79 m well. The bomb tritium did not reach the 87.5 m well and deeper wells at the Higashu-kurume site. These observation facts may indicate that some silt beds have a function as an aquiclude that restricts groundwater flow and lateral groundwater flow as well as the downward groundwater flow is dominate in the confined aquifer. Therefore it should be concluded that the calculated rate of recharge assuming the only downward groundwater flow is not the real rate of recharge.

CONCLUSION

Long-term tritium concentration records from 1969 to 1997 were used to estimate recharge to confined aquifers in Metropolitan Tokyo. The depth of penetration of bomb tritium into ground was used to calculate the rate of recharge to a confined aquifer. The calculated rate of recharge to confined aquifers in Tokyo was found to range from 493 to 1752 mm/y assuming the only downward groundwater flow. However, the time variations of tritium concentration at the Higashi-yama and Higashi-kurume observation sites indicates that some silt beds function as an aquiclude that restricts groundwater flow and lateral groundwater flow as well as the downward groundwater flow is dominate in the confined aquifer in Tokyo. Therefore it should be concluded that the calculated rate of recharge assuming the only downward groundwater flow is not the real rate of recharge.

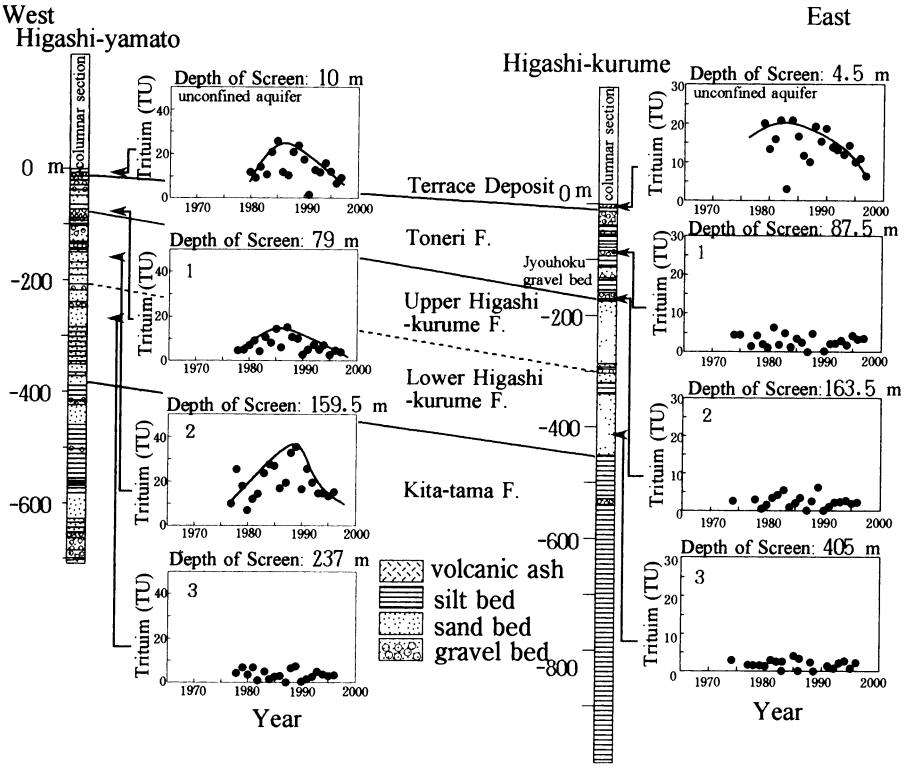

Fig.5 Variation with time of the tritium concentration at the Higashi-yamat and Higashi-kurume observation sites in Musashino uppland

REFRENCES

1. Kayane, I (1980):Hydrology, Taimeidou, Tokyo, 272p.(in Japanese)
2. Ishii, M., Endo, T., Kawashima, S. and Kawai, M.(1976):Studies on the mechanism of artesian water flow(1), Annual Report I.C.E. of TMG, S50, 183-205.(in Japanese)
3. Endo,T(1978):Stratigraphy and geologic strucure of the Quaternary system in the underground of the Tokyo district, Geological Society, Vol.84, No.9, 505-620.(in Japanese)
4. Sindo, S(1972):Groundwater in the Southern Kanto Plane, Jp. Geotec. Soci., 20-5(171), 25-36.
5. Kawashima, S., Kawai, M. and Hamada, J.(1996):Characteristics of Groundwater in Wards District, Tokyo, Annual Report I.C.E. of TMG, H8, 217-231(in Japanese)
6. Kimura, S.(1971):Study of groundwater flow by tritium concentration in water(I), Bulletin of the National Reseach Institute of Agricultural Engineering, No.9, 1-46.(in Japanese)
7. Anders, G. and Egger, R.(1985) : A new tritium interface method for determinants the recharge rate of deep groundwater in the Bavarian Molasse Basin. J. Hydrol., 82, 27-38.

MODELING OF A KARST DRAINAGE RESPONSES WITH RESERVOIRS IN THE ITXINA KARSTIC AQUIFER (BASQUE COUNTRY, SPAIN)

Jaime Gárfias[1], Hilario Llanos[2] and Ismael Herrera[3]

[1] Faculty of Engineering (CIRA). Autonomous University of the State of Mexico, Cerro de Coatepec S/N, C.P. 50130. Toluca, México
[2] Department of Geodynamics, Faculty of Sciences, University of the Basque Country. Apdo: 644. Bilbao, Spain.
[3] Institute on Informatics, Applied Mathematics and Systems (IIMAS), Apdo. 22-582, México, D.F. 14000, México

Abstract. The aim of this study is to apply a parsimonious hydrologic model to the Itxina karstic aquifer, capable of predicting changes in discharge resulting from variable inputs (recharge). The Itxina aquifer is divided in four cells corresponding to distinct recharge areas. Each cell was treated as a tank to characterize the conditions within cell. In the model when the reservoir boundaries coincide with the position of the siphons, the signal simulated is sensitive to input pulses of the recharge. The good agreement between predicted and measured discharges demonstrates the ability of the model to simulate the flow in the Itxina aquifer. These results demonstrated that the hydraulic conductivity increases downstream within the aquifer. The hydraulic conductivities obtained by numerical calibration varied between 4.2×10^{-3} m/s upstream of the Itxina aquifer, 6.0×10^{-2} m/s in the central region, and 9.5×10^{-1} m/s in the lower region of the aquifer. These values seem reasonable because the underground features in the principal caves show that the density of caves increases downstream in the Itxina aquifer.

Key words. Karst, Modeling, Reservoir, Spring, Itxina Aquifer, Basque Country.

INTRODUCTION

A growing concern with groundwater contamination by agricultural chemicals and potential spills of hazardous materials, calls for some method of prediction and possible tools for remediation. This is especially applicable in the case of a karstic aquifer, which is known to be highly vulnerable to contamination. However, the lack of spatial knowledge in the karst parameters, and the relative unpredictability and the extreme heterogeneity in aquifer properties, has often discouraged researchers from attempting to model such aquifers.

In most cases, hydrologic interpretations are based on the analysis of recession hydrographs by using the different hydrograph separation methods [1], statistical analysis of the whole spring hydrograph [2,3], or analysis of transfer functions between input (infiltration) and output (spring hydrograph) obtained by black-box models [4] used time moment analysis to relate a time series of inputs (recharge) to a series of outputs (spring flow). Simple regression models also have been used to predict water levels in karst aquifers [5]. The limitation of these global models is because they lack predictive power.

Direct verification of interpretations based on global methods is obviously very difficult because of the scarcity of empirical observations in real karstic aquifers. In the other hand, conventional groundwater models are overly difficult for this task given the uncertainties in parameterization and

the difficulties associated with estimating changes in recharge characteristics. In addition, most of the studies are ideal simulations, which frequently do not represent the natural system accurately. Consequently, the main goal of this paper is to apply a parsimonious hydrologic model for the Itxina karstic aquifer, capable of predicting changes in discharge resulting from changes in the inputs (recharge). This modelling effort is to demonstrate the applicability and practical use of the modelling concepts for the simulation of groundwater flow, while retaining the simplicity resulting from using lumped regional scale parameters.

DESCRIPTION OF THE STUDIED AREA

The aquifer of Itxina, located in the Basque province of Vizcaya, is represented by a flat area of triangular geometry and rough relief, known as mountains of Itxina, whose highest points are the peaks of Aitzkorrigane (1090 *m.a.s.l.*), Lekanda (1308 *m.a.s.l.*) and Ipergorta (1225 *m.a.s.l.*). Sideways it shows a divergent hydrographical network, structured in two watersheds. That way, while to the north, the superficial flows are piped by the Nervion and Ibaizabal rivers, to the south the draining is done towards the Zadorra river, through the Bayas river. In the same way we could emphasise the existence of the depression known as Campas of Arraba, which is characterized for having an own internal draining net which comes to an end at the feet of the mountains of Itxina (Fig. 1).

The aquifer of Itxina is represented by a 6,15 km^2 outcrop of reef limestone which can go over 300 meters of width. It shows a free aquifer kind typology, with a pending structure, and gets characterized for showing high permeability levels for karstification and fracturation, what makes the infiltration to be fast. With a rain of about 1300 mm with an almost full infiltration of it, its underground resources can be estimated as about $7.7x10^6$ m^3/year, which discharge is done in a minority way by the springs. In general, such sources show low volume and a great irregularity which workings would be associated to the draining of low structures and near depressions.

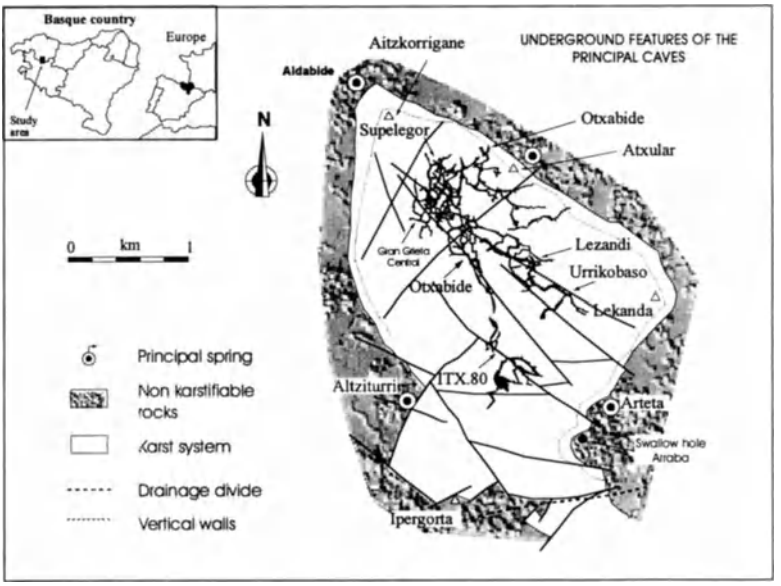

Fig. 1. Geological description of the study area and simplified plans of the morphology of the karst aquifer.

The most important spring of the aquifer is the source of Aldabide, located in the north end of the massive and in the lower height of it (725 *m.a.s.l.*). Through this point the main discharge of the massive of Itxina (85% of the resources) is done, with an average annual volume next to 250 *l/s*. It is a spring characterized by important volume oscillations, with response times of few hours, which show the low regulation capacity of the aquifer, shown in other studies [6, 7, 8]. In the same way, can be said that the water in the aquifer is taken through wide conduits according to a general circulation scheme, in north-north-west direction, from its south-eastern extremity, in the sinks existing in the Campas of Arraba, to the source of Aldabide, main collector of the aquifer.

Model formulation

In order to understand the movement of storm pulses in the basic model, the aquifer prototype is translated into four zones of different type and complexity. Upstream of the Itxina aquifer (Campas de Arraba), this watercourse drains entirely in the swallow hole (Arraba). Cave investigations and underground flow show that preferential flow directions between the Campas de Arraba and the Aldabide spring are related to the high permeability zones and the existence of rapid flow channels running in direction of the two siphons (Figure 2). The first siphon is located at ITX-80 (820 *m.a.s.l.*), and the second is located at Otxabide (797 *m.a.s.l.*). Therefore, the geometrical model of the structure of the karst can be used to show that the Aldabide spring is supplied by four reservoirs. The first in the shallow hole at Arraba, the second in the siphon ITX-80, the third in the siphon Otxabide, and the last in the Aldabide spring. The waters of these four reservoirs mingle downstream to form the waters at the Aldabide spring. These reservoirs are fairly evenly spaced which suggested the use of a four-cell model to predict the behavior of the aquifer.

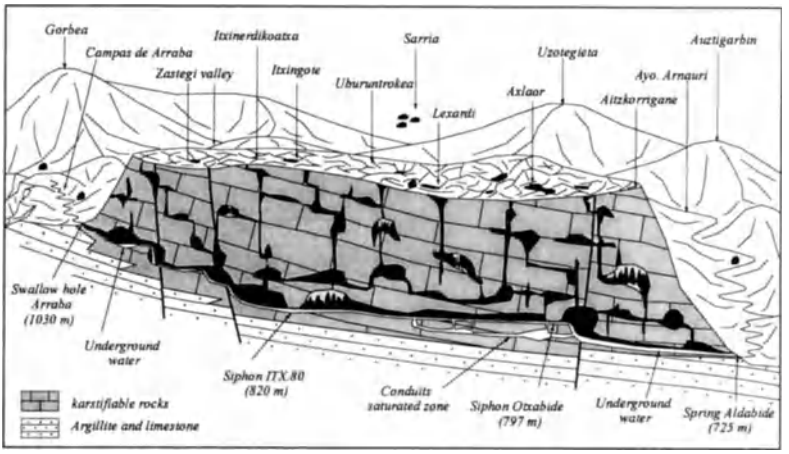

Fig. 2. Conceptual model of the karstic network of the Itxina aquifer.

Each cell is treated as a tank, which is, assigned an effective area (equivalent to the product of specific yield and surface area). At the present time, piezometric data and hydraulic conductivity measurements are not available owing to the topographical difficulties and the cost of drilling wells in mountainous areas with difficult access. The only hydrological information available for a long enough period of time is the daily spring discharges. Data for the period that ranges between January 1982 and June 1984, as well as the daily rainfall data from the precipitation station at Gorbea (Zastegui Valley) for the same period, have been used. A schematic diagram of the model is shown in Figure 3.

The model describes flow between the cells using Darcy's Law. The hydraulic conductivity was assigned to the boundaries between cells which was the method employed by [9], and the saturated thickness of the upstream cell was used to calculate the transmissivity. All external model boundaries were treated as no-flow boundaries, so there are only three boundaries where flow occurs. Flow rate across each internal boundary was calculated as:

$$Q_G = Kwb\left(\frac{\Delta h}{l}\right), \quad (1)$$

where Q_G is the groundwater flow rate across the boundary, w is the width of the boundary, Δh is the head difference across the boundary, b is the saturated thickness of the upstream cell, and l is the distance between the key wells in each cell.

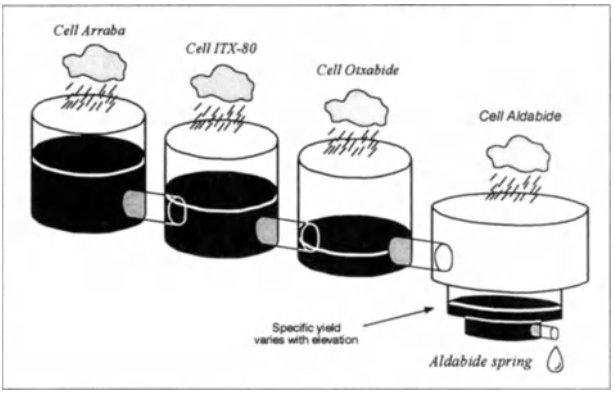

Figure 3. Schematic diagram of the aquifer model.

MODEL CALIBRATION AND RESULTS

To determinate aquifer properties during the study period, data from five events were used for model calibration. These events occurred between January 1982 to June 1984. Rainfall data, which was also available at this time, was also collected. The average discharge for the five events was 0.336 $m^3 s^{-1}$, with a maximum recorded discharge of 4.7 $m^3 s^{-1}$ and a minimum of 0.009 $m^3 s^{-1}$.

For most groundwater modeling efforts, a model with a fixed structure is selected and parameters are chosen through the calibration process to achieve the best fit with measured field data. In this case, a number of different model structures were evaluated and within each case, parameters were selected to achieve optimum calibration. In this case, analyses were carried out for three situations to determine which model more accurately fitted the data. For this purpose, different simulations were made using three options that can modify a storm pulse moving through the model. The first situation (run 1) is a model with two reservoirs representing flow moving from a karst system. The second (run 2) is a system with four reservoirs that allow for overflow in the system. Finally, the third (run 3) is a system in which four reservoirs plus the vertical variation in aquifer properties in the last reservoir. These simulations were used to understand the variations due to input, and variations in the number of reservoirs.

Figure 4 shows three runs of the calibration process for October 1 to November 20, 1982. The first simulation involves two reservoirs, the second simulation four, and the last simulation uses four reservoirs plus the vertical variation of the aquifer properties of the last reservoir. For the first simulation, the response is erratic and overestimates the peak for the final pulse in the series. In addition, it was found that a lag period exists between the peak observed time and the peak simulated time. This is likely due to the lack of regulation with two reservoirs. For the second simulation, the regulation and the lag are improved. However, the sensitivity of the model with variations of input intensity was found to be not considerable. It is interesting to note the difference between run one and the run three, where the last fit introduce the vertical variation of the aquifer properties. The ability of the last scheme to perform is strongly supported by the hypothesis that the siphons were the controlling mechanism in the system during storm events. These results are the similar to findings by [10], who used a system theorize of three reservoirs to obtain the same suggestions. In [10] case, the series system acts as a feedback mechanism in the conduit system. In his configuration, the smallest section controls the response with a single configuration of four reservoirs with aquifer characteristics changing in the last reservoir. The signal simulated is also sensitive to input pulses of the rainfall.

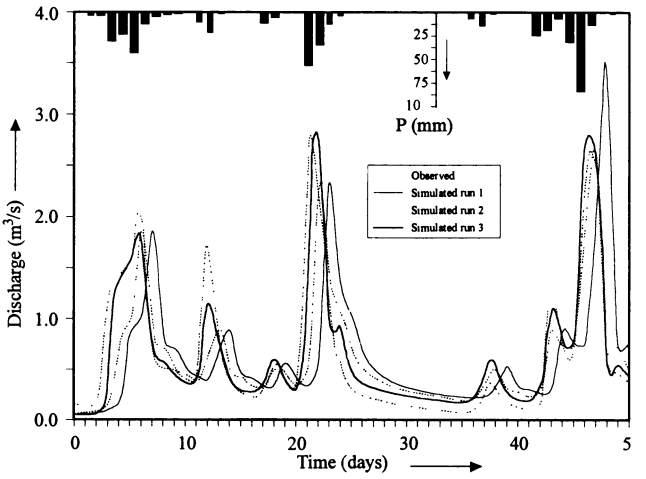

Fig. 4. Observed and model-simulated daily discharge at Aldabide spring between October 1 and November 20, 1982.

The hydraulic conductivities varied between 4.2×10^{-3} *m/s* upstream of the Itxina aquifer, 6.0×10^{-2} *m/s* in the central region, and 9.5×10^{-1} *m/s* in the lower region of the aquifer. These findings have been used as representative values of the hydraulic conductivity, which demonstrates its usefulness in problems concerning groundwater resource evaluation. The hydraulic conductivities obtained are a result of the varying contributions of fractures (conduits) and regional matrix (fissure) in the system.

CONCLUSIONS

The presented results demonstrate that even a karst aquifer can be successfully modelled with a parsimonious model, which has the ability to accurately predict water movement in this complex karst aquifer. The study developed a lumped parameter model for the Itxina aquifer. When faced with the task of modeling extremely complex flow system, the natural tendency is to develop a

more complex model. However, this research shows that a very simple model can provide useful information about the behavior of such a system. The results provide a quantitative tool to assess spring hydrograph, and illustrate mechanisms that can generate observed responses, which have previously been qualitatively interpreted.

The aquifer was divided into four cells, each of which is treated as a tank. This model differs from previous models in that it allows properties within the cell to vary with water elevation. A comparison of model predictions with historical data for five events for the period January 1982 to June 1984 demonstrate its accuracy. The results obtained by calibration of the model indicate that hydraulic conductivity increases downstream within the aquifer. This seems reasonable because the density of caves at the Itxina aquifer increases downstream of the cave system. This simple representation of the hydrologic system produced accurate results with fewer data requirements and calibration parameters than traditional groundwater models. Because of the horizontal stratification of the formation, vertical changes in aquifer properties have a greater influence on aquifer behavior than does horizontal variation. As water levels rise, caves, conduits, and other stratigraphic features, which submerged strongly, affect flow and storage in the aquifer. In fact, when the reservoir boundary coincide with the position of the siphons, the signal simulated is sensitive to input pulses of the rainfall.

ACKNOWLEDGEMENTS. The authors express your gratefulness to the National Sciences Council and technology (CONACyT) and to the University of the Basque Country (UPV) by the financing conceded to the research projects 3642-A financed by CONACyT and to the project UPV-EHU 001.154EA061-95 financed by the University of the Basque Country. The authors wish to thank M. E. Barrett at the University of Texas at Austin for their valuable comments. We would also like to thank D. Rudolph at the University of Waterloo for their thoughtful reviews of this paper.

REFERENCES

[1] Bonacci, O. 1993. *Karst springs hydrographs as indicators of karst aquifers*. J. Hydrol. Sciences, 38 (1-2): 51-62.

[2] Mangin, A. 1984. *Pour une meilleure connaissance des systèmes hydrologiques à partir des analyses corrélatoire et sprectrale*. J. Hydrol. 67: 25-43.

[3] Dreiss, S.J. 1982. Linear kernels for karst aquifers. Water Resour. Res., 18(4): 865-876.

[4] Dreiss, S.J. 1989. *Regional scale transport in a Karst aquifer: 1. Component separation of spring flow hydrographs*. Wat. Resour. Res., Vol. 25 (1), pp. 117-125.

[5] Zaltsberg, E.A. 1984. *Forecast of Karst water levels*. In: A. Burger and L. Dubertret (Editors). Hydrogeology of Karstic Terrraines. International Contributions to Hydrogeology, Heise, Hannover, pp. 40-42.

[6] Antigüedad I. (1986). Estudio Hidrogeológico de la Cuenca Nervión-Ibaizábal. Tésis Doctoral Universidad del País Vasco–Euskal Herriko Unibertsitatea, 320 pp. Leioa, Bizkaia.

[7] EVE (1992). Investigación Hidrogeológica del Area de Itxina. Ente Vasco de la Energía, Eusko Jaurlaritza-Gobierno Vasco, Bilbao-Bilbo (informe inédito).

[8] Llanos H. y Garfias J. (1996). Reconstitución de Hidrogramas de Manantiales de la Unidad Hidrogeológica del Macizo del Gorbea (País Vasco). In Contribuciones a la Investigación y Gestión del Agua Subterránea, pp. 115-130. (I. Morell y J.R. Fagundo, eds.). Universitat Jaume I. Castellón, España.

[9] Prickett, T.A. and C.G. Lonnquist. 1971. *Selected digital computer techniques for groundwater resource evaluation.* Illinois State Water Surv. Bull., 55: 1-62.

[10] Halihan, T. and C. M. Wicks, J.F. Engeln. 1998. *Physical response of a karst drainage basin to flood pulses: example of the Devil's Icebox cave system (Missori, USA).* J. hydrol. 204, pp. 26-36.

Groundwater Pollution and Remediation Technologies

Correlation of Optimal Salinity as Function of Water/Oil Ratio in Brine/Surfactant/Alcohol/Oil System

Truong Hong Tien[1], Emiko Katayama[1], Mehdi Bettahar[2] and Uichiro Matsubayashi[2]

[1]Department of Civil Engineering, Nagoya University, Furo-cho, Chikusa-ku, Nagoya 464-8603, Japan
[2]Research Center for Advanced Waste and Emission Management, Nagoya University, Furo-cho, Chikusa-ku, Nagoya 464-8603, Japan

ABSTRACT. Results of investigation on the effects of water/oil ratio (*WOR*) in groundwater on phase behavior of the system containing brine, an anionic surfactant, alcohols and different oils were presented. The results showed that the effect of *WOR* and salinity on the phase behavior of this system is analogous. Increasing the *WOR* also changes the system from Winsor I → Winsor III to Winsor II. The higher the *WOR*, the lower the salinity required to produce the middle-phase microemulsion, but the narrower the salinity range for the three-phase region. The *WOR* term was correlated with the function of optimal salinity (S^*) through the coefficient of *WOR* (k_a). This correlation can be used to select the surfactant/alcohol formulation potentially effective for aquifer remediation.

KEY WORDS: surfactant, middle-phase, optimal salinity, water-oil ratio, oil fraction.

INTRODUCTION

The efficiency of pump and treat methods for remediation of soil contaminated with non-aqueous phase liquids (NAPLs) is often limited due to their low aqueous solubility and relatively large interfacial tensions (IFTs) with water [1,2]. To overcome these limitations, different innovative technologies such as surfactant flushing [3,4], cosolvent (alcohol) flushing [5,6,7] or combination of both [8,9,10] have been developed. In most cases, the systems using the mixture of surfactant and alcohol have shown high efficiency than that with the use of surfactant or alcohol, separately. The latter technique is based on the ultralow IFTs and high solubilizing properties of middle-phase microemulsion coexisting with both oil- and water-excess phases.

The formation of the middle-phase microemulsion depends on many factors, such as surfactant structure, alcohol type and concentration, oil type, salinity and temperature. In free alcohol system, the effect of water oil ratio (*WOR*) on the phase behavior can be neglected, changing the *WOR* does not change the system type. But this is not the case when the alcohol presents in the system, because heavy alcohols (medium and longer chain length) dissolve mainly in the oil phase, changing the *WOR* tends to change the co-surfactant (alcohol) concentration in both oil- and water-rich phases, which in turn can change the type of system [11]. However, in all studies relating to phase behavior of the brine/surfactant/alcohol/oil system, the effect of *WOR* was not considered. Salager et al [11] had developed an empirical correlation capable for predicting the phase behavior of multicomponent systems containing anionic surfactants, brine, alkanes and various alcohols, but this correlation is valid only for *WOR* equal 4. Kahlweit [12] fixed *WOR* at 1 when discussing on how to prepare the microemulsion at prescribed temperature, oil and brine.

Because the residual oil content existing inside the porous media is a function of the pore structure, nature of contaminants and temperature, the surfactant/alcohol formulation optimized at particular

WOR may not be applicable for all cases. The objectives of this paper are therefore: (1) to study the effect of *WOR* on the phase behavior of brine/surfactant/alcohol/oil system; (2) to correlate the *WOR* term with other variables of optimum formulation. This study is a supplementing part to the work of Salager et al [11] where the effect of *WOR* on system phase behavior is considered.

BACKGROUND

A systematic approach for designing surfactant systems to produce ultralow IFTs is the observed relationship between IFT and the formation of the middle-phase microemulsion (or Winsor III) (Fig. 1). A microemulsion is thermodynamically stable emulsion [13]. If surfactant is hydrophilic (more soluble in water than in oil), and is in the form of oil-swollen micelles in the aqueous phase, one find oil in water (O/W) microemulsion (or Winsor I); if it is lipophilic (more soluble in oil than in water), and is found in the form of water-swollen reverse micelles in the oil phase, one find water in oil (W/O) microemulsion (or Winsor II). In Winsor III system, the surfactant has nearly equal affinity for both oil and water phases [12,14]

The water-oil IFT (γ_{wo}) is much reduced when the middle phase is formed, and is minimized at the center of three-phase region where approximately equal volumes of oil and water are dissolved in the middle phase [14,15]. This minimum water-oil IFT is also characterized by the point, at which the IFTs between the middle-phase and excess oil (γ_{mo}) and water phases (γ_{mw}) are equal. In the three-phase region, all the IFTs are much lower than those achieved in Winsor I and Winsor II. For this reason, the middle-phase microemulsions have been promoted for both enhanced oil recovery and aquifer remediation.

Because, the lower the water-oil IFT, the less energy would be required to push the residual oil from the pores, and consequently the higher the efficiency of the surfactant formulation, for the constant conditions of surfactant/alcohol concentrations, oil type, *WOR* and temperature, the system is optimum, when water-oil IFT reaches to its minimum value (γ_{min}). The salinity associated with that formulation is called as optimal salinity (S^*) [11,14]. As the variables of the formulation are changed, the system will move to another optimum state with its new optimum parameters (S^*, γ_{min}). Thus, both γ_{min} and S^* are function of surfactant, alcohol, oil, *WOR* and temperature.

By considering the effects of these variables independently, Salager et al [11] had found that at *WOR* = 4, the S^* can be expressed by the following empirical correlation

$$Ln S^* = K(ACN) + f(A) - \sigma + a_T (T - 25) \tag{1}$$

where K is constant depending on the surfactant type; $f(A)$ is a function of heavy alcohol and its concentration in aqueous solution; σ is a parameter characteristic of surfactant; ACN is alkane carbon number, e.g. the number of carbons in the hydrocarbon chain; a_T is the temperature coefficient; T is the current temperature. At 25^0C, the graphical representation of the equation (1) is shown in Fig. 2.

For crude oil and mixture of pure hydrocarbons, an equivalent alkane carbon number ($EACN$) can be assigned as in equation (2) [15].

$$(EACN)_m = \Sigma X_i (EACN)_i \tag{2}$$

Where $(EACN)_m$ and $(EACN)_i$ are the equivalent alkane carbon numbers for the oil mixture and component i, respectively; X_i is the mole fraction of the component i in the mixed oil phase; that is,

$\Sigma X_i = 1$. Thus, $(EACN)_m$ can be substitute into equation (1), resulting in

$$LnS_m^* = K(EACN)_m + f(A) - \sigma + a_T(T - 25) \quad (3)$$

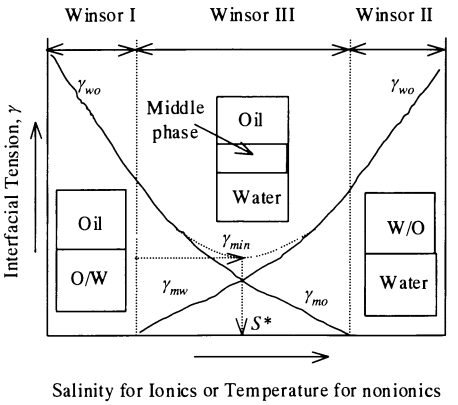

Fig. 1. Relationship of phase behavior and interfacial tension

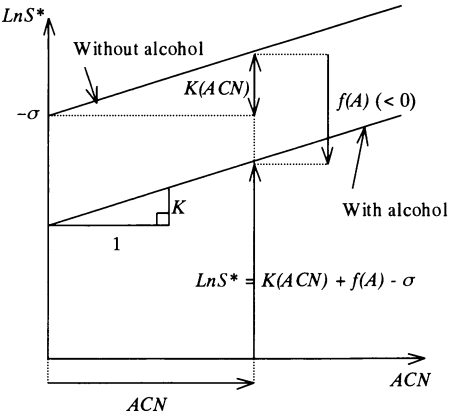

Fig. 2. Relationship between variables of optimum surfactant/alcohol mixture

The significance of equations (1) and (3) is that these correlations link the variables that produce an optimal formulation. However, the term *WOR* is not included in these correlations. The experiments described below were designed to study the effect of *WOR* on the phase behavior and to correlate it with the function of *S**.

EXPERIMENTAL SECTION

Chemicals

Sodium Dodecyl BenzeneSulfonate (SDBS) in purity of 95% is selected as surfactant. 2-butanol and *n*-pentanol in purity > 99% were used as co-surfactants for producing middle-phase microemulsions. Three saturated hydrocarbons (alkanes): *n*-decane, *n*-dodecane and *n*-tetradecane in purity > 99% and diesel oil were used as testing contaminants. The contaminants were dyed with Oil-Red-O, so that appearance of the different phases could be observed quantitatively. All these chemicals were purchased from Tokyo Kasei Kogyo Company and used without further purification. Sodium chloride in purity of 99% was used as electrolyte and water was distilled for preparation of aqueous solution.

Methodology

In order to investigate the relationship between *S** and *WOR*, salinity scan were conducted for a range of *WOR*. Batch experiments were conducted in 100ml-bottles capped to prevent volatilization losses. For each *WOR*, the experiments were carried out with different *n*-pentanol concentrations and oil types, while maintaining a constant concentration of SDBS (10g/l). The classical Winsor type I-III-II transitions were obtained by salinity scan. All bottles were shaken multiple times, and were equilibrated for at least one week in a temperature controlled room. The occurrence and

disappearance of middle phase were verified by visual observation and the S^* were determined as the midpoint of three-phase region.

The model parameters were determined by the same method of Salager et al [11] with taking a secondary standard for $f(A)$ (= -0.16) for 30g/l of 2-butanol. This experiment was carried at *WOR* of 4 and SDBS concentration of 10g/l. For determination of temperature coefficient a_T, the experiments were repeated at different temperatures.

RESULTS AND DISCUSSION

Effect of *WOR* on the S^*

Fig. 3 shows the phase diagram S^*-*WOR* for *n*-decane. It is found that the effects of salinity and *WOR* on phase behavior of brine/surfactant/*n*-pentanol/*n*-decane are the same. With increasing *WOR*, the system phase behavior changes from Winsor I → Winsor III to Winsor II.

When the hydrophilic character of surfactant is heavily balanced, surfactant dissolves in the water phase forming O/W microemulsion (Winsor I). Increasing the *WOR* tends to increase the *n*-pentanol concentration in the oil phase which makes the nature of water and oil phases become less dissimilar. This is because *n*-pentanol dissolved in the oil, performs as co-oil to decrease the lipophilic character of the oil. Thus, with increasing *WOR*, the surfactant has the tendency to move to the oil phase. At some oil fraction, when balance of hydrophilic-lipophilic characters of surfactant molecules takes place, surfactant molecules move to the water-oil interface forming the middle-phase microemulsion (Winsor III). At sufficiently high *WOR*, the system is overoptimum, and the surfactant dissolves in the oil phase forming a reverse micelles (Winsor II or W/O microemulsion).

Correlation of S^* and *WOR*.

The plots of LnS^* versus *ACN* with 30g/l of 2-butanol (at 15°C and 25°C) and without alcohol (at 25°C) are shown in Fig. 4. The parameters of the model are found as σ = -3.525, K = 0.13±0.04, a_T = 0.0073 when S^* is expressed in gram per liter.

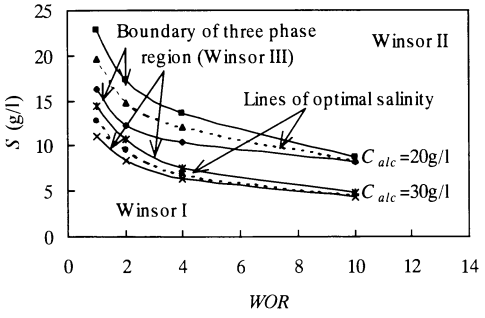

Fig. 3. The phase diagram S^*-*WOR* for *n*-decane at different concentrations of *n*-pentanol

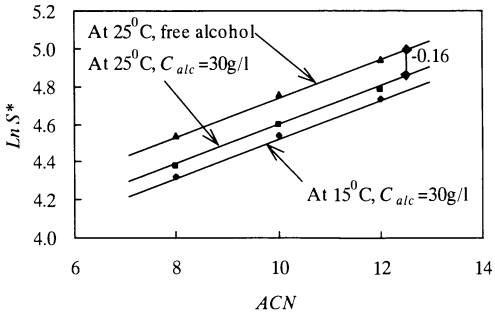

Fig. 4. LnS^* vs *ACN* for determination of model parameters

Since the plots of LnS^* versus WOR are nonlinear, an alternative is made to correlate the S^* with WOR through the oil fraction (S_O) which is defined as ratio of oil volume to the total volume of the system.

$$S_O = 1/(1+WOR) \tag{4}$$

The optimal salinity, S_x^* at any oil fraction, $S_O = x$ can be correlated with S^* at $S_O = 0.2$ (or $WOR = 4$) as

$$LnS_x^* = LnS_{0.2}^* + \Delta LnS^* = LnS_{0.2}^* + \frac{\Delta LnS^*}{x - 0.2}(x - 0.2) \tag{5}$$

By setting $k_a = \Delta \ln S^*/(x\text{-}2)$ called as coefficient of WOR, the equations (1) and (3) will be

$$LnS^* = K(ACN) + f(A) - \sigma + a_T(T - 25) + k_a(x - 0.2) \tag{6}$$

$$LnS_m^* = K(EACN)_m + f(A) - \sigma + a_T(T - 25) + k_a(x - 0.2) \tag{7}$$

Fig. 5 shows S^* for different concentrations of n-pentanol as function of S_O. Interestingly, all curve are straight, but not parallel lines. The positions of the straight lines shift downward and right on the graph with increased alcohol concentrations.

The slope of the straight lines is the coefficient of WOR (k_a). The plots of k_a and $f(A)$ versus concentrations of n-pentanol are shown in Fig. 6. The results show that k_a is a function of n-pentanol concentration only, it is independent with salinity, and oil type. In free alcohol system, changing the WOR does not change the system behavior, so k_a is equal zero. With presence of n-pentanol, k_a measures the angle of the straight lines from the position for alcohol-free system. The Fig. 6 also indicates that the effect of n-pentanol concentrations on the values of k_a and $f(A)$ are inverse. With increasing the n-pentanol concentration, k_a is increased, but $f(A)$ is decreased.

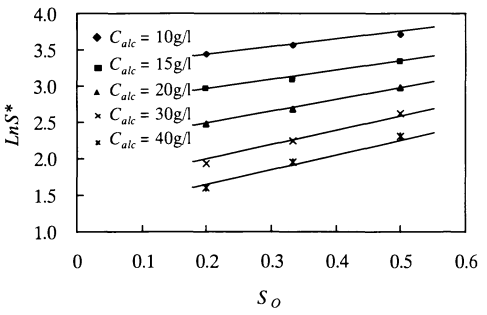

Fig. 5 . LnS^* vs WOR for n-decane with different concentrations of n-pentanol

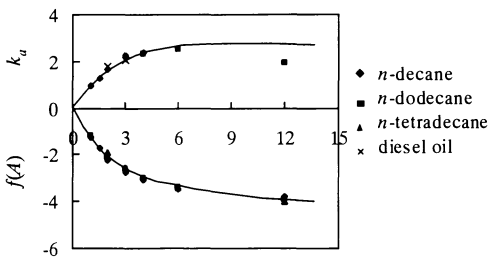

Fig. 6 . $f(A)$ and k_a for different concentrations of n-pentanol

CONCLUSION

In this research, results of batch experiments have been presented which were conducted to investigate the effect of *WOR* on the phase behavior of systems containing brine, an anionic surfactant, alcohols and different oils. The results demonstrated that the effect of *WOR* on the phase behavior of the system is analogous with that of salinity and alcohol. Increasing the *WOR* also causes the system change from Winsor I → Winsor III to Winsor II. The higher the *WOR*, the lower the salinity required to produce the middle-phase microemulsion, but the narrower the salinity range of the three-phase region. Based on this, the *WOR* term was correlated with the function of optimal salinity (S^*) through the coefficient of water oil ratio (k_a). This correlation can be used to select the surfactant/alcohol formulation potentially effective for aquifer remediation.

When applying the microemulsion for remediation of the soil, in general, the temperature, geologic conditions of the site with known composition of the oil and that of the brine are prescribed. Wanted is to find an efficient mixture of surfactant and co-surfactant, which can produce middle-phase microemulsion. The correlations allow one to estimate the values of the adjustable variables (for example, *n*-pentanol concentration) needed to obtain an optimum formulation. If more than one variable will be adjusted, the best optimum formulation can be selected according to the supplementary criterion, such as reduced adsorption, minimum interfacial tension, or any other practical economic criterion.

ACKNOWLEDGEMENTS: This research was supported by the Ministry of Education, Science, Sport and Culture (Monbusho). The authors are indebted to Mr. Y. Inoue and Mss. V.T.H. Minh, for their assistance with these experiments.

REFERENCES

1. Mackay DM, and Cherry JA (1989) J Environmental Science and Technology 23(6): 630-636
2. Grimberg SJ, Miller CT, and Aitken MD (1996) J Environmental Science and Technology 30: 2967-2974
3. Pennel KD, Jin M, Abriola LM, and Pope GA (1994) J Contaminant Hydrology 16: 35-53
4. Desphpande S, Shiau BJ, Wade D, Sabatini DA, and Harwell JH (1999) J Water Research 33(2): 351-360
5. Brandes D and Farley KJ (1993) J. Water Environmental Research 65(7): 869-878
6. Imhoff PT, Gleyzer SN, McBride JF, Vancho LA, Okuda I, and Miller CT (1995) J Environmental Science and Technology 29(8): 1966-1976
7. Lunn SRD and Kueper BH (1997) J Water Resource Research 33(10): 2207-2219
8. Desnoyers JE, Quirion F, Hetu D, and Perron G. (1983) J Canadian Chemical Engineering 61: 672-679
9. Bettahar M, Schafer G., and Baviere M (1999) J Environmental Science and Technology 33(8): 1269-1273
10. Jawitz J W, Annable MD, Rao PSC, and Rhue RD (1998) J Environmental Science and Technology 32(4): 523-530
11. Salager JL, Morgan JC, Schechter RS, Wade WH, and Vasquez E (1979) J Society of Petroleum Engineers 19: 107-115
12. Kahlweit M (1995) J Physical Chemistry 99: 1281-1284
13. Rosen MJ, (1988) Surfactant and interfacial phenomena – second edition. Wiley Edition , pp 207-239
14. West CC, Harwell JH (1992) J Environmental Science and Technology 26(12): 2324-2330
15. Shiau BJ, Sabatini DA, Harwell JH, and Vu DQ J Environmental Science and Technology 30: 97-103

Installation of a Permeable Groundwater Treatment Wall and Its Remedial Effects

Makoto Nakashima[1], Dai Sakamoto[1], Satoshi Imamura[2] and Masanori Negishi[2]

[1] Kokusai Kogyo Co., Ltd., Geo-Environmental Engineering Dept., 3-2 Kojimachi, Chiyoda-ku, Tokyo 102-0083, Japan
[2] Taisei Co., Technology Research Center, 344-1, Nase-cho, Totsuka-ku, Yokohama, Kanagawa 245-0051, Japan

Abstract. In order to prevent groundwater contamination of chlorinated organic compounds from flowing outside of the facility property, a permeable treatment wall using zero-valent iron was installed downgradient of the contaminant source. The permeable groundwater treatment wall consisted of block-style reactive zones, installed in a zigzag-shifting disposition. Each reactive zone segment was approximately 0.6 m thick, 3.0 to 6.0 m long, and 7.0 m deep. The reactive zones are intended to clean up the contaminated groundwater passing through the shallow boulder gravel aquifer. Remedial effectiveness has been confirmed through monitoring. The concentrations of tetrachloroethylene (PCE), trichloroethylene (TCE) and cis-1,2-dichloroethylene (cis-1,2-DCE) in the treated water were confirmed to be below the levels set by the Japanese Environmental Quality Standards for Groundwater (EQSG).

Key words. groundwater contamination, zero-valent iron, permeable treatment wall

INTRODUCTION

Basically, corrective action for soil and groundwater contaminated by TCE and other volatile chlorinated organic compounds emphasizes treatment of the contaminant source zone. But where contaminant sources are beneath buildings and removal is difficult, it is often more practical to prevent the contamination from flowing off-site than to remove the contaminant source. Recently, a new method to keep contaminated groundwater from flowing off-site, using permeable groundwater treatment walls and "funnel and gate" systems has come into favor and examples of installation of these systems have increased in Europe and America [1].

"Permeable groundwater treatment walls" are a technology used to clean up contaminated groundwater by a reactive zone, installed in the pathway of the contaminants. The hydraulic conductivity of the reactive zone is larger than that of the adjoining aquifer.
This method has the advantage of being able to remediate contaminated soils in-situ, with little or no maintenance. In the case of remediation of chlorinated volatile organic compounds, it is possible to convert the contaminants to harmless species using elementary (zero-valent) iron powder, as has been reported by Senzaki [2]. This method is now widely used at many sites in Europe and America [1]. Prior to the implementation of a permeable reactive wall at the site described in this report, only one pilot study using the same methodology has been carried out in Japan [3].

The authors installed a permeable reactive treatment wall to prevent the off-site migration of volatile chlorinated compounds in the groundwater, and are monitoring the effectiveness of this countermeasure. In this paper the permeable reactive treatment wall will be introduced and its effectiveness estimated, based on the results of the monitoring data.

REACTIONS IN A PERMEABLE TREATMENT WALL

It was reported that under the presence of elementary iron, chlorinated volatile organic compounds undergo rapid dechlorination reactions [2]. When elementary iron gets in contact with water, anodic and cathodic polarization occurs at the iron metal surface, causing dechlorination reactions by reduction- and oxidation-(Redox) processes, as shown in Fig. 1.

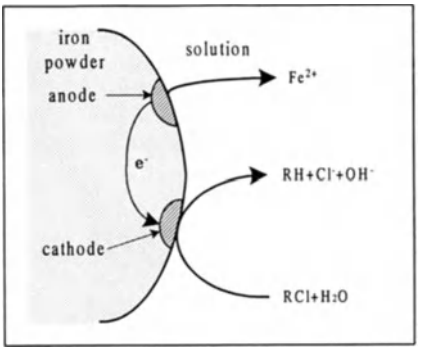

Fig. 1. Reduction and oxidation model of chlorinated organic compounds.

Dechlorination reactions of volatile chlorinated organic compounds by elementary iron powder have been studied by many scientists [4~9], who generally conclude that the dechlorination is caused by Redox-reactions, but there are many obscure points about the reaction mechanisms and the intermediate products. In particular the relation of contact time with the iron powder and the resulting intermediate products and, for instance, the degradation mechanisms of ethylene to ethane are unknown.

SITE DESCRIPTION AND INSTALLATION OF A PERMEABLE TREATMENT WALL

Site Description

The site where the Permeable Treatment Wall was installed is located on the lower rim of an alluvial fan, a shallow aquifer, consisting of large boulders, mixed with sand and gravels. The hydrogeologic structures and the process of contamination are outlined schematically in Fig. 2. The main aquifer consists of an 4.5 to 6 m layer of boulders, gravels and sand, with boulder diameters ranging from 30 to 50 cm. The lower boundary of the main aquifer is a clay layer located approximately 7 m below ground surface. The aquifer is partly covered by clayey soil lenses to a depth of 1 ~ 2.5 m below surface. Artificial fill covers these natural layers.

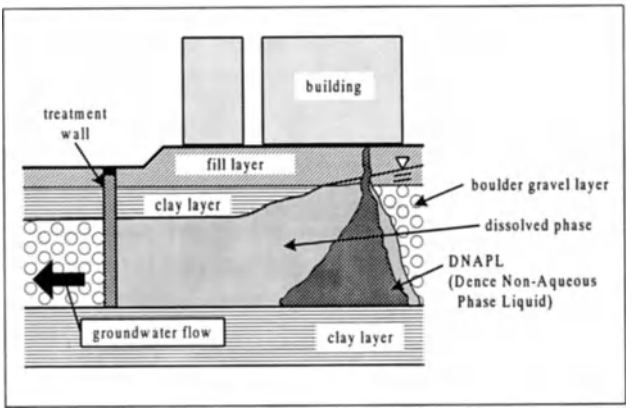

Fig. 2. Schematic profile of hydrogeologic structures and the process of contamination.

At more than two points on the site, a release of PCE to the aquifer has occurred beneath the factory facilities. The contamination plumes in the groundwater have joined and migrated to the site boundary. This information has been obtained by the following investigations: document & data study, soil gas analysis, drilling, and groundwater contamination analysis. The groundwater table contour map and PCE concentration contour map are shown in Fig. 3. The hydraulic permeability of the main aquifer (boulder, mixed with gravels and sand) is about 0.9×10^{-5} to 4.5×10^{-5} m/s, evaluated

by slug tests in monitoring wells BP1 ~ BP5, which were screened at depths from 3.5 to 7 m. Additionally, boreholes GW1 ~ GW14 were drilled for groundwater investigation to multiple depths, using a Geoprobe direct push system. In these boreholes, monitoring wells were installed with a screened depth of 4.5 to 5 m.

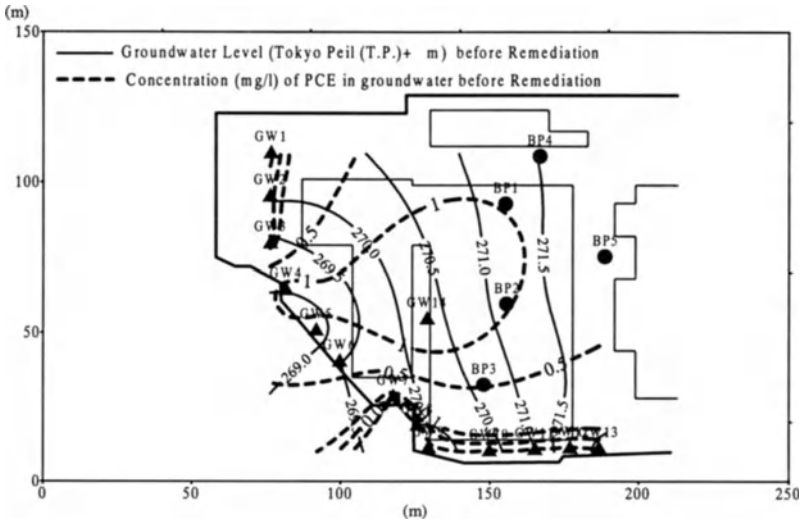

Fig. 3. Groundwater level and PCE distribution in groundwater before installation of the permeable treatment wall.

Selection of the Remediation Method

A factory building with a main production line is located above the groundwater contamination plume. It was difficult to drill inside the buildings and install extraction wells for countermeasures. The migration of the groundwater contamination in the direction of an existing well presented an environmental risk. For this reason a method that could remediate all groundwater and release the treated water under natural conditions was preferred. The permeable treatment wall, installed down-gradient of the contamination plume, was judged to be most effective for this purpose. From the results of the groundwater quality investigation prior to the installation of the permanent treatment wall, the groundwater exhibits the following properties: Dissolved oxygen (DO) was 1.2 to 1.75 mg/l and the pH was about 7.4 to 7.5 on average. The maximum PCE concentration 1.938 mg/l was found in borehole GW4.

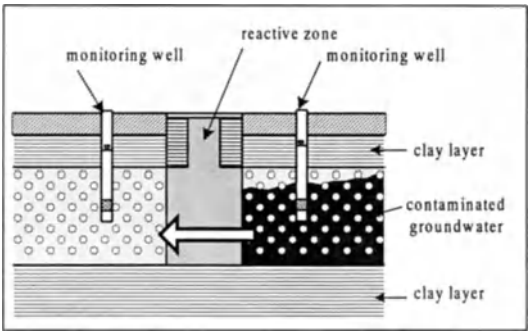

Fig. 4. Profile sketch of the permeable treatment wall

Installation of the Permeable Treatment Wall

Fig. 4 shows a profile sketch of the permeable treatment wall. Fig. 5 shows the corresponding location map and the groundwater table contour map 147 days after installation. The permeable treatment wall has a thickness of more the 0.6 m, with segment lengths varying from 3 ~ 6 m and a

height of about 7 m. The individual segments are arranged in two lines and their interim spaces are shifted in a zigzag pattern. Thus the contaminated groundwater will pass through at least one segment. This pattern allowed us to prove the effectiveness of the permeable treatment wall before the installation was completed for the total area.

The reactive material was made of small broken stones mixed with 20 percent by weight elementary iron powder. Each segment hole was excavated by a backhoe to a depth of 7 m, the upper boundary of the impermeable clay layer, and refilled with the reactive material up to 0.1 m below ground surface, with a thickness of at least 0.6 m. The chemical composition of the iron powder was 92.05% elementary iron, 2.5% nickel, 5.45% copper, with a specific surface area of 0.052 m^2/g. Using a thickness of more than 0.6 m is expected to result in a residence time of at least 2 days with a groundwater flow velocity of 1×10^{-5} m/s and a groundwater gradient of 1/40. These values are calculated on the assumption of a maximum groundwater velocity 10 times the Darcy-velocity of 2.5×10^{-6} m/s. The annular space around the reactive segments was refilled with (iron-free) small broken stones in the area of the aquifer and with excavated materials in the area of the surface clay layer and the artificial fill. A 0.1 m thick sand layer covered the top of the permeable reactive wall.

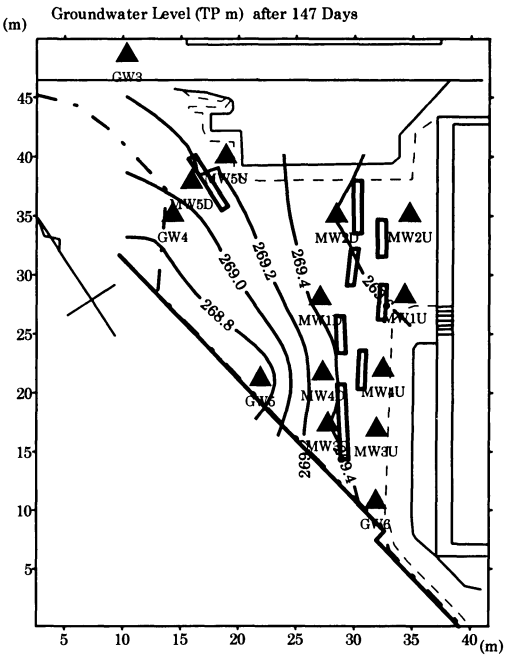

Fig. 5. Plan view of permeable treatment wall segments and the groundwater table contour map (147 days after installation)

Generally, it is difficult to install a permeable reactive wall in a sandy gravel layer containing such large boulders [3] as those found at this site. However, the feasibility of the applied installation method was confirmed. Fife pairs of monitoring wells were installed with one well up-gradient (MW1U ~ MW5U) and one well down-gradient (MW1D ~ MW5D) of the permeable reactive wall to confirm it's remedial effectiveness. The screen of monitoring well MW1D was set at a depth of 3.3 ~ 5.25 m, whilst the other wells were screened between 4.0 ~ 4.5 m below surface.

As estimated from the monitored groundwater levels in each well, the groundwater velocity was about 1.38×10^{-7} to 6.44×10^{-7} m/s. All contaminated groundwater passes through the permeable treatment wall as shown in Fig. 5.

MONITORING THE REMEDIAL EFFECTIVENESS

In Fig. 6, the temporal development of the concentration of cis-1,2-DCE, TCE and PCE in the groundwater of wells GW14, MW1D, MW4U and MW4D is plotted. GW14 is located 30 m up-gradient of the permeable treatment wall. Time 0 was the day when installation of the treatment wall was started. The contaminant concentrations in the up-gradient wells, GW14 and MW4U, changed due to groundwater recharge by rainfall. Nevertheless the down-gradient concentrations of PCE and cis-1,2-DCE in MW1D decreased constantly. The initial concentration of PCE in MW1D before the

installation was 0.072 mg/l but it fell below EQSG of 0.01 mg/l after 70 days. After 147 days it was only 0.002 mg/l, 2.8% of the initial concentration. In the period of from 133 days to 323 days, the contaminants concentrations of the groundwater in well MW4D were below EQSG (PCE : 0.01 mg/l, TCE : 0.03 mg/l, cis-1,2-DCE : 0.04 mg/l), and remediation efficiency was at least 99% for PCE, 96% for TCE and 90% for cis-1,2-DCE.

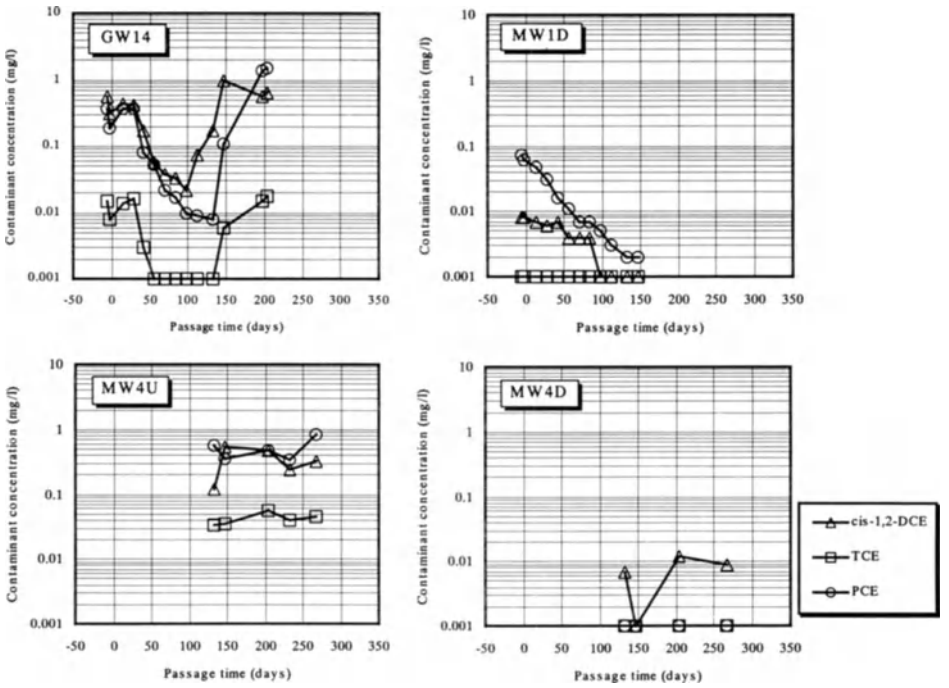

Fig. 6. Change of cis-1,2-DCE, TCE and PCE concentrations in groundwater after installation of the permeable treatment wall.

Fig. 7 compares the up- and down-gradient contaminant concentrations, after an operation time of 147 days. As estimated from the monitored groundwater levels in each well, the groundwater velocity was about 1.38×10^{-7} to 6.44×10^{-7} m/s. All contaminated groundwater passes through the permeable treatment wall as shown in Fig. 5. As shown in Fig. 7, the permeable treatment wall works properly to remediate PCE, TCE and cis-1,2-DCE. Regarding PCE and TCE, both contamination levels are below EQSG in all down-gradient monitoring wells (MW1D ~ MW5D), thus the remediation goal was achieved. The cis-1,2-DCE

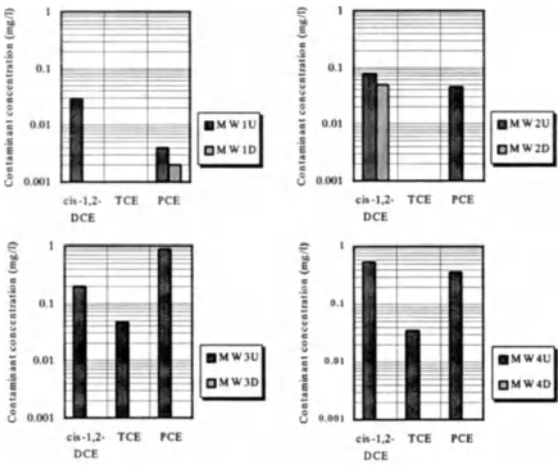

Fig. 7. Comparison of groundwater concentration between up- and downgradient side of the permeable treatment wall (147 days after installation)

concentration shows degradation, compared to the up-gradient concentration. But, in MW2D, the concentration level of cis-1,2-DCE still remains above EQSG (0.04 mg/l), because cis-1,2-DCE is a secondary byproduct of the slow TCE, PCE degradation process. Two samples were also taken from monitoring wells MW1D and MW3D, and analyzed for vinyl chloride (VC) but levels were found to be below the detection limit.

Durability of the treatment wall was predicted by the reaction model of Shimomura et al. [10]. The parameters were estimated by column experiment using on-site groundwater. It was predicted that the durability of the treatment wall is large enough to prevent the out-flow of contaminated groundwater with concentration levels exceeding the EQSG for approximately 17000 days (about 47 years), even in case, that the groundwater velocity is ten times higher than the measured average groundwater velocity on the site [11].

CONCLUSIONS

Successful remediation of contaminated groundwater spreading from the source zone beneath a facility was achieved by installation of a permeable treatment wall containing zero-valent iron. The remedial effectiveness was confirmed by monitoring results from up- and down-gradient wells. Down-gradient concentrations were below the EQSG levels. The reliability of such systems was calculated [11] with a remediation effectiveness prediction model, developed by Shimomura et al. [10]. When demolition or reconstruction activities will take place on the site, additional countermeasures, such as excavation of the hot spot area, could be performed with minimal costs. Meanwhile the permeable treatment wall gives the company the advantage of solving the problem completely without interrupting their on-site business activities.

REFERENCES

1. U.S.EPA (1998) : Permeable Reactive Barrier Technologies for Contaminant Remediation. EPA/600/R-98/125
2. Senzaki T(1995) Koatsu Gas, 32, 604-608 (in Japanese)
3. Negishi M, Shimomura M, Imamura S (1999) The Foundation Engineering & Equipment, Monthly, 1999-1, 63-65 (in Japanese)
4. Senzaki T, Kumagai Y (1988) Kogyo Yosui, 357, 2-7 (in Japanese)
5. Senzaki T, Kumagai Y (1989) Kogyo Yosui, 369, 19-25 (in Japanese)
6. Senzaki T (1991) Kogyo Yosui, 391, 29-35 (in Japanese)
7. Orth WS, Gillham RW (1994) Environ. Sci. Technol., 30, 66-71
8. Gillham RW (1996) In: Aral MM (Ed) Advances in Groundwater Pollution Control and Remediation. Kluwer Academic Publishers, pp249-274
9. Matheson LJ, Tratyek PG (1994) Environ. Sci. Technol., 28, 2045-2053
10. Shimomura M, Imamura S, Negishi M, Lee C (1998) Jour. of Groundwater Hydrology, 40, 445-454 (in Japanese with English abstract)
11. Nakashima M., Sakamoto D., Negishi M, Shimomura M (submited) Jour. of Groundwater Hydrology (in Japanese with English abstract)

Groundwater Quality Evaluation with Special Reference to Fluorosis and Nitrate Pollution - A Case Study

Anil Abbi. Ph.D.

Tropical Research and Development Centre, 57/C, 18th Main, BSK-I stage, Bangalore-560 050, INDIA

ABSTRACT. Despite a seeming abundance, India's groundwater resources are not inexhaustible. Moreover the sustainable development of our groundwater resources is increasingly threatened by Municipal, Industrial and Agricultural sources. As the public becomes increasingly concerned about water quality and quantity, a greater demand is placed on scientists to provide scientific information on which decisions regarding the health and management of water resources are based.

This research paper describes the preliminary results of a study attempting to evaluate the long term water quality situation and health hazards in the eastern part of the Dharmapuri district,Tamil Nadu, India. The study also aimed at increasing understanding of the distribution of fluoride in the surface and groundwater, its source, its effects on human beings and animals, and proposing preventive and curative measures if possible. This study also indicated the occurrence of a high quantity of nitrate in the ground water samples. For this reason, the paper mainly deals with the Fluorosis problem and nitrate pollution in the study area. Fluoride concentration exceeding the desirable limit (0.6 to 1.2 mg/ltr) in sixteen samples is a major health hazard has lead to primary dental florosis amongst the villagers. All the samples showed more than 0.6 mg/ltr and six samples exceeded the highest permissible level of 1.2 mg/ltr. The nitrate concentration in seven groundwater samples exceeded the WHO maximum permissible limit of 45 Mg/litre. This was the first time such a high nitrate concentration in groundwater was observed in the region and it requires immediate action to provide safe drinking water for the rural community.

KEYWORDS :Groundwater, fluorosis, nitrate pollution, water treatment.

INTRODUCTION

The rural community mainly depends upon groundwater for drinking and other domestic uses. Ground water has the properties of dissolving, and carrying in solution, a variety of chemical and other materials. It is well established that deficiencies or toxicity of elements may cause health hazards both in animals and in human beings. For example, Fluorosis and incidence of goiter are among the many diseases which can be studied through preparation of multi-elemental atlases by geochemical mapping, and this will be of great help in defining problems and demarcating potential areas of risk groups. The presence of high nitrate concentration normally indicates pollution of ground water at some stage of its history. Since the presence of excess nitrate ions is deleterious to health, their occurrence in high concentrations in natural water is a matter of great concern to environmental scientists.

GEOGRAPHICAL SITUATION

The area falls between latitude 12° 11' 30" to 12° 19' North and longitude 78° 3' to 78° 17' 30" East, in the Eastern part of Dharmapuri District, Tamil Nadu. The area is a plain covering about

308 sq.kms. In the central part of the area there is a small river flowing that forms the main drainage network. Agriculture is the principle activity in the district. The major soil types are mainly mixed loam red ferruginous and black soil. The area enjoys a tropical climate, being hot and dry for the greater part of the year. The temperature ranges from 20° to 40°C. The average rainfall (1970 - 1998) of this area is 825 mm per annum and the area receives rainfall through both south-west and north-east monsoons. The intensity of precipitation is erratic and its areal distribution varies from place to place and from year to year. The principal crops of this area are Paddy, Maize, Sorghum, Bajra, Ragi, Pulses and Groundnut.

GEOLOGICAL SITUATION

The study area forms a part of Archaean sheild of peninsular India. The area is underlain mostly by crystalline rocks of Archaean age and recent alluvium, which is restricted to the course of larger streams. The general foliation of the rocks runs NNE-SSW with dips to ESE. The occurrence and behaviour of ground water are controlled by the hard crystalline rock formations such as granites, gneisses and charnokites. Important source of ground water in the area is the return seepage from irrigation, along with downward percolation of influent stream runoff. The rainwater harvesting ponds/tanks form the permanent source of surface water which help in recharging of groundwater in the area[1].

METHODOLOGY

Sixteen water samples were collected in well cleaned and pretreated double -stoppered polythene bottles of two liter capacity from the existing tubewells and from an open well in different villages. The water samples were analysed to test the quality of the water with special reference to Fluoride and Nitrate problems. The water quality details are given in Table-1 and the chemical parameters are compared with drinking water standards of the World Health Organisation (WHO) and of the Indian Standard Institute (ISI), both of which indicate maximum permissible limits.

QUALITY OF GROUNDWATER

The quality of groundwater in few villages of Dharmapuri District was studied with a view to evaluating the suitablilty of this groundwater for domestic and irrigation purposes. The analytical data revealed that the groundwater in the surveyed villages is alkaline with pH values ranging from 7.1 to 7.7. The electrical conductivity of water in this zone ranges from 624 to 2538 micro mhos/cm at 25^0 C and falls beneath the "good" to "maximum permissible" limits according to the WHO standards. The total hardness of the water ranges from 218 to 838 mg/litre and in some samples, it exceeds maximum permissible limits of the WHO standards. The water is moderately hard and in some places it is highly brackish. The chloride concentrations range between 30 to 552 mg/litre. The other constituents, such as Ca and Mg, are within the maximum permissible limits of WHO standards, except at one place called, Kodiyur where Ca is excessive. Moderately high concentrations of fluoride in groundwater were observed in most of the locations. Sulphate is within the permissible limits, except at one location. High nitrate content was observed in most of the samples, may be due to the usage of large quantities of fertilisers for agricultural purposes. In general, groundwater in the study area is good and is suitable for irrigation purposes. The poor quality of groundwater, resulting from the occurrence of fluoride, is a local feature due to constant interaction with source rocks rich in fluoride bearing minerals and the occurrence of high nitrate levels may be due to the application of large amounts nitrogenous fertilizers. This pollution of groundwater with high Nitrate needs immediate attention and proper treatment so as to provide good quality safe water.

Table -1. Results of the Groundwater Quality Analysis and Comparison with WHO & ISI Standards

Sl No	Sample Location	Ca mg/ltr	Mg mg/ltr	Na mg/ltr	K mg/ltr	HCO3 mg/ltr	Cl mg/ltr	SO4 mg/ltr	F mg/ltr	NO3 mg/ltr	TDS mg/ltr	TH mg/ltr	PH
1	Melur	115.2	81.2	215.0	102.0	378.0	480.0	120.0	0.84	127.80	1549	622	7.1
2	Pudur	35.2	31.5	187.0	98.0	774.0	52.0	35.2	1.44	5.11	950	218	7.7
3	Sellankottai	192.8	47.1	188.0	140.0	326.0	532.0	120.0	1.20	136.30	1624	676	7.2
4	Maravadi	66.4	136.0	155.0	6.0	474.0	388.0	52.8	1.52	110.80	1362	726	7.4
5	Gollahalli	56.0	29.2	77.0	5.0	334.0	100.0	20.0	0.92	29.80	576	260	7.7
6	Guttahalli	168.0	17.5	124.0	45.0	288.0	316.0	54.4	0.80	127.80	1044	492	7.4
7	Indamangalm	13.6	62.2	61.0	5.0	378.0	40.0	27.2	1.36	20.45	552	290	7.5
8	Krishnapuram	169.6	15.5	263.0	51.0	340.0	470.0	88.0	1.04	102.20	1453	488	7.3
9	Mallikottai	33.6	111.2	166.0	11.0	270.0	164.0	440.0	1.28	1.70	1179	542	7.6
10	Nilampatti	73.6	16.5	65.0	6.0	318.0	50.0	23.2	0.70	93.71	553	252	7.2
11	Nattam	18.4	76.8	99.0	19.0	294.0	162.0	127.2	1.36	0.85	799	362	7.4
12	Maddankottai	58.4	74.3	99.0	6.0	300.0	216.0	96.0	0.68	21.30	891	452	7.5
13	Sellankottai	23.2	34.5	40.0	6.0	238.0	30.0	42.0	0.96	31.52	399	200	7.6
14	Naganur	12.8	50.5	137.0	20.0	390.0	136.0	37.6	1.16	29.80	722	240	7.6
15	Agraharam	36.8	62.7	38.0	1.0	234.0	92.0	34.3	0.52	41.74	525	350	7.5
16	Kodiyur	228.0	65.1	80.0	11.0	294.0	400.0	128.4	0.84	93.71	1336	838	7.3
	W.H.O standards	200	150	--	--	--	600	400	0.8 -1.78	45	1500	500	6.5- 9.2
	ISI standards	200	100	--	--	--	1000	400	1.5	45	1500	600	8.5-9.2

Occurrence of Fluoride: Fluoride is so highly reactive that it is never encountered in its elemental gaseous state, except in some industrial processes[2]. It occurs in the earth's crust, notably as fluorspar, cryolite and fluorapatite. These fluoride minerals are nearly insoluble in water. Fluoride is encountered in water when conditions favour its dissolution from fluoride bearing minerals. Occurrences of excess fluoride bearing waters were reported by many research workers in Andhra Pradesh, Bihar, Gujarat, Haryana, Karnataka, Madhya Pradesh, Maharashtra, Orissa, Punjab, Rajasthan, Tamil Nadu and Uttar Pradesh. There are an estimated 8700 villages in India which have problems of excessive fluoride in water, affecting 2.5 million people. Fluorine in the exogenic cycle of this fluorosis belt is almost entirely derived from granitic and pegmatitic rocks. There is no evidence of any addition of fluoride into the environment by artificial means either by industry or by any other sources. The principal fluorine bearing minerals such as fluorite and fluorapatite, are responsible for a high concentration of fluoride under normal pressure and temperature conditions, whereas refractory minerals like hornblende, Mica and Epidote will not release fluoride under normal temperatures. The factors that govern the distribution of fluoride in natural waters are dependent on amount of fluorine in the source rocks and soils, and the duration of contact of water with the rocks and soils. Systematic data on variations in fluoride content of groundwater with different seasons are not available for this area. Finally, it may be noted that the high incidence of fluorosis is because of a variety of factors such as geological, geochemical, climatological, social and economic conditions. The natural ocurrence of high fluorine content in groundwater is an environmental hazard.

Significance of fluoride: Fluoride plays a significant role in affecting human health, to varying degrees depending upon its concentration in groundwater. It is well established that element deficiencies or toxicity may cause health hazards both in animals and human beings. Fluoride acts as a two-edged sword: High doses (i e., above 1.2 mg/litre) of it lead to tooth and bone fluorosis and low doses (i.e., below 0.6 mg/litre can cause dental caries. Researche carried out on the effect of fluoride concentration in potable water around 1mg/litre reduced dental caries by reducing the solubility of tooth enamel to acid and also acting as an inhibitor of the bacterial enzymes responsible for the production of the acid which attacks the enamel. However, a higher concentration, viz. 1.5 mg/litre or above, results in staining of the tooth enamel while at still higher levels, viz. 5 to 10 mg/litre of fluoride, pathological changes such as stiffness of the back and difficulty in performing natural movements occur with sustained use.

The desirable limit for fluoride in drinking water is 0.6 to 1.2 mg/litre (ISI,1983)[3]. If the limit is below 0.6 mg/litre, the water source should not be rejected but suitable public health measures should be undertaken. The maximum limit may be extended to 1.5 mg/liter if no alternative source is available. The highest desirable levels according to the Indian Council of Medical Research are 1.0 and 1.5 mg/litre respectively. According to the WHO guidelines for drinking water quality(1982)[4] and the Water Technology Mission of the Government of India, the permissible limit for fluoride in drinking water is 1.0 mg/litre. It can be extended to 1.5 mg/litre if there is no alternative source in the village. The water needs treatment if the level is above this limit.The analytical results of the present investigation reveal that the fluoride concentration in the shallow aquifers in some of the areas is well within the permissible limits (0.6 to 1.2 mg/litre, ISI 1983). In some villages, however it has exceeded WHO and ISI drinking water standards and treatment is required urgently.

Nitrate Pollution and its impact on human beings: The hydrogeochemical investigations on groundwater samples of the study area revealed the presence of high nitrate content. In recent years there has been an increased use of agricultural chemicals, notably pesticides and fertilisers. Farmers apply fertilizers extensively on crop lands. Their extensive use, however creates some problems. Nitrates are especially susceptible to leaching with each rainfall and they subsequently enter the groundwater. Where they are extensively used, they appear in well water (Sample No.16). Nitrates are of special concern but they generally find their way into waterways

from feedlots, not from excessive or improperly timed fertilizer use. Nitrates in drinking water can cause Methemoglobinemia in babies (Blue Babies) because, in an infants stomach, the nitrate NO3- is converted into Nitrite (NO2-), which acts on the blood hemoglobin to form methemoglobin[5]. Hence the study of nitrate in potable water assumes a great importance. The present study indicates that nitrate concentrations of groundwater are over 100 mg/litre in several places in the study area and concentrations as high as 136.30 mg/litre have been observed, whilst a maximum permissible limit of 45 mg/litre is suggested by WHO. The behaviour of nitrate ions is similar to that of chloride ions. Nitrate salts usually have a high solubility and are not absorbed by the clays present in the soils of the area.

Nitrate content in groundwater serves as a basis for detecting pollution. Most of the samples of groundwater drawn from the boredwells showed an occurrence of Nitrate ranging from 1.70 to 136.30 mg/litre. These wells are located near to the cultivable lands where large quantities of inorganic fertilizers and pesticides are used. These chemicals pollute the well-water through percolation. This high level of Nitrate should be considered a serious problem for further future development of drinking water. The occurrence of high nitrate content may be the result of continuous application of inorganic fertilizers in these regions.

CONCLUSIONS AND RECOMMENDATIONS

The present water quality situation in easternpart of the Dharmapuri District is under great threat. The high fluoride content in the groundwater of this area has affected villagers in the form of primary level of fluorosis resulted in stained and darkened tooth enamel. Though there no proper health survey has been conducted with respect to the nitrate pollution problem, death of fishe in one open well (Sample No -16) was observed. Regular monitoring of water quality is recommended to improve understanding of nitrate pollution in the groundwater in these villages and in the surrounding region. The high fluoride content in the drinking water should, also be given attention and defluoridated water should be provided for drinking purposes in the rural areas. In addition to these actions a proper survey is recommended to study the negative impact of Nitrate pollution on public health in the areas affected.

REFERENCES

1. R.Chakrapani (1982), Hydrogeological Conditions in Dharmapuri District, Tamil Nadu, Report of CGWB, Hyderabad,
2. G.W.Nawlakhe and R.K.Bulusu((1989), Water Treatment Technology for Removel of excess Fluoride, IGW-89, NGRI,Hyderabad pp.815-827,
3. ISI (1983), Indian Standard Specification For Drinking Water, IS-10500, Indian Standards Institute, New Delhi.
4. WHO (1971), International Standards For Drinking Water(Geneva 1971) Third Edition.
5. N.C.Ghose and C.B.Sharma(1986), An Integrated Study of the pollution of Dugwells around Patna, Bihar, GSI memoir-5, Bangalore.

A designing method for in-situ bioremediation of groundwater with evaluation of transport characteristics in aquifers

Mitsutoshi Nakamura[1], Junichi Kawabata[1] and Tatsushi Kawai[1]

[1] Environmental Engineering Department, Kajima Technical Research Institute, Tokyo, JAPAN

ABSTRACT. Solute transport analysis is performed to design an effective in-situ bioremediation system for contaminated groundwater with chlorinated hydrocarbon such as trichloroethylene etc. The principal consideration involved in the design of in-situ bioremediation is two-fold: one is to understand the chemical and biological conditions in an aquifer, which allow the most efficient performance of bioremediation; the other is how to make such a condition by an artificial groundwater systems. The contaminated groundwater to be cleaned up should be mixed efficiently with the stimulated microorganisms. It should be designed only through the solute transport analysis based on a properly characterizing of transport parameters specific to a site. This study reviews methods of mixing a few kinds of solutes to enhance the microbial degradation activity in an in-situ aquifer, which is to be effective for trichloroethylene in groundwater. It then proposes a method of evaluating the key elements in dealing with mixture in an aquifer bioremediation, which is transport characteristics such as dispersion, retardation effect etc. Solute transport analyses are carried out, assuming various solutes injected into the aquifer through a well during the treatment process. In so doing, this study presents the basic design principles of in-situ bioremediation.

Key words. Groundwater contamination, Solute transport analysis, Bioremediation, Trichloroethylene, In-situ tracer test

INTRODUCTION

There are many ways to remediate groundwater. Directly extracting methods such as soil vapor extraction and pump and treat method etc., have been quite often used where the contamination level is very high which is always observed around leaking points. Such physical methods are efficient for lowering the concentration of contaminants to a certain level. However, it is difficult to make them work efficiently in low level of contamination. It is due to the heterogenity in aquifers, sorption of contaminants to soil particles, retention of contaminants due to physical interactive characteristics between contaminants and soil particles (governed by surface tension, wet angle.) and other factors.

In-situ bioremediation is a method detoxifying contaminants by artificially activating microbial degradation of organic contaminants. Once a biodegradable condition is satisfied, degradation of contaminants proceeds more and more efficiently with lowering of concentration or molecular weight of organic contaminants. Hence, bioremediation is inherently an effective method under condition that the concentration of organic contaminants is relatively low.

For a specific design of the in-situ bioremediation system, the following items are important as design conditions:

(i) The necessary conditions to activate microbial degradation in an aquifer. That is, necessary concentration of substrate and of nutrients to activate microorganisms, and also the duration time of activity

(ii) Physical conditions such as permeability and solute transport characteristics, which are essential to predict injected solutes movement and the degree of mixture among them in aquifers, quantitatively.

Of the two, microbial activation characteristics mentioned in the item (i) will be clarified through biological treatability tests using in-situ soil. For the item (ii) an evaluation on the solute transport characteristics in the aquifer would be necessary in order to assess controllability of the injected solute concentration and a mixture condition of injected plural solutes.

This paper classifies typical methods for in-situ bioremediation, and discusses methods for evaluation of solute transport characteristics in an aquifer, which is a practical key factor for designing remediation system. Furthermore, solute transport analysis based on the evaluated characteristics is performed, and then methods for designing remediation systems are generally described.

IMPORTANCE OF EVALUATION ON SOLUTE TRANSPORT

There are basically two methods of in-situ bioremediation. The biostimulation process in which indigenous microorganisms are multiplied rapidly by supplying substrates, such as methane and oxygen in the case of TCE co-oxidation essential for the multiplication and nutrients such as phosphates that activates microorganism's growth. The other method is the bioaugmentation process in which microorganisms are directly injected into the aquifer for microbial degradation of contaminants.

Of the two, the stimulation process requires a system design for controlling mixture condition and concentration of several solutes in an aquifer. Using the system designed as such, it would also be possible to activate introduced microorganisms in the augmentation process. If a design method for the stimulation process is established, it can also be applied to the augmentation process; for this reason, this study mainly deals with the stimulation process.

Figure 1 shows a design process for an in-situ bioremediation system with using an artificial groundwater flow, as proposed by the author. This paper presents the investigation results by following this flow diagram.

EVALUATION OF SOLUTE TRANSPORT CHARACTERISTICS IN AN AQUIFER

In-situ tracer tests by the continuous injection method. (Test methods) The tracer tests were performed to evaluate solute dispersion characteristics generally in an artificial groundwater flow. The test was made to run through an unconfined aquifer consisting of homogeneous diluvial fine sand (permeability coefficient is about $2.1*10^{-3}$ cm/s). An apparatus capable of continuous tracer injection at a constant flow rate into the injection well was used for this test. Figure 2 shows an outline of the tests and ground conditions. The tests were performed in the following processes:

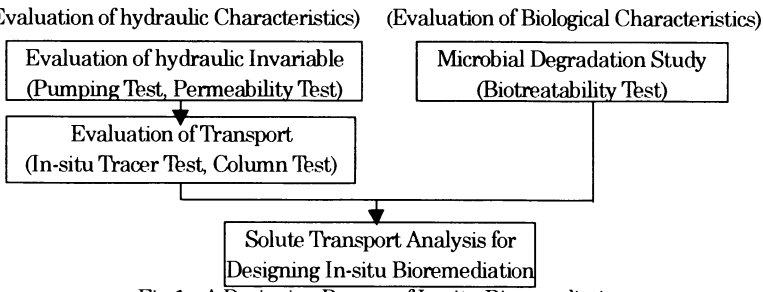

Fig.1 A Designing Process of In-situ Bioremediation

(i) an artificial groundwater flow was generated by pumping from the pumping well at a rate of 6.7 l/min.(which is 80 % of the maximum pumping capacity for the well)
(ii) after the groundwater level stabilized, 800ppm NaCl solution (EC=1.2 mS/cm) was injected continuously into the injection well, at a rate of 1 l/min.
(iii)Changes in electrical conductivity with time at the two observation wells located downstream.

(Test results) Figure 3 shows the test results. Break-through curves that indicate tracer arrivals are clearly observed in each observation well. Also shown are the values of dispersivity compatible with the break-through curves, obtained through two-dimensional advective-dispersive analyses. The analyses were performed after calculating actual flow rate and effective porosity, assuming as an arrival time the instance when relative concentration (the ratio assuming the concentration at a time of injection as 1.0) became 0.5 in each observation well. The values obtained for the effective porosity based on the break-through curve for each well are fairly consistent. On the other hand, the values of dispersivity tend to be greater as the distance from the injection well increases.

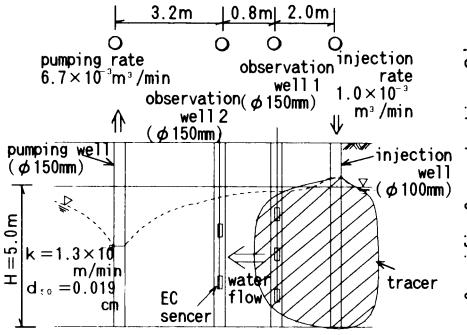

Fig.2 Outline of a In-situ Tracer Test by Continuous Injection

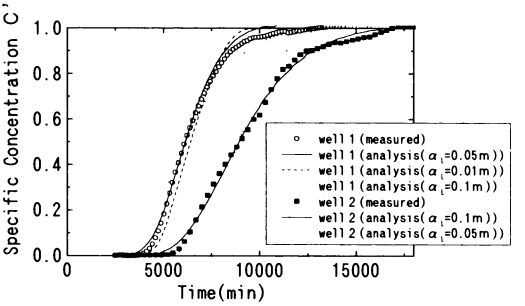

Fig.3 Breakthrough Curve of Tracer Test (at Observation Well1,2)

Evaluation of dispersivity. Figure 4 shows the results of laboratory column tests performed in the past by the author[1], which is rearranged to indicate relationship between the ratio of dispersion coefficient D_l to kinematic viscosity coefficient ν and the Reynolds number Re. Also shown in the figure are empirical formulae obtained using glass beads. It has, generally, positive correlation with each other. The solute dispersion is caused by actual flow rate distribution in the pores among soil particles. Dispersion coefficient obtained in the present tests was higher than those obtained using the empirical formulae. The author believes this is because actual diluvial sand layers have particle distribution similar to those shown in Figure 3, and their dispersivity is higher than that in a porous media consisting of glass beads. Figure 5 shows relationship between the observation scales L (the distance that the tracer travels) and each of the dispersivity values obtained from the laboratory column tests and in-situ tracer tests for this study, and those of an aquifer with identical particle sizes and density. Also plotted in the figure are the values of dispersivity obtained from other laboratory column tests and in-situ tracer tests performed in the past [2]. The graphs indicate that dispersivity is strongly affected by the observation scales L, when the observation scales L is greater than 1 m. Also shown are reorganized equations according to Nueman or Arya[3]. The relationship between the dispersivity obtained from the laboratory column tests and in-situtracer tests corresponds relatively well to equation by Nueman in

this observaton scale. If the in-situ bioremediation process is designed in larger scale, because of the larger permeability of the site, the scale of measurement also should be wider. The scale dependent dispersivity is obtained statistically by Nueman. The results indicate that the dispersivity may be selected based on this equation for practical point of view.

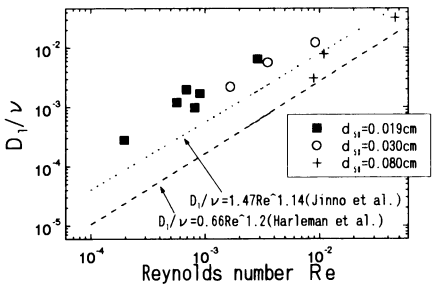

Fig.4 Estimated Coefficient of Dispersion in Relation to Reynolds Number [1]

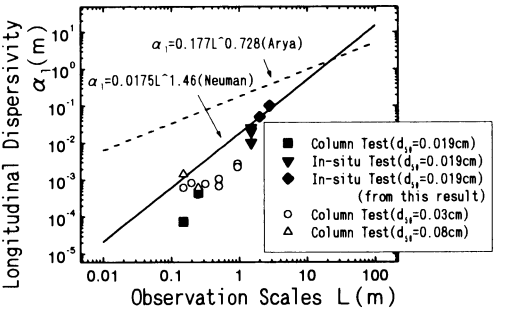

Fig.5 Relationship between Dispersivities and Observation Scales

ANALYSES FOR DESIGNING IN-SITU BIOREMEDIATION SYSTEMS

Conditions for the investigation. The effect of biostimulation method is strongly affected by the mixture situation among substrates and nutrients, which should be injected for activating indigenous indigenous microorganisms, and by the frequency of contacts between the activated microorganisms and the contaminants. From a viewpoint of the system design, it is important that injected solutes should be efficiently mixed in an aquifer, not in a well. Because well clogging should occur due to simultaneous injection with mixed solutes into a well. Thus, the following two schemes, in which solutes are injected spatially apart or with a lapse in time, were devised as two basic methods for efficient mixing: scheme A in which several wells are used for injection; and scheme B in which pulse injection is performed intermittently. In other words, it is fundamental, for designing an efficient remediation system, to clarify the mixing characteristics of injected solutes in aquifers as for the schemes A and B.

For this purpose, a general discussion is presented on mixing characteristics and effects through solute transport analyses, assuming the application of the two methods in various aquifers. Figure 6 and Table

Table 1 Designing Conditions

Scheme A	Case1	Case2	Case3	Scheme B	Case4	Case5
Injection Method	multi-wells, continuous injection			Injection Method	alternate pulsing injection	
Permeability (cm/s)	10^{-3}	10^{-2}	10^{-1}	Permeability (cm/s)	10^{-3}	
Dispersivity (m)	0.01	0.5	5	Dispersivity (m)	0.01	
Pumping Rate (l/min)	18	200	2000	Pulsing Time(min)	500	5000
Injection Rate (l/min)	3	30	300	Injection Rate (l/min)	3	3

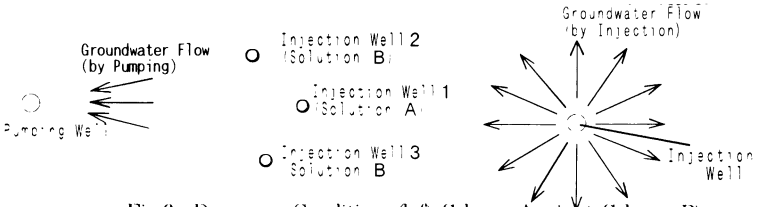

Fig.6 Designing Conditions (left: Scheme A, right: Scheme B)

1 shows the conditions of analyses. The values for pumping rate, injection rate, and distance among wells are selected appropriately in accordance with the specific permeability for each aquifer (H=10m). The time required for solute transport from the injection well to the pumping well was set between 10 to 14 days, which are feasible duration for practical management under given conditions. In other words, the area to be investigated expands with larger permeability. The values for dispersivity were determined based on Figure 4, and according to the extent of the area to be investigated. The values one tenth of longitudinal dipersivity were used as horizontal dispersivity. For solute transport analyses, upwind finite element method was utilized, which was developed by authors.

The results of investigation. Figure 7 show the example of solute transport analysis. From the results of biological treatability tests using aquifer's sand[4], microbial degrading activity will reach to the sufficient level under the condition that oxygen and methane are mixed at concentrations greater than 10% of saturation. This condition is applied to the designing condition of the in-situ bioremediation. The figures indicate areas where solutes injected from the injection wells dispersed at concentrations greater than 10 % of each saturated solution. The regions where these solutes mixed, or the areas with highly activated microorganisms, are also shown. The results of analyses, along with microbiological point of view, are summarized in Table 2.

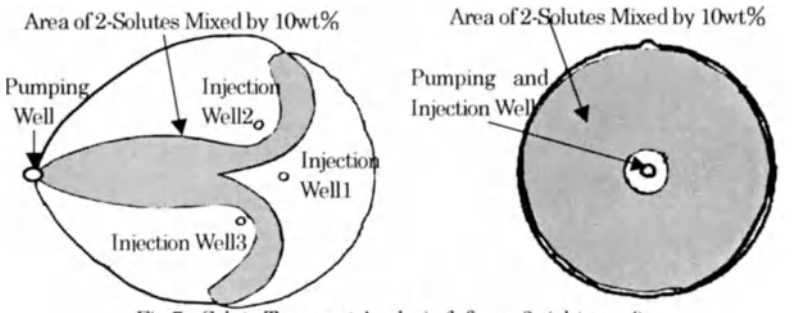

Fig.7 Solute Transport Analysis (left:case3,right:case4)

Table 2 Comparison of Designing Conditions A & B

	Scheme A
Merits	Solutes are constantly supplied for exposure to microorganisms, and multiplication of the organisms and degradation may be easily controlled by adjusting injection rates and amount. Injection equipment can be easily operated and managed.
Demerits	Transversal dispersion makes mixing difficult, and the ratio of injected substrates effectively used to activate microorganisms is low.The method is very inefficient in grounds with permeability coefficient of 10^{-2} cm/s or less.
	Scheme B
Merits	Mixing is accomplished through longitudinal dispersion, and if microorganisms are maintained active as bacterial cells, they can easily contact and mix with the contaminants in groundwater. Injected substrates are effectively used, and mixing efficiency increases as injection intervals are made shorter.
Demerits	In cases with short injection intervals, permeability might be lowered due to clogging.

A SUMMARY OF IN-SITU BIOREMEDIATION SYSTEM DESIGN

Basic conditions for designing systems: It is important to clarify mixture conditions of injected solutes in an aquifer, as well as characteristics of activated microorganisms and duration of biodegrading activities in order to design an efficient in-situ bioremediation system to cope with groundwater contaminated with petroleum hydrocarbons or chlorinated organic compounds.

Importance of solute transport analyses and the investigation results: It is necessary to evaluate transport characteristics, quantitatively, in aquifers in order to clarify mixture conditions of injected solutes. The results of this study suggested that not only the particle size but also the particle distribution affect dispersivity. Dispersivity is also positively correlated with distance of tracer travels even within a relatively homogeneous aquifer. For a practical purpose, it is possible to adopt the values of dispersivity, which are decided from the relationship in Fig.5 and Fig.6

Results of injected solute transport analyses: Solute transport analyses are performed, which is based on the evaluation of transport characteristics, which is mentioned above. Results indicated that in a ground with permeability coefficient of about 10^{-3} cm/s, longitudinal dispersion should be used to mix the solutes efficiently: that is, a pulsing injection system would be necessary to make an effective bioremediation system. On the contrary, It is possible to use transversal dispersion when the permeability coefficient of an aquifer is about 10^{-1} cm/s. That is, simultaneous injection of each solute from different wells are possible to use in a system, which may avoid complicated controlling of pulsing injection.

ACKNOWLEDGMENT

The author is grateful that some part of the test data and simulation results in the study were allowed to be cited from a national research project entitled "Development of Remedial Technologies for Soil Contamination (In-situ Soil Bioremediation)",which is entrusted to Research Institute of Innovative Technology for the Earth (RITE) by New Energy and Industrial Technology Development Organization (NEDO).

REFERENCE

1.Nakamura & Kawabata; Evaluation Method of Transport Characteristics in Groundwater Flow, The 53th Annual Conference of The Japan Society of Civil Engineers, 1998

2.Kawabata & Nakamura; Evaluation of contaminated transport characteristics through in-situ tracer test and column test, Geo-environmental Engineering; Contaminant Ground: Fate of Pollutants and remediation, pp99-105, 1997.

3.Xu & Eckstein; Use of least-squares method in evaluation of relationship between dispersivity and field scale, groundwater, vol.33, No.6, pp905-908, 1995

4.Eguchi,M. and Sasaki,S. : Biotreatability Studies for Remediation of TCE-Contaminated Groundwater, The Proceedings of The First International Conference on Remediation of Chlorinated and Recalcitrant Compounds, pp187-192, 1998

Groundwater Contamination from Agro-chemicals in Irrigated Environment : *Field Trials*

Jehangir Khan Sial[1] and Sajid Mahmood[2]

[1]Director Research/Chairman, Department of Structures and Environmental Engineering, University of Agriculture, Faisalabad, Pakistan.
[2]Lecturer, Department of Irrigation & Drainage, University of Agriculture, Faisalabad, Pakistan.

ABSTRACT: This paper highlights on the increasing fears that chemicals in agriculture have found their way into drinking water causing health complications. In fact, many chemicals have not had these effects but waiting to do so by moving into groundwater, sinking slowly and finally going into taps. Nitrate fertilizer is largely blamed for these fears. Use of fertilizer obviously would increase manifold to meet the food needs arising out of population explosion and it would further aggravate the situation. Therefore, the use of chemicals in agriculture presents a global alarm particularly for Pakistan where environmental degradation is rampant and unfortunately least attended. It necessitates development of Best Management Practices (BMP's) to reduce groundwater contamination resulting from application of agricultural chemicals especially the fertilizer. The study conducted at the University of Agriculture for reducing fertilizer pollution of groundwater is presented in this article.

Key words. Water pollution, Fertilizer, Nitrates, Irrigation, Contamination.

INTRODUCTION

Among all the agricultural concerns, agro-chemicals have given rise to grave environmental contamination. An unthoughtful use of chemicals may render agricultural land, water and air inefficient for supporting life. It is unfortunate that most of the public environmental protection programs are urban-oriented, whereas the pollution and its direct effects in the local sectors are ignored. As much as 50 to 70% of the water resources are polluted due to contamination from agricultural activities (Lal and Stewart, 1994). This paper presents an attempt to discuss agriculture oriented environmental problems and highlights the experiments conducted to realize the Best Management Practices BMP's) to mitigate groundwater contamination.

Agro-chemicals: The agro-chemicals can be grouped into two broad categories i.e. biocides and fertilizers. Biocides are man made products such as insecticides, herbicides, fungicides, rodenticide, etc. They are poisonous substances deliberately disseminated to exploit their toxic properties. They cause pollution when they reach wrong targets. After a continuous use, these toxic chemicals are found in waters, air, soil and in the bodies of fish, birds, worms, eggs, in many human beings, mother's milk and possibly tissues of the unborn child. Some pesticides destroy enzymes, and block energy generating oxidation processes and initiate malignancy in the cells.

Dichloro-diphenyl-trichloroethylene (DDT) is, perhaps,s the most notorious chemical. It was used to kill both medical and agricultural pests saving millions of human lives as well as many from starvation. However, its indiscriminate over-use has caused worldwide environmental contamination and death of non-target organisms. Almost every body in the world has a measurable amount of DDT and its breakdown products. Toxic effects of DDT have migrated from areas of application to remote places. Even Alaskan Eskimos have traces of DDT in their body fat. DDT is strongly adsorbed to soil particles that make their way into rivers through soil erosion. Lakes, bays and reservoirs all tend to become traps for DDT because of large volume of sediments continually deposited in them. DDT attacks nervous and reproductive systems of human body. DDT can harm phytoplankton by inhibiting its photosynthesis and upset the O_2 balance of atmosphere (Anonymous, 1989). However, use of DDT has been banned and risk of its hazard is reducing. The level of global contamination resulting from the use of biocides needs no further emphasis. Some of the remedial measures to eliminate/reduce the hazards are as under:

- A better control over the disposal and dispersal of the chemical
- Use of carefully designed and calibrated spraying and dusting machines with possibly electrostatic spraying to magnetize spray drops and reduce drift losses.
- Field applications supervised by trained/qualified personnel.
- Use of protective devices e.g. mask, gloves, long boots, etc.
- Avoid long exposures of field workers to active material
- Scientific research to dig up new substances that may replace poisonous synthetic biocides.

Fertilizers Pollution: Use of fertilizers in agriculture is recognized as a potential source of water pollution. High Nitrate-nitrogen (NO_3-N) concentrations found in surface and groundwater is currently receiving considerable attention. A certain portion of
(NO_3-N) pollution comes from the use of agricultural fertilizers which can enter directly from the fields into the streams or underground sources. Report on water quality deterioration in Lake Biwa (Japan) showed that the drainage from agricultural land contributed to 47% and 23% of the total nitrogen and phosphorus respectively (Misawa and Kondoh, 1992). Groundwater pollution is of increasing concern in Pakistan as about 60 to 70% of the drinking water comes from wells (Sial et al. 1993). Pollution of drinking water supplies is being reported frequently.

At the University of Agriculture, Faisalabad, a study was conducted by taking 150 samples of drinking water from different parts of Faisalabad city. The results indicated higher nitrate contents in water of localities fed from industrial effluent, whereas areas with better drainage contained lower nitrate contents. Similar were the results from WASA tube-wells in the urban area (Yaqoob, 1990). No study, however, was available for the agricultural fields under the conditions of this region for understanding the leaching behavior of nitrates. Thus studies were planned to investigate the effect of varying amounts of tillage, nature of implements, doses of fertilizers, depth of irrigation and time of sampling after the fertilizers, depth of irrigation, and time of sampling after the fertilizer application. The nitrogenous fertilizers were applied under varying

soil and crop conditions at different places. For various treatments, the water samples were collected using porous cups and soil/water samples were analyzed for (NO_3-N) contents.

RESULTS AND DISCUSSION

In one of the experiments, five tillage treatments namely tine cultivator, sweep cultivator, disk harrow, M.B. plow and chisel plow were selected for comparing their effects on nitrate leaching. Fifteen plots, each measuring 57 x 10 m^2 in size, were used for making three replications of each treatment. All the plots were prepared once with their designated implements. At the time of wheat planting, 125 kg/ha of Diammonium Phosphate (DAP) was applied after seed-bed preparation with two sweep cultivations to all the plots. First, water sampling was carried out two weeks after DAP application at 0-30, 30-60, 60-90, 90-120 and 120-150 cm depths. Secondly water samples were taken one month after the application of urea (125 kg/ha) and a surface irrigation of 10 cm. The samples were analyzed for (NO_3-N) contents using Disulphonic acid method. The data on (NO_3-N) contents were analyzed statistically.

Nitrate-nitrogen contents present at different soil depths, two weeks after application of Diammonium phosphate (DAP), are given in Table 1. The data show higher contents of (NO_3-N) in the top soil layers. This was obvious as neither irrigation was applied nor any precipitation occurred during this time interval to transport the fertilizer downward. Mean (NO_3-N) contents in various soil layers after the application of urea with first irrigation are given in Table 2.

Analysis of variance of the data after irrigation indicated that the effect of depth of soil on (NO_3-N) contents tested statistically significant. A comparison of the values of (NO_3-N) contents before and after irrigation suggests that maximum concentration of (NO_3-N) was present in upper 0-60 cm layer. A noticeable leaching appears to have occurred upto 90 cm. Traces of nitrates were, however, found upto 150 cm soil depth just with a conventional dose of fertilizer and a single 10 cm irrigation. The exponential nature of data with increasing depth of soil further revealed that (NO_3-N) would even leach beyond 150 cm. This downward movement of nitrates would perhaps continue in the irrigations to follow. In case, this trend persists in our agricultural fields year after year, then the day is not too far when groundwater reservoir would be badly polluted.

The effect of tillage implements tested statistically non-significant. This was expected as there was little evidence for the nitrate concentration in each treatment to differ. The main focus was to study nitrate leaching behavior for view point of implement-depth interaction. A significant implement-depth interaction suggested that various tillage practices managed nitrates differently at each soil depth. However, sweep and tine cultivators showed better results compared with other implements. Sweep tilled plots were better than tine cultivation in retaining NO_3-N in the top (0-60 cm) soil layer. It is apparent that sweep cultivation can be considered as an appropriate tillage practice among the treatment included in this experiment. In short, the following conclusions were drawn from this study.

Table 1. Nitrate-nitrogen (ppm) for various tillage treatments (before irrigation)

Tillage treatment	Depth (cm)				
	0-30	30-60	60-90	90-120	120-150
a.Narrow time cultivator	10.6	3.54	2.13	1.13	0.53
b.Sweep cultivator	8.13	4.67	1.80	0.73	0.73
c.disk harrow	7.66	2.26	2.00	0.67	0.46
d.Moldboard (M.B) plough	6.86	2.60	1.20	0.40	0.00
e.Chisel plough	7.80	5.73	0.54	0.34	0.20

Table 2. Nitrate-nitrogen (ppm) for various tillage treatments (after irrigation)

Tillage treatment	Depth (cm)				
	0-30	30-60	60-90	90-120	120-150
a.Narrow time cultivator	8.33	5.40	2.53	1.46	0.67
b.Sweep cultivator	9.73	7.60	2.40	1.60	0.00
c.disk harrow	5.06	4.46	3.00	1.34	0.60
d.Moldboard (M.B) plough	4.86	2.86	1.54	1.06	0.34
e.Chisel plough	6.13	4.40	2.00	0.53	0.43

1. A normal 10 cm irrigation played a significant role in the downward movement of nitrates
2. Sweep cultivators and narrow tine were considered relatively appropriate for retaining nitrates in the 0-60 cm soil layer compared with other implements.
3. A noticeable leaching of nitrates was observed upto 90 cm after irrigation, whereas traces of nitrates upto 150 cm soil depth were observed. The nitrate contents exponentially decreased with the depth of soil. An extrapolation of this trend suggests nitrates would certainly move too far from soil depths considered here.

Another experiment was conducted on an area of 0.87 ha divided into three blocks and 24 plots. Begin text of second succeeding pages here. Do not leave additional margins inside the frame. At the University of Agriculture Faisalabad. Two tillage techniques (Sweep cultivator, Chisel Plow), two levels of surface irrigation (5 cm deep six irrigation and 10 cm deep four irrigation and two doses of fertilizer (split dose and normal dose) were compared to study their effects on NO_3-N leaching. Soil water samples were collected to determine the NO_3-N from the porous cups installed at 30, 60 and 120 cm depths at both head and tail ends of all the plot. Nitrate-nitrogen concentration of soil water samples were then detected adopting Hydrazine Reduction Method.

Field studies indicated that tillage treatment had significant effect on NO_3-N leaching. At 30 cm depth mean NO_3-N concentration in sweep cultivated plots were higher than those of the chisel plowed plots. However, higher NO_3-N concentration detected at 60 and 120 cm depths in chisel plowed plots illustrated migration of nitrates to lower depths. This is due to low density of deep soil layer and more pore space available for water and solute movement. Whereas, sweep cultivator generated low soil densities only near the surface and high soil densities underneath. Hence, sweep cultivator offered a better tillage option to reduce NO_3-N leaching away from the root zone.

Heavy irrigations produced loss of water through deep percolation and enhanced nitrate leaching. Whereas, light but frequent irrigations confined the nitrates in only upper soil layers. Similar to the pattern observed in sweep cultivation, light irrigations showed more nitrates at 30 cm depth, while at 60 and 120 cm depths higher NO_3-N concentration was observed for heavily irrigated plots. Light irrigations settled about 9.2% less NO_3-N concentration upto 120 cm depth. Results revealed that light but frequent irrigations held more nutrients within the root zone of the soils and thus proved to be a preferable alternative.

Comparatively more nitrate concentration were detected in upper soil layers even after the last irrigation in the split fertilized plots. About 19.4% less nitrate leaching was observed for split application compared with normal or conventional application. Split application checked fertilizer leaching by providing less amount of fertilizer exposed to the leaching agents. Hence, split fertilization proved useful by keeping most of the nitrates in the root zone for a longer period of time. In surface irrigation, the advancing sheet of water transported nitrates towards tail end of the plots. Tail ends showed 4.9% more nitrates than the head ends of the plots. This effect might be due to high solubility of nitrates in water. Therefore, medium length of plots with low grade are advisable to reduce transport of nutrients to tail ends. Results provided the following conclusions:-

1. Sweep cultivation proved a better tillage option to minimize NO_3-N leaching from the root zone.
2. Light but frequent irrigations checked nitrate movement to the deeper soil strata.
3. Split application of fertilizer reduced NO_3-N leaching and nitrate redistribution to deep-seated soil mantle.

The results of the present studies evidenced leaching of nitrogenous fertilizer in the form of NO_3-N upto 150 cm soil depth. Of about 30% of 41 million acres surveyed had water table within 150 cm from ground surface in Pakistan (Anonymous, 1989); apparently a sizeable part of our subsurface water reservoir is under direct threat of fertilizer pollution. Presently, Pakistan on the average uses 56 kg ha^{-1} of fertilizer as against 779 kg ha-1 in Holland (Sial et al. 1992). Thus the situation may further worsen as the use of fertilizer increases manifold in the years to come. Measures need to be taken to reduce the irreversible pollution of subsurface water. Unfortunately most of our anti-pollution programs are either urban or industry oriented and agricultural sector

is absolutely neglected. Drainage, tillage, irrigation, crop rotation and fertilizer practices need to be managed in order to reduce threat of fertilizer on subsurface water pollution. In particular, the present investigation suggests that improved practices of soil, water and fertilizer management may effectively reduce NO_3-N leaching and safeguard our soil and water environment.

GENERAL RECOMMENDATIONS

If the present trend in modernization of agriculture continues, pollution issues will become increasingly complicated in the future. What general model be adopted to minimize the pollution is rather more important than identification of problems. The following submissions provide a guideline to plan environmental strategies:

1. Important enough is to realize the fact that environmental protection is more of necessity than luxury. Good environment is key to sustainable development.
2. Availability of trained specialists is necessary for the successful execution and assessment of environmental projects. Thus, initiation of formal educational programs will be needed.

REFERENCES

1. Anonymous. (1989). International Waterlogging and Salinity Research Institute (IWASRI). Annual Report, Lahore, Pakistan.

2. Lal, R. and B.A. Stewart. (1994). Soil Processes and Water Quality - Advances in Soil Science. CRC Press Inc. Florida, pp. 409-427.

3. Misawa, S. and T. Kondoh. (1992). The Water quality problems in paddy irrigation and drainage. In: Murty V.V.N. and K. Koga (eds) " Soil and Water Engineering for Paddy Field Management" Proceedings International Workshop Jan. 28-30, 1992 A.I. T., Bangkok, Thailand.

4. Sial, J.K., M.A. Abbas and M.A. Sargana. (1991) Agricultural Impact on Environmental Pollution. Paper presented on "World Environmental Day, June 5, 1991" at Pearl Continental, Lahore.

5. Sial, J.K., F.H. Khan, N. Ahmad and S. Mahmood. (1992). Fertilizer-A Big Water Pollutant. Pakistan Journal of Agricultural Sciences. 29(4): 321-324.

6. Sial, J.K., S. Mahmood, N. Ahmad and M.S. Sabir. (1993). Nitrate-Nitrogen Management for Groundwater Quality. Proceedings of the International Symposium on Environmental Assessment and Management of Irrigation and Drainage Projects, CEWRE, UET, Lahore. (2): 48-54.

7. Yaqoob, M. (1990) Environmental Pollution and its Control in Pakistan. Human Environmental Cell, University of Agriculture, Faisalabad, Pakistan.

In-situ Electrokinetic Remediation of Soil and Water in Aquifer Contaminated by Heavy Metal

S. Shiba[1], Y. Hirata[1], and T. Seno[2]

[1] Department of Chemical Engineering, Graduate School of Osaka University, Toyonaka, Osaka 560-8531, Japan
[2] Department of Systems Engineering, Graduate School of Shizuoka University, Hamamatsu, Shizuoka 432-8561, Japan

Abstract. The electrokinetic method for the remediation of contaminated aquifers is realized by applying a fixed low voltage direct current between an anode and a cathode placed into the contaminated zone. The purge water is injected into the anode well and drawn out from the cathode well with the pollutants. Therefore the application of this method to in-situ remediation of aquifers is relatively simple. This method can be applied effectively to remove heavy metals. These cannot be decomposed by other methods such as bioremediation, although this method can be used also for decontamination of organic chemicals in aquifers. However, the variations of the operational variables of this method have not been made clear, because this method is relatively new and is an inovative technique. In order to investigate the operational variables of electrokinetic remediation, a mathematical model has been constructed based on the physico-chemical transport process of heavy metals in the pore water of a contaminated aquifer. The transport of heavy metals is driven not only by the hydraulic flow due to the purge water, but also by electromigration caused by the electric potential gradient. The electric potential between the anode and the cathode is the important operational variable for electrokinetic remediation. From the numerical simulations using this model it is confirmed that remediation starts from the upstream anode and the heavy metal is gradually transported downstream towards the cathode and is drawn out through the purge water.

Key words. Electric potential gradient, Electromigration, Ionized heavy metal, Porous medium, Soil and groundwater purification

INTRODUCTION

The need for water resources is increasing more and more not only in developed countries but also in developing countries. Groundwater is utilized as one of the important water resources supplementing surface water. However, in many aquifers groundwater has been seriously contaminated by the migration of various hazardous organic and inorganic chemicals from the disposal of municipal and industrial wastes. The increase in water demand makes it urgent to clean up contaminated groundwater and soil immediately.

Many new techniques have been presented for the remediation of groundwater and soil. Among them, one of the most cost-effective in-situ technologies is electrokinetic remediation. However, understanding of electrokinetic remediation is not only experimentally but also theoretically quite insufficient. This is because the technique is relatively new and innovative, although the electrokinetic method has been utilized previously in civil engineering for dewatering soil. This paper aims to develop a mathematical model based on physico-chemical mass transport theory and to simulate the nonsteady characteristics of the electrokinetic remediation. Only a few studies ([1], [2], [3], [6], [7], [8], [9] and [10]) can be utilized for comparison with the mathematical model.

The electrokinetic method consists of installing electrodes (anode and cathode) into the aquifer zone requiring treatment, which is saturated with groundwater or purge water, and applying a fixed low voltage direct current between the electrodes, as shown in Figure 1. Heavy metals are typically ionized into cations in groundwater (e.g., Cu^{2+}, Pb^{2+}, and so on). Purge water is injected into the anode well and contaminant-concentrated water is drawn out from the cathode well. The injection of purge water causes a hydraulic flow from the anode to the cathode. The electrokinetic driving force, which acts on the ionized heavy metal (cation), is superposed on the hydraulic flow so that the heavy metal is accelerated and migrates to the cathode well where it can be swept out of the contaminated aquifer.

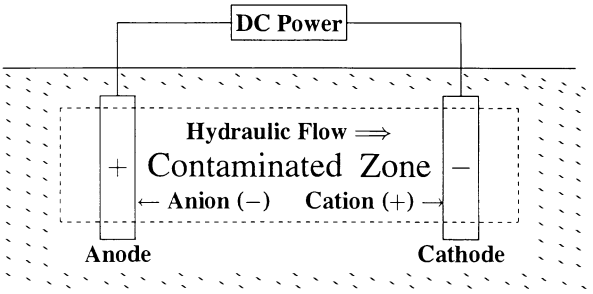

Fig. 1. Schematic Representation of Electrokinetic Remediation. Chemicals, i.e., cations (heavy metals) and anions are transported by the hydraulic flow due to the injection of purge water in conjunction with electromigration due to the applied electric potential.

MATHEMATICAL MODEL OF ELECTROKINETIC REMEDIATION

Governing Equation. The model developed here is composed of a kind of advective diffusion equation and its boundary conditions. In pore water, cations migrate to the cathode and anions migrate to the anode. Under steady uniform flow, the equation of conservation of mass, which considers the advection, dispersion, and sorption for chemical species k in saturated homogeneous isotropic media, can be described as follows [8]:

$$\frac{\partial}{\partial t}(\mathrm{n}\mathrm{Rd}_\mathrm{k}C_\mathrm{k}) + \frac{\partial}{\partial z}\{(u_\mathrm{S} - u^*_\mathrm{ezk})C_\mathrm{k}\} = \mathcal{D}^*_\mathrm{k}\frac{\partial^2 C_\mathrm{k}}{\partial z^2} + \mathrm{n}R^\mathrm{aq}_\mathrm{k} \qquad (1)$$

where C_k = concentration of species k (mol/L); u_S = pore flow velocity (cm/s); n = porosity of soil (−); Rd_k = retardation factor (−); R^aq_k = molar rate due to liquid-phase chemical reactions (mol/L/s); and $\mathcal{D}^*_\mathrm{k}$ and u^*_ezk = effective diffusion coefficient and effective electromigration velocity, respectively, as:

$$\mathcal{D}^*_\mathrm{k} = \frac{\mathrm{n}}{\tau^2}\mathcal{D}_\mathrm{k}\,; \qquad u^*_\mathrm{ezk} = \frac{\mathrm{n}}{\tau^2}u_\mathrm{ezk} \qquad (2), (3)$$

where τ = tortuosity obtained experimentally (−); $\mathcal{D}_\mathrm{k}$ = diffusion coefficient of species k in pore water (cm^2/s); and u_ezk = electromigration velocity (cm/s).

Retardation factor. The chemical reaction is composed of a homogeneous liquid-phase reaction, which generates the molar rate R^aq_k in pore water, and a heterogeneous adsorption-desorption reaction between pore water and soil, which generates the molar rate R^sp_k. The retardation factor Rd_k is introduced to consider R^sp_k (Inoue and Kaufman [4]). The retardation factor is defined by:

$$\mathrm{Rd}_\mathrm{k} = 1 + \frac{(1-\mathrm{n})\rho}{\mathrm{n}}\mathrm{Kd}_\mathrm{k}\,; \qquad \mathrm{Kd}_\mathrm{k} = \frac{\partial s_\mathrm{k}}{\partial C_\mathrm{k}} \qquad (4), (5)$$

where ρ = density of soil solids (g/cm^3); $\mathrm{Kd_k}$ = distribution coefficient of species k (L/g); and s_k = absorbed concentration of species k per unit mass of soil solid (mol/g). The adsorption isotherms between s_k and C_k are generally expressed by a linear function.

Electromigration velocity. The electromigration velocity u_{ezk} plays an important role in the remediation and is given by:

$$u_{ezk} = \frac{\mathrm{F}}{\mathrm{RT}} z_k \mathcal{D}_k \frac{\partial \phi}{\partial z}\,; \qquad \frac{\partial \phi}{\partial z} = -\frac{\mathrm{RT}}{\mathrm{F}}\,\mathrm{f}(t,z) \tag{6),(7}$$

$$\mathrm{f}(t,z) = \frac{\left[\sum (z_k \mathcal{D}_k^* \frac{\partial C_k}{\partial z}) + 10^3 \frac{i_S^*}{\mathrm{Fn}}\right] - u_S \sum (z_k C_k)}{\sum (z_k^2 \mathcal{D}_k^* C_k)}\,; \quad i_S^*(t) = \frac{\mathrm{n}}{\tau^2} i_S(t) = \frac{\mathrm{n}}{\tau^2}\frac{I(t)}{A} \tag{8),(9}$$

where F = Faraday's constant (C/mol); R = universal gas constant (J/K/mol); T = water temperature ($^\circ$K); z_k = charge number of species k (−); ϕ = electric potential (V); and i_S^* = effective current density (A/cm^2). The factor 10^3 multiplying i_S^* is introduced since C_k is specified in mol/L as usual practise. Since $i_S(t) = I(t)/A$, $i_S^*(t)$ is given by Eq(9), where $I(t)$ = electric current from power unit (A) and A = cross sectional area of soil column (cm^2).

Electric potential. Integrating Eq(7), $\phi(t,z)$ along the experimental column is estimated by:

$$\phi(t,z) = \phi(t,0) - \frac{\mathrm{RT}}{\mathrm{F}} \int_0^z \mathrm{f}(t,z)\,\mathrm{d}z \tag{10}$$

Then the potential difference E (Volts) applied betweeen the anode ($z = 0$) and the cathode ($z = L$), which is taken to be an operational variable, is obtained by:

$$E(t) = \phi(t,0) - \phi(t,L) \tag{11}$$

Initial condition. The initial condition for the governing equation, Eq(1), specifies the concentrations of chemical species in the pore water at $t = 0$ and is simply given by:

$$C_k = C_{k0} \qquad \text{at} \qquad t = 0 \tag{12}$$

Boundary conditions. At the anode, $\mathrm{H_2O}$ gives electrons to the electrode, as described by Eq(13). At the cathode, $\mathrm{H_2O}$ takes electrons from the electrode and releases hydrogen gas and $\mathrm{OH^-}$, as described by Eq(14).

$$2\mathrm{H_2O} - 4\mathrm{e^-} \rightarrow \mathrm{O_2(g)} + 4\mathrm{H^+}\,; \quad 2\mathrm{H_2O} + 2\mathrm{e^-} \rightarrow \mathrm{H_2(g)} + 2\mathrm{OH^-} \tag{13),(14}$$

The production rate of $\mathrm{H^+}$ at the anode and of $\mathrm{OH^-}$ at the cathode can be expressed in terms of their fluxes as follows:

$$J_{\mathrm{eH}}^* = 10^3 \frac{i_z^*}{z_H \mathrm{F}}\,; \qquad J_{\mathrm{eOH}}^* = 10^3 \frac{i_z^*}{z_{OH}\mathrm{F}} \tag{15),(16}$$

where i_z^* = effective electric current density. J_{eH}^* and J_{eOH}^* are superposed on J_H^* (for $\mathrm{H^+}$) and J_{OH}^* (for $\mathrm{OH^-}$), respectively. Then, the boundary conditions in terms of fluxes of chemical species can be stated as ($i_z^* = i_S^*/\mathrm{n}$; $z_H = +1$; and $z_{OH} = -1$):

$$\frac{\partial(D_k^* C_k)}{\partial z} + (u_S - u_{ezk}^*) C_k = \left\{ \begin{array}{ll} u_S C_k^{\mathrm{dN}} + 10^3 \frac{i_S^*}{\mathrm{Fn}}\,, & \text{for } \mathrm{H^+} \\ u_S C_k^{\mathrm{dN}}\,, & \text{for others} \end{array} \right\} \quad \text{at } z = 0 \tag{17}$$

$$-\frac{\partial(D_k^* C_k)}{\partial z} + (u_S - u_{ezk}^*) C_k = \left\{ \begin{array}{ll} u_S C_k - 10^3 \frac{i_S^*}{\mathrm{Fn}}\,, & \text{for } \mathrm{OH^-} \\ u_S C_k\,, & \text{for others} \end{array} \right\} \quad \text{at } z = L \tag{18}$$

Dimensionless governing equation. Eq(1) can be solved numerically using the initial condition, Eq(12), and the boundary conditions, Eqs(17) and (18). For the convenience of numerical calculation, the following dimensionless variables and constants are introduced:

$$\widehat{C}_{\mathrm{k}} = \frac{C_{\mathrm{k}}}{C_0}\,; \qquad \widehat{t} = \frac{\mathcal{D}_0 t}{\mathrm{nRd}_0 L^2}\,; \quad \widehat{z} = \frac{z}{L}\,; \qquad \widehat{\phi} = \frac{\mathrm{F}}{\mathrm{RT}}\,\phi \qquad (19),(20),(21),(22)$$

$$\widehat{\mathcal{D}}^{\star}_{\mathrm{k}} = \frac{\mathcal{D}^{\star}_{\mathrm{k}}}{\mathcal{D}_0}\,; \qquad \widehat{u}_{\mathrm{S}} = \frac{L}{\mathcal{D}_0} u_{\mathrm{S}}\,; \qquad \widehat{u}^{\star}_{\mathrm{ezk}} = \frac{L}{\mathcal{D}_0} u^{\star}_{\mathrm{ezk}} \qquad (23),(24),(25)$$

$$\widehat{R}^{\mathrm{aq}}_{\mathrm{k}} = \frac{L^2}{\mathcal{D}_0 C_0}(\mathrm{n} R^{\mathrm{aq}}_{\mathrm{k}})\,; \qquad \widehat{\mathrm{Rd}}_{\mathrm{k}} = \frac{\mathrm{Rd}_{\mathrm{k}}}{\mathrm{Rd}_0}\,; \qquad \widehat{i} = 10^3 \frac{L}{\mathrm{nF}\mathcal{D}_0 C_0}\, i \qquad (26),(27),(28)$$

where L = distance between anode and cathode (cm); and subscript "$_0$" denotes the standard quantity for normalization. The dimensionless form of the governing equation becomes:

$$\frac{\partial(\widehat{\mathrm{Rd}}_{\mathrm{k}}\widehat{C}_{\mathrm{k}})}{\partial \widehat{t}} + \frac{\partial}{\partial \widehat{z}}\left\{(\widehat{u}_{\mathrm{S}} - \widehat{u}^{\star}_{\mathrm{ezk}})\widehat{C}_{\mathrm{k}}\right\} = \frac{\partial^2}{\partial \widehat{z}^2}(\widehat{\mathcal{D}}^{\star}_{\mathrm{k}}\widehat{C}_{\mathrm{k}}) + \widehat{R}^{\mathrm{aq}}_{\mathrm{k}} \qquad (29)$$

Chemical reactions. The contaminat treated here is copper sulfate (heavy metal). In this case the chemical reactions in the pore water can be expressed as follows:

$$\mathrm{CuSO_4} \rightleftharpoons \mathrm{Cu^{2+}} + \mathrm{SO_4^{2-}} \quad (\mathrm{K_1})\,; \qquad \mathrm{H_2SO_4} \rightleftharpoons \mathrm{H^+} + \mathrm{HSO_4^-} \quad (\mathrm{K_2}) \qquad (30),(31)$$

$$\mathrm{HSO_4^-} \rightleftharpoons \mathrm{H^+} + \mathrm{SO_4^{2-}} \quad (\mathrm{K_4})\,; \qquad \mathrm{H_2O} \rightleftharpoons \mathrm{H^+} + \mathrm{OH^-} \quad (\mathrm{K_W}) \qquad (32),(33)$$

where $\mathrm{K_1}$, $\mathrm{K_2}$, $\mathrm{K_4}$, and $\mathrm{K_W}$ are dissociation constants. The concentrations are defined as follows:

$$(C_1,\, C_2,\, C_3,\, C_4,\, C_5,\, C_6) = ([\mathrm{CuSO_4}], [\mathrm{Cu^{2+}}], [\mathrm{SO_4^{2-}}], [\mathrm{HSO_4^-}], [\mathrm{H^+}], [\mathrm{OH^-}]) \qquad (34)$$

NUMERICAL SIMULATION

The simulations were carried out under the following conditions: column length (L) = 40 cm; cross-sectional area of column (A) = 100 cm^2; porosity (n)= 0.4; tortuosity (τ) = 1.5; flow rate (Q) = 0.01 cc/s; applied voltage (E) = 5 V; inflow acidity (pH) = 7; and initial acidity of pore water (pH) = 6. Figure 2 reveals that the distributions of Cu^{2+} concentration ($\widehat{C}_2$) in the column are almost linear.

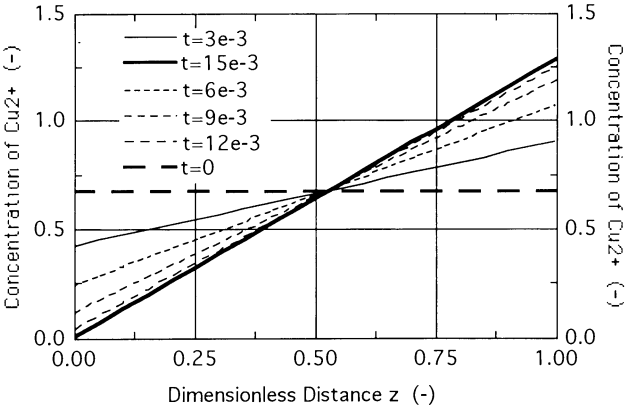

Fig. 2. Distribution of Cu^{2+} concentration between anode and cathode.

Time variation of the anode (upstream) and of the cathode (downstream, i.e., effluent) concentration of Cu^{2+} are shown in Figure 3. From these figures it can be seen that copper is removed from the anode (upstream end) and it is transported and accumulated near the cathode. In addition, with time, the anode concentration decreases whilst the cathode concentration increases. These distributions accord qualitatively with the experimental results for heavy metals obtained by Nekrasova and Korolev [5] using a one-dimensional column. Distribution of pH between the anode and the cathode is shown in

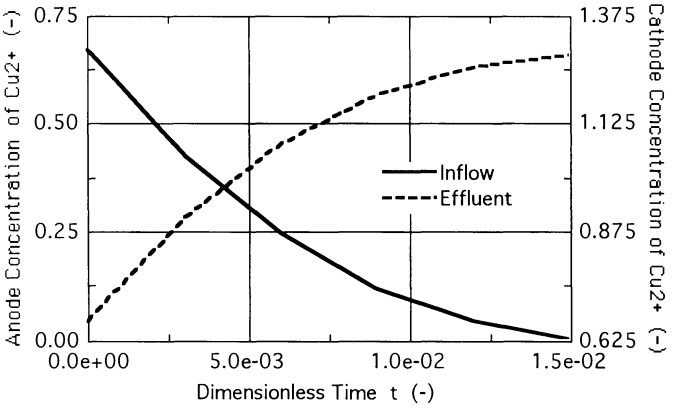

Fig. 3. Time variation of Cu^{2+} concentration at anode and cathode.

Figure 4. Since hydrogen ion, H^+, is produced at the anode and hydroxyl ion, OH^-, at the cathode, it is supposed that, with the passage of time, pH at the anode should decrease and pH at the cathode should increase, i.e., pH distribution curves are expected to have an ascending gradient and exhibit an acid front (sharp increase of pH in the distribution). Figure 5 demonstrates the time variation of electrical

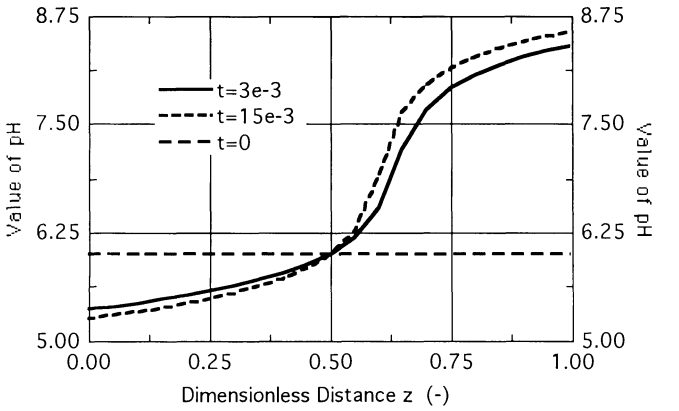

Fig. 4. Distribution of pH between anode and cathode.

potential (voltage) distribution in the column. The initial distribution is linear. However, the distribution curve expands upward in the upstream region (less steep than initial distribution), and contracts to the initial line (steeper than initial distriution) in the downstream region. The steepest portion corresponds to the pH jump in Figure 4. This means that, with the passage of time, the electric resistance

is concentrated near the pH jump portion and then, in the upstream region of the column before the pH jump, the resistance becomes smaller than the initial resistance. The decrease in resistance may be due to increase in the ion density of pore water.

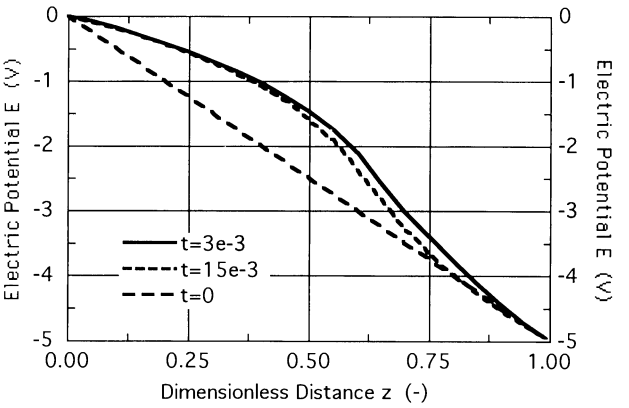

Fig. 5. Distribution of electric potential E between anode and cathode.

CONCLUSIONS

From the numerical simulation of decontaminating heavy metal (copper sulfate) from soil, using a 1-D mathematical model, it may be concluded that:
(1) Electrokinetic remediation is theoretically proved to be effective for removal of heavy metals in aquifers;
(2) The pH distribution in the column is well simulated numerically by the mathematical model; and
(3) The electric resistance of the column becomes smaller than the initial resistance in the upstream region (before the pH jump) and becomes larger in the downstream region .

REFERENCES

1. Alshawabkeh, A. N., Acar, Y. B., (1992) Environ. Science Health A27: 1835-1861
2. Bruell, C. J., Segall, B. A., Walsh, M. T., (1992) J Environmental Engineering ASCE 118: 68-83
3. Eykholt, G. R., Daniel, D. E., (1994) J Geotechnical Engineering ASCE 120: 797-815
4. Inoue, Y., Kaufman, W. J., (1963) Health Physics 9: 705-715
5. Nekrasova, M. A., Korolev, V. A., (1997) In: Marinos, P. G. et al (eds) Engineering Geology and the Environment Vol.2, pp.2047-2052
6. Rodsand, T., Acar, Y. B., Breedveld, G., (1995) In: Acar, Y. B., Daniel, D. E. (eds) Geoenvironment 2000 Vol.2, pp.1518-1534
7. Segall, B. A., Bruell, C. J., (1992) J Environmental Engineering ASCE 118: 84-100
8. Shapiro, A. P., Renaud, P. C., Probstein, R. F., (1989) Physico Chemical Hydrodynamics 11: 785-802
9. Penn, M., Savvidou, C., (1997) Marinos, P. G. et al. (eds) Engineering Geology and the Environment Vol.2, pp.2081-2086
10. Taha, M. R., Acar, Y. B., Gale, R. J., (1997) Marinos, P. G. et al. (eds) Engineering Geology and the Environment Vol.2, pp.2209-2214

Use of Global Optimisation Technique in Groundwater Pumping Strategy for Plume Removal

Shreedhar Maskey, Andreja Jonoski and Dimitri P. Solomatine

International Institute for Infrastructural, Hydraulic and Environmental Engineering (IHE), Hydroinformatics Section, P. O. Box 3015, 2601 DA, Delft, The Netherlands.

ABSTRACT: The remediation of groundwater contamination by pumping and injection is generally a long-term strategy and requires a huge amount of money. Aquifer cleanup time is a highly non-linear function of pumping rates and well locations, and there exist multiple local minima. The objective of a cleanup strategy often involves minimising or constraining the cleanup time or cleanup cost. Linear programming and non-linear optimisation techniques used in practice cannot guarantee a global solution. In this study, a Global Optimisation (GO) technique is used to minimise both cleanup time and cleanup cost, taking pumping rates and/or well locations as decision variables. Two contaminated aquifers are considered – one real and one hypothetical. The models, MODFLOW and MODPATH, developed by the United States Geological Survey (USGS) are used for groundwater flow and particle tracking, and the code, GLOBE, developed by IHE, Delft is used as a GO tool. The technique essentially involves the coupling of MODFLOW and MODPATH with GLOBE so as to run them in a loop. Results are compared using four algorithms, namely Genetic Algorithm (GA), Adaptive Cluster Covering (ACCO), Controlled Random Search (CRS4) and Multis. Results, in all cases, show that both cleanup time and cleanup cost can be reduced significantly using this technique.

KEY WORDS: global optimisation, groundwater, multiple extrema, particle tracking, plume.

INTRODUCTION

The contamination of groundwater is a widespread problem and requires a huge amount of money for its remediation. In practice, many different approaches are used to design the 'best' remediation strategy. In the United States, contaminant removal to clean up the aquifer is the approach most typically sought by members of the public affected by groundwater contamination. The objective of this approach is to remove as much contamination as possible by pumping and injection, and return the groundwater to its original quality. For the engineering design of the cleanup procedures, a simulation and optimisation method is widely used in which the simulation is carried out with commonly available groundwater models for flow and transport while the optimisation is based on standard linear programming and non-linear optimisation tools[1].

Some examples of application of this approach are discussed in references [2], [3], [4], [5] and [6]. However, because of the fact that the problem of optimising the pumping strategy for the contaminant plume removal is highly non-linear and nonconvex, some researchers have used randomised search techniques, usually GA. For example, [7] presented an outer approximation method, [8] used a differential GA and [9] presented a similar approach using GA in conjuction with a dual reciprocity boundary element method. In addition, [10] coupled groundwater flow and solute transport codes MODFLOW and MT3D with GA for optimisation and applied them to a hypothetical and a field scale problem. [11] presented a new approach for repeatedly and successively obtaining the solutions of a linear forward simulation model subject to successive

perturbations. [12] and [13] used artificial neural networks (ANN) together with GAs for the optimal design of groundwater remediation schemes.

This paper presents the use of different Global Optimisation (GO) algorithms to determine the optimised combination of pumping rates and well locations for the removal of a contaminant plume. Simulation is carried out assuming that the contaminant transport travel times are based on advection alone. Four global optimisation algorithms, namely GA, ACCO, CRS4 and Multis are used. MODFLOW and MODPATH are used for groundwater flow and particle tracking respectively, and GLOBE is used for optimisation. All publications cited above using GO algorithms calculate the objective function based on the aquifer cleanup cost over a fixed period of time. Sometimes, however, it is necessary to clean up contamination as fast as possible for reasons not directly related to costs, such as legal requirements or public relations campaigns [3]. Therefore, in this study, the simulation-optimisation calculation is carried out for both cases: (1) with aquifer cleanup **time**, and (2) with aquifer cleanup **cost** as objective functions. The method is illustrated with applications to both a hypothetical and a real aquifer.

SIMULATION-OPTIMISATION

Flow and Particle Tracking Models. In the plume removal by pumping/injection system, pumping rates and well locations are major decision variables. For a given set of decision variables a flow model updates the hydraulic head (a state variable) and a particle tracking model computes the particle travel time and path lines. The total cleanup time of a contaminant plume by pumping can be viewed as a function of the transport of particles defined at the plume boundary. When all particles have reached a pumping well, the plume is said to be removed. Hence, the travel time of the slowest particle is assumed to be the total cleanup time. Considering the transport by advection only, the time it takes for a particle to flow to a pumping well is given by the integral along the particle flow path S(q) as follows [3]:

$$t(q) = \int_s \frac{1}{v(q)} ds \qquad (1)$$

where: q = vector of pumping and injection rates; t(q) = travel time of the particle; v(q) = velocity in the direction of flow; ds = incremental distance in the direction of flow; and S(q) = length of particle flow path.

Global Optimisation. Global optimisation is aimed at finding the best solution of constrained optimisation problems which (may) have various local optima [14]. GO techniques have particular advantages for problems in which other optimisation techniques are not of much help due to the existence of multiple extrema and/or difficulties in defining functions analytically. A GO problem with box constraints can be considered as: find an optimiser x^* such that

$$f^* = f(x^*) = \min_{x \in X} f(x) \qquad (2)$$

where the objective function $f(x)$ is defined in the finite interval (box) region of the n-dimensional Euclidean space as:

$$X = \{x \in \Re^n : a \le x \le b \quad (componentwise)\} \qquad (3)$$

This constrained optimisation problem can be transformed to an unconstrained optimisation problem by introducing a penalty function with a high value outside the specified constraints. In cases when the exact value of an optimiser cannot be found, we speak about its estimate and, correspondingly, about its minimum estimate [15]. Comprehensive description about the algorithms used in this study is found in [15].

Coupling of MODFLOW and MODPATH with GLOBE. Using the GLOBE system as an optimiser requires coupling it with the simulation model so that they execute as a single application without the necessity of interactive input during computation. To do this, two sets of executable programs are needed. The first program converts the GLOBE output file (searched values of parameters) as an input file to MODFLOW, whereas the second program takes the output from MODPATH and computes the objective function value to feed to GLOBE. The coupled model starts from GLOBE and runs in a loop until the selected algorithms generate an acceptable solution and a stopping criterion is met.

Optimisation Problem Formulation. Two separate optimisation problems are formulated : (1) for minimisation of cleanup time, and (2) for minimisation of cleanup cost (establishment cost and operation plus maintenance cost of pumping and wells). In both cases, pumping rates and well locations are decision variables. Upper and lower limits in pumping rates and specified area for well locations are considered as constraints. In addition, in the case of cost minimisation the limitation in cleanup time is also introduced as a constraint.

Optimisation of cleanup time. If the aquifer cleanup time is to be minimised, the objective function and the constraints can in general be defined as:

minimise: $t = f(q_1, q_2, ...q_n, c_1, r_1, c_2, r_2, ...c_n, r_n)$ (4)

subject to: $q_{min} \le (q_1, q_2, ...q_n) \le q_{max}$, $c_{min} \le (c_1, c_2, ... c_n) \le c_{max}$ and $r_{min} \le (r_1, r_2, ... r_n) \le r_{max}$. Where t = cleanup time; $q_1, q_2, ...q_n$ = pumping rates in wells 1, 2,...n; $c_1, c_2, ...c_n$ = column number (on grid) of wells 1, 2, ... n; $r_1, r_2, ... r_n$ = row number (on grid) of wells 1, 2, ... n; q_{min}, q_{max} = minimum and maximum ranges in pumping rates; c_{min} , c_{max} = ranges in column number for well locations; and r_{min} , r_{max} = ranges in row number for well locations

Optimisation of cleanup cost. The well installation cost (capital cost) and the operation and maintenance cost per year (annual cost) can be expressed as a function of total pumping rates as:

Capital cost = $c_1 \sum_{i=1}^{n} q_i^m$ (5)

Operation and maintenance cost per year = $c_2 Q^r$ (6)

The constants c_1 and c_2 depend on the unit rates (per unit pumping rate) of capital cost and annual cost respectively. The coefficients m and r are generally less than unity and they account for the rate of change (generally decrease) in per unit capital and annual costs respectively with respect to the increase in total pumping rate. Q is the total pumping rate of all wells and q_i are the pumping rates of individual wells with n being the number of wells. Thus, for the optimisation of total cost of well installation and pumping the objective function can be expressed as a function of pumping rates. Expressing the total cost in present worth the objective function and the constraints are defined as:

Minimise: $c_1 \sum_{i=1}^{n} q_i^m + c_2 \sum_{k=1}^{t} \frac{c_3 Q^r}{(1+D)^k}$ (7)

subject to: $t \le t_{max}$

The constraints in pumping rates and position arrays apply similarly as in the optimisation of cleanup time. In the above equation: t is the cleanup time in years, D is the discount rate (discounted from k^{th} year) and c_3 is the coefficient that takes the value unity if k is a whole number and has the value of the fraction part of k otherwise. The t_{max} is the maximum limit in cleanup time. If the resulting cleanup time is greater than the maximum limit the coupled model generates a high value of the cost outside the constraint limit (a penalty) as an objective function value.

APPLICATION EXAMPLES

Hypothetical aquifer. A hypothetical unconfined aquifer system is formulated. The total size of this aquifer is 1500 m x 1500 m with an average depth of 34.5 m. In plan, a square uniform grid size of 20 m x 20 m is used. Two types of boundary conditions, impervious (or zero flux) at two sides and constant head boundaries at the other two sides are specified. The hydraulic conductivity varies from 2 m/day to 30 m/day. The effective porosity of the soil is taken as 0.2 and recharge of 0.0005 m/day is specified throughout the area. A contaminant plume is defined in the middle of the aquifer, which covers 28 grids. In order to illustrate graphically the relationship between pumping rates and plume removal time, a plot of cleanup time against two varying pumping rates (say A and B) is shown in Fig. 1. Pumping is done by four wells with two wells pumping at a constant rate of 1000 m^3/day (11.57 L/s).

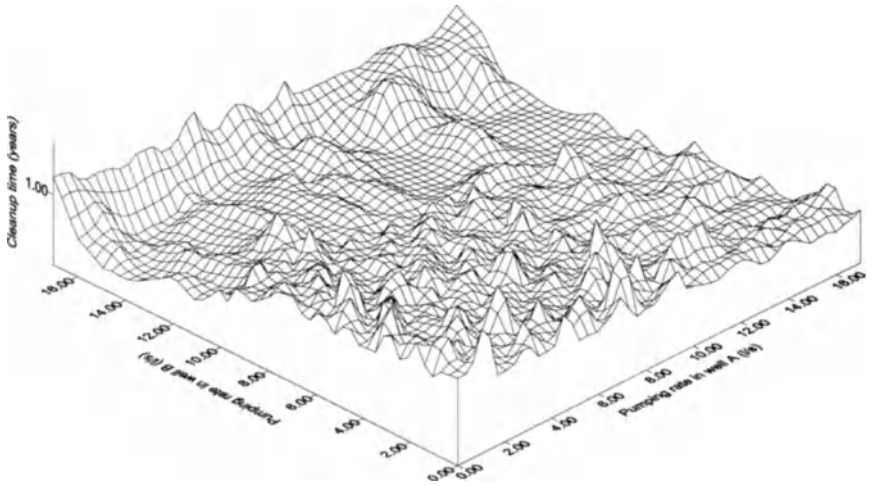

Fig 1. An illustration of nonconvex function of aquifer cleanup time and pumping rates.

Optimisation and results. Optimisation is carried out to minimise: (1) cleanup time and (2) cleanup cost with pumping rates and well locations as decision variables. In both cases, four wells are used for pumping. For each well, the range of pumping rates is defined from 0.0 (no pumping) to 1500 m^3/day. First, cleanup time is calculated without using the optimisation technique, keeping the maximum pumping rate (1500 m^3/day) in all wells with initially assumed locations. The cleanup time for this case is found to be 1080 days. Then the GO technique is applied by varying only pumping rates and fixing well locations as initial. The best optimal solutions (aquifer cleanup time) given by all four algorithms are in the range of 200 days with total pumping rates (sum of pumping rates of four wells) between 3580 to 4620 m^3/day. All optimal solutions and corresponding total pumping rates are significantly lower than the cleanup time of 1080 days resulted by the total pumping rate of 6000 m^3/day. These results are given in Table 1. In this case, CRS4 gives the best result (188 days), requiring 658 model runs, and ACCO is the fastest, requiring only 353 model runs. Optimisation is also carried out varying both the pumping rates and well locations. In this case the best solution given by CRS4 dropped to 151 days.

Table 1. Cleanup time optimisation- pumping rates as decision variable.

GO algorithms	Number of model run	Cleanup time (days)	Pumping rates (m^3/day)				
			Well-1	Well-2	Well-3	Well-4	Total
Without optimisation		1039	1500	1500	1500	1500	6000
GA	509	192	1210	1070	1100	740	4120
ACCO	**353**	191	1480	1000	950	1190	4620
CRS4	658	**188**	1170	1120	1070	760	4120
Multis	1583	207	390	1290	930	970	3580

The aquifer system is then optimised in the total cost of cleanup with the objective function defined by Eq. (7). In this case, only the pumping rates are taken as decision variables. The coefficients c_1 and c_2 are taken as 300 and 730, respectively assuming the resulting cost in US dollars. The coefficient m is taken as 0.75 whereas the r is taken equal to 1. The annual discount rate D is taken as 8.0 %. In addition to the limit in maximum pumping rate of 1500 m^3/day, the maximum limit in cleanup time of 5 years is introduced as a constraint. This means that the optimum cleanup cost is sought so as to remove the plume within the maximum time span of 5 years. Among the three algorithms used, CRS4 results in the best solution with the cleanup cost of US$ 13 280 (Table 2). This solution removes the plume in 1482 days (4.06 years).

Table 2. Cleanup cost optimisation- pumping rates as decision variables.

GO algorithms	Number of model run	Cleanup cost (US$)	Cleanup time (days)	Pumping rates (m^3/day)			
				Well-1	Well-2	Well-3	Well-4
GA	668	13 904	462	55	83	1350	0.0
ACCO	**315**	15 462	455	28	1461	55	28
CRS4	473	**13 280**	1482	28	28	413	28

Real aquifer. A contaminated aquifer at Semtin, in the outskirts of Pardubuce town, Czech Republic is considered. All data regarding this aquifer including boundary conditions, simulated hydraulic heads, hydraulic conductivity etc. are taken from [16]. This aquifer is contaminated primarily due to the waste disposal from chemical industries. The area covered by the plume is shown in Fig. 2.

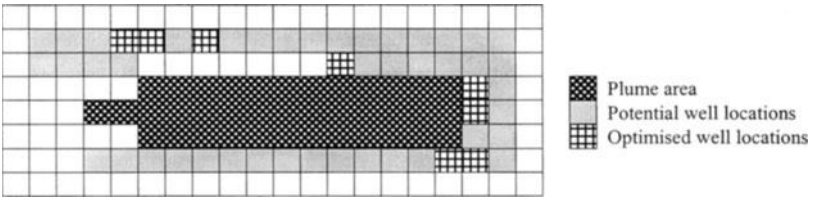

Fig 2. Plume area, potential well locations and optimised well locations given by GA.

Optimisation and results. In this aquifer area, as given by test wells [16], the maximum yield from each well is only 25.92 m^3/day (0.3 L/s). Therefore, to consider pumping rates as a decision variable has no significance. It is for this reason that the optimised solution is computed considering only the well locations as a decision variable. Nine pumping wells are assumed and the constant pumping rate of 25.92 m^3/day is assigned to each well. In this case, optimisation in

cleanup time is carried out using two algorithms: GA and ACCO. For the initially located well positions the resulting cleanup time is 35 years. The optimal solutions given by GA and ACCO are 13 and 14.8 years respectively, and these results were obtained after 1158 and 860 model runs respectively. Fig. 2 shows the optimised well locations given by GA within the potential locations together with the plume.

CONCLUSIONS

This study proves that the optimisation of pumping and injection strategy for contaminated groundwater remediation is a problem of multiple extrema (global optimisation problem) and shows the applicability of global optimisation techniques in such problems. It also shows that the cleanup time and therefore the cleanup cost are very susceptible to both pumping rates and well locations. Satisfactory results are obtained both in the minimisation of cleanup time and cleanup cost taking pumping rates and/or well locations as decision variables. The optimum solutions obtained from different algorithms are quite close but require noticeably different number of model runs. It is necessary to note that in different cases, the best results are obtained from different algorithms. In the examples used, ACCO was the fastest to reach the solution requiring, on average, less than two thirds of the number of model runs of GA and CRS4.

REFERENCES

1. Gorelick SM, Freeze RA, Donohue D and Keely JF (1993) Groundwater Contamination: Optimal Capture and Containment. Lewis Publishers.
2. Bogacki W and Daniels H (1989) Optimal Design of Well Location and Automatic Optimisation of Pumping Rates for Aquifer Cleanup. Proc., Int. Symposium on Contaminant Transport in Groundwater, 363-370.
3. Greenwald RM and Gorelick SM (1989) J. Hydrology 107: 73-98.
4. Chang L-C, Shoemaker C A and Liu PL-F (1992) Water Resour. Res. 28: 3157-3173.
5. Jonoski A, Zhou Y and Nonner J (1997) Hydrological Sciences J. 42: 937-953.
6. Willis R and Yeh WW-G (1987) Groundwater Systems Planning and Management. Prentice-Hall, Inc., pp 337-342.
7. Karatzas GP and Pinder GF (1993) Water Resour. Res. 29: 3371-3378.
8. Aral MM and Guan J (1996) Computational Methods in Water Resources XI: 349-357.
9. El Harrouni K, Ouazar D, Walters GA and Cheng AH-D (1996). Engineering Analysis with Boundary Elements 18: 287-296.
10. Wang M and Zheng C (1997) Ground Water 35: 757-764.
11. Wang PP and Zheng C (1998) Advances in Water Resources 21: 499-508.
12. Rao Z-F and Jamieson DG (1997) Hydrology and Earth System Sciences 1: 345-356.
13. Rogers LL, Dowla FU and Johnson VM (1995) Environ. Sci. Technol. 29: 1145-1155.
14. Pinter JD (1996) Global Optimisation in Action. Continuous and Lipschitz Optimisation: Algorithms, Implementation and Applications. Kluwer Academic Publishers, pp 3-7, 351-360.
15. Solomatine DP (1999) J Global Optimization 14: 55-79.
16. Nemecek J, Myl J and Nawalany M (1993) Optimal Control of the Contamination Plume under the Semtin Waste Disposal Site. TNO Environmental and Energy Research, TNO-report OS 93-58A.

Numerical Simulation of Nitrate Transport with Unsaturated Flow Condition in Volcanic Soils

Naoki Yamashita[1] and Satoru Sugio[2]

[1]Graduate School of System Eng., Miyazaki Univ., 1-1 Gakuen-Kibanadai-Nishi, Miyazaki, JAPAN 889-2192
[2]Dept. of Civil & Environmental Eng., Miyazaki Univ., 1-1 Gakuen-Kibanadai-Nishi, Miyazaki, JAPAN 889-2192

ABSTRACT. The groundwater contamination caused by NO_3-N is one of the environmental problems in the agricultural field. In the southern part of Kyushu Island in Japan, the unconfined aquifer is contaminated by NO_3-N. In this paper, NO_3-N transport in two types of volcanic soil was investigated In order to understand NO_3-N transport process in unsaturated flow condition, two experimental works were carried out under precipitation condition using vertical columns filled up with soils. Simulated rainfall of NO_3-N solution was generated on the top of columns. From the experiments, percolation processes of NO_3-N in the soils were observed. In addition, the experimental results were simulated by means of one-dimensional numerical model. In the model, advection-dispersion and biochemical reaction term taking heterotrophic processes into consideration was described. According to the simulated results, it was clarified that the characteristics of NO_3-N transport in each soil deeply depend on the biochemical reaction and the activity of bacteria in Shirasu was not as robust as it was in Ando soil.

Key Words. Groundwater contamination, Vertical column, Unsaturated seepage flow, biochemical reaction term

INTRODUCTION

The southern part of Kyushu Island in Japan has over 2,500 mm of annual precipitation and consists of thick aquifers with high permeability. These hydrologic conditions are suitable for ground water storage. All of water in this region depends on the groundwater resource. However, groundwater contamination caused by NO_3-N has been disclosed in the recent years around the local shallow aquifers, and the expansion of the contamination in the future is worried about [1]. According to the field research, it was pointed out that one of the causes in the contamination was considered by penetration of NO_3-N with rainwater in overload use of barnyard manure on the farmland [2]. Therefore, NO_3-N transport process under the ground is important to understand the contamination. The soils in this region include mainly two types of volcanic soil; that is, Ando soil and Shirasu. Ando soil covered all of ground surface in southern part of Kyushu Island and Shirasu formed thickly under Ando soil. NO_3-N transport in Ando soil during cultivation activity has been investigated up to now [3] [4] [5]. According to these studies, it was discussed that Ando soil contains plenty of bacteria and nitrification-denitrification processes, which were important for NO_3-N, were active. NO_3-N transport in Shirasu has not been investigated yet To understand NO_3-N transport process with unsaturated flow condition in each soil, laboratory experiments were carried out by means of vertical columns filled up with the soils. The experiment results were simulated using one-dimensional numerical model including the additive terms of advection-dispersion and biochemical reaction with unsaturated flow condition.

EXPERIMENT OF TRNSPORT IN VERTICAL COLUMNS

The experiments of NO_3-N transport were performed under precipitation condition by means of 155 cm and 305 cm vertical columns filled up with Ando soil and Shirasu, respectively. These soils were collected from actual field. The columns are made from plastic pipe of 14.3 cm in diameter Simulated rainfall in constant intensity was generated from the top of column. Firstly, simulated rainwater was applied for 10 days. Secondly, NO_3-N solution of constant concentration was applied for some days, and finally simulated rainwater was applied again up to the end of experiments. Experimental conditions are shown in Table 1. For the flow boundary, water table of constant level was set up at the bottom of column. Soil solution at each depth point of column, as shown in Fig.1, was gathered by means of soil moisture sampler with porous cup. Fig.2 and Fig.3 show the measured results of NO_3-N concentration with time at each depth point in Ando soil and Shirasu, respectively.

Table 1. Experimental conditions of NO_3-N transport

	Column length (from surface to water table)	Rainfall intensity	NO_3-N concentration	Loading term of NO_3-N solution
Ando soil	155 cm	5.4 mm/h	118.3 mg/l	3 days
Shirasu	305 cm	5.0 mm/h	100 0 mg/l	5 days

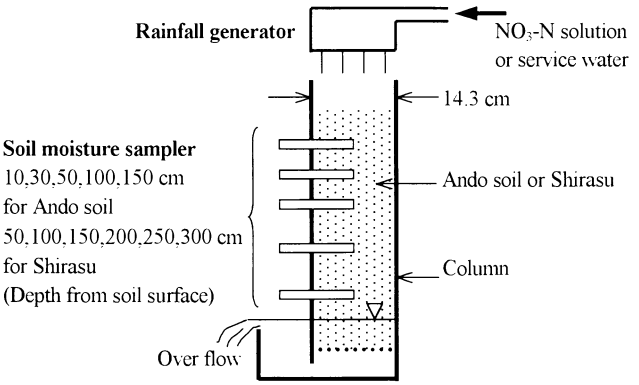

Fig.1. Experiment system with column

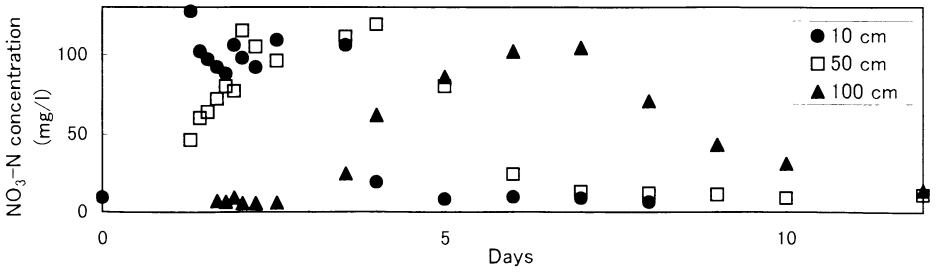

Fig.2. Measured concentration of NO_3-N at 10, 50, 100 cm depth in Ando soil

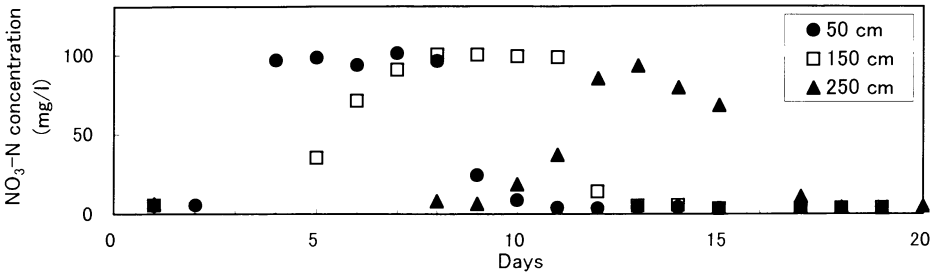

Fig. 3. Measured concentration of NO_3-N at 50, 150, 250 cm depth in Shirasu

NUMERICAL SIMULATION OF TRANSPORT

One-dimensional numerical model was introduced to simulate NO_3-N unsaturated transport observed in the experiments. In the model, the following terms are adopted for the description of NO_3-N transport [6][7] 1) advection or convection, which is the migration of solute with the unsaturated seepage flow 2) hydrodynamic dispersion, which is consisted of molecular diffusion and mechanical dispersion 3) biochemical source or sink, which is the interaction of nitrate, oxygen, organic carbon and bacteria. Finite difference method was used for numerical solution [8][9]. The governing equation for the unsaturated seepage flow is expressed by:

$$C_u(\psi)\partial\psi/\partial t = \nabla(k_u(\psi)\nabla\psi - k_u(\psi)) \tag{1}$$

where, C_u is rate of water content, ψ is capillary suction head and k_u is unsaturated hydraulic conductivity. Unsaturated seepage characteristics were expressed by the parameters of Van Genuchten equation [10] as following equations:

$$\begin{aligned} &S_e = \left[1/\left(1+|\alpha\psi|^n\right)\right]^m \quad , \quad k_u/k_s = S_e^{1/2}\left[1-\left(1-S_e^{1/m}\right)^m\right]^2 \quad , \quad m = 1-1/n \\ &S_e = (\theta-\theta_r)/(\theta_s-\theta_r) \end{aligned} \tag{2}$$

where, k_s is saturated hydraulic conductivity, θ is volumetric water content, θ_s is saturated water content to approximate to the value of porosity, θ_r is residual water content.

The NITRAT developed by Kinzelbach (1991) is one of the useful numerical models to simulate multi-species transport in saturated groundwater flow [11]. The computer code of NITRAT modified to unsaturated flow condition was used for the calculation of transport. This model describes heterotrophic processes, which takes the interaction of oxygen, nitrate nitrogen, organic carbon and bacteria into account. A set of governing equations are:

$$\partial(\theta NO_{3,u})/\partial t = -\nabla(qNO_{3,u}) + \nabla(\theta D(v)\nabla NO_{3,u}) - \theta\beta(NO_{3,u} - NO_{3,bio}) \tag{3}$$

$$\partial(\theta O_{2,u})/\partial t = -\nabla(qO_{2,u}) + \nabla(\theta D(v)\nabla O_{2,u}) - \theta\beta(O_{2,u} - O_{2,bio}) \tag{4}$$

$$\partial(\theta C_{org,u})/\partial t = -\nabla(qC_{org,u}) + \nabla(\theta D(v)\nabla C_{org,u}) - \theta\beta(C_{org,u} - C_{org,bio}) \tag{5}$$

$$\partial NO_{3,bio}/\partial t = -\gamma_{den}/Y_{den} - \gamma_{aer}\ Y_{aer} + \beta(NO_{3,u} - NO_{3,bio}) \tag{6}$$

$$\partial O_{2,bio}/\partial t = -\gamma_{aer}/Y_{aer} + \beta(O_{2,w} - O_{2,bio}) \quad (7)$$

$$\partial C_{org,bio}/\partial t = -\gamma_{den}/Y_{den} - \gamma_{aer} Y_{aer} + f_{live}\gamma_{dec} + \beta(C_{org,w} - C_{org,bio}) \quad (8)$$

$$\partial(X_{aer} + X_{den})/\partial t = \gamma_{aer} + \gamma_{den} - \gamma_{dec} \quad (9)$$

where, NO_3, O_2, C_{org} and X are the concentration of nitrate nitrogen, oxygen, organic carbon and bacteria, respectively. The subscripts *w*, *bio*, *aer* and *den* indicate pore water, biophase, aerobic and denitrifying, respectively. v is the seepage velocity, q (= $v\,\theta$) is the volumetric water flux, $D(v)$ (= a_L v+D_M) is dispersion coefficient, a_L is dispersion constant, D_M is molecular diffusion constant, β is exchange coefficient between pore water and biophase, Y is yield coefficient, f is utilizable portion of dead bacteria. γ defined as growth rate of bacteria is also expressed by the following equations:

$$\gamma_{aer} = \mu_{\max}^{aer}[1 - F(O_2)]\frac{C_{org}}{(K_c^{aer} + C_{org})}\frac{NO_3}{(K_{NO_3}^{aer} + NO_3)}\frac{O_2}{(K_{O_2}^{aer} + O_2)}X_{aer} \quad (10)$$

$$\gamma_{den} = \mu_{\max}^{den}F(O_2)\frac{C_{org}}{(K_c^{den} + C_{org})}\frac{NO_3}{(K_{NO_3}^{den} + NO_3)}X_{den} \quad (11)$$

$$\gamma_{dec} = \lambda(X_{aer} + X_{den}) \quad (12)$$

where, $\mu_{\max}$ is maximum growth rate of bacteria, K_i is half-velocity concentration for species i, λ is first-order decay coefficient, $F(O_2)$ is oxygen dependent weight.

Unsaturated seepage parameters were identified from experiments and tests as shown in Table 2 [12][13]. The initial concentration and the boundary condition of organic carbon and oxygen at ground surface are set as shown in Table 3. For the initial concentration of NO_3-N, measured values of each depth point were applied.

Table 2. Unsaturated seepage parameters

	k_s	θ_s	θ_r	a	n
Ando soil	1.12×10^{-3} cm/s	0.66	0.36	0.0370	3.80
Shirasu	2.25×10^{-4} cm/s	0.52	0.29	0.0286	4.78

Table 3. Initial and boundary values

	NO_3-N	O_2	C_{org}
Initial values	5.0-10.0 mg/l	0.5 mg/l	1.0 mg/l
Boundary values at the ground surface	0-118.3 mg/l	0.5 mg/l	1.0 mg/l

SIMULATED RESULTS

The biochemical parameters applied to the numerical model are shown in Table 4. Fig.4 shows the measured and simulated results in each depth point of vertical columns The simulated results agreed completely with the measured results except for the case of 150 cm depth in Ando soil. It is considered that the disagreement at 150 cm is caused by error of experiments but not by simulation. In the biochemical parameters, the bacteria concentration X was modified by trial method and finally decided

Table 4. Biochemical parameters used to NITRAT

Parameters	Values	Parameters	Values	Parameters	Values
β	10.0	X	3.0 or 0.3 mg/l	K_C^{aer}	0.76 mg/l
Y_{den}	0.4	a_L	0.01 m	K_C^{den}	0.5 mg/l
Y_{aer}	0.09	$K_{NO_3}^{aer}$	7.0 mg/l	$\mu_{\max}^{aer}$	0.64 1/d
f_{use}	0.9	$K_{NO_3}^{den}$	7.0 mg/l	$\mu_{\max}^{den}$	0.3 1/d
λ	0.2 1/d	$K_{O_2}^{aer}$	0.6 mg/l		

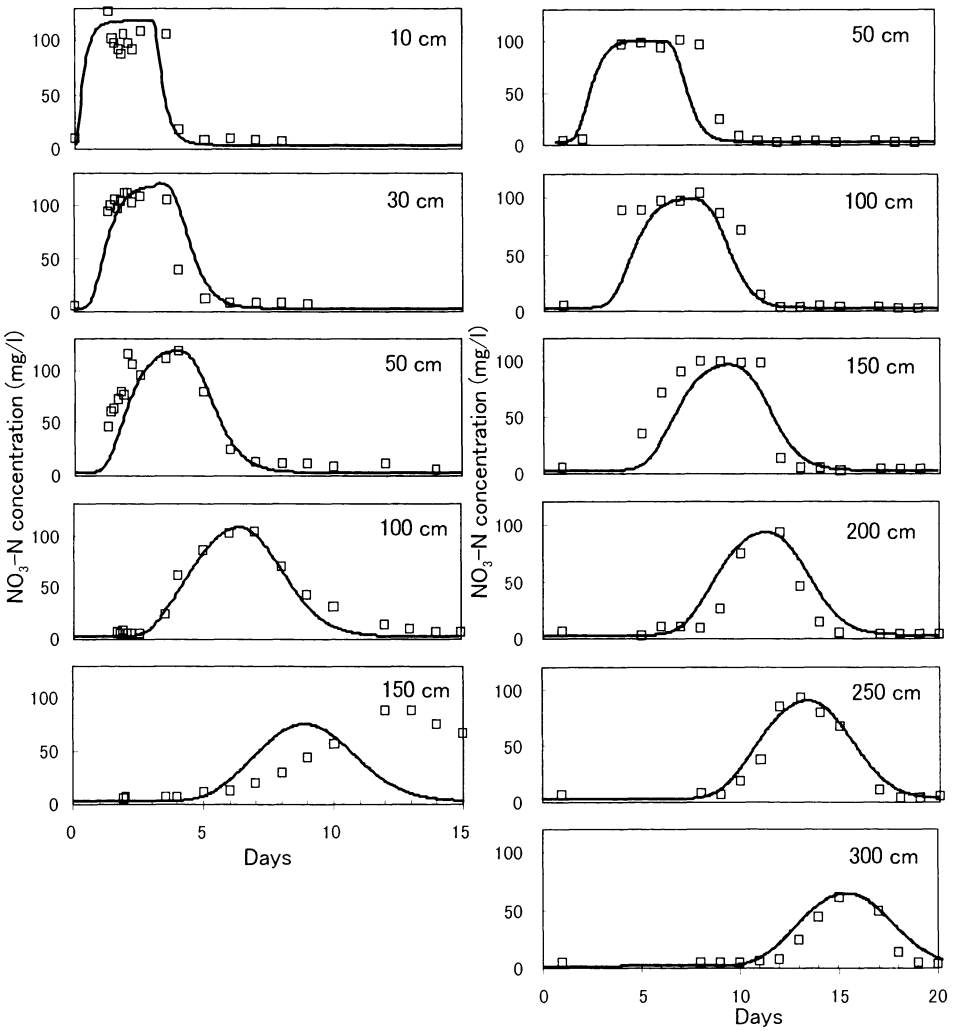

Fig.4. Measured and simulated concentration of NO_3-N at each depth point
(The left side is for Ando soil and the right side is for Shirasu in the figure. Solid lines show the simulated results and plotted marks indicate the measured results)

as 3.0 for Ando soil and 0.3 for Shirasu. This means that the difference of NO_3-N transport in Ando soil and Shirasu is deeply depends on the bacteria concentration X. Because the value of X controls the growth rate of bacteria as shown in equation (10), (11) and (12), X corresponds to the activity of bacteria in soil. Therefore, it can be recognized that the activity of bacteria in Shirasu was not as robust as it was in Ando soil.

CONCLUSION

The characteristics of NO_3-N transport in two types of volcanic soil were understood by means of numerical simulation taking biochemical source-sink term into consideration. According to the simulation applied with various values of bacteria concentration X, application of the bigger values of X generated the smaller values of NO_3-N concentration in the soil solution. The results show that simulated denitrification process depends on the value of X. The value of X in Shirasu was small compared to it in Ando soil. From the results, in the contaminated area in the southern part of Kyushu Island where Shirasu is thickly accumulated, it is estimated that the decrease of NO_3-N in Shirasu is not expected any more. In order to protect the groundwater from contamination in this region, it is emphasized that NO_3-N concentration in the soil is measured for all of the farmlands and the quantity of NO_3-N that percolate under the ground is controlled by managing the amount of barnyard manure loaded to the every farmland.

REFERENCES

1. Environmental Division of Miyakonojo City (1994) The promoting project of Groundwater Conservation in Miyakonojo City, pp 32-35
2. Yamashita N, Sugio S (1999) Movement of applied nitrogen in forage crops field, Proc. of Annual Meeting of Western Division of JSCE, pp 216-217
3. Sugio S, Imamura T (1991) Dissolution of fertilizer in Ando soils, Jour. of Groundwater Hydrology, Vol.33, No.3, pp 155-164
4. Kobayashi Y, Oshima H, Hasegawa I, Niimi H (1995) Dynamics of nitrogen in fields cultivated with forage crops in the warm and rainy region of Japan, The Bulletin of the Kyushu National Agricultural Environment Station, No.29, pp 109-162
5 Sugio S (1997) Experiments and numerical simulations of nitrate transport in Ando soil, Proc. 27th Cong. of IAHR, Theme C, pp 301-306
6. Momii K (1991) Computational methods for Groundwater analysis (10), 2-1. Fundamentals of solute transport analysis, Jour. of Groundwater Hydrology, Vol.33, No.2, pp 115-122
7. Nishigawa M, Hishiya T, Hashimoto N, Kohno I (1995) The numerical method for saturated-unsaturated fluid-density-dependent groundwater flow with mass transport, Jour of Geotechnical Eng., JSCE, No.511/III-30, pp 135-144
8. Bresler E (1973) Simultaneous transport of solute and water under transient unsaturated flow conditions, Water Resour. Res., Vol 9, No 49, pp 975-986
9 Nofziger D L, Rajender K, Sivaram K Nayudu, Pei-Yao Su (1989) CHEMFLO, One-dimensional water and chemical movement in unsaturated soils, U S. Environmental Protection Agency, pp 1-17
10. Van Genuchten, M Th (1980) A closed-form equation for predicting the hydraulic conductivity of unsaturated soils, Soil Sci. Am. Jour , Vol.44, No 5, pp 892-898
11. Kinzelbach W, Schäfer W (1991) Numerical modeling of natural and enhanced denitrification processes in aquifers, Water Resour. Res., Vol.27, No.6, pp 1123-1135
12. Sugio S, Okabayashi T (1994) Unsaturated permeability of Shirasu and its in-situ measuring methods, Jour. of Hydraulic, Coastal and Environmental Eng., JSCE, No.503/ II -29, pp.39-47
13 Yamashita N, Sugio S (1998) Measurement of NO_3-N in farm of Ando soil, Proc. of Annual Meeting of JSCE, pp 430-431

The Effect of an Heterogeneous Hydraulic Conductivity Field on the Spread of a Contaminant Plume in a Porous Aquifer: A Case Study in Portugal

Luís Ribeiro

CVRM-Geosystems Center, Instituto Superior Técnico
Av. Rovisco Pais, 1049-001 Lisboa, Portugal

ABSTRACT. A great majority of the areas selected by man for waste disposal sites purposes have been insufficiently characterized from the hydrogeological point of view. This ignorance and/or negligence has, in the past resulted in negative repercussions to the Environment. In order to better understand the flow and the movement pollutants through aquifers in the neighborhood of these sites, it is necessary to have an adequate description of an aquifer heterogeneity, especially as regards the identification of the impermeable boundaries between hydrostratigraphic units. These can vary strongly in thickness and can also be geometrically anisotropic and present different features concerning its neighborhood relationships. In a 1st phase, to take into account these special features, a 3D inter-correlation structural model was built. For this purpose, a non-parametric geostatistical methodology, based on an indicator approach, was applied to a coded lithological data extracted from borehole logs. After validation of the structural model with the experimental data, it was used to simulate the main hydrogeological units and to infer the stratigraphic boundaries. In a 2nd phase, the equiprobable images generated by a stochastic simulation technique are used as input to the mass transport model, previously implemented for the site. The results of various deterministic model runs constitute predictions of the influence of the spatial variability of the hydrogeological system on the uncertainty of the contaminant pathways and travel times. The proposed methodology was used to predict the impact of a waste disposal site in a porous aquifer in an area near Lisbon, Portugal

KEY WORDS: Groundwater pollution, waste disposal, heterogeneity, geostatistics, mass transport

INTRODUCTION

In order to better understand the flow and the movement of pollutants through aquifers in the vicinities of waste disposal sites it is necessary to have an adequate description of the aquifer heterogeneity in terms of the spatial distribution of the hydrostratigraphic units..

In a preliminary hydrogeological characterization and in the great majority of case studies, the only available hydrogeological data is lithological logs obtained from boreholes. Because we deal with an invisible resource, there is a growing need to obtain images that could reflect the uncertainty of the subsurface architecture. The interconnectedness of the hydrofacies influences the spatial patterns of hydraulic conductivity (K) and, consequently, they condition the pathways and travel times of the pollutant.

More and more, geostatistical techniques, are becoming preferred tools to perform adequate hydro-stratigraphic inter-correlations based on the lithological data extracted from well logs. For this purpose, the stratigraphic levels are coded according to a given lithological classification system, either in a binary way, as impermeable and permeable units [1, 2, 3] or using three distinct levels: impermeable, moderately permeable and very permeable [4].

In order to predict the uncertainty of the leachate plume dispersion, it is imperative to use together a mass transport model, which simulates the physical-chemical pollution processes in the aquifer media, and a stochastic model capable of generating various images of the heterogeneity of the system.

The goal of this paper is to apply a geostatistic-deterministic methodology to study the influence of spatial variability of hydro-stratigraphic units on the prediction of uncertainty of plume dispersion into an aquifer in the vicinity of a landfill.

GEOSTATISTICAL SIMULATION

The Geostatistical Conditional Simulation (CS) methodology is a Monte Carlo type technique with two important features: i) - it takes account of spatial correlations between parameter data and, ii) - the simulated variables are consistent with the measured ones at observed locations.

The visualization of several simulations gives an idea of the uncertainty of the phenomenon. These realizations were achieved by stochastic simulation algorithms and represent equally probable high-resolution models of the spatial distribution. Each simulation is conditioned in the sense that the resulting images maintain the hard data values at theirs respective locations. The simulated values of the variable also have the same statistical distribution and correlation structure as the true field. These are good representations of reality in some global sense and they measure the spatial uncertainty. In short, we can say that each CS is a different version of reality. Furthermore, the alternative images of a particular parameter produced by CS can be processed through a groundwater flow simulator to yield the corresponding measure of uncertainty of the response function [5].

A complete description of the model of uncertainty can be achieved by using a non-parametric approach called Indicator Geostatistics. This involves the calculation of the probability distribution function of the unknown value at any location, conditioned to the available information. A special coding must be used, to estimate the uncertainty in the hydrostratigraphic correlations. This is can be applied by assigning binary indicator values to impermeable and permeable levels based on a lithological classification system, using data extracted from borehole logs. This will reveal details that can be used to infer changes in deposition environments and to describe the boundaries of the units. By using these categorical variables the indicator formalism can provide an estimation of the probability that the sediment at a specific location is of a relatively high permeability.

HYDROGEOLOGICAL DATA

The site under study, named Vale de Milhaços, is located in the Setúbal Península near Lisbon, (see Figure 1). In this area two waste disposal sites, I and II, exist. The aquifer is unconfined and is one of the units of the Miopliocene groundwater system of Tejo extending over an area of 35km. From the lithological point of view it consists of sand, silty sands, gravel, sandstones and clays associated in an interbedded architecture with a total average thickness of 100m. Topographic gradients are about 4% and 8% SW. It is a highly permeable area, with well productivities of around 2 to 20 litres/sec.

Data from 84 borehole logs were discretized into 1m intervals. In consequence 5809 new data locations were obtained. Following a binary lithological classification criterion we have assigned

the following values to each location: 0 = impermeable and 1 = permeable. About 53% of the material. In the area is permeable.

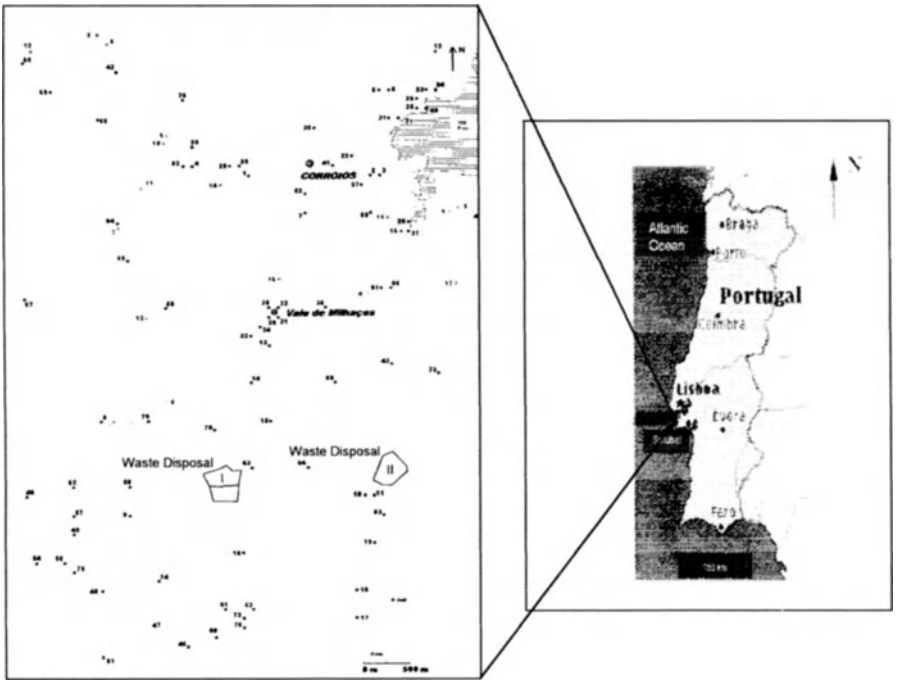

Fig. 1. Area under study, showing the 2 waste disposal sites and the locations of the lithological logs

INDICATOR STRUCTURAL ANALYSIS

After the coding process was completed, the 3D spatial correlation structure of the lithological units was described by means of variograms of the indicator variable. Structural analysis was performed in approximately horizontal and vertical directions. No significant geometric anisotropy was detected in the 2D horizontal plane. Only significant vertical range anisotropy ratios were found between the horizontal and vertical variograms. In the latter ones a two nested structure was detected with ranges of around 15 and 70m. The nugget effect is about 10% of the total variance. The variograms were modeled by spherical functions.

SPATIAL PATTERNS OF HYDRAULIC CONDUCTIVITIES

Using the above models we have performed an indicator simulation for the waste disposal sites area using a 20m X 100m X 0.5m grid with a total of 210000 nodes. For the calculations we have used the SISIM software, a sequential indicator simulation algorithm from the GSLIB package [6]. Due to the indicator coding used each simulated value represents the probability of finding at a specific depth, a lithological material of highest permeability.

For contaminant transport modeling purposes, maps of the spatial distribution of K are required. In order to obtain such maps probabilities were multiplied by a value of 0.001 m/s, which is the value of K corresponding to the highest permeable material existing in the aquifer, viz. clean sand. Figure 3 displays four spatial distribution patterns of K. They correspond to four simulations obtained for a cross–section of 600m X 120m in landfill area I (Fig.2).

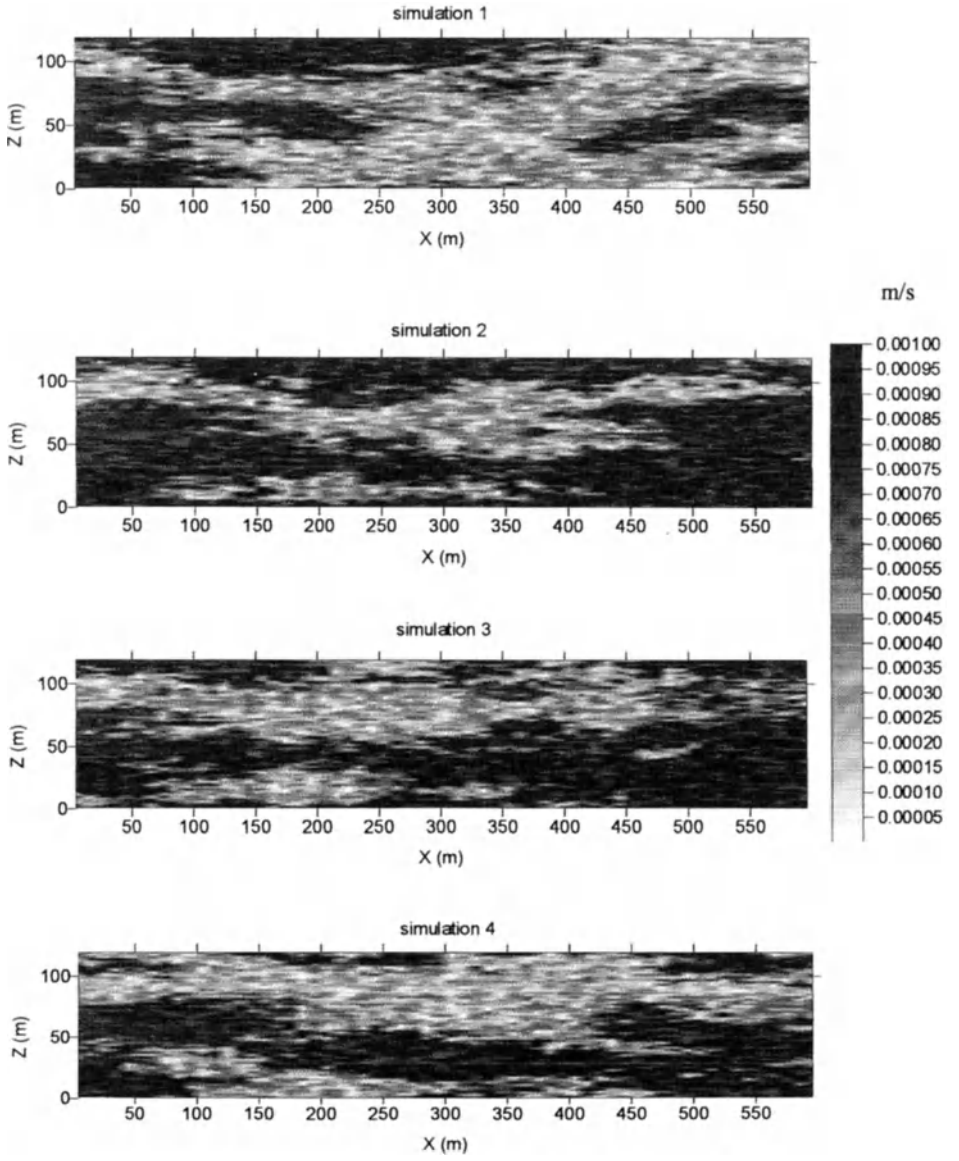

Fig. 2. Simulated images of the distribution of K along a cross-section through the landfill area

PREDICTION OF THE UNCERTAINTY OF LANDFILL PLUME DIFFUSION

A groundwater flow simulation was performed under steady-state conditions with an imposed hydraulic gradient observed in the field (5/1000). Because of its importance to public health we selected the mercury (Hg), one of the waste disposal constituents, as a potential pollutant

The advective-dispersive solute transport was simulated using the following parameters: Porosity = 30%; Molecular diffusion coefficient = 5x 10^{-10} m^2/s; Longitudinal dispersivity coefficient: 10m Transverse dispersivity coefficient: 0.5m. Continuous injection was estimated as 0.1 g/day and the total simulation time was set at 30 days.

Figure 3 displays the different shapes of plume dispersion resulting from the influence of the spatial variability of K on the pollutant preferential pathways in the aquifer. These images show either a plume spreading preferentially through the vertical direction (simulation 1) or through the groundwater flow direction (simulation 4). Note that, for the sake of clarity the images were restricted to the landfill area.

According to the Portuguese drinking water rules, the maximum admissible value for Hg is 0.001 mg/l.

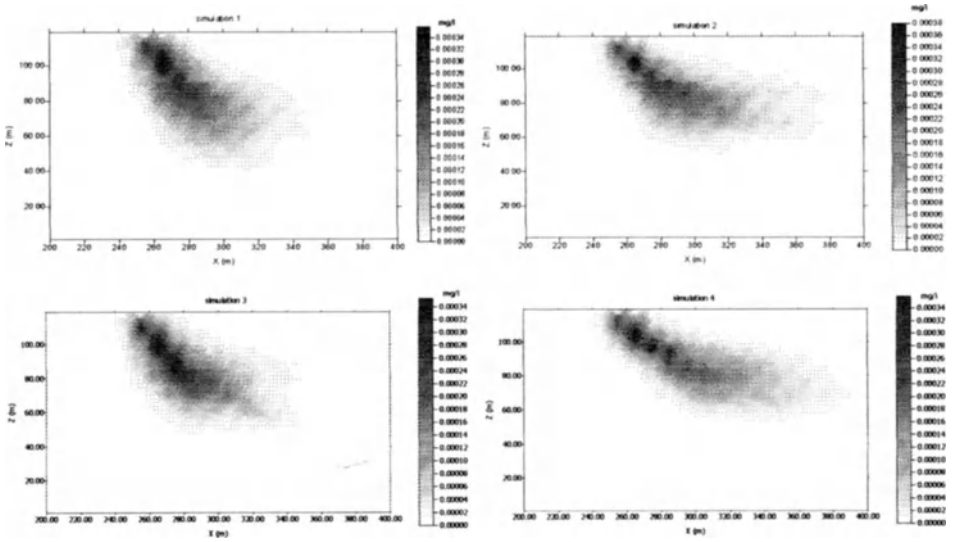

Fig. 3. Effect of the spatial variability of K on the spread of a contaminant plume as a result of a continuous source

Another example of the influence of aquifer heterogeneity on solute transport is given by the breakthrough concentration curves, Figure 4, observed at a monitoring point situated 40 m from the injection location at a depth of 20 m. They clearly show that the contaminant display distinct concentration rates, according to the spatial patterns of K used in the numerical simulation.

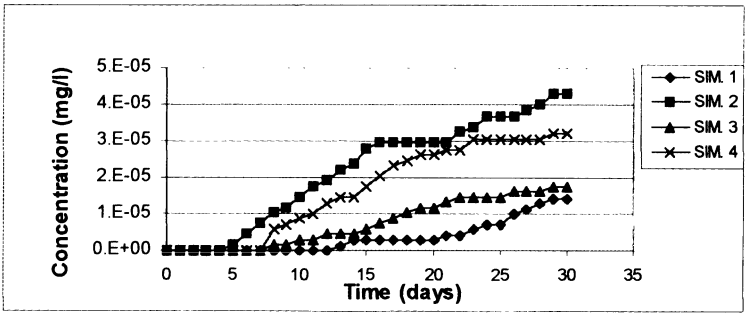

Fig. 4. Effect of the spatial variability of K on the breakthrough concentration curves observed at a monitoring station

CONCLUSIONS

Results of this study show clearly the influence of the spatial variability of hydraulic conductivity on the shape of pollution dispersion plume caused by a waste disposal site. The proposed methodology consists in the joint use of two models, one that deals with the uncertainty, the other with the deterministic aspects.

Because aquifers are hidden systems with sparse data we must generate hypothetical probabilistic representations of their heterogeneity, which image is a plausible version of the unknown subsurface reality. Indicator Geostatistics proved to be a powerful tool to achieve this objective

When this stochastic technique is associated with a traditional mass transport model we have, at last, a straightforward procedure for analyzing different groundwater pollution scenarios taking into account the uncertainty of the spatial variability of hydrostratigraphic units.

REFERENCES

1 Johnson, N.M. (1995) Characterization of alluvial hydrostratigraphy with indicator variograms. Water Resour. Res., 31(12), 3217-3227.

2 Johnson,N.M.,Dreiss,S.J. (1989) Hydrostratigraphic interpretation using indicator geostatistics, Water Resour. Res., 25(12), 2501-2510.

3 Ribeiro L., Pina P., Muge F. (1997) Contribution of indicator geostatistics and mathematical morphology to the characterization of aquifer heterogeneities in the vicinities of waste disposal sites - Proc. International Symposium Engineering Geology and the Environment, vol. 2, pp.2127-2132, Athens, Greece, Balkema ed..

4 Muge F., Ribeiro L., Pina P., Oliveira V. (1997) Morphological characterization of the spatial variability of hydrostratigraphic units. Proc. 5th International Geostatistics Congress, Wollongong, Australia, vol.2, pp.1134-1148, Kluwer Academic Publishers,.

5 Ribeiro L.(1993) A geostatistical-deterministical methodology for evaluating predictive uncertainty of saltwater intrusion from leakage. Proc. International Conference on Groundwater Quality Management, GQM93, Talinn, Estonia, IAHS publication n° 220, pp.271-280

6 Deutsch, C.V., Journel, A.G. (1992) GSLIB : geostatistical software library and user's guide, 340p., Oxford University Press.

Significance of Pore-Scale Dispersion and Sorption Kinetics for Solute Flux in Heterogeneous Aquifers.

Aldo Fiori[1] and Sten Berglund[2]

[1]Dipartimento di Scienze dell'Ingegneria Civile, Universita' di Roma Tre, I-00146 Rome, Italy
[2]Department of Civil and Environmental Engineering, Royal Institute of Technology (KTH), SE-10044 Stockholm, Sweden

Abstract. Analytical expressions for the statistics of mass fluxes of nonreactive and reactive solutes in presence of pore-scale dispersion are presented, where the reactive solutes undergo first-order sorption kinetics. The developments which lead to the analytical formulation of the solute flux are rigorous in the first-order analysis framework. The methodology is illustrated for a two-dimensional aquifer, assuming that the source is of small transverse extent compared to the heterogeneity length scales. The examples show that pore-scale dispersion has a small effect on the mean point flux, whereas the point flux variance shows much larger sensitivity to the Peclet number. The variance reduction first decreases as the reaction rate increases from the nonreactive limit, but for equilibrium reactions it is of the same order as for nonreactive solutes.

Key words: Groundwater Transport, Groundwater Quality, Stochastic processes

INTRODUCTION

Various modeling approaches have been employed for studying the concentration fluctuations in the subsurface (e.g. [1,2,3,4,5,6,7,8,9,10]). In some of these studies, it was shown that the variance of the local concentration is highly sensitive to pore-scale dispersion. However, current subsurface transport models that account for the effect of pore-scale dispersion are limited to the resident concentration of nonreactive solute. In most applications, the contaminants of interest are affected by mass transfer reactions, and in many cases these reactions exhibit kinetic effects. Moreover, for risk assessment of groundwater contamination, as well as for setting regulatory standards, the contaminant flux (or discharge) across compliance boundaries (or discharge areas), is the quantity of prime importance; the flux is either used directly in risk assessment models, or indirectly for computing the statistics of the flux-averaged concentration. In the present study, a model for computing the mass flux statistics in heterogeneous aquifers, accounting for the effect of pore-scale dispersion, is presented. The model is applicable for nonreactive as well as for reactive solute. We combine here the basic Lagrangean methodologies as proposed by Dagan and Fiori [11] and Cvetkovic and Dagan [12], extending and reformulating these in a more general and comprehensive fashion. For a more detailed description of the underlying theory, we refer to [13].

We consider an aquifer of spatially variable hydraulic conductivity, K, and steady groundwater flow, uniform in the mean. The logconductivity, $Y = \ln K$, is modeled as a stationary, normally distributed random field, resulting in a random velocity field in the aquifer. The logconductivity field is thus characterized by its statistical moments, i.e. the mean $\langle Y \rangle$, the variance σ_Y^2, and the two point correlation $\langle (Y(\mathbf{x}) - \langle Y \rangle)(Y(\mathbf{x}+\mathbf{r}) - \langle Y \rangle) \rangle = C_Y(\mathbf{r})$. Here, $\mathbf{x}(x_1, x_2, x_3)$ and other similar variables are defined in a Cartesian coordinate system.

The governing balance equations are

$$n\frac{\partial C}{\partial t} + \nabla \cdot \mathbf{Q} = -n\frac{\partial N}{\partial t} \quad ; \quad F\left(\frac{\partial N}{\partial t}, N, C\right) = 0 \tag{1}$$

where C and N are the mobile and immobile concentrations (mass per unit volume of fluid), respectively, n is the porosity, and the function F is a general expression for mass transfer that relates $\partial N/\partial t$ to C and N in a deterministic manner. Thus, we assume that mass transfer is characterized by spatially constant (effective) parameters, and we also restrict the present study to linear mass transfer processes.

The vector $\mathbf{Q}$ is the solute mass flux, defined as $\mathbf{Q} = nC\mathbf{V} - n\mathbf{D}_d \cdot \nabla C$, where $\mathbf{V}$ is the seepage (pore) velocity, and $\mathbf{D}_d$ is the pore-scale dispersion tensor. The velocity $\mathbf{V}$ is a steady-state stationary random space function satisfying the continuity equation $\nabla \cdot (n\mathbf{V}) = 0$. The statistics of $\mathbf{V}$, which depend on the statistics of the logconductivity Y, are assumed to be known. Without loss of generality, we assume $\langle \mathbf{V} \rangle = \mathbf{U}(U, 0, 0)$, i.e. the coordinate axis x_1 is aligned with the constant mean velocity. The solution of (1) is sought in the Lagrangean framework (e.g. [12,14]). If a continuous injection within the area A_0 is considered, where A_0 is normal to the x_1 direction and located at $x_1 = 0$, the initial and boundary conditions assume the following form: $C(0, x_2, x_3, t) = C_0(x_2, x_3, t)$ (for $x_2, x_3 \in A_0$), and $C(\mathbf{x}, 0) = 0$ (for $x_1 > 0$).

LAGRANGEAN SOLUTION OF THE PROBLEM

The transport problem is cast in the Lagrangean framework by considering the trajectory of a nonreactive solute particle defined at the pore-scale and originating from $\mathbf{x} = \mathbf{a}$ at $t = 0$, i.e. $\mathbf{X}_t(t; \mathbf{a})$. The trajectory can be written as the sum of two components: (i) a large-scale advection displacement $\mathbf{X}$, and (ii) a pore-scale dispersion (hereinafter PSD) component $\mathbf{X}_d$, of zero mean. This is the starting point in pore-scale models of dispersion, e.g. [15]. The "total" trajectory $\mathbf{X}_t = \mathbf{X} + \mathbf{X}_d$ satisfies the following differential equation $d\mathbf{X}_t/dt = \mathbf{V}_t(\mathbf{X}_t) = \mathbf{V}(\mathbf{X}_t) + \mathbf{u}_d$, subject to the initial condition $\mathbf{X}_t(0) = \mathbf{a}$, where $\mathbf{V}$ and $\mathbf{u}_d$ are the large-scale advective and PSD velocity field, respectively. The PSD velocity $\mathbf{u}_d$ has a support much smaller than that of $\mathbf{V}$, and can thus be modeled as a "white noise" process, of zero mean and a Dirac covariance function. Thus, PSD has a vanishing support, and as a consequence the associated process is ergodic in the sense that ensemble and space averaging can be exchanged for any finite spatial support. This is consistent with our assumption that the minimum support scale of practical interest is of the order of the Darcy scale, by definition much larger than the pore scale.

Thus, PSD is modeled as an advective process, and the partial differential equation satisfied by the concentration c is written as a pure advective-reactive one, as follows:

$$\frac{\partial c}{\partial t} + \mathbf{V}_t \cdot \nabla c = -\frac{\partial N}{\partial t} \tag{2}$$

where PSD is embedded in the pore-scale velocity field $\mathbf{u}_d$ in $\mathbf{V}_t = \mathbf{V} + \mathbf{u}_d$. In writing (2), we assume that the macroscopic process that represents the reaction through the term $\partial N/\partial t$ in (1) is the same as that acting at the pore-scale. The concentration c can be viewed as the one pertaining to a solute particle of the size of the pore. The derivation of the solution of (2) greatly simplifies by switching to the coordinates: $\tau_t(x_1; \mathbf{a})$ (denoted as travel time to a control plane located at x_1), and $\eta_{ti}(x_1; \mathbf{a})$ $(i = 2, 3)$ (the particle displacement in the same control plane); these quantities are related to the trajectory through the following relations [12]: $X_{t1}(\tau_t; \mathbf{a}) = x_1$ and $\eta_{ti}(x_1; \mathbf{a}) = X_{ti}(\tau_t; \mathbf{a})$ (for $i = 2, 3$), obtaining for a particle moving

along its streamline (see [12,16] for the details)

$$\frac{\partial c}{\partial t}+\frac{\partial c}{\partial \tau_t}=-\frac{\partial N}{\partial t} \qquad (x_2=\eta_{t2},\ x_3=\eta_{t3}) \tag{3}$$

In words, the transport equation along a streamline of the steady velocity field is formally identical with the one prevailing in one-dimensional transport.

The solution of (3) for an instantaneous injection of the mass $dM=n(\mathbf{a})\,C_0(\mathbf{a})\,d\mathbf{a}$ at $t=0$ in the volume element $d\mathbf{a}$ at $\mathbf{a}$ can be written as $c(t,\tau_t)=dM\,\gamma(t,\tau_t)/dS$, where γ is a function that accounts for the reaction and $dS=n(\mathbf{x})\,V_{t1}(\mathbf{x})\,dA$ is the constant water discharge along the streamtube. Note that dM/dS is a ratio of quantities associated with a single streamtube, and not a differentiation. Using the above expressions for dM and dS, the longitudinal solute flux, $q=ncV_{t1}$ resulting from injection at $\mathbf{a}$ can be expressed as [12]

$$q(\mathbf{x},t)=n(\mathbf{a})\,C_0(\mathbf{a})\,d\mathbf{a}\,\gamma(t,\tau_t)\,\delta(\mathbf{y}-\boldsymbol{\eta}_t) \tag{4}$$

where the relation $1/dA\rightarrow\delta(\mathbf{y}-\boldsymbol{\eta}_t)$ for $dA\rightarrow 0$ has been used. For linear sorption kinetics, considered here, γ is the solution of (3) supplemented by $\partial N/\partial t=k(K_dC-N)$ for a unit instantaneous injection. The solution for a continuous injection within the plane A_0, located at $x_1=0$, and time interval Δt is readily derived from (4) by substituting $d\mathbf{a}=V_{t1}(\mathbf{b})\,dt_0d\mathbf{b}$ (here $\mathbf{b}$ is the generic coordinate of a point at the injection plane) and integrating over $d\mathbf{b},dt_0$ which yields

$$q(\mathbf{x},t)=\int_0^{\Delta t}\int_{A_0}Q_0(\mathbf{b},t_0)\,\gamma(t,\tau_t)\,\delta(\mathbf{y}-\boldsymbol{\eta}_t)\,d\mathbf{b}dt_0 \tag{5}$$

where $Q_0=nV_{t1}C_0$ is the flux at the injection plane, and τ_t is the advective travel time from that plane to the control plane at x_1.

Since the flux (5) is a random variable, the next step is the characterization of its statistical moments, namely the mean and the variance; these are obtained through ensemble averaging over the random variables pdfs of τ_t and $\boldsymbol{\eta}_t(\eta_{t2},\eta_{t3})$. Statistical averaging leads also to the definition of the Darcy-scale solute flux Q, because the PSD contribution is also averaged. The flux expected value is thus calculated by averaging (5) over τ_t and $\boldsymbol{\eta}_t$, which are approximately independent random variables under the first-order approximation (see [17]). In the following, we denote the pdfs of the variables $\tau_t,\boldsymbol{\eta}_t$ as $g(\tau_t;x_1,Pe)$ and $f(\boldsymbol{\eta}_t;x_1,\mathbf{b},Pe)$, respectively. If the solute is continuously released with the rate function $\varphi(t)\,[T^{-1}]$, we can write $Q_0(\mathbf{b},t)=\rho_0(\mathbf{b})\,\varphi(t)$, with ρ_0 being the areal mass density in the source plane; inserting the former and the pdfs f,g in (5) and integrating, we obtain:

$$\langle Q(\mathbf{x},t)\rangle=\int_0^{\infty}\int_{A_0}\rho_0(\mathbf{b})\,\Gamma(t,\tau_t)\,g(\tau_t;x_1,Pe)\,f(\mathbf{y};x_1,\mathbf{b},Pe)\,d\mathbf{b}\,d\tau_t \tag{6}$$

where $\Gamma(t,\tau_t)=\int_0^{\Delta t}\varphi(t_0)\,\gamma(t-t_0,\tau_t)\,dt_0=\varphi*\gamma$. In a similar vein, the expression for the flux variance $\sigma_Q^2\equiv\langle Q^2\rangle-\langle Q\rangle^2$ can be computed with the aid of the two-particles joint pdf of $\tau_{tI},\boldsymbol{\eta}_{tI}$ and $\tau_{tII},\boldsymbol{\eta}_{tII}$, which are the travel times and the transverse displacements of two particles originating at $\mathbf{x}=\mathbf{b}_I$ (subscript I) and $\mathbf{x}=\mathbf{b}_{II}$ (subscript II) at $t=0$. As mentioned before, $\tau_t,\boldsymbol{\eta}_t$ are approximately independent, and we can write the joint pdf as the product of the pdfs related to each variable, i.e. $h_2(\tau_{tI},\tau_{tII},\boldsymbol{\eta}_{tI},\boldsymbol{\eta}_{tII};x_1,\mathbf{b}_I,\mathbf{b}_{II})=g_2(\tau_{tI},\tau_{tII};x_1,Pe)\,f_2(\boldsymbol{\eta}_{tI},\boldsymbol{\eta}_{tII};x_1,\mathbf{b}_I,\mathbf{b}_{II},Pe)$, with g_2,f_2 denoting the two-particles pdfs of the variables $\tau_t,\boldsymbol{\eta}_t$. Introducing the latter in (5) and squaring the resulting expression, the following formula for σ_Q^2 is obtained:

$$\begin{aligned}\sigma_Q^2(\mathbf{x},t)\;=\;&\int_0^{\infty}\int_0^{\infty}\int_{A_0}\int_{A_0}\rho_0(\mathbf{b}_I)\rho_0(\mathbf{b}_{II})\Gamma(t,\tau_{tI})\,\Gamma(t,\tau_{tII})\,g_2(\tau_{tI},\tau_{tII};x_1,Pe)\\&\cdot f_2(\mathbf{y},\mathbf{y};x_1,\mathbf{b}_I,\mathbf{b}_{II},Pe)\,d\mathbf{b}_I\,d\mathbf{b}_{II}\,d\tau_{tI}\,d\tau_{tII}-\langle Q(\mathbf{x},t)\rangle^2\end{aligned} \tag{7}$$

Expressions (6,7) provide the statistical moments of the solute flux, which will serve as a basis for the application illustrated in the next section.

APPLICATION EXAMPLE

The aim of this Section is to illustrate a particular application of the proposed methodology and to show the combined effects exerted by hydraulic conductivity heterogeneity, PSD and sorption reactions on the solute flux statistical moments. We consider a two-dimensional, statistically isotropic medium with a uniform line source at $x_1 = 0$, centered at $x_2 = b = 0$, of length H and with a constant mass density at the source $\rho_0(b) = \rho_0 = const$, which releases mass into the transport domain during a finite injection time. In the following, we assume that the transverse extension of the source is small compared to the logconductivity integral scale I_Y. This assumption implies that the Darcian velocities spanned by the particles trajectories originating from the source line are strongly correlated, and so are the statistical moments of τ_t, η_t. The consequence is that the moments of the two particles pdfs f_2, g_2 do not depend on the separation distance $b_I - b_{II}$. It should also be noted that the above assumption has no influence on the mean flux calculation.

We finally obtain through (6,7) the following expressions for the expected flux and variance:

$$\langle Q(\mathbf{x},t)\rangle = \rho_0 \int_0^\infty \Gamma(t,\tau_t)\, g(\tau_t; x_1, Pe)\, d\tau_t \cdot \int_{-H/2}^{H/2} f(x_2; x_1, b, Pe)\, db \tag{8}$$

$$\begin{aligned}\sigma_Q^2(\mathbf{x},t) &= \rho_0^2 \int_0^\infty \int_0^\infty \Gamma(t,\tau_{tI})\,\Gamma(t,\tau_{tII})\, g_2(\tau_{tI},\tau_{tII}; x_1, Pe)\, d\tau_{tI} d\tau_{tII} \\ &\cdot \int_{-H/2}^{H/2}\int_{-H/2}^{H/2} f_2(x_2, x_2; x_1, b_I - b_{II}, Pe)\, db_I db_{II} - \langle Q(\mathbf{x},t)\rangle^2 \end{aligned} \tag{9}$$

We consider reversible mass transfer in the form of first-order sorption kinetics, for which process the function F (1) can be expressed as $F \equiv \partial N/\partial t - k_1 C + kN \equiv \partial N/\partial t - k(K_d C - N)$ where k_1 and k are the forward and backward rate coefficients, respectively, and $K_d = k_1/k$ is the equilibrium distribution coefficient (dimensionless). Furthermore, solute injection is assumed to take place at a constant rate during the time interval Δt, equal to $1/\Delta t$. This implies that we can use superposition of continuous injections to obtain the following expression for the reaction-release function: $\Gamma(t,\tau_t) = \Gamma^*(t,\tau_t)/\Delta t$ for $0 < t < \Delta t$, and $\Gamma(t,\tau_t) = [\Gamma^*(t,\tau_t) - \Gamma^*(t-\Delta t,\tau_t)]/\Delta t$ otherwise, where the function Γ is given by [18]

$$\begin{aligned}\Gamma^*(t,\tau_t) &= H(t-\tau_t)\exp[-(kK_d\tau_t + k(t-\tau_t))] \\ &\cdot \left\{ I_0\left[2k\sqrt{K_d\tau_t(t-\tau_t)}\right] + \psi[k(t-\tau_t), kK_d\tau_t] \right\}\end{aligned} \tag{10}$$

where I_0 is the modified Bessel function of the first kind of order zero, $H(\cdot)$ is the Heaviside step function, and $\psi(u,v) = \exp(u)\int_0^u \exp(-s)\, I_0(2\sqrt{vs})\, ds$. We assume that the total travel time and transverse displacements two-particles pdfs $g_2(\tau_{tI},\tau_{tII})$, $f_2(\eta_{tI},\eta_{tII})$ are bivariate-lognormal and bivariate-normal, respectively, and thus characterized by the first- and second-order moments of the variables. These moments are evaluated through the procedure illustrated in [11,13], assuming an exponential isotropic logconductivity covariance and an isotropic PSD tensor. The latter assumption is not critical, since it has been shown that longitudinal PSD has negligible impact on the results [19,20,21,22].

DISCUSSION OF RESULTS AND CONCLUSIONS

As an application, we consider a source size of $H/I_Y = 0.5$, where I_Y is the logconductivity integral scale, and a control plane at distance from the source of $x_1 = 10I_Y$. Furthermore, the logconductivity variance is $\sigma_Y^2 = 0.5$ and the duration of the injection pulse is $\Delta tU/I_Y = 0.1$. Some of the integrations in (8,9) could be solved exactly, while the remaining are performed numerically; the moments characterizing f, g, f_2, g_2 are evaluated through the procedure in [13].

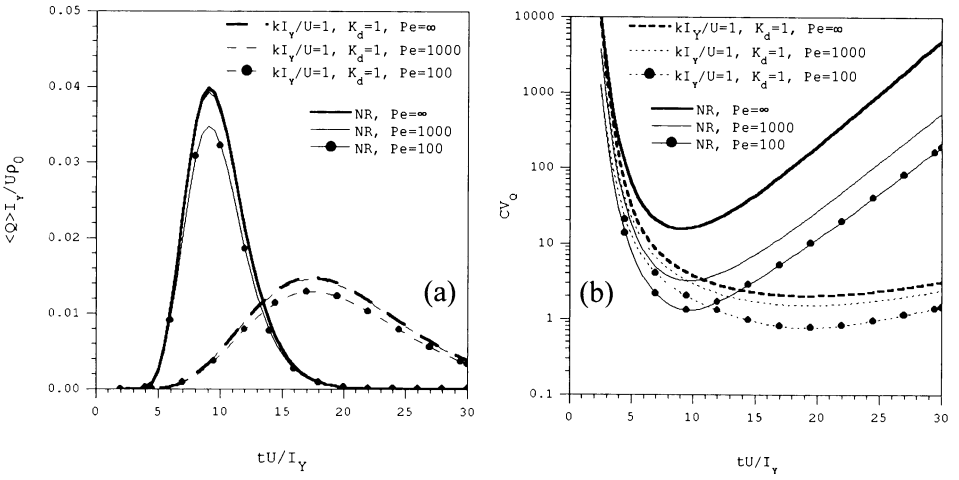

Fig. 1. Solute flux mean (a) and coefficient of variation (b) for a continuous injection of duration $\Delta tU/I_Y = 0.1$ as a function of time for different combinations of reaction parameters and Peclet numbers; $\sigma_Y^2 = 0.5$, $H = 0.5I_Y$, $x_1 = 10I_Y$, $x_2 = 0$; NR = nonreactive.

Figure 1a shows the dimensionless mean flux as a function of time for different parameter combinations; i.e. for conservative and reactive solutes with $Pe = UI_Y/D_d = 100$, 1000, ∞. Analyzing first the conservative case, it is seen that pore-scale dispersion has a limited effect on $\langle Q \rangle$; the maximum $\langle Q \rangle$ for $Pe = 1000$ and $Pe = 100$ are 98% and 88% of that for infinite Pe, respectively. Hence, to get a significant decrease in the mean point flux a much lower Peclet number than 100 is needed. This result is similar to that obtained for the mean point concentration of a conservative solute [5]. A similar effect of PSD is observed when the reaction is included with different mass transfer rates (Figure 1a). The effect of PSD is even smaller than for nonreactive solute in such cases, although approximately the same in relative terms.

The situation is different when dealing with the flux standard deviation σ_Q (9) or, alternatively, the flux coefficient of variation $CV_Q = \sigma_Q / \langle Q \rangle$ (Figure 1b). For the considered Peclet numbers ($Pe = 100, 1000$), PSD strongly reduces the flux coefficient of variation of the conservative solute, and more drastic reductions are observed for lower Pe. For the nonreactive transport cases at hand, the effect of pore-scale dispersion is to reduce the CV_Q corresponding to the maximum mean flux to about 20% ($Pe = 1000$) and around 8% ($Pe = 100$) of the coefficient of variation for infinite Pe. Such an influence of pore-scale dispersion on nonreactive solute transport has also been observed for the second moments of the point concentration [5], confirming that the impact of PSD on higher-order moments of point concentration and flux is quite relevant.

A reduction of σ_Q and CV_Q caused by pore-scale dispersion is also observed for reactive solutes. However, the infinite-Pe flux standard deviation for a kinetically sorbing solute is considerably smaller than that for a nonreactive solute, because the addition of the (deterministic) sorption process diminishes the effect of advection variability [*12*]. Figure 1b shows that for the case $kI_Y/U = 1$, PSD reduces the coefficient of variation corresponding to the maximum mean flux to about 50% ($Pe = 1000$) and 33% ($Pe = 100$) of CV_Q for infinite Pe, these reductions being significantly smaller than those obtained for nonreactive solute. Results for different reaction rates (not shown in the Figure) indicate that the PSD-related reduction in CV_Q diminishes as the reaction rate coefficient increases from the nonreactive limit ($k \to 0$). However, under equilibrium conditions ($k \to \infty$) the smoothing effect of the reaction vanishes, the solute pulse being shifted with the retarded velocity $U/(1 + K_d)$, and the variance reduction is of the same order as that for the nonreactive case. Thus, there exists a finite sorption rate for which the effect of PSD at a given time has a minimum.

The conclusion is that pore-scale dispersion affects the solute flux statistical moments, primarily its variance. Expressions (6,7) may serve as useful tools for predicting statistical moments of the conservative or reactive solute flux in heterogeneous aquifers.

ACKNOWLEDGMENT

The authors wish to thank Vladimir Cvetkovic and Gedeon Dagan for their helpful suggestions and support of this research.

REFERENCES

1. Dagan G, (1982) Water Resour Res 18: 835-848
2. Dagan G, (1984) J Fluid Mech 145: 151-177
3. Dagan G, Cvetkovic V, Shapiro A, (1992) Water Resour Res 28: 1369-1376
4. Andricevic R, (1998) Water Resour Res 34: 1115-1129
5. Dagan G, Fiori A, (1997) Water Resour Res 33: 1595-1606
6. Kabala Z J, Sposito G, (1994) Water Resour Res 30: 759-768
7. Kapoor V, Gelhar L W, (1994) Water Resour Res 30: 1789-1801
8. Hu B X, Deng F W, Cushman J H, (1995) Water Resour Res 31: 2239-2252
9. Miralles-Wilhelm F, Gelhar L W, (1996) Water Resour Res 32: 3451-3459
10. Pannone M, Kitanidis P K, (1999) Water Resour Res 35: 623-634
11. Fiori A, Dagan G, Concentration fluctuations in aquifer transport: A rigorous first-order solution and applications, in review
12. Cvetkovic V, Dagan G, (1994) J Fluid Mech 265: 189-215
13. Fiori A, Berglund S, Cvetkovic V, Dagan G, Statistics of reactive solute flux in aquifers: Combined effect of pore-scale dispersion and sampling, in review
14. Dagan G, (1989) Flow and Transport in Porous Formations. Springer-Verlag, New York
15. Saffman P G, (1960) J Fluid Mech 2: 194-208
16. Cvetkovic V, Dagan G, (1996) Proc R Soc London A 452: 303-328
17. Dagan G, (1982) Water Resour Res 18: 835-848
18. Thomas H C, (1948) Ann N Y Acad Sci 49: 161-182
19. Berglund S, Fiori A, (1997) Water Resour Res 33: 399-405
20. Fiori A, (1996) Water Resour Res 32: 193-198
21. Naff R L, (1990) Water Resour Res 25: 1013-1026
22. Neuman S P, Winter C L, Newman C M, (1987) Water Resour Res 23: 453-466

Longitudinal Dispersivity of Partially Saturated Sand Packed into Air Suck Column

T.Sato[1], H.Tanahashi[2] and M.Shibata[1]

[1]Department of Civil Engineering, Gifu University, Yanagido 1-1, Gifu 501-1193, JAPAN
[2]Department of Civil Engineering, Shinshu University, Wakasato 500, Nagano 380-8553, JAPAN

ABSTRACT. Dispersion coefficient has been estimated from the best fitting of one-dimensional convection-dispersion model with laboratory experiments in transport of aqueous constituent through sand column. Suction is applied to the bottom to get rid of the end effect and to keep constant in water saturation throughout the column. The Toyoura sand was packed and sodium chloride solution was supplied with steady state flow condition. The experimental results indicated that the dispersion coefficient increases dependently on the decrease of water saturation and a linear relationship exists between dispersion coefficient and average pore water velocity when dispersion coefficient is evaluated at the same water content. The study highlights the linear increase of dispersivity, which is defined by the dispersion coefficient divided by the average pore water velocity, as water saturation decreasing. Physical meaning of this tendency is considered by the shape of breakthrough curve describing concentration distribution at solute front.

KEY WORDS: air suction, degree of water saturation, dispersion coefficient, partially saturated sand, pore water velocity

INTRODUCTION

Flow of water through fully or partially saturated soil is often considered as bulk movement, which can be described by Darcy's law. This description becomes inadequate for the purpose of movement of transient dissolved solutes and chemical processes. It has been of interest to measure the ionic or molecular tracer concentration distribution moving through soil so that solute transport can now be understood on the basis of mathematical descriptions for miscible displacement Several literatures have been published for aqueous constituents in unsaturated soil from view points of miscible displacement. Nielsen and Biggar[1] reported the shape of breakthrough curve measured at bottom of partially saturated soil column. They revealed breakthrough curve with more gentle slope and large amount of pore volume to be perfectly displaced by solution Krupp and Elrick[2] compared breakthrough curve of partially saturated glass beads with saturated. They described that it continuously shifts to the left with decrease of water saturation De Smedt and Wierenga[3] discussed breakthrough curve by using the mobile-immobile model to estimate effects of stagnant zone within pore water on solute transport. They introduced interesting conclusions that twenty times of dispersion coefficient are estimated in unsaturated soil when the one-dimensional convection-dispersion model for mobile water(M-model) is applied, however, almost the same values are given by MIM-model Sato et al.[4] and Kotani and Yao[5] showed that dispersion coefficient becomes larger in unsaturated soil than that in saturated one and it tends to increase with increase of pore water velocity when we consider at an identical water saturation.

The purpose of this study is to make clear the effects of water saturation on dispersion coefficient. Bresler[6] may be the first researcher to describe dispersion coefficient as the function of pore water velocity and volumetric water content His literature, however, intensively focussed on the

dependency of molecular diffusion onto water content but does not address dispersion coefficient. There were no publications discussing the effects of water saturation on the shape of breakthrough curve under steady state condition. Transient behavior is one of key issues in transport of aqueous chemicals from ground surface to aquifer so that the magnitude of dispersion coefficient plays an important role in variably saturated subsurface region where water movement is affected by precipitation or by dehydration due to evaporation.

LABORATORY EXPERIMENT SETUP

A device for laboratory column is described in Fig.1. The Toyoura sand, of which particle size varies from 110 to 420 μm, was packed into a column with saturation at density of 1.55g/cm^3, which was kept at constant for all test cases. Drinking water was pumped up and supplied to the top of the soil sample at a constant flow rate. Pore water was drained from the bottom. A steady state condition was confirmed after the effluent volume equals to the influent. Solution of 0.0282N NaCl was supplied as a tracer instead of drinking water at the same flow rate after reaching steady state flow condition. Drained water flowed into fraction collector to measure concentration of chloride ion. The measurement was made on the basis of argentometric method. Concentration of background was also measured by drinking water before starting test. Air suction was applied to the sample at the bottom to eliminate the end effects and to keep a constant value in water content throughout the column. Magnitude of applied vacuum was determined from water saturation and flow rate for a given test condition.

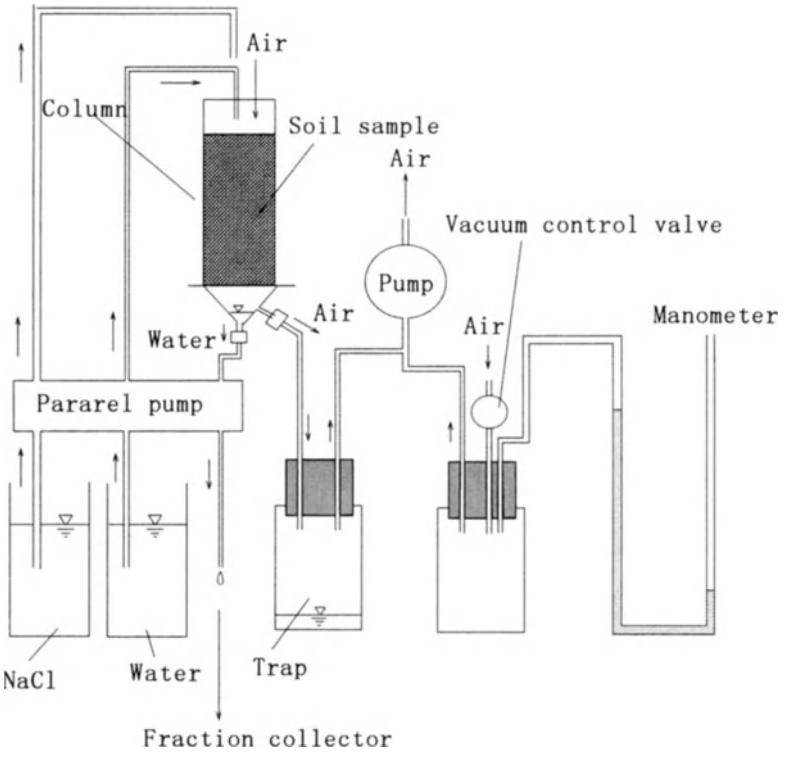

Fig.1. Experimental setup for laboratory column test

DEGREE OF SATURATION AND BREAKTHROUGH CURVE

Water content was measured at each depth of the column after test operation. Distribution of water saturation was well controlled by air suction with keeping a constant level along the whole length as shown in Fig.2. Experiments in both cases in the figure were carried out at the same average pore water velocity. The figure shows that applied vacuum determines magnitude of water saturation when discharge rate is identical. Concentration measures were aimed to draw breakthrough curve at the exit of column. Breakthrough curve in Fig.3 shows the transient behavior of tracer displacing with pore water in sand column. They were obtained at the exit of column with different values of water saturation under the identical pore water velocity. The vertical axis shows the relative concentration defined by ratio of Cl^- in effluent with respect to influent. The horizontal axis is pore volume, which is defined as vt/L, in which v: average pore water velocity, t: time since beginning of solution inflow and L: column length. It is convenient to describe the experiments by these two axes for characterization of solute transport affected by macroscopic flow condition.

The two cases, of which test condition is the same in column length and velocity, show different shape of breakthrough curve. Continuous lines in this figure are mathematical solutions of one-dimensional convection-dispersion model being fitted to the experimental values. The test results imply that the curve rotates clockwise with a decrease in water saturation. Breakthrough took place in Sr=49.4% earlier than in Sr=88.4%. The amount of pore volume to reach 1.0 relative concentration becomes larger in Sr=49. 4% than Sr=88.4%. These results indicate that preferential flow arises and displacement does not smoothly occur as water saturation decreasing.

RELATION AMONG DISPERSION COEFFICIENT, WATER SATURATION AND VELOCITY

Dispersion coefficient was determined by fitting one-dimensional convection-dispersion model to the experimental data. Breakthrough curves were analyzed in details to estimate dispersion coefficient. The test was made while keeping a constant in flow rate and water saturation. The model is available to analysis of unsaturated soil as well as fully saturated one. Terms of the application are uniformity of volumetric water content and discharge velocity throughout the column. This is one of important conditions in this type of column tests for the estimation of transport characteristics. The best fitting was made around 0.9 of relative concentration to reduce errors due to lack of measured values around 0.5 of relative concentration and uncertainty of argentometric method at beginning of breakthrough.

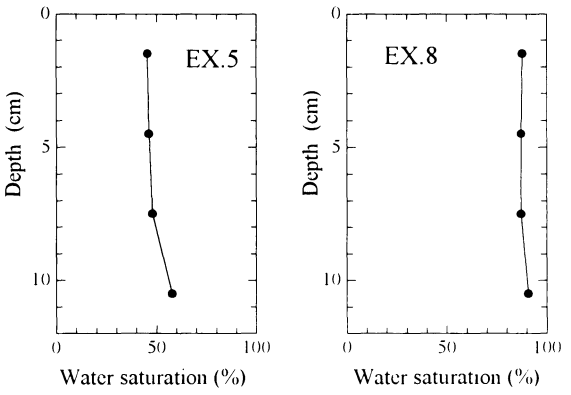

Fig.2. Water saturation in sand column

Estimated values of dispersion coefficient are displayed with reference to average pore water velocity in Fig.4. Straight lines are regression of the almost same water saturation. Dispersion coefficient increases linearly with pore water velocity on every straight line. The slope, however, tends to be steeper with decrease of water saturation except of more than Sr=70%. There were no measures less than 0.1 cm/min of pore water velocity. According to the famous literature describing relation in the Peclet number and the ratio of dispersion coefficient to molecular diffusion [6], the region less than 0.1 cm/min becomes the so called diffusion controlled, which means that dispersion coefficient is given as a function of molecular diffusion and tortuosity. Thus dispersion coefficient is equal within this region, independent of pore water velocity. This is well understanding of the regression within the region of more than 0.1 cm/min in pore water velocity described by Fig.4. The relation is delicate in the region of more than 70% of water saturation. The line of Sr=100% becomes inverse to that of Sr=70%. This results from difference of column length. The test was made by 24cm of column length for saturated soil. The test was 12 cm for Sr=70%. The exact relation for this range of high water content, using the test series of the same column length, will be provided in future.

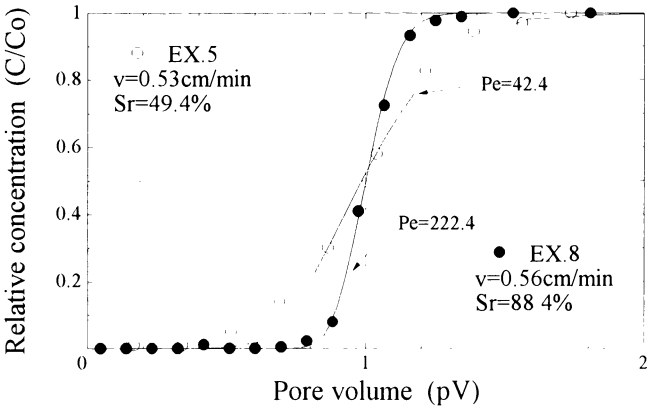

Fig.3. Breakthrough curve

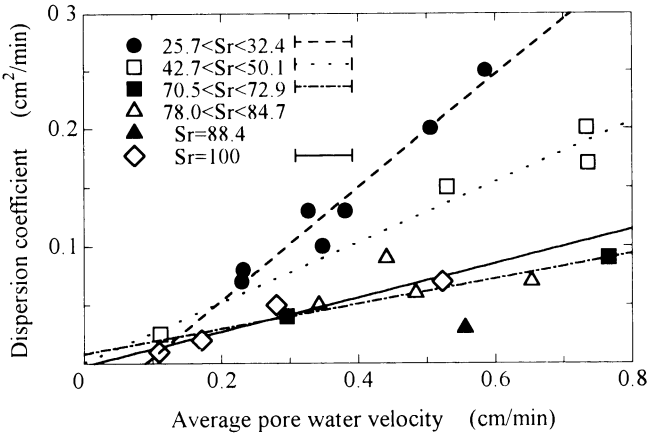

Fig.4. Relation between dispersion coefficient and average pore water velocity

The column Peclet number, which is defined as vL/D, in which v: average pore water velocity, L: column length and D: dispersion coefficient, becomes almost the same on the regressions for the experiments with the same column length as shown in Fig.5. The shape of breakthrough curve becomes identical when the column Peclet number is the same [7]. This implies that the breakthrough curve has an intrinsic shape, dependent on soil type, pore structure, characteristics of flow, etc., if the same column length is selected for tests. Fig.5 shows that non-homogeneity emerges in sand column at low rate of water saturation. Furthermore it shows the dependency of breakthrough curve on column length. The tests were made by the use of two different types of column length. The column Peclet number becomes larger in the case of L=24cm than L=12cm. Breakthrough curves observed with sand column at low saturation show an early breakthrough followed by a long tail which reflects the slow equilibration of the stagnant part of the column by diffusion. The figure also implies that short column is difficult to avoid deviation due to transverse dispersion. Schwartz and Smith[8] concluded that the diameter of the column is required at greater than 30 times of the particle size for neglecting of wall effects on uniformity of flow condition. The characteristic length may be larger than 12cm for averaging scale of non-uniformity in flow through the column. The tests were made by using 50mm diameter column which is greater than 30 times of particle size of the sand.

Dispersivity was estimated from definition of D/v in which D: dispersion coefficient and v: average pore water velocity. Spatial variance or distribution of location of chemical species at the front is given by $\sigma^2 = 2\alpha L$ in which σ: standard deviation of spatial distribution of chemical species, α: dispersivity and L: location. Dispersivity is one of important properties to guess the extent of contaminated soil by aqueous constituents. The experiments in Fig.6 show interesting prospects for estimation of pollutant progress. Dispersivity tends to increase linearly with the decrease of water saturation and does not strongly depend on pore water velocity. The experiments at Sr=100% were obtained from the tests with different column length Thus the former description may not be applied to the sand with more than 90% of water saturation. Independent behavior of dispersivity on pore water velocity implies that spatial distribution of chemical species can be uniquely determined by location and it does not depend on travel time from contamination source. Furthermore, the linear increase implies that the spatial distribution of the front goes to linearly expand with decrease of water saturation.

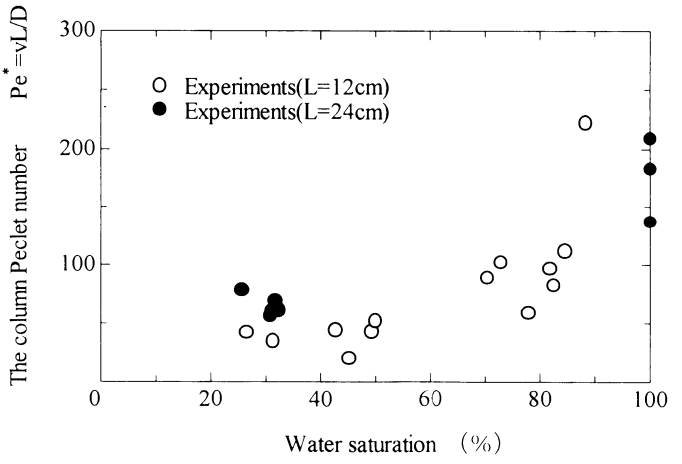

Fig.5. Relation between the column Peclet number and water saturation.

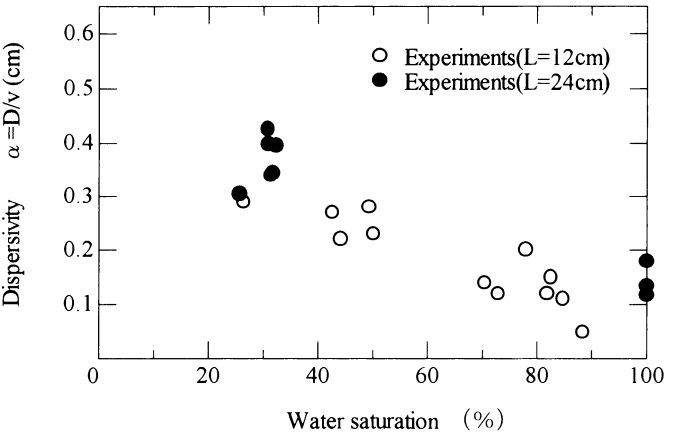

Fig.6. Relation between dispersivity and water saturation

CONCLUDING REMARKS

Dispersion coefficient was evaluated from the best fitting of one-dimensional convection-dispersion model to the experiments of laboratory column test for the Toyoura sand by using chloride ion as a non-reactive tracer. The experimental results imply strong effects of water saturation on hydrodynamic dispersion as well as pore water velocity. The conclusions described this paper are;

(1)Dispersion coefficient increases linearly with pore water velocity if water saturation is identical,

(2)Dispersivity increases with decrease of water saturation but does not depend on pore water velocity within the range of 0.1-0.6cm/min, and

(3)The column Peclet number decreases with decrease of water saturation as well as column length at low degree of saturation.

REFERENCES

1.Nielsen DR, Biggar JW (1961) Miscible displcement in soil: 1. Experimental information. Soil Science Society of American Proceedings 25(1): 1-5.

2.Krupp HK, Elrick DE (1968) Miscible displacement in an unsaturated glass bead medium. Water Resources Research 4(4): 809-815.

3.De Smedt F, Wierenga PJ (1984) Solute transport through columns of glass beads, Water Resources Research 20(2): 225-232.

4.Sato K, Muraoka K, Ito Y (1985) Dispersion coefficient of solute in unsaturated flow. Tsuchi-to-Kiso 47(9): 45-50

5.Kodani Y, Yano T (1988) Measurement of salt dispersion coefficients in unsaturated soils by the steady state method. Bull. Sand Dune Research Inst. Tottori University 27:1-7.

6.Bear J (1972) Dynamics of fluids in porous media. American Elsevier: 607.

7.Rose DA, Passioura JB (1971) The analysis of experiments on hydrodynamic dispersion. Soil Science 111(4): 252-257.

8.Schwartz CE, Smith JM (1953) Flow in packed beds. Int. Eng. Chem. 45: 1209-1218.

Geochemical Behavior of Trace Vanadium in the Spring, Groundwater and Lake Water at the Foot of Mt. Fuji, Central Japan

Koshimizu S.[1] and Tomura K.[2]

[1]Yamanashi Institute of Environmental Sciences, Kamiyoshida, Fujiyoshida, Yamanashi 403-0005, Japan

[2]Institute for Atomic Energy, Rikkyo University, Nagasaka, Yokosuka, Kanagawa 240-0101, Japan

ABSTRACT. The behavior of trace vanadium in natural water samples such as underground water, spring, river and lake water from the Kofu basin and the foot of Mt. Fuji, central Japan was geochemically investigated. Trace vanadium was determined by neutron activation analysis or inductively coupled plasma mass spectrometry. We found distinct differences in vanadium concentration in the water samples between the foot of Mt. Fuji and the Kofu basin. The difference was essentially explained by geological and geochemical characteristics in the areas examined. Further, we discussed the utilization trace vanadium concentrations to the hydrographic studies of the natural waters(underground water, river water and lake water) in the various locations at the foot of Mt. Fuji. The concentration values of trace vanadium of the spring water were in a relatively narrow range. This result suggests that vanadium is leached out through the simple interaction between underground water and Mt. Fuji volcanic rocks. The analytical data of the five lakes at the foot of Mt. Fuji show slightly less homogeneous distribution pattern, compared with that of the spring and ground waters. The informations of trace vanadium were useful as a sensitive indicator to trace the migration of natural water and elucidate the origin of the lakes water.

KEY WORDS: vanadium, ground water, spring, lake, river, basalt, Mt.Fuji

INTRODUCTION

Vanadium is one of the most important elements in biological and environmental sphere. From geological and geochemical viewpoints, the concentration of this element in rocks and waters can also provide us with much informations about their nature and history. It is recognized that the vanadium content is higher in basic igneous rocks such as basalts and gabbro than acidic rocks[1] and the vanadium content of natural water can be influenced by geological nature of sampling locations.

Mt Fuji is the largest composite stratovolcano in Japan and spews a large amount of volcanics. These volcanics have mainly chemical characteristics of typical island arc basalts. There are many springs on the

ring around Mt. Fuji with the radius of 10-20 km. At the northern foot of Mt. Fuji, the five lakes were formed by lava flows in the 9th and 10th centuries[2,3]. It is necessary for the clarification of their lakes water origins to analyze chemically various kinds of natural water such as spring, lake and river water as well as underground water from the many locations surrounding Mt. Fuji. Vanadium is most important trace element for basic rocks and has been determined by colorimetric analysis, catalytic methods, neutron activation analysis(NAA) and inductively coupled plasma mass spectrometry(ICP-MS)[4,5,6,7,8,9]. We have determined vanadium for various kinds of geochemical samples by NAA and ICP-MS and found that the vanadium concentrations are relatively higher in the natural water collected near Mt. Fuji.

On the other hands, the concentrations of vanadium are lower in the five lakes water than in the ground and spring water around Mt. Fuji. The analytical values of vanadium of the lake water might be expected to be interpreted from the dilution effects; the mixing of water with a relatively low concentration of vanadium such as rain and river water and the underground water with high vanadium concentration would result in the water of the five lakes. In the present study, the origin of water in the five lakes around Mt. Fuji has become clear on the basis of their vanadium concentrations.

VANADIUM CONCENTRATION OF WATER SAMPLES IN CENTRAL JAPAN

To determine trace vanadium in natural water and tap water samples, preconcentrational neutron activation analysis(NAA) was used. Tap water samples were collected in a lot of locations in Central Japan[7]. These tap water are originated from the different geological locations (ground water, spring water and river water). The analytical results of these samples show that the vanadium contents in natural water range widely: vanadium concentration is higher in the eastern location samples such as around Mt. Fuji, Mt. Akagi and Mt.Yoneyama area than in the western area of Central Japan[Fig. 1]. Especially, the tap water collected from the locations surrouding Mt. Fuji contains vanadium of much higher concentration. This regional difference in the vanadium concentration in water might be explained by vanadium in geological rocks and sediments in the area the water sample was collected. It has been known that the basaltic geology around Mt. Fuji originated from eruptive materials containing vanadium in a higher level. On the

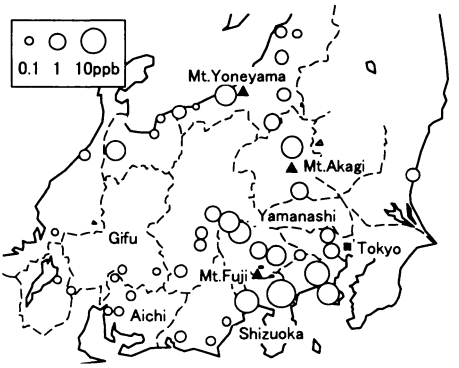

Fig.1 Vanadium concentrations in tap water at the various locations in central Japan after Sakai,et al.(1997).

other hand, a lower amount of vanadium should be explained by the geological conditions in Aichi and Gifu Prefectures and the western part of Shizuoka Prefecture belonging to the western area of Central Japan, whose geologies are mainly granitic and sedimentary.

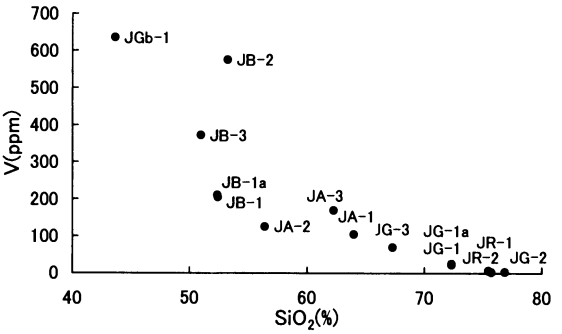

Fig.2 Plots of vanadium vs. SiO_2 for JGS igneous rocks(Imai et al.,1995).

Chemical analysis of elements in standard rocks was compiled[1]. The concentration data of many elements other than vanadium in standard rocks were summarized in that report. Using these data, vanadium has most negative correlation with SiO_2 in igneous rocks[Fig. 2].

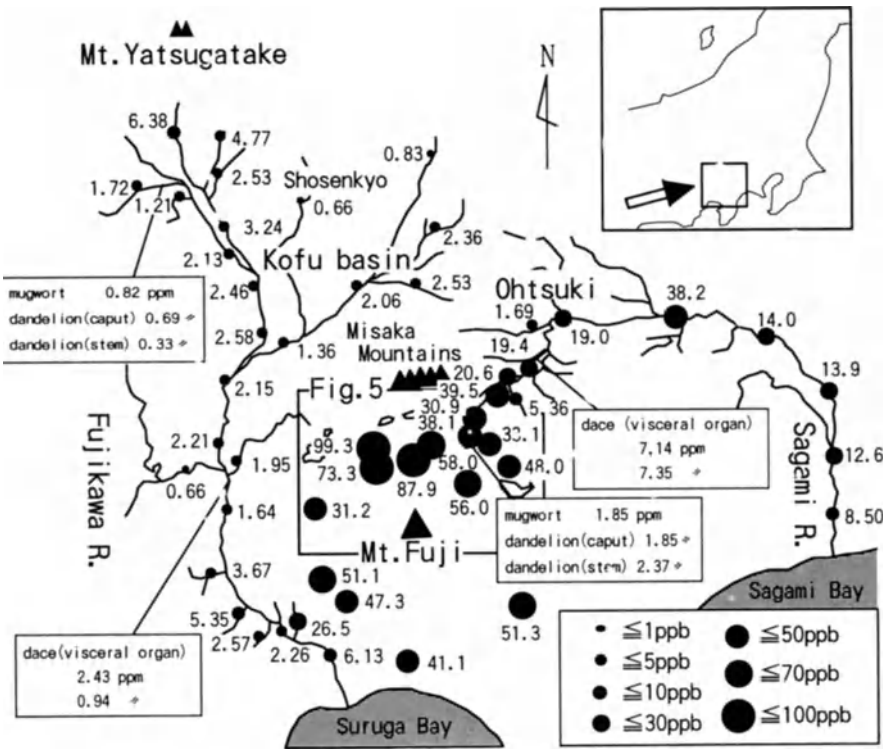

Fig.3 Vanadium concentrations in underground and river water, plants and fish from various locations at the foot of Mt.Fuji and in the Kofu basin.

Thus, it is expected that the larger content of vanadium in the soils or rocks, the higer the concentration in the natural waters. It seems to be explained by considering that vanadium in soils or rocks should be leached into ground and spring waters through the interaction with rain or snow.

ORIGIN OF TRACE VANADIUM IN WATER SAMPLES AT THE FOOT OF Mt. FUJI

We have measured and reported the vanadium concentrations in ground, spring and lake water sampled collected in a lot of locations around Mt. Fuji[6,7]. Then, the regional concentration differences of vanadium in river water were elucidated by us [8,1,9], who compared the Fuji River with the Sagami River. All these analytical results are summerized in Fig. 3, in which the cause of differences was explained by geological and geochemical differences in the areas examined. It is recognized that the Kofu basin and area around Mt.Yatsugatake consists of mainly granite and andesitic rocks with a low concentration of vanadium and the foot of Mt. Fuji consists of mainly basalt with a high amount of it.

Mt. Fuji is the largest basaltic stratovolcano in Japan, whose geology and petrography was studied by many researchers[2,3,10,11]. Based on theses investigations, the present feature of Mt. Fuji is divided into the two sequence layers: those formed before and after about 11000years B.P. called the former Older Fuji volcano and the latter Younger Fuji volcano, respectivelly. It is recognized that water percolates easily through Younger Fuji volcano because it mainly consists of lava and volcanic ash. The surface layer of the Older Fuji volcano is composed of a mudflows and pyroclastic deposits, resulting in an impermeable layer. The rain or snow permeates the Younger Fuji volcano layer on the impermeable Older Fuji volcano surface, resulting ground water falling down along the Older Fuji volcano surface. Accordingly, the ground water spouts out in the form of springs or falls at the foot of Mt. Fuji, where the boundary between the Older Fuji volcano and Younger Fuji volcano layers is exposed [Fig. 4].

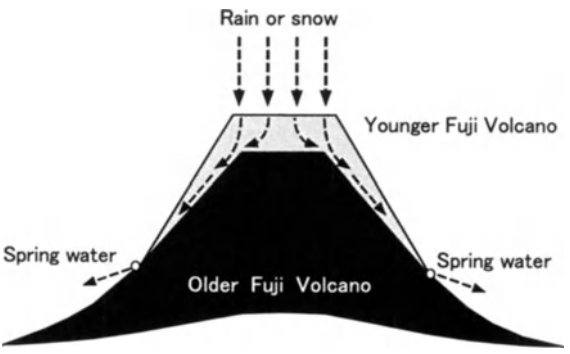

Fig.4 Conceptual feature of Mt.Fuji and water flowing

The concentrations of vanadium in these spring waters were within a narrow range from 31 to 56 ppb. The analytical values of vanadium of grownd water at the northern foot of Mt. Fuji were also within a narrow range from 58 to 99 ppb, showing slightly higer than those of springs. Based on these analytical data, it

might be explained that the vanadium of spring waters was decreased by addition of surface water and/or rain(snow) with a low amount of vanadium to the grownd water travelling through the Younger Fuji Volcano layer. From the vanadium concentration decreases, the spring waters seem to be brought by mixing of about 55% of ground water and 45% of rain or surface water, the vanadium concentration in which is assumed to be 0ppb.

On the other hand, the water from the lake surrounding Mt. Fuji, such as Motosu, Shoji, Sai, Kawaguchi and Yamanaka, were from 0.6 to 5.2 ppb in average with a narrowly ranged, respectively[Fig.4]. Although the five lakes water, located at the northern foot of Mt. Fuji, is believed to be essentially composed of ground water, the vanadium data of five lakes do not suport this hypothesis. The lower vanadium values of the five lakes water may be explained that the origin of the water is not ground water from Mt. Fuji, but other water such as rain with low vanadium contents. The water of these five lakes is formed by mixing river and rain water with low vanadium concentration and the ground water with high vanadium.

It is geohistorically recognized that the five lakes were formed by lava flows in the area between Mt. Fuji and Misaka mountain ranges[2,3]. Since the bottoms and walls of the western four lakes are partly made of the Misaka Group composed pyroclastic and volcanic rocks whose minerals were andesitic and subjected to alternation, the Misaka Group is impermeable for water. Therefore, the water with a low

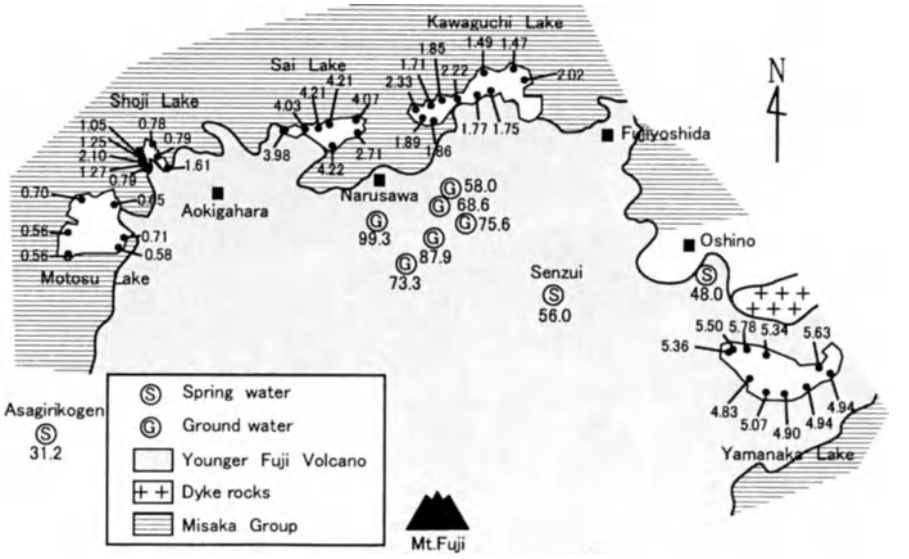

Fig.5 Sampling locations around five lakes at the northern foot of Mt.Fuji.

concentration of vanadium falls down on the surface of Misaka Mountain Layer and flows into the four lakes easily. We estimated that the most part of water in each lakes is from the water falling down on the surface of Misaka Mountain and less part of the water is from the ground water and/or spring water at the foot of Mt. Fuji. The vanadium content of Yamanaka lake in eastern end of the five lakes is higher than that of other four lakes in western part excepting Sai lake. This shows that Yamanaka and Sai lakes were influenced more strongly by the ground and spring water from Mt. Fuji.

When the average vanadium contents of underground or spring waters at the northern foot of Mt. Fuji and that of rain water are 53.5 and 0 ppb, the fractions of underground water to each five lake waters calculated from the vanadium dilution were only 1.2, 2.2, 3.4, 7.3 and 9.8 % for Motosu, Shoji, Kawaguchi, Sai and Yamanaka lakes, respectively. Here, the average lake vanadium concentration values (0.63, 1.2, 1.84, 3.92 and 5.23 ppm V) for Motosu, Shoji, Kawaguchi, Sai and Yamanaka lakes were divided by 53.5 ppb V for the average spring water vanadium concentration value.

REFERENCES

1. Imai N., Terashima S., Itoh S. and Ando A.(1995) 1994 compilation values for GSJ reference samples," Igneous rock series".Geochemical Jour., 29: 91-95.
2. Hamano K. (1988) Mt. Fuji -Its geohistory-. Kajima Press, Tokyo.
3. Machida H.(ed.) (1994) The Picture Atlas of Mt. Fuji. Dohosha, Tokyo.
4. Okabe S. and Morinaga T. (1968) Determination of vanadium and molybdenum in river water samples at the mouth of Suruga Bay. Nihon kagaku zashi, 89, 284-287.
5. Okabe S., Shibasaki M., Oikawa T., Kawaguchi Y. and Nihongi H. (1981) Geochemical Studies of Spring and Lakewaters on and around Mt. Fuji(1). Jour. Fac. Marine Sci. Tokai Univ., 14, 81-105.
6. Sakai Y., Ohshita K., Tomura K. and Koshimizu S. (1994) Determination of vanadium in water samples by NAA after chemical preconcentration. Bunseki Kagaku, 43, 919-924.
7. Sakai Y., Ohshita K., Koshimizu S. and Tomura K. (1997) Geochemical study of trace vanadium in water by preconcentrational neutron activation analysis. Jour. Radioanal. Nucl. Chem., 216, 203-212.
8. Koshimizu S., Sakai Y., Tomura K. and Ohshita K. (1998) Earth environmental study for influence to health - on the geochemical migration of trace vanadium-. Jour. Earth Environment, 2, 215-220.
9. Koshimizu S., Kyotani T. and Iwatsuki M. (1998) Geochemical study of trace element concentrations in water samples from Fuji and Sagami Rivers by Inductively Coupled Plasma Mass Spectrometry. National Meeting of the Chemical Society of Japan (Abstract), I, 205.
10. Tsuya H. (1940) Geological and petrological studies of Volcano Fuji III: Geology of the southwestern foot of volcano Fuji. Bull. Earthq. Res. Inst. 18, 419-445.
11. Miyaji N. (1988) History of Younger Fuji Volcano. Jour. Geol. Soc.Japan, 94, 433-452.

A case study using a soil gas extraction method for the remediation of a site contaminated by chloro-organic compounds

Teruo Ohora and Kouhei Okumura

OYO Corporation, Environmental Engineering Division, 2-61-5, Toro cho, Oomiya 330-8632 Japan

Abstract. Research was conducted on the mechanism of groundwater contamination by tetrachloroethylene (hereinafter abbreviated as PCE) which had occurred in Shimousa plateau, Chiba Prefecture, Japan [4] . The study showed that about 90% of the contamination is distributed within an area of approximately 1,400 m^2 centered on a dry-cleaning plant site in soil with an unsaturated zone (vadose layer) that extends to nearly 10 m deep. Remediation measures based on the soil gas extraction method were applied to the contaminated soil of the unsaturated zone. To increase the extraction flow rate, knowledge of the distinct extraction characteristics of each stratum was exploited to select the extraction procedure best suited to each stratum. For example, the "*adjacent wells open*" extraction procedure was adopted for the Joso clay stratum while the "*three point simultaneous*" extraction procedure was used for the first sand stratum. The remediation measures succeeded in cleansing the contaminated soil in the unsaturated zone from an initial soil gas concentration that was as high as 12,000 ppm to a level below 10 ppm. This paper reports the remediation results obtained and introduces a system for the automatic measurement of suction level and extraction flow rate adapted to each stratum's individual extraction characteristics.

Key words . Tetrachloroethylene (PCE), Extraction, Remediation, Extraction flow rate, Contamination

OUTLINE OF CONTAMINATION

Planar distribution.
To comprehend the planar distribution of contamination and the source of PCE infiltration, surface soil gas concentrations in the dry cleaning plant site and in the surrounding land were measured at the intersections of a 2 m grid using detection tubes located 85 cm below GL. The contamination source location and the limits of the contaminated area determined from these measurements are shown in Fig.1.

Vertical distribution of contamination.
The results of the detection tube analysis (elution concentration), carried out on uninterrupted core samples, are shown in Table 1. The strata directly below the pollution source (bore hole B1) showed the highest level of pollution (max Dss1; 150 mg/L).

Estimation of the total amount of PCE at the site.
To examine remediation measures and evaluate their effectiveness, the existing amount of PCE in the strata was estimated from the measured planar and vertical distributions of PCE

concentration in each stratum combined with the stratum's wet density.
The total amount of PCE in the soil was found to be 435 kg, about 396 kg of which is in the unsaturated soil zone (vadose layer) above the groundwater table (located approximately 11 m below GL), with the remainder, 39 kg, in the saturated zone, below the groundwater table.

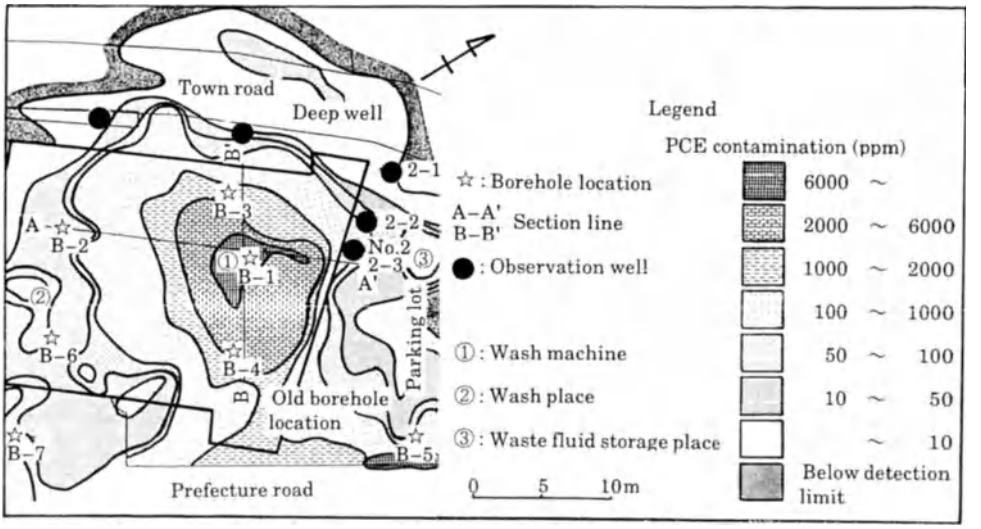

Fig. 1. Contours of PCE concentration in the soil gas

Table 1. Measured PCE concentration (mg/L) in each formation, for each bore hole

Stratum repartition	B-1	B-2	B-3	B-4	B-5	B-6	B-7
Fill soil and Kanto loam layer (Bs, Lm)	0.75 to 21	ND to 0.34	0.050 to 0.70	0.13 to 1.0	0.005 to 0.27	ND to 0.080	ND to 0.013
Joso clay layer (Tc)	25 to 28	0.047 to 0.66	0.54 to 1.4	0.64 to 1.0	0.69 to 1.6	0.013 to 0.34	ND to 0.008
Upper part 1st sand layer (Dss1)	0.22 to 150	0.012 to 0.66	0.24 to 1.4	0.096 to 1.6	0.011 to 0.67	0.022 to 0.60	0.004 to 0.18

Application of the soil gas extraction method and its effectiveness in stratified soil

Pollution by chloro-organic compounds and effectiveness of remedial measures

Since each contaminated soil site has a different set of factors that significantly affect remediation, such as stratum conditions and groundwater levels, it is difficult to define precisely beforehand what research and remediation measures are most appropriate in any given case. The soil gas extraction method has been field-proven in the U.S. for the removal of chloro-organic compounds and the method is also rated effective for this purpose by the EPA [1,3].

Remediation efficiency, however, varies considerably, depending on soil permeability and concentration of the contaminant, as well as on the kind of contamination and the physico-chemical form it takes[2]. Accordingly, a soil gas extraction method in which a large quantity of contaminated soil gas can be extracted at low vacuum pressure from a wide area was applied using an apparatus equipped with a vacuum pump, as shown in Fig.2.

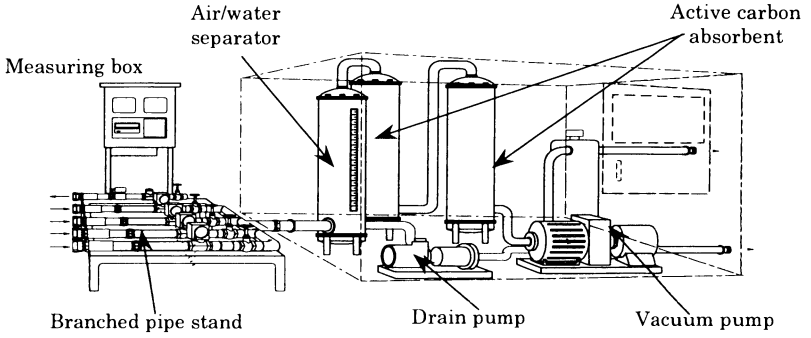

Fig. 2. Schematic diagram of soil gas extraction apparatus

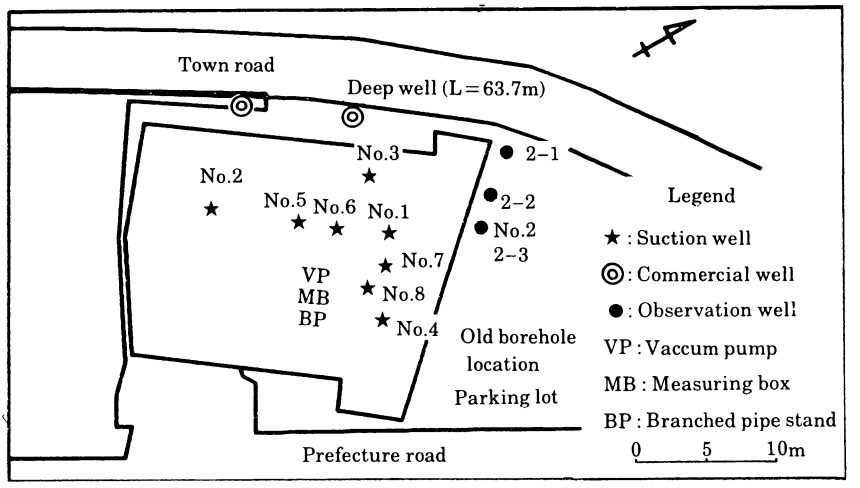

Fig. 3. Location of extraction wells and apparatus

Extraction characteristics of each stratum

(1) Location of suction wells:

The layout plan showing the location of the eight suction points in the affected zone is given in Fig.3. Each point has three soil gas suction wells: hole A [upper part of the first sand stratum (Dss1): 10 m deep], hole B [Joso clay stratum (Tc): 5 m deep] and hole C [Kanto loam layer (Lm): 2.5 m deep].

(2) Soil gas extraction characteristics:

Measurements (not shown) of extraction flow rates made using a stepwise change of suction

pressure (*step extraction test*) lead to the following conclusions:

a) In the Kanto loam layer, a high extraction flow rate was obtained at high suction (large negative pressure).

b) In the Joso clay layer, the extraction flow rate increased much less with increasing suction.

c) In the upper part of the first sand layer, the extraction flow rate was 30-50% higher than in the Joso clay layer, for the same suction.

d) In all the strata, as shown in Figure 4, the extraction coefficient, defined as the ratio of the extraction flow rate in L/min to the applied suction (kPa), increased when the a lesser suction was applied.

In addition, measurements of the propagation of negative pressure during continuous extraction at constant suction (*continuous extraction test*), shown in Fig. 5, indicated that:

a) In the Kanto loam layer, the extraction radius was small because of inflow of air from the surface of the earth.

b) Even when a high suction was used in the Joso clay layer, the extraction flow rate and affected radius were small because of the low permeability of this soil.

c) The upper part of the first sand layer is overlain by the much less permeable Joso clay layer and the area of sand affected by the extraction was large.

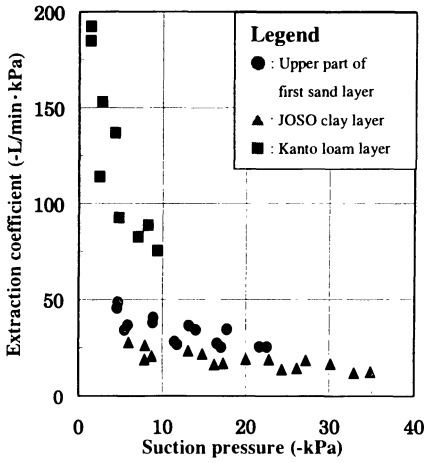

Fig.4 Relationship between extraction coefficient and applied suction

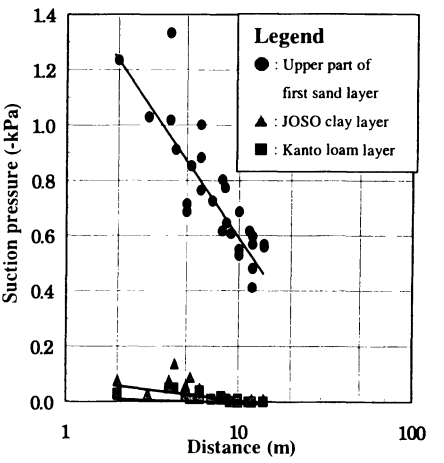

Fig.5 Effect of suction on radius of extraction zone

Effectiveness of improved soil gas extraction measures.

The relationship between suction and extracted flow rate, shown in Figure 5, indicates that smaller suction produces a lower flow rate but a higher extraction coefficient. Based on these findings, attempts were made to obtain low extraction pressures and to increase the extraction efficiency by :

a) opening certain nearby wells in addition to the active suction well ("*adjacent wells open*" extraction).

and

b) extracting gas simultaneously from several neighbouring wells ("*multiple wells simultaneous*" extraction).

Tables 2 and 3 show that for both the "*adjacent wells open*" extraction case and the "*multiple wells simultaneous*" extraction case, the extraction coefficient was indeed increased by these procedures, as was the extracted gas concentration, and remediation was accelerated as a result.

Table. 2 Extraction performance using the "*adjacent wells open*" extraction procedure

Stratum	Well status	Suction pressure (-kPa)	Extraction flow rate (L/min)	Extraction coefficient (-L/min·kPa)	PCE concentration (ppm)
Joso clay layer	Adjacent wells Closed	15.8	527	33.4	1800
	Wells (B2～B8) Open	11.0	584	53.2	2900
Upper part of 1st sand layer	Adjacent wells Closed	16.1	546	33.9	980
	Wells (A2～A8) Open	14.8	566	38.2	1500

Table. 3 Extraction performance using the "*three simultaneous wells*" extraction procedure

Stratum	Well status	Suction pressure (-kPa)	Extraction flow rate (L/min)	Extraction coefficient (-L/min·kPa)	PCE concentration (ppm)
Kanto loam layer	No. 1 well alone	5.47	664	121	500
	No 1 plus two additional C wells	5.45	800	147	560
Joso clay layer	No. 1 well alone	15.8	527	33.4	1800
	No 1 plus two additional B wells	21.5	759	35.3	2100
Upper part of 1st sand layer	No. 1 well alone	16.1	546	33.9	980
	No 1 plus two additional A wells	17.4	774	44.6	1400

Results of remediation measures

Approximately 420 kg of PCE was collected by extracting a total of 146,445 Nm^3 of PCE-polluted soil gas over a period of 8 months, during which time the system was operated a total of 3174 hours. As a result, the surface soil-gas concentration significantly decreased and eventually reached a level below the detection limit of 10 ppm. PCE elution concentrations of soil samples retrieved from test borings dropped to less than 0.01 mg/L except at a point about 1 m below the ground surface (Kanto loam layer) where the value remained near 0.2 mg/L, and at a point about 6 m deep (upper part of the first sand layer) where the concentration decreased to 0.05 mg/L.

CONCLUSION

Measures were devised to efficiently collect PCE distributed within the vadose soil layer above the groundwater table in three contaminated strata using the soil gas extraction method. The main conclusions of this study are as follows:

Extraction characteristics of each stratum

a) In the Kanto loam layer, a large extraction flow rate was achieved at high suction and, in this case the highest extraction coefficient was also achieved with values in the range 85.2 ~ 108 L/min·kPa. On the other hand, the radius of the zone affected by the extraction was only about 13 m.

b) In the Joso clay layer, the extraction flow rate was small, even with high suction and the extraction coefficient, 23 ~ 35 L/min·kPa, was the lowest of the three soils. The extraction-affected zone was also smallest, extending to about 12 m.

c) In the upper part of the first sand layer, as a result of the sealing effect of the weakly permeable Joso clay layer, the extraction coefficient was 34 ~ 45 L/min·kPa while the extraction-affected zone extended to nearly 50 m.

Effectiveness of improved soil gas extraction procedures

a) In every stratum, a smaller suction produced a higher extraction coefficient. The extraction coefficient improved by 30-50 % when the suction was decreased from 10 kPa to 5kPa.

b) In addition, the extraction coefficient was increased by both the "*adjacent wells open*" and the "*three point simultaneous*" extraction procedures. In the Joso clay layer, using the "*adjacent wells open*" procedure, the extraction coefficient increased from 33 ~ 53 L/min·kPa . In the upper part of the first sand layer, the extraction coefficient was increased from 34 ~ 45 L/min·kPa by using the *three point simultaneous* extraction procedure.

REFERENCES

1. Yoshikazu Suzuki, Yasuo Harada, Jyun-ichi Murata, Kenzi Satoh and Hisashi Nirei (1992) Effectiveness of absorbing method for the contaminated ground air in the vadose zone on geo-pollution site. The Proceedings of the Second Symposium on Geo-environments, The Committee of Environmental Geology, Geological Society of Japan, Tokyo, November 1992, pp.65-70.

2. Yoshikazu Suzuki, Kenzi Satoh, Hisashi Nirei, Yasuo Harada, Jyun-ichi Murata and Kunitoshi Matunobu (1992), The absorbing method for the Contaminated Ground-air by Volatile Organic Compounds. The Symposium on Remediation for Contaminated Sediments and Ground Water, Kanto Branch, Geological Society of Japan, June 1992, pp.55-64.

3. Y.Sasaki, S.Kinbara (1992), The cleanup of contaminated soils by vacuum extraction technique. The Symposium on Remediation for Contaminated Sediments and Ground Water, Kanto Branch, Geological Society of Japan, June 1992, pp.75-80

4. Shigehisa Hamada, Akira Tanimoto and Hideo Wakasa (1991), Groundwater contamination by the organic chloride compounds - a case study on Shimousa upland, Chiba, in Japan. The Proceedings of the First Symposium on Geo-environments, The Committee of Environmental Geology, Geological Society of Japan, Tokyo, November 1991, pp.65-70.

Estimation of Air-Water Interfacial Area in Unsaturated Porous Medium: A New Experimental Approach

A.H.M. Faisal Anwar[1], Mehdi Bettahar[2] and Uichiro Matsubayashi[2]

[1]Department of Civil Engineering, Nagoya University, Furo-cho, Chikusa-ku, Nagoya 464-8603, Japan
[2]Research Center for Advanced Waste and Emission Management, Nagoya University, Furo-cho, Chikusa-ku, Nagoya 464-8603, Japan

ABSTRACT. Air-water interfacial area (a_0) was estimated using a surfactant (surface-active agent) adsorption concept in unsaturated porous medium by a new experimental technique. Sodium dodecylbenzene sulfonate (SDBS) was selected as anionic surfactant and a glass bead of size 425-600μm (d_{50}=0.50mm) was chosen as the porous medium. Sorption of surfactant onto the solid surfaces was evaluated by miscible displacement under water saturated conditions using nonreactive NaCl and reactive SDBS, and was found to be zero for the glass bead surfaces. The number of surfactant monomers adsorbed onto the air-water interface per unit area was determined by Gibbs isotherm. The main experiment was done in a column composed of several rings where the medium was made unsaturated step by step from the saturated condition to allow the surfactant monomers to be adsorbed at the air-water interface in a regular fashion. After the column reached equilibrium and became homogeneous, the rings were dismantled and the total amount of surfactant in each ring as well as the surfactant concentration in the aqueous phase was determined by the two-phase Hyamine 1622 titration method. Finally, based on these estimated parameters, the air-water interfacial area was determined and the values obtained were found to support the general concept of decreasing a_0 with increasing water saturation, S_w. The surface area of the solid (75cm^2/cm^3), estimated from extrapolation of the experimental data (a_0~S_w) at S_w=0, was found to be close to the geometrically calculated area (76cm^2/cm^3), which proves the validity of the method.

KEYWORDS: Interfacial area, Unsaturated, Surfactant, Sorption, Titration

INTRODUCTION

A porous medium consists of a solid phase and void spaces. These void spaces are extremely complex interconnected pores, which are occupied by one or more fluids, usually water and air. When these fluids completely fill the voids, the soil is termed either saturated or dry. In the unsaturated case, both water and air co-exist as two separate immiscible fluid phases in the pore spaces. The area of this air-water interface is one of the fundamental hydrologic parameters that describe the complexity of the pore-scale distribution of air and water in unsaturated porous media. This area plays a significant role in many flow and transport processes, especially during the remediation of volatile organic contaminants in the vadose zone, where interphase mass transfer is important [1,2].

Karkare and Fort [3] were the first researchers to estimate this parameter experimentally. In their study, the effect of water insoluble surfactant on water movement was investigated and they reported that a reproducible critical quantity of surfactant is necessary to move water. The air-water interfacial area was calculated as being equal to the number of molecules of surfactant required to just initiate the water movement multiplied by the area occupied by each molecule in the air-water interface. Recently, a new miscible displacement experimental procedure has been developed [4]

using an interfacial tracer to estimate the air-water interfacial area, and it has been applied to estimate the fluid-fluid interfacial area in porous media [5,6]. In this paper, a new experimental method to estimate the air-water interfacial area is proposed. During the unsaturated flow of a surfactant solution in a porous medium, some surfactant monomers are adsorbed onto the solid surfaces and onto the air-water interface, while some others remain in the aqueous phase [7]. The mass adsorbed onto the solid surfaces can be calculated following the procedure of miscible displacement under water-saturated conditions [4]. The total mass of surfactant in these three phases can be extracted and then be analyzed by the two-phase Hyamine 1622 titration method [8]. The number of surfactant monomers adsorbed onto the air-water interface per unit area is determined from the Gibbs adsorption equation. Thus, the air-water interfacial area can be calculated from the amount of surfactant adsorbed onto the air-water interface divided by the number of monomers per unit area.

BACKGROUND OF THE METHOD

The surfactant molecules have a strong tendency to accumulate in an oriented fashion in interfacial regions such as solid-liquid, liquid-liquid or air-liquid interfaces [9]. In an unsaturated soil-water system with surfactant concentration C_s (C_s<CMC, Critical Micellar Concentration), it is usually found that some surfactant monomers remain in the liquid phase while others are adsorbed onto the solid-liquid and air-liquid interfaces respectively. This phenomenon is illustrated in Fig. 1 schematically.

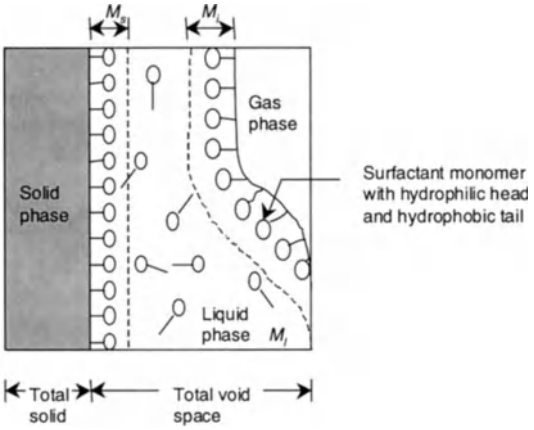

Fig. 1. Schematic representation of surfactant monomers distribution in different phases in unsaturated soil-water system.

The total surfactant mass per unit volume, M_t (mol/cm^3) in such a system can be expressed as:

$$M_t = M_s + M_i + M_l \tag{1}$$

where, M_s and M_i are the surfactant mass adsorbed per unit volume at the solid-liquid and air-liquid interfaces, respectively (mol/cm^3) and M_l is the surfactant mass per unit volume (mol/cm^3) in the liquid phase. In order to find out the air-liquid interfacial area in an unsaturated porous medium, it is usually assumed that surfactant molecules forms a monolayer coverage at the air-liquid interface

and that each molecule occupies a known molecular area [5]. This provides a simple way to estimate the surfactant mass adsorbed onto the air-water interface in an unsaturated soil-water system. The air-water interfacial area in such system may be expressed as:

$$a_0 = \frac{M_i}{\Gamma} \tag{2}$$

where a_0 is the air-water interfacial area per unit volume of porous medium (cm^2/cm^3) and Γ is the surface (excess) concentration of the surfactant which is equal to the number of molecules adsorbed per unit area (mol/cm^2). Γ is usually determined from the Gibbs adsorption equation, for the case of common background electrolyte concentration [9], using the relationship between surface tension, σ, and the bulk surfactant concentration, C_s:

$$\partial\sigma = -RT\Gamma\partial(\ln C_s) \tag{3}$$

where R is the ideal gas constant and T is the temperature in ^0K.

EXPERIMENTAL MEASUREMENTS

Materials

The porous medium consisted of glass beads size in the range 425-600μm (d_{50}=0.50mm). An anionic surfactant, sodium dodecylbenzene sulfonate (SDBS) (purity>95%; CMC=414mg/l) was chosen as the surface reactive tracer, and sodium chloride (NaCl) was selected as the surface non-reactive tracer. NaCl was also used to maintain a constant background Na^+ concentration (counter ion of SDBS). In order to titrate the anionic surfactant, Hyamine 1622 was used as the cationic surfactant in the presence of a color indicator and a solvent. Dimidium bromide, disulphine blue, ethanol and sulfuric acid were used to prepare the color indicator [8] and dichloromethane was used as the solvent [10]. Deionized water was used to prepare all the solutions.

Column experiments

The experimental setup was made with several pieces of stainless steel rings of 3cm length and 9.6cm inner diameter, carefully joined together by Teflon tape (Fig. 2). The column, initially filled with water, was packed successively with the dry glass beads in small increments and tapped at the bottom. The bulk density and the saturated hydraulic conductivity measured for the porous medium were $1.53g/cm^3$ and 0.023cm/s respectively.

In order to estimate the adsorption of the surfactant onto the glass bead surfaces, a miscible displacement experiment was carried out under water-saturated conditions using SDBS and NaCl as surface reactive and surface non-reactive tracers, respectively [4]. The unsaturated experiments were conducted directly from the saturated condition and the same surfactant solution was recycled in order to estimate the surfactant mass adsorbed onto the air-water interface. At first, SDBS solution (with constant Na^+ concentration) was recycled under saturated conditions with unit hydraulic gradient (i.e. way I is closed; Fig. 2). Then, to make the column unsaturated, the flow rate was decreased stepwise but was kept constant during each step to ensure steady flow. This helped to form a constant air-water interfacial area inside the porous medium. Thus, concentration of surfactant became steady and homogeneous inside the system. After establishing steady equilibrium conditions in the system, the column was dismantled. Three wet glass bead samples of about 25-30g were collected from each ring to ensure reproducibility. These glass bead samples were set aside

and used to extract the total mass of surfactant present inside the medium. The rest of the glass bead from each ring was weighed and put in the oven at 110^0C for 24 hours. After titration, collected glass bead samples (25-30g) were also oven dried at the same temperature for 24 hours and the total volumetric water content for each ring was evaluated gravimetrically.

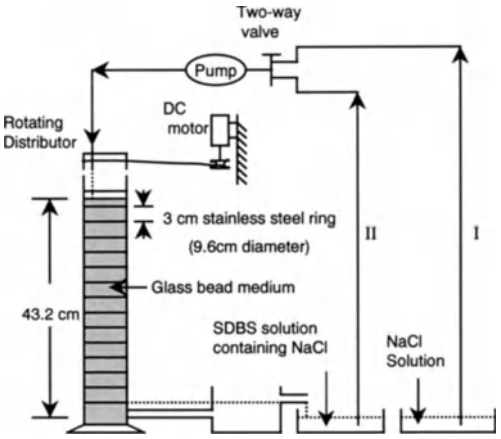

Fig. 2. Scheme of the experimental setup.

Extraction and two-phase titration process

About 25ml of NaCl solution (the same as the background electrolyte concentration of SDBS) was added to the collected glass bead samples and the samples were vigorously shaken for about 1 minute. All the surfactant monomers present in the three phases (solid, aqueous and interface) were diluted in the aqueous solution and the supernatant phase was immediately extracted by a pipette to another bottle for analysis by the Hyamine 1622 titration method [8]. About 10ml of aqueous phase solution was collected from the outlet tank at the end of the experiment and was analyzed by the same procedure in order to obtain the SDBS concentration in the liquid phase.

Measurements of surface tension

The Gibbs adsorption equation was developed by measuring the surface tension, σ of surfactant solution with a different concentration (0-450mg/l) under a constant temperature (20 ± 1^0C). The surface tension, σ, of SDBS solution containing the same common Na^+ ion concentration was measured by the Wilhelmy plate method [11] with the help of a surface tensiometer. First, the platinum Wilhelmy plate was cleaned, burned on a Bunsen burner and 3/4 of the area of the plate was wetted by the SDBS solution. The plate was hung on a balance and the solution level was automatically increased until it touched the plate. The weight increase was recorded by an electronic balance and was converted to surface tension directly.

RESULTS AND DISCUSSION

Surface (excess) concentration, Γ

Surface tension data, measured for different surfactant concentrations with constant background Na^+ concentration was plotted and Γ, calculated from the fitted equation, was estimated to be 2.87×10^{-10} (mol/cm^2). This result can be used to calculate the area occupied per molecule of surfactant at the interface as $10^{16}/N\Gamma$ where, N is Avogadro's number. This area was calculated to be 58(Å^2), which was in an agreement with the areas listed for different anionic surfactants in the literature [9].

Adsorption onto the solid surfaces

SDBS sorption onto the solid surfaces was tested by a miscible displacement experiment under water saturated conditions and found to be zero (i.e. $M_s = 0$), which was in an agreement with the results obtained by other researchers [5,6].

Extraction and titration process

First, the glass beads were calibrated for extraction and titration processes. 25g of dry glass beads was contaminated with a known mass of SDBS solution for two days and analyzed by two-phase titration, as described above. The calibration curve comparing measured and actual mass of surfactant (mg) per gram of glass beads is shown in Fig. 3. Using the samples collected during dismantling the column, the SDBS mass was estimated by titration and was converted to actual mass using the calibration curve of Fig. 3. Later, this mass (mg/g) was converted into the total mass of surfactant (M_t) using the dry weight of soil for each ring. The same calibration procedure was also used with the aqueous phase solution (without the porous medium). Afterwards, the actual liquid phase surfactant concentration obtained by titration was estimated using the calibration and was subsequently converted into M_l.

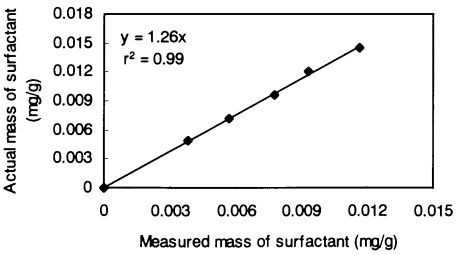

Fig. 3 Calibration for titration process

Air-water interfacial area

The air-water interfacial area, a_0, calculated with these parameters using equations (1) and (2), is shown in Fig. 4. The results are in general agreement with those obtained by others [4,12,13,14] and exhibit decreasing a_0 with increasing saturation, S_w. The air-water interfacial area calculated for zero saturation was compared with that of the solid specific surface area, which was calculated by conventional method [15]. The experimentally calculated value (75cm^2/cm^3) was found to be close to the geometrically calculated value (76cm^2/cm^3), which supports the belief that reasonable estimations of a_0 can be obtained with this technique.

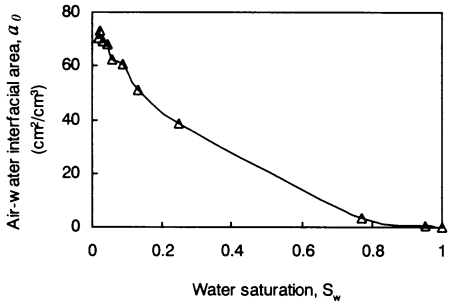

Fig. 4. Air-water interfacial area with water saturation

CONCLUSIONS

A new experimental method was described to estimate, the air-water interfacial area (a_0) using a surfactant adsorption concept. Surfactant molecules added to the unsaturated soil-water distribute themselves in three phases, i.e. adsorption on soil particle surfaces, on air-water interfaces, and as monomers in soil-water. The methodology describes how to determine the surfactant mass from these three phases. The air-water interfacial area was then calculated from the amount of SDBS adsorbed onto the air-water interface and the number of SDBS monomers per unit area. The results obtained by this method showed that, in general, a_0 decreases with increasing water saturation, S_w. The specific surface area of the solid fraction, estimated from the extrapolation of the experimental data (a_0~S_w) at S_w=0, was found to be close to the geometrically calculated area. Thus it is concluded that a reasonable estimate of a_0 in unsaturated porous media can be obtained by this method.

REFERENCES

1. Miller CT, Poirier-McNeill MM, Mayer AS (1990) Water Resources Research 26 (11): 2783-2796
2. Wilkins MD, Abriola LM, Pennell KD (1995) Water Resources Research 31 (9): 2159-2172.
3. Karkare MV, Fort T (1996) Langmuir 12: 2041-2044.
4. Kim H, Rao PSC, Annable MD (1997) Water Resources Research 33 (12): 2705-2711.
5. Saripalli KP, Kim H, Rao, PSC, Annable MD (1997) Environmental Science and Technology 31 (3): 932-936.
6. Saripalli KP, Rao PSC, Annable MD (1998) J of Contaminant Hydrology 30: 375-391.
7. Schaefer CE, Unger DR, Kosson DS (1998) Water Resources Research 34 (10): 2529-2537.
8. Brewer PI (1972) J. of Institute of Petroleum, 58 (559): 41-46.
9. Rosen MJ (1989) Surfactant and interfacial phenomena. John Wiley, pp 436.
10. Bettahar M, Schafer G, Baviere M (1999) Environmental Science and Technology 33(1-8): 1269-1273.
11. Adamson AW, Gast AP (1997) Physical chemistry of surfaces. John Wiley, pp 784.
12. Reeves PC, Celia MA (1996) Water Resources Research 32 (8): 2345-2358.
13. Bradford SA, Leij FJ (1997) J. of Contaminant Hydrology 27: 83-105.
14. Cary JW (1994) J of Contaminant Hydrology 15: 243-248.
15. Dullien FAL (1979). Porous media: Fluid transport and pore structure. Academic, pp 396.

The Lysimeter Experiments and Numerical Simulations on Behavior of DNAPL in the Unsaturated Zone

Masahito Yoshimura[1], Changyuan Tang[1] and Yasuo Sakura[2]

[1]Graduate School of Science and Technology, Chiba University
[2]Department of Earth Science, Chiba University
1-33, Yayoi-cho, Inage-ku, Chiba, Japan, 263-8522

Abstract. Lysimeter experiments were conducted to study the behavior of NAPLs in unsaturated zone by simulated rain. TCE and Bromide were used in the experiments to trace the behavior of DNAPL and water respectively. Soil properties such as porosity and hydraulic conductivity were measured at nine depths. Soil water potential was measured with tensiometers and soil water contents were checked by a nuclear soil water meter and TDR. The water was sprinkled from the top of the lysimeter during the ten experiments. At the beginning of the first experiment, pure TCE and bromide-dated water were put at the surface of lysimeter. Soil water and soil gas in the unsaturated zone were sampled and analyzed during and after rain events. Soil water content increased as lapsed time from 20 % to 30 % approximately. By comparing the velocity of infiltrating water with that of TCE, it was found that pure TCE liquid did not always move straight downward immediately and TCE gas moved more quickly than water in the unsaturated zone where TCE gas migration was important. Using experimental results, some numerical simulations were carried out to reveal the behavior of TCE in both gaseous phase and dissolution phase. Compared the vertical profile of TCE concentration experimented and that of calculated, some parameters such as diffusion coefficient, partition coefficient and decay coefficient have been derived.

Key words. Lysimeter experiments, Numerical simulations, DNAPL, Unsaturated zone

INTRODUCTION

Soil and groundwater contamination by organic solvents, gasoline, petroleum products and similar nonaqueous phase liquids (NAPLs) tend to degrade sensible environment after leaking storage tanks, pipelines, chemical waste disposal facilities and surface spills. In spite of the aqueous solubility of these organic liquids contamination is a low existence in subsurface as NAPLs, it is still large enough to degrade water quality. The mobility of liquid contaminants depends on spilled volume in site and, its physico-chemical properties as well as the hydraulic properties of porous media [1,2].

Several investigations have been conducted on behavior of NAPLs spilling problems. When a spill front from a large liquid release passes through the unsaturated zone, the liquid contaminants may form a continuous phase, filling a large fraction of the void volume. After the spill front has passed, a discontinuous phase is more likely to exist. If the trapped ganglion is in the vertical length, the relationship between the ganglion vertical dimensions and porous media assumed that stable TCE ganglia can be up to 2 m in vertical length for fine sand with a grain size of 0.1 mm [1]. The inclusion of volatilization, gas-liquid partitioning, and advection in the gas phase is necessary for accurate determination of the fate VOC in variably saturated media [3]. Furthermore numerical analysis for vertical transport including effect of rainfall was conducted [4]. The field and laboratory observations and the review of multiphase flow theory are both very perceptive of dominant mechanisms and are clear about uncertainties which arise in real field situations and which, for the most part, are still unsolved [5,6].

Natural subsurface systems are heterogeneous in nature. Some works have been done to show that the heterogeneous nature of field-scale systems probably causes the nonequilibrium conditions typically encountered in the field [7,8]. Despite the fact that several studies of behavior of NAPLs in unsaturated zones have been undertaken, there is still a relatively poor understanding of the processes at both field scale and laboratory scale. Many laboratory-scale systems have typically been using homogeneous porous media with experimental length scales in the order of centimeter.

The goal of this work is to gain an improved understanding of DNAPL migration in the unsaturated zones. In this work, by experiments in simulated rain were conducted to study the behavior of trichloroethylene (TCE) using Lysimeter in simulated rain. Next, we tried to describe experimental results by considering differences between TCE migration and the infiltration velocity of water. Based on the experimental results, some numerical simulations were carried out to reveal the behavior of TCE in the gaseous phase and dissolution phase to identify soil and component properties.

MATHEMATICAL MODEL FOR MULTIPHASE FLOW

The mass conservation equations for water (w), organic liquid (o) and air (a), assuming an incompressible porous medium, incompressible liquid phase and compressible gas phase, may be written in summation convention for a two dimensional Cartesian domain as [9].

$$\phi\frac{\partial S_w}{\partial t} = -\frac{\partial q_{wi}}{\partial x_i} + \frac{R_w}{\rho_w} \qquad (1) \qquad\qquad \phi\frac{\partial S_o}{\partial t} = -\frac{\partial q_{oi}}{\partial x_i} + \frac{R_o}{\rho_o} \qquad (2)$$

$$\phi\frac{\partial \rho_a S_a}{\partial t} = -\frac{\partial \rho_a q_{wi}}{\partial x_i} + R_a \qquad (3)$$

where Φ is porosity, S_p is the p-phase saturation, x_i (and x_j) are Cartesian spatial coordinates (i,j=1,2), q_{pi} is the Darcy velocity of phase p in the i-direction, ρ_p is the density of phase p, R_p is the net mass transfer per unit porous media volume into (+) or out of (-) phase p, and t is the time.

Relationships between phase permeabilities, saturations and pressures are described by a three phase extension of the van Genuchten model [10]. To describe the saturation-capillary pressure relations, we introduce capillary presuure heads defined by

$$h_{aw} = h_a - h_w \qquad (4) \qquad\qquad h_{ao} = h_a - h_o \qquad (5) \qquad\qquad h_{ow} = h_o - h_w \qquad (6)$$

where $h_p = p_p/\rho_w g$ with P_p the p-phase pressure, ρ_w the density of water, and g the gravitational acceleration and p=a (air), o (oil) or w (water).

Darcy velocities in the p-phase are defined by

$$q_{pi} = -K_{pij}\left\{\frac{\partial h_p}{\partial x_j} + \rho_{rp} u_j\right\} \qquad (7)$$

where K_{pij} is the p-phase conductivity tensor, $h_p = P_p/g\rho_w$ is the water height-equivalent pressure head of phase p where P_p is the p-phase pressure, g is gravitational acceleration and ρ_w is the density of pure water, ρ_p is the density of phase p, $\rho_{rp} = \rho_p/\rho_w$ is the p-phase specific gravity, and $u_j = \partial z/\partial x_j$ is a unit gravitational vector measured positive upwards where z is elevation.

A model for transport of NAPL constituents that can partition among water, oil, air and solid phases is described. To model component transport, continuity and mass flux equations for each partitionable component in each phase must be specified. Mass conservation of species α in the p-phase requires that

$$\phi\frac{\partial C_{\alpha p} S_p}{\partial t} = -\frac{\partial J_{\alpha pi}}{\partial x_i} + R_{\alpha p} + \gamma_{\alpha p} \qquad (8)$$

where $C_{\alpha p}$ is the concentration of the noninert α component in p-phase expressed as the mass of α per phase volume [ML^{-3}], $J_{\alpha pi}$ is the mass flux density of α in p-phase per porous media cross section in the i-direction [$ML^{-2}T^{-1}$], $R_{\alpha p}$ is the net mass transfer rate per porous medium volume of species α into (+) or out of (-) the p-phase [ML^{-3}], and $\gamma_{\alpha p}$ is the net production (+) or decay (-) of α within phase p per porous medium volume due to reactions within the p-ohase [ML^{-3}] described subsequently by

$$\gamma_{\alpha p} = -\mu_{\alpha p} C_{\alpha p} \tag{9}$$

where $\mu_{\alpha p}$ is an apparent first-order decay coefficient.

The governing equation in this formation have been solved using a finite element method with spatial derived terms of equations approximated by asymmetric upstream-weighting functions developed by Huyakorn and Nikuha [11], while the remaining terms are handled using linear basis functions. These numerical simulations are carried out to by fineite element code of multiphase flow and multicomponent transport (MOFAT)[12].

LYSIMETER EXPERIMENTS

Materials and method. Experiments of infiltration were conducted with the lysimeter of sand volume 120cm×120cm×210cm illustrated in Fig. 1. Tensiometers, soil water samplers and gas samplers were set at 10 depths. Water content was measured by a nuclear water meter and five

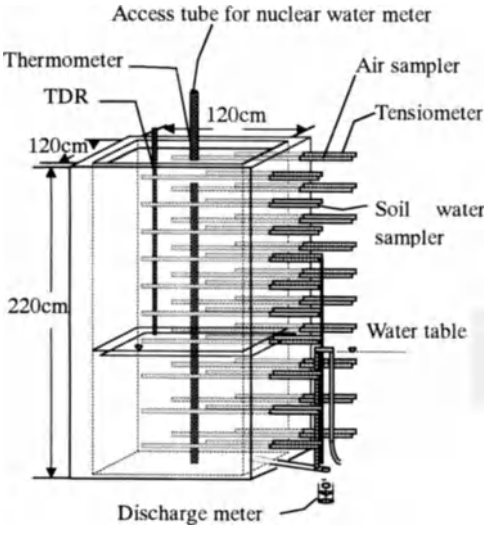

Fig. 1. Schematic diagram of lysimeter used in the experiments

Table 1. Depth at which sensors were setup

Sensors	Setup depth
	cm
Tensiometer, Soil water sampler, Gas sampler	10,32,55,77,100,122, 145,167,190,212
TDR	10,32,55,77,100,122

Table 2. Event conditions

Stage NO.	Time	Rainfall
	min	mm/min
Stage 1	Water distribution	-
Stage 2	TCE infiltration	-
Stage 3	0 – 80	0.417
.	4,000 – 4,080	0.417
.	10,080 – 10,160	0.417
.	15,560 – 15,640	0.417
.	19,940 – 20,020	0.417
.	24,200 – 24,280	0.417
.	29,980 – 30,060	0.417
.	34,340 – 34,420	0.417
.	41,540 – 41,620	0.834
.	52,580 – 52,660	0.209

TDR(time domain reflectometer) sensors. Those locations are shown in Table 1. Soil suctions, temperatures and effluent water from the bottom of the lysimeter were measured automatically and recorded in a data-logger. Hydraulic potentials were calculated by setting the lysimeter surface as zero cm. Trichloroethylene (TCE) and sodium bromide (NaBr) were used to trace the behavior of DNAPL and water. The water was sprinkled from the top of the lysimeter

Table 3. Soil properties used in experiments and simulations

Depths from the surface	Hydraulic conductivity	Porosity	Water saturation	β	n
m	m/day	-	-	m^{-1}	-
0 – 0.21	2.71	0.48	0.15	5.0	2.65
0.21 – 0.44	2.50	0.44	0.15	5.0	1.75
0.44 – 0.66	1.04	0.42	0.15	5.0	1.48
0.66 – 0.89	1.91	0.40	0.15	5.0	1.31
0.89 – 1.11	1.20	0.42	0.15	5.0	1.32
1.11 – 1.34	1.62	0.37	0.15	5.0	1.28
1.34 – 1.67	6.32	0.38	0.15	5.0	1.30
1.67 – 2.10	6.32	0.38	0.15	5.0	1.75

with an intensity of 25 mm/h which were 33.3 mm in the first eight experiments, and 66.6 mm and 15.6 mm in the last two experiments respectively shown in Table 2. At the beginning of the first experiment, 2,420ml pure TCE and bromide-dated water were put into at the depth of 10 cm from the top of the lysimeter. The TCE used here was analytical-grade produced by Wako Pure Chemical Industries. Table 3 shows soil properties used in experiments and simulations shown in Table 3. Soil water and soil gas in the unsaturated zone were sampled during and after rain events. Soil water was extracted by n-Hexane and analyzed by gas chromatography on Shimadzu GC-14B equipped with a flame ionization detector (FID). Soil gas was analyzed by a gas chromatography on Nihondenshi GC-311 equipped with a photon ionization detector (PID). Variations of bromide concentration in soil waters were analyzed with an ion chromatography on Shodex.

RESULTS AND DISCUSSION

Relationship between the movements of water and TCE. Fig. 2 shows the variations of soil water content during experiments including ten rain events. Initial soil water content at the surface was less than 20%. It increased with deepening. After supplying with rainwater, soil water content increased to 30 %. The variations of hydraulic potential at the beginning of experiments were almost the same at every depth, which means no vertical flow movement occurs. Additionally, vertical profiles for bromide of the soil water are shown in Fig. 3. The graph illustrates the velocity of water infiltrated was 5 cm/day and 3 cm/day during the first ten days and the second ten days respectively. Fig. 4 shows the variations of vertical distribution for TCE gas concentrations. Before pouring TCE liquid into the lysimeter, TCE gas concentration was 0 ppm at all depths. As soon as experiments were conducted, TCE gases were detected at 32 cm and 55 cm depths with the concentrations of 0.034 ppm and 0.006 ppm. About five days later, TCE gases were found as 0.041ppm and 0.029ppm at 100cm and 122 cm depths respectively. This fact indicates that there is possibility of quick movement in gaseous phase TCE into the unsaturated zone. By considering the rain, it can be stated that the

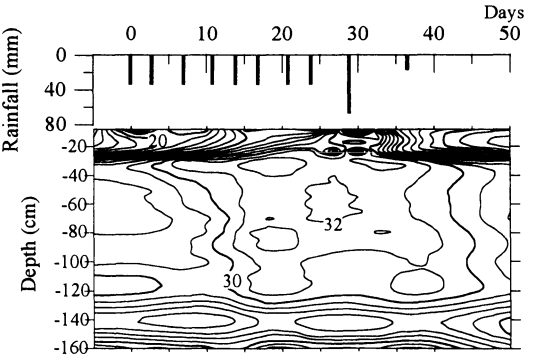

Fig.2. Variations of soil water content (%)

movement of TCE gas corresponds well with that of the infiltrating water. Fig. 4 shows iso-concentration line for zero ppm shifts down quickly from five to ten days and around 25 days. By comparing the vertical profile of bromide and TCE, it is revealed that pure liquid does not always move straight downward to a water table and remains at the top of layer. The front of bromide matches well with the depths where the TCE concentration is about 20 to 50 ppm. This result means that TCE moves more quickly than water in the unsaturated zone where gaseous TCE exists. This movement is considered to be a result of pushing both TCE-dissolved-water and TCE gas downward by infiltrating water.

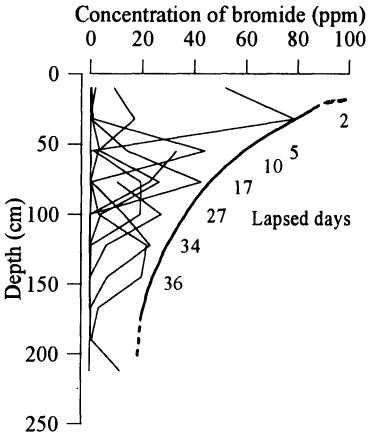

Fig. 3. Variations of profile for bromide

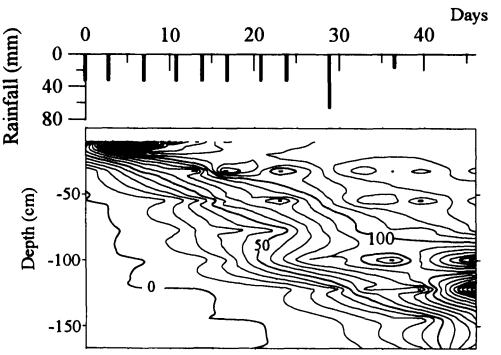

Fig. 4. Variations of vertical distribution for TCE gas concentration (ppm)

Soil properties derived from calculation. First, two stages are adopted to explain the initial water distribution and TCE liquid infiltration. Fig. 5 expresses the result in stage 1 and 2. Stage 1 accounts for the volumetric water content at the condition before supplying of water from the top of the surface with a water table at the depth of 170 cm. The diamond and the dotted line show experimental and calculated results, respectively. The VG (van Genuchten) – model [10] was used to simulate the water content. Prior to the occurrence of oil at a given location, the system is treated as a two-phase air-water system described as followed

$$\bar{S}_w = \left[1 + (\beta h_{aw})^n\right]^{-m} \qquad (10)$$

where $S_w=(S_w-S_m)/(1-S_m)$ is the "effective" water saturation, S_m is the "irreducible" water saturation, β [L^{-1}] and n[-] are porous medium parameters and m=1-1/n. In order to bring calculating results to fit our experimental results, β and n is adjusted as can be seen in Table 3. Results between 40 cm and 110 cm agreed well. In stage 2, TCE liquid was added under a constant head of h_0=0 cm. Other boundaries for oil and water were no flow. Transport was not considered during Stage 2. Total duration of stage 2 was only 0.0001 day. The straight line in Fig. 5 shows the depth of infiltration of total liquid. The depth of TCE gas agreed well with the calculated depth of total liquid saturation. Using experimental results, numerical simulations were carried out to reveal the behavior of TCE in both gaseous-phase and

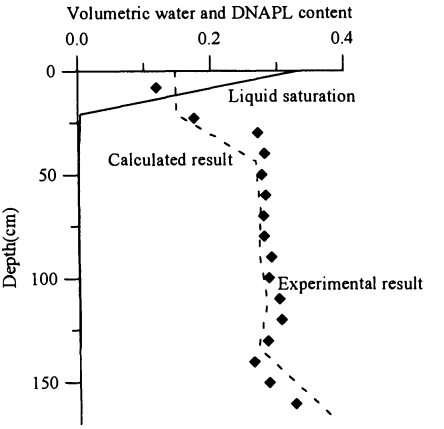

Fig. 5. Result of Stage 1 and 2

The diamond and dotted line were obtained from the experiment and the calculation respectively. The straight line shows the calculated infiltration depth of total liquid.

dissolution phase based on different soil properties at each depth in Stage 3. Compared the vertical profile of TCE concentration experimented and that of calculated, some parameters such as diffusion coefficient, partition coefficient and decay coefficient have been derived.

CONCLUSIONS

The following conclusions were derived from this study.
Lysimeter experiments were conducted to study the behavior of DNAPL in unsaturated zone with simulated rain.

1. Pure TCE liquid did not always move straight downward immediately.
2. TCE gas moved more quickly than water in the unsaturated zone where TCE migration in the gas phase was important.

Compared the vertical profile of the TCE concentrations experimented and that of calculated,

3. Parameters such as diffusion coefficient, partition coefficient and decay coefficient have been derived.

ACKNOWLEDGMENTS

The authors gratefully acknowledge Professor, Emeritus Shindo, S. of Chiba University, and Professor Hirata, T. of Wakayama University for discussing the results.

REFERENCES

1. Hunt, J. R., N. Siltar, and K. S. Udell (1988) Nonaqueous phase liquid transport and cleanup, 1, Analysis of mechanisms, Water Resour. Res.,24, 1247-1258, 1988
2. Warren J. Lyman, Patrick J. Reidy, Benjamin Levy (1992) Mobility and Degradation of Organic Contaminants in Subsurface Environments, C. K. SMOLEY, INC, pp153-176
3. B. E. Sleep and J. F. Sykes (1989), Modeling the Transport of Volatile Organics in Variably Saturated Media, Water Resour. Res., 25, 81-92
4. Nobuaki EGUSA, Tatemasa HIRATA and Changyuan TANG (1997), Vertical transport of chlorinated hydrocarbons in unsaturated zone, Proceedings of hydraulic engineering, JSCE, 41, pp569-574
5. Schwille, F. (1967) Petroleum contamination of the subsoil-A hydrological problem, in The Joint Problems of the Oil and Water Industries, Proceedings of a Symposium, edited by P. Hepple, pp.23-54, Institute of Petroleum, London
6. van Dam, J., The migration of hydrocarbons in water-bearing stratum (1967), in The Joint Problems of the Oil and Water Industries Proceeding of a Symposium, edited by P. Hepple, pp. 55-88, Institute of Petroleum, London
7. Christakos, G (1992) Random Field Models in Earth Sciences, Academic Press, San Diego, California, USA.
8. Mayer, A. S. & Miller, C. T (1996) The influence of mass transfer characteristics and porous media heterogeneity on nonaqueous phase dissolution, Water Resour. Res.,32, 1551-1567
9. Parker, J. C.(1989) Multiphase flow and transport in porous media, Reviews of Geophysics, 27,311-328
10. M. TH. van Genuchten (1980) A Closed-form Equation for Predicting the Hydraulic Conductivity of Unsaturated Soils, Soil Sci. Am. J., 44, 892-898
11. Huyakorn, P. S. and K. Nilkuha (1978) Solution of transient transport equation using an upstream weighted finite element scheme. Apple. Math. Modeling. 3:7-17
12. A.K. Katyal, J.J. Kaluarachchi and J.C. Parker (1991) MOFAT: A two-dimensional finite element program for multiphase and multicomponent transport, program documentation and user's guide, EPA/600/2-91/020

Underground Development and Groundwater Technologies

Experimental Study on Gas Seepage in Rock

Kuniaki SATO[1] and Masahiko EBARA[2]

1 Member of IAHR, Hydroscience & Geotechnology Laboratory, Faculty of Engineering, Saitama University, 255 Shimo-ohkubo, Urawa, Saitama, 338-8570 JAPAN
2 Design Office, Civil Engineering Dept., Electric Power Development Co., Ltd., 6-15-1 Ginza, Chuo-ku, Tokyo, 104-8165 JAPAN

ABSTRACT. In order to investigate the characteristics of gas seepage in rock, laboratory tests on one-dimensional seepage were carried out for several columnar rock samples (andesites, granites and tuffs). The permeabilities of gas seepage in dried and saturated rocks are discussed based on test results and theoretical approach. Nonlinear relationships between seeping gas flow rate and acting pressure were obtained experimentally, and the intrinsic permeabilities lay in the range from 10^{-19} to 10^{-15} m^2 for the rock specimens employed in these experiments.

KEY WORDS: gas seepage, permeability, laboratory test, underground storage

INTRODUCTION

Many large-scale underground caverns have been constructed in Japan for energy storage, hydroelectric power stations etc. Especially in point of the energy storage, crude oil has been stored in underground rock caverns since 1993, after successful completion of the Kikuma Test Project [1], [2]. The feasibility of storing liquefied petroleum gas (LPG) has also been demonstrated in a pressurized rock cavern [3], and underground storage projects of LPG are already under way in this country. An underground cavern at a pilot plant for investigating more efficient electric power generation by using compressed air energy storage and gas turbine system (CAES-G/T) is under construction to test performance and reliability in northern Japan [4].
In the underground storage of compressed air, LPG and other fuel products, the water-seal system has earned popularity due to low cost. In order to maintain reliable underground storage, it is very important and essential to keep the water-seal system safe. Therefore, several laboratory tests and field investigations on gas seepage phenomena through rock masses have been carried out by several authors [5], [6]. Unified design criteria against gas leakage have, regrettably, not been established for lack of basic knowledge of gas seepage as well as parameterization. In the water-seal system, gas or air tightness is required for both fractures and texture of rock.
In the present study, the laboratory tests focus on dynamic characteristics of gas seepage in rock itself. Rock specimens used in the tests are andesite, tuff and granite, three typical rocks in Japan.

THEORETICAL BASIS OF GAS SEEPAGE

Taking the basic nature of gas seepage into consideration, the fundamental equation of seepage is expressed by Eq. (1), which is derived from equations of continuity, motion (Darcy's law) and a state equation of gas [7]. Eq. (1) is known as Leibenzon's unsteady seepage equation of a gas.

$$\mathrm{div}(\mathrm{grad}\ P) - \frac{\lambda \cdot \mu_g}{K \cdot \beta(1+n)} \left(\beta \frac{1+n}{n} \right)^{1/(1+n)} \cdot P^{-n/(1+n)} \cdot \frac{\partial P}{\partial t} = 0 \ , \qquad (1)$$

$$P = \frac{n}{\beta(1+n)} p^{1+1/n}, \tag{2}$$

in which λ, K, μ_g, β and p are effective porosity, intrinsic permeability, the coefficient of gas viscosity, a constant and absolute pressure, respectively. The exponential parameter n depends on compressibility of the gas. When the process is isothermal, n equals unity. If the change in gas state is adiabatic, n will be c_p/c_v, in which c_p and c_v are the specific heat of the gas at a constant pressure and at constant volume, respectively. Generally if the isothermal assumption is adopted in gas seepage, n equals unity. Under this assumption, the fundamental equation, a steady pressure distribution and steady gas flow rate are given by Eqs. (3), (4) and (5).
According to these equations, it is obvious that the pressure distribution is nonlinear along depth z, and the air flow rate Q_g is proportional to the square of the pressure difference $(p_l-p_0)^2$, in deviation from Darcy's law.

$$\frac{\partial^2 p^2}{\partial z^2} - \frac{2\lambda \cdot \mu_g}{K} \frac{\partial p}{\partial t} = 0, \tag{3}$$

$$p^2 = \frac{z}{l}(p_l^2 - p_0^2) + p_0^2, \tag{4}$$

$$Q_g = \frac{K \cdot A}{2\mu_g p_a} \frac{p_0^2 - p_l^2}{l}, \tag{5}$$

where Q_g, z, l, A and p_a are gas flow rate at atmospheric pressure (1atm=101kPa), coordinate along the axis of rock, length, cross sectional area of rock and reference pressure (=1atm), respectively. Pressure p_o and p_l express those at depth $z=0$ and $z=l$.
The correlation between Darcy's permeability k and intrinsic one K is written,

$$k = \frac{K\rho g}{\mu}, \tag{6}$$

where ρ, g and μ are density of fluid, acceleration of gravity and coefficient of viscosity, respectively.
Gaseous fluid generally has large compressibility, and density greatly depends on the degree of pressure. Nevertheless, viscosity is not highly dependent on compressibility. It is thus reasonable to employ intrinsic permeability to evaluate the permeability of porous media in gas seepage phenomena.

LABORATORY TESTS

A set of laboratory tests in one-dimensional gas seepage was carried out to obtain the intrinsic permeability of several rock samples and to investigate relationships between pressure and gas flow rate. The tests also aimed at discovering how intrinsic permeability relates to porosity and water content. The permeability of steady state air flow was evaluated under a constant atmospheric temperature.

TEST APPARATUS AND PROCEDURE

The appearance and configuration of the testing apparatus are as shown in **Photo.1** and **Fig.1**. The apparatus basically consists of a pressure cell ④, a compressed air tank ⑧, measuring instruments ③,⑥ and gas regulator ⑦, and it has a maximum testing pressure of 10 MPa. The accuracy in minimum pressure is 0.01 MPa. Two air flow meters measure up to 10 cm^3/min and 100 cm^3/min in accordance with flow rate.

As shown in **Fig.1**, a required loading pressure acts on the top of the specimen, and pressure at the bottom is kept to be constant in atmosphere. A circumferential sidewall of the specimen in the pressure cell is confined by water pressure using a rubber membrane so as to prevent gas leakage along the sidewall of specimen.

Testing procedures are as follows: The water content of the specimen was kept either dried or saturated at the initial stage. A required loading pressure was put on the top of the specimen after setting confined pressure through a rubber membrane. The loading pressure was charged from 0.5 MPa up to 7 MPa in 12 steps. Steady state air flow for each step was measured when constant after an elapsed time of 15 minutes. The same procedure was repeated for different kinds of testing rocks under a constant temperature room (20℃).

Photo.1 Appearance of test apparatus

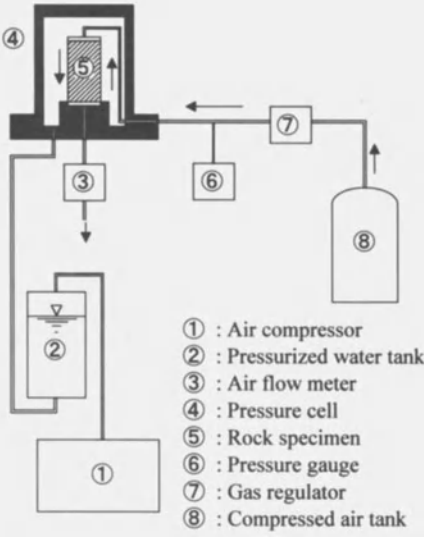

Fig.1 Test apparatus configuration

ROCK SAMPLES

Rock samples tested in the experiment were andesites collected from Emochi and Shinkomatsu, tuffs from Izu and Shirakawa, and granites from Teisen and Inada in Japan. All samples were columnar shape, 5 cm in diameter and 10 cm in height. The physical properties of each rock type and cement mortar are listed in **Table 1**. It can be recognized from the table that the density of plutonic rocks like granite is higher than that of volcanic rocks and that the porosity of the volcanic rocks is smaller. Three photographs of typical rock specimens are shown in **Photo.2**.

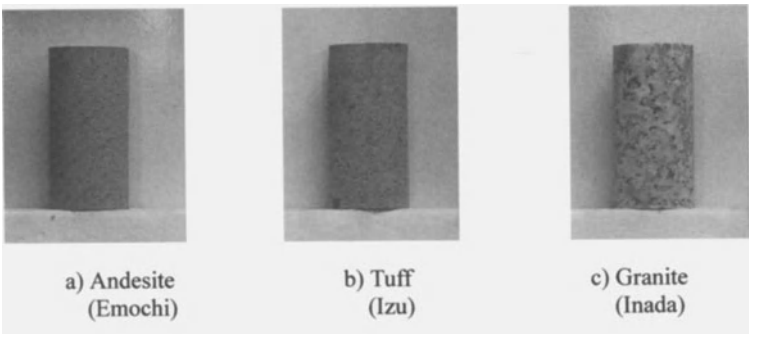

Photo.2 Appearance of rock specimens

TESTING CONDITIONS

Gas seepage tests were carried out for seven rock specimens in dried and saturated conditions. At the initial state of water content, the "dried" condition was attained by drying 24 hours at a temperature of 110℃, and the "saturated" rock samples were prepared by submerging and vacuuming in a water tank for a week. To avoid entrapped air in pores, prudent care was taken before each gas seepage test.

GAS SEEPAGE CHARACTERISTICS OF ROCK

The intrinsic permeabilities of dried rocks (K_d) obtained in the test are in the range from 10^{-19} m^2 to 10^{-15} m^2 (corresponding to 10^{-12} m/sec～10^{-8} m/sec in Darcy's permeability at kinematic viscosity $\nu_{20℃}$) as shown in **Table 1**. As a tendency, the intrinsic permeability (K_d) increases as effective porosity increases. The intrinsic permeabilities of saturated rocks (K_{sat}) range from 10^{-19} m^2～10^{-16} m^2 and the K_{sat}/K_d ratio ranges from 0.03 to 0.43. Similar results have also been reported by Sakaguchi et al., in a laboratory test using andesite, granite and sandstone [8].

Table 1 Physical properties and intrinsic permeabilities obtained in laboratory tests

Rock sample	Dry density (g/cm^3)	Effective porosity (%)	Intrinsic permeability for dried rock K_d (m^2)	Intrinsic permeability for saturated rock K_{sat} (m^2)
Andesite (Emochi)	2.15	12.96	$5.349x10^{-18}$	$3.070x10^{-19}$
Andesite (Shinkomatsu)	2.63	3.54	$1.013x10^{-16}$	$4.019x10^{-17}$
Tuff (Izu)	1.99	22.43	$1.103x10^{-17}$	$2.840x10^{-19}$
Tuff (Shirakawa)	2.03	21.30	$3.306x10^{-15}$	$3.217x10^{-16}$
Granite (Teisen)	2.70	0.74	$9.044x10^{-19}$	$3.030x10^{-19}$
Granite (Inada)	2.62	0.67	$5.805x10^{-19}$	$2.501x10^{-19}$
Cement mortar	1.83	23.57	$4.700x10^{-16}$	$3.072x10^{-18}$

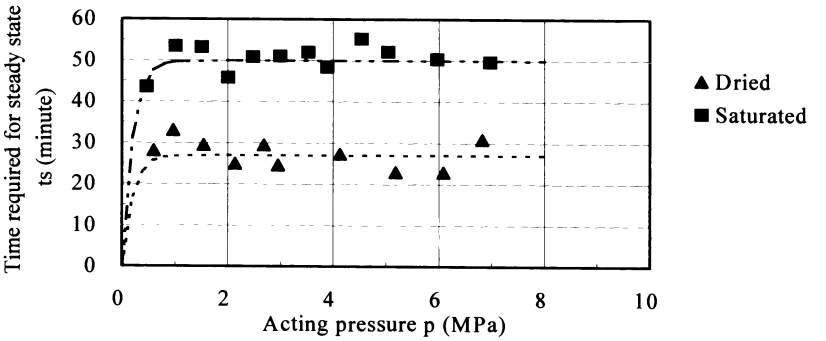

Fig.2 Two typical experimental relationships between acting pressure p and stability time ts reaching steady state gas seepage for andesite (Emochi)

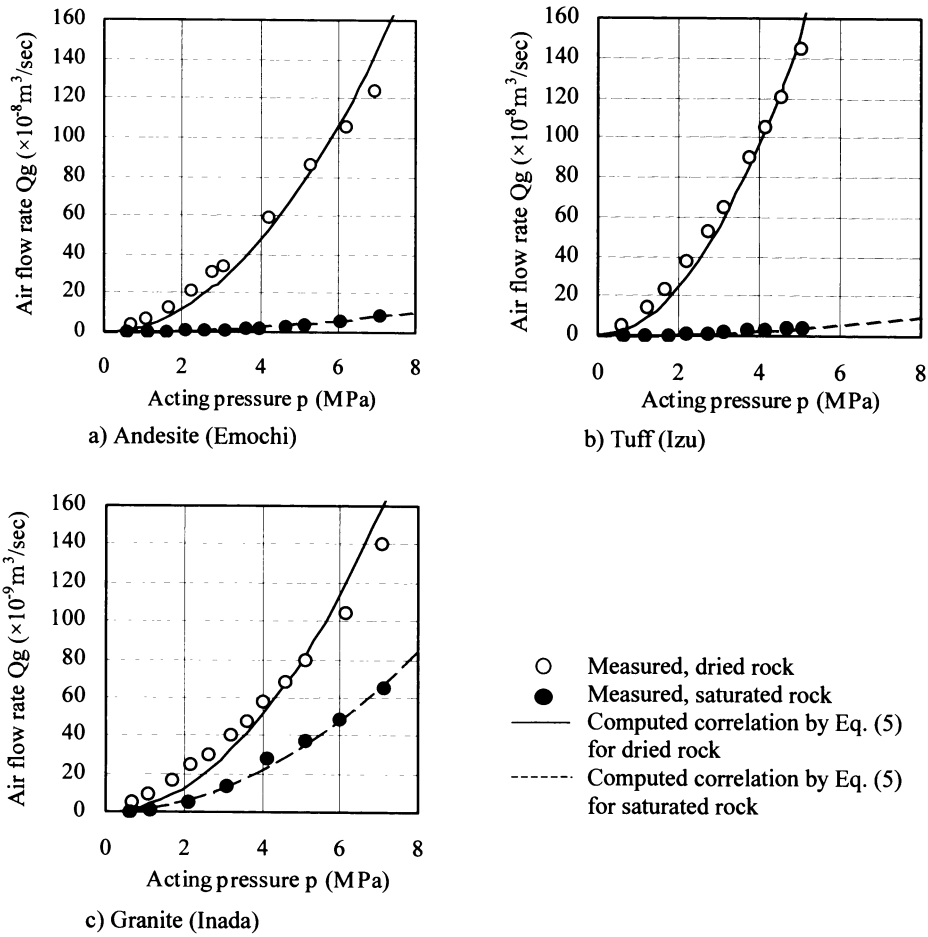

Fig-3 Relationships between acting pressure p and air flow rate Qg

In the seepage process of pressurized air, the time required for a steady flow rate was approximately 27 minutes for dried andesite (Emochi) as shown in **Fig.2**.
The elapsed time for seepage to arrive at steady state is noteworthy. The mechanism behind this phenomenon involves that stable air pressure in pores is attained by successive, steady increments in seepage over time in dried rock. Namely, the formation of steady state air pressure requires a certain amount of time. Similarly, the time until constant seepage flow was observed to be around 50 minutes for the saturated andesite (Emochi) as well. The reason for this lies in the fact that the pore water in specimen is continuously squeezed out and replaced by air.
Fig.3 shows typical relationships between gas flow rate (Q_g) and acting pressure p for different rocks at both dried and saturated conditions. A set of experimental flow rates (Q_g) for each tested rock is compared with theoretical ones computed from Eq. (5) by substituting the averaged intrinsic permeability K. A good agreement between experimental and theoretical results is clearly recognized.

CONCLUSION

To keep the water-seal system safe, the gas or air tightness is required for both fractures and texture of rock mass. In the study, the laboratory tests focus on finding intrinsic permeabilities of several rocks and attaining correlations between pressure and air flow rate.
The test results can be summarized as follows:

1) The intrinsic permeabilities K range from 10^{-19} m^2 to 10^{-15} m^2 for dried rock samples and from 10^{-19} m^2 to 10^{-16} m^2 for saturated rock samples. The ratio of K_{sat} / K_d is 0.03～0.43.
2) In dried rock, the intrinsic permeability increases with increasing effective porosity.
3) Experimental results between air flow rate Q_g and acting pressure p agree well with the theoretical correlations derived from Eq. (5).

The authors would like to express their thanks to The Central Research Institute of Electric Power Industry for technical support and facilities for research.

REFERENCES

1. Miyashita K. et al., (1983) An investigation of geomechanics and hydraulics around an underground crude oil storage cavern, Int. Sym. on Field Measurements in Geomechanics, 1117-1126, Zurich
2. Hoshino K. and Makita T., (1990) Construction of large underground caverns for the storage of crude oil in ductile rocks of Miocene volcanism, Proc. of 6th Int. Congress of Engineering Geology, 2587-2592
3. Tokimasa H., (1993) Demonstration plant outline on LPG underground storage technology, J. of Japan Tunneling Assoc. (in Japanese), Vol.24, No.5, 389-395
4. Ishihata T., (1997) Underground compressed air storage facility for CAES-G/T power plant utilizing an airtight lining, News J., ISRM, Vol. 5, No.1, 17-21
5. Aberg, B., (1977) Prevention of gas leakage from unlined reservoirs in rock, Rock Store '77, Stockholm, 175-189
6. Nakagawa K. et al., (1986) Prevention of leakage of compressed air stored in unlined rock caverns (in Japanese), JSCE, 370/III-5, 233-241
7. Aravin, V.I. amd Numerov, S.N., (1965) Theory of fluid flow in undeformable porous media, Israel Program for Scientific Translation, Jerusalem, 54-97
8. Sakaguchi T. et al., (1992) Fundamental study of gas seepage in rock and open-crack (in Japanese), JSCE, 445/III-18, 17-25

An Investigation on Uplift Forces Acting on Water Structures' Floors

M. A. Ashour and F. K. Abd El-Sayed

Civil Eng. Dept., Faculty of Eng., Assiut University, Assiut, Egypt

Abstract. Till now theoretical values of uplift forces are used in the design of water structures floors regardless of the effect of local conditions on the design parameters. The work presented herein attempts to provide a better understanding of the uplift characteristics under such floors and to clarify to what extent the experimental results obtained are compatible with theories of the behavior of uplift forces. The results obtained gave an explicit range of distribution of the uplift forces in both longitudinal and transverse directions and showed good agreement with previous research. The study included the effect of using a cut-off, either at the beginning or at the end of the floor, as well as the effect of the underlying pervious layer thickness.

Key words. Uplift forces, Cut-off , Water structures

INTRODUCTION

Water structures are generally subjected to upstream water levels that are higher than downstream levels. Sometimes water levels vanish in certain circumstances such as repair periods. These structures are usually built on a pervious soil where water percolates underneath the floor. For this reason, the floor represents one of the most important parts of such structures. Certain provisions should be taken to overcome the upward directed forces acting on the floor as well as undermining the floor near the downstream exit. In the design of solid floors, Bligh [1], assumed that the horizontal and vertical contact surface length between the floor and subsoil represents the length of the path followed by filtering particles of water. This is called the creep line. He also assumed that the head loss per unit length is constant throughout the length of the creep line, in both horizontal and vertical directions. A certain coefficient, C_B, governs the minimum floor length to guard against undermining, according to Bligh's simple empirical formula:

$$L_P = C_B.H_d \qquad (1)$$

where L_P is the length of percolation creep line measured along the perimeter of contact between soil and floor, H_d is the maximum differential head, and C_B is Bligh's coefficient. Values of C_B depend upon type of soil and range between 7.0 and 15.0. Therefore, the hydraulic gradient, H_d/L_P which equals $1/C_B$, must be kept below a certain limit to ensure safety against piping. Lane [2], considered that the water follows the path of least resistance, contrary to Bligh's assumption that water follows the line of creep. Lane suggested that, in calculating the length of creep, one should discriminate between vertical and horizontal surfaces, greater weight being attributed to vertical than horizontal because, firstly, local soil settlement (roofing) beneath the floor following construction is dangerous and is akin to a piping failure. This can not occur on vertical or steeping sloping faces since the voids would be immediately filled again owing to the ability of earth to maintain a steep slope. Another reason is that in stratified soils resistance is greater in the vertical direction than in the horizontal. Therefore Lane chose a one-to three

efficiency ratio of horizontal to vertical length of floor, considering all sloping contacts less than 45° to be added to the vertical sum, as represented by the relation:

$$L_t = \frac{L_x}{3} + L_y \qquad (2)$$

where L_t is the total considered contact length of percolation, L_x is the sum of horizontal contacts and sloping surfaces with a slope less than 45° to the horizontal, and L_y is the sum of vertical contacts and sloping ones with a slope of more than 45°. The safe total length L_T, according to Lane is therefore:

$$L_T = C_L.H_d \qquad (3)$$

where C_L is Lane's coefficient. Values of C_L range between 1.6 and 8.5, depending upon the type of subsoil. Bligh's assumption, previously mentioned, met with much adverse criticism because exact mathematical solutions, carried out later [3, 4, 5] showed that the hydraulic slope is not constant along the entire length of the floor, as he assumed. In addition, it has been found that soil can resist values of hydraulic slope greater than what he stated. Also, it has been found that the resistance to the flow of water in the vertical direction is much greater than that in the horizontal direction. Because of these considerations, Lane introduced his theorem discussed previously. The main aim of the experimental study presented here is to obtain a better understanding of the characteristics of the longitudinal and transverse distribution of uplift forces on a floor in one of the most critical situations where the upstream water level is maximum while there is no water at the downstream end. In the present investigation, both length and thickness of the floor are kept constant while the upstream water level, relative depth of a cut-off placed at either the beginning or end of the floor, and relative depth of the pervious sandy layer underneath the floor are variable. Till now, no exact solution is available to determine the effect of plane drainage located anywhere between two end cutoffs of a flat floor founded on permeable soil of finite depth. An accurate solution has been obtained using conformal mapping by Kumar et al. [4]. Equations for uplift pressure below the floor and exit gradient are given.

EXPERIMENTAL WORK

The experimental set up is shown in Fig. 1. Tests were carried out in the Irrigation and Hydraulic Laboratory of the Civil Eng. Dept., Assiut University, Assiut, Egypt. In the channel shown in Fig. 1, a two centimeter thickness floor rested on a pervious layer of sand. Three layers of sand with different thickness (10, 20, and 30 cm) were used. A gate was erected upstream on this floor to maintain a maximum upstream water level, H_o, of 40 cm. To get the mean upstream water depth a side well was connected to the channel through three openings flushed from the bottom, by a pipe 12 mm diameter. For measuring the values of uplift pressure acting on the floor in both longitudinal and transverse directions, a plate with twenty one holes was prepared to fix the piezometer nozzles, as shown in Fig. 2. The piezometers were connected with plastic hoses to glass tubes mounted on a wooden board covered with a squared paper (1.0x1.0 mm grid).

RESULTS AND DISCUSSION

From the data collected the following results were calculated:

All dimensions in m

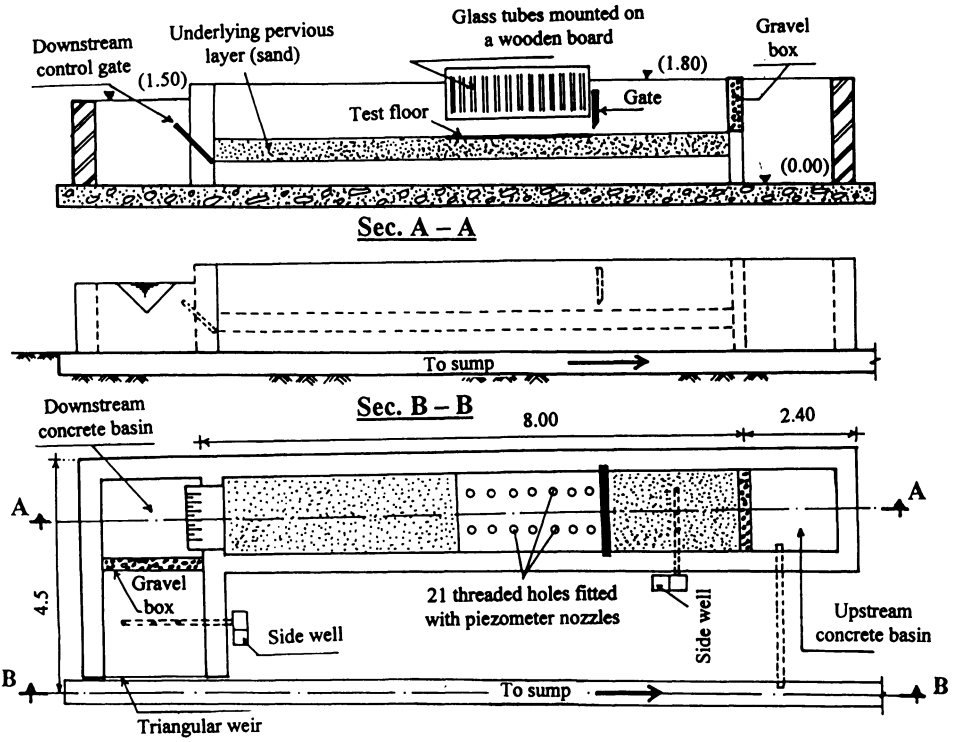

Fig. 1. Schematic sketch of the experimental channel.

Figure 3 shows the relationship between the relative observed uplift pressures U/H_o and the relative values of longitudinal distances x/L, where U is the uplift pressure measured through the piezometer holes, H_o is the maximum upstream water level, x is the distance from the gate, and L is the floor length. Four values of H/H_o namely, 1.0, 0.8, 0.6, and 0.4 were considered, where H is the upstream water depth. Each point indicated on the four curves, is the average of the three measured values located in the transverse direction. It is clear that, at a certain value of x/L, as the ratio H/H_o increases, the ratio U/H_o increases too. It can also be seen that the uplift pressure at the beginning of the floor is about 92% of the upstream applied water head while this value reaches about 26% at the downstream end of the tested floor length.

All dimensions in cm

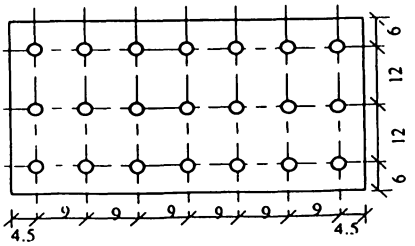

Fig. 2. Location of piezometer holes.

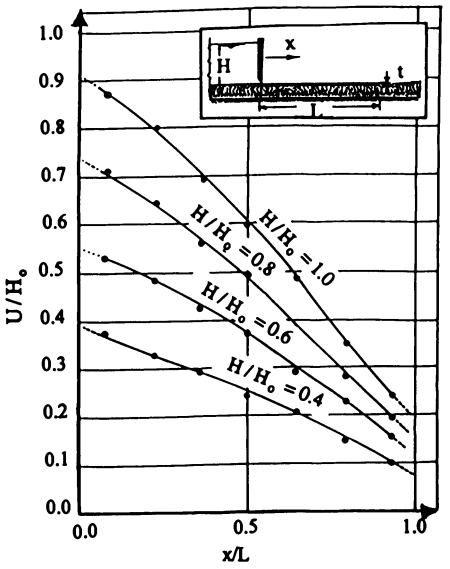

Fig. 3. Longitudinal distribution of uplift pressure below the floor.

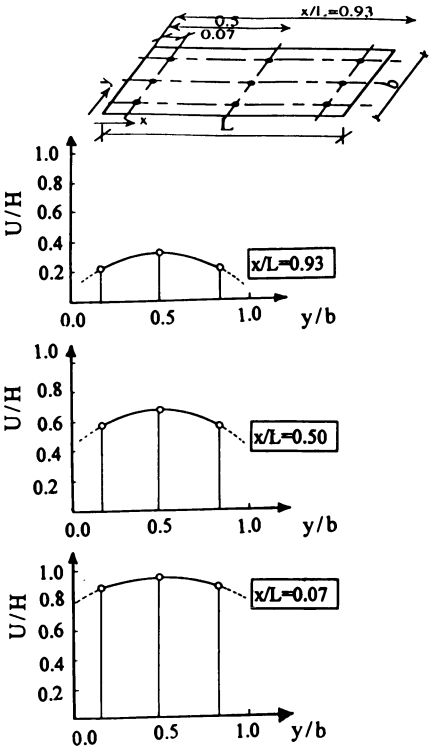

Fig. 4. Distribution of uplift pressure in transverse direction ($H/H_0 = 1$).

Figure 4 shows the relationship between U/H and distance y/b in the transverse direction at distances of the gate x/L equal to 0.07, 0.5, and 0.93. It can be seen that the uplift force in the center is bigger than at the edges and that the rate of difference increases with increase of x/L. The difference is found to be about 12% at $x/L = 0.07$, while this value reaches about 26% at $x/L = 0.93$.

For different values of x/L, Fig. 5 shows, the relationship between U/H and relative depth of a cut-off placed at the end of the floor length, denoted by d/t, where d is the cut-off depth and t is the floor thickness. From Fig. 5, it can be concluded that, at any value of x/L, the existence of a cut-off at the end of the floor increases the uplift pressure. Also, as the relative depth of this cut-off increases, the relative uplift pressure increases too. It is also worth mentioning that the rate of increase of U/H increases with increase of x/L.

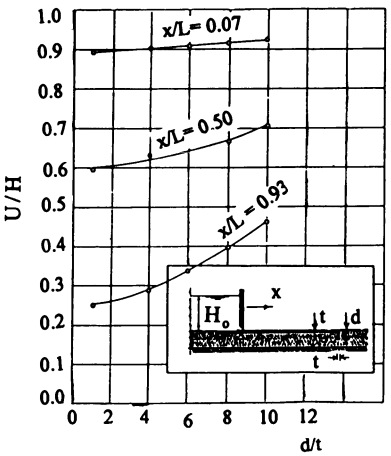

Fig. 5. Effect of relative depth of cut-off at the end of floor on the relative uplift pressure ($H/H_0 = 1$ and $T/t = 10$).

Figure 6 shows the relationship between U/H and relative depth, d/t, of a cut-off placed at the beginning of the floor, for different values of x/L. Form Fig. 6 it can be concluded that, at any value of x/L, the existence of a cut-off at the beginning of the floor decreases the uplift pressure. In addition, as the relative depth of the cut-off increases, the relative uplift pressure decreases. It is also clear that the rate of decrease of U/H decreases as x/L increases, which confirms the great advantage of a cut-off of suitable relative depth, if placed at the beginning of the floor.

For comparison, three curves relating U/H with x/L are plotted in Fig. 7 representing the case of using a cut-off at the beginning, a cut-off at the end of the floor, and the case of no cut-off. From this figure it can be seen that using a cut-off at the beginning of the test floor significantly reduces the relative uplift pressure over the entire length of the floor, starting by a reduction value of about 32% and ending by a value of about 54%. Meanwhile, using a cut-off at the floor end increases the relative uplift pressure starting by a small increase of about 2% and ending by a value of about 32%. This can be attributed to the fact that the use of a cut-off at the beginning of the floor elongates the percolation path underneath the floor, leading to a reduction in uplift pressure. But the use of a cut-off at the floor end, although having a positive influence on decreasing the exit gradient, has the negative effect decreasing the uplift forces under the floor. This is, perhaps, due to rebound of the seepage flow resulting from the cut-off obstruction to this flow.

The relationship between the relative uplift pressure and the relative values of longitudinal distances, for three values of T/t (5, 10, 15) where T is the depth of the pervious layer underneath the floor, is given in Fig. 8. It can be seen that increasing the relative value T/t increases the relative value of uplift pressure. Within the tested range of underlying layers' thickness, it was found that T/t and the relative uplift pressure are related approximately linearly.

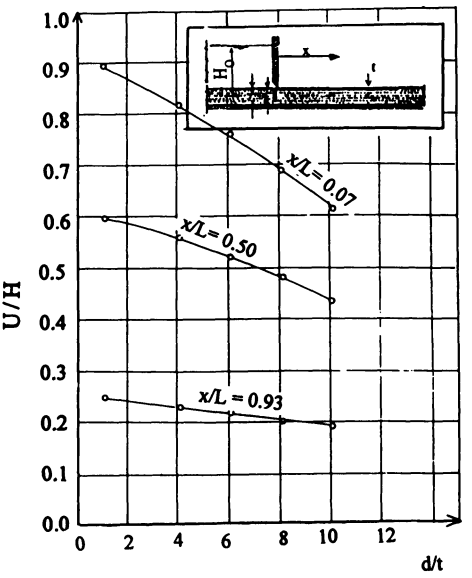

Fig. 6. Effect of relative depth of cut-off at the beginning of the floor on the relative uplift pressure ($H/H_o = 1$ and $T/t = 10$).

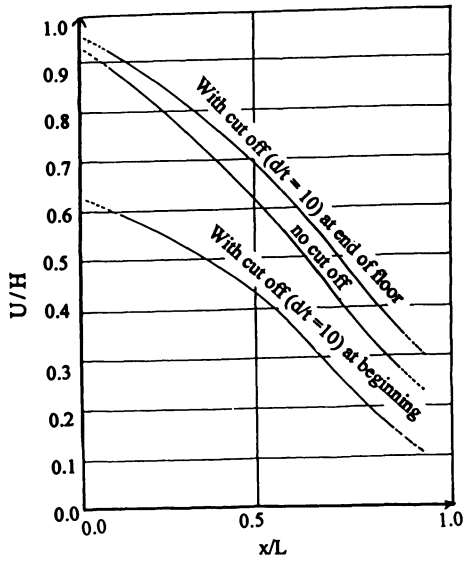

Fig. 7. Comparison curves between uplift forces under a floor with and without cut-off ($H/H_o = 1$).

CONCLUSIONS

The experimental results obtained strongly support the theoretical behavior described by Kumar et al. [4]. The following conclusions can be drawn:

1) Placing a cut-off at the beginning of water structures floors significantly improves the uplift characteristics under such floors. A reduction of about 32% was achieved just down stream a cut-off having a depth equal to 10 times the floor thickness. Therefore it is recommended to use a cut-off at the mentioned location in the design of floors subjected to high values of uplift pressures.
2) The use of a cut-off at the end of water structures floors has an adverse effect on the uplift pressure underneath such floors.
3) The thicker the underlying pervious layer is, the higher the values of uplift pressure will be.
4) The distribution of uplift pressure in the transverse direction proved to be non-uniform: bigger at the center while smaller towards the edges. The difference in uplift forces between center and edges reached about 26% at the end section of the test floor.

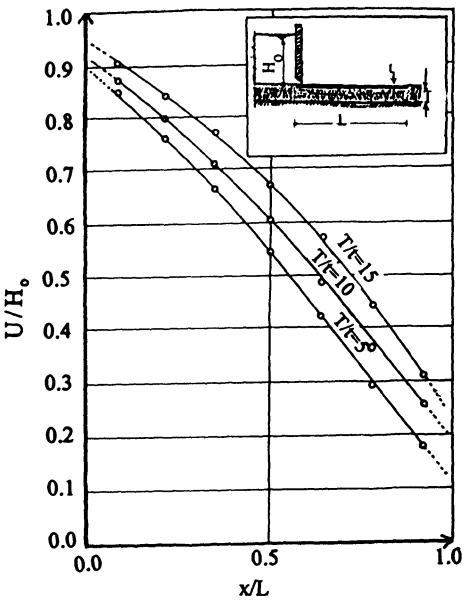

Fig. 8. Effect of relative depth of underneath pervious layer on uplift pressure ($H/H_o = 1$).

REFERENCES

Books.

1- Bligh, (1910) The practical design of irrigation works. 2nd edition, pp 108, Cited from [6]
3- Grishin MM, (1982) Hydraulic structures. Vol. 1, Mir Publishers, Moscow
6- Lelivasky S, (1957) Irrigation and hydraulic design. Vol. 2, London, pp 37-113

Journal papers.

2- Lane EW, (1932) Security from under seepage. J Trans. Am. Soc. C.E. pp 1269, Cited from [6]
4- Kumar A, Singh B, Chawla AS, (1986) Design of structures with intermediate filters. J Hydraulic Engineering, ASCE, Vol. 112, No. 3

Edited works.

5- Salem MH, Salama MM, El-Giddawy E, (1990) Seepage under hydraulic structures for different arrangements of riprap and filters. National seminar on Physical Response of the River Nile to interventions, Proceedings Cairo

The Long-Term Piping behind the Concrete Lining of a Tailrace Canal with High Diurnal Drawdown; Beresti Canal Case

Gheorghe Armencea[1], Emil Neagoe[2] and Ion Moraru[3]

[1] Technical University of Civil Engineering, Hydraulic and Environmental Protection Department, Bucharest, 124 Lacul Tei, Sector 2, 72302, Romania
[2] Hidroelectrica, Piatra-Neamt Division, Piatra - Neamt, Romania
[3] Institute of Hydroelectrical Studies and Design, Hydraulic Laboratory, 5-7 Vasile Lascar, Bucharest,79669, Romania

ABSTRACT. The paper describes the methodology and the results of a field study which was initiated when large zones of Beresti hydropower canal lining were cracking.The operation of the Beresti tailrace has the following features. For the peak demand, the discharge of Q=330 m^3/s flows with a mean depth of about 4.5 m. The diurnal water tide has a peak of 3.0 m. The rate of drawdown was of about 1.8-3.0 m/h, for unrestricted shut down of the two turbines.
After 5-6 years of operation, in some zones of the canal slope the concrete slabs cracked and many of them collapsed. Field study was carried out in 1995. Two sections were chosen for detailed measurements; they were instrumented with an array of piezometers. In embankment and weeper stand pipe piezometers were installed, and beneath the lining, on the back side of slabs, boundary piezometers were placed. The transient water table in canal and bank soil was simultaneously recorded. The seepage flow gradients could be determined and, in the first stage of the drawdown, their values were larger than the critical gradients of soil in the weeper zone. The piping phenomenon caused extended holes of 0.2 - 0.3 m deep.
Analyses of soil samples, collected from the holes, found the presence of an armouring layer on the hole perimeter. This fact put forward that the fine sand washing ceased after forming of a natural filter.

KEY WORDS. Piping, tailrace lining ageing, rapid drawdown, transient groundwater flow, field study of pore water pressure

INTRODUCTION

Tailraces bears some water levels fluctuation brought about by surge waves.. In general, the height of the wave is of the order of half meter. The Beresti tailrace, of 4.5 km. long and 40 m. in width has a diurnal water level variation of 3.0m high. The Beresti hydropower station is the last one of a chain of medium head hydro development of the Siret river- Romania. Until the completion of the downstream reservoir, the operation of the tailrace has been characterized by this unusual drawdown (Fig. 1).

After some years of operation, large areas in the drawdown zone presented serious damages of the concrete slabs which lines the banks; the aspect of such areas on the left bank is exposed in Fig.2 The task to state the main cause of that event was difficult because, at the first glance, the damaged areas were distributed at random and the aspect of damages was diverse, from slabs' displacements to slabs' fractures and foundation material erosion.

A field study of the unsteady open–channel flow and the induced transient groundwater flow was undertaken in the summer of 1995. The paper describes the results of a parallel recording of the

tailrace water levels and the transient pore water pressure in the vicinity of the concrete sheet, on the left bank. The diagrams and the schemas of the actual seepage flow elucidated the stages of the long-term internal erosion, which was manifested by an extended cavity behind the slab.

MEASUREMENT SECTIONS

At the beginning of the field study, the only information on the implied phenomena were that the damaged areas were lying in the upstream half of the canal length; there, according to the hydraulics rules the height of the drawdown has the maximum value. In this zone was chosen one section at the distance of 2.7 km from the power station; which is referred to as Section A. The second section was placed at the last third of the canal length, where the damages were absent; this section is referred to as Section B. In the Table 1 are presented some features of these measurement sections, which proved to be very different from each other .

Table 1 Topographical features of the measurement sections

Symbol	Distance km	Drawdown rate	Drawdown height	Water TWL , m	Groundwater GWL, m	Weeper level m
Section A	2.760	2.9 m	3.0 m/h	93.0	c.. 91.5	91.5
Section B	3.600	2.3 m	1.6 m/h	92.5	c.. 91.3	92.0

The economics of the field study did not allow to extend the number of the measurement sections though the third one would have played the role of witness section.. The data in TAble 1 shows that the initial rate of drawdown in section A has been about double the section B value
We have to mention that these drawdown values were practised in the first years of the turbines operation; after occurrence of the cracks the power station staff diminished these rates, but without an evident influence on the course of events.

SITE INSTRUMENTATION

The design of lining was conceived so that every slab, with dimensions of 4.0x5.0x0.15 m, should have a weeper of 0.20 m in diameter, in the center of the area. In general, only one weeper opening lies in the drawdown zone. The weepers placed under canal static water level was not detected and investigated. The phreatic line in the riverain land was recorded intermittently (Fig. 1)

The measurement sections were instrumented with an array of three hydraulic piezometers; marked in Fig. 3 with P and S. One electrical piezometers, marked with letter C, was used to verify the time of response of the hydraulic piezometers P_6 The features of the installed piezometers are synthesized in Table 2.

Table 2 The characteristics of the installed piezometers

Section	Code	Type	Tip elevation, m	Diameters	Soil type	Place
A	P1	Standpipe	90.20	3/8"	Alluvial	Joint
	P3	Standpipe	90.50		Deposits	Weeper
	P4	Standpipe	90.80		(Fig.5)	Weeper
	P5	Standpipe	92.03			Weeper
B	P6	Standpipe	91.15	3/8"	Alluvial	Weeper
	S1	Nylon	90.30	0.8mm	Deposits	Slab back
	S2	Nylon	90.96			Slab back
	S3	Nylon	91.34			Weeper

The piezometers at the boundaries were coded with S. It consists of a bronze box, with geotextiles membrane, which was inserted in the back side of the concrete slab. The piezometer tube was brought up the slope, and the pore water pressure was measured in the transparent tube. Parallel records of the open-channel water level and the pore water pressure were performed during drawdown period, which lasted about two hours. Some records of the phreatic line variation were made, but the groundwater wave propagation was not studied.

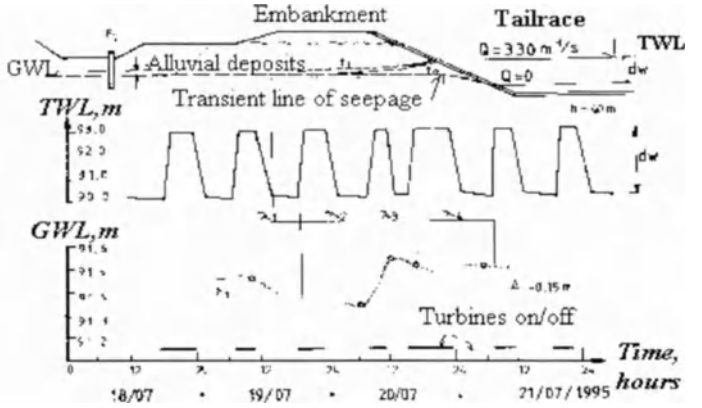

Fig.1. The control water levels of the unsteady open – channel and bank seepage flows

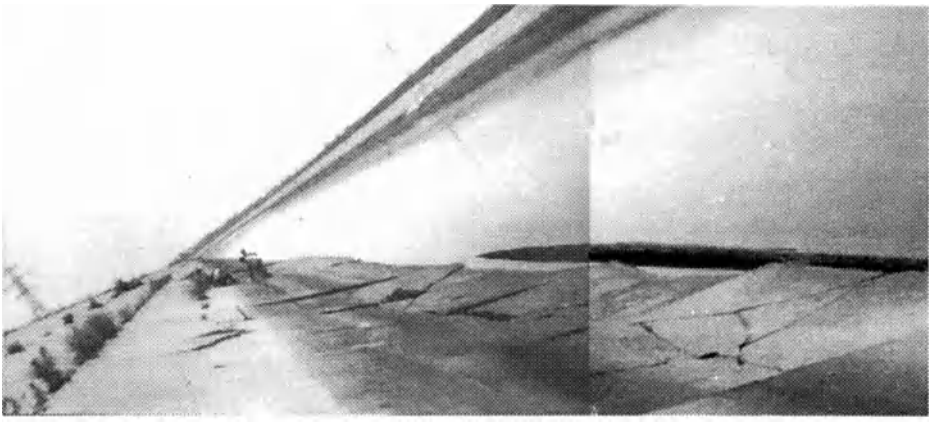

Fig. 2 View of the left bank lining in the drawdown area at the section A

MEASUREMENT RESULTS

The first field measurements were carried out in the section A. The representation of the piezometric levels versus time (Fig.3,4) showed a trend somewhat unexpected: a very rapid decreasing of the pore water pressure in P1, where the piezometric levels have been close to open–channel water levels (Fig. 4b). The results from the Section B seemed more consistent with classical theory of groundwater flow.

The diagrams of the piezometric levels as a function of three stages of canal drawdown has been presented in Fig.3. The axis of representation has the depression lines at the left, and the tailrace water levels at the right; the time origin , in general, has been the turbine shut down moment.

The marked difference between the drainage of the groundwater in the two sections suggested, at the field study time, to inspect in detail the weepers. At the section A, the hole from the bottom of the opening W4 proved to be not o local one, but an extended up and lateral, in the form of semicircle with the radius of about 2.0 m (Fig.3b). The presence of the cavity elucidated the groundwater flow features in section A.

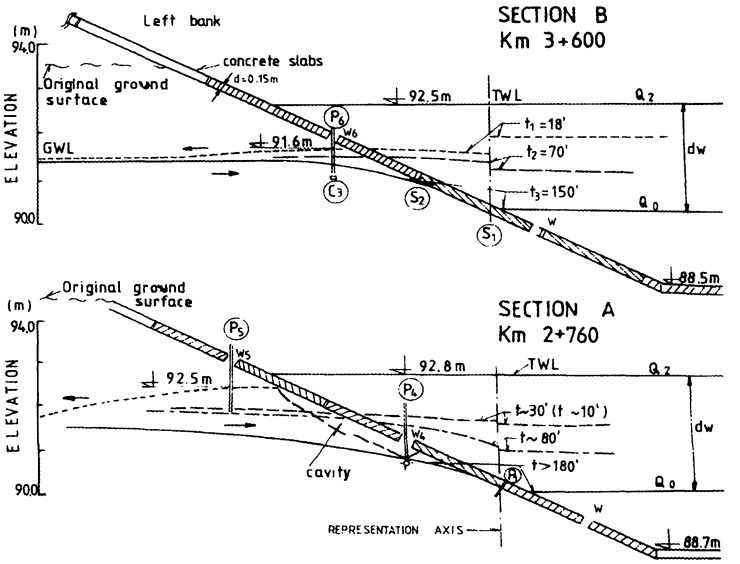

Fig. 3. Diagrams of the characteristic phases of unsteady flow in tailrace and left bank .

TRANSIENT GROUNDWATER FLOW

Seepage aspects. The detailed records of piezometric levels beneath the concrete slab (Fig.4) show that in the main phase of transient flow, when relative rapid changes of pore water pressure take place, the groundwater flows by the following mechanism. In the section B, the flow in the vicinity of the slab is underpressure. In the section A, a free surface flow, with a depression line imposed by the cavity, shows a low influence of the lining sheet.
In section B, the pressure variation in all piezometers is very slow and the piezometric levels are practically the same along the back of the slab. The diagram of piezometric levels in section A shows that the water pressure decreases down the slope, with the last point P1, very close to control water level..

The two schemes based on the data in Fig 4 would be considered as the initial and final type of groundwater flow in the left bank alluvial deposits: one at the beginning of canal operation and the other at present. The inspection of the slab weepers reveals that all weepers with vegetation, as the sign of an efficient filter at the orifice opening, were remaining at the initial aspect of flow. The weepers without vegetation presented inner holes and cavities with various stages of development, which changed the aspect of groundwater flow. This fact has explained that random presence of weeper filter determined at random places of lining damages due to the collapse of the slabs.

Flow gradients. During the drawdown, the maximum seepage flow gradient might be considered to occur when the tailrace water level has been at the weeper elevation. The field records came to light the head values of about H= 0.8 – 1.0 m. Under the hypothesis of a flow net generated by a spherical sink [1], the gradient has been of bout i=0.45 – 0.48.

For the section with cavity the discharge through the weeper was no longer through porous media; it was like a reservoir orifice discharging in atmosphere. This type of pressure flow lasted 3-5 minutes. After this phase the seeping flow has been of free surface type with the top flow line containing the point P1, which did not manifest any pressure on back side of the slab. Under the hypothesis of a permanent seepage flow the gradients were computed by means of a software [6] based on the boundary element method [5]. The maximum values of about i= 1.0 – 1.1 are found in the vicinity of the discharge point on the slope

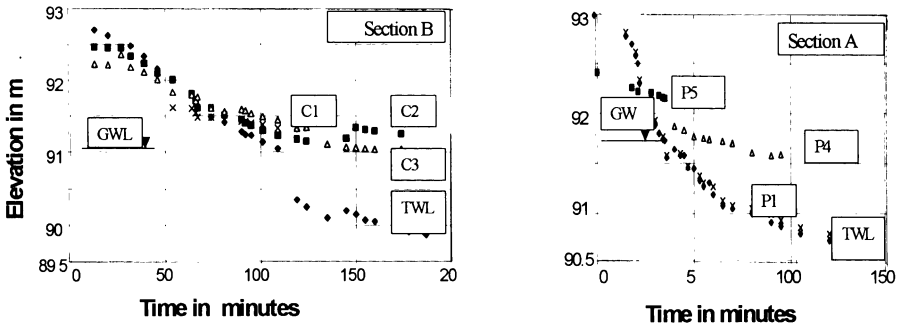

Fig.4. Diagrams of the piezometric levels as a function of time

INTERNAL EROSION DEVELOPMENT

Grain size curves. Some samples of bank material were taken from weeper hole (Fig. 5). The sample characterizing the undisturbed alluvial deposits, in which the canal had been excavated, was analyzed by means of the geometrical criterion of the granular material resistance to 'suffosion' (piping). This method was proposed by Cistin and Ziems and was used by the German researchers [3]. The bank material resulted to be very susceptible to internal erosion [7].

Critical gradients. The fore-mentioned method consist of two steps: the first verifies the property of the soil to form a natural filter; the second step makes the comparison between the seepage flow gradients and critical gradient values. The method offers a synthetic table of values for critical gradients as a function of flow direction [3]. The Delft laboratory's researchers elaborated graphs and formulas for critical gradients, on the base of a careful model study [4].

The site topography favored to perform an *in situ* experiment on critical gradient value, in our case. In S1 point an hole of 5 cm in diameter was drilled into the slab. The fine sand material with the sieve curve in Fig 5 was discharged under an head of about H=0.7 m. For a spherical flow net, the direction of the flow carrying the fine sand has been uncertain. The experiment allowed us to assume only that the piping would progress under similar head, in this soil..

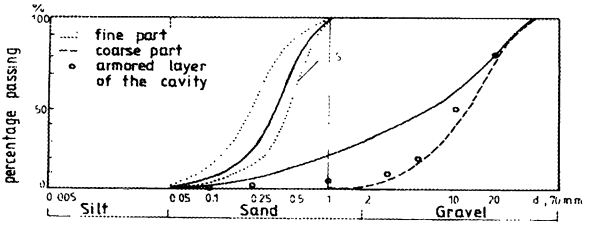

Fig.5. Grain size distribution curves of the bank material and the armouring layer of the weeper perimeter

Long-term piping evolution. The seepage gradients of flow towards weeper orifice were greater than critical ones in the upstream half of the canal length. The internal erosion started at all weepers without filter. The inspection of cavities aspect showed that a thin armouring layer was present at the base of the cavity, in front of the orifice. Up the slope, the perimeter was paved with a layer of grains finer than that marked with circles on Fig.5, but greater than the initial grain size curve. The analyze of this natural filters was not carried out, but by analogy with the river bed armouring, it might be supposed that the internal erosion process has been in final stage, due to self paving of the cavity perimeter.

COMMENTS

The field study results focussed the attention on the weeper's aspects. The careful inspection revealed that all weepers without vegetation and filters presented cavities which brought about the collapse of the slabs

The hazard placed the weeper elevations at a relative lower level in the zone with high transient groundwater levels; a water head of about 1.0 m, during active phase of the drawdown, drove a seepage flow with gradients that overpasses the critical gradients.

The theoretical schemes of groundwater flows may help elaborating a general frame of the piping phenomenon, but without efficient capabilities to evaluate the actual evolution of the cavities in the field conditions. The general rules concerning the necessity of the efficient filters could have prevented the extended internal erosion due to transient seepage in the Beresti tailrace.

REFERENCES

1.Cioc D. (1975) Hidraulica , Ed. Tehnica , Bucuresti (in Romanian)
2.Cedergreen H. (1973) Seepage control in earth dams. Casagrande memorial volume. John Willey &Sons N. Y
3.Armbuster H, Troger M. (1992) Underground erosion caused by raised levels of impounded rivers. Proc of the First International Conference – Geo–filters, Karlsruhe
4.de Graauw A, van der Meulen T, van der Does de Bye M.(1983) Design criteria for granular filters. Delft Publication No. 287
5.Brebia C (1978) The boundary element methods for engineers, London
6.Armencea G, Caprita D. (1997) Seepage through a slit of a cutoff wall . Computational method Comparison. Hidrotehnica Vol.42 Special Issue (edited by Romanian Committee on Large Dams)
7. Armencea G. (1995) The study of the transient seepage flow at the Beresti tailrace. Technical Report, Hydraulic Laboratory, IHSD, Bucharest

Interaction Between Surface and Subsurface Water

Determination of Groundwater Seepage into a River by Radon-222 Concentration in Water

Hiromasa HAMADA, Satoshi NIHIRA[1)] and Masato ASANO[2)]

1) National Research Institute of Agricultural Engineering, 2-1-2, Kannondai, Tsukuba, Ibaraki, 305-8609, Japan
2) Hokuriku regional agricultural administration office, 2-2-60, Hirosaka, Kanazawa, Ishikawa, 920-8566, Japan

Abstract

In Japan, the amount of infiltration from paddy fields is about 50 billion m^3 per year, and most of the infiltration flows into rivers. It is necessary to determine groundwater seepage into rivers in order to use water resources effectively. Generally, river discharge is measured to determine groundwater effluent. The practice is, however, very troublesome and not conducted easily. Furthermore, the results tend to contain errors and cannot be used to clarify groundwater seepage behavior. To solve these problems, the authors directed their attention to radon-222 (^{222}Rn), and measured the concentration in a river.

^{222}Rn is a radioactive gas generated by the alpha decay of radium-226 (^{226}Ra) in strata, and it dissolves in water. Since the origin of ^{222}Rn is ^{226}Ra underground, the concentration in groundwater is higher than in river water. ^{222}Rn concentration in a stream decreases exponentially due to dispersion to the atmosphere and radioactive decay of ^{222}Rn. Therefore, the increase of ^{222}Rn concentration in a stream implies that groundwater seeps into the river.

The authors chose the Tedori River as a test area, where many paddy fields exist, and measured ^{222}Rn concentration in river water during irrigation and non-irrigation periods. As a result, in the Tedori River, ^{222}Rn concentration in the irrigation period was higher than in the non-irrigation period. The concentration at some observation points during the irrigation period was more than 100 times that during the non-irrigation period. The reason is that paddy field irrigation recharged the groundwater and increased seepage into the river.

Key words. groundwater, ^{222}Rn, irrigation, recharge

Introduction

In Japan, about 60% of the annual water use is for paddy field irrigation [1]. Most of the irrigated water infiltrates underground, and it is said that the amount is more than 50 billion m^3 per year [2]. Much of this infiltrated water, however, flows into rivers in a short time. It is necessary to determine groundwater seepage into a river in order to use water effectively. A conventional method of estimating it is to measure discharge of the river and/or levels of river water and groundwater. The measurement of discharge is, however, very troublesome and can not be conducted easily. Water level data can be obtained only from a limited number of points, because drilling an observation well is very costly. Moreover, these results tend to contain errors and it is difficult to determine groundwater seeping into a river. To solve these problems, the authors directed their attention to radon-222 (^{222}Rn) in water and determined groundwater effluent from the variation of ^{222}Rn concentration in river water.

Characteristics of ^{222}Rn

^{222}Rn is a radioactive gas generated by the decay of radium-226 (^{226}Ra) in strata. ^{222}Rn dissolves in water, while it decays with a half life of 3.8 days. Since the rate of decaying atoms is proportional to the number of existing ones, the concentration in groundwater rises according to the growth curve of radioisotopes and finally achieves the equilibrated value. In two to three weeks, ^{222}Rn concentration reaches equilibrium and the value depends on the content of ^{226}Ra and the specific surface area of the strata. Using these characteristics, ^{222}Rn was applied to the analysis of groundwater. Hoehn et al. calculated the velocity of river water effluent from the increase of ^{222}Rn concentration in groundwater [3]. Kimura et al. applied similar techniques to analyzing leakage of reservoir water [4].

Since the origin of ^{222}Rn is ^{226}Ra underground, ^{222}Rn concentration in groundwater is 10～100 times as high as that in river water. Thus, groundwater seepage into a river is indicated when ^{222}Rn concentration in river water increases along the stream. Rogers A. S. measured ^{222}Rn concentration in a stream and determined the section where groundwater seeped into the river [5]. Ellins et al. and Hamada et al. quantified groundwater effluent from water and ^{222}Rn balance equations [6] [7]. Though there have been some researches on analysis of the interaction between river water and groundwater using ^{222}Rn, the results pertain to only one season and there has not been an analysis of groundwater effluent from the seasonal change of ^{222}Rn concentration in river water. In Japan, there are many paddy fields, which implies that groundwater seepage into rivers increases during the irrigation period. The authors analyzed groundwater effluent measuring ^{222}Rn concentration in river water during irrigation and non-irrigation periods.

Field investigation

The Tedori River Basin, Ishikawa Prefecture was chosen as a study site. The geological structure is a several tens of meters gravel layer, which is an aquifer (Fig.1) [8]. There are many paddy fields in the Tedori River Basin and recharging groundwater by irrigation was expected. The irrigation starts in April and ends in September. The groundwater level rises during the irrigation period and falls during the non-irrigation. Fig.2 shows the relationship between the levels of the Tedori River and groundwater [9]. This figure which was made by the Hokuriku regional agricultural administration office was the only information available on levels of the Tedori River and groundwater. Groundwater rose by about 5m during the irrigation period, but even the highest level was lower than that of the river water, which indicated that there was no groundwater effluent but river water influent. However, the limited data was insufficient to confidently analyze the relationship between the river water and groundwater in the Tedori River Basin. For a more-detailed analysis, the authors measured the ^{222}Rn concentration in the river water.

Field investigations were carried out in early-irrigation (May), late-irrigation (August) and non-irrigation periods (November). The toluene extraction method was adopted to ^{222}Rn measurement [10]. In a field, 10l of sample water and 150ml of toluene containing scintillators (4.0 g/l of PPO and 0.01 g/l of POPOP) were mixed in a closed vessel. 100ml of toluene was collected into a 100ml-Teflon vial. The sample was brought to the laboratory, and the radioactivity from ^{222}Rn and its daughters was measured by a liquid scintillation counter for 50 minutes. On the basis of the count rate, ^{222}Rn concentration was calculated by four corrections, i.e., extraction, decay, counting efficiency and background. The detection limit is about 0.003Bq/l.

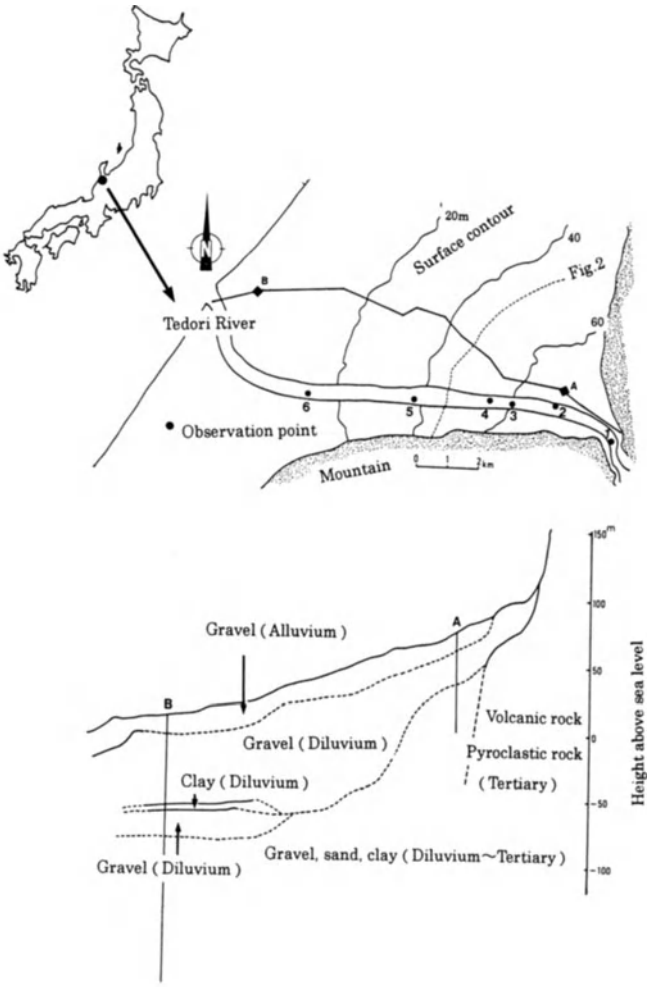

Fig.1. Tedori River Basin and its geological structure.

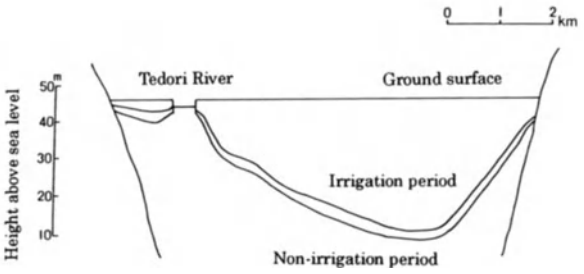

Fig.2. Relationship between the levels of Tedori River and groundwater.

Results and discussion

Fig.3 shows the results of the investigations. The ^{222}Rn concentration was lower than 0.1 Bq/l during the early-irrigation and the non-irrigation periods. During these periods, the amount of groundwater seepage is very small and negligible compared to that of river water. In the late-irrigation period, ^{222}Rn concentrations at all observation sites increased, especially at site 3 and site 4; their ^{222}Rn concentrations were over 100 times higher than those of other periods. From this result it is obvious that much groundwater seeped into the river during the late-irrigation period. The groundwater level rose after the start of irrigation and became highest before the end. It is inferred that the groundwater level in the late-irrigation period was higher than the river water level and that groundwater seeped into the river. The sections where a lot of groundwater flows into the river are the section 1-4 and 5-6 (Fig.3), in which ^{222}Rn concentrations increased. Though it was impossible to determine groundwater seepage from the relationship between river water and groundwater levels, the measurement of ^{222}Rn concentration in river water was helpful to increase understanding of groundwater seepage.

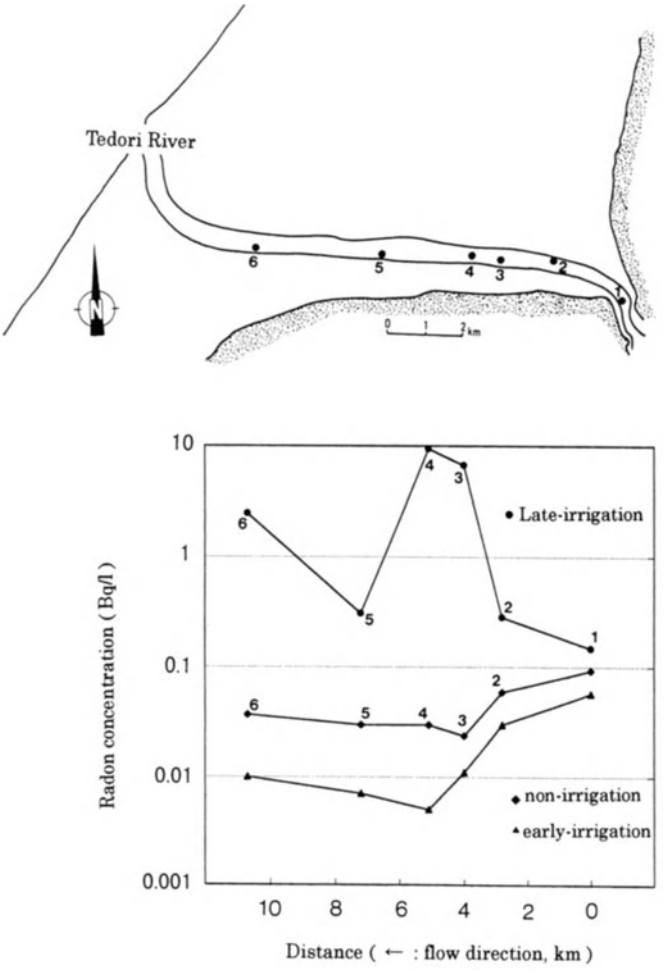

Fig.3. Radon concentration in Tedori River.

Assuming that river water is a mixture of a surface stream and groundwater and that the ^{222}Rn concentration in a stream is zero, it is possible to estimate the groundwater proportion in river water during the late-irrigation period. The ^{222}Rn concentration in groundwater for this period was about 20Bq/l. On the basis of this value, groundwater proportions were calculated in Table1. At site 4, the groundwater component was about 50% of the total amount of river water.

Table 1. The rate of groundwater component in late-irrigation period.

Site	Radon concentration (Bq/l)	Groundwater proportion (%)
1	0.146	1
2	0.282	1
3	6.69	33
4	9.42	47
5	0.303	2
6	2.48	12

Radon concentration in groundwater was 20 Bq/l.

Conclusion

The authors measured the seasonal variation of ^{222}Rn concentration in river water in order to analyze the interaction between river water and groundwater. It was confirmed that groundwater seepage into the river occurred by recharge from paddy field irrigation and it was possible to calculate the rates of groundwater components to the total river water. It was shown that much groundwater seeped into the river during the late-irrigation period, even though this could not be detected by measurement of groundwater and river water levels. It is concluded that the measurement of ^{222}Rn concentration in river water is useful to determining groundwater seepage into rivers.

Acknowledgment

We would like to acknowledge the useful suggestions for this research from Dr Takami Komae and Dr Masayuki Imaizumi, the staff of the National Research Institute of Agricultural Engineering. We would also like to thank Mr Motoi Kotoku and Mr Takashi Arakawa, former staff of the Hokuriku Regional Agricultural Administration Office, and Mr Michiaki Konno, of the Hokuriku Regional Agricultural Administration Office, for their assistance with the field investigations.

REFERENCES

1) National Land Agency (1998) Water Resources in Japan, pp3-67 (in Japanese)
2) Research Group on Groundwater for Agriculture (1986) Groundwater in Japan, Chikyusya, Tokyo, pp952-974 (in Japanese)
3) Hoehn E, von Gunten HR (1989) Radon in groundwater : a tool to assess infiltration from surface waters to aquifers, Water Resour. Res.: 1795-1803
4) Kimura S, Komae T (1978) Application of environmental radon-222 to some cases of water circulation, Natural Radiation Environment Ⅲ: 581-599
5) Rogers AS (1958) Physical behavior and geologic control of radon in mountain streams, US Geol. Survey Bull. 52-E: 187-210
6) Ellins KK, Roman-Mass A, Lee R (1990) Using ^{222}Rn to examine groundwater/surface discharge interaction in the Rio Grande de Manati, Puerto Rico, J. Hydrol.: 319-341
7) Hamada H, Komae T (1994) Analysis of exchange between river water and groundwater using radon-222, Water Down Under'94: 115-120
8) Watanabe K, Yamazaki Y. (1974) Hydrology and geology in an alluvial fan – A case study of Tedori-river alluvial (Ⅰ), Water Science: 1-25, (in Japanese)
9) Hokuriku regional agricultural administration office (1996) Technology of enhancement of groundwater recharge, pp1-30 (in Japanese)
10) Noguchi M (1964) New method of radon activity measurement with liquid scintillation, Radioisotopes: 362-366, (in Japanese)

Interaction between Fresh Groundwater and Salt Sea Water in Heterogeneous Freshwater Coastal Aquifer

A.P. Frolov and I.O. Yushmanov

Water Problems Institute, Russian Academy of Sciences,
3, Gubkina str., Moscow, 117735 Russia

ABSTRACT. A two-dimensional model is developed to simulate saline water intrusion into highly-inhomogeneous confined and unconfined coastal aquifers. The model is based on the system of equations describing the motion of a variable-density fluid with advective diffusion of dissolved salts, which is solved numerically by the finite-difference technique. The model potentialities are demonstrated by examples of intrusion into aquifers with layered structure and into those containing screening inclusions.

KEY WORDS: Coastal aquifers, sea water intrusion, inhomogeneous media, mathematical model

INTRODUCTION

The extent of sea-water penetration into the shore depends on a large number of factors, among which, of considerable importance, are the rate of groundwater withdrawal and the structure of water-bearing aquifers. The length of the intrusion zone is negligible in thin aquifers with low permeability, whereas in highly-permeable aquifers with large thickness this length can reach several kilometres. In multi-stratum systems comprising a number of layers separated by relatively impermeable interbeds, an intrusion tongue will form in each layer. Hydrodynamic analysis of this kind of system is more intricate, because the fluid leakage through interbeds separating the adjacent layers has to be taken into account. Long Island (Lusozynski, N.J., Swarzenski, W.V., 1962) and coastal aquifers of the Mediterranean (Schmorak, S., Mercado, A., 1969) represent typical examples of a multilayer intrusion zone. An attempt to theoretically study multilayer intrusion zones was made by Todd, D.K. and Huisman, L. (1959), where the intermediate layers were assumed to be absolutely impermeable. Collins, M.A. and Gellhar, L.W. (1971) used the hydraulic approximation to consider the zone of sea-water intrusion into an aquifer separated by a semi-permeable interbed. The finite-element technique used Huyakorn, P.S., et al (1987) to obtain a solution to the three-dimensional problem, taking into account effect of discharging wells in layered media. Souza, W.R. and Voss, C.I. (1987) studied the distribution of concentrations in the case of complicated hydrogeological conditions, where a highly-permeable anisotropic horizon is overlain by relatively impermeable sedimentary rocks and their interface is of a rather arbitrary form. Aquifers can also include individual geological formations with different permeability. Sugio, S. (1987) and Fitts, G.R (1987) suggested the prevention of intrusion by way of forming "subsurface dams" hindering the

penetration of sea water into fresh-water coastal aquifers. In these cases, the hydraulic conductivity in Darcy's law varies both vertically and horizontally.

MATHEMATICAL FORMULATION

The most general mathematical model of the process of sea-water intrusion into a fresh-water coastal inhomogeneous aquifer is a system of equations describing fluid motion with advective diffusion of dissolved salts (Khublaryan, M.G., Frolov, A.P., 1988; Khublaryan, M.G.,Churmaev, O.M., Yushmanov, I.O.; 1984; Reilly, T.E., 1990; Senger, R.K., Fogg, G.E., 1990; Inouchi, K., Kakinumas, T., Sawa, M., 1989; Nishikawa, T., 1997). The intrusion model considered below is based on the generalised law of motion of a fluid whose density is determined by the concentrations of dissolved substances. The model can describe both confined and unconfined groundwater flows in inhomogeneous and anisotropic aquifers.

Let us represent the fresh-water head in the following form

$$\Psi(X,Y,T) = \frac{P(X,Y,T)}{\rho_0 g} + Y \ , \qquad (1)$$

ρ_0 = density of fresh water,
g = acceleration due to gravity,
X, Y = horizontal and vertical co-ordinates,
$P(X,Y,T)$ = pressure at the point (X,Y),
T = time.

The generalised Darcy's Law for variable-density fluid motion in an inhomogeneous anisotropic aquifer has the form:

$$Q = -A(\nabla P + \rho g) / \mu(\rho) \qquad (2)$$

Q = the specific flux vector with components Q_x, Q_y in the directions of X, Y coordinates,
$\mu(\rho)$ = the fluid dynamic viscosity,
$\rho = \rho_0(1 + \varepsilon C)$ = the variable density of the fluid, where $\varepsilon = (\rho_s - \rho_0)/\rho_0$, and
$A(K_x,K_y)$ = the permeability tensor of water-bearing rocks, where K_x,K_y - hydraulic conductivity in the directions of X, Y coordinates.

The equation of continuity for an incompressible variable-density fluid in an undeformable porous medium has the form:

$$\nabla(\rho Q) = 0 \qquad (3).$$

For relative concentration $C = (S - S_0)/(S_s - S_0)$ the equation of conservation of dissolved pollutant (sea-water salts) can be written in the form:

$$\nabla(D\nabla C) - \nabla(VC) = \partial C / \partial T \qquad (4)$$

S = salt concentration in the mixture of fresh and sea water,
S_s, S_0 = salt concentration in the ambient sea and fresh water, respectively,
$V = Q / n$,
n = the effective porosity of water-bearing rocks,
D = the hydrodynamic dispersion tensor.

Equations (3)-(4) are connected by the dependence of fluid density on dissolved sea salt concentration, and hence cannot be solved separately.
Let us formulate boundary conditions for this system of equations.
In the case of intrusion, if R is the height of the boundary between the groundwater flow and the saline-water reservoir, wherever $Y < R$ sea water flows into the aquifer, while for $Y > R$ groundwater discharges into the sea.
On the confining layer ($Y=0,\ 0 < X < L$), (L is the size of the domain in question) the flow $Q_y = 0$, or in accordance with (1)

$$\partial\psi / \partial Y + \varepsilon C = 0 \qquad (5)$$

(on this boundary, the flow can be assumed nonzero Q_y).
At the top of the confined bed ($Y=L,\ 0 < X < L$) the flow of fluid also is equal either to zero or to a given function.
In the case of unconfined flows, we have $P = 0$, or $\psi = Y = \Phi(X,T)$ on the free surface of groundwater flow $Y = \Phi(X,T)$.
For the equation of dissolved salt transport, eqn. (4), on the free surface, assuming the availability of infiltration flow with contaminant concentration C_{inf}, the following boundary condition holds:

$$D\partial C / \partial N = E_N (C - C_{inf}) , \qquad \text{where}$$

$E_N = w/(1 + (\partial\Phi / \partial X)^2)^{-0.5}$,
$\partial / \partial N$ = inner normal derivative to the boundary,
E_N = infiltration recharge for a unit of free surface length,
w = infiltration recharge for the soil horizontal surface.

The motion of the free surface is described by the following equation

$$n\partial\Phi / \partial T = -K_y(\partial\psi / \partial Y + \varepsilon C) + K_x(\partial\psi / \partial X)(\partial\Phi / \partial X) + w$$

As for the side (vertical) segments of the boundary, either head ψ or flow rate Q_x is known on the landward part of it, whereas on the seaward part, below the sea level, $Y = d_s$, the pressure is distributed hydrostatically, i.e., for $X = 0,\ 0 < Y < d_s$

$$P = \rho g(d_s - Y) \qquad (6)$$

In the case of unconfined flow at the site of surface seepage ($X = 0,\ d_s < Y < \Phi(0,T)$) we have $P = 0$.
Various types of boundary conditions can be applied to the equation of dissolved salt transport. Sousa, W.R. and Voss, C.I. (1987) subdivided them into three groups, depending on what is

specified: the concentration, the diffusion flux, or the total flux of dissolved substances through the boundary. The boundary conditions used for mass transport, equation (4), are as follows. It is assumed that fresh water with concentration S_0 enters the aquifer from the land side, that is, the dimensionless concentration equals zero on the land-side boundary. From the sea side, the boundary conditions have the form:

$$C = 1,\ X = 0,\ 0 < Y < R$$
$$\partial C / \partial T = 0\ ,\ R < Y < d_s$$

At the base of the aquifer $0 < X < L,\ Y = 0,\ \partial C / \partial Y = 0$. For confined flows we have, at the top of the aquifer, $0 < X < L,\ Y = L,\ \partial C / \partial Y = 0$.
The initial condition for the problem is the initial distribution of the concentration $C(X,Y,0) = C_0$; in the case of an unconfined aquifer it also necessary to specify the position of the free surface $\Phi(X,0) = \Phi_0(X)$.

The boundary-value problem was solved by numerical methods. Elliptic equation (3) was solved by the iteration relaxation method (Yanenko, 1967). All partial derivative equations were solved by the method of decomposition with respect to spatial variables (Khublaryan et al, 1984). The longitudinal-transverse sweeping scheme was chosen for equation (3), and the implicit decomposition scheme for equation (4).

RESULTS AND DISCUSSION

The suggested technique was used to calculate the intrusion of sea water into inhomogeneous confined aquifers and to assess the effect of the coefficients of conductivity and dispersion on the zone of intrusion.
The model was tested by correlation of the simulation results with data from (Kohout, F.A., 1960), where sea-water intrusion was studied in the Biscayne coastal aquifer near Cutler, Florida. This aquifer is composed of soluble limestones and calcareous sandstones, and is up to 30 m thick. A rather long diffusion zone is detected, where the salinity changes from that of fresh water to that of sea (Atlantic) water. A vast recirculation zone of saline water is found to form in this case. Fig. 1 compares the results of our finite-difference simulation of the salt concentration distributions in the circulation zone and the field data by Kohout (1960) (the numbers on the curves denote concentration). The simulation results in this layered aquifer are found to be in rather good agreement with field data, especially near the aquifer bed.
To take into account the layered structure of the aquifer two different values of hydraulic conductivity were used: $K_{up} = 0{,}01 * K_{low}$.
Fig. 2 shows the distribution of concentration in an aquifer with a rectangular semipermeable barrier occupying part of the aquifer thickness.
On the same Fig. 1 and Fig. 2 the curves of C=0,25 and C = 0,75 for homogeneous media are also shown.
The influence of layered and inhomogeneous aquifer structures on the sea salt distribution is clearly seen.

CONCLUSION

The calibration of the model has been done on the field data of Biscayne coastal aquifer, and simulation analysis shows, that the aquifer has a complicated multilayer structure. The examples

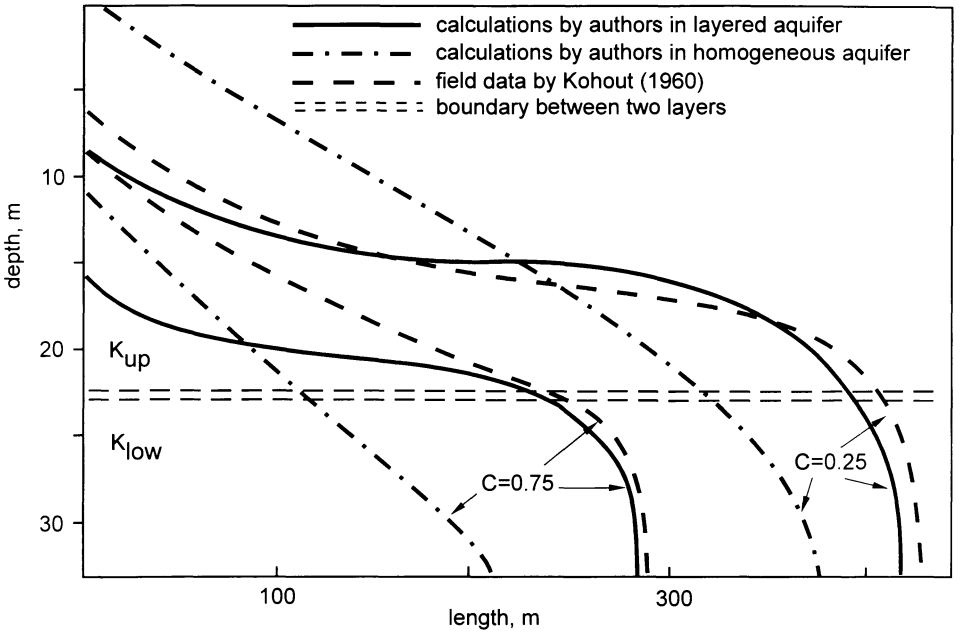

Fig. 1. Comparison of field data and calculated results of salt concentration in a coastal aquifer (Kutler, Florida).

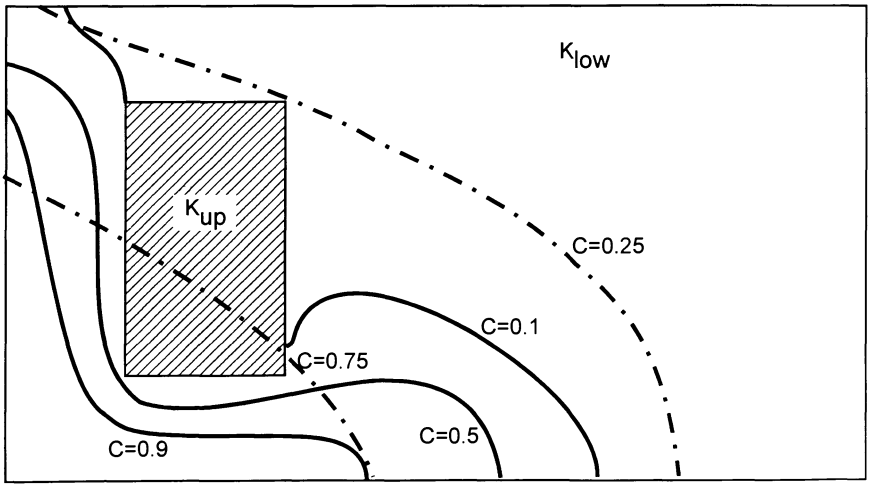

Fig. 2. Influence of semipervious subsurface barrier on the seawater intrusion in a coastal aquifer.

presented suggest that the problem of simulation of intrusion into inhomogeneous aquifers and its implementation make it possible to efficiently simulate different hydrogeological conditions, with respect to the problems of water use in coastal zones, and groundwater protection against pollution by sea-water salts.

REFERENCES

Bear, J., Zaslavsky, D., and Irmay, S., (1968). Physical Principles of Water Personal and Seepage. UNESCO, Paris.

Collins, M.A. and Gellhar, L.W., (1971). Seawater intrusion in layered aquifers. Water Resour. Res., vol. 7, no. 4, 971-979.

Fitts C.R. Analitic Modeling of Impermeable and Resistant Barriers. Ground Water, 1997, vol. 35, no. 2, 312-317.

Groundwater Problems in Coastal Areas, Paris: UNESCO, 1987.

Huyakorn, P.S., Andersen, P.F., Mercer, J.W., and White, H.O. (1987). Saltwater intrusion in aquifers. Development and testing of a three dimensional finite-element model. Water. Resour. Res., vol. 23 ,no. 2, 293-312.

Inouchi K., Kakinuma T., Sawa M. Model Analysis of Seawater Intrusion into Saturated and Unsaturated Domains. Jpn. J. Limnol. 1989, vol. 50, no. 3, 207-217.

Khublaryan, M.G. and Frolov, A.P. (1988). Modelling the Processes of Intrusion into Estuaries and Aquifers, Nauka P.H., Moscow.

Khublaryan, M.G., Churmaev, O.M., and Yushmanov, I.O. (1984). The investigation of hydrodynamic problem for filtration and convective diffusion in heterogeneous and anisotropic porous media. Water Resources, Nauka P.H., Moscow, no. 3, 23-29.

Kohout F.A. (1960). Flow pattern of fresh water and salt water in the Biscayne aquifer of Maiami area, Florida. Int. Assoc. Sci. Hydrol. Publ., 52, 440-448.

Lee, C.-H., Cheng, R.T.-S. (1974). On seawater encroachment in coastal aquifers. Water Resour. Res., vol. 10, no. 5, 1039-1045

Lusozynski, N.J., Swarzenski, W.V. (1962). Fresh and salty groundwater in Long Island. J. Hydraul. Div. Proc. ASCE, 1962, vol. 88, no. 4, 173-194.

Nishikawa T. Testing Alternative Conceptual Models of Seawater Intrusion in a Coastal Aquifer Using Computer Simulation, Southern California, USA.. Hydrogeology J., 1997, vol. 5, no. 3, 60-74.

Reilly, T.E. (1990). Simulation of dispersion in layered coastal aquifer systems. J. Hydrol., vol. 114, 211-228.

Schmorak, S. and Mercado, A. (1969). Upconing of fresh water-seawater interface below pumping wells field study. Water Resour. Res., vol. 5, no. 6, 1290-1311.

Senger, R.K., Fogg G.E. (1990). Stream functions and equivalent freshwater heads for modelling regional flow of variable-density groundwater. Water Resour. Res., vol. 26, no. 9, 2089-2106.

Souza, W.R. and Voss, C.I. (1987). Analysis of an anisotropic coastal aquifer system using variable-density flow and solute transport simulation. J. Hydrol., vol. 92, 17-41.

Sugio S. (1987) Effectiveness of semi-pervious Barrier on protection ground water reservoir against sea water intrusion. Memoirs of Fac. Eng., Miyazaki Univ., no. 17, Miyazaki.

Todd, D.K. and Huisman, L. (1959). Groundwater flow in the Netherlands coastal dunes. J. Hydraul. Div. Proc. ASCE, vol. 85, no. 7, 63-81.

Yanenko, N.N. (1967). Method of rational steps for solving multidimensional problems in mathematical physics. Nauka P.H., Novosibirsk.

Hydraulic Analysis on Stream-Aquifer Interaction by Storage Function Models

Morihiro Harada[1], Mohamed M. Hantush[2] and Miguel A. Mariño[3]

[1] Department of Civil Engineering, Meijo University, Tenpaku, Nagoya 468-8502, Japan
[2] Kerr Environmental Research Center, US Environmental Protection Agency, Ada, OK 74820, USA
[3] Department of Land, Air and Water Resources and Department of Civil and Environmental Engineering, University of California, Davis, CA 95616, USA

Abstract. To improve the river environment in an urbanized basin, it is important to restore the hydrologic relationships between streams and aquifers. In this paper, the dynamic interaction between them, the so-called "bank storage effect," is analyzed based on hydraulic models of a stream-aquifer system. In particular, linear and nonlinear storage function models are used in order to express the stream flow. It is shown that bank storage by the aquifer fulfills the functions to control the fluctuation of the stream flow.

Key words. stream-aquifer interaction, bank storage effect, river environment, groundwater discharge, storage function model

INTRODUCTION

In the natural hydrologic cycle, surface and subsurface water in a watershed are closely related and interact with each other. However, their relationships are affected by human activities. For instance, as the impervious area of a basin spreads due to urbanization, rainfall recharge into unconfined aquifers decreases and consequently the stream flood hazard increases. By renovating channels for flood control, natural streams are reconstructed into artificial channels. As a result, water exchange between stream and aquifer may be impacted and altered. It is well known that small streams in a city become drainage channels in rainy days and run dry in non-rainy days. In order to improve such a river environment, it is necessary to recover the natural water cycle in the watershed by recognizing the hydrologic connection between streams and aquifers.

Although the relationship between a stream and an aquifer has been investigated from various angles [1][2][3], most of the researches dealt with merely the response of an aquifer to fluctuation in the stream stage. At alluvial plains, however, the relationship between the two is interactive and the water exchange between them depends on their relative hydraulic state. Therefore, it is necessary that the stream-aquifer interaction is evaluated by solving two governing equations of the stream flow and the groundwater simultaneously. The purpose of this paper is to clarify a potential role that the aquifer plays for regulating the stream flow, the so-called "bank storage effect" [4], by expressing the stream flow in the storage function model.

FUNDAMENTAL EQUATIONS

Stream Flow. Let us consider a combined system of a stream channel and an unconfined aquifer as shown in Fig. 1. For simplicity, it is assumed that the channel has width B, slope I_o and straight reach length L, and the aquifer is of semi-infinite lateral extent on a horizontal base. Now, an inflow rate $I(t)$ at the upstream end of the channel reach, we seek the effect of the aquifer on the outflow rate

$O(t)$ at the downstream end. At time $t = 0$, it is also assumed that $I(t)$ is equal to $O(t)$ and the stream stage is in equilibrium with the water-table in the aquifer. For storage volume in the reach, $S(t)$, and groundwater discharge from both sides of the aquifer into the channel, $Q_r(t)$, the fundamental equations of the stream flow take the following form:

$$\frac{dS(t)}{dt} = I(t) - O(t) + Q_r(t) \qquad (1)$$

$$S(t) = kO(t)^p \qquad (2)$$

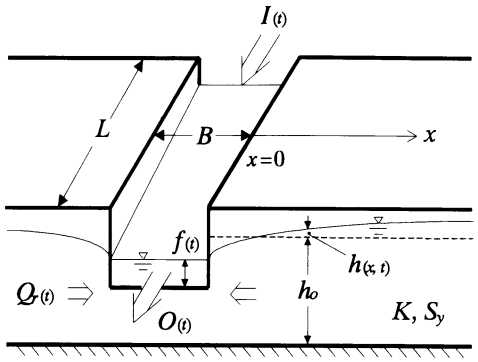

Fig. 1. Schematic of stream-aquifer system.

where k and p are coefficients of the storage function, $p = 1.0$ in the linear flood routing, $p = 0.6$ in the nonlinear flood routing based on the Manning formula. $S(t)$ can be expressed as $S(t) = Af(t) = BLf(t)$, where A is horizontal area in the reach and $f(t)$ is depth of the stream flow assumed to be uniform along the reach length.

Groundwater Flow. Generally speaking, the groundwater around the stream is three-dimensional flow with vertical velocity. However, in the case that the aquifer thickness is three times smaller than the channel width, the flow may be regarded as horizontal and that the Dupuit-Forchheimer assumption may hold [5]. Moreover, in the case that water-table fluctuation h is smaller than the average depth h_o, the Boussinesq equation of unconfined flow may be linearized. Based on these assumptions, the fundamental equation for one-dimensional flow toward the channel takes the following form:

$$\frac{\partial h(x,t)}{\partial t} = \frac{Kh_o}{S_y}\frac{\partial^2 h(x,t)}{\partial x^2} + \frac{r_e(x,t)}{S_y} \qquad (3)$$

where K is the hydraulic conductivity of the aquifer, S_y is the specific yield of the unconfined aquifer, $r_e(x, t)$ is the recharge rate from above, x is horizontal coordinate measured in orthogonal direction from the channel, and $h(x, t)$ is the water-table elevation relative to the initial equilibrium elevation. The initial and boundary conditions are adopted as shown in Fig. 1, $h(x, 0) = 0$, $h(0, t) = f(t)$, $h(\infty, t) = 0$, and $r_e(x, t) = 0$. Thus, it can be shown that the variation of $h(x, t)$ due to $f(t)$ is formulated by the Duhamel theorem as:

$$h(x,t) = \int_0^t U(x,t-\tau)\frac{\partial f(\tau)}{\partial \tau}d\tau, \qquad U(x,t-\tau) = \frac{2}{\sqrt{\pi}}\int_{\frac{x}{2\sqrt{\kappa(t-\tau)}}}^{\infty} e^{-\xi^2}d\xi = \operatorname{erfc}\left(\frac{x}{2\sqrt{\kappa(t-\tau)}}\right) \qquad (4)$$

where $\kappa = \frac{Kh_o}{S_y}$, and erfc(-) denotes the complementary error function. The groundwater discharge $Q_r(t)$ into the channel reach L from both sides of the aquifer can be obtained as follows:

$$Q_r(t) = 2 \times Lh_o \cdot K\left.\frac{\partial h(x,t)}{\partial x}\right|_{x=0} = -2L\sqrt{\frac{S_y K h_o}{\pi}}\cdot\int_0^t \frac{1}{\sqrt{t-\tau}}\frac{\partial f(\tau)}{\partial \tau}d\tau \qquad (5)$$

From eqs.(1), (2), and (5), it is evident that both the stream flow and the groundwater discharge are interacts through the stream stage $f(t)$.

LINEAR STORAGE FUNCTION MODEL

For a linear storage function of the stream flow, $p = 1.0$ in eq. (2), Morel-Seytoux [6] obtained a closed-form solution of the interaction problem. Though it was a leading achievement, unfortunately the mathematical forms are slightly inadequate. Thus, we will rederive more accurate forms here.

Expressing the response of the channel depth $f(t)$ to the inflow $I(t)$ by the convolution integral with the response kernel $u(t)$, the outflow $O(t)$ is rewritten as follows.

$$O(t) = \frac{S(t)}{k} = \frac{A}{k} f(t) = \frac{A}{k} \int_0^t u(t-\tau) I(\tau) d\tau \tag{6}$$

The equation which $u(t)$ should satisfy becomes the following by substituting eqs. (2) and (5) into (1).

$$A\left(\frac{df(t)}{dt} + \frac{f(t)}{k} \right) = I(t) - 2L\sqrt{\frac{S_y K h_o}{\pi}} \cdot \int_0^t \frac{1}{\sqrt{t-\tau}} \frac{\partial f(\tau)}{\partial \tau} d\tau \tag{7}$$

Eq. (7) is a linear integral differential equation that can be solved by the Laplace transform method. Expressing the Laplace transform of $f(t)$ by $\mathbf{L}\{f(t)\} = F(s)$, and taking $f(0) = 0$ into consideration, the Laplace transform of the above equation can be shown to be

$$F(s) = \frac{\mathbf{L}\{I(t)\}}{A\left(s + \frac{1}{k} + \frac{2L}{A}\sqrt{S_y K h_o}\sqrt{s} \right)} \tag{8}$$

Since the Laplace transform of $f(t)$ in eq. (6) is $F(s) = \mathbf{L}\{I(t)\} \cdot \mathbf{L}\{u(t)\}$, as compared it with the above equation, $\mathbf{L}\{u(t)\}$ can be expressed as

$$\mathbf{L}\{u(t)\} = \frac{1}{A\left(s + \frac{1}{k} + 2\sqrt{\frac{S_y K h_o}{B^2}}\sqrt{s} \right)} \tag{9}$$

$$\therefore \quad u(t) = \mathbf{L}^{-1}\left\{ \frac{1}{A\left(s + \frac{1}{k} + 2\sqrt{\frac{S_y K h_o}{B^2}}\sqrt{s} \right)} \right\} = \mathbf{L}^{-1}\left\{ \frac{1}{2A\sqrt{\frac{S_y K h_o}{B^2} - \frac{1}{k}}} \left\{ \frac{1}{\sqrt{s}+b} - \frac{1}{\sqrt{s}+a} \right\} \right\} \tag{10}$$

where $a = \sqrt{\frac{S_y K h_o}{B^2}} + \sqrt{\frac{S_y K h_o}{B^2} - \frac{1}{k}}, \qquad b = \sqrt{\frac{S_y K h_o}{B^2}} - \sqrt{\frac{S_y K h_o}{B^2} - \frac{1}{k}}$ (11)

By using a table of the inverse Laplace transform [7], $u(t)$ is given as

$$u(t)=\frac{1}{2A\sqrt{\frac{S_y K h_o}{B^2}-\frac{1}{k}}}\left\{ae^{a^2t}\,\mathrm{erfc}\left(a\sqrt{t}\right)-be^{b^2t}\,\mathrm{erfc}\left(b\sqrt{t}\right)\right\} \tag{12}$$

Consequently, by substituting eq. (12) into eq. (6), one can calculate the response of the outflow $O(t)$ to any fluctuation of the inflow $I(t)$. Assuming a combined system with a small stream and a highly permeable aquifer, let us evaluate the response kernel $u(t)$. Values of parameters are supposed to be B = 10 m and k = 1 hr for the channel, S_y = 0.2 and h_o = 10 m for the aquifer. For the aquifer hydraulic conductivity, two cases of K = 0 (without aquifer) and K = 50 m/hr are considered. Fig. 2 shows difference of $u(t)$ by the aquifer hydraulic conductivity K. According to this figure, it appears that the response kernel in case of K = 50 m/hr reduces more rapidly initially than in the case of K = 0. This reflects the initial impact of lateral flow to the aquifer on the attenuation of the inflow $I(t)$.

The linear response models as stated above is easily applicable to evaluate the bank storage effect. However, we should notice that the solution (12) is valid only when

$$\frac{S_y K h_o}{B^2}>\frac{1}{k} \tag{13}$$

Since this condition may be very restrictive because it corresponds to the case of a channel with narrow width and an aquifer with high conductivity and large porosity, we cannot recognize eq. (12) to be a general solution of the bank storage problem. In addition, since this solution is based on the linear storage function, the stream stage fluctuates in proportion to a variation in the stream flow rate. Thus, it is possible that eq. (12) overestimates the exchange between the stream and the aquifer. We will consider a universal nonlinear model in the following section.

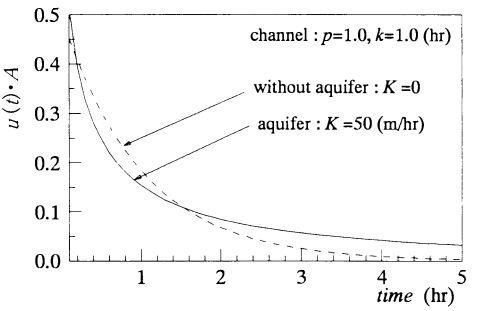

Fig. 2. Linear response function of outflow to inflow.

NONLINEAR STORAGE FUNCTION MODEL

Numerical Method. Applying Manning's formula to eq. (2), $p = 0.6$ and $k = n^{0.6}B^{0.4}I_o^{-0.3}L$, in which n is the channel roughness, are obtained [8]. In other words, since the storage function is nonlinear, it is difficult to obtain the analytical solution. Thus, we will attempt to obtain a numerical solution by linearizing the fundamental equation. By replacing of $y(t) = O(t)^p$, eq. (1) is rewritten as

$$k\frac{dy(t)}{dt}=I(t)-y(t)^{1/p}+Q_r(t) \tag{14}$$

Expanding the right-hand side in Taylor series about y_*, which is the value of y at $t^*=t-\Delta t$, in which Δt is chosen to be sufficiently small, and ignoring the higher-order terms,

$$\frac{dy(t)}{dt}-a\;\;y(t)=\frac{1}{k}\left\{I(t)-b+Q_r(t)\right\},\quad a=-\frac{1}{kp}y_*^{\left(\frac{1}{p}-1\right)},\quad b=\left(1-\frac{1}{p}\right)y_*^{\frac{1}{p}} \tag{15}$$

Noting that the left-hand side of eq. (15) is equal to $e^{at}\frac{d}{dt}\left(e^{-at}y(t)\right)$, then, by integrating in time, we have

$$y(t)=e^{at}y(0)+\int_0^t e^{a(t-\tau)}x(\tau)d\tau,\quad x(t)=\frac{1}{k}\{I(t)-b+Q_r(y(t))\} \tag{16}$$

$Q_r(y(t))$ can be rewritten by substituting $f(t)=\frac{k}{A}y(t)$ into eq.(5):

$$Q_r(t)=Q_r(y(t))=-\frac{2Lk}{A}\sqrt{\frac{S_y K h_o}{\pi}}\cdot\int_0^t\frac{1}{\sqrt{t-\tau}}\frac{\partial y(\tau)}{\partial\tau}d\tau \tag{17}$$

Replacing time t in eq. (16) by discrete times i = 0, 1, 2,$\cdots$, m,$\cdots$ with increment T, the equation to be solved becomes

$$y_m=\phi^m y_0+\sum_{i=1}^{m}\phi^{i-1}\gamma x_i,\quad \phi=e^{aT},\quad \gamma=\frac{1}{a}\left(e^{aT}-1\right),\quad x_i=\frac{1}{k}\left(I_i-b+Q_{ri}\right) \tag{18}$$

Evaluation of Bank Storage Effect. As in the linear case, we evaluate the bank storage effect for a similar stream-aquifer system. For the aquifer it is assumed that S_y = 0.2, h_o = 10 m and K = 0, 1, 10 m/hr. For the channel, assuming p = 0.6 as mentioned earlier, B = 20 m, I_o = 1/1000, L = 4 km, and n = 0.03 in m-sec unit system, the value of k becomes k = 100 in m-hr unit system.

Fig. 3 shows differences of the outflow $O(t)$ for different aquifer hydraulic conductivity when the inflow I (t) is given by a leftmost curve in the figure. From the figure, it is recognized that in the case of higher conductivity, the peak of the curve $O(t)$ decreases and the tail of the curve becomes milder. This may be caused by increased exchange between the stream and the aquifer due to a higher conductivity (Fig. 4). According to Fig. 4, the groundwater discharge $Q_r(t)$ changes its flow direction from negative to positive in response to the fluctuation of the stream stage. In other words, this implies that in the combined system of the channel and the highly permeable aquifer, the latter may absorb the fluctuating inflow and regulate the stream outflow.

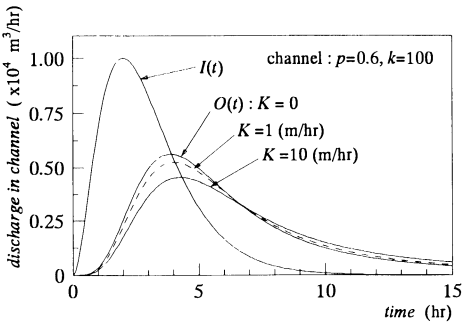

Fig. 3. Effect of aquifer hydraulic conductivity K on stream outflow rate in channel.

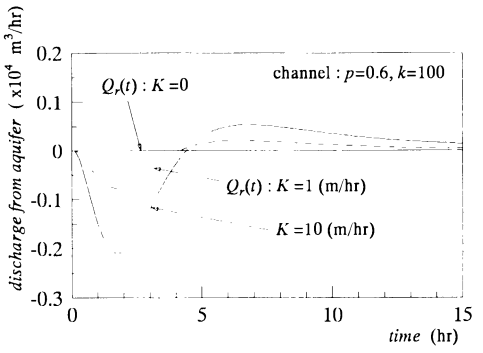

Fig. 4. Effect of aquifer hydraulic conductivity K on groundwater discharge from aquifer into channel.

Fig. 5 shows differences of the outflow $O(t)$ for different channel roughness in two cases of the

aquifer hydraulic conductivity K. Assuming the Manning's roughness n = 0.01, 0.03, 0.06 for same shape of the channel, values of k are k = 50, 100, 150. According to the figure, as k becomes larger, $O(t)$ gets increasingly attenuated with the outflow regulated over a longer period of time. This effect by k is considered to be natural because of increase of friction resistance in the channel. In the channel with larger roughness, it is expected that the exchange with aquifer may become more active due to increased stage fluctuation. In the figure, however, differences of $O(t)$ are almost similar in case of various k. This implies that the amplified effect of the stream stage by the channel roughness does not significantly affect the evaluation of the bank storage effect.

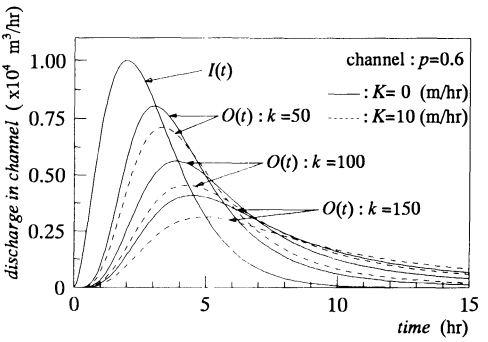

Fig. 5. Effect of channel roughness on stream outflow rate in two cases of aquifer hydraulic conductivity K.

CONCLUSION

To gain a basic understanding of a river environment in a watershed, relationships between streams and aquifers have been analyzed by using storage function models. It was shown that the existence of an aquifer with a high hydraulic conductivity fulfills the function of regulating the stream flow rate by the bank storage effect. Since this investigation merely dealt with an aspect of the behavior of the stream and the groundwater in a watershed, it is evident that additional work using different approaches is necessary.

ACKNOWLEDGEMENTS

We thank H. Basagaoglu, UC Davis, for his helpful suggestions with previous work.

REFERENCES

1. Hall FR, Moench AF (1972) Application of the convolution equation to stream-aquifer relationships. Water Resources Research, 8(2), pp 487-493
2. Mariño MA (1975) Digital simulation model of aquifer response to stream stage fluctuation. J Hydrology, 25, pp 51-58
3. Hantush MM (1987) Stochastic model for the management of a stream-aquifer system. MS Thesis, Univ. of California at Davis, pp 46-61
4. Freeze RA, Cherry JA (1979) Groundwater. Prentice Hall, pp 226-227
5. Bouwer H (1978) Groundwater Hydrology. McGraw-Hill, pp 268-279
6. Morel-Seytoux HJ (1979) Cost effective methodology for stream-aquifer interaction modeling and use in management of large-scale systems. Hydrowar Program Report, Colorado State Univ. at Fort Collins, pp 59-62
7. Oberhettinger F, Badii L (1973) Tables of Laplace Transforms. Springer-Verlag, p 229
8. Chow VT, Maidment DR, Mays LW (1988) Applied Hydrology. McGraw-Hill, pp 282-283

Investigation of Saline Water Intrusion into Aquifer by Using Resistivity Method

Masayuki Ishii[1], Taro Oka[2], and Kunio Otoshi[3]

[1]Faculty of Life and Environmental Science, Shimane Univ, 1060 Nishi-kawatsu-cho, Matsue, Shimane 690–8504, Japan
[2]Disaster Prevention Research Institute, Kyoto Univ, Gokasho, Uji, Kyoto 611–0011, Japan
[3]Faculty of Agriculture, Kochi Univ, 200 Mononobe-cho, Nankoku, Kochi 783–0093, Japan

ABSTRACT. Investigation of saline water intrusion into coastal aquifer is carried out in a coastal area where productions of rice, fruits and vegetables take place. Rice paddy fields are irrigated from a river, but fruit and vegetable productions use much quantity of groundwater, causing saline water intrusion. Groundwater is becoming unsuitable for agricultural use due to its salinity. Electrical soundings by resistivity method are carried out, and the results are analyzed using curve matching method. Vertical distributions of resistivity beneath measurement points are obtained, and a deep layer of low resistivity is found. Near the coast, its depth is shallow and its resistivity is high. Furthermore, below the point farthest from the coast, such a layer is not observed. It is concluded that the layer of low resistivity is intruded by saline water. The saline water is estimated to intrude through the riverbed, as well as the bottom of the sea. Where fruits and vegetables are mainly produced using large quantity of groundwater, the saline water sits especially shallow. The curve matching method is widely used to estimate the depth and the resistivity of the layers, but the estimation tends to be subjective. A new method with a numerical analysis and Standard Powell's method is proposed.

KEY WORDS. saline water intrusion, electrical sounding, numerical method, optimization

INTRODUCTION

Groundwater has been widely used as one of the most important water resources. Recently, serious problems are being caused by the improper and the excessive uses of groundwater. The intrusion of saline water into aquifers is a typical and common problem in coastal areas.

When heavy saline water intrudes under fresh groundwater, the boundary line between them raises with the decline in groundwater level. In coastal areas, where the quantity of groundwater use is large, the interface of saline water and fresh groundwater rises so high that the continuous use of groundwater becomes difficult and/or impossible. Moreover, much time is needed to recover from this kind of problem.

In this study, a method of investigation using the resistivity method is presented and discussed. Electrical soundings are carried out at several points along the coastal area of Haruno Town in Kochi Prefecture, Japan. The results are analyzed by the curve matching method to detect a layer of saline water and to estimate its depth. After discussing the problems with the curve matching method, including the lack of objectivity, another method is presented with a numerical analysis and optimization.

VERTICAL ELECTRICAL SOUNDINGS

In the resistivity method, which is a kind of electrical sounding, the difference in electrical potential between electrodes applied to the ground is measured, and the resistivity of the

ground is estimated[1]. The resistivity is affected not only by minerals in the layer, but also by its porosity, water content, and the concentration of ions in the pore water. Thus, it is possible to estimate these values from the resistivity. Since the resistivity of saline water is much smaller than that of rock, sand, and fresh water, the resistivity method is suitable for the investigation of saline water intrusion.

In this study, Wenner's arrangement of electrodes, shown in Fig. 1, is used for the investigation. Two potential electrodes, P_1 and P_2, are placed between two current electrodes, C_1 and C_2, and the spaces between the four electrodes are equal. With electric current I between C_1 and C_2, and the difference in electric potential V between P_1 and P_2, the resistivity of the ground is calculated using the following equation:

$$\rho_a = 2\pi a \frac{V}{I} \tag{1}$$

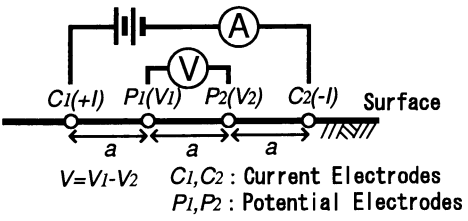

Fig. 1: Schematic diagram of electrical sounding

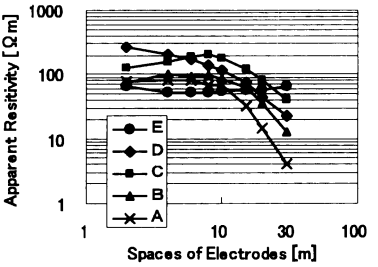

Fig. 2: Results of electrical soundings

This equation is derived with the assumption that the resistivity is uniform over the entire area where the current passes. Its extent depends upon the space between the current electrodes, and the current reaches deeper with wider spaces. Therefore, the resistivity of the upper layer can be measured with a narrow space, and the resistivity affected mostly by deep layers is obtained with a wide space.

Fig. 2 shows curves of electrode spaces a and the apparent resistivities ρ_a drawn on log-log section paper. In a case where the underground constitution and its resistivity are almost uniform, the apparent resistivity does not change with the electrode space, like Curve E in the figure. Curve D shows the results of the upper layer with the high resistivity and the lower layer with low resistivity. The middle layer has the highest resistivity and the lower layer has the lowest resistivity among the three, thus, the apparent resistivity changes like Curve C. With vertical electrical soundings, the vertical constitution is investigated with different spacings of electrodes using these characteristics. It is possible to investigate three-dimensional constitutions by making vertical soundings at many points.

The curve matching method is widely used to estimate the resistivities of layers from the results of the vertical soundings. By matching the curve of the results with the standard curves and finding a curve to coincide with the results, the resistivities of the upper and the lower layers and the depth of the boundary can be estimated. It is also possible to estimate the resistivity and the depth of three or more layers using auxiliary curves.

SITES AND RESULTS OF INVESTIGATIONS

The investigation is carried out in Haruno Town in Kochi Prefecture, Japan, whose location is shown in Fig. 3. In this coastal area, production of fruits and vegetables using hothouses take

place, as well as rice production in paddy fields. The rice fields are irrigated from a river, but the agriculture with the hothouses uses a great quantity of groundwater, causing saline water intrusion. The groundwater is becoming unsuitable for agricultural use due to its salinity.

Fig. 3: Location of investigated area

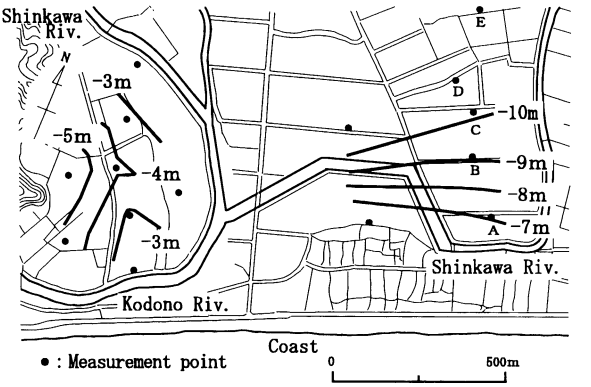

Fig. 4: Measurement points and depth of saline water in March of 1998

The points of the investigation conducted in March of 1998 are shown in Fig. 4. At each point, eight measurements with varying spacings between electrodes a, ranging from 2 m to 30 m, are carried out. Apparent resistivities are calculated for all the measurements by Eq.(1). Among them, the results obtained at Points A to E are shown in Fig. 2. Point A is the nearest to the coast, B is the next closest, and E is the farthest from it. Except for Point E, apparent resistivities become lower with wider electrode spaces, showing the existence of a deep layer of low resistivity. On the other hand, such a layer is estimated not to exist below Point E or to be deeper than a measurable depth.

At Points A to C, apparent resistivities take their maximum values when the spacing between electrodes is around 8 m, and lower rapidly with an increase in the width of the spaces. These facts show that three layers of different resistivities exist beneath these points. Furthermore, it is estimated that the resistivity of the middle layer is the largest and that of the deepest layer is the smallest. Under the assumption of a three-layered constitution, the resistivities of the layers below every measurement point are estimated by the curve matching method.

The results obtained for Points A to D are shown in Fig. 5. Beneath the points far from the coast, the boundary between the second and third layers sits deep in the ground. Furthermore, the resistivity of the third layer, ρ_3, is much smaller than those of the other layers. The results of boring investigations show that thick layers of gravel stratify below this area, so the difference in resistivity is caused by the difference in the resistivity of the pore water. It is concluded that the concentration of ions in the pore water is the highest in the deepest layer.

To ensure that the resistivity of the groundwater in the investigated area is mainly affected by dissolved salt, the relationship between the resistivity of pumped water and the concentration of chloride ions, measured by liquid chromatography, is examined. As shown in Fig. 6, the concentration of chloride ions is high in the groundwater with low resistivity. It is concluded that, in the investigated area, the concentration of dissolved salt in groundwater can be estimated by measuring its resistivity. Based on these discussions, the third layer of low resistivity is estimated to be intruded by saline water.

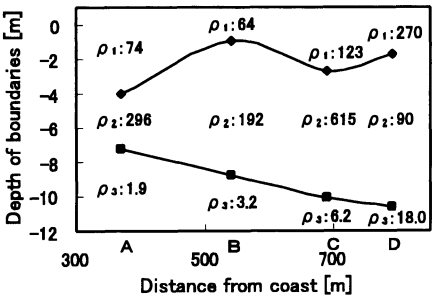

Fig. 5: Depth and resistivity of three layers

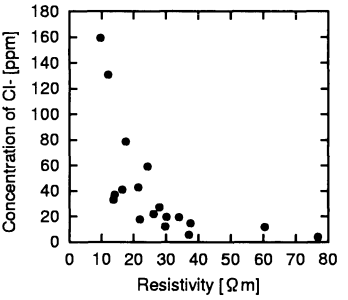

Fig. 6: Resistivity and concentration of chloride ions of pumped water

For each measurement point, except E, the depth of the saline water is estimated using the curve matching method and shown in Fig. 4. In the eastern part of the investigated area, saline water is supposed to intrude from the seabed because its depth becomes deep beneath the points far from the coast. In the western part, the depth of the saline water is estimated to be shallower than that in the eastern part. The saline water is also supposed to intrude through the riverbed, because it is especially shallow near the river.

Another investigation was carried out in August of 1999, and the results are shown in Fig. 7. Compared to the results from the March study, the layer of saline water is shallower, since the quantity of groundwater use is smaller and the groundwater level is higher in August. As in March, no saline water is observed below Point E, and the depth in the western part is shallower than that in the eastern part. Below the rice fields in the eastern part, the depth of the saline water is especially deep. The groundwater level there is expected to be high due to the water infiltrating from the fields.

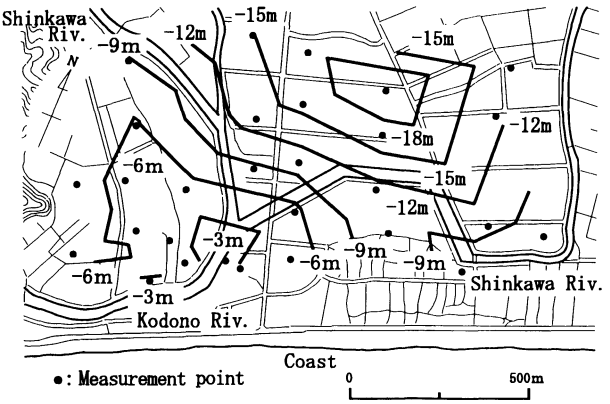

Fig. 7: Measurement points and depth of saline water in August, 1998

ESTIMATION OF RESISTIVITY BY POWELL'S METHOD

With the curve matching method, it seems that different investigators usually obtain varying resistivities and depths of layers from the same investigative results. Since the curve of the apparent resistivity and electrode spaces do not match perfectly with the standard curve, the matching tends to be subjective. Using a method with a numerical analysis and optimization, the distribution of resistivity can be determined objectively.

Fig. 8 shows the distribution of electric potential in a vertical plane caused by an electric current between electrodes C_1 and C_2. The depth and the resistivity of the layers affect both the distribution of electric potential and the difference in potential between P_1 and P_2. If the conditions of an analysis are identical to those of an investigation, the same distribution and difference in potential are obtained by the analysis. Therefore, modifying the conditions of the analysis for the same difference in potential with the investigation allows the actual resistivities below the investigated site to be obtained. The vertical two-dimensional finite element analysis and Standard Powell's method[2] are used for this purpose.

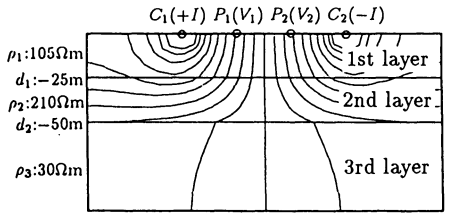

Fig. 8: Electric potential caused by electrical sounding

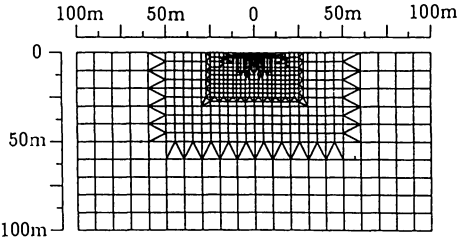

Fig. 9: Finite element mesh used in vertical two dimensional analysis

In vertical soundings, measurements with varying electrode spaces are carried out at one investigation site. Resistivities and depths of layers must be determined so that similar differences in potential are analyzed for each measurement. The error in differences to be minimized is defined as Eq.(2). N is the number measurement points, and the superscripts O and A mean the value obtained by observations and analyses, respectively.

$$E_r = \sqrt{\sum_{i=1}^{N} \left\{ \left(\frac{V}{I}\right)_i^O - \left(\frac{V}{I}\right)_i^A \right\}^2} \tag{2}$$

In the actual measurement, three-dimensional distribution of electric potential are generated, thus, a two-dimensional analysis with identical resistivity distribution causes different electric potential. To compare the V/I of a two-dimensional analysis, V/I by a measurement must be multiplied with $4 \log 2 \cdot a$ before substituting Eq.(1)[3].

Using the described method, the distribution s of resistivity are estimated from the results of the August investigation. The electric potential is analyzed using the finite element mesh shown in Fig. 9, which has fine divisions near the electrodes. Since the distance between two current electrodes becomes 90 m at the maximum, the analyzed region is 200 m wide and 100 m deep. The number of nodes is 853 and the number of elements is 912. The resistivity of each element is defined as the resistivity of the layer in which the element exists. For an element which belongs to two layers, the resistivity is calculated and defined proportionally to their areas in the element.

Since the number of layers is assumed to be three as in the curve matching method, three resistivities and two depths of boundaries are to be estimated. Eight measurements are carried out for each point, and the number of unknowns is smaller than the number of conditions. The estimation of these values is expected to be possible. In Standard Powell's method, the initial values for all unknowns must be specified. In this study, the resistivities and the depths obtained by the curve matching method are used.

The depth of saline water below all measurement points is estimated and shown in Fig. 10. Compared to the results by the curve matching method in Fig. 7, the depth is shallower for

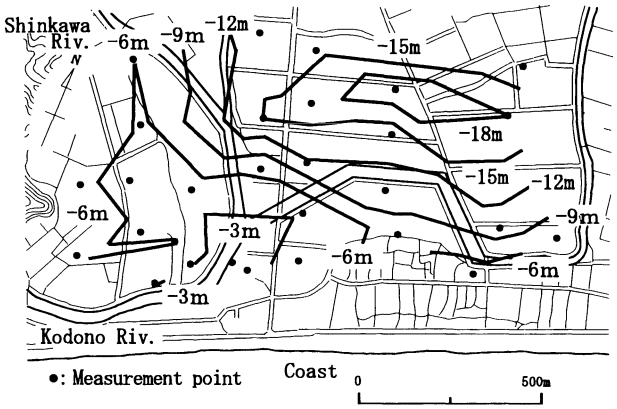

Fig. 10: Depth of saline water estimated by optimization

most of the measurement points. In particular, the depth for the point at the northern end of the western part is estimated to be shallow, which shows the intrusion from the river bed.

CONCLUSION

Electrical soundings resulting from the resistivity method are applied to the investigation of saline water intrusion in Haruno Town, Kochi Prefecture, Japan. The results obtained by two investigations, conducted in March and in August, are shown, and the differences are discussed. An alternative method for estimating the resistivity and the depth of the layers with a numerical method and optimization is proposed and applied.

This study is concluded as follows:

1. The electrical soundings obtained with the resistivity method are carried out in the coastal area of Haruno Town, Kochi Prefecture, Japan. A deep layer of low resistivity is found near the coast and is estimated to be a layer intruded by saline water.
2. The resistivity and the depth of the layers are obtained using the curve matching method to estimate the depth of the saline water. In the western part of the investigated area, where the quantity of groundwater use is large, the depth of the saline water is shallower than in the eastern part.
3. From the August investigation, when the quantity of groundwater use is small, the depth of the saline water is estimated to be shallow even in the eastern part where there is little groundwater use. Infiltrating water from rice paddy fields is supposed to raise the groundwater level and lower the saline water level.
4. The resistivity and the depth of layers are estimated with a numerical analysis and optimization from the results of the soundings. With this method, they can be determined more objectively than with the curve matching method.

REFERENCES

1. Sasa K, Ashida Y, Sugano T (1993) Physical soundings for construction and disaster prevention, Morikita Publishing Company, pp.128–158 (in Japanese).
2. Kadoya M, Nagai A (1979) Kyoto University Disaster Prevention Research Institute Annuals 22(B–2): 209–224 (in Japanese).
3. Ishii M, Oka T, Otoshi K. (1998) Estimation of saline water intrusion by electrical soundings, JSIDR Applied Hydrology 11: 23–29 (in Japanese)

Groundwater Flow Systems in Yoro River Basin Estimated from Stable Isotope, Subsurface Temperatures and MODFLOW

Dim Jules Rostand[1], Michiaki Konno[2], Akinobu Miyakoshi[1] and Yasuo Sakura[3]

[1]Graduate School of Science and Technology, Chiba University, Chiba 263-8522, Japan
[2]Hokuriku Regional Agricultural Administration Bureau, Kanazawa 920-8566, Japan
[3]Department of Earth Sciences, Faculty of Science, Chiba University, Chiba 263-8522, Japan

ABSTRACT. Yoro river basin is located at the center of Boso peninsula, Chiba prefecture. Its area is 250 Km^2, with maximum width of about 10 Km, length of 40 Km, then a relative height of 360 m and, a slope of 0.5 degree dipping northwards to the Tokyo bay. The topography of the area has been classified from South to North into three groups: Kazusa hills, Shimosa upland and alluvial plain. These geomorphological units belong respectively to the geological features of Kazusa group, Shimosa group and alluvium. From oxygen isotope analysis and subsurface temperature distribution, three groundwater flow systems of almost equivalent concentration of oxygen isotope are distinguished: the regional, intermediate and local. Natural recharge areas consist of zones of low subsurface temperature and, discharge areas of zones of high temperature. The regional and intermediate flow systems are recharged upstream of Yoro river basin at Kazuasa hills and, discharged respectively near the seashore and the middle of the basin through the kasamori formation (top layer of Kazusa group composed of muddy strata). The flow of discharging groundwater is at the origin of high subsurface temperature areas. The local flow system recharges at the Shimosa upland (midstream) and discharges at the alluvial plain (downstream river basin). These flow systems have been confirmed by a 2-D steady state numerical simulation using the MODFLOW program on a cross-section along the main groundwater flow direction .

KEY WORDS: Groundwater flow system, Temperature, Oxygen isotope, Model, Measurements

INTRODUCTION

Yoro river basin (Fig.1 and 2) is known for its artesian wells (which can reach 600 m depth) bored by the "Kazusa Bori" drilling bamboo method. This method started to be performed around a hundred years ago. For a proper use and control of groundwater, a sufficient knowledge of its flow system is necessary. The present work analyzes distribution of subsurface temperatures and hydraulic heads then, isotopic oxygen contrast, with the aim of clarifying the existing groundwater flow systems of the Yoro sedimentary basin. A 2-dimensional flow simulation model performed on a vertical cross-section along the main water flow direction confirms the presence of these systems. Results of this simulation show the dependence of groundwater flow patterns on geological conditions.

MEASUREMENTS AND PROCESSING METHODS

Subsurface temperature. Subsurface thermal measurements generally made in observation wells assume equilibrated thermal state between water and the surrounding solid material. Temperature measurements in this study were carried out in 13 observation wells. 10 of them were less than 300 m deep while, the 3 others had depths of 600 m (two wells) and 2000 m. The equipment used for the measurements was a digital

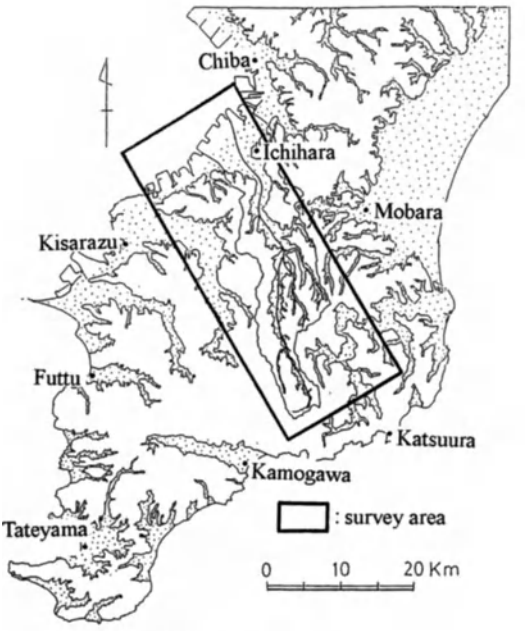

Fig. 1. Location of Yoro river basin

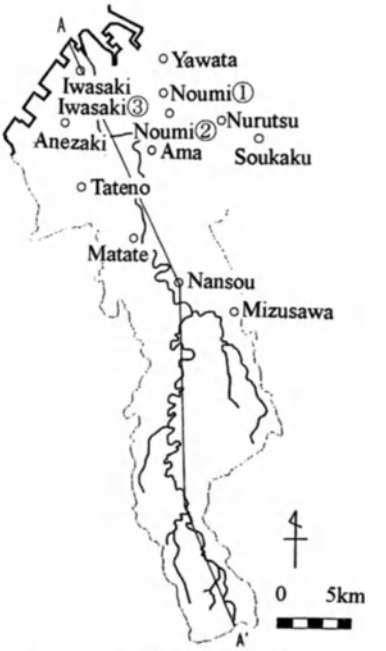

Fig. 2. Location of observation boreholes

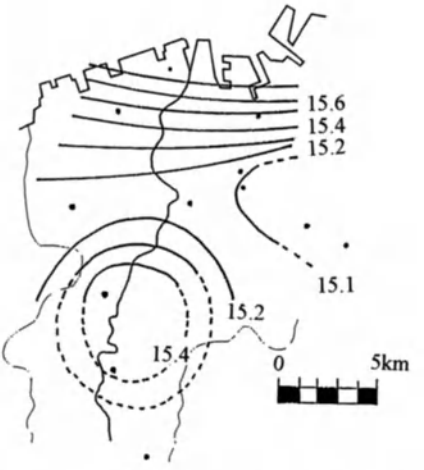

Fig. 3. Subsurface thermal distribution at –100m elevation

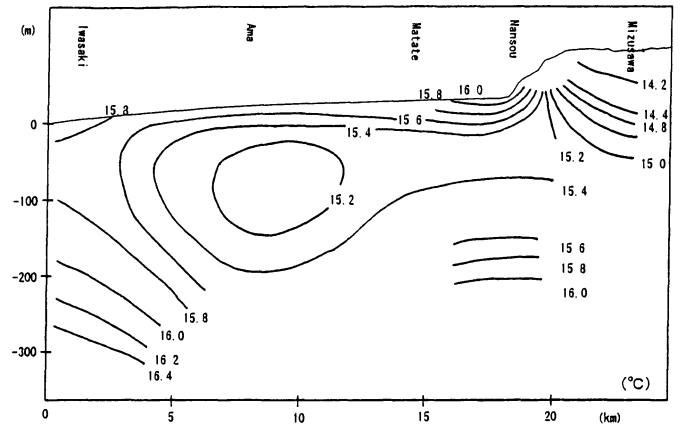

Fig. 4. Distribution of temperatures along A-A' cross-section

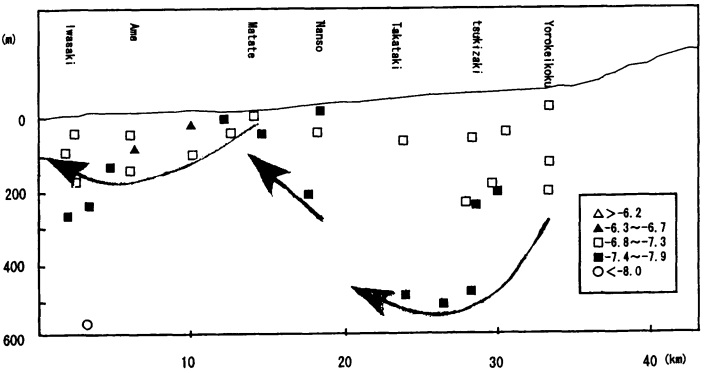

Fig. 5. Oxygen isotopic distribution along A-A' cross-section

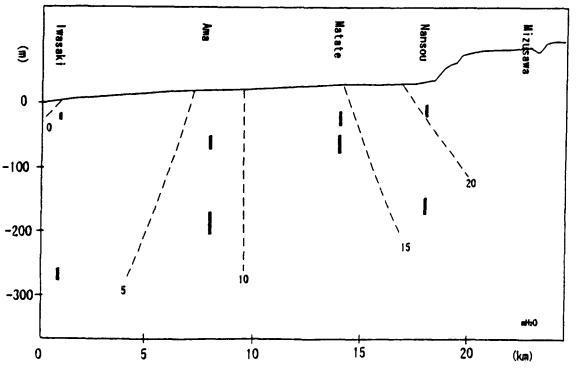

Fig. 6. Hydraulic head distribution along A-A' cross-section

thermister thermometer (resolution of 0.01°C) attached to a cable of 600 m length. Data were recorded from the water table till the bottom of the hole, every 2 meter interval downward in the relatively shallow boreholes (Anezaki, Iwasaki, Yawata, Ama, Matate, Nansou, Tatsuno, Nomi①, Nurutsu and Mizusawa) and, till 600 m depth , with a 5 meter interval in the 3 relatively deep boreholes (Iwasaki③, Noumi② and Soukaku)

Areal and vertical subsurface thermal distribution. Figure 3 shows horizontal distribution of temperatures at an altitude of 100 m below sea level. It is observed on this figure that there is a gradual increase of temperatures from highlands to seashore. Temperatures also increase towards the center of the basin (Matate and Nansou). High thermal and lowland areas, characteristic of natural discharge co-exist with low thermal and highland areas consisting of natural recharge zones. The flow system expressed by this distribution shows that water recharging upstream of Yoro river basin, discharges near the seashore. A 2-dimensional temperature distribution (Fig.4) along the South-North main groundwater flow direction A-A' cross-section of figure 1 shows the increase of temperatures with decreasing topography. This means, recharge takes place near Mizusawa, area located on highlands of the basin's median sites and where subsurface temperatures are relatively low. And, discharge occurs near Iwasaki, which is a lowland zone at the proximity of the seashore showing relatively high temperatures.

GROUNDWATER FLOW CONDITIONS

Oxygen isotope contrast. Oxygen isotopic analysis shows the existence of two different flow systems as illustrated on figure 5. One is the intermediate flow system, recharging at Yoro upstream area and discharging at Matate located at the median of the basin. The other is the local flow system, recharging mid area of Yoro river basin and discharging around the seashore. Each of these flow systems has almost the same oxygen isotope concentration.

Simulation model. As seen in the previous sections, the general flow direction estimated through subsurface temperature distribution and oxygen isotope contrast now clearly appears. A 2-dimensional numerical model (using a finite difference approach) was built along A-A' cross-section representing the main water flow direction, in order to simulate field distribution of hydraulic heads. MODFLOW program was used to run the steady state simulation exercise. The head change criterion for closure was set at 1.0×10^{-4} m. Theoretical background of this process can be found in [2] where the Richard formula (3) is derived from Darcy's law (1) and continuation equation (2) is solved through the finite difference approach. For the 2-dimensional case, this stands as:

$$V_x = K_x(x,y)\frac{\partial \varphi}{\partial x} \qquad \cdots\cdots\cdots (1)$$

$$\frac{\partial V_x}{\partial x} + \frac{\partial V_y}{\partial y} = 0 \qquad \cdots\cdots\cdots (2)$$

$$\frac{\partial}{\partial x}\left[K_x(x,y)\frac{\partial \varphi}{\partial x}\right] + \frac{\partial}{\partial y}\left[K_y(x,y)\frac{\partial \varphi}{\partial y}\right] = 0 \qquad \cdots\cdots\cdots (3)$$

Where Vx and Vy represent groundwater velocity in the respective x and y directions, Kx and Ky are hydraulic conductivities in the respective x and y directions and φ is hydraulic head. The observed field hydraulic head distribution along the main groundwater flow direction (cross-section A-A') is presented on figure 6. To build the model, a constant horizontal grid interval 500 m is set. While the vertical grid spacing comprises three sub-regions: 10 m interval above 0 m altitude, 50 m interval between the sea level

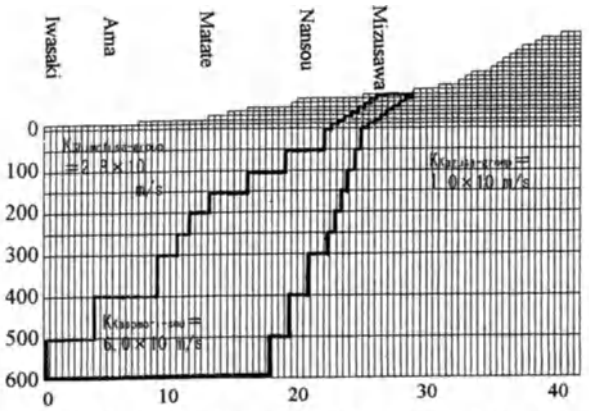

Fig. 7. Hydrogeological properties along A-A' simulation area

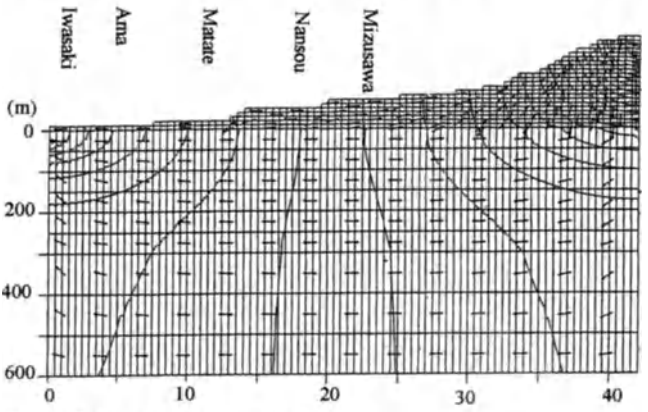

Fig. 8. First case simulation results

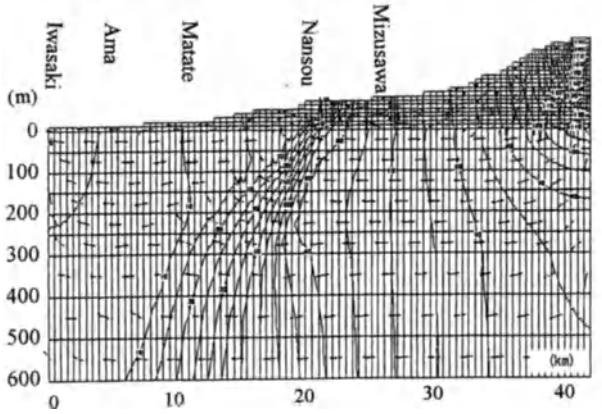

Fig. 9. Second case simulation results

and 300 m beneath and, 100 m interval between –300 and –600 m altitude (Fig.7). Boundary conditions stand as follows: for the upper boundary, an average yearly amount of 600 mm of recharge supplies the water table. This value was taken from recharge rates evaluated by [3]. Lower boundary: below 600 m depth, circulation of water is assumed to be very limited and negligible. This depth is therefore considered as a no flow boundary. Lateral boundaries: constant hydraulic heads were assigned under seashore location (left lateral boundary). Those values were estimated from the nearest observational wells of different depths. No flow condition was assumed for the right lateral boundary located upstream. Hydraulic conductivities chosen for the main geological features of this section have been deduced from aquifer test results [3]. These are (Fig.7): Shimosa group: 2.8×10^{-4} m/s, Kasamori layer (upper part of Kazusa group): 6.0×10^{-6} m/s and, lower part of Kazusa group: 1.0×10^{-5} m/s.

Results of simulation. The 2-dimensional groundwater flow simulation results of A-A' cross-section of Yoro river basin are presented in two modeling cases illustrating different hydrogeological conditions. For the first case (Fig.8), an average permeability coefficient of 1.0×10^{-5} m/s was imposed without distinction, on the different geological terrains of the basin. Results show that only the regional flow system can be recognized. In the second case (Fig.9), a clear illustration of the three flow systems recognized through subsurface temperature distribution and isotopic oxygen contrast is drawn by the distribution of flow line vectors. For this case, geological differences of the basin's formations were considered. Therefore, hydraulic conductivities used were those noted on the previous paragraph recognizing 3 main geological structures (Shimosa and Lower Kazusa groups and, Kasamori layer). The results of this last case confirm the interpretations made previously on the existence of regional, intermediate and local groundwater flow systems. The regional flow system is recharged on Kazusa hill and discharged near the seashore. The intermediate flow system is recharged at Yoro upstream and discharged at Nansou through Kasamori aquiclude layer. The local flow system is recharged at the mid area of Yoro river basin and discharged at the surroundings of the seashore.

CONCLUSION

The current study was based on measurements of subsurface temperatures, hydraulic heads and concentrations of oxygen isotope. Its target was to identify groundwater flow systems and clarify hydrogeological characteristics of the Yoro river basin. The results obtained can be summarized as: areas of high subsurface temperatures existing near the seashore are of discharging character. While, low temperatures of southern highlands are the recharging areas. Groundwater flows mainly from South to North. Finally, simulation results when they take into account specific geological features of the river basin confirm the existence of three flow systems as inferred by thermal analysis and oxygen isotope study.

References

1. Dominico, P.A & Palciauskas, V.V.(1973) Theoretical analysis of forced convective heat transfer in regional groundwater flow. Geol.Soc.Amer.Bull.**84**: 3803-3814
2. Freeze & Witherspoon (1966) Theoretical analysis of regional groundwater flow: 1-Analytical and numerical solutions to mathematical model. Wat Resour.Res.**2**: 641-656.
3. Kondo, A.(1985) Water balance of the groundwater basin in Ichihara region, Chiba prefecture. Jap. Ass. Groundwater Hydrol. **27**(3): 73-87
4. Parsons, M.L (1970) Groundwater thermal regime in a glacial complex. Wat. Resour. Res.**6**(6): 1701-1720

Climate Change Impacts in Regional-Scale Aquifers: Principles and Field Application

Hugo A. Loaiciga[1]

[1]Department of Geography, University of California, Santa Barbara, California 93106 USA.

ABSTRACT. $1xCO_2$ and $2xCO_2$ global circulation model (GCM) climate simulations were expressed in terms of scaling ratios and coupled with historical time series of normal and extreme climate periods. The scaled time series created global warming scenarios in regional karst aquifer which were then used to estimate ground-water recharge and to simulate ground-water flow and springflow for a range of pumping levels. GCM and ground-water pumping sensitivity of aquifer management strategies were identified. Methods and models to link climate change to regional aquifer response are examined in this work.

KEY WORDS: climate change, regional aquifer, aquifer recharge, karst aquifer, streamflow.

INTRODUCTION

Study objectives, climate scenario, and regional aquifers

This article presents an approach to investigate water resources impacts of climate change in regional aquifers. A regional aquifer is defined as one in which the longitudinal dimensions (x and y coordinates) are on the order of tens of kilometers while the vertical (z) coordinate is a fraction of the x and y dimensions, typically on the order of hundreds of meters. This means that aquifer flow is well-characterized as a 2-dimensional (x;y) process in which the hydraulic head is represented as an averaged value over the z coordinate. The Ogallala aquifer of the Great Plains regions of the United States and the Edwards Balcones Fault Zone (BFZ) of south-central Texas are two cases in point. The Edwards BFZ aquifer is one of the most productive karst aquifers in the world [1], with average annual recharge during normal precipitation years on the order of 9.9×10^8 m^3. Regional aquifers are important contributors to water supply, and in some cases provide a substantive share of the water used in large regional economies. Thus, it is important to investigate how these aquifers respond to short-term (seasonal) or long-term (intra-annual) climate variations. In this article we focus on the so-called "$2xCO_2$" global-warming scenario, in which the climate of the earth is simulated by global circulation models (GCMs) under conditions which correspond to double CO_2 atmospheric concentration relative to the base level of 355 ppmv (which approximates that of 1990, see [2]). Some authors speculate that the $2xCO_2$ scenario may be realized within one or two centuries [2]. New evidence regarding the global $2xCO_2$ budget suggests more complex feedbacks between atmospheric CO_2, soils, vegetation, and the ocean than originally understood [3]. This new evidence has cast doubts on whether the steady-state $2xCO_2$ climate scenario will ever be realized by human action alone within the next few centuries. This work reports an approach to estimate likely aquifer responses to the $2xCO_2$ scenario and highlights the effect of climate versus human impacts on aquifer yield. Our methodology is applicable to transient as well as steady-state climate variations, and it is not limited to $2xCO_2$ estimates.

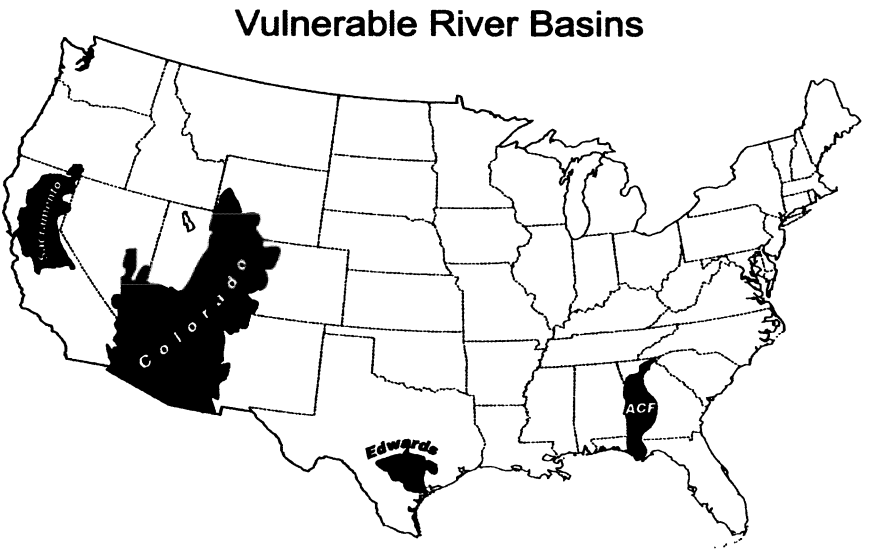

Fig. 1. Watersheds vulnerable to climatic change in the United States.

CLIMATE-CHANGE VULNERABILITY AND THE EDWARDS BFZ AQUIFER

Figure 1 shows a map of four U.S.A. watersheds considered highly vulnerable to climatic change and climatic variability [3]. They were identified based on analysis of multiple vulnerability factors which included: (i) water resources implications of changes in water supply; (2) ecosystem dependence on hydrologic regime modification; (3) institutional issues surrounding adaptive strategies to climatic modifications. The Edwards BFZ aquifer of south-central Texas was ranked as the most vulnerable watershed to climate change in the United States. This watershed's hydrologic regime is dominated by the strong interaction of streamflow seepage into the Edwards BFZ aquifer, the evolution of hydraulic head in the recharge zone and the confined zone of the aquifer, large-scale ground water pumping (currently on the order 4.9×10^8 to 6.2×10^8 m^3 yr^{-1}) and springflow discharge along a series of large springs located in the discharge zone of the aquifer.

Figure 2 shows a schematic of the recharge mechanism in the Edwards BFZ aquifer. The right portion of Figure 2 shows the current mechanism of recharge in the Edwards BFZ aquifer by means of streamflow seepage into the outcropping Edwards limestone. Streamflow is measured upstream (Q_U) and downstream (Q_D) of the recharge area in several streams which run through the Edwards aquifer. Runoff generated within the recharge area (Q_I) adds to streamflow. The recharge R in the outcrop area is given by $R = Q_U + Q_I - Q_D$. Q_I is estimated as a fraction of the upstream flow (Q_U) scaled by the ratios $A_I/A_U \cdot P_I/P_U$, in which A_I, A_U, P_I, and P_U are the drainage area in the recharge zone, the drainage area upstream of the recharge zone, the precipitation in the

recharge zone, and the precipitation in the drainage upstream of the recharge zone, respectively [1]. Thus, $Q_I = Q_{RU} \cdot A_I/A_U \cdot P_I/P_U$.

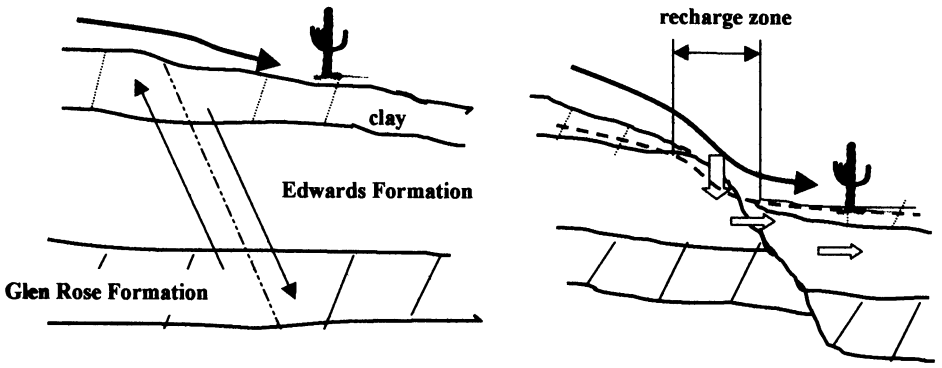

Fig. 2. Recharge mechanism in the Edwards BFZ aquifer. The karstified Edwards limestone was exposed by normal faulting. Streamflow which was previously kept flowing over the del Rio clay was then able recharge the limestone aquifer by seepage (right). The unconfined aquifer in the recharge zone becomes confined downgradient from the outcrop area (see hydraulic head dashed line). Drawing not at scale.

The recharge discharge (confined) zones of the Edwards BFZ aquifer have surfaces of 2.9 x 10^3 and 13.0 x 10^3 mi^2, respectively. Because of the relative magnitudes of the horizontal and vertical dimensions, ground water flow in the study area is well-described by the following transient-flow equation:

$$\frac{\partial}{\partial x}\left(T(x,y)\frac{\partial h}{\partial x}\right)+\frac{\partial}{\partial y}\left(T(x,y)\frac{\partial h}{\partial y}\right)=S(x,y)\frac{\partial h}{\partial t}+N(x,y) \qquad (1)$$

in which T is transmissivity, h is the hydraulic head, S is the storage coefficient, and N is the net ground water flux per unit area of aquifer (includes pumping, springflow, and recharge). Equation (1) was discretized according to a (fully-implicit) finite-difference scheme and coded into a Fortran program named GWSIM IV ([1] and [5]). Figure 3 shows the one-layer, finite difference, grid which consists of 30 rows and 81 columns. The layer represents the Edwards (limestone) Formation (see Figure 2). Transmissivity (T), storage coefficient (S), pumping (Q), and recharge (R) are variable within the aquifer and are input cell by cell according to the spatial variability dictated by field measurements. The time step in the finite-difference discretization is one month. The effect of climate change is introduced through climate scaling factors as explained below.

CLIMATE SCALING FACTORS AND 2xCO_2 RECHARGE

Climate change is quantified in terms of scaling factors that involve 1x CO_2 and 2xCO_2 GCM-simulated temperature, precipitation, and streamflow. The 1xCO_2 GCM simulation corresponds to the 1990 CO_2 atmospheric concentration (≈ 355 ppmv). Scaling factors are used in two ways to generate climate-change scenarios from historical time series. The first consists of multiplying a historical time series by the corresponding scaling factor (or scaling ratio in this case). Using streamflow (Q) as an example, the equation used to generate the 2xCO_2 streamflow scenario is as

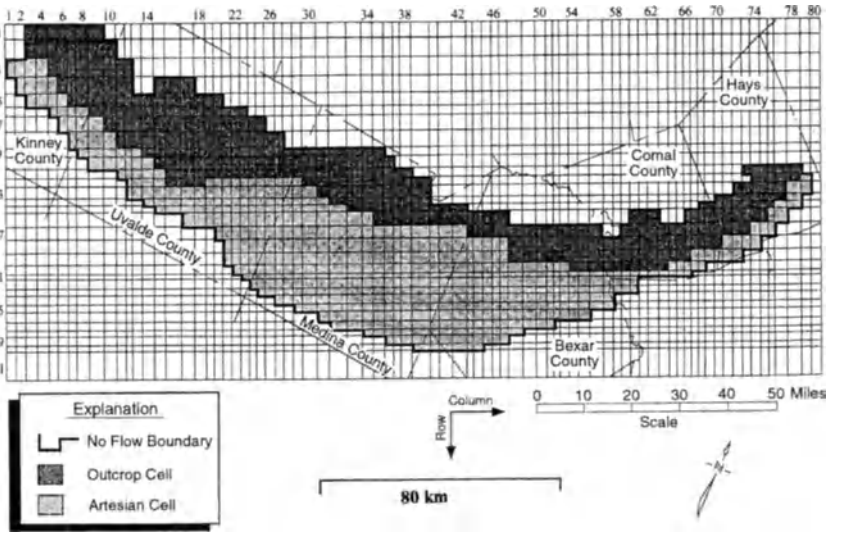

Fig. 3. The finite-difference grid of the Edwards BFZ aquifer model [5].

follows:

$$Q_{2xCO_2 scenario} = \frac{Q_{2xCO_2}}{Q_{1xCO_2}} \cdot Q_{historical} \qquad (2)$$

If the GCM-simulated Q_{1xCO2} and Q_{2xCO2} are unbiased and independent estimators of streamflow under 1 x CO_2 and 2 x CO_2 conditions, respectively, then, the expected value of the estimated streamflow $Q_{2xCO2scenario}$ is equal to the 2 x CO_2 streamflow mean (μ_{2xCO2}), i.e., $Q_{2xCO2scenario}$ is an unbiased estimator also. It is implied in the latter statement that $Q_{historical}$ and Q_{1xCO2} have identical expected values which are both equal to the historical mean. Precipitation and other climatic variables are scaled in a manner similar to that used to scale streamflow. With the streamflow scaling factors available, then the aquifer recharge is scaled to 2xCO2 conditions by the following expression :

$$R_{2xCO_2} = \frac{Q_{2xCO_2}}{Q_{1xCO_2}} [Q_U + Q_I - Q_D] \qquad (3)$$

Pumping is specified to be consistent with the estimated water use at the time of simulation. For example, our 2xCO_2 pumping scenario has been established at 7.84 x 10^8 m^3 yr^{-1}, which is the farthest reaching estimate (year 2050) currently available for the study area. Once scenario recharge and pumping are created, one can simulate aquifer impacts.

The climate scaling factors were obtained from a database developed by the U.S. National Center for Atmospheric Research (NCAR, [7]). The database, called VEMAP (Vegetation/ Ecosystem Modeling and Analysis Project), relied on seven leading GCMs to generate coarse-grid forcing

climatic output for the USA under $1xCO_2$ and $2xCO_2$ conditions. Their outputs served then as forcing conditions to a regional climate model for the coterminous USA which produced climates scaling factors at a scale of 0.5° latitude x 0.5° longitude. Figure 4 shows the VEMAP grid overlain on the Edwards BFZ aquifer.

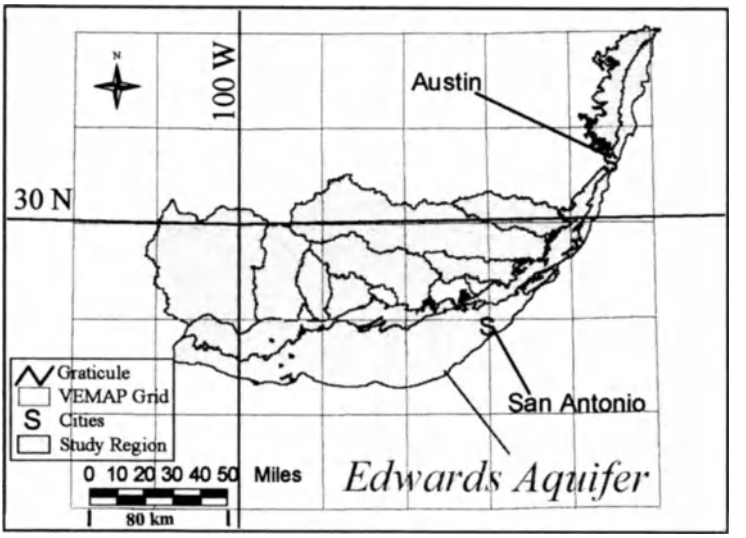

Vemap coverage

Figure 4. The VEMAP grid overlain on the Edwards BFZ aquifer [1].

RESULTS AND CONCLUSIONS.

Figure 5 shows the minimum springflows at two of the major springs found in the Edwards aquifer's discharge zone, the San Marcos and Comal Springs, as a function of annual pumping rate in a $2xCO_2$ drought climate scenario. The drought scenario in a warmer climate was obtained by scaling ground water recharge during the critical drought period from 1947 through 1959 with $2xCO_2$ scaling factors as dictated by equation (3). The San Marcos and Comal springs are of significance with respect to water supply and ecological criteria, and are good indicators of the aquifer's hydraulic and ecologic status. The results of Figure 5 correspond to climatic scaling factors obtained from one of the seven GCMs in the VEMAP database, namely, the United Kindom Meteorological Office (UKMO) GCM. Results are available for all the other GCMs, but space limitations constraint us to present only one set of GCM results. The UKMO GCM is of particular interest because it predicts median $2xCO_2$ moisture supply in the study area relative to the predictions of the other GCMs. Thus, the UKMO results can be seen as an average scenario relative to more extremes ones. Figure 5 shows springflow minima and the reference target springflow of 7.34×10^6 m^3/month, which is considered adequate to maintain aquatic habitat viability in the discharge zone. Figure 5 indicates that minimum reference springflow at Comal springs is met whenever the annual pumping rate is kept at approximately 1.23×10^8 m^3 yr^{-1} or less under drought in a $2xCO_2$ era. This compares with the current pumping of about 6.2×10^8 m^3 yr^{-1} and with predicted year 2050 pumping of 7.84×10^8 m^3 yr^{-1}. San Marcos minimum reference

springflow, on the other hand is not met under drought $2xCO_2$ for any level of pumping, pointing to challenging habitat management considerations. Other simulations were done using base periods of normal (as opposed to drought) climate. Those results, not shown here, indicate the predominant effect that pumping has on aquifer response compared to the impacts of climate change on available surface moisture. The approach herein presented can be extended to any other type of regional aquifer to explore the simultaneous impacts of ground-water and climate forcing.

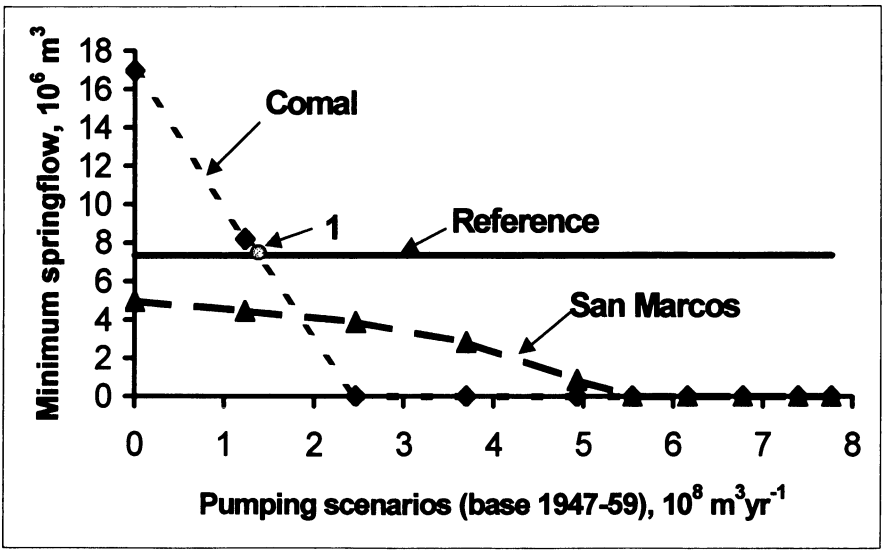

Fig. 5. Minimum monthly springflows based on UKMO general circulation model (GCM).

REFERENCES

1. Loaiciga, H.A., Maidment, D.R. and Valdes, J.B. (1999) Climate change impacts in a regional karst aquifer, Texas, USA, Journal of Hydrology, in press.
2. Houghton, J.T., Meira Filho, L.G., Callander, B.A., Harris, N., Kattenberg, A., and Maskell, K. (1996). Climate Change, 1995. Cambridge University Press, Cambridge, UK.
3. Loáiciga, H.A., Maidment, D.R., Valdes, J.B., Roos, M., and Wood, E.F. (1996). Report of the case study selection team. Report ASCE/USEPA Climate Change Cooperative Agreement, Am. Soc. Civil Engrs., Reston, Virginia, USA.
4. Loaiciga, H.A., Valdes, J.B., Vogel, R., Garvey, J., and Schwarz, H. (1996). Global warming and the hydrologic cycle. Journal of Hydrology 174:83-128.
5. Thorkildsen, D., and McElhaney, P.D. (1992). Model refinement and application for the Edwards BFZ aquifer in the San Antonio region. Texas Water Development Board Report 340, Austin, Texas, USA.
6. Texas Water Development Board. (1997). Water for Texas-GP-6-2, Austin, Texas, USA.
7. Kittel., T.G.F., Rosenbloom, N.A., Painter, T.H., Schimel, D.S. et al. (1995). The VEMAP integrated database form modeling United States ecosystem/vegetation sensitivity to climate change. J. Biogeography 22:857-862.

Simulation of Conservation of a Spring in Groundwater Recharge by Rainwater

Yosihisa Ando[1], Kazumasa Fujimura[2], and Tomohei Kobayashi[3]

[1]Department of Civil Engineering, Graduate School of Engineering, Tokyo Metropolitan University, Hachioji City, Tokyo 192-0397, Japan.

[2]Department of Civil Engineering, Faculty of Physical Sciences and Engineering, Meisei University, Hino City, Tokyo 191-8506, Japan.

[3]Gifu Land Development Authority, Gifu City, Gifu 500, Japan.

ABSTRACT. In this study, the conservation of a spring in groundwater recharge by rainwater is investigated using a hydrological model which includes the direct runoff, infiltration, evapotranspiration, groundwater recharge, and groundwater runoff for simulating the total runoff from the rainfall. The Kokubunji basin is chosen the study area. In the basin, the direct runoff from impervious areas discharges to one main stream, and the groundwater runoff originates from the unconfined aquifer. We assume that the groundwater runoff rate is proportional to the second power of the amount of stored groundwater, and the groundwater recharge is proportional to the soil moisture excess. The total runoff is simply obtained from the sum of the direct runoff and the groundwater runoff. The groundwater recharge in the Kokubunji basin is restricted because of permeable inlets through which the rainwater from roofs penetrates into the soil. Hydrological data from a rain gauge and a stream flow gauge in the area are used for analyses of the rainfall-runoff relationship. Computations were carried out by using the 1995's hydrological data for 1000, 2000, 3000, and 4424 permeable inlets. The effects of the conservation of the spring in groundwater recharge by rainwater increase 26%, 52%, 78%, and 116% to the total runoff for 1000, 2000, 3000, and 4424 permeable inlets, respectively.The hydrological model has good applicability when calculated at intervals of one hour.

KEY WORDS: spring, groundwater recharge, rainwater, simulation, hydrological model

INTRODUCTION

In this paper we present a hydrological simulation of the water cycle of a spring in groundwater recharge by rainwater. The spring belongs to the Kokubunji basin, and is one of the springs in an upland region of Tokyo, Japan. Ando [1] developed a hydrological water budget model with a groundwater component in the Kokubunji basin. Ando et al. [2] developed a lumped groundwater component model in the Kokubunji basin. In this paper, the authors propose an improved hourly-lumped hydrological budget model in the Kokubunji basin and simulate the effects of the conservation of the spring in groundwater recharge by rainwater.

DESCRIPTION OF THE KOKUBUNJI BASIN

The Kokubunji basin is located in the western suburbs of Tokyo and has a catchment area of about 41 hectares. The spring that drains the terrace is one of the many terrace springs that flow into the Noh river. Fig.1 shows an outline of the Kokubunji experimental basin; the groundwater table contour was drawn based on the groundwater level data for 12th December 1982. The groundwater flows from the west of the basin to the east and emerges as a spring and a stream. The basin is equipped with both a rain gauge and a streamflow gauging station. The groundwater divide was delineated from a study of the geology of the basin, which consists of a loam formation, a sand and gravel formation, and a compacted clay formation (see Fig. 2). The sand and gravel formation acts as an unconfined aquifer for groundwater flow, and the compacted clay formation functions as an impermeable layer.

HOURLY HYDROLOGICAL MODEL

The hourly hydrological model is a combination of direct runoff, infiltration, evapotranspiration, groundwater recharge, and groundwater runoff (see Fig. 3). Direct runoff occurs in impervious areas (*Ad*) near the stream. *Ad* is equal to 4123 square meters (1% of the basin). *P'imp* (rainfall in the impervious area near the stream) becomes direct runoff (*D'imp*), including a loss estimate of *L* =2mm [3]. *Pi(t)* (rainfall in the pervious area) becomes *I(t)* (infiltration into the soil) when *Pi(t)* is less than *R* (infiltration capacity of ground surface). *R* becomes *I(t)* when *Pi(t)* is greater than *R*. *R* is equal to 10mm/h [4]. When *Ms* and *Ms'* represent soil-moisture storage, *Ms'(t)* is shown in Fig.3. *E(t)* represents evapotranspiration from the infiltration area. Evapotranspiration (*E(t)*) is calculated using Hamon's formula [5]. The relationship between *Ms'(t)* and *G(t)* is shown in Fig.3, where *Mn* is equal to 200mm, β is equal to 0.1, *g* is equal to 0.5mm/h, and *h* is equal to 5mm. These values are the same as those for the Nagayama experimental basin [3]. Groundwater runoff (*Qg(t)*) originates from the unconfined aquifer. The recession equation of groundwater runoff from unconfined aquifers was theoretically obtained by Takagi[6]. It may be stated as

$$Qg(t)= Q_0 / (1 + Au\sqrt{Q_0}t)^2$$

where Q_0 is the value of groundwater runoff at time $t=0$ and *Au* is the recession constant of groundwater runoff from unconfined aquifers. The relation between groundwater runoff and groundwater storage、as presented by Coutagne[7] and Ding[8], is given as

$$Qg(t)=Au^2\ Sg(t)^2$$

where *Sg(t)* is the groundwater storage, and *Au* is equal to 0.016. Total runoff (*Q(t)*) is the sum of direct runoff (*D'imp(t)*) and groundwater runoff (*Qg(t)*). The observed and calculated hydrographs , which show good agreement, are shown in Fig. 4. Therefore, the hourly hydrological model has good applicability to the Kokubunji basin.

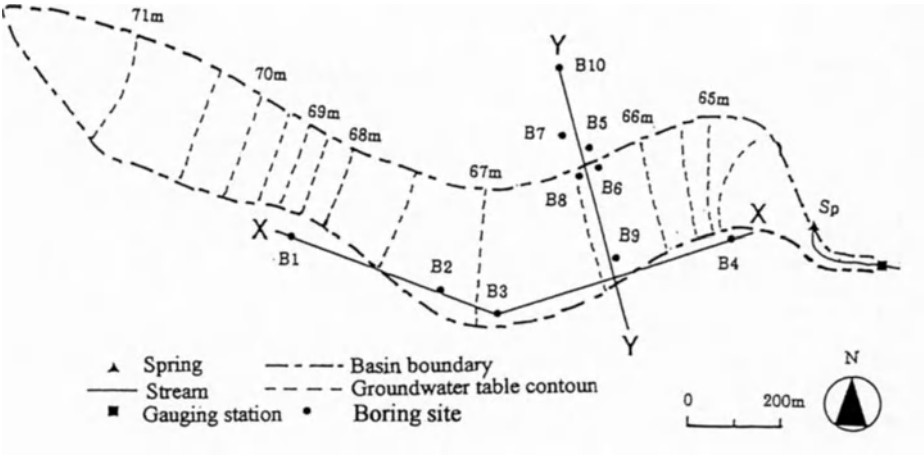

Fig. 1 . Outline of the Kokubunji experimental basin

(a) Geological cross section of X-X line

(b) Geological cross section of Y-Y line

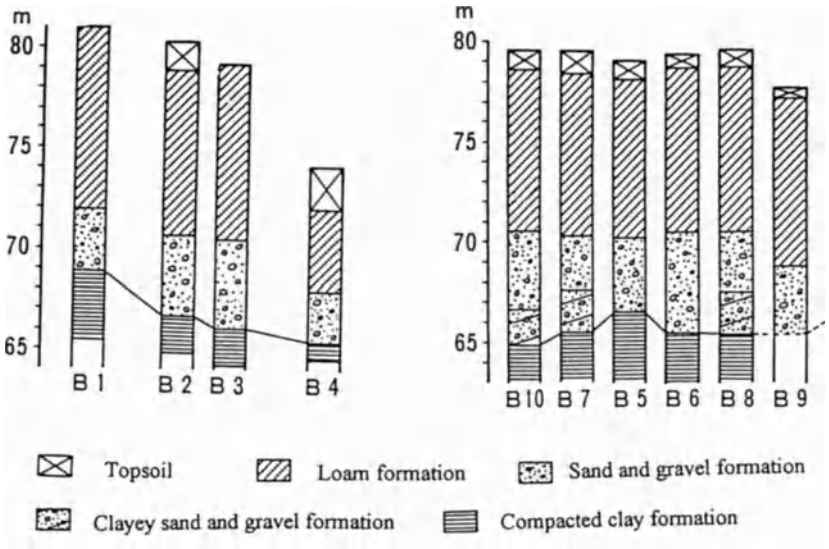

Fig. 2. Geological cross sections

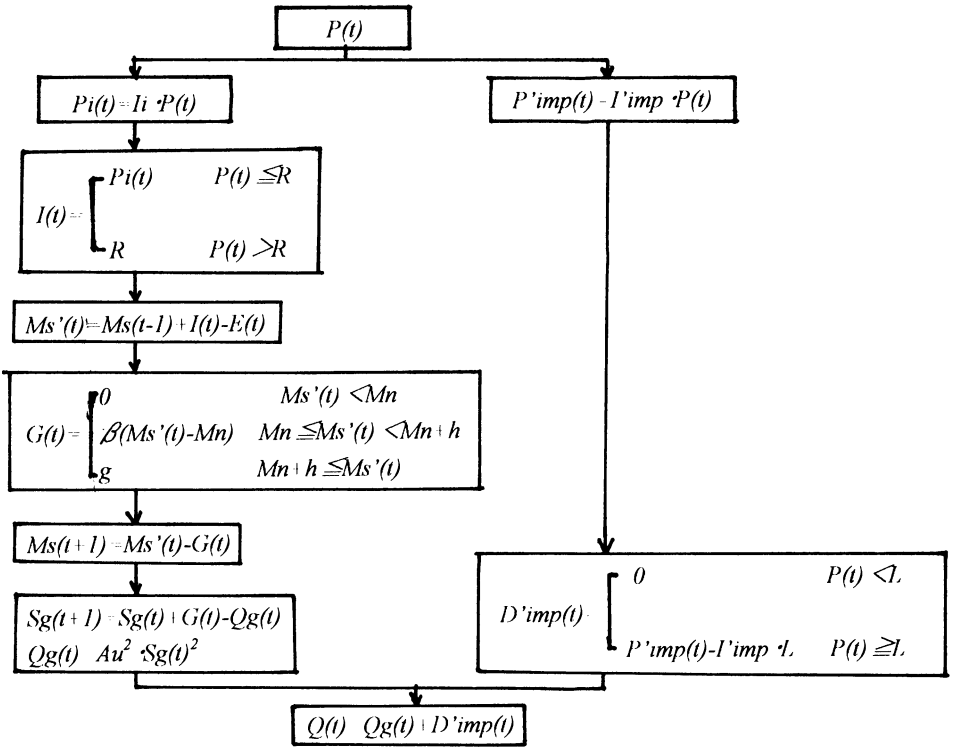

P:Rainfall
Ii:Ratio of the pervious area to the catchment area
I'imp:Ratio of the impervious area nearthe stream to the catchment area
I:Infiltration
Ms,Ms':Soil moisture storage
E:Evapotranspiration
Mn:Normal soil moisture
G:Groundwater recharge
g:Capacity of groundwater recharge
h:Constant of soil moisture excess
R: Infiltration capacity of ground surface
β: Constant of groundwater recharge
Sg: Groundwater storage
Qg: Groundwater runoff
Au: Recession constant of groundwater runoff from unconfined aquifer
I': Loss in the imperviousarea near the stream
D'imp: Direct runoff contributing to the stream
Q: Total runoff
t: Time step(in this case, 1hr)

Fig. 3. Sequence of the hourly hydrological model of the Kokubunji basin

SIMULATION OF CONSERVATION OF A SPRING IN GROUNDWATER RECHARGE BY RAINWATER

Groundwater recharge by rainwater is restricted to the rain falling on roofs because of water quality. Assuming 1000, 2000, 3000, and 4424 permeable inlets, simulation using the above hourly hydrological model was carrried out during 1995. The count of 4424 permeable inlets corresponds to 100% of the roofs in the Kokubunji basin being covered by permeable inlets. Fig. 5 shows examples of the results of the simulation of conservation of the spring in groundwater recharge by rainwater. Effects of the conservation of a spring through groundwater recharge by rainwater were a 26% increase of total runoff for 1000, 52% increase for 2000, 78% increase for 3000, and 116% for 4424 permeable inlets. These results indicate that the number of permeable inlets significantly affect the results.

CONCLUSION

The authors aim at simulating the conservation of a spring in groundwater recharge by rainwater. The spring belongs to the Kokubunji basin, and is one of several springs in an upland region of Tokyo , Japan. The Kokubunji basin is located in the western suburbs of Tokyo and the catchment area is about 41 hectares. A rain gauge and a streamflow gauge are equipped in the basin. The hydrological model is a combination of direct runoff, infiltration, evapotranspiration, groundwater recharge, and groundwater runoff.

1. The hourly hydrological model has good applicability to the spring (the Kokubunji basin).
2. Simulation using the above hourly hydrological model was carried out, and a significant increase of total runoff when there are permeable inlets for rainwater on roofs was confirmed.

REFERENCES

1. Ando Y (1988) Proc.of the International Symposium on Interaction between Groundwater and Surface water, pp.261-268
2. Ando Y, Miyata T, Komiya T (1999) Handbook and Proc. of Water 99 Joint Congress, pp.609-614
3. Ando Y, Musiake K, Takahasi Y (1984) J of Hydrology, 68, pp.61-83
4. Ando Y, Nabeyama T, Nishijima S (1993) IAHS Publication No.216, pp.403-408
5. Hamon W R (1961) Estimating potential evapotranspiration, Proc. of ASCE, pp.107-120
6. Takagi F (1966) Proc. JSCE, pp.1-11 (in Japanese)
7. Coutagne A (1948) Houille Blanche, Sept.-Oct., pp.3-23 (in French)
8. Ding J Y (1966) Discussion of "inflow hydrographs from large unconfined aquifers", J. Irrig. Drain. Div., Proc. ASCE, 90 (IR1), pp.104-107

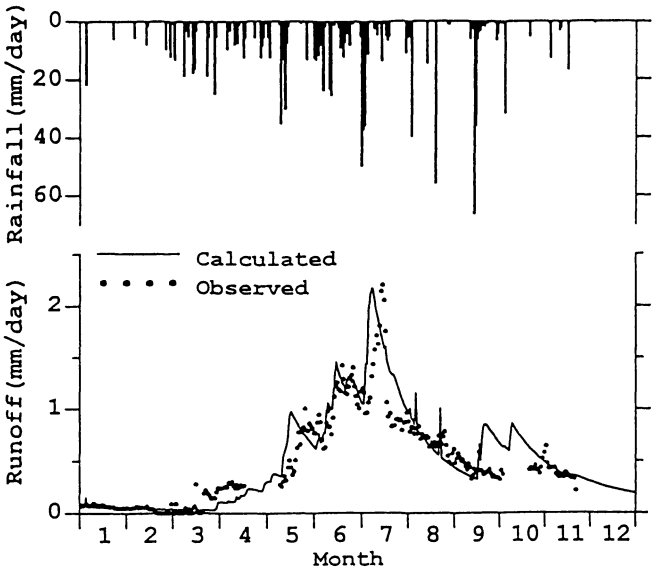

Fig . 4. Observed and calculated hydrographs for 1995

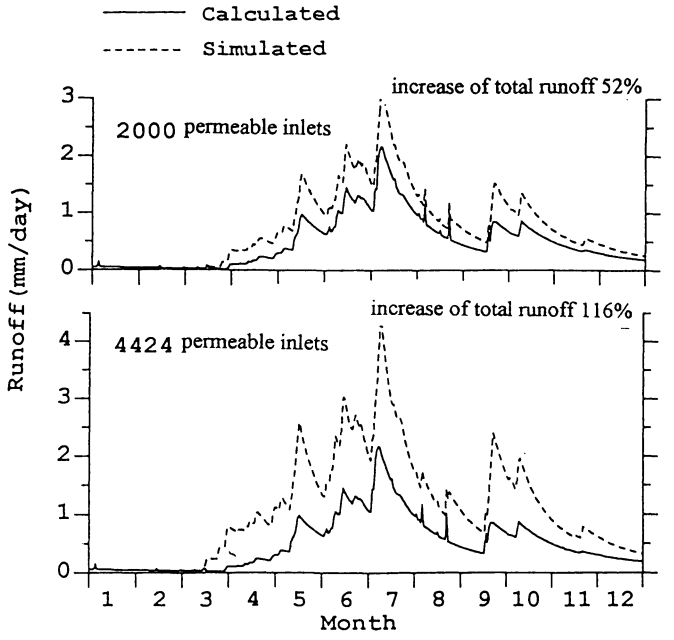

Fig. 5. Results of simulation of conservation of a spring in groundwater recharge by rainwater

Numerical Simulation of Groundwater Flow in Multi-layered Aquifers with a Distributed Hydrological Model

Yangwen Jia[1], Guangheng Ni[2], Yoshihisa Kawahara[3] and Tadashi Suetsugi[3]

[1]JST Domestic Research Fellow, Public Works Research Institute, Ministry of Construction, Asahi 1, Tsukuba, Ibaraki 305-0804, Japan.
[2]Exchange Researcher, Public Works Research Institute, Ministry of Construction, Asahi 1, Tsukuba, Ibaraki 305-0804, Japan.
[3]Division of Urban River, Public Works Research Institute, Ministry of Construction, Asahi 1, Tsukuba, Ibaraki 305-0804, Japan.

ABSTRACT: In this study, a distributed hydrological model is applied to the Ebi river catchment by coupling computation of surface water with simulation of multi-layered groundwater. The distributed hydrological model is grid-based and able to model spatially variable water and heat processes with complex land covers. Taking into account of recharge from unsaturated soil layers and lifted groundwater as source terms, a two-dimensional simulation of multi-layered aquifers is performed for groundwater flow to consider the interactions between surface water and groundwater. The Ebi river catchment has an area of 27 km^2 and is located in the Funabashi and Kamagaya cities, Chiba prefecture, Japan. It is one of the pilot catchments set by Ministry of Construction to study hydrological cycle. The groundwater aquifers in the catchment include one unconfined aquifer and two confined aquifers. The soil of unconfined aquifer varies from the Kanto-loam to the alluvial soil, the Joso clay or the Narita sand whereas that of confined aquifers is mainly the Narita sand. The distributed hydrological model is applied to the catchment with a grid cell size of 50m and a time step of 1 hour. The simulation of 5 years from 1992 to 1996 is performed and tested against the measurement. The comparison of water balance in wet 1993 with that in dry 1994 is also conducted to see the effect of weather change on groundwater and other hydrological components. With the further urbanization in future, countermeasures such as infiltration facilities are highly required to conserve the groundwater and to improve the hydrological cycle in the catchment.

KEY WORDS: groundwater, hydrological cycle, urbanization, Ebi river, distributed model

INTRODUCTION

The hydrological cycle is greatly changed with the rapid urbanization in catchments. The groundwater outflow decreases and groundwater levels become lower while the river flood become bigger and quicker because of increased impervious area. The purpose of this study is to make clear the hydrological cycle and groundwater flow in the rapidly urbanized Ebi river catchment, and to provide basic information for the conservation countermeasures of hydrological cycle in the catchment.

The map of the Ebi river catchment is shown in Fig.1. It is located in the Funabashi and Kamagaya cities, Chiba prefecture, Japan. It is one of the pilot catchments set by Ministry of Construction to study hydrological cycle in details. It has an area of 27 km^2. There are 6 rain gauges inside or near the catchment, one of which is the Funabashi AMeDAS station with the observations of temperature, wind and sunshine. The annual average precipitation over the past 10 years is 1360 mm. There are 3 gauges of river water level and discharge. The land use and elevation data are based on the Fine Digital Information System (FDIS). The catchment is adjacent to the Tokyo bay and land elevations are quite low (0~33m). There are 4 kinds of soils considered in the study, the

dominant ones of which are the Kanto loam and the Alluvial soil. Based on the geological boring data, aquifers in the catchment show a multi-layered structure. The boundary of groundwater flow shows a little larger than the catchment boundary according to the measurement of groundwater levels as shown in Fig.1.

According to the prediction by the local government, about 5.7 km^2 forest, paddy or drought farmland will be developed to housing area from 1993 to 2035, the population will reach 261,000 from 203,000 and the coverage rate of sewer system will attain 100% from 10% (in population). To study the impacts of urbanization on groundwater and hydrological cycle and to propose countermeasures, a robust simulation model is required to develop and verify.

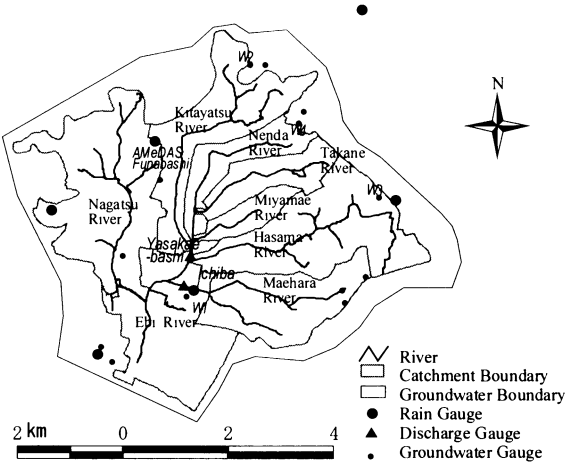

Fig.1 The map of the Ebi river catchment.

MODEL STRUCTURE

The details of model structure are referred to Jia and Tamai (1998). In this study, modification is added to groundwater simulation. By adding another confined aquifer and directly calculating groundwater outflow to rivers, groundwater simulation becomes quasi-3 dimensional and physically based.

The diagram of the model vertical structure inside a grid cell utilized in this study is shown in Fig.2 (a). Land use is at first summarized into 3 groups, namely a water body group, a soil-vegetation group and an impervious area group. The soil-vegetation group consists of bare soil, tall vegetation (forest or urban trees) and short vegetation (grass or crops). The impervious area group consists of impervious urban cover and urban canopy. Evapotranspiration and latent heat flux are computed by the Penman-Monteith equation, infiltration excess during heavy rains is simulated by a generalized Green-Ampt model (Jia and Tamai, 1997) whereas saturation excess during the remaining periods is obtained by balance analysis in unsaturated soil layers. Surface temperature is solved by the Force-Restore method.

The diagram of the model horizontal structure inside a catchment is shown in Fig.2 (b). River flow routing is conducted for every sub-catchment and a main channel using the kinematic wave method. Overland flow is simplified as lateral inflow to rivers because the concentration time is estimated to be shorter than the simulation time interval in this study. Taking into account of recharge from unsaturated soil layers and lifted groundwater as source terms, a quasi-3 dimensional simulation is performed for groundwater flow to consider the interactions between surface water and groundwater by using the following Boussinesq equations (Zaradny, 1993):

Unconfined aquifer
$$C_u \frac{\partial h_u}{\partial t} = \frac{\partial}{\partial x}(k_u h_u \frac{\partial h_u}{\partial x}) + \frac{\partial}{\partial y}(k_u h_u \frac{\partial h_u}{\partial y}) + (Q_3 + WUL - RG - Per - E) \quad (1)$$

Confined aquifers
$$C \frac{\partial h}{\partial t} = \frac{\partial}{\partial x}(kD \frac{\partial h}{\partial x}) + \frac{\partial}{\partial y}(kD \frac{\partial h}{\partial y}) + (Per - GWP - Perc) \quad (2)$$

where C_u is the specific yield, C the storage coefficient, h_u and h the groundwater heads in the unconfined aquifer and confined aquifers respectively, k_u and k the hydraulic conductivities of unconfined aquifer and confined aquifers respectively, D the thickness of confined aquifers, Q_3 the recharge from unsaturated soil layers, RG the groundwater outflow to rivers, WUL the water use leakage, GWP the pumped groundwater, Per and $Perc$ the percolation to the aquifer below and E is the evapotranspiration from groundwater (when groundwater level is high).

Water exchange between river and groundwater is calculated according to the hydraulic conductivity k_b of riverbed material and difference between river water level H_r and groundwater level h_u:

$$RG = \begin{cases} k_b A_b (h_u - H_r)/d_b & h_u \geq H_r \\ -k_b A_b & h_u < H_r \end{cases} \tag{3}$$

where A_b is seepage area of the riverbed and d_b is the thickness of riverbed material.

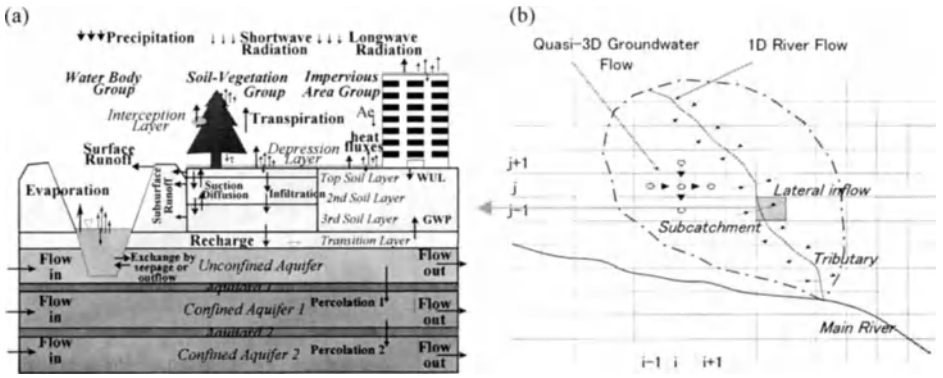

Fig.2 The diagram of model structure: (a) vertical structure inside a grid cell, (b) horizontal structure.

APPLICATION

The above model is applied to the Ebi river catchment with a grid cell size of 50m and a time step of 1 hour. The simulation of 5 years from 1992 to 1996 is performed. The characteristic curves of soil ~ moisture and hydraulic conductivity parameters are referred to Herath, Musiake and Hironaka (1992). Aquifer data are based on geological boring data. The unconfined aquifer with a thickness of 2-17 m is constituted of the Kanto loam, the Narita sand and the alluvial soil. The hydraulic conductivity of unconfined aquifer is around 5×10^{-4}cm/s and the specific yield is related to groundwater level and soil moisture in unsaturated layers. When groundwater level falls or it is 2m below ground surface, the specific yield is set as 0.01, a deduced effective porosity of the Kanto loam or the Narita sand. When groundwater rises near to ground surface, it is set as the difference of saturated soil moisture and soil moisture in unsaturated layers. Below the unconfined aquifer is an aquitard constituted of the Joso clay with a thickness of 5-10m and a hydraulic conductivity of around 1×10^{-6}cm/s. Two confined aquifers with a thickness of 100-400m are mainly constituted of the Narita sand and their specific storage is set as 0.0005/m.

Fig.3 shows the comparison of simulated groundwater levels with the observed ones at 4 wells (their positions are referred to Fig.1). It can be seen that the variation patterns are almost same. Here the groundwater level is the elevation above the sea level of the Tokyo bay.

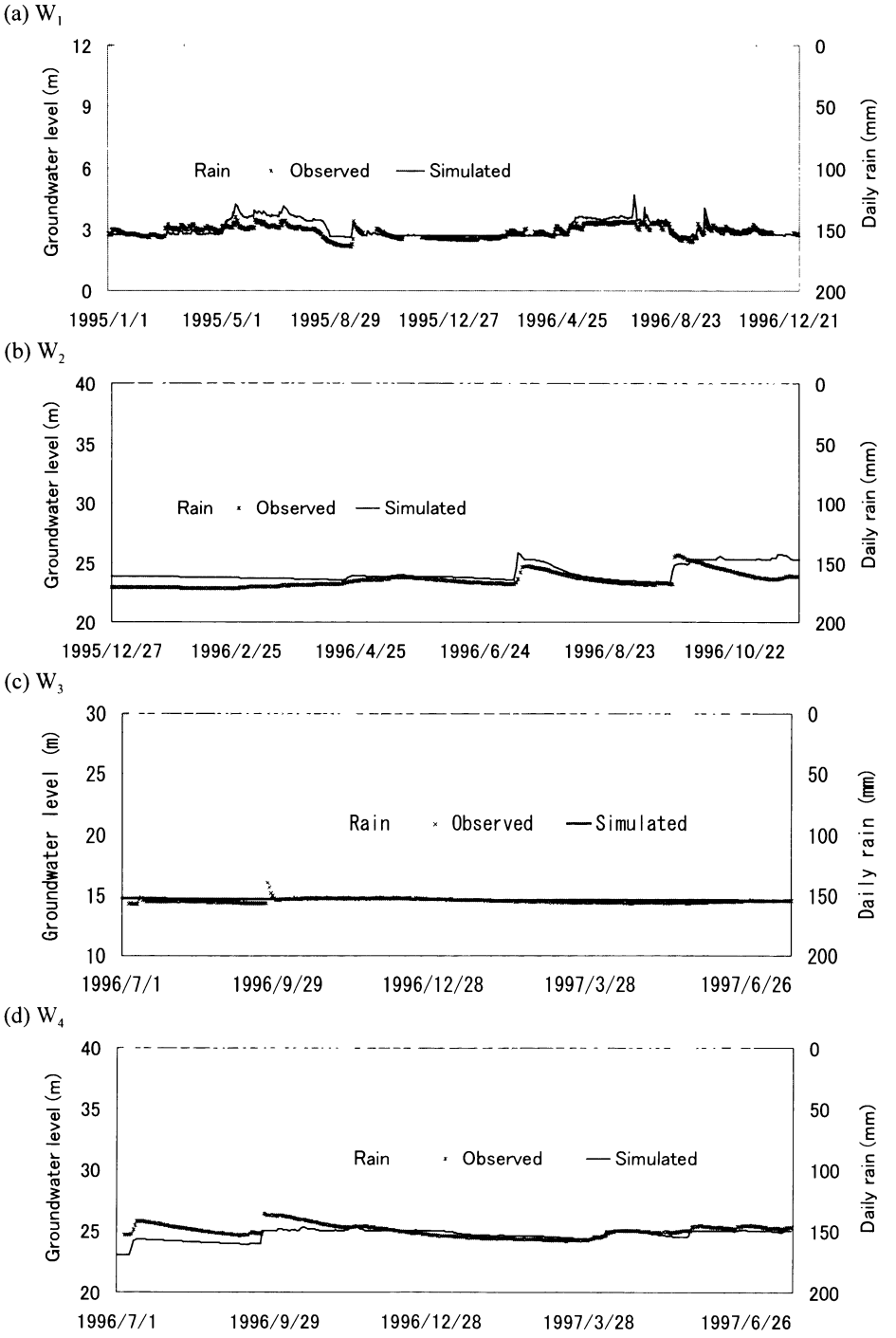

Fig.3 Groundwater levels at (a) W_1 well, (b) W_2 well, (c) W_3 well and (d) W_4 well.

Contour lines of groundwater level in the catchment are shown in Fig.4. The simulated result of the top confined aquifer is compared with the measurement at 112 private wells in winter of 1996. Though there are obvious differences between them, the distribution patterns are similar, namely the groundwater level become lower from upstream area to downstream area (refer to Fig.1 at same time). In addition to the imperfect of model itself, the differences are also related to the complicity of actual aquifers in the catchment. Though most of the wells take groundwater from the top confined aquifer, some take groundwater from unconfined aquifer.

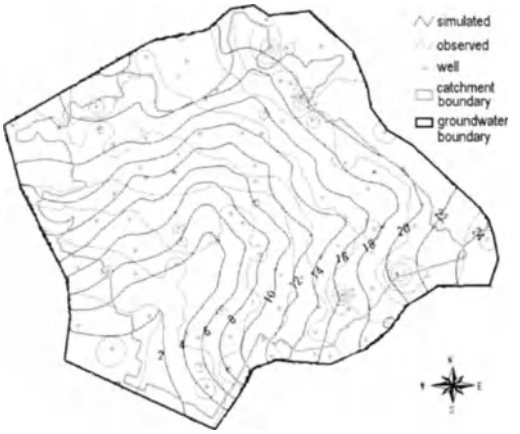

Fig.4 Contour lines of groundwater level on Jan.25, 1996 (Unit: m).

In addition, from Fig.5 it can be seen that the simulated daily discharges match well with the observed ones at the Yasakaebashi station, which is located at the middle reach of Ebi river (see Fig.1) and has a control area of 8.3 km^2. The simulated annual discharges in 1993, 1994 and 1995 are 1851mm, 1373mm and 1414mm respectively whereas the observed ones are 1617mm, 1285mm and 1404mm respectively, which means relative errors ranging from 0.7% to 12.6%.

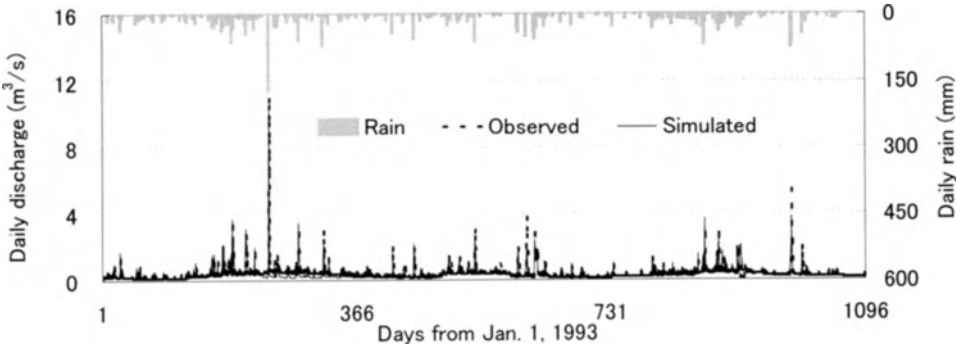

Fig.5 Daily discharges at the Yasakaebashi station of Ebi river.

The comparison of annual water balances in 1993 and 1994 is shown in Fig.6 to see the effect of weather change on groundwater and other hydrological components. 1993 is a wet year with annual precipitation of 1463mm whereas 1994 is a dry year with annual precipitation of 980mm. From the figure it can be seen that the ratios of evapotranspiration, surface runoff and infiltration to precipitation are roughly 32%, 53% and 23% in 1993 in the Ebi river catchment. Compared with natural catchments, the surface runoff shows a higher ratio where infiltration shows a lower value, which illustrates the impact of urbanization in the catchment. In addition, groundwater flow is only 1/4 of sewerage to rivers, which indicates a water quality problem during clear days. In addition, in the dry 1994 the annual recharge to groundwater decreases 167mm (46%) and the groundwater outflow decreases 25mm, which makes river base flow become less and degrade the water quality further. On the other hand, the surface runoff decreases 301mm whereas the evapotranspiration has no big change. With the further urban development and especially the construction of separate sewer system, if the treated wastewater is directly discharged to the Tokyo

bay, the river base flow will further decrease, which will bring a serious environmental problem in the catchment. Therefore, to conserve the groundwater and river environment, countermeasures such as installation of infiltration facilities, re-use of treated wastewater and construction of detention ponds etc. are highly expected.

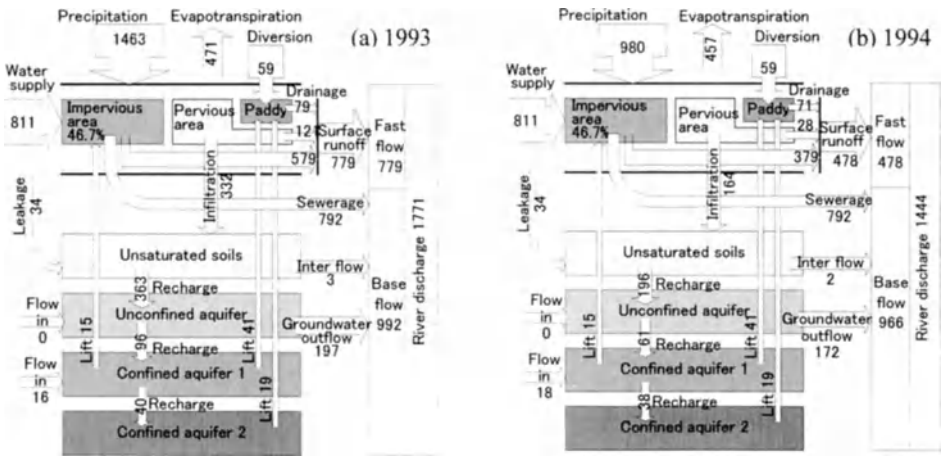

Fig.6 Comparison of annual water balances in 1993 and 1994 (Unit: mm).

CONCLUSIONS

A distributed hydrological model is applied to simulate groundwater flow and water balance in the Ebi river catchment with reasonable results obtained. The comparisons of simulated groundwater levels and river discharges with the observed values show the rationality of the model. The comparison of water balance in wet 1993 with that in dry 1994 is also conducted and it shows the effect of weather change on groundwater and other hydrological components. To conserve the groundwater and river environment the countermeasures such as implementation of infiltration facilities etc. are thought to be highly required and their effect estimation will be conducted in the study of next step.

ACKNOWLEDGMENT

The authors give their sincere thanks to Prof. K. Musiake, Tokyo University and Urban River Division, Chiba Prefecture and Association for Rainwater Storage and Infiltration Technology, Japan for providing valuable observation data in the Ebi river catchment.

REFERENCES

1. Jia Y and Tamai N (1998) Integrated analysis of water and heat balances in Tokyo metropolis with a distributed model, J. Japan Soc. Hydrol. & Water Resour. 11-2, 150-163
2. Herath S, Musiake K and Hironaka S (1992) Field estimation of saturated conductivity using borehole test, influence of unsaturated flow and soil anisotropy, Ann. J. Hydraul. Eng., JSCE, 36: 435-440
3. Jia Y and Tamai N (1997) Modeling infiltration into a multi-layered soil during an unsteady rain, Ann. J. Hydraul. Eng., JSCE, 41: 31-36
4. Zaradny H (1993) Groundwater flow in saturated and unsaturated soil, Balkema, pp.66-82

Study on Interaction between Surface and Subsurface Flows using Conjunctive Flow Model

Masaru Morita[1], Ben Chie Yen[2]

[1]Shibaura Institute of Technology, Department of Civil Engineering, 3-9-14, Shibaura,Minato-ku, Tokyo 108, Japan
[2]University of Illinois at Urbana-Champaign, Department of Civil Engineering, Urbana, IL 61801,USA

ABSTRACT. The interaction between the surface and subsurface flow components plays an important role especially in initial loss and overland flow initiation at the early stage in rainfall events. Therefore, coupling of the surface and subsurface flow submodels is necessary in more comprehensive and sophisticated watershed modeling to deal with the interaction theoretically. We already proposed the conjunctive 2-D surface and 3-D subsurface flow model using an approximate version of the Saint-Venant equations to simulate the two-dimensional unsteady surface flow and a modified version of Richard's equation for the three-dimensional unsaturated and saturated unsteady subsurface flow [1, 2]. This paper shows a further development of the conjunctive model and focuses on the interaction between surface and subsurface flow components. The interaction of the two components is directly related to the estimation of effective rainfall or initial loss of hyetographs. In the conjunctive model the interaction is formulated using the comparison of the two parameters, "rainwater supply" and "infiltrability (infiltration capacity) ". The model reproduces the initiation of overland flow and initial loss process and contributes to more precise and reliable estimation of effective rainfall than the usual methods using the empirical formulas in watershed modeling.

KEY WORDS: conjunctive model, effective rainfall, infiltration capacity

INTRODUCTION

Initial loss, infiltration, and overland flow initiation are familiar to us and can easily be observed on pervious surfaces around our residences at the early stage in rainfall events. These hydrological processes are typical examples of an interaction between surface and subsurface flows. The interaction, however, has been disregarded in watershed modeling. Instead, most of the models separate the surface and subsurface flow components, calculating the effective rainfall using the empirical formula such as Horton's infiltration equation. For more sophisticated models using nonlinear partial differential equations for surface and subsurface flows, the common boundary condition as an interface of the two flow components has not been treated theoretically in the numerical calculations and the surface and subsurface flows have been ' eternally connected' [3].

In this paper, we show a conjunctive 2-D surface and 3-D subsurface flow model. The conjunctive model couples the two flow components with a common boundary condition set on the comparison between infiltrability (infiltration capacity) and rainwater supply at each time step in the numerical calculation. After formulating the conjunctive model, we applied the model to simulate the interaction between surface and subsurface flows: initial loss, infiltration and overland flow initiation.

GOVERNING EQUATIONS AND NUMERICAL METHODS

For the conjunctive model, we apply an approximated dynamic wave equation used in the diffusion flow model [4] – appropriately named the non-inertia model - for the two-dimensional

surface flow, and a modified version of Richard's equation for the three-dimensional subsurface flow.

<Surface Flow>
The continuity equation for two-dimensional surface flow is described as

$$\frac{\partial h}{\partial t}+\frac{\partial}{\partial x}(uh)+\frac{\partial}{\partial y}(vh)+i-r=0 \tag{1}$$

where h = flow depth normal to surface; u and v = cross sectional average velocities in the x and y directions ; i = infiltration rate; r = rainfall intensity.
Momentum conservations equation can be written in the non-inertia approximation form.

$$\frac{\partial h}{\partial x}-S_{ox}+S_{fx}=0 \tag{2}$$

$$\frac{\partial h}{\partial y}-S_{oy}+S_{fy}=0 \tag{3}$$

where S_{ox} and S_{oy} = bottom slopes in the x and y directions ; S_{fx} and S_{fy} = friction slopes in the x and y directions, respectively.
The friction slopes are obtained from the Darcy-Weisbach formula.

$$(S_{fx},S_{fy})=\left(f_d\frac{u^2}{8gh}\,,\,f_d\frac{v^2}{8gh}\right) \tag{4}$$

The friction resistance coefficient f_d is calculated as a function of the Reynolds number : $\boldsymbol{R}= VR/\nu$; where V is the magnitude of flow velocity, R hydraulic radius, ν kinematic viscosity.

$$f_d=\frac{24}{\boldsymbol{R}} \qquad \text{for} \quad 0<\boldsymbol{R}<500 \tag{5}$$

$$f_d=\frac{0.223}{\boldsymbol{R}^{0.25}} \qquad \text{for} \quad 500<\boldsymbol{R}<30\,000 \tag{6}$$

$$f_d=\frac{1}{4}\left[-\log\left(\frac{k_s}{12R}+\frac{1.95}{R^{0.95}}\right)\right]^{-2} \qquad \text{for} \quad \boldsymbol{R}>30\,000 \text{ and } k_s/R<0.05 \text{ (Yen [5])} \tag{7}$$

Using surface elevation H instead of flow depth h in Equation (1) - (3), the governing equation for surface flow can be represented as follows:

$$\frac{\partial H}{\partial t}=\frac{\partial}{\partial x}K_x\frac{\partial H}{\partial x}+\frac{\partial}{\partial y}K_y\frac{\partial H}{\partial y}+r-i \tag{8}$$

where K_x and K_y are described by the equation (9) and calculated by the Reynolds number $\boldsymbol{R}$.

$$(K_x,K_y)=\left(\sqrt{\frac{8gh^3}{f_d}}\left|\frac{\partial H}{\partial x}\right|^{-\frac{1}{2}},\sqrt{\frac{8gh^3}{f_d}}\left|\frac{\partial H}{\partial y}\right|^{-\frac{1}{2}}\right) \tag{9}$$

In the non-linear equation (8), the diffusively coefficients, K_x and K_y change with flow depth and flow velocity.

<Subsurface Flow>
The equation for three-dimensional subsurface flow is represented on the basis of Richard's equation [6].

$$\frac{\partial H}{\partial t} = \frac{\partial}{\partial x}\alpha_x(\theta)\frac{\partial H}{\partial x} + \frac{\partial}{\partial y}\alpha_y(\theta)\frac{\partial H}{\partial y} + \frac{\partial}{\partial z}\alpha_z(\theta)\frac{\partial H}{\partial z} \tag{10}$$

$$\alpha_i(\theta) = K_{si} K_r / (\partial\theta/\partial P) \tag{11}$$

where H = piezometric head; K_{sx}, K_{sy}, and K_{sz} = saturated permeabilities in the x, y, and z directions; K_r = relative permeability ; P = capillary pressure head; θ = volumetric moisture content ; $\theta = n\,S$; n = soil porosity ; S = saturation degree. Piezometric head H has the relation with P : $H = P + z$. Equation (10) can be applied to both saturated groundwater flow and unsaturated soil water flow. Except for the case of initial loss, the effect of surface flow on the subsurface flow can be treated by the surface boundary condition: flow depth.

The governing equations (8) and (10) for surface and subsurface flows are written in the form of heat diffusion equation. The numerical methods for two- and three-dimensional heat diffusion equations, therefore, can be applied to solve these equations. The ADE method of Larkin [7] was selected through the investigation of the numerical methods [2].

COUPLING OF SURFACE AND SUBSURFACE FLOW COMPONENTS

For coupling the surface and subsurface flow models together, we set the common boundary condition, comparing the rainwater supply and the demand of infiltration capacity or infiltrability I_p. The procedure of the conjunctive model calculation is described as follows:

1. Calculate the infiltrability I_p using the equation (12). The infiltrability is the potential infiltration rate under the condition of given surface water depth and soil water content just below the surface.

$$I_p = 0.5\,(K_s+K_1)(Y - H_1) / \Delta z \tag{12}$$

where K_s = saturated permeability ; K_1 and H_1 = permeability and piezometric head at the first node in the z direction ; Y = water depth at the surface calculated as

$$Y = h + r\,\Delta t \tag{13}$$

where h = water depth at a previous time step; r = rainfall intensity; Δt = time increment. The water depth h should be zero until overland flow occurs.

2. Calculate the modified rainfall intensity or rainwater supply as

$$R_s = Y/\Delta t = r + h / \Delta t \tag{14}$$

3. Compare the infiltrability I_p with the rainwater supply R_s.

4. If the infiltrability I_p is larger than the rainwater supply R_s, set the boundary condition at the surface for equation (10) as follows:

$$H_0 = H_1 + 2.0\,(R_s\,\Delta z) / (K_s+K_1) \tag{15}$$

In this case, infiltration rate equals to rainwater supply.

5. If the infiltrability I_p is less than the rainwater supply R_s, set the surface boundary condition as $H_0 = Y$.

6. Calculate the piezometric head H by equation (10) under the surface boundary condition from step 4 or step 5.

7. Go back to step 1 in the case of step 4. In the case of step 5, on the other hand, go on to surface flow calculation by equation (8) with the flow depth modified by the infiltration rate, and then go back to step 1 with new flow depth h.

At each time step, we compare the infiltrability and the rainwater supply and then set the right boundary condition for subsurface flow calculation. The infiltrability changes in time with surface water depth and soil moisture content just below the surface and thus controls the interaction between surface and subsurface flows.

SIMULATION OF INTERACTION BETWEEN SURFACE AND SUBSURFACE FLOWS

The conjunctive model was tested using the laboratory experimental data by Smith and Woolhiser[8]. Fig.1 shows the comparison between the observed and calculated hydrographs under constant rainfall intensity of 9.9 inch/hr. To save space, we omit the description of the experiment. Although the difference in the time of overland flow initiation is recognized between the two hydrographs, the calculated hydrograph reproduces the experimental data satisfactorily.

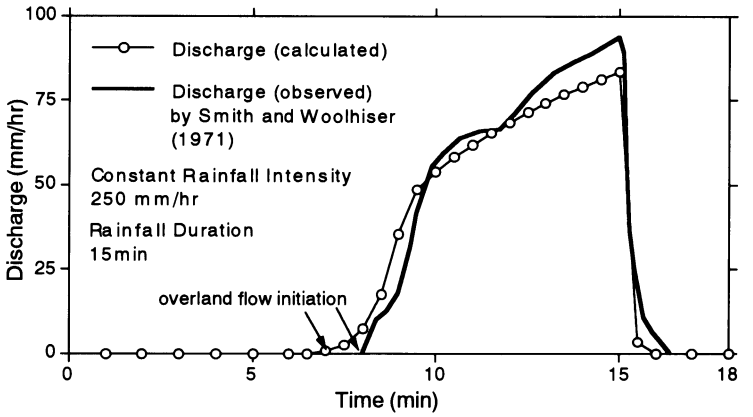

Fig.1 Comparison of Calculated Values with Experimental Data by R.E.Smith and D.A. Woolhiser

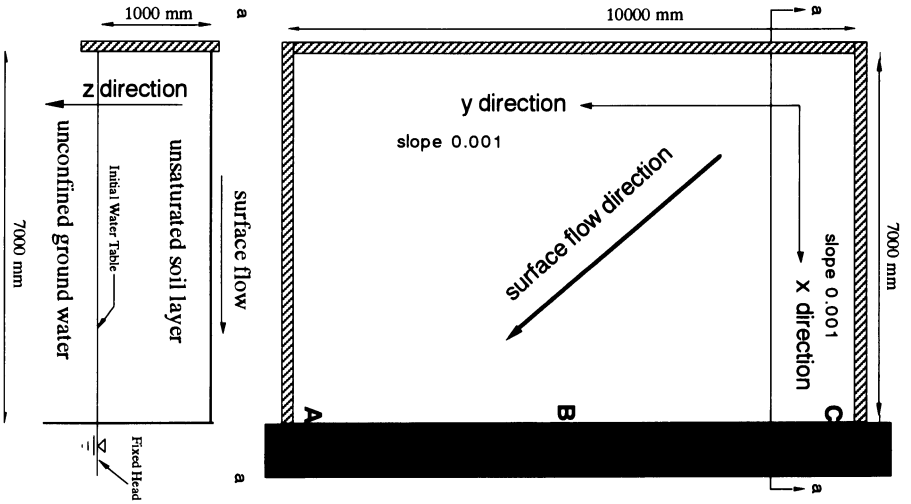

Fig.2 Surface Drainage Area for Conjunctive Model Simulation (right : top view, lower : cross sectional view)

After testing the model, we carried out simulation calculations of infiltration and overland flow. Fig.2 shows a top view of an analyzed drainage area. The surface flow area is 7.0 m by 10 m and has the slopes 0.001 in both of x and y directions. Under the top view, the cross sectional view features the soil layer and the water table of unconfined groundwater. For the application of the

model, we assumed a homogeneous, isotropic porous body of stable soil layer. The soil has, according to the linearized equation of Philip [9], idealized hydraulic properties : $\alpha = K(dP/d\theta) = K_s K_r(dP/d\theta) = 2.5\text{mm}^2/\text{s}$, $k = dK/d\theta = (K_s/n)dK_r/dS = 0.05\text{mm/sec}$. These properties mean that the soil may be classified as fine silt rather than sand. Under the linearized condition the moisture diffusivity coefficient α is set to be constant, but the relative permeability K_r change with S and P. For the numerical calculation of the surface flow equation (8), the drainage area has the space increments $\Delta x = \Delta y = 0.5$ m, and the boundary conditions; top, leftmost, and bottom boundaries in the top view of Fig.2 are closed and rightmost boundary is open to the channel. In the calculation of subsurface flow, space increments are $\Delta x = \Delta y = 0.5$ m and $\Delta z = 0.01$ m. Besides we set $S = 0.2$ ($t = 0$, $0 < z < 1$m) as initial condition and $S = 1.0$ ($t > 0$, $z = 1$m) as bottom boundary condition. The hydrographs calculated under the triangular hyetograph with a peak rainfall intensity 100 mm/hr and under the rectangular hyetograph with a constant rainfall intensity 100 mm/hr are shown in Fig.3 and Fig4, respectively. The figures describe rainfall intensity, surface flow discharge, surface infiltration rate, infiltrability, and flow depth at point A,B,and C.

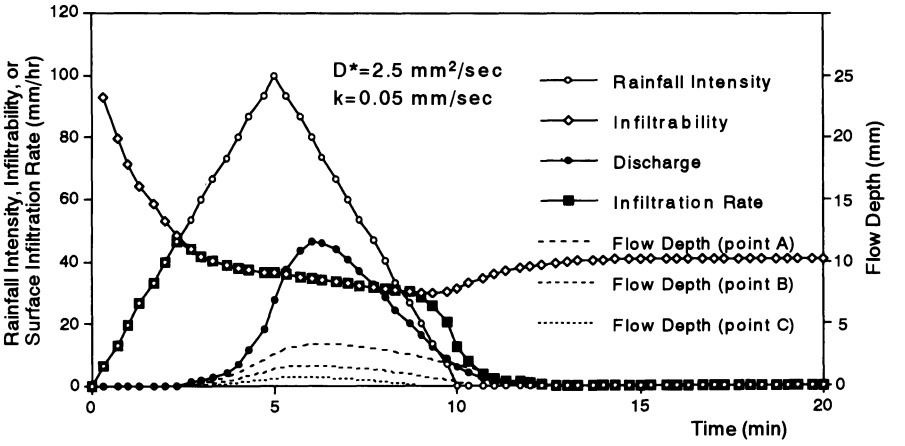

Fig.3 Calculated Hydrograph under Triangular Hyetograph

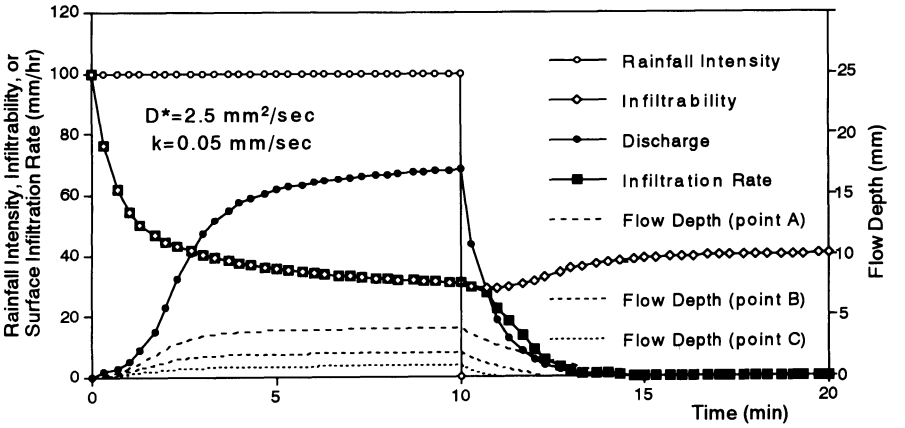

Fig.4 Calculated Hydrograph under Rectangular Hyetograph

In Fig.3 we easily recognize initial loss process in the first 2 minutes, when the infiltration rate is identical with the rainfall intensity or rainwater supply. During the initial loss process, the infiltrability is always larger than the rainwater supply. The infiltrability curve monotonously decreases in the same manner as Horton's empirical formula curve. At the time when the infiltrability curve crosses the rainfall intensity line of the hyetograph, the overland flow just initiates and has the peak discharge around 6 minutes just behind the peak rainfall intensity. Fig.3 also shows the surface flow depths at point A, B, and C. The flow depth at point A is the largest and the depths at point B and C follow in this order. The three flow depth curves indicate the initiations and terminations of overland flow are different in time at the three points. In the calculation, we found some part has overland flow and the other part has no water on the surface. The surface flow submodel thus simulated the two-dimensional overland flow.

The hydrograph calculated under the rectangular hyetograph with a constant rainfall intensity is also presented in Fig.4. The overland flow initiates simultaneously with rainfall and the infiltration rate monotonously decreases more rapidly than that in Fig.3. In the conventional approach such as Horton's equation, the same soil condition produces the same infiltration capacity. The conjunctive model, however, gives different infiltration capacities for different hyetographs as shown in Figs. 3 and 4. This is because the conjunctive model directly and theoretically deals with the interaction between surface and subsurface flows.

CONCLUDING REMARKS

We showed how to deal with the interaction between surface and subsurface flows, and introduced and defined the infiltrability I_p to compare with rainfall intensity. Using this coupling method, the 2-D surface and 3-D subsurface flow conjunctive model was formulated and the numerical calculation procedure of the model was also presented. Furthermore, we applied the conjunctive model to the drainage area after testing the model and thus simulated the 2-D surface and 3-D subsurface flows. The simulation results showed the infiltrability, the infiltration, and the overland flow and explained the mechanism of initial loss and overland flow initiation theoretically.

REFERENCES

1. Morita M, Nishikawa R, Yen BC (1996) Application of Conjunctive Model to Infiltration Trench. Proceedings of 7th International Conference on Urban Storm Drainage, Hanover : 527-532
2. Morita M, Yen BC (2000) Numerical Methods for Conjunctive 2-D Surface - 3-D Subsurface Flow Model. International Journal for Numerical Methods in Fluids, accepted.
3. Freeze RA (1972) Role of Subsurface Flow in Generating Surface Runoff: 1. Base Flow Contribution to Channel Flow. Water Resources Research 8 : 609-623
4. Akan AO, Yen BC(1981) Mathematical Model of Shallow Water Flow Over Porous Media. Journal of the Hydraulics Division ASCE 107: 479-494
5. Yen BC (1991) Hydraulic Resistance in Open Channels in Channel Resistance: Centennial of Manning's Formula ed. by B.C.Yen. Water Resources Publications, Highlands Ranch, Colorado : 15
6. Eagleson PS (1970) Dynamic Hydrology, MacGraw-Hill Book Co., Inc., New York
7. Larkin BK (1964). Some Stable Explicit Difference Approximation to the Diffusion Equation. Mathematics of Computer 18 : 196-202
8. Smith RE, Woolhiser DA (1971) Overland Flow on an Infiltrating Surface. Water Resources Research 7: 899 - 913
9. Philip JR (1969) Theory of Infiltration, in Advances in Hydroscience 5, V.T.Chow,ed., Academic Press, New York : 216-295

Diurnal fluctuations of soil temperature, vapor pressure and evaporation in bare soils

Yasuhide Takano[1], Teruyuki Fukuhara[2] and Kuniaki Sato[3]

[1]Program for Doctor's Degree, Graduate School of Engineering, Fukui University, 3-9-1 Bunkyo, Fukui 910-8507, Japan
[2]Department of Architecture and Civil Engineering, Faulty of Engineering, Fukui University, 3-9-1 Bunkyo, Fukui 910-8507, Japan
[3]Hydroscience and Geotechnology Laboratory, Faculty of Engineering, Saitama University, 255 Shimo-ohkubo, Urawa, Saitama 388-8570, Japan

ABSTRACT. In order to better understand post-irrigation drying phenomena, micro-meteorological observations and heat and moisture transfer measurements in soil under bare surface conditions were carried out in the United Arab Emirates (U.A.E). Soil temperature, relative humidity in soil pores and volumetric water content were measured by thermo-hygrometers and thermal conductivity probes.
This paper describes a mathematical model to analyze heat and moisture movement in the near-surface soil layers resulting from the evaporation that occurs during the post-irrigation drying phase. The validity of the proposed model was shown by comparing numerical with experimental results concerning diurnal variations of temperature, moisture content and vapor pressure profiles.
It is concluded that the proposed simulation model is a valid tool that can be used to estimate the evaporation flux in unsaturated soils.

KEY WORDS. evaporation, heat and moisture transfer, internal evaporation, coupled numerical computation

INTRODUCTION

Arid regions, which cover one third of the total land on earth, are potentially attractive places for plant production because they are rich in solar energy needed to facilitate photosynthesis. Revegetation in arid regions could become an important key to solving global environmental problems such as the food crisis and global warming. The sustainability of agriculture in arid regions depends critically on economizing irrigation water, i.e. on the optimal usage and management of groundwater. In order to better understand post-irrigation drying phenomena, micro-meteorological observations and heat and moisture transfer measurements in soil under bare surface conditions were made continuously in the United Arab Emirates starting in 1996. A Soil Thermo-Hygrometer Method (STHM) was used in the field for the first time at this site. Fukuhara et. al. [1] applied the STHM to laboratory drying experiments using soil columns, and the vertical profile of vapor pressure was obtained. Consequently it was shown that the vapor density reaches a maximum at the interface between the dry surface layer and the capillary layer beneath it and that the evaporation rate could be calculated with acceptable accuracy assuming a linear vapor density profile in the dry layer.

Knowledge of moisture content and temperature is important for the analysis of drying-evaporation phenomena. A comprehensive theory of heat and moisture movement in porous media was proposed by Philip and de Vries [2]. In their now classical model, moisture movement is considered to be a composite of vapor and liquid flows in which the liquid flow compensates for the change of mass between liquid and vapor resulting from internal evaporation. In this way the internal evaporation does not appear in the moisture conservation equation and this makes computation more convenient. Takano et. al. [3] developed a mathematical model to analyze heat, liquid water and water vapor movement in a soil column associated with evaporation from soil pores at the interface between the dry and capillary layers. In this model, the internal evaporation rate is taken to be proportional to the product of a) the vapor pressure difference between the soil pores and the surface of the water films surrounding the soil particles and b) the liquid-vapor interfacial area. As a consequence, the energy equation and the mass balance equations for liquid and water vapor can be solved simultaneously.

This paper describes the diurnal variations of heat and moisture movement in the near-surface soil layers resulting from the evaporation that occurs after watering the soil surface and discusses the validity of the proposed model by comparing numerical results with experimental measurements of temperature, moisture content and vapor pressure distributions.

THEORETICAL CONSIDERATIONS

In the proposed model the internal evaporation is expressed as a function of vapor pressure, P_v, and volumetric water content, θ_l, so that temperature, T, P_v and θ_l can be calculated simultaneously without using Kelvin's relation.

Theory of liquid water transfer. The equation of conservation of mass for liquid water, including the sink term associated with internal evaporation, is given by

$$\frac{\partial(\rho_l \theta_l)}{\partial t} = -\frac{\partial m_l}{\partial z} - E_v \tag{1}$$

where, t = time (s); ρ_l = density of liquid water (kg/m^3); m_l = mass flux density of liquid water (kg/m^{2}s); E_v = internal evaporation rate per unit volume (kg/sm^3) and z = vertical coordinate (m). Note that ρ_l is a function of T only. E_v is a function of both θ_l and P_v.

Expanding Eq.(1) using to Darcy's law, yields

$$\rho_l\left(\frac{\partial \theta_l}{\partial \psi}\right)\frac{\partial \psi}{\partial t} + \theta_l \frac{\partial \rho_l}{\partial t} = \frac{\partial}{\partial z}\left[\frac{\rho_l K K_{rl} g}{\nu}\left(\frac{\partial \psi}{\partial z} + 1\right)\right] - E_v \tag{2}$$

where, K = saturated hydraulic conductivity (m/s); K_{rl} = relative hydraulic conductivity; g = acceleration due to gravity (= 9.8 m/s^2); ν = dynamic viscosity of liquid water (m^2/s) and ψ = matric potential (m). Note that K_{rl} is a function of θ_l, and ν is a function of T, while ψ is a function of both θ_l and T.

Theory of water vapor transfer. As is done for water vapor transfer in the Philip and de Vries model, the time rate of θ_v, can be expressed as the sum of terms involving the second derivatives of T and θ_l with respect to z. However, since P_v is much easier to measure than θ_v, P_v is selected as the dependent variable to be solved for instead of θ_v.

Combining the equation of state with the Fickian diffusion equation, the mass flux density of water vapor in the soil, m_v is written as follows

$$m_v = -D_{atm}\,\xi\,\eta(\varepsilon - \theta_l)\frac{\partial\left(P_v / R_v \tilde{T}\right)}{\partial z} \tag{3}$$

where, m_v = mass flux density of water vapor in the soil (kg/m^{2}s); ε = porosity; D_{atm} = diffusivity of water vapor in atmosphere (m^2/s); ξ = correction coefficient for liquid-vapor interfacial area (net interfacial area / apparent area); η = tortosity (= 0.67); R_v = gas constant of water vapor (= 461.52 J/kgK) and $\tilde{T}$ = absolute temperature (= T+ 273.15K). The value of ξ for Toyoura standard soil ranges between 2 and 3, according to our experiments [4] and turns out to be of the order of $(dT/dz)_a/dT/dz$ (the suffix a refers to air in soil pores) defined by Philip and de Vries [2]. In the present paper ξ = 2.0 is used. Note that D_{atm} is also a function of $\tilde{T}$. Further information on this dependence is given, for example, in reference [3].

The internal evaporation acts as a source term in the equation of conservation of mass of water vapor and the basic equation becomes

$$\frac{\partial\left[P_v(\varepsilon - \theta_l)/R_v\tilde{T}\right]}{\partial t} = \frac{\partial}{\partial z}\left[D_{atm}\,\xi\,\eta(\varepsilon - \theta_l)\frac{\partial\left(P_v / R_v \tilde{T}\right)}{\partial z}\right] + E_v \tag{4}$$

Theory of heat transfer. In principle, the heat flux density, q_h, includes contributions from both heat

conduction and sensible heat. Sensible heat associated with vapor movement is, however, small and can be ignored. Thus q_h, simplifies to

$$q_h = -\lambda \frac{\partial T}{\partial z} + (\rho_l c_l) V_l (T - T_0) \quad (5)$$

where, q_h = heat flux density (W/m^2); λ = thermal conductivity (W/mK); c_l = specific heat of liquid water (J/kgK); V_l = velocity of liquid water (m/s) and T_0 = arbitrary reference temperature (℃).

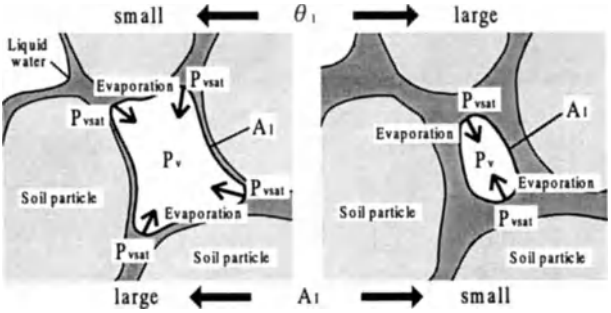

Fig. 1 Concept of internal evaporation

λ basically depends on T and θ_l. The effect of T on λ is, however, negligibly small for the usual range of diurnal temperature variation but λ increases significantly with θ_l in the range of $\theta_c \leqq \theta_l \leqq \varepsilon$. θ_c is the lower limit of θ_l below which there is no movement of liquid water.

Taking into account the latent heat associated with internal evaporation, LE_v, the equation of conservation of thermal energy becomes

$$\frac{\partial [(\rho c) T]}{\partial t} = \frac{\partial}{\partial z}\left[\lambda \frac{\partial T}{\partial z} - (\rho_l c_l) V_l (T - T_0)\right] - LE_v \quad (6)$$

where, (ρc) = volumetric heat capacity of wet soil (J/m^{3}K) and L = latent heat of vaporization (J/kg).

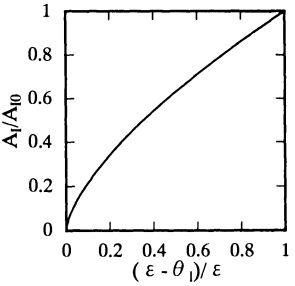

Fig. 2 Relationship between A_l and $(\varepsilon - \theta_l)$

Mechanism of internal evaporation. Internal evaporation may take place at the surface of the water films surrounding the soil particles, i.e. at the liquid-vapor interfaces, and this is essentially the same mechanism as for surface evaporation from the boundary between a soil surface and the atmosphere.

According to **Fig. 1**, it can be surmised that the evaporation rate should be proportional to the driving force for vapor movement, i.e. to the difference between the vapor pressure in the soil pore space, P_v, and that at the surface of the water films surrounding the soil particles, P_{vsat}, and, in addition, it will be proportional to the liquid-vapor interfacial area, A_l. P_{vsat} is the saturated vapor pressure, which is only dependent on T.

Thus the internal evaporation rate per unit volume, E_v,may be written as follows:

$$E_v = \gamma A_l (P_{vsat} - P_v) \quad (\theta_l \geqq \theta_c) \quad (7)$$

where γ = constant of proportionality with units (s/m^4) and θ_c is assumed to be a critical volumetric water content corresponding to the condition where the vapor pressure at the surface of the soil particles begins to decrease below the saturation value. Futagami et. al [5] determined θ_c experimentally using a thin soil layer and found that the relative humidity of the soil surface decreases suddenly when θ_l becomes smaller than a clearly defined value, θ_c. Based on their result $\theta_c = 0.04$ is used in this paper.

Fig. 2 shows the relationship between A_l and $(\varepsilon - \theta_l)$ calculated by Slichter's theory [6], but A_l and $(\varepsilon - \theta_l)$ are normalized by the surface area of spherical soil particles A_{l0} and ε, respectively. The curve can be approximated by a power law formula $A_l \propto (\varepsilon - \theta_l)^m$, and for the range of θ_l appropriate to this paper, a value $m = 1$ is adequate. Finally, E_v can be expressed as follows:

$$E_v = (\varepsilon - \theta_l) K_G (P_{vsat} - P_v) \quad (\theta_l \geqq \theta_c) \quad (8)$$

where K_G = coefficient of internal evaporation (s/m^2). Note that $E_v < 0$ means internal condensation. From

our previous experiment using Toyoura standard soil [3], K_G was found to be 1×10^{-5} s/m^2. The value used here is proposed tentatively and it would be desirable to undertake more detailed studies of K_G and θ_c using other kinds of soils.

Boundary conditions. The soil surface control volume is a layer of thickness Δz_s and the surface temperature can be calculated from the surface heat conservation equation,

$$(\rho c)_s \frac{\partial T_s}{\partial t}\Delta z_s = R_n - H - LE_s + G_s \tag{9}$$

where, R_n = net radiation (W/m^2); H = sensible heat transferred by air flow (W/m^2); LE_s = latent heat transferred by evaporation from the soil surface, and G_s = ground heat flux density conducted across the bottom of the surface layer (W/m^2). The suffix s refers to the surface layer.

The evaporation flux density from the soil surface, m_{vs}, can be calculated by the $\alpha-\beta$ method. The wetness functions α and β are dependent on θ_l. Further information on these relationships is given in reference [5].

The coupled equations for liquid water, water vapor and heat transfer, Eqs. (2), (4) and (6) are simultaneously solved by the Integrated Finite Difference Method. The model was used to simulate diurnal variations of ψ, P_v and T using input data measured at our U.A.E. field site.

MEASUREMENT TECHNIQUES

The experiment was begun at a test site (area: 600 m^2) of the Hamuraniyah Agriculture Experimental station in March, 1996. In the Hamuraniyah area there are two principal types of soils: sandy soil, and sandy loam. At the test site, a 1.2 m uniform sandy soil fill was placed over the native soil. The native soil consists of sandy loam, probably interspersed with sandy layers, and with the groundwater table located between 90 ~ 150 m below the surface. The measurements discussed in this paper only involve the sandy fill layer.

The meteorological observation system is comprised of global radiation, long-wave radiation, and albedo meters, anemometers, thermo-hygrometers and heat-probe type soil moisture sensors. Both global radiation and long-wave radiation meters were placed at a height of 1.5 m above the ground surface, while one anemometer was set at a height of 0.3 m and the other at 1.5 m. Air temperature and relative humidity profiles were measured with thermo-hygrometers, placed at heights of 0.02, 0.05, 0.1, 0.2, 0.4, 0.6, 0.8 and 1.0 m above the ground surface. Soil pore vapor densities were obtained using thermo-hygrometers embedded at depths of 0.02, 0.05, 0.1, 0.2, 0.4, 0.6, 0.8 and 1.0 m below the surface. Liquid soil moisture content profiles were measured using heat probe type soil moisture sensors, inserted at depths of 0.02, 0.05, 0.1, 0.15, 0.2, 0.3, 0.4 and 0.6 m. The albedo meter was placed at a height of 0.5 m above the ground

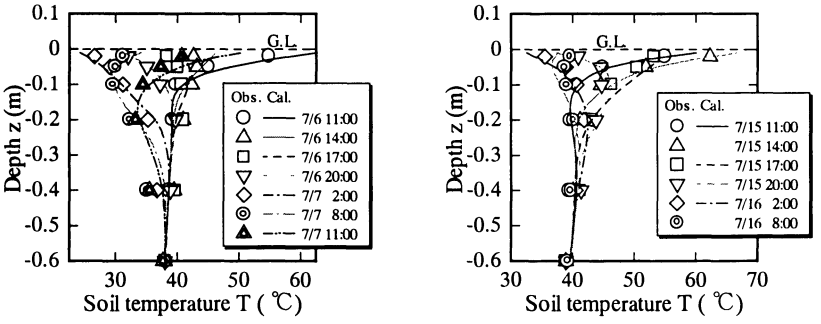

(a) 7/6 11:00~7/7 11:00 **(b)** 7/15 11:00~7/16 8:00

Fig. 3 Time variations of soil temperature profile

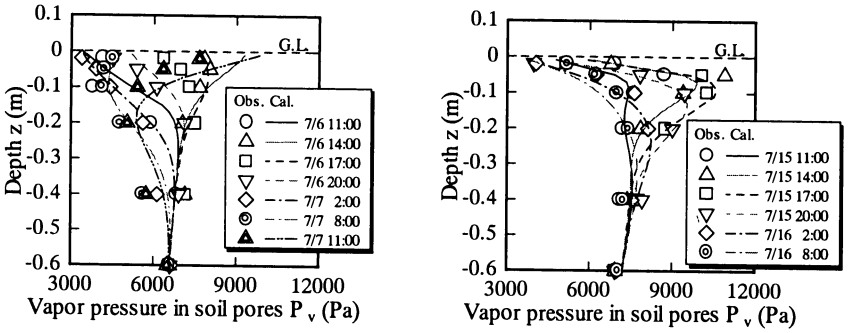

(a) 7/6 11:00～7/7 11:00 (b) 7/15 11:00～7/16 8:00

Fig. 4 Time variations of vapor pressure in soil pores profile

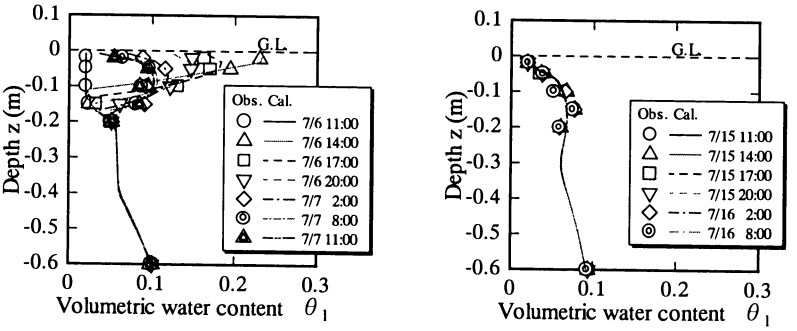

(a) 7/6 11:00～7/7 11:00 (b) 7/15 11:00～7/16 8:00

Fig. 5 Time variations of volumetric water content profile

surface. Because of unreliable line voltage conditions, battery operated data logging equipment was used. All data were sampled and stored at 30-minute intervals. The data were downloaded to a portable computer during regular, monthly site visits. For further details on the measurement techniques, the reader should see reference [7].

The irrigation water was sprinkled at a rate of 1.4 ℓ/m^2min. from 11:00 July 6. The water temperature was 37℃ and duration of irrigation was 4 minutes.

COMPUTATIONAL RESULTS AND DISCUSSIONS

Figs. 3(a) and **(b)** show the comparison of observed and calculated diurnal variations of soil temperature for the periods July 6 to July 7 and July 15 to July 16, respectively. **Fig. 3(a)** shows the thermal behavior for the first 24 hours starting immediately after watering. **Fig. 3(b)** shows the corresponding diurnal temperature variations 9 days later. Immediately after watering, a rapid decrease of soil temperature is observed near the soil surface as a result of sensible heat transfer to the cooler irrigation water and because of the latent heat loss associated with evaporation. The thermal behavior for the first one day after watering was well reproduced by the computations. As regards the diurnal variation 9 days later, the temperature profiles computed at several different times throughout the day agreed closely with the measured ones, as shown in **Fig. 3(b)**. Since the soil surface was dry at this time (see **Fig. 5(b)**), the daytime soil surface temperature was higher than in **Fig. 3(a)**.

Figs. 4(a) and **(b)** show the vertical profile of vapor pressure at the same times as those in **Fig. 3**. The depth of maximum vapor pressure, P_{vmax}, moves downward from the soil surface as time elapses, and this suggests a shift from soil surface evaporation to internal evaporation. This vapor pressure behavior is also

reproduced by the present model.

Figs. 5(a) and **(b)** represent the calculated and measured change with time of vertical profiles of volumetric water content, θ_l, for the same time periods as above **Fig. 3**. It can be seen that the liquid water propagates downward with the passage of time and that θ_l at the soil surface gradually decreases as a consequence of the surface evaporation. The thickness of the surface dry layer became 4 cm 9 days later. The present model was able to correctly reproduce the growth of the surface dry layer and the computed result (solid lines) agrees well with the observations. This implies that reliable estimates of evaporation flux may be computed using such a model.

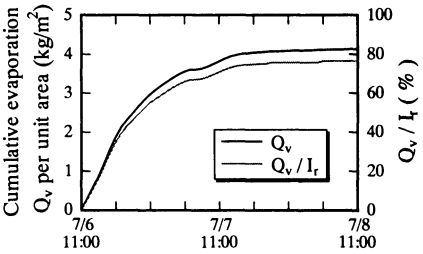

Fig. 6 Time variations of Q_v and Q_v/I_r (7/6 11:00~7/811:00)

Finally, **Fig. 6** shows the time variation of the cumulative evaporation, Q_v, per unit area after watering. The ratio of Q_v to the irrigation discharge, I_r, per unit area, i.e. Q_v/I_r is also plotted in the same figure. An initial constant-rate stage lasts for 8 hours and then, as the soil surface becomes drier, the evaporation flux density falls substantially below the potential evaporation flux density. The total loss of irrigation water resulting from evaporation may reach as much as 60% within 15 hours after watering.

CONCLUSIONS

In order to better understand post-irrigation drying phenomena, micro-meteorological observations and heat and moisture transfer measurements in soil under bare surface conditions were carried out in the United Arab Emirates. Time variations of soil temperature, relative humidity in soil pores and volumetric water content were measured at different depths in the ground. A mathematical model was proposed to analyze heat, liquid water and water vapor movement in soil associated with evaporation and was used to simulate diurnal variations of ψ, P_v and T after watering using data from the U.A.E. field site.

The simulated diurnal variations of vertical profiles of soil temperature, vapor pressure in soil pores and volumetric water content agreed well with observations. It is concluded that the proposed simulation model is adequate to estimate the evaporation flux during the post-irrigation phase and, additionally, that the present experimental techniques are a valid contribution to improving the comprehension of drying processes of near surface soil layers in arid regions.

REFERENCES

1. Fukuhara, T., Sato, K. and Baba, T. (1994) : Movement of water vapor in sand column and mechanism of evaporation, Journal of Hydroscience and Hydraulic Engineering, Vol.12, No.1, pp.47-55.
2. Philip, J. R. and deVries, D. A. (1957) : Moisture movement in porous materials under temperature gradients, Trans. Amer. Geophys. Union, Vol.38, pp.222 - 232.
3. Takano, Y., Fukuhara, T. and Sato, K. (1999) : Simultaneously coupled analysis of heat, liquid water and water vapor movement in dry-unsaturated soil layer, Journal of Hydraulic, Coastal and Environmental Engineering, JSCE, No.635/II-49 (in Japanese, now printing).
4. Fukuhara, T., Sato, K. and Imai, T. (1994) : Interaction between evaporation, movement of water vapor and heat transfer in sand layer under constant meteorological conditions, Journal of Hydraulic, Coastal and Environmental Engineering, JSCE, No.503/II-29 pp.29-38 (in Japanese).
5. Futagami, S., Takano, Y., Fukuhara, T. and Sato, K. (1997) : Heat and moisture transfer between sand surface and atmosphere by surface layer model -Consideration of thickness of sand layer by $\alpha-\beta$ method-, Annual Journal of Hydraulic Engineering, JSCE, Vol.41, pp.37-42 (in Japanese).
6. Slichter, C. S. (1899) : Theoretical investigation of the motion of ground waters, The 19th Ann. Rep. U.S. Geophys. Survey., pp.304-319.
7. Takano, Y., Fukuhara, T. and Sato, K. (1999) : Considerations of seasonal micro-meteorological characteristic in the United Arab Emirates and evaporation-drying after watering the soil by the "soil thermo-hygrometer" method, Journal of Japan Society of Hydrology and Water Resources, Vol.12, No.4,1999.

Modeling Groundwater Flow in an Unconfined Aquifer in an Alluvial Fan

Ali M. Elhassan[1], Akira Goto[2] and Masakazu Mizutani[2]

[1]United Graduate School of Agricultural Sciences, Tokyo University of Agriculture and Technology, Mine machi 350, Utsunomiya City, Tochigi 321-8505, Japan
[2]Department of Environmental Engineering, Faculty of Agriculture, Utsunomiya University, Mine machi 350, Utsunomiya City, Tochigi 321-8505, Japan

ABSTRACT. In alluvial fans, paddy field irrigation plays an important role in the hydrologic system both as a source of recharge to the shallow aquifer and as a cause of discharge by pumping. This fact has emphasized the need for reliable estimates of groundwater recharge and discharge in modeling regional groundwater flow in alluvial fans. In this study a modified tank model, which estimates groundwater recharge and withdrawal by pumping is combined with a transient, two-dimensional groundwater flow model in an unconfined aquifer. The modified tank model calculates percolation to the shallow aquifer from paddy fields and non-paddy fields separately. The modified tank model also calculates the amount of groundwater pumped for paddy fields irrigation. Distributed groundwater recharge and groundwater withdrawals are calculated at each node in the groundwater flow model grid based on paddy field area around the node. The model was applied to Nasunogahara alluvial fan, Tochigi Prefecture, Japan. Water table elevations are calculated for two years, 1991-1992, on a daily basis. Results of the model application indicate that the model is able to describe the actual behavior of the aquifer. The calculated water table elevations showed a fairly good agreement with the observed ones at four observation wells. These results confirm the usefulness of combining tank model calculation with the groundwater flow model.

KEY WORDS. Groundwater flow model, Unconfined aquifer, Alluvial fan, Modified tank model, Paddy field irrigation.

INTRODUCTION

Groundwater recharge and discharge are the major components of the water budget in aquifers, therefore adequate estimates of recharge and discharge, based upon hydrological processes, are crucial in groundwater modeling and its applications. In previous studies concerning modeling regional groundwater flow, groundwater recharge and discharge were simulated as separate

processes without considering their hydrologic interaction. Groundwater recharge was usually estimated by empirical methods, supported by site-specific investigations. Empirical methods have limited applications where there is soil and land use heterogeneity as well as large spatial and temporal variability in irrigation deliveries [1]. Additionally, due to the absence of wells extraction records, it is difficult to estimate the amount of water pumped from the aquifer.

The purpose of this study is to establish a regional, transient groundwater flow model in an unconfined aquifer in an alluvial fan and to improve the estimation of groundwater recharge and extraction for irrigation by combining a conceptual rainfall-runoff model, tank model, with the groundwater flow model.

MODEL DEVELOPMENT

Groundwater flow model. The current model is developed assuming that the aquifer is single-layered, isotropic and heterogeneous and the flow is two-dimensional. The partial differential equation that governs the flow in the aquifer is Boussinesq equation for two-dimensional, transient flow in an unconfined aquifer [2]:

$$\frac{\partial}{\partial x}\left(k\frac{\partial h^2}{\partial x}\right)+\frac{\partial}{\partial y}\left(k\frac{\partial h^2}{\partial y}\right)=S_y\frac{\partial h}{\partial t}-R \qquad \text{..... (1)}$$

where h is the pressure head, k is the hydraulic conductivity, x and y are the spatial coordinates, S_y is the specific yield of the aquifer, t is time and R is the source-sink term. Equation (1) is solved using an implicit finite difference scheme (Crank-Nicolson) and Gauss-Seidel iteration technique.

Tank model application. Goto and Sawata developed a modified tank model [3], whose upper tanks consist of a paddy field tank and non-paddy field tanks, (Fig.1), for assessing the water balance in an alluvial fan. The model was applied successfully to calculate run-off discharges to rivers in Nasunogahara alluvial fan, Japan. In this study, the modified tank model calculates the percolation rate from the upper tanks to the shallow groundwater tank for both paddy fields and non-paddy fields respectively, (Fig.1). To calculate the recharge flux at each node in the finite difference grid, paddy field area around each node is estimated and used to overcome the lumped nature of the tank calculation. Then the recharge is calculated using the following equation,

$$\mathrm{Rch} = \mathrm{pp} \times \mathrm{percoP} + (1 - \mathrm{pp}) \times \mathrm{percoNP} \qquad \text{..... (2)}$$

where *Rch* is the recharge per unit aquifer area, *pp* is the paddy field area around each node in the FDM grid, *percoP* is the percolation per unit paddy field area, and *percoNP* is the percolation per unit non paddy field area. The modified tank model is also used to calculate the amount of groundwater withdrawals. To calculate the amount of water pumped, a certain ponding depth is assumed to exist in the paddy fields during the irrigation period. Pumping starts when the water

level in the paddy field tank is less than the assumed level. The water pumped at specific node in the FDM grid is calculated using the paddy field area (*pp*) around the node as in the following equation:

$$W = P \times pp \qquad \text{..... (3)}$$

where W is the amount of water pumped per unit aquifer area and P is the amount of water pumped per unit area of paddy field area.

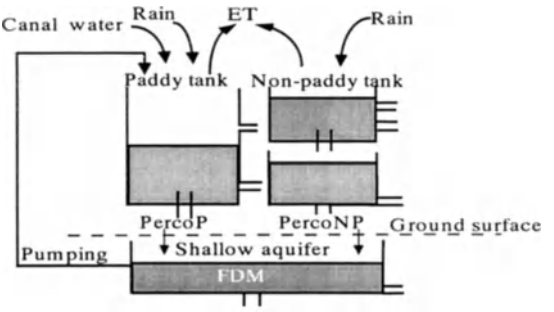

Fig. 1. Combination of the modified tank model calculation with the groundwater flow model

Calculation of the source-sink term (R) in the groundwater flow model. The source-sink term (R) in the groundwater flow equation, Eq. (1), is calculated per unit aquifer area using the following formula:

$$R = Rch - W - Q_S \qquad \text{..... (4)}$$

The term Q_S represents the groundwater discharge by natural springs, which is of great importance in the hydrologic scheme of alluvial fans and it can be calculated using the following equation:

$$Qs = CD(H_{WT} - H_{SR}) \qquad \text{if } H_{WT} \geq H_{SR} \qquad \text{..... (5)}$$

where H_{WT} is the groundwater table elevation, H_{SR} is the lowest ground surface elevation around nodes and CD is a conductance factor which is determined during the calibration of the model.

STUDY AREA

The present study took Nasunogahara alluvial fan, Tochigi prefecture, Japan, as the study area (Fig. 2). The fan has a total area of about 40,000 ha, 37% of the total area are paddy field areas. The area is bounded by two river systems, Hoki River to the west and Naka River to the east.

Between these two rivers, Sabi River had developed the fan. In the upper area of its stream, Sabi River usually has no water on its riverbed. When runoff water from the mountains (in the northern-western part of the fan) flows to Sabi River, water disappears from the riverbed surface to subsurface because of the high permeability of its coarse gravel formation. River water can be seen in the upper part of the river only after floods. Part of Sabi River's water that flows under the ground appears again to the riverbed surface in the lower part and the rest recharges the groundwater along the river. In this model nodes of Sabi River through which water flows under the ground are treated as natural replenishment sources. The mean annual rainfall of the area is about 1500 mm. About 80% of the rain precipitates in summer and autumn, from June to October. Nasunogahara canals irrigation system, Fig 2, has an important role in the hydrologic scheme of the fan. It supplies stable amount of water for irrigating the paddy fields in the upper area of the fan. The water infiltrating from these paddy fields is an important source of groundwater recharge. In the lower area of the fan, water pumped from the unconfined aquifer is the major source for irrigation.

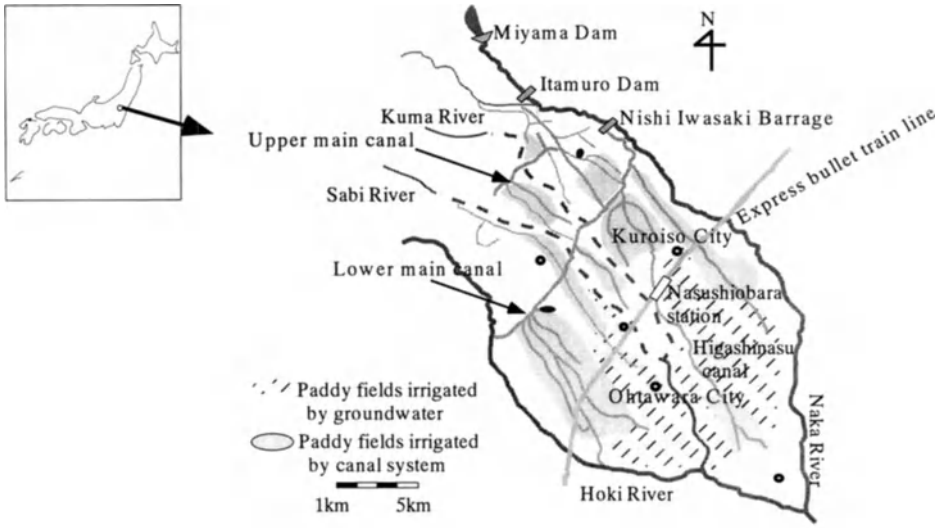

Fig. 2. Outline of Nasunogahara alluvial fan, Tochigi Prefecture, Japan, and its irrigation system

MODEL APPLICATION

A grid consisting of 396 cells is covering the area divided with a regular nodal spacing of 1-km. Prescribed head boundaries were assigned along Hoki River and the lower part of Naka River. The boundaries between the mountainous area and the fan at the northern-western part and the upper part of Naka River were treated as a no flow boundaries because of the presence of a confining layer, Kuroiso volcanic brecca. The simulation was done for a period of two years,

1991-1992, using a one-day time step. The sources and values of the hydrological data used for the model application are summarized in Table 1.

Table 1. Summary of hydrological data used for the model application

Parameter	Source of data	Value
Hydraulic conductivity (m/d)	Fujinawa model [4]	100, 84.5, 58- upper, central and lower*
Specific yield	Kanto Agricultural Bureau investigation report	0.05- 0.1
Fixed head boundary	Hydrogeological maps	1.5 m- 3 m
Elevation of impervious layer	Hydrogeological maps	400m (upper*)- 120 (lower*)
Tank model parameters & inputs	Goto and Sawata model [3]	-
Paddy field %	Topographical maps	-
Initial head configuration	Steady-state flow model	-

* Upper: upper part of the fan, Central: central part of the fan and Lower: lower part of the fan.

RESULTS AND DISSCUSION

The model calculates the variation of groundwater table elevation with time throughout the fan area. Comparisons of calculated groundwater table elevations with observed ones at four observation wells are shown in Fig. 3. Generally the results of the comparison shows a fairly good agreement between the calculated and the observed values, although the model is not fully calibrated, i.e. the model was only calibrated using different values of the conductance term CD. It appears that the model has the ability to describe the seasonal variation of the water table elevation of the aquifer satisfactorily. It is noticed that the water table level increases during the irrigation season, which lasts from April to August, and comes down during the non-irrigation period, Fig. 3. The ability of the model to describe the actual behavior of the aquifer is thought to be mainly due to the comprehensive assessment of the different sources of groundwater recharge such as irrigation water, river water and rainfall. Although the model results are able to describe the seasonal groundwater table changes, differences between the observed and calculated water table elevations are recognized. The causes of these differences are guessed to be:

1. Simulation of the prescribed head boundaries as a temporally fixed head boundaries; and
2. Errors in the estimation of some model parameters.

CONCLUSION

A regional, transient groundwater flow model in an unconfined aquifer in an alluvial fan was established. A modified tank calculation was combined with the groundwater flow model to

assess groundwater recharge and groundwater withdrawal for irrigation. The paddy field area around each node in the flow model grid is estimated and used to overcome the lumped nature of the tank calculation. The model was applied to Nasunogahara alluvial fan, Japan. Calculation of water table elevations for two years was obtained as model outputs. Comparisons between the model calculated groundwater elevations and the observed ones showed a fairly good agreement, which indicates that the model is able to describe the actual behavior of the aquifer sufficiently. Based on the results, the following conclusions can be reached:

1. The usefulness of combining tank calculation with the groundwater flow model to assess the source-sink term was confirmed; and
2. The basic structure of a groundwater flow model that considers surface water-groundwater interaction was established.

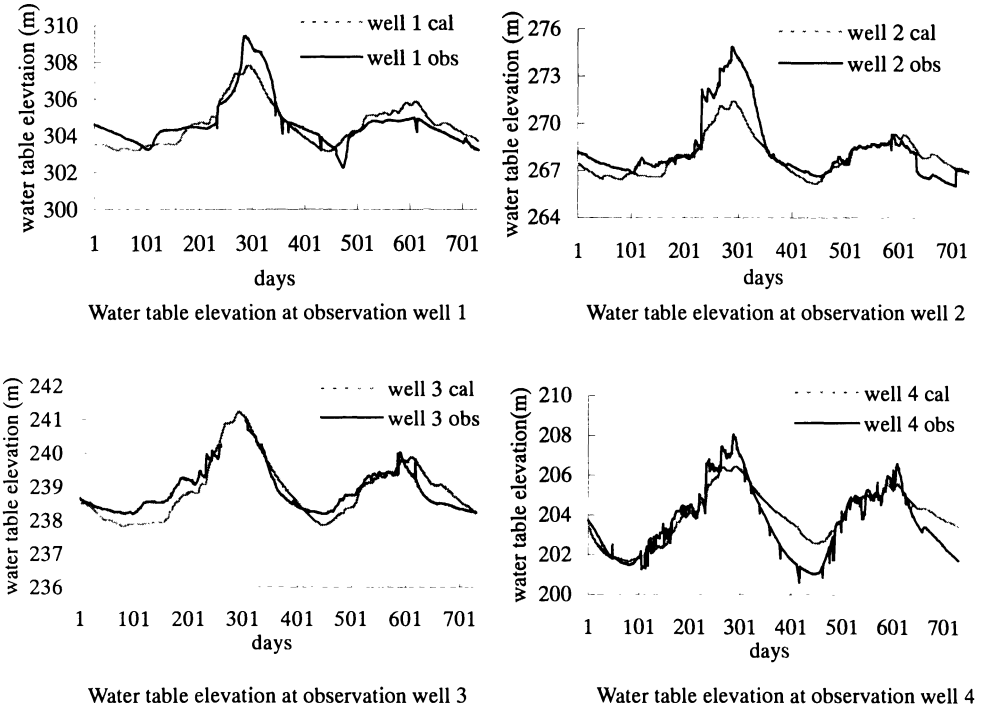

Fig. 3. Comparisons of calculated and observed water table elevations at 4 observation wells, 1991-1992

REFERENCES

1. Chiew F, Mcmahon T (1990) J Hydrology 114: 285-304
2. Anderson M, Woessner W (1991) Applied groundwater modeling. Academic press, pp 12-27
3. Goto A, Sawata A (1999) Transactions of the 17th ICID congress, Granada, Spain, pp 48-62
4. Fujinawa K (1981) bull. Natural resources, institute of agricultural Eng. Japan 21: 127-141.

EXTREME CAPACITY OF UNCONFINED AQUIFERS WITH ACCRETION

Sergej Belov [1], Nobuo Fujii [1], and Anvar Kacimov [2]

[1] Dept. of Information Systems Engineering, Osaka Sangyo University, Nakagaito 3-1-1, Daito-shi, Osaka, 574, Japan
[2] Dept. of Soil & Water Sciences, P.O. Box 34, Al-Khod 123, Sultan Qaboos University, Sultanate of Oman

ABSTRACT. Two dimensional – Darcian flows in unconfined and incompressible homogeneous isotropic aquifers with infiltration-evaporation distributed above the water table are studied theoretically. In a steady state regime the method of isoperimetric estimation is applied to calculate the saturated volume (capacity) using the Dupuit-Forchheimer assumption. The cross-sectional area of the flow domain is fixed and the capacity reaches its extremum for a circular plan section. The method of shape variations and the Fourier series are applied to derive chain inequalities for the capacity. For cyclostationary variations of accretion formulated as a linear source-sink above the water table between two reservoirs, a linear potential model is used to calculate the oscillating water table. A time and space averaged deviation of the water table is selected as a capacity. A certain water depth in the adjacent reservoirs provides the maximum of the capacity.

KEY WORDS: phreatic surface, infiltration, saturated thickness, optimization

INTRODUCTION

The paucity of data in subsurface hydrology requires qualitative assessments of flow and transport characteristics. In this paper we study analytically a steady state phreatic surface flow with uniform infiltration (the Poisson equation) and a cyclostationary flow in a porous formation in which the water table is subject to periodic accretion (the Laplace equation). Our goal is to optimize the flow domain, i.e., to establish what domain provides an extremal value of a posed criterion under given restrictions. Optimal values are used for isoperimetric estimations.

UNIFORM INFILTRATION

It is to be steady 2-D flow in a homogeneous unconfined aquifer of conductivity k and porosity m. Infiltration of constant intensity ϵ^* is uniformly distributed over the water table. Fig. 1a shows a plan view, D, of the aquifer, section '1-1' indicates an arbitrary vertical cross-section. Fig. 1b shows a cross-section where the water table elevation above a horizontal impermeable bed is $u(x, y)$. Flow is discharged into a drainage network, Γ. The water level u_Γ coincides with u in adjacent points and is constant (assume $u_\Gamma = 0$). We neglect seepage faces near points E and F. Furthermore, we assume that the area S of D is known. In terms of the Dupuit-Forchheimer model the mass conservation in the aquifer gives

$$\Delta u^2 = -2\epsilon \tag{1}$$

where $\epsilon = \epsilon^*/k$. Along Γ, the constant level condition holds

$$u = 0 \tag{2}$$

Recently eqns. (1)-(2) have been used [1,2] to determine u in watersheds of various shapes and stream network configurations. The boundary-value problem (1)-(2) has been studied in the theory of elasticity [3].

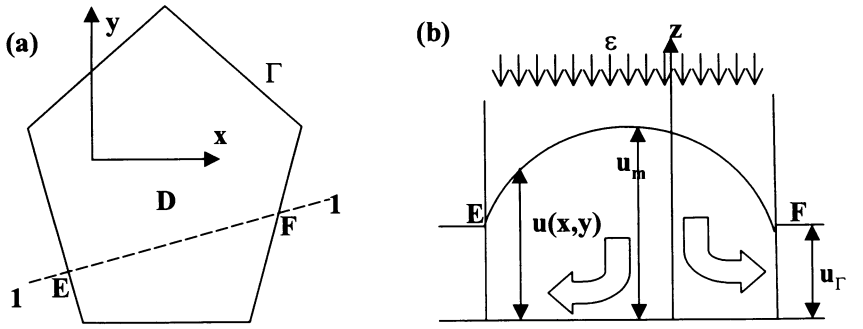

Fig.1 Drainage zone, plan view (a) and cross-section (b)

Exact solution of (1)-(2) is not always necessary (information on ϵ^*, k, and D is very approximate) for hydrologists because they are often only interested in estimating of characteristics of the groundwater mound, which rises between drains as curve EF shows in Fig.1. The choice of these characteristics depends on their modeling goals. For example, the maximum water table elevation $u_m = max_D u(x,y)$ (Fig.1 b) is important, if water logging is of concern. We calculated this maximum u_m for three domains: a rectangle $a \times b$, a sector of radius a and angle α, and the Filon lens [3] with circular boundaries of radius a_c and b_c. The dimensionless maximal height $u_m/(\epsilon\sqrt{S})$ for the rectangle is shown in Fig.2 (curve 1) as a function of a/b and the maximum is reached at $a/b = 1$. For the sector, this height is shown as a function of α/π and the maximum is reached at $\alpha \approx 1.48$. Curve 3 in Fig.2 shows $u_m/(\epsilon\sqrt{S})$ of the Filon lens as a function of b_c/a_c, which varies from 0 to 2. The maximum is at $b_c = 0$ when the lens degenerates into a circle.

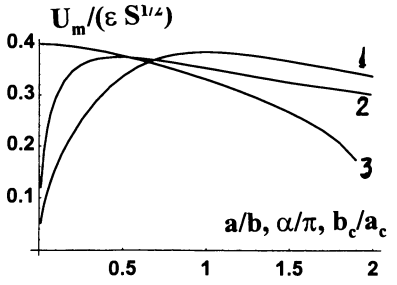

Fig.2 Maximal nondimensional water table elevation for a rectangular domain (1), a sector (2), and a filon lens (3)

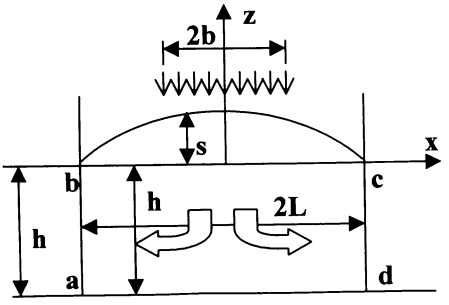

Fig.3 Strip accretion, cross-section

Another characteristic, the total amount of ground water stored in the aquifer J, is used for water budget calculations. This volume for the mound in Fig.1:

$$J(D) = m \int \int_D u(x,y)dxdy \tag{3}$$

Instead of calculating the double integrals in (3) we use the isoperimetric estimations based on domain optimization. We determine the bounds for a physical characteristic, which is difficult to measure or evaluate directly (J in our case), using another physical quantity, which can be readily measured or calculated (S).

Eq.(3) shows that J is a functional i.e. depends on the shape of D. Clearly, the solution of the boundary-value problem (1)-(2) depends on this shape, too.

At given S the minimum of $J(D)$ is zero (for example, for very thin domains $u \to 0$ everywhere within D). Introduce $J^* = J/m$ and $u_1 = u^2/(2\epsilon)$, designating for brevity any point (x,y) as x, and use the sign of simple integrals instead of double integrals. Thus we determine Γ, posing maximum of J^* at a given S.

In terms of variational calculus the problem is singular. For regularization we consider a set of problems

$$J^*(D,\alpha_0) = \int_D \sqrt{u_1(x)}\, dx \tag{4}$$

$$\Delta u_1(x) = -1 \quad (x \in D), \tag{5}$$

$$u_1(x) = \alpha_0 > 0 \quad (x \in \Gamma). \tag{6}$$

$$I(D) \equiv \int_D dx = S. \tag{7}$$

Theorem. A circle provides maximum (at least local) of J^* for any $\alpha_0 > 0$.

Proof of the theorem: By Ω we denote the circle with its center at origin and its radius R, where $R = \sqrt{\frac{S}{\pi}}$. We show how any disturbance of the circle reduces the criterion J^*. For this purpose, we consider another domain Ω_h with its boundary Γ_h given by

$$r = R + h(\phi), \tag{8}$$

where h is some small $C^{2,\gamma}$ function. Let u_h be the solution of the boundary-value problem (5), (6) on the domain Ω_h. Using the Lagrangian function we can rewrite the difference of the criterion up to the second order of accuracy

$$J^*(\Omega_h,\alpha_0) - J^*(\Omega,\alpha_0) = \int_{\Omega_h} (u_h(x))^{\frac{1}{2}}\, dx - \int_{\Omega} (u(x))^{\frac{1}{2}}\, dx$$

$$= \frac{R}{2\alpha_0^{\frac{1}{2}}} \int_\Gamma F^2\, ds - \frac{4}{R}((\frac{R}{4}+\alpha_0)^{\frac{1}{2}} - \alpha_0^{\frac{1}{2}}) \int_\Gamma F \frac{\partial F}{\partial n}\, ds - \frac{1}{8}\int_\Omega \frac{F^2}{u_1^{\frac{3}{2}}}\, dx + \beta(h)\int_\Gamma h^2\, ds, \tag{9}$$

where $u_1 = \frac{1}{4}(R^2 - r^2) + \alpha_0$ is the solution of (5), (6) on the circle Ω, F is so-called variation of the solution which satisfies the following boundary-value problem

$$\Delta F = o(x \in \Omega), \tag{10}$$

$$F = \frac{1}{2}h; (x \in \Gamma). \tag{11}$$

and $\beta(h) \to 0$, if $\|h\|_{C^{2,\gamma}} \to 0$.
Using the Fourier series we rewrite the boundary conditions (11) as

$$F(1,\phi) = \frac{1}{2}h(\phi) = \sum_0^\infty (a_n \cos n\phi + b_n \sin n\phi), \tag{12}$$

Then, we can rewrite expression (9)

$$\begin{aligned} &J^*(\Omega_h,\alpha_0) - J^*(\Omega,\alpha_0) \\ &= \sum_1^\infty \pi(a_n^2+b_n^2)\left(\frac{R}{2\alpha_0^{\frac{1}{2}}} - \frac{4n}{R}((\frac{R}{4}+\alpha_0)^{\frac{1}{2}} - \alpha_0^{\frac{1}{2}}) - \frac{1}{8}\int_0^R \frac{r^{2n+1}}{(\frac{1}{4}(R^2-r^2)+\alpha_0)^{\frac{3}{2}}}\,dr\right) \\ &+\beta(h)\sum_1^\infty \pi(a_n^2+b_n^2) = \sum_1^\infty \pi(a_n^2+b_n^2)G(n,\alpha_0) + \beta(h)\sum_1^\infty \pi(a_n^2+b_n^2) \end{aligned} \tag{13}$$

where we neglected a_0 in the sums above because of the constraint (7).
By direct computations we obtain

$$G(1,\alpha_0) = 0, \quad G(n+1,\alpha_0) < G(n,\alpha_0), \quad n \geq 1 \quad G(n,\alpha_0) < 0, \quad n \geq 2 \tag{14}$$

We have recently shown [4] that $n = 1$ in the sums above corresponds to translations of the circle and, therefore, the coefficients a_1, b_1 can be eliminated after appropriating translation of the origin of coordinates. Hence

$$J^*(\Omega_h,\alpha_0) - J^*(\Omega,\alpha_0) = \sum_2^\infty \pi(a_n^2+b_n^2)G(n,\alpha_0) + \beta(h)\sum_2^\infty \pi(a_n^2+b_n^2) < 0, \tag{15}$$

for domains, which are geometrically, close enough to a circle. The theorem is thereby proved. Now we can write following inequalities

$$J^*(\Omega_h) < J^*(\Omega_h,\alpha_0) < J^*(\Omega,\alpha_0) = \frac{\pi(R^2+4\alpha_0)^{\frac{3}{2}}}{3} - \frac{8\pi\alpha_0^{\frac{3}{2}}}{3} \tag{16}$$

Since we assumed α_0 to be an arbitrary small parameter we can return to the original problem with parameters S, ϵ, m. We obtain the following relationships

$$J(\Omega_h) = J(D) \leq J(\Omega) = \frac{m\pi(2\epsilon)^{\frac{1}{2}}R^3}{3} = \frac{mS^{\frac{3}{2}}(2\epsilon)^{\frac{1}{2}}}{3\pi^{\frac{1}{2}}}, \tag{17}$$

which can serve for practical estimations of the mound volume.

PERIODIC INFILTRATION-EVAPORATION

Let us consider an aquifer *abcd* of horizontal dimension $2L$ based on an impermeable bottom *ad*. The aquifer contacts two draining channels *ab* and *cd* where the water level h is constant (Fig.3 shows a cross-section). Replenishment/evaporation is distributed along a strip of width $2b$ (symmetric about the channels). The accretion rate is $\epsilon = \delta \sin \omega t$ at $|x| < b$ and $\epsilon = 0$ at $|x| > b$, where ω is the frequency, $2T = 2\pi/\omega$ is the period, δ is a small non-dimensional

parameter defined according to [7] as $\delta = max|s(x,t)|/h$. The water table $h + s(x,t)$ moves due to periodic accretion.
Various models have been developed for transient phreatic surface flows [5,6]. We use a linear potential model [5] in the study. The velocity distribution and $s(x,t)$ for this flow were determined in [7]. As an integral criterion we adopt the capacity C of the mound:

$$C = \frac{1}{L^2 T} \int_0^T \int_{-L}^{L} s(x,t) dx dt \tag{18}$$

The value of C is an analogue of J from the previous section. The question is: which geometrical (h) and climatological (T) parameters give an extreme value of C? This problem is similar to one in heat conduction [8].
According to [7] the water table elevation is:

$$s^*(x,t) = \frac{4\delta p}{m\pi} \sum_{n=1}^{\infty} \frac{(-1)^{n+1}}{2n-1} \sin\frac{(2n-1)\pi b^*}{2} * \sin\frac{(2n-1)\pi(x^*+1)}{2} \frac{A_{2n-1}\sin(\pi t^*/p) + \cos(\pi t^*/p)}{1 + A_{2n-1}^2} \tag{19}$$

where

$$A_{2n-1} = \frac{(2n-1)p}{2m} \tanh\frac{(2n-1)\pi h^*}{2}$$

Here the nondimensional values are overstarred. All geometrical sizes are related to L, the nondimensional half-period is $p = Tk/L$, and time is $t^* = tk/L$.
From (18)-(19) we can calculate:

$$C = \frac{32\delta^*}{\pi^3} \sum_{n=1}^{\infty} \frac{(-1)^{n+1} A_{2n+1}}{(2n-1)^2\sqrt{1 + A_{2n-1}^2}} \sin\frac{(2n-1)\pi b^*}{2}$$

Fig.4 shows the free surfaces at $\beta^* = 0.1, p = 1, h^* = 0.1, m = 0.3$ plotted at $t^* = 0.0, 0.25, 0.5, 0.75, 1.0$, curves 1-5, respectively ($\delta = 0.1$). Fig.5 shows the functions $C(h^*)$ at $p = 2, \quad m = 0.3$ for three values of $b^* = 0.1, 0.5, 0.9$ (curves 1-3, respectively). For our data the pairs of maximal capacity (C_{max}, h^*_{max}) are (0.016, 0.207), (0.075, 0.201), (0.112,0.193). The horizontal velocity distribution U/k along cd is shown in Fig.6 as a function of y^* for the same parameters as in Fig.4. The graphs illustrate the deviation of U from a constant. Note, that in the Dupuit-Forchheimer model U is postulated to be constant along all vertical lines. When outflow into the draining channel occurs, the main concern is the maximum of U, which controls the seepage erosion stability. From Fig.6, this maximum "travels" along the slope during one cycle.

CONCLUSION

We studied a steady Dupuit-Forchheimer flow with a uniform accretion and formation of a groundwater mound, which is discharged into a drainage. The Poisson equation for the squared water table height can be treated by the method of shape variations. We studied different plan sections contoured by a drainage line and showed that a circular flow domain provides an extremum to the total amount of water stored in the mound. For a cyclostationary

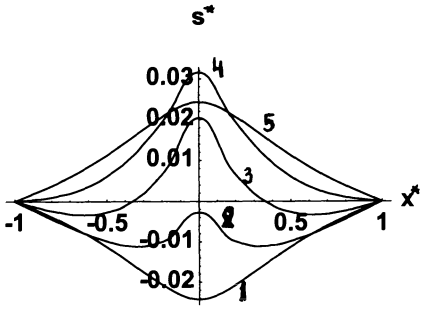

Fig.4 Water table elevations at t=0.0, 0.25, 0.5, 0.75, 1.0 (curves 1-5)

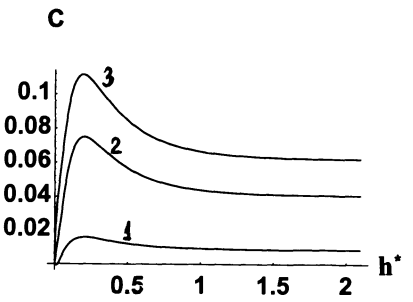

Fig.5 Capacity as a function of undisturbed saturated thickness at b=0.1, 0.5, 0.9 (curves 1-3)

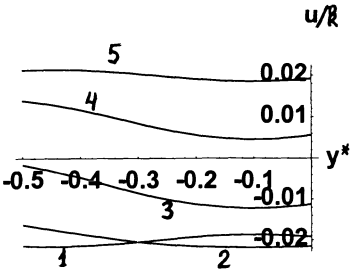

Fig.6 Horizontal velocity along the outlet section as a function of depth

accretion along the water table we applied a linear potential model and analyzed the amount of water in storage during one cycle of accretion. This volume as a function of the water level in the draining reservoirs has a non-trivial maximum.

REFERENCES

1. Youngs EG (1992) Patterns of steady groundwater movement in bounded unconfined aquifers. J. Hydrol. 131: 239-253
2. Haitjema HM, Kelson VA (1996) Using the stream function for flow governed by Poisson's equation. J. Hydrol. 187: 367-386
3. Timoshenko SP, Goodier JN (1970) Theory of Elasticity. McGraw-Hill.
4. Belov SA, Fujii N (1997) Symmetry and sufficient conditions of optimality in a domain optimization problem. Control and Cybernetics 26: 1-12
5. Polubarinova-Kochina PYa (1977) Theory of Ground Water Movement. Nauka.
6. Turner IL, Coates BP, Acworth RI (1996) The effects of tides and waves on water-table elevations in coastal zones. Hydrogeology J. 4: 51-69.
7. Nimr AE (1972) Effect of accretion on dynamics of groundwater between two channels. Water Resour. Res. 9: 1058-1064.
8. Magyari E, Keller B (1998) The storage capacity of a harmonically heated slab revisited. Int. J. Heat Mass Transfer 41: 1199-1204.

Biological Treatment of Groundwater

Harri Seppänen

Water Protection Association of the River Vantaa and Helsinki Region
Ilmalankuja 2 E, 00240 Helsinki, Finland

ABSTRACT. All ground water aquifers are multiform biological systems. Taking into account the environmental requirements of different microbes it is possible to utilise certain microbes to solve many ground water quality problems. The most common problems are excessive iron and manganese concentrations in the ground water. Nitrate is an increasing problem in many countries. Using microbes it is possible to reduce the nitrate concentration in ground water to acceptable levels.

KEY WORDS: ground water, iron, manganese, nitrate, biological treatment

INTRODUCTION

Ground water is a living ecosystem. The quality of the ground water varies both in horizontal and vertical directions. Ground water aquifer is very often horizontally stratified because of density or temperature differences. Colder water is always found beneath warmer water and denser water containing high concentrations of iron, manganese or salts is found in deeper layer. In some cases the quality differences may be observed in wells which are situated very close each other. The distance between two wells may be even less than ten meters.

Living organisms affect the quality of ground waters. The effect of microbes and even higher organisms may be either direct or, in many cases indirect. Typical direct effects are related to circulation of nutrients and other inorganic and organic compounds in ground waters. The main processes are oxidation and reduction of organic and inorganic compounds. In indirect effect living organisms alter their environment suitable for pure chemical reactions.

This paper is not any special research rapport. The purpose of this paper is to summarise some important microbiological observations made during many ground water researches in Finland.

DIRECT EFFECTS OF MICRO-ORGANISMS

If the effect of living organisms is direct concerning changes of the oxidation state of elements, it means that the metabolic end products of very specialised organisms are simple inorganic compounds [1].

Nitrogen cycle

Ammonification:

$$\text{Organic Nitrogen} \rightarrow NH_3$$

Ammonification is one of the most important decomposition processes in nature. Ammonification is possible in aerobic or anaerobic environments. The biological spectrum of ammonification is wide. In practice this means that the process is possible in quite extreme environmental conditions. There

are bacteria capable of decomposing organic nitrogen to ammonia almost in every environmental conditions.

Nitrification:

Phase 1 *Nitritation*: $NH_4^+ + 1½\ O_2 \rightarrow NO_2^- + H_2O$

Nitritation is the first step in oxidation of inorganic NH_4^+-nitrogen to NO_2^--nitrogen. The process is strictly aerobic. There are a group of very special bacteria capable of maintaining this process. A typical species is *Nitrosomonas*.

Phase 2 *Nitratation*: $NO_2^- + ½\ O_2 \rightarrow NO_3^-$

Nitratation is the second step in oxidation of inorganic nitrogen. In this step nitrite-nitrogen, NO_2^- is oxidised to nitrate-nitrogen, NO_3^-. The process is also strictly aerobic. There are a group of very special bacteria capable of maintaining this process. A typical species is *Nitrobacter*.

Denitrification: $NO_3^- \rightarrow NO_2^- \rightarrow N_2O \rightarrow N_2$

Denitrification is a anaerobic process. In anaerobic environments chemically bound oxygen e.g. NO_3^- is absolutely necessary. In denitrification, NO_3^-oxygen serves as the electron acceptor whilst organic material ($C_6H_{12}O_6$) acts as the electron donor.

$12\ NO_3^- + C_6H_{12}O_6 \rightarrow 12\ N_2 + 6\ CO_2 + 6\ H_2O$

Sulphur cycle

Decomposition of sulphur containing organic compounds:

Organic sulphur $\rightarrow$ H_2S
(Proteins)

$2\ (CH_2O) + H_2SO_4 \rightarrow 2\ CO_2 + 6\ H_2O + H_2S$

Oxidation of H_2S: $H_2S + ½O_2 \rightarrow S^0 + H_2O$; $S^0 + 1½\ O_2 + H_2O \rightarrow H_2SO_4$

Carbon cycle

Decomposition of organic carbon: Organic carbon $+ O_2 \rightarrow CO_2 + H_2O$

Decomposition of organic carbon to inorganic CO_2-carbon is a very common process in the living world. For heterotrophic organisms this biochemical "burning" of organic material yields the energy needed for metabolism for heterotrophic organisms and the end product of oxidation is carbon dioxide.

Formation of the methane:

Complex organic Compounds	→ Acid production	Organic Acids	→ Methane production	$CH_4 + CO_2$

In anaerobic conditions decomposition of organic compounds yields both carbon dioxide and methane. The methane fermenting bacteria can utilise only very simple substrates in fermentation. A typical compound is acetate.

Oxidation of methane:

$CH_4 + O_2 \rightarrow 2(CH_2O) + 3CO_2 + H_2O$

Oxidation of methane to carbon dioxide is an aerobic process. The process is relatively fast in nature.

INDIRECT EFFECTS OF MICRO-ORGANISM

Very often living organisms affect the chemical reaction indirectly. In practice this means that the metabolism of microbes make their environment suitable for some pure chemical oxidation and reduction processes of simple inorganic compounds [1]. Some precipitation and dissolution processes depend on the chemical character of the environment.

The metabolism of microbes changes the redox-potential and pH of the environment. Some processes may increase the pH (ammonification) while others may decrease the pH (decomposition of organic compounds resulting in the formation of CO_2). The precipitation and dissolution of some inorganic compounds depends on the pH.

Oxidation of reduced iron and manganese

Iron occurs in two states of oxidation in nature, divalent (ferrous) and trivalent (ferric). One state can be converted into the other by the exchange of an electron: $Fe^{2+} \rightarrow Fe^{3+} + e^-$

The oxidation of reduced iron and manganese may be described by chemical equations. It is possible to calculate the amount of chemical energy released in these processes. It seems that the bacteria can not utilise this energy for their metabolism. In the oxidation of reduced iron and manganese compounds the role of micro-organisms is more or less indirect.

Reduction of oxidised iron and manganese

Iron and manganese in ground water originate mainly from mafic silicate minerals and sulphides in bedrock and superficial deposits [3] [4]. As a consequence of environmental and biological processes, most of the relatively rapidly formed iron and manganese minerals in ground water are poorly ordered and readily soluble in slightly reducing conditions [5] [6]. Enzymatic reduction of ferric iron in nature seems to be a prominent phenomenon, however, indirect mechanisms of ferric iron cannot be ignored [7].

Bacteria play only a secondary role in the reduction of ferric iron to ferrous iron. Heterotrophic bacteria consume dissolved oxygen from their environment, decreasing the redox-potential to the level where the ferric iron is reduced to ferrous iron.

IRON CYCLE IN NATURAL CONDITIONS

As rain water hits the surface of the earth it is saturated with oxygen. A part of the water percolates into the ground. Initially it has to penetrate through the upper layer of the earth. A characteristic of the humus containing surface soil layer is the abundance of different heterotrophic organisms,

bacteria, protozoa and even higher organisms, which consume the dissolved oxygen from the percolating water. Carbon dioxide is produced as an end product of their metabolism. Because waters often have low buffer capacity, the pH of the water decreases. The water becomes aggressive. Since both iron and manganese are present practically everywhere in the crust, they become soluble in the water as bicarbonates. Living organisms play only a secondary role in this process.

The solubility of iron correlates with the redox potential of the environment. The ground water contains soluble iron and manganese in significant amounts only when the redox level decreases below +230 mV [8] [9][10] [11]. If the redox potential is above + 230 mV, both iron and manganese are in an oxidized state and are precipitated on soil particles.

There are many technical applications of these natural processes for removing iron and manganese from ground water. These can be divided into two categories: methods applied on the surface of the earth in specially constructed filter basins and methods applied directly in the aquifer.

MICRO ENVIRONMENTS

With chemical analyses it is possible to get only a coarse picture of the very complicated microbiological system of an aquifer. Chemical analyses give results only for the macro environment. In fact, all microbiological processes take place in very small micro environments. In these micro environments strictly anaerobic processes are possible within aerobic macro environments. Even one dead algae cell may serve as a suitable anaerobic micro environment for an anaerobic bacteria. In practical applications of natural processes the idea of micro environments must always be taken into account.

TREATMENT METHODS

Filtration

In conventional filtering processes sand, or active carbon are the most common filter bed materials. Often the filtration processes are divided into two categories, slow and rapid. Slow filtration is considered to be a biological and rapid filtration a more or less physical treatment unit. Actually filtration, either slow or rapid, is always a biological treatment unit. Both sand and active carbon filters are occupied by millions of living organisms. It is even impossible to prevent the bacteria to grow in filter beds. The main type of micro-organisms in filtration are heterotrophic bacteria which decompose organic material. The main purpose of filtering processes is to reduce the amount of organic carbon. The metabolic products of these bacteria are simple inorganic compounds such as carbon dioxide, ammonia and sulphates.

Floating filters can be used to prevent clogging of the filter bed. Iron and manganese bacteria are sessile organisms that grow and attach themselves on the solid surfaces of filter media. In floating filters, the filter material is lighter than water [12].

Re-infiltration

Re-infiltration is a modification of the conventional filter method. That has been applied for iron and manganese removal from ground water. In this method iron and/or manganese bearing water is pumped up from the aquifer and filtered back to the aquifer through sand-filtration. Iron and manganese bacteria living on soil particles oxidise and precipitate reduced iron and manganese compounds around cells and sheaths.

Artificial recharge

Artificially recharge is one modification of biological filtration. The method depends on the quality of infiltrated water. Water containing high amounts of humus material may cause problems because humus is a very stable organic material. Only few microbes are able to decompose humus compounds.

In general, water is infiltrated using infiltration basins. Clogging of basins during artificial recharge is one of the problems. Assimilating algae biomass increases the oxygen content of the infiltrated water and decreases the concentration of dissolved nutrients that are assimilated to the biomass. On the other hand, algae growth increases both amount and types of soluble organic compounds in the water. Later the microbial decomposition of these compounds consumes oxygen and, as a consequence, iron and manganese become soluble and deteriorate the water quality.

Water may be spread directly on the ground surface using special nozzles. In these cases the quality of the soil is very important. All organic soil of whatever kind must be taken away from the infiltration field. The most convenient soil type is gravel.

Vyredox-method

Vyredox-method was developed in 1970-1971 in Finland [11] [13]. Nowadays there are many different application of this method. The basic principle of all applications is, however, the same.

The Vyredox-method is based on the idea of oxidising and precipitating iron and manganese in the ground. This is accomplished in practice by pumping into the ground water that is free from iron and manganese and is saturated with oxygen into the ground. With this artificial oxidation, a steady gradient between anaerobic and aerobic environments is formed in the ground. Iron and manganese are oxidized, precipitated and adsorbed on soil particles in the oxidized zone and are easily soluble on the reduced side.

NITROGEN PROBLEMS

The increase of nitrogen content in ground waters is, presently, a world wide problem. This problem will become more and more serious in the future. Causes of the increase of nitrogen are fertilisers and the over all pollution of the soil. The maximum acceptable nitrate concentration in potable water is 50 mg/l. If the concentration exceeds this limit water is no longer suitable for drinking water purposes.

The most practical method for removing reduced ammonium-nitrogen from water is by stripping with air. Removing oxidized nitrate nitrogen from water is possible only with biological methods. Denitrification, $NO_3 \rightarrow N_2$ is a well known process in waste water technology. The same process can be applied in ground water technology as well.

In Bisamberg, Austria, a raw water nitrate (NO_3^-) concentration of 52 mg/l is reduced to 19 mg/l utilising the denitrification process [14]. It is possible the construct a biological filter for nitrogen removal, or nitrogen can be removed in situ, as was discussed earlier in contact of iron and manganese removal methods.

The main reason for increasing the amount of nitrate nitrogen in the aquifer is the lack of a suitable

electron donor. It can be said that the ground water is too pure! To solve the nitrate problem, the ground water must be polluted to a certain degree.

Introducing organic matter into the aquifer, denitrification process can be started and maintained in operation. It is important that the added organic compound not be harmful or toxic. Ethanol is one compound applied in practice. The ethanol dosage must be adjusted to such a level that all of it is consumed from the water before the water is pumped to consumers.

CONCLUSIONS

Microbes are the really busy workers in nature. Assuming that the chemical process and all environmental requirements of the microbes including nutrients and other growth factors are known it is possible to isolate a special type of bacterium to solve different ground water quality problems. In the future it is even possible to specialize microbes with gene manipulation.

Metabolism of microbes may affect the environment in such a manner that it may restrict their activity. The buffer capacity of ground water is in general low. Therefore it is often necessary to increase the buffer capacity artificially. It is not question only of the buffer capacity of the water but more often problems may arise in the micro scale in the immediate vicinity of single bacterium cells. In this context the chemical composition and the physical structure of the filter material play an important role.

Making the environment suitable for their metabolism and multiplication, it is possible get a lot of useful co-workers to solve many chemical problems existing in ground waters. In fact the solution of many problems can be achieved only by microbes.

REFERENCES

1. Seppänen, H., (1988b). Ground Water – A Living Ecosystem.- Wat. Sci. Tech. Vol 20. No 3:95-100.
3. Marmo, V., (1958). Pohjavesien ja kasvintuhkien käytöstä malminetsinnässä. In : Marmo,V. (Ed)Geokemiallinen ja biogeokemiallinen malminetsintä.- Geotek. Julk. 61:55-120.
4. Rönkä, E., Uusinoka, R. And Vuorinen, A., (1981). Geochemistry of Ground Water in the Precambrian Crystalline Bedrock of Finland in Relation to the Chemical Composition of the Reservoir Bedrock.- Publ. Water Res.Inst. Natl. Board of Waters Finland, 38:41-53.
5. Carlson, L., Vuorinen, A., Lahermo, P. and Tuovinen, O., (1980). Mineralogical, geochemical and microbiologi cal aspects of iron deposition from ground water.- In : Trudinger, P. A. Walter, M. R. And Ralph, B. J. (Eds.).- Biochemistry of Ancient and Modern Environments. Aust. Acad. Sci. Canberra. Springer Verlag, Berlin, 255-364.
6. Carlson, L. and Schwertmann, U., (1981). Natural ferrihydrites in surface deposits from Finland and their associa tion with silica.- Geochim. Cosmochim Acta. 45:421-429.
7. Echrlich, H.L. (1981). Geomicrobiology, New York 393.
8. Mortimer, C.H. (1941). The exchange of dissolved substances between mud and water in lakes.- J. Ecol. 31: 280-329.
9. Hem, J.D. (1960). Restrains on dissolved ferrous iron imposed by bicarbonate redox-potential and pH.- U.S. Geol. Survey water supply paper 1459, b:33-55.
10. Morris, J.C. and Stumm W., (1967). Redox equilibria and measurements of potentials in the aquatic environment.- equilibria concepts in natural water systems.- (ed. by . R.F. Gould). Am. Chemic. Soc. Publ. Washington D.C. 270-285.
11. Hatva, T., Niemistö, L. and Seppänen, H. (1973). Examination and removal of iron in ground water.- Aqua Fennica 1973, 82-94.
12. Seppänen, H., (1988a). Biological treatment of ground water in basins with floating filters.- The role of micro-organisms in floating filters.- Wat. Sci. Tech. Vol 20. No 3:185-187.
13. Hallberg, R. And Martinell, R., (1976).Vyredox – In Situ Purification of Ground Water.- Ground Water, Vol. 14 Nro 2: 1-6.
14. Jechlinger, G., Eibl, W. And Martinell R., (1998). NITREDOX in situ treatment plant, case study from Bisamberg.- Vatten 54: 61-66.

Numerical Simulation of Water–Gas Flow and Transport Processes in Coastal Aquifers

Reinhard Hinkelmann[1], Hussam Sheta[1], Rainer Helmig[1], Eberhard J. Sauter[2], Michael Schlüter[2]

[1]Institut für ComputerAnwendungen im Bauingenieurwesen, Technische Universität Braunschweig, Pockelsstr. 3, 38106 Braunschweig, Germany, e-mail: (r.hinkelmann, h.sheta, r.helmig)@tu-bs.de
[2] GEOMAR Forschungszentrum für Marine Geowissenschaften, 24148 Kiel, Germany, email: (esauter, mschlueter)@geomar.de

ABSTRACT. In this paper a two–phase / three–component model concept for simulating interaction processes of fresh water, salt water, and methane in coastal aquifers is presented. The numerical algorithm which is part of the simulator MUFTE–UG is briefly explained. If methane occurs in very low concentrations and builds no gas phase, the model concept is simplified to one–phase / three component. For this case a reasonable agreement of computations and measurements was obtained in the range of available data. The simulations showed that certain concentration profiles can be caused by hydraulic conditions and not only by reaction processes as supposed before. If methane occurs as a gas phase, it has a significant influence on the results.

KEY WORDS: water–gas flow, methane migration, multiphase / multicomponent model

INTRODUCTION

Field measurements at several locations in coastal zones of the Baltic and North Sea have detected submarine groundwater fluxes into surface water. These locations are called vents. The transport of methane, nutrients, and contaminants involved has a considerably larger influence on the water quality in coastal areas than it has been expected up to now. To get closer insight into these complex phenomena (see fig. 1), to predict future trends, and to develop suitable remediation measures, numerical models as well as monitoring tools are developed and adapted to the special problems in coastal subsurface systems. This paper focuses on the numerical simulation of fresh water, salt water and methane interaction processes at vent and non–vent locations. The computations are based on a two–phase / three–component model approach and are partially compared with field measurements.

For modelling salt water intrusion processes into fresh water, a one–phase / two–component model concept (phase: water; components: water, salt) should be applied in most cases (e.g. Oldenburg & Pruess (1995 [1]), Hinkelmann et al. (1999 [2])). If methane is integrated in the simulations, two situations must be distinguished. At low concentrations, methane is soluble in water. Then it builds no further phase, but a third component. Such situations require a one–phase / three component model (phase: water, components: water, salt, methane). If the maximum solubility is exceeded, methane is changing into the gas phase and a two–phase / three–component model approach (phases: water, gas; components: water, salt, methane) is necessary (e.g. Pruess (1991 [3]), Helmig (1997 [4])).

The paper is organized as follows: In chapter 2 the governing equations and the numerical algorithm are explainded, while the field measurements are briefly described in chapter 3. Chapter 4 contains some applications analyzing different phase situations and varying flow regimes. In chapter 5 conclusions are drawn.

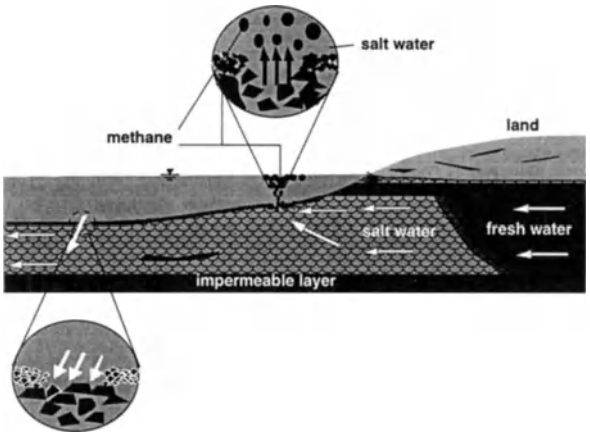

Figure 1: Interaction of fresh water, salt water and methane in a coastal aquifer

NUMERICAL ALGORITHM

Governing equations for a two–phase / three–component model concept

The balance equations for the flow of three components (f: (fresh) water, s: salt, m: methane) in two fluid phases (w: water, g: gas) in porous media is given by the conservation of mass (eq. 1) for each component κ:

$$\frac{\partial(\phi \rho_\alpha S_\alpha X_\alpha^\kappa)}{\partial t} + \nabla \cdot \{\rho_\alpha \mathbf{v}_\alpha X_\alpha^\kappa - \mathbf{D}_\alpha^\kappa \nabla (\rho_\alpha X_\alpha^\kappa)\} = q_\alpha^\kappa \qquad in \quad \Omega x I; \quad \alpha = w, g \tag{1}$$

In this equation ϕ denotes porosity, ρ density, S unknown saturation, X unknown mass fraction, t time, $\mathbf{v}$ *Darcy* velocity vector, $\mathbf{D}$ hydrodynamic dispersion tensor, q source or sink term, Ω space dimension, and I time dimension. The velocity vector of each phase α is determined by the *generalized Darcy law* (eq. 2):

$$\mathbf{v}_\alpha = -\frac{k_{r\alpha}}{\mu_\alpha} \mathbf{K} (\nabla p_\alpha - \rho_\alpha g) \tag{2}$$

In equation 2 k_r stands for relative permeability, μ dynamic viscosity, $\mathbf{K}$ absolute permeability tensor, p unknown pressure and g gravity. In addition, three algebraic relations close the system: The mass fractions add up to one in each phase (eq. 3), the void space in the porous medium is completely filled (eq. 4), and the difference of the pressure at every point is a function of the capillary pressure p_c (eq. 5):

$$X_\alpha^f + X_\alpha^s + X_\alpha^g = 1; \quad \alpha = w, g \tag{3}$$

$$S_w + S_g = 1 \tag{4}$$

$$p_g - p_w = p_c \tag{5}$$

According to Oldenburg & Pruess (1995 [1]), the density of the water phase ρ_w can be formulated as a function of the mass fractions and the density of fresh water and salt water (concentrated brine, see eq. 6):

$$\frac{1}{\rho_w} = \frac{X_w^f}{\rho_f} + \frac{X_w^s}{\rho_s} \tag{6}$$

The hydrodynamic dispersion tensors of the components in two phases are functions of other variables (e.g. Oldenburg & Pruess (1995 [1])) for which information is lacking. Therefore, they are assumed to be constant. There exist different functions to describe the *constitutive relations* for the relative permeability / saturation $k_{rw}(S_w)$ and $k_{rg}(S_g)$ as well as for the capillary pressure / saturation $p_c(S_w)$. The solution processes of water in the gas phase and methane in the water phase are generally described by *Raoult's law*, which can be simplified to the *Henry law* by low concentrations. Finally, *Dalton's law* of partial pressures is required.

For the solution of these coupled non–linear partial differential equations, initial and boundary conditions must be given. Depending on the processes, i.e. if no gas phase occurs, the model concept is reduced to one–phase / three–component. The choice of the primary variables is determined by appropriate boundary conditions. Further information is given in Helmig (1997 [4])) and Atkins (1996 [7])).

Discretization and Solvers

In this paper two–dimensional examples consisting of quadrilaterals are investigated. The partial differential equations are discretized in space by a finite volume–based method, a so–called *box scheme*. For the flux terms a *fully upwind technique* is applied. The time is discretized with an *implicit Euler scheme*.

The discretizations described above lead to nonlinear and sparse systems of algebraic equations for every time step, which may have a large number of unknowns. Therefore, an outer *Newton iteration* is combined with an inner *conjugate gradient* or *multigrid solver*. The techniques explained here as well as a number of variants are part of the modular program system MUFTE–UG for simulating multiphase flow, transport, and energy processes in heterogeneous porous media (Helmig, (1997 [4]), Helmig et al., (1998 [5])).

MEASUREMENTS

The major task of the joined EU project Sub-GATE is to investigate submarine groundwater fluxes and transport from methane–rich coastal sedimentary environments (Sauter & Schlüter (1999 [6])). Within this work, a number of field measurements are carried out, and some monitoring tools are developed or adapted to the special situations at vent locations.

One task of this project consists of continuously monitoring fluid flow at vent sites. The vent sampler enables a quantification of the advective upward fluid flow and determines boundary conditions for the numerical simulations. One interesting result is the fact that the vertical flow velocities from groundwater into surface water are comparatively high with up to 1cm/s, and thus are in the range of the horizontal flow velocities in the surface water.

In the geochemical task group sediment and pore water sampling at vent and non–vent locations have been conducted in order to describe the geochemical fluxes through the sediment–water in-

face. Some of the measurements are shown in figure 3 and are compared to the numerical computations. Vents have been detected at many locations, and as they don't only occasionally occur, they have a greater influence on the methane cycle in coastal environments than assumed in the past. Some open questions remained, e.g. concerning the vertical methane distributions. Solely looking on the measurements it was supposed that methane formation and oxidization must occur. Further informations are given in Sauter & Schlüter (1999 [6]).

APPLICATIONS

The system shown in figure 2 was chosen for simulating the first vertical meter of a submarine coastal aquifer in the Eckernförder Bucht, Baltic Sea, Germany. The sediment is highly porous $\phi = 0.9$, and the permeability was estimated at $K = 10^{-8}m^2$ and constant. Quasi one–dimensional upward vertical flow situations were investigated. Therefore, the system width was chosen to be $1m$, and the left and right boundaries are closed. On the upper boundary, a twenty meter salt water column with a salinity of $7^o/_{oo}$ was given and the methane concentration was set to zero. It is assumed that the salinity is mainly determined by chloride. For a given mole mass of water $0.018kg/mol$, $7^o/_{oo}$ are equivalent to $0.007/0.018 = 0.39mol/l = 390mmol/l$ (see fig. 3). On the lower boundary, fresh water ($\rho_w = 1000kg/m^3$, $\mu_w = 10^{-3}Pa/s$) discharge according to the vent sampler measurements of $q_w^f = 10.8l/(m^2h)$ for a vent location, $q_w^f = 4.0l/(m^2h)$ for a partial vent location, and $q_w^f = 0.1l/(m^2h)$ for a non–vent location, as well as the methane fluxes were determined as the boundary conditions. The density of the concentrated brine in equation 6 was set to $\rho_s = 1025kg/m^3$ (see Oldenburg & Pruess (1995 [1])). For the gas phase, the density was $\rho_g = 0.68kg/m^3$ and the dynamic viscosity $\mu_g = 10^{-5}Pa/s$ (see Atkins (1996 [7])). In the dispersion tensors only molecular diffusion was taken into account, $D_w^s = 6.6 \cdot 10^{-6}m^2/s$ and $D_w^m = 9.0 \cdot 10^{-10}m^2/s$ (see Atkins (1996 [7])). As initial conditions, the system was filled with fresh water (without methane). The system was discretized with 100 quadaratic elements in the vertical as well as in the horizontal direction, i.e. 10000 elements.

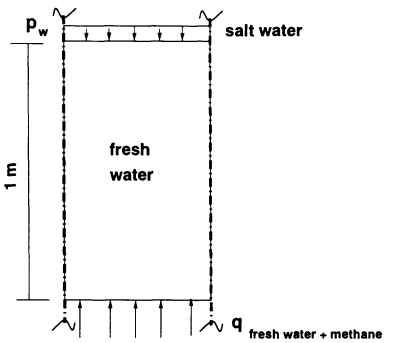

Figure 2: System set up, initial and boundary conditions

One–phase / three–component model

Due to the higher density, salt water is flowing downwards into the system, while fresh water and methane is coming up. After some time, a steady state solution is obtained for all three cases. A methane flux of $q_w^m = 0.015mol/(m^2h)$ lead to a reasonable agreement between computations and

measurements for the three locations (see fig. 3). The maximum solubility of methane in water, which is a function of pressure and temperature (see Atkins (1996 [7])), is never exceeded during the simulations. In the vent location, methane shows little variation over the depth – the computed decrease to zero in the upper $10cm$ is caused by the boundary condition –, while chloride drops down to about a third of the bottom water concentration due to the comparatively high advection. In the non–vent location, methane drastically decreases from nearly the maximal solubility to zero, and there is little variation in the chloride distribution, which is near to the bottom water concentration due to very small advection. For the partial vent, the results are found in between. The computed methane profiles are fully developed by hydraulic conditions. Methane formation and oxidization, which will be quantified in the close future, may have an influence on the methane distribution. However, as assumed before, it must not be mainly responsible for it.

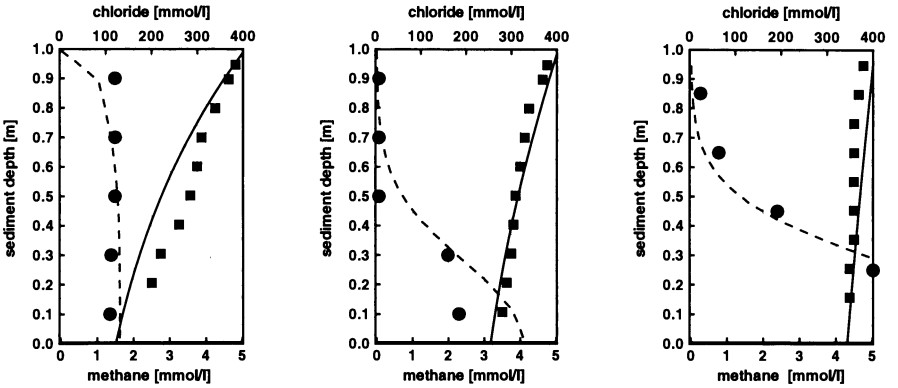

Figure 3: Chloride and methane profiles; left: vent, middle: partial vent, right: non–vent; computations: full lines (chloride), dashed lines (methane); measurements: squares, dots

Two–phase / three–component model

As methane is expected to be found as a gas phase at other locations, which will be investigated in the near future, we started with some test cases. For simplification, we neglected the component methane in the water phase and the components water and salt in the gas phase. The methane flux given at the inflow boundary leads to concentrations which are much higher than the maximum solubility in water. Although the prinicipal system behaviour can be compared to the one of the last subsection, the higher methane flux has a significant influence on the chloride and methane distribution, as shown for a vent location in figure 4. When compared to the results for the vent in figure 3 (left), chloride (component in the water phase) is partially displaced by the increased methane flux. It has nearly disappeared at the bottom of the system and has the same prescibed value at the top. Methane (main component in the gas phase) shows a constant profile again. But it has a much higher concentration due to the higher prescribed flux.

CONCLUSIONS

The numerical simulator MUFTE–UG is capable to deal with interaction processes of fresh water, salt water, and methane in coastal aquifers. Depending on the methane concentration, a one–phase / three component or a two–phase / three–component model approach must be applied. For the first

approach, a reasonable agreement between comptutations and measurements was obtained. But it must be mentioned that certain model parameters and boundary conditions had to be estimated, as information was lacking. The simulations showed that certain concentration profiles can be fully caused by hydraulic conditions and not only by reaction processes as supposed before. If methane occurs as a gas phase, it has a significant influence on the results. Future numerical work will deal with the integration of reaction processes.

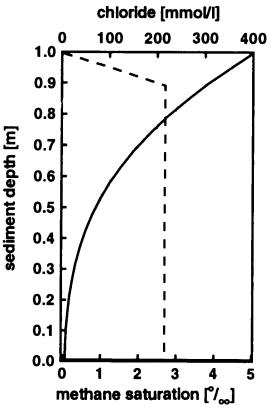

Figure 4: Computed chloride (full line) and methane profile (dashed line) for vent location

ACKNOWLEDGEMENT

This paper presents results of the research project Sub-GATE which is funded by the EU within the ELOISE project.

REFERENCES

1. Oldenburg CM, Pruess K (1995) Dispersive Transport Dynamics in a Strongly Coupled Groundwater–Brine Flow System. *Water Resources Reserach*, **31**(2), 289–302

2. Hinkelmann R, Sheta H, Class H, Helmig R (1999) A Comparison of Different Model Concepts for Salt Water Intrusion Processes. ModelCARE 99, International Conference on Calibration and Reliability in Groundwater Modelling, Zürich, Schweiz

3. Pruess K (1991) TOUGH 2, A General–Purpose Numerical Simulator for Multiphase Fluid and Heat Flow. Lawrence Berkeley Laboratory, University of California

4. Helmig R (1997) Multiphase Flow and Transport Processes in the Subsurface – A Contribution to the Modeling of Hydrosystems. Environmental Engineering, Springer–Verlag, Berlin, Heidelberg, New York

5. Helmig, R. et. al (1998) Architecture of the Modular Program System MUFTE–UG for Simulating Multiphase Flow and Transport Processes in Heterogeneous Porous Media. Mathematische Geologie, Band **2**

6. Sauter E, Schlüter M (1999) Sub-GATE, Summary Progress Report (End of year 1). Technical Report, GEOMAR, Kiel, Germany

7. Atkins PW (1996) Physikalische Chemie, 2. Auflage. Weinheim, New York, Basel, Cambridge, Tokyo

Groundwater Recharge Study and Simulation
- Kamphaeng Phet Case Study -

Sucharit Koontanakulvong[1] and Chokchai Suthidhummajit[2]

[1]Water Resources Engineering Department, Faculty of Engineering,
Chulalongkorn University, Phyrathai Rd., Patumwan, Bangkok, Thailand 10330.
[2]Chula Unisearch, Chulalongkorn University, Banthatthong, Patumwan, Bangkok,
Thailand 10330.

ABSTRACT. The feasibility of groundwater recharge scheme had been proposed to study in Kamphaeng Phet Province, about 400 km. north of Bangkok. The general movement of groundwater in the province was analysed and simulated from the data of the watertable monitoring program. Field experiment on artificial basin recharge was conducted and proved to be effective though sediment clogging issue was left to be solved. Water balance study from simulation results during the year 1997-2002 revealed that agricultural water use is the main reason for the decrease in groundwater table with the rate of 1-2 meters annually. To mitigate the situation, pumping control and/or groundwater recharge schemes are simulated and proposed in order to maintain the groundwater table as in the year 1997.

KEY WORDS. groundwater, simulation, water balance, recharge

INTRODUCTION

Water demand in domestic, industrial and agricultural uses gradually increases with the development of socio-ecomonics. This caused the decrease in groundwater table in many area in Thailand [1] and made people in rural area, who mainly rely on shallow well, suffer from water shortage especially during dry season [2].

Groundwater recharge scheme had been proposed to study in Kamphaeng Phet Province in order to mitigate the water shortage problem in the long term. Groundwater table monitoring program was executed during the year 1995 to 1997 and the data were collected and used to understand and simulate the general conditions of groundwater in the Province. Field experiment on gravity recharge was also conducted to investigate the recharge effectiveness and efficiency.

This paper summarized the study results of groundwater movement in the Province and the water balance analysis during the year 1997 to 2002. The effects of pumping control and groundwater recharge schemes were studied by computer simulation, using the data from field experimental recharge basin, to find suitable means to maintain groundwater table as in the year 1997.

GROUNDWATER MOVEMENT IN THE PROVINCE

Kampheng Phet Province is located in the northern part of Central region of Thailand with the distance of about 374 km from Bangkok. The total area of the Province is 8,623 sq. km with the average annual rainfall of about 1,300 mm and the anuual evaporation rate of about 1,460 mm. Topographically, the western part is a mountainous area with small hills in the Northwest. The basin slope decreases towards the East with an alluvial floodplain near the Ping River starting from the central part of the Province.
Geologically, rocks in Precambrain Era could be found in the mountainous and hilly areas in the West and Northwest, where Quaternary deposits (both terrace and alluvium) are found to be laid

on the rock layer in the plain area, covering most of the area in the Province. Groundwater aquifer is found in the Quaternary deposits starting from the area of Muang District and spreading towards in the East and both sides of the Ping River in the central area. There are three aquifer layers, i.e., an unconfined layer (from 4.0 to 12.0 m deep), two confined layers (from 8.0 to 40.0 m deep and from deeper from 40.0 m).

To understand the movement of groundwater in the Province, past records of water table data were collected from thounsands of well log and 42 monitoring wells were selected and monitored monthly during August 1996 to March 1998. Fig. 2 shows the contour of groundwater table in the Province monitored in monthly basis. It is clear that the groundwater in the Province flows from the West to East direction and the trend of water table decreases by time, i.e., 0.2-3.8 meters annually. There is a seasonal cycle especially in the inner area from the river, i.e., with the range of 1 - 4 meters during rainy and dry seasons [3].

GROUNDWATER SIMULATION

The simulation of groundwater movement in the province was conducted by using the models called GMS/MODFLOW [4] and data from pumping test and field survey on water use [5]. The simulation was conducted under the following conditions: specified head in the West, general head conditions in the East, no flow boundary on other sides, pumping rate from the survey data and mesh configuration (2 layers, 2500 grids with size of 1.5 x 2.5 sq.km.) as shown in Fig. 1. The model calibration was conducted to estimate the hydraulic conductivity, transmissivity and pumpage ratio in the steady state and estimate the storage coefficient in the transient state. The calibrated parameters: hydraulic conductivity (K)=70 m/day, tranmissivity (T)=560 m^2/day, Specific storage (S)=0.0034 (1st layer), 0.0015(2nd layer), percentage of pumping= 50%(rainy), 10%(dry), leakage between layer= 2x10exp-6 per day, gave figures with the same order as to the field pumping test results. The simulation of groundwater was then conducted to

(a) verify the calculation results during Jan 95 to Apr. 97,
(b) simulate the groundwater situation next 5 years during May 1997 to Apr. 2002 under 0, 2, 6, 10% pumping rate annual increase and to analyse water balance in the area,
(c) simulate the groundwater situation next 5 years during May 1997 to Apr. 2002 under10, 30, 50% pumping rate annual decrease.

The simulation verification, in general, gave a fairly good trend between the computed and observed water table with the range of 0.6 to 6.1 meters. However some certain points gave significant differences on water table which is attributed to the assumption of average pumpage rate over the area. From the next 5 years simulation, groundwater table under 0, 2, 6, 10% pumping rate annual increase will decrease annually in the range of 0.4 to 1.9 meters. Table 2 gives the water balance analysis results from the calculations. It can be seen from the table that water storage in the aquifer always shows a decrease trend, i.e., the pumping volume is greater than the natural inflow. In case the pumping reduction scheme is imposed, water table in the year 2002 is still lower than level in 1997 by 2 - 4 meters even with 10% pumping reduction and water table in the year 2002 becomes higher than level in 1997 by 0 - 6 meters and 6 - 18 meters with 3% and 5% pumping reduction respectively. The study proposed that the water table will recover to be as in the year 1997 if 5% annual reduction in pumping rate can be imposed, though this high rate reduction scheme for pumping seems to be hardly implemented when considered from the practical aspect.

RECHARGE STUDY AND SIMULATION

To cope with the increase of water demand and groundwater table drawdown, various studies on recharge possibility in Thailand such as well injection [6], recharge rate determination [7], recharge scheme design [8] etc., had been conducted. In the study, a field experimental recharge

was executed to confirm the recharge rate and investigate relevant issues to be prepared before actual implementation and simulation of various recharge schemes were conducted to find the suitable measures in the area.

A recharge basin sized 10 x 50 x 3 meters was excavated and a 6" well was drilled after proper field survey and log drilling to locate the suitable site in order to test the gravity recharge feasibility. Water from a nearby irrigation canal was drawn and filtered by basin bed sand and slow sand filter tank before recharging into recharge basin and well respectively. The recharge rate for basin and well types were found to be 0.34 and 4.95 cm/min respectively. The experimental results in the pilot area satisfactorily proved the effectiveness of recharging by gravity recharge method for the area, however, the main obstacles for implementation are the availability and quality of raw water, groundwater table, rapid growing of grass and sediment clogging [9]. The laboratory experiment on recharge was also conducted to study the relationship of recharge rate and sand grainsize and it is found that the unit recharge rate is affected by the grainsize, distribution of sand and groundwater table [10].

Since in the study area, the drawdown issue takes place in two main locations, i.e., area near the Ping River (Muang District) and inner cultivated area (Zaigarm and Larnkrabu Districts) with different characteristics mainly due to hydrogeological conditions and agricultural practices in dry season, hence the recharge should be implemented by basin recharge in the area near the river and by well injection recharge in the inner area respectively. Simulation on recharge schemes under such conditions was conducted with various percentage of demand increase in order to estimate the recharge rate needed and its impacts. From the simulation results, the influential area from recharge operation is quite limited near the recharge location, i.e. , 2 to 3 kilometers from the recharge location. Fig 3 and Table 2 show the influential area and the increase of water table under the basin recharge scheme of 500,000 m^3/day and under the well injected recharge scheme of 10,000 m^3/day with various increase percentage in pumping rate respectively. As a result, with the recharge rate proposed, groundwater table in the province can still be controlled as in the year 1997 with the pumping increase not more than 10 % annually. The recharge schemes of gravity type with the rate of 500,000 m^3/day such as river bed improvement, retention pond near river etc., and well injected type with the rate of 10,000 m^3/day are then proposed for further more detailed study before actual implementation in order to balance groundwater storage with water demand increase in the province.

CONCLUSIONS AND RECOMMENDATIONS

From the study, the following conclusions and recommendations can be drawn.

1) The movement of groundwater in the Province, from the monitoring data, showed the pattern of moving from the west towards the east and the water table at present in average is lowering with the rate of 1 - 2 meters per year.
2) From the simulation, it is found that groundwater is not balancing, i.e., water pumping out is more that natural recharge which is attributed mainly from agricultural activities in dry season. Proper pumping control should be considered and implemented. To balance the water supply and demand in the province, the reduction in pumping control of 5% annually is recommended.
3) From the recharge field study, gravity recharge scheme can be effectively implemented in the area near the Ping River as long as raw water quantity and quality can be provided. The cautions on site selection, easy routined maintenance and cleaning up basin shape, sediment clean up after excavation should be paid attention during the design and construction phases.
4) Within 10% annual increase in pumping, groundwater table in the Province can be controlled as in the year 1997 if recharge schemes, i.e., 500,000 m^3/day of gravity

recharge near river area and 10,000 m^3/day of well injected recharge for inner area, are implemented.

5) Computer models, GMS and MODFLOW, are shown to be good tools to handle huge amount of hydrogeological data and groundwater simulation, though the effect of mesh size and mesh configuration for recharge calculation is still needed improvement.

REFERENCES

1. Mineral Resources Department (1999), Preliminary Study on Groundwater Recharge Design for Environment Conservation, Inception Report, prepared by Chula Unisearch, Chulalongkorn University, June (in Thai).
2. Public Works Department (1998), Groundwater Conservation and Rehabilitation in Kampheng Phet Province, Final Report, prepared by Chula Unisearch, Chulalongkorn University, Apr. (in Thai).
3. Chaiyuth S., Sucharit K.(1998), The evaluation of Groundwater Conservation and Rehabilitation Project in Kampheng Phet Province, Water Resources Eng. Dept. Chulalongkorn University, Dec. (in Thai).
4. Sucharit K., Chokchai S.(1999), Application of GMS/MODFLOW in Groundwater Simulation, Proc. Nat. Conf. of Civil Eng., Engineering Institute of Thailand, Mar., pp. 26-34 (in Thai).
5. Chindasanguan, S.(1997), Simulation of Groundwater Condition in Kampheng Phet Province, Master Thesis, Graduate School on Water Resources Eng., Chulalongkorn University (in Thai).
6. Ramnarong V.(1988), Subsurface Injection of Storm Water Runoff into an Underground Storage of Bangkok, Proc. Int. Sym. on Artificial Recharge of Groundwater, Anaheim, California, Aug. 23-27, pp,. 145-156.
7. Sucharit K.(1999), Determination of Groundwater Gravity Recharge Rate, Proc. Sym. Mineral, Energy and Water Resources of Thailand: Towards the Year 2000, Oct 28-29, Chulalongkorn University, Thailand.
8. Mineral Resources Department (1999), Potential Water Resources Development for Industrial Use in Bangkok Metropolitan Area, Draft Final Report, prepared by Chula Unisearch, Chulalongkorn University, July (in Thai).
9. Sucharit K., Chaiyuth S.(1999), Experimental Results of Basin Recharge Project in Kamphaneg Phet Province: Thailand, Proc. Int. Conf. on Water Resources Management in Intermontane Basin, Chiengmai University, Thailand, Feb , pp. 261-275.
10. Thirachit C.(1998), The Relationship of Gravity Groundwater Recharge Rate and Grainsize Distribution, Master Thesis, Graduate School on Water Resources Eng., Chulalongkorn University, (in Thai).

ACKNOWLEDGEMENT

The authors would like to express sincere gratitude to the Division of Groundwater Development, Public Works Department, Ministry of Interior, for financing the project execution and for providing valuable data and field assistances. Special thanks are also extended to the faculty staff, graduate students namely, Mr. Sont Chidsanguan, Mr. Tirachit Chitraporn from the Water Resources Engineering Department, Chulalongkorn University in conducting field and laboratory experiments, monitoring and assisting in the preparation of the study report.

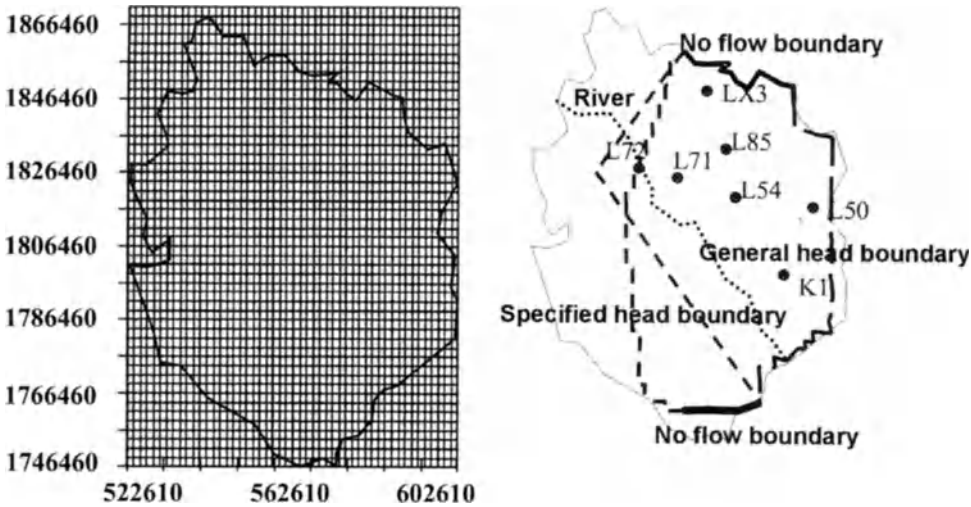

Fig 1. Grid, boundary conditions and reference stations

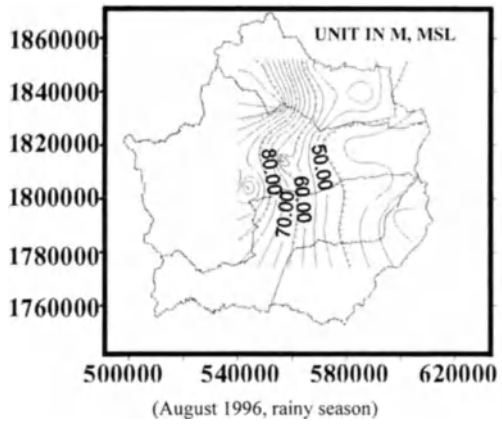

Fig 2. Groundwater table in the Province (rainy season)

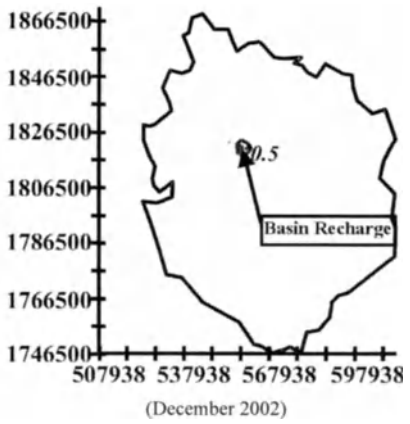

Fig 3. Water Table increase after recharge (December 2002)

Table 1. Water Balance Analysis Results

	Normal State (0% increase)		5% Pumpage Reduction	
IN (5 years)	Storage	= 5.94850E+08	Storage	= 5.27340E+08
	Constant Head	= 8.43820E+08	Constant Head	= 8.15270E+08
	Wells	= 0.00000E+00	Wells	= 0.00000E+00
	Recharge	= 7.28040E+08	Recharge	= 7.28040E+08
	River Leakage	= 2.28520E+08	River Leakage	= 1.89937E+08
	Head Dep Bounds	= 1.99860E+07	Head Dep Bounds	= 1.24550E+07
	Total In	= 2.41520E+09	Total In	= 2.27250E+09
OUT (5 years)	Storage	= 5.45030E+08	Storage	= 5.13210E+08
	Constant Head	= 7.87070E+07	Constant Head	= 8.00140E+07
	Wells	= 8.48970E+08	Wells	= 7.21630E+08
	Recharge	= 0.00000E+00	Recharge	= 0.00000E+00
	River Leakage	= 7.94530E+08	River Leakage	= 8.06730E+08
	Head Dep Bounds	= 1.47980E+08	Head Dep Bounds	= 1.50900E+08
	Total Out	= 2.41520E+09	Total Out	= 2.27250E+09
IN-OUT/year	Storage	= 9.96400E+06	Storage	= 2.82600E+06
	Constant Head	= 1.53023E+08	Constant Head	= 1.47051E+08
	Wells	=-1.69794E+08	Wells	=-1.44326E+08
	Recharge	= 1.45608E+08	Recharge	= 1.45608E+08
	River Leakage	=-1.13202E+08	River Leakage	=-1.23359E+08
	Head Dep Bounds	=-2.55988E+07	Head Dep Bounds	=-2.76890E+07
	In-Out	= 0.00000E+00	In-Out	= 0.00000E+00

Table 2. Water Table Change due to Recharge

Annual Pumping Increase Percent	year	Water Table Increase (m)						
		Reference Stations						
		L72	L71	L54	L50	LX3	L85	K1
0%	1998	0.02	0.33	1.75	0.354	0.18	0.80	0.17
	2000	0.01	0.48	2.26	1.05	0.58	1.31	0.48
	2002	0.03	0.57	2.42	18.22	0.71	1.05	0.60
2%	1998	0.01	0.32	1.75	0.45	0.21	0.67	0.16
	2000	0.03	0.57	2.27	1.04	0.66	1.29	0.40
	2002	0.01	0.57	2.42	1.20	0.70	1.45	0.60
6%	1998	0.02	0.46	1.76	0.46	0.18	0.80	0.16
	2000	0.01	0.52	2.27	1.04	0.58	1.31	0.50
	2002	0.01	0.57	2.42	1.21	0.66	1.46	0.60
10%	1998	0.01	0.31	1.75	0.45	0.17	0.79	0.16
	2000	0.01	0.51	2.26	1.05	0.58	1.30	0.48
	2002	0.01	0.58	2.43	1.21	0.69	1.45	0.61

Remarks: Basin recharge rate = 500,000 m^3/day and injection recharge rate = 10,000 m^3/day.

A Simulation Study on the Heat and Vapor Transfer at the Ground Surface

Vu Thanh Ca

Department of Civil and Environmental Engineering, Faculty of Engineering, Saitama University, Urawa, Saitama 338-8570, Japan.

ABSTRACT. A numerical model is developed for the simulation of heat and moisture transfer above and below the ground surface. In the soil, the equations coupling the processes of heat and moisture transfer are solved to get the temperature and the moisture content at the ground surface, which are necessary for the computation of the heat and moisture fluxes. The sensible heat flux and evaporation rate at the ground surface are evaluated based on the bulk type formulas and by an improved k-ε model for the transport of momentum, heat and water vapor in the atmospheric surface layer. The accuracy of the numerical model was verified using field experimental data on the temperature and water content at the soil surface and different depths under the ground surface. Based on the numerical model, the accuracy of the flux-gradient method for the prediction of evaporation from the ground surface is investigated.

KEY WORDS: atmospheric surface layer, evaporation resistance, flux variance approach, surface-layer similarity, k-ε model.

INTRODUCTION

The study of heat and moisture transfer at the ground surface, or in other way, the sensible heat transport and evaporation, is very important for an accurate weather, climate and water resources forecasting. The flux-variance approach for the prediction of sensible heat transport and evaporation rate is based on the assumption of a dynamical similarity between the momentum, heat and water vapor transport near the ground surface. This implies a similarity in the distributions of the source or sink at the ground surface for the momentum, heat and water vapor. This assumption is usually satisfied for a sufficiently wet porous ground surface under heating, where exists an abundant source for water vapor. However, when the ground surface becomes drier, the evaporation rate may decrease significantly and in many occasions, approach zero, accompanying an increase in the ground surface temperature. It means that there is a significant difference in the vertical distributions of air temperature and moisture content; and this may lead to a considerable error in the prediction of the evaporation rate using the similarity law

In many field experiments, sensible heat and latent heat fluxes at the ground surface are evaluated based on wind velocity, humidity and air temperature, measured at a reference height, and humidity and temperature at the ground surface. In the flux-variance method, this is carried out using the Monin-Obukhov similarity law with the assumption of negligible horizontal advection. This assumption is usually not satisfied since the surface samples in the experiments are not wide enough. Thus, to reduce possible errors caused by the violation of this assumption, the reference height must be lower enough.

Another difficulty for an accurate prediction of the evaporation rate at the ground surface is the method for evaluation of water vapor density at a dry ground surface. Many models for the coupling of under ground heat and moisture flow [1,7,8] can compute the matric potential at the ground surface. Then, with the assumption of a local equilibrium between liquid and vapor phases

within surface pores, the vapor density $\rho_{vs}(T_s)$ at the ground surface temperature T_s and relative humidity h in surface pores can be expressed as

$$\rho_{vs}(T_s) = \rho_0(T_s)h, \qquad h = \exp(\psi g / R_w T_{ks}) \tag{1}$$

where $\rho_0(T_s)$ is the saturated vapor density at temperature T_s, ψ the water potential at the ground surface, g the gravitational acceleration, R_w the gas constant for water vapor and T_{ks} the absolute temperature of the ground surface.

Kondo and Saigusa [4] pointed out that although equation (1) is adequate for calculating the relative humidity of the air immediately above the water surface within soil pores, its extension for the calculation at the ground surface is questionable. If the surface is dry, there will be an imbalance in the supply of vapor from the surface and its upward diffusion. Thus, the assumption on a local equilibrium between the liquid and vapor phases is violated, and equation (1) is not valid for the evaluation of relative humidity at the ground surface. According to Lee and Pielke [5], the value of h computed by Eq. (1) will be overestimated when the soil moisture availability drops to around the soil wilting point. This may cause another error in the computation of the evaporation rate for any flux-variance method.

The purpose of this study is to investigate possible errors in the computation of the evaporation rate at the ground surface with the similarity approach under different conditions. The study is conducted based on a numerical model, coupling under ground heat and moisture transfer and the transfer of momentum, heat and moisture in the atmospheric surface layer. The numerical model can also provide the wind velocity, potential air temperature and humidity at a reference height, closed enough to the ground surface to minimize the influence of advection on the evaluation of sensible and latent heat using the flux-variance method.

NUMERICAL MODEL

The numerical model in this study comprises two models: a model for the coupling of vertical one-dimensional subsurface heat and moisture transfer [1] and a model for the transport of momentum, heat and moisture transfer in the atmospheric surface layer.

Coupling the subsurface heat and moisture transfer

The vertical one-dimensional subsurface heat and moisture transfer model, employed in this study is the same as that in Asaeda and Vu [1]. The governing equations of the model are as follows.
Equation for subsurface water transfer

$$\left[\left(1-\frac{\rho_v}{\rho_l}\right)\frac{\partial\theta}{\partial\psi}+\frac{\theta_a}{\rho_l}\frac{\partial\rho_v}{\partial\psi}\right]\frac{\partial\psi}{\partial t}+\left[\left(1-\frac{\rho_v}{\rho_l}\right)\frac{\partial\theta}{\partial T}+\frac{\theta_a}{\rho_l}\frac{\partial\rho_v}{\partial T}\right]\frac{\partial T}{\partial t}$$

$$=\frac{\partial}{\partial z}\left[\left(K+D_{\psi v}\right)\frac{\partial\psi}{\partial z}+\left(D_{Tv}+D_{Ta}\right)\frac{\partial T}{\partial z}\right]+\frac{\partial K}{\partial z}, \tag{2}$$

and the accompanying equation for heat transfer

$$\left[C+L_e\theta_a\frac{\partial\rho_v}{\partial T}-\left(\rho_l W+\rho_v L_e\right)\frac{\partial\theta}{\partial T}\right]\frac{\partial T}{\partial t}+\left[L_e\theta_a\frac{\partial\rho_v}{\partial\psi}-\left(\rho_l W+\rho_v L_e\right)\frac{\partial\theta}{\partial\psi}\right]\frac{\partial\psi}{\partial t}$$

$$=\frac{\partial}{\partial z}\left[\lambda\frac{\partial T}{\partial z}+\rho_l\left(L_e D_{\psi v}+gTD_{Ta}\right)\frac{\partial\psi}{\partial z}\right]-C_l q_m\frac{\partial T}{\partial z}, \tag{3}$$

where ρ_l is the density of liquid water; θ and θ_a are respectively the underground liquid water and air content; T is the ground temperature; $D_{\psi v}$ and D_{Tv} are the water potential head diffusivity and

temperature diffusivity of vapor in the ψ-T system, respectively; D_{Ta} is a transport coefficient for absorbed liquid water flow due to thermal gradient; K is the hydraulic conductivity; λ accounts for the combined effects of simple Fourier heat diffusion and latent heat transport by temperature-induced vapor diffusion; L_e is the latent heat of vaporization of water; C_l is the specific heat of liquid water; g is the gravitational acceleration; q_m is the vertical flux of water vapor; t is time; and z is the vertical coordinate.

Neglecting the sensible heat transport by the evaporated water vapor, the ground surface boundary conditions for equations (2) and (3) are as

$$q_m = e, \qquad -\lambda \frac{\partial T}{\partial z} = S(1-\alpha) + R_{Ln} - H - L_e e, \tag{4}$$

where e is the evaporation rate at the ground surface; S and R_{Ln} are respectively the total solar radiation and net longwave radiation flux at the ground surface; α is the short wave reflectivity of the surface; and H is the sensible heat flux at the surface.

All coefficients in Eqs. (2) and (3), and the total solar radiation and net longwave radiation at the ground surface are evaluated follows Asaeda and Vu [1].

The transfer and momentum, heat and moisture in the atmospheric surface layer

The model for the momentum, heat and moisture transfer in the atmospheric surface layer used in this study is a k-ε model. The Reynolds averaged equations, governing the turbulent transport of momentum, heat and moisture in the atmospheric surface layer over an assumed horizontally homogeneous ground surface, are as

$$\frac{\partial U}{\partial t} = \frac{\partial}{\partial z}\left(\nu_t \frac{\partial U}{\partial z}\right), \tag{5};$$

$$\frac{\partial T_p}{\partial t} = \frac{\partial}{\partial z}\left(\kappa_t \frac{\partial T_p}{\partial z}\right), \tag{6};$$

$$\frac{\partial \rho_v}{\partial t} = \frac{\partial}{\partial z}\left(\kappa_t \frac{\partial \rho_v}{\partial z}\right) \tag{7};$$

$$\frac{\partial k}{\partial t} = \frac{\partial}{\partial z}\left(\frac{\nu_t}{\sigma_t}\frac{\partial k}{\partial z}\right) + P + G - \varepsilon, \tag{8};$$

$$\frac{\partial \varepsilon}{\partial t} = \frac{\partial}{\partial z}\left(\frac{\nu_t}{\sigma_\varepsilon}\frac{\partial \varepsilon}{\partial z}\right) + \frac{\varepsilon}{k}\left[C_{1\varepsilon}P + (1-C_{3\varepsilon})G - C_{2\varepsilon}\varepsilon\right] \tag{9};$$

$$P = \frac{1}{2}\nu_t\left(\partial U/\partial z\right)^2, \tag{10a};$$

$$G = -g\kappa_t\left(\beta \partial T_p/\partial z + 0.61\partial \rho_v/\partial z\right), \tag{10b};$$

$$\nu_t = C_\mu k^2/\varepsilon, \tag{11a};$$

$$\kappa_t = \nu_t/P_{rt}. \tag{11b}$$

In Eqs. (5) to (11), U and T_p are the ensemble averaged horizontal wind velocity and potential temperature, respectively; ν_t and κ_t are respectively the eddy viscosity and diffusivity; k and ε are respectively the turbulent kinetic energy and its dissipation rate; σ_t(=1), σ_ε(=1.33), $C_{1\varepsilon}$(=1.44), $C_{2\varepsilon}$(=1.92) and $C_{3\varepsilon}$(= $C_{1\varepsilon}$ for stable stratification, and =0 for unstable stratification) are closure coefficients; and P_{rt} is the turbulent Prandtl number. In this study, the traditional standard k-ε model is improved based on the work of Launder [5] for the computation under stratification. With the assumption of near-equilibrium shear flow, where transport effects on vertical fluxes can be negligible, and isotropic dissipative motions, Eqs. (12) and (13) are obtained

$$C_\mu = \frac{\phi\left(1.59 - 5.22R_f\right)\left(0.53 - 0.94R_f\right)}{\left[1.59 + R_f\left(3\phi + 1.5\phi\ \ P_{rt} - 5.22\right)\right]\left(1 - R_f\right)}, \qquad P_{rt} = P_{rt0}\frac{1.59 - R_f\left(1.5\phi_T + 2.82\right)}{1.59 + R_f\left(3\phi - 5.22\right)} \tag{12}$$

where ϕ_T =1/3.2, ϕ=0.2, and R_f is the Flux Richardson number, defined as

$$R_f = \beta g \frac{1}{P_{rt}} \frac{\partial T_{pv}/\partial z}{\left(\partial U/\partial z\right)^2} \tag{13}$$

The boundary conditions for Eqs (5)–(9) are as follows. The values of wind velocity, air temperature and vapor density at every time step are specified at the top of the computational domain while the turbulent kinetic energy and its dissipation rate at this point are interpolated

from their respective values in the computational domain. A no-slip boundary condition and a zero vertical gradient of turbulent kinetic energy are applied at the ground surface while the turbulent kinetic energy dissipation rate is evaluated based on the Kolmogorov hypothesis; the potential temperature is set equal to the ground surface temperature; and the vapor density is evaluated using Eq. (1). The momentum, sensible heat and latent heat fluxes at the ground surface are evaluated using the wind velocity U_1, potential temperature T_{p1} and vapor density ρ_{v1} at the first computational mesh above ground surface as

$$\tau_0 = -\rho_a u_*^2, \quad u_* = U_1\kappa/\left[\ln(z_1/z_0) - \Phi_m(z_1/L)\right], \quad L = \frac{-\rho_a u_*^3}{\kappa g\left(H/C_p T_{pa} + 0.61e\right)} \tag{14}$$

$$H = \rho_a C_p u_* T_{p*}, \qquad T_{p*} = (\kappa/P_{rt0})(T_{ps} - T_{p1})/\left[\ln(z_1/z_{0t}) - \Phi_t(z_1/L)\right] \tag{15}$$

$$L_e e = L_e \rho_a u_* \rho_{v*}, \qquad \rho_{v*} = (\kappa/P_{rt0})(\rho_{vs} - \rho_{v1})/\left[\ln(z_1/z_{0v}) - \Phi_v(z_1/L)\right] \tag{16}$$

where z_0, z_t and z_m are respectively the roughness length for momentum, heat and vapor; subscripts s and 1 respectively denote values at the surface and at a reference height z_1; and the stability functions for momentum, heat and vapor for unstable stratification are as [2]

$$\Phi_m = \ln\left[\frac{(1+x_m)^2(1+x_m^2)}{(1+x_{0m})^2(1+x_{0m}^2)}\right] - 2\arctan(x_m) + 2\arctan(x_{0m})$$

$$\Phi_h = 2\ln\left[\frac{(1+x_t^2)}{(1+x_{0t}^2)}\right], \qquad \Phi_v = 2\ln\left[\frac{(1+x_v^2)}{(1+x_{0v}^2)}\right], \tag{17}$$

and for stable stratification

$$\Phi_m = -\beta_m(\zeta - \zeta_m), \qquad \Phi_t = -\beta_t(\zeta - \zeta_t), \qquad \Phi_v = -\beta_v(\zeta - \zeta_v) \tag{18}$$

Numerical scheme

A finite element scheme is adopted for the spatial discretization of Eqs. (2) and (3) in the soil domain. A smallest mesh of 1cm is used near the ground surface, where the variables change most rapidly. The mesh increases with the increase of depth. A finite volume scheme is employed for the spatial discretization of Eqs. (5)-(9) in the air domain. A smallest mesh size of 3 cm is used near the ground surface; and the mesh size increases linearly with the distance from the ground surface. A second order accurate Crank – Nicholson scheme is used for the time discretization. Since various parameters in Eqs. (2) - (3) and Eqs. (5)–(18) are functions of other unknown variables, an iterative computation is needed.

COMPUTATIONAL RESULTS AND DISSCUSSIONS

The numerical model has been verified with observed data on the soil temperature and water content at the ground surface and different depths, obtained from a field experiment in Tsukuba City, Japan. The model has also been verified with observed data on the temperature and moisture content at various porous pavement samples, obtained from field experiment in Kuki City, Japan. Due to the page limitation, results of the verification process are not presented in this report. However, results of the computation (not shown) reveals that the model is capable of simulating the heat and water vapor transfer at the ground surface with acceptable accuracy. Thus, the model is used to investigate the vertical distribution of potential air temperature and water vapor density near the ground surface, and the accuracy of the flux-variance method for the computation of the evaporation rate at a bare soil surface.

The surface used in the computation was assumed as bare soil, which resembles the bare soil

surface in the field experiment in the Tsukuba City. The height of roughness element is assumed of 0.7cm, which corresponds to a momentum roughness length z_{0m} of 1mm. The roughness length for heat and water vapor are evaluated based on z_{0m} and the roughness Reynolds number, following [2,3]. A wind velocity of 1.5m/s at the height of 1.5 m above ground surface is assumed unchanged with time for whole computational period. The time variations of air temperature and relative humidity used in the computation are shown in Fig. 1. The computation was carried out for two cases. Initial soil surface volumetric moisture contents of 0.143 and 0.01 were assumed for case 1 and case 2, respectively. The porosity of the soil is assumed as 0.33.

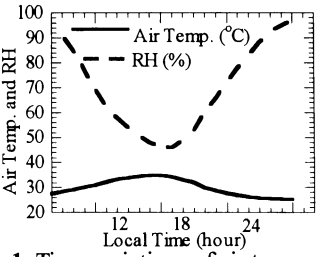

Fig. 1. Time variations of air temperature and wind velocity

Fig. 2 and Fig. 3 respectively show the vertical distributions of potential temperature and water vapor density for case 1 at different times. From Fig. 3, it can be seen that at 12 a.m., the water vapor density at the soil surface reaches more than 0.035(kg/kg), and there is a very steep gradient of water vapor density just at the soil surface. The vertical distribution of potential air temperature in Fig. 2 shows that it is significantly different from that for the water vapor density.

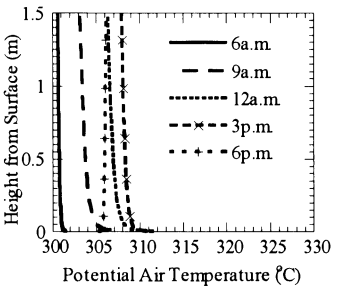

Fig. 2. Vertical distribution of potential air temperature for case 1.

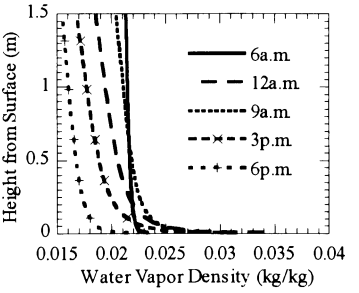

Fig. 3. Vertical distribution of water vapor density for case 1.

Fig. 4 shows the computed energy budget at the ground surface for case 1. As in the figure, the latent heat flux evaluated by equation (16) using the water vapor density at the soil surface and at 1.5m height reaches its maximum of 700W/m^2. Thus, it is evident that the water vapor density at the ground surface, evaluated based on equation (1), and consequently the evaporation rate at the ground surface, are over estimated. The overestimation of the sensible heat flux leads to a very cool ground surface even at noon. It is noted that Eqs. (15)-(16) for the computation of sensible heat and latent heat fluxes are based on an assumption of steady vertical distribution of wind velocity, air temperature and humidity, which is not satisfied since the temperature and vapor density at the ground surface and upper boundary change continuously. Theoretically, the error caused by this assumption is smaller with smaller reference height. To investigate this kind of errors in more details, two reference heights were used in the computations. Computed results show that ratio of the sensible heat flux, computed by Eq. (15) using the potential air temperature and wind velocity at two reference heights of 1.5m and 1.5cm is 1.24. At the same time, ratio of the latent heat fluxes, computed by Eq. (16)

using the two reference heights, is 1.29. As stated previously, there is an overestimation of the latent heat flux if the reference height of 1.5m is used. Thus, it seems that the values of sensible heat and latent heat, evaluated using wind velocity, air temperature and humidity at the reference height of 1.5cm is better. Also, as discussed previously, with the assumption of negligible horizontal advection, lower reference height can produce more accurate results. These findings should be investigated further more using detailed field experiment data.

To improve the computation for the latent heat flux at the ground surface, a factor of the form $(\theta/\theta_{sat})^m$ (where θ_{sat} is the saturated volumetric moisture content at the ground surface), accounting for the resistance to evaporation at the ground surface is multiplied to the right hand side of Eq. (16). Results of the computation show that the value of m=2 provides the best fit with the experiment data.

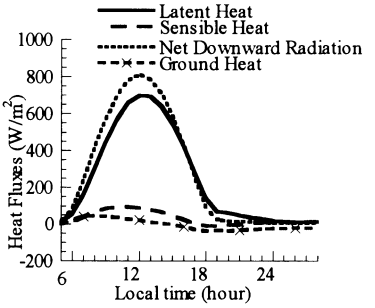

Fig. 4. Energy budget at the ground surface without evaporation resistance (case 1).

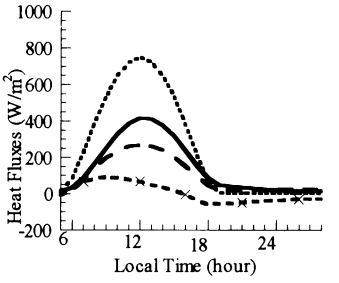

Fig. 5. Energy budget at the ground surface with evaporation resistance (case 1).

The computed energy budget at the ground surface with accounting for the evaporation resistance shown in Fig. (5) reveals that reasonable results are obtained.

Computational results for the dry surface also confirms the above findings.

CONCLUSION

The accuracy of the flux-variance method for the computation of the sensible and latent heat fluxes at the ground surface is investigated by employing a numerical model. It was found that for a dry ground surface, the resistance to evaporation must be accounted for in the computation of the evaporation rate at the ground surface using this method.

REFERENCES

1. Asaeda T. and Vu T.C. (1993) Boundary-Layer Meteorol., 65, 159-179.
2. Brutsaert W. (1982) Evaporation into the Atmosphere. Theory, History and Application. D. Reidel Pub. 299 pp.
3. Hignett P. (1994) Boundary-Layer Meteorol., 68, 225-236.
4. Kondo J. and Saigusa (1994) J. Meteor. Soc. Japan, 72(3), 413-420.
5. Launder B.E. (1975) J. Fluid Mech., 67, 569-581.
6. Lee T.J. and R.A. Pielke (1992) J. Appl. Meteor., 31, 480-484.
7. Milly, P.C.D. (1984) Water Resour. Res., 20,(8), 489-498.
8. Phillip J.R. (1957) J. Meteor., 14, 354-366.
9. Ye Z. and R. Pielke (1993) J. Atmos. Sci., 32, 1248-1258.

An Engineering Approach towards Appropriate Hydrological Water Cycle in Urban Areas : First Report

Masahiro Imbe[1],Yutaka Nakano[1],Noriyuki Nakashima[2],Sigeru Nakamura[2] and Daikichi Ogawada[2]

[1]Association for Rainwater Storage and Infiltration Technology, 3-7-1, Kojimachi, Chiyoda-Ku, Tokyo 102-0083, Japan
[2]Nippon Koei Co. Ltd., 5-4, Kojimachi, Chiyoda-Ku, Tokyo 102-8583, Japan

Abstract. This paper presents an engineering approach for planning comprehensive mitigation measures to improve the hydrological water cycle deteriorated due to urbanization. The hydrological water cycle is closely related to the aqua environment which supports sustainable city activities, creates a natural amenity, and derives the friendly relationship between residents and water. In order to study this in more detail, the Shingasi River basin was selected as a study area, which is located in the suburbs of Tokyo metropolitan region and has a catchment area of 390 km^2. The practical study was conducted based on the standard investigative procedure. The hydrological water cycle was evaluated for the past and present condition and its condition in the future was predicted by means of a numerical method. The goal of a project for implementing the mitigation measures should be set up carefully to be understood by both government and local residents. In order to satisfy the project goals, various measures including rainwater storage and infiltration facilities were taken into account. The co-operative system was proposed for getting consensus among the governments and the local residents. It is also pointed out that great effort should be paid for creating the positive activity of the organizers and interpreting the engineering assessment to be understandable for all the relevant members.

Key words. hydrological water cycle, water environment, engineering assessment, consensus building, comprehensive master plan

INTRODUCTION

Urbanization generally boosts expansion of urban areas, improvement of lifestyles, high population density and high grade of land utilization. Those urbanization processes have resulted in an expansion of impermeable areas such as roofs and pavements, an increase in water demand, an increase in industrial and domestic waste water and a reduction of water surface areas and green lands. The phenomena tend to distort the appropriate hydrological water cycle and bring about the following six issues to be solved [1] : 1) Increase of ordinary water discharge, 2) Flood control, 3) Conservation and development of water resources, 4) Conservation and revival of ecological system, 5) Pollution control and 6) Improvement of heat environment.

In order to implement a policy for solving these issues, the Ministry of Construction in Japan set up a committee to draw up a manual for planning the renewal of hydrological water cycle in urban areas. The paper [2] explains the design concept authorized by the committee which was finally involved into the manual [3]. According to the paper [2], the word of "hydrological water cycle" is useful for the discussion among the people with different backgrounds to plan the comprehensive measures to improve the aqua-environment. The paper [2] also proposes an investigation procedure as shown in Fig.1.

Recently, an interim report "How should an appropriate water cycle be in river basins." [4], proposed in July,1998 by the sub-committee of water cycle, the River Council for river control, provoked the necessity of a sustainable water cycle. This report [4] also pointed out that comprehensive master plans for appropriate water cycle should be urgently drafted for urbanized areas which suffer from serious problems concerning the deterioration of water cycle.
This paper presents only the preliminary consideration applied for the study area in order to draft a comprehensive master plan for an appropriate water cycle. This study is supposed to continue in order to finalize the comprehensive master plan.

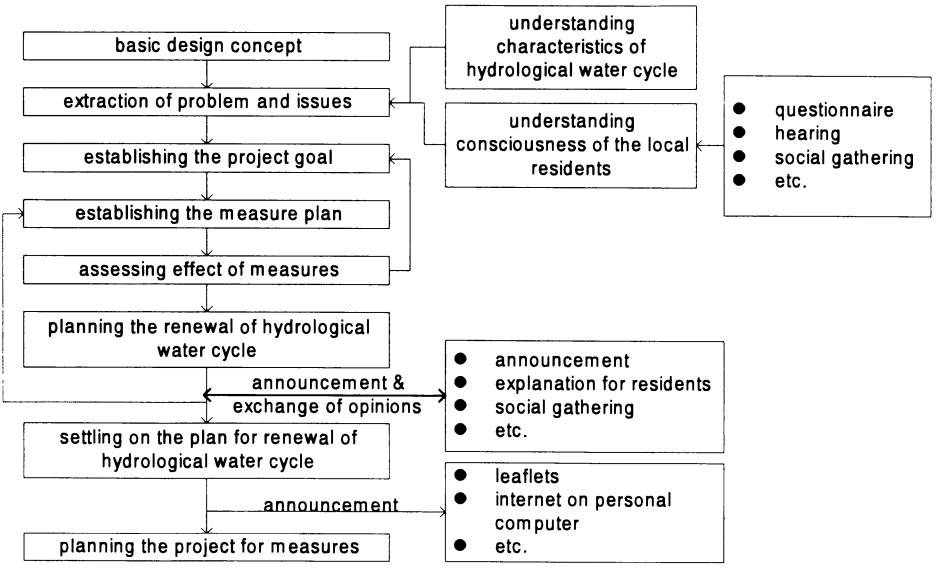

Fig.1. Investigation procedure for planning the renewal of hydrological water cycle

OUTLINE OF STUDY AREA

The Shingasi River of the study area is a tributary of the Arakawa River and runs northeast of Tokyo. Most of the catchment area belongs to Saitama prefecture and has been rapidly urbanized since the 1950s when the Tokyo metropolitan area widened to involve this area. The Shingasi River has five major tributaries namely Shirako River, Kurome River, Yanase River, Sunagawabori River, and Furo River. The basic urbanization data are tabulated in Table 1.

Table 1. Basic urbanization data for the Shingasi River Basin (as of 1990)

Items	Shirako	Kurome	Yanase	Sunagawabori	Furo	Others	Total
Basin Area (km^2)	25.0	37.6	95.5	44.0	56.6	131.2	389.8
River Length (km)	10.0	19.1	26.8	17.7	17.0	20.1	34.6
Population (1000 persons)	294	277	527	170	163	471	1902
Ratio of Urbanization (%)	59.6	44.4	40.9	25.7	28.6	39.5	38.5
Ratio of Sewerage Propagation (%)	91.7	77.6	74.3	71.1	55.5	77.0	76.2

The Shingasi River Basin comprises two different areas, lowland and terrace. The lowland is of an alluvium spread along the main stream. The terrace occupies a large area along the tributaries. The gradient of the basin is 1/1000 to 1/4000 in the main stream areas, and 1/100 to 1/400 in the tributary areas.

The lowland areas are covered with silty soil. The terrace areas are covered with a layer of the Kanto loam which is 2 to 10 meters thick with a gravel layer approximately 30 meters thick underneath. Groundwater levels are generally low, about 5 to 10 meters below the surface. The direction of the groundwater aligns with the configuration of the land. Saturated hydraulic conductivities are approximately 1×10^{-3} to 5×10^{-2} cm/s in the Kanto loam, 1×10^{-4} cm/s in the silt and 1×10^{-2} cm/s in the gravel. Fig.2 shows the distribution of the contour line of the unconfined groundwater and the saturated hydraulic conductivities of the surface soil.

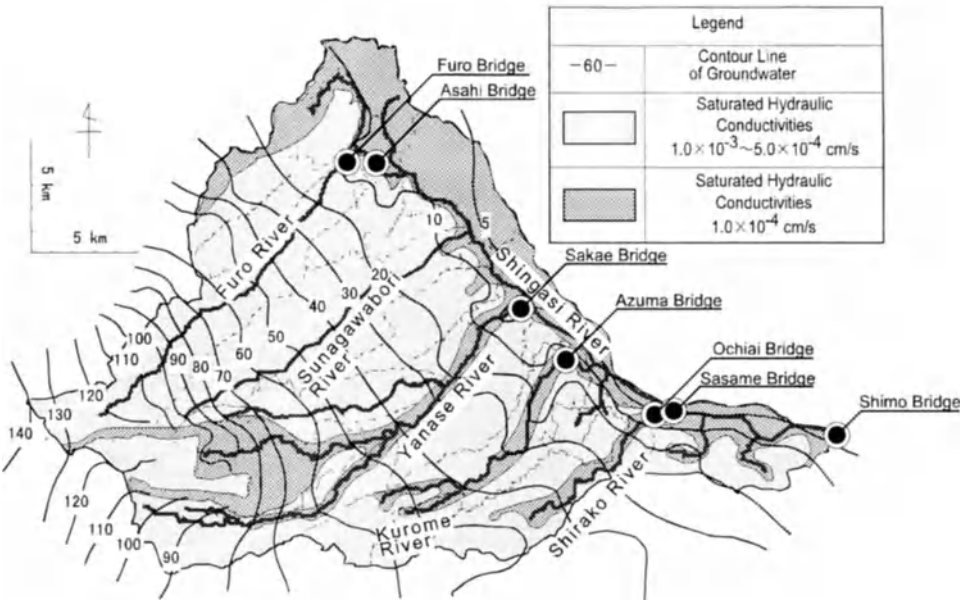

Fig.2. Contour lines of the unconfined groundwater and saturated hydraulic conductivities of the surface soil

EXTRACTON OF PROBLEMS AND ISSUES

Changes of water cycle in the Shingasi River Basin, from the past to the present as well as changes predicted in the future, have been estimated by focusing on the influential factors. The quantitative estimation was conducted by applying the simulation model which represents the physical characteristics of the natural flow mechanism of a river basin [5]. The past refers to around the year 1945 when the basin was assumed to be in a natural state. The future is supposed to be the year 2025 when urbanization will have further progressed.

Increase of peak flood flow ; Due to the expansion of impermeable areas and the improvement of urban storm drainage systems, the present peak flood flow is estimated to be 1.5 times that in 1945 and it is predicted to increase in the future as shown in Fig.3(a).

Increase of water demand ; Water transmitted from outside of the basin is significant due to the industrial and living uses. In the future, all the water supply is predicted to rely on the transmitted water from outside of the basin and it is equivalent to the water volume of the precipitation inside this area as shown in Fig.3.(b).

Deterioration of water quality ; Due to the discharge of waste water, the water quality of the river has been deteriorated as shown in Table.2. The river water used to be utilized for the agricultural and living use but not now. In proportion to the deterioration of water quality, the area for habitat of animals and plants is decreased and the river has already lost the function as the water amenity for the local residents.

Decrease of base runoff ; The decrease of rainwater infiltration and the bypass of the sewerage system have caused the decrease of base runoff as shown in Fig.3.(c). In addition to the absence of water amenity, the utilization of water for emergency has become difficult.

Decline of groundwater level and dry-up of spring water ; Excess pumping of groundwater lowers the groundwater level and causes ground subsidence. In addition to the excess pumping, the decrease of rainwater infiltration dries up spring water and reduces groundwater flow into the

rivers. Fig.3.(d) shows the change in groundwater level and Fig.3.(e) shows the change in spring water discharge.

Change of climate ; The decrease of green land and water surface (marsh, river etc.) and the increase of exhaust heat cause the change in heat environment. Fig.3.(f) shows the change in evaporation quantity.

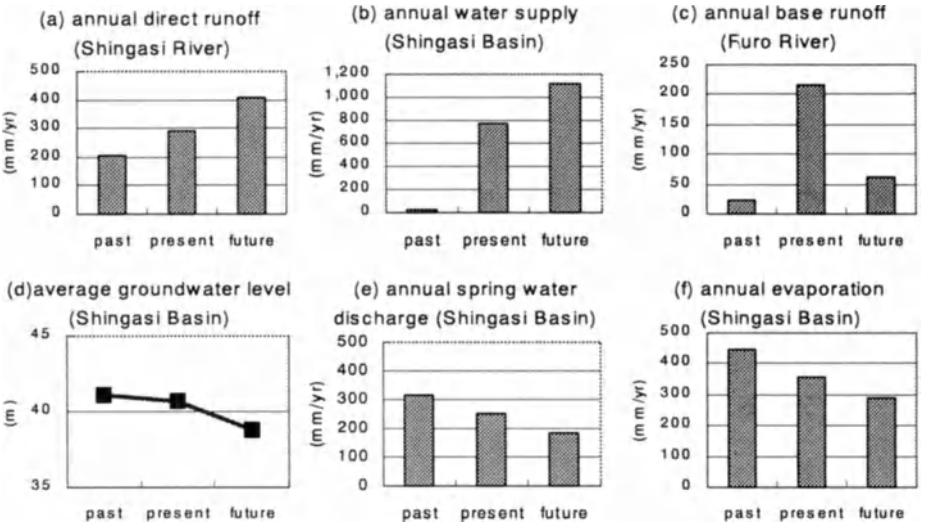

Fig.3. Transition of hydrological quantity and quality from past to future

Table 2. Water quality (Biochemical Oxygen Demand : BOD) of dominant rivers in Shingasi River Basin

name	observation point	observed value(mg/l)
Furo River	Furo Bridge	28.7
Yanase River	Sakae Bridge	11.2
Kurome River	Azuma Bridge	12.0
Shirako River	Ochiai Bridge	6.4

name	observation point	observed value(mg/l)
Shingasi River	Asahi Bridge	9.1
	Sasame Bridge	8.0
	Shimo Bridge	6.4

BASIC IDEA FOR SETTING UP PROJECT GOALS

Before setting up the various measures for improving the water cycle, appropriate project goals should be set based on the extracted problems and issues. The viewpoints for the desirable image of the catchment area can be classified into two types. One is the effect directly derived by the improvement of water cycle and the other is the effect indirectly derived. In other words, one is the quantitative index for the amount of water or the water quality such as water discharge, groundwater level, biochemical oxygen demand (BOD) etc., which is rather an engineering approach. The other is the environmental condition related with aqua-culture, ecological system, water amenity etc., which is more understandable for ordinary inhabitants in spite of the difficulty for the quantitative estimation. It is very important to explain the relationship between the improvement of water cycle and the life of inhabitants and to present project goals that we understandable for not only engineers but also ordinary inhabitants.

It is necessary to consider various viewpoints such as the past condition, the intention of inhabitants, the political goals and the ability of implementation, etc., to set up the appropriate target values.

Table 3. Relation between available measures and quantitative effects

Available Measures \ Quantitative Effects		flood discharge	influential factor: quantity of infiltration	discharge and quality of ordinary	influential factor: quantity and quality of sewage	influential factor: quantity and quality of treated water	influential factor: quantity and quality of spring water	influential factor: quantity of water intake from river	water demand and supply	groundwater level and spring water discharge / quality	influential factor: quantity and quality of waterworks	influential factor: quantity of leakage from	influential factor: ground water quantity of pumping water from	influential factor: seapage into sewerage quantity of groundwater	influential factor: quantity and quality of ground water flow through a boundary of basin	quantity of evapotranspiration
river improvements	improvement of river channel	○														
	regulating reservoir	○														
	natural river channel bond						○				○					
	diluent flume			○												
	clarification of river or pond directry			○												
	effective utilization of river water			○				○					○			
sewerage improvements	improvement of rainwater drinage	○												○		
	improvement of sewerage system					○								○		
	propagation of advanced treatment					○										
	effective utilization of treatment water					○										
	renewal of sewer channel					○	○							○		
rainwater storage and infiltration	propagation of rainwater infiltration facility	○	○				○				○					○
	propagation of rainwater storage facility	○														
conservation of green zone and agricultural land	conservation of green zone		○				○				○					○
	conservation of agricultural land		○				○				○					○
effective utilization of water resource	rationalization of water utilization				○	○		○	○			○				
	utilization of rainwater							○	○							
	utilization of waste water				○	○		○	○							
conservation of groundwater	regulating for or monitoring ground water pollution						○			○						
	providing a groundwater cultivating facility, maintenance of spring outlet		○				○									
	monitoring groundwater level						○			○						
	regulating for pumping up ground water						○	○					○			
reduction of pollution load	promoting combined septic tank				○											
	regulating for or monitoring water waste				○											
urban afforestation	providing public gardens		○				○				○					○
	afforestation along with road		○				○				○					○
	afforestation on building		○				○				○					○

SETTING UP MEASURES

The available measures and their quantitative effects are listed in Table 3. The quantitative indexes are classified into either the effect directly specified or the effective factor related indirectly with the specified effect. For example, the influential factor of a quantity of infiltration is related with various effects such as flood discharge, ordinary river discharge and groundwater level. It means that the infiltration facility is effective for not only flood control but also aqua-environment. The various measures listed in Table 3 should be allotted among the government, inhabitants, and private enterprises depending on their characteristics.

CO-OPERATIVE SYSTEM FOR DRAFTING MASTER PLAN

In order to build the consensus of the master plan among the government, the inhabitants, and the enterprises, a co-operative system should be carefully constructed. Under this co-operative system, the master plan should be authorized by the river council which consists of the representatives from the Ministry of Construction, the local governments, and the tributary working groups.

Before the river council finalizes the master plan, the each tributary working group should build the consensus through the discussion among the academic advisories of professors, the administrative officers of relevant local governments, and some local residents. During this process, it is also very important to encourage the relevant members through social gathering, explanation and discussion, symposium, festival and so on.

CONCLUSIONS

This paper indicates the investigative procedure and consideration to draw up the master plan for the appropriate hydrological water cycle. The problems and issues of the water cycle in the Shingasi River Basin were extracted and explained in this first report.

According to the future schedule, many steps of discussion should be done under the co-operative system presented in this paper in order to build the consensus among the governments, the inhabitants and the enterprises. To make the results successful, the desirable image of water cycle should be discussed from the various view points not only with the governments but also with the local residents.

It is also important to select the most suitable plan among the various alternatives. The effectiveness of each alternative can be calculated, but in order to make the master plan comprehensible, reasonable and sympathetic, the great effort should be paid for producing the positive activity of the co-operative system and interpreting the engineering assessment to be easily understandable for all the relevant members.

REFERENCES

1. Imbe M., Ohta T., Takano N. (1995) Methodological approach to improve the hydrological water cycle in urbanized areas, Proceedings on the Second International Conference on Innovative Technologies in Urban Storm Drainage, Lyon, France, pp37-44
2. Musiake K., Kubota M., Imbe M., Takano N., Dan T. (1999) Design concept for renewal of hydrological water cycle in urban area, Proceedings on the 8th International Conference on Urban Storm Drainage, Sydney, Australia, Vol.1, pp232-239
3. The Ministry of Construction in Japan (1998) The Manual for Planning the Renewal of Hydrological Water Cycle in Urban Areas (in Japanese)
4. The Sub-committee of Water Cycle under the River Council for River Control (1998) How should an appropriate water cycle be in river basins, The Interim Report (in Japanese)
5. Nakamura S, Saito M, Herath S. (1996) Development and applications of a physically based distributed catchment model in urban area, International Conference on Urban Engineering in Asian Cities in the 21st Century, proc. vol. II, pp. F. 128-223

Planning for Renewal of the Hydrological Cycle in Hillside Developments

Jun Matsushita, Takayoshi Nagai and Mitsuo Adachi
Department of Urban Improvement, Saitama Regional Branch, Urban Development Corporation
1-10-1 Numakage, Urawa City, Saitama, Japan 336-0027

Abstract. It is well known that urban development on hillsides affects the hydrological cycle. In this study, the influence of urban development on the water balance was assessed using a runoff analysis for an actual field case. Based on these analytical results, a hydrological cycle maintenance system was built in order to minimize the influence of development on the water balance of the area. The system, which consists of a combination of water storage and infiltration facilities, was designed to maintain the normal water discharge rates occurring in small channels, to enhance the degree of safety from flooding, to recharge the ground with rainwater and to ensure the availability of water sources for disaster prevention.

Key words. Urban hydrological cycle, Infiltration and storage facilities, Urban development.

INTRODUCTION

During the rapid economic growth period which began in the 1950s, major cities in Japan experienced rapid shifts of population towards urban centers, and demand for housing in and around large cities increased accordingly. In the past 40 years, a government-affiliated company, the Urban Development Corporation (UDC), has implemented numerous urban development projects in nearly 270 locations (covering approximately 38,000 ha). The urbanization of river basins has, however, resulted in significant increases in storm water runoff. In the 1960s, the storm water storage method, which aims to reduce storm water discharge into rivers by temporarily storing the storm water within the built-up area, was proposed to cope with the problem of increased runoff.

By the mid-1980s, the general public became highly conscious of environmental problems and began to demand environmentally sound development involving special environmental measures to ensure simultaneous conservation of landscapes, hydrological cycles and ecological systems. In 1994, the Ministry of Construction formulated its "Basic Environmental Policy" which indicates the importance placed on conserving and restoring natural hydrological cycles by providing storm water storage and infiltration facilities in river basins.

In accordance with, or in anticipation of national policy, UDC has initiated various projects that introduce comprehensive measures for flood, low water and water environment control. As part of its community development, UDC has designated model areas and has been working on projects for the integration of storm water retention facilities, the construction of infiltration facilities and the restoration of streams. In 1996 UDC formulated its "Guidelines for Environmentally Sound City Development" which take the hydrological cycle into consideration in anticipation of greater public demand. Since then, UDC has been working towards the goal of maintaining and restoring the hydrological cycle in urban developments.

The term "environmentally sound" has two facets: "trying to live in harmony with nature" and "aiming to reduce environmental loading". The specific goals to be attained for "living with nature" are the conservation and restoration of the original land and water environments. This paper reports on the work that is underway to restore a water environment in the Hannou-okawara area of Saitama Prefecture starting from an analysis of the hydrological cycle of the zone under development.

OVERVIEW OF HANNOU-OKAWARA AREA

Profile of the development area

The Hannou-okawara area, Fig. 1, lies on a hillside about 45 km to the south of inner Tokyo in Okumusashi Prefectural Natural Park. The development zone, (total land area 137.7 ha), is a part of a planned community, "Hannou Big Hills", that will eventually have a population of about 8,000

people. The zone slated for development slopes down towards the southeast and the northeast. In this region, lies Mt. Ryugai, surrounded by valleys formed by the Osawa (A) and Tonoyashiki Streams (B). The bedrock geology of the area consists mainly of sandstone, slate, and a Mesozoic chert formation, the Chichibu belt. The hill slopes are formed by bedrock covered with loam and talus deposits, while the bedrock in the flat area is covered with streambed and terrace deposits.

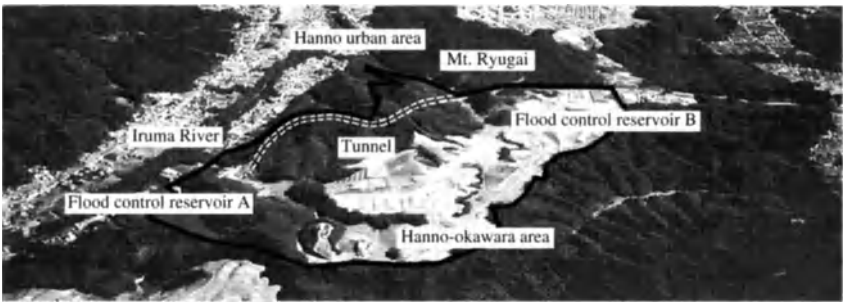

Fig 1. Hannou-okawara area

Outline of the scheme for an environmentally sound city

The aim of the project is tot build a multifunction city that has not only a good living environment but also a high concentration of recreational, research and development, educational, and other functions. The most important goal of this community building scheme is "environmental friendliness". With a view to promoting systematic conservation and restoration of the natural environment, work is now underway to create a green and high-quality water environment.

Conservation and restoration of greenery

The community building scheme aims to conserve the existing rich natural environment and ultimately achieve a green coverage ratio of 43%. Since conservation of greenery also leads to conservation of the water environment, efforts to restore lost vegetation are doubly beneficial.

Flood control reservoirs were constructed at the valley entrances of the Osawa Stream and the Tonoyashiki Stream to retain storm water in times of flood. To conserve the existing greenery on the hillsides, the two reservoirs were interconnected by a tunnel. This method has made it possible to conserve 4.5 ha of existing green slopes. In addition, to permit plant growth, the revetments of the flood control reservoirs were built with permeable material. Since site preparation inevitably creates large, bare slopes that are inhospitable to plants, prior to selecting the actual construction method, different greening techniques were evaluated at an adjacent test site.

Conservation of the water environment

It was foreseen that the planned development would reduce the normal discharge from the rivers originating in the area, as well as groundwater runoff. Measures now being taken to conserve the water environment include not only the maintenance of normal stream discharge but also restoration of the groundwater recharge function, creation of waterside spaces for recreation, pedestrian walkways and ecological protection zones, as well as the development of sources of water for disaster prevention.

HYDROLOGICAL CYCLE RESTORATION SYSTEM

At present, the Hannou-okawara area is mostly covered with trees, and changes caused by development are likely to have a major impact on the hydrological cycle and the ecosystem of the area. To permit relevant measures to be taken to guard against the negative effects of development, the present condition of the hydrological cycle was first analyzed, the consequences of development were estimated, and hydrological cycle maintenance measures were then proposed consistent with the basic concepts of community development.

Goals of hydrological cycle restoration

Since loss of pervious areas and removal of vegetative cover associated with site preparation cause major changes in the water environment it was decided to make effective use of storm water. To this end, a hydrological cycle restoration system consisting of a combination of storm water storage and infiltration facilities was conceived, and the following goals were set:

- Maintenance of low water flow in the stream (maintenance of pre-development normal discharge)
- Groundwater recharge through storm water infiltration
- Creation of waterside spaces with hydrophilic properties
- Enhanced factor of safety from inundation for all sewers (1/10 for sewer mains)
- Securing sources of water for disaster prevention (40 m^3 of stored water within a radius of 100 m)

Hydrological cycle modeling

Water balances both before and after the development were estimated using a model capable of quantifying direct runoff, groundwater runoff, and evapotranspiration. The water balance equation is as follows:

$$P-(D+Q_g+E)=\Delta M_s+\Delta S_g \tag{1}$$

where P = rainfall, D =direct runoff, Q_g = groundwater runoff, E = evapotranspiration, ΔM_s = change of soil moisture content in the unsaturated zone, ΔS_g = change of groundwater storage.

The hydrological cycle model was constructed by dividing the catchment area into pervious areas and impervious areas. In modeling pervious areas, a two-stage tank analogue was assumed. It was also assumed that part of the infiltrating water returns to the atmosphere by evapotranspiration and the rest, when the water-holding capacity of the soil is exceeded, runs off as either direct runoff or groundwater runoff. In modeling the impervious areas, it was assumed that direct runoff occurs when the loss associated with surface depressions has been exceeded, and that the amount of direct runoff is equal to the volume of rainwater. Both leakage from unconfined aquifers to deeper strata and groundwater inflow from outside the catchment area are assumed negligible. The model can be represented mathematically by equation (2):

(Pervious areas)

For the upper tank ;

$$\frac{dM_s}{dt}=\begin{cases} I_iP-I_iE-G-D_1 & (M_s \geqq S_{max}) \\ I_iP-I_iE-G & (M_n < M_s < S_{max}) \\ I_iP-I_iE & (M_s \leqq M_n) \end{cases}$$

$$G=\begin{cases} 0 & (M_s < M_n) \\ \beta(M_s-M_n) & (M_s \geqq M_n) \end{cases}$$

$$D_1=\begin{cases} 0 & (M_s \leqq S_{max}) \\ M_s-M_n & (M_s > S_{max}) \end{cases} \tag{2}$$

For the lower tank ;

$$\frac{dS_g}{dt}=G-Q_g \qquad (M_n < M_s < S_{max})$$

$$Q_g=A_u{}^2\ S_g{}^2$$

(Inpervious areas)

$$D_2=\begin{cases} 0 & (1.0-I_i)P \leqq L \\ (1.0-I_i)P-L & (1.0-I_i)P > L \end{cases}$$

The model and its parameter values (see inset, Fig.2) were verified by comparison of calculated runoff predictions with measured values. For purposes of verification, the catchment area and the infiltration area ratio I_i were determined from the topography and land preparation plan while values for the loss associated with surface depressions were taken from past case study data. The unconfined recession constant A_u was calculated from recession curves for dry weather measurement data because unconfined groundwater recesses fractionally. The groundwater recharge constant β was assumed to be equal to 1.0. The minimum water-holding capacity M_n, and the maximum storage volume S_{max}, were chosen by trial and error to match the hydrograph of actual wet-weather runoff.

Figure 2 shows the general agreement of the model with the measured values of runoff for the Tonoyashiki catchment area. While the model can not, of course, accurately represent the peaks the overall agreement is satisfactory for the present purposes.

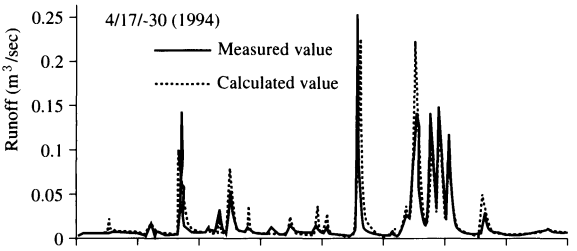

Model parameters (Tonoyashiki Stream)

Catchment area	50.8ha
Infiltration area ratio (Ii)	68.5%
Unconfined recession constant (A_u)	0.1
Depression loss (L)	2.5mm
Minimum water-holding capacity (M_n)	20.0mm
Groundwater recharge constant (β)	1.0
Maximum storage volume (S_{max})	100mm

Fig 2. Results of model verification

Flow regime and water balance before and after development

The above model was used to estimate the flow regime and water balance before and after development of the Osawa and Tonoyashiki projects. It was assumed that only the infiltration area ratio and the evapotranspiration area ratio were affected by development, as indicated in Table 1. All other parameters were assumed to remain the same as in the model calibration calculation.

Table 1. Area parameters before and after development

Flow regime	Osawa Stream catchment area		Tonoyashiki Stream catchment area	
	Before developmemt	After developmemt	Before developmemt	After developmemt
Catchment area	49.7ha	60.0ha	52.2ha	60.5ha
Infiltration area ratio (I_i)	96.8%	19.2%	94.6%	30.0%

As shown in Table 2 and Figure 3, the results also indicate that runoff in the area would increase in times of flood but decrease under normal conditions. The differences in runoff before and after development are, however, not large. This is probably because the water-holding capacity of the ground in the infiltration areas is so small that infiltrating rainwater runs off as groundwater.
Estimates of the annual water balance indicated that, while the runoff percentage would increase considerably because of the increased area of impervious surface, evapotranspiration and groundwater runoff would decrease.

Table 2. Comparison of flow regimes before and after development (m^3 /day)

Flow regime	Osawa Stream catchment area		Tonoyashiki Stream catchment area	
	Before development (49.7ha)	After development (60.0ha)	Before development (52.2ha)	After development (60.5ha)
Maximum flow	47,810	57,643	50,315	52,537
Normal flow (185-day flow)	268	149	299	208
Low water level flow (275-day flow)	95	55	101	73
Drought flow (355-day flow)	18	6	19	14
Minimum flow (365-day flow)	12	4	11	10
Runoff percentage (%)	65	92	65	88

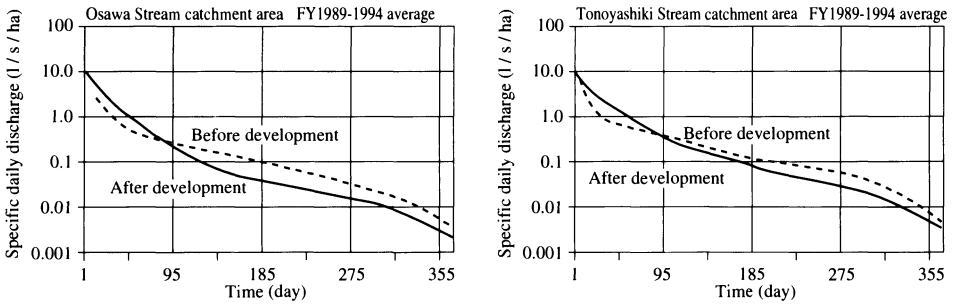

Fig 3. Flow regime diagrams

Types of facilities

The hydrological cycle restoration system specifically designed for restoration of the water environment comprises the following facilities:

- Triple tank system (used to provide storage capacity for flood control, to store water for disaster prevention, and to provide water for environmental purposes)
- Underground crushed stone reservoir
- Infiltration facilities

This system is illustrated schematically in Fig. 4 while Table 3 shows the size requirements calculated for these facilities for the Osawa and Tanoyashiki developments described here.

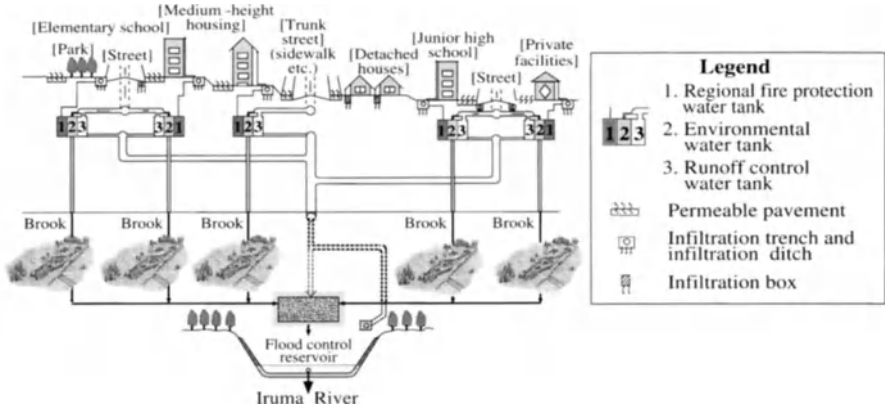

Fig. 4 Hydrological cycle restoration system

Table 3. Sizes of storage / infiltration facilities

	Storage facilities	Infiltration facilities
Osawa Stream catchment area	5,150m^3	196.26m^3/hr
Tonoyashiki Stream catchment area	4,800m^3	136.46m^3/hr

System evaluation

Normal discharge of water channels can be ensured by constructing a hydrological cycle restoration system. As shown in Fig. 5, water balance can, potentially, be improved significantly. According to this figure, in the case of the Osawa Stream catchment area, groundwater runoff can be doubled by providing a hydrological cycle maintenance system, although the pre-development condition cannot be restored. Direct runoff after development will reach about nine times the pre-development level if no corrective measures are taken, but this can be reduced by about 20% if a hydrological cycle maintenance system is provided.

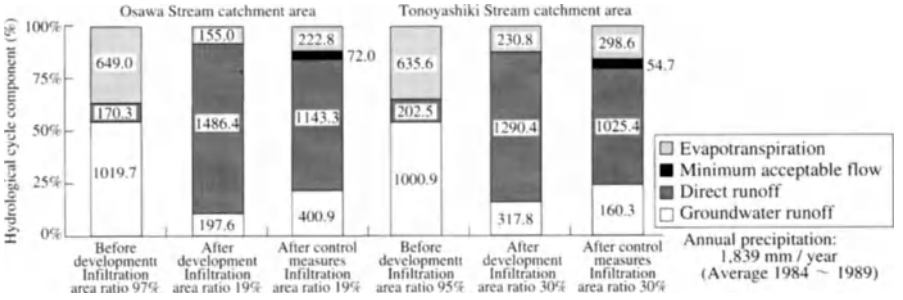

Fig 5. Results of water balance calculations

Present and planned construction activities

To secure minimum channel discharge under normal conditions, an underground crushed stone reservoir, filled with locally excavated crushed stone, Fig 6, is now under construction directly upstream of the flood control reservoir B. The next step, to be taken in conjunction with sewerage improvement, is to construct a triple storage tank system, which will provide storage capacity for flood control as well as store water for environmental control and for disaster prevention. Infiltration basins will be constructed as well.

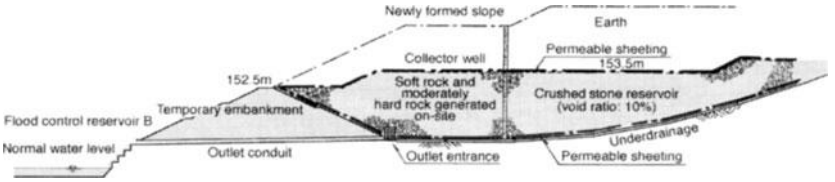

Fig 6. Profile of underground crushed stone reservoir now under construction

CONCLUSION

The Urban Development Corporation (UDC) analyzed the runoff mechanism in a hillside area using a tank model. The tank model was used firstly to estimate the influence on the hydrological cycle of changes in topography and in ground surface cover resulting from development and, subsequently, to devise corrective measures.

- Urban development on the hillside is likely to reduce pervious areas, thereby causing not only decreases in the normal discharge of the rivers (channels) but also decreases in evapotranspiration and groundwater runoff.
- To reduce the influence on the water balance, a hydrological cycle restoration system consisting of a combination of distributed storage facilities and infiltration facilities was proposed.
- Although the water balance cannot be restored to the original pre-development state , the discharge in the channels under normal conditions can be maintained by constructing a hydrological cycle restoration system.
- This system will also be effective in restoring groundwater runoff.

UDC is implementing various measures in many parts of the country, including the Hannou-okawara area, to attain the goal of "building environmentally friendly communities". The project reported in this paper is just one example of such schemes. UDC will continue to work on the research and development of techniques suited to characteristics of individual districts in order to create a better living environment.

Acknowledgment

The author would like to thank Prof. Kuniaki Sato, Faculty of Engineering, Saitama University, the Ministry of Construction and the Saitama Prefectural Government who have provided invaluable and generous suggestions in connection with the preparation of this paper.

Bibliography

1. Ando Y, Mushiake K, Takahashi Y. (1983). Modeling of hydrological processes in a small natural hill slope basin, based on the synthesis of partial hydrological relationships. Journal of Hydrology, 64, pp. 311-337.
2. Housing and Urban Development Corporation: A study report on the hydrological cycle maintenance system in Hannou-okawara area. Oct. 1995. Saitama Branch UDC, Japan, pp.33-44. (in Japanese)
3. Matsuda, S. 1995. A study on development and integration of hydrological cycle restoration system in connection with urban development. Water Science, Institute of Water Utilization No. 226-229.(in Japanese)
4. Matsushita, J., Go-o, K. and Shigeta, T. : A Study on stream restoration project for Tama New Town B-4 district (Live Nagaike) and development process of hydrological cycle restoration system. July, 1998, Water Science, Institute of Water Utilization No. 244-245. (in Japanese)

Reliability of Numerical Methods and Scaling in Geohydraulics

Integrating GIS Data with 3D Finite Element Groundwater Models

Norman L. Jones[1], Alan M. Lemon[2], and Cary A. Talbot[3]

[1] Associate Professor, Environmental Modeling Research Laboratory, Brigham Young University, Provo, Utah 84602, USA.
[2] Research Associate, Environmental Modeling Research Laboratory
[3] Research Hydraulic Engineer, US Army Engineer Waterways Experiment Station, Vicksburg, Mississippi 39180, USA.

Abstract. In this paper we describe a new approach to generating 3D finite element models using GIS data and triangulated irregular networks (TINs). The GIS objects are vector-based feature objects and include points, arcs, and polygons. The model boundary, recharge zones, streams, lakes, and other boundary condition and source/sink data are described using the GIS objects. The stratigraphy is modeled using TINs constructed from borehole data. The GIS objects are then used in conjunction with the TINs to generate the 3D mesh. The mesh precisely matches the model and interior boundaries and it is refined around wells in the mesh interior. Once the mesh is constructed, the boundary conditions and source/sink terms are automatically transferred from the GIS objects to the nodes and faces of the mesh. The conversion method is designed to handle complex boundary conditions including exit face boundaries, flux boundaries, and multi-level head dependent boundaries.

Key Words. GIS, finite element, FEMWATER, GMS, modeling

INTRODUCTION

While most ground water models use the finite difference approach, the finite element method has several advantages for 3D ground water modeling. The unstructured nature of the finite element mesh makes it possible to refine the grid locally around wells or other locations where steep gradients are expected. The unstructured mesh also allows for precise matching of model boundaries and interfaces between adjacent stratigraphic units. A drawback of the finite element approach is that constructing 3D meshes and assigning boundary conditions can be difficult when modeling sites with complex boundaries, large numbers of sources and sinks, and complicated stratigraphic relationships.

In this paper we describe a new approach to generating 3D finite element models using GIS data and triangulated irregular networks (TINs). The GIS objects and the TIN define a mesh-independent representation of the model that includes material zones, boundary conditions, and sources and sinks. These data can be used to automatically generate a mesh and assign model parameters to nodes and elements.

Since the data are stored independently of the finite element mesh, the GIS and TIN data represent a conceptual model of the site being studied. The conceptual model approach has numerous advantages over the traditional method for building ground water models. With the traditional method, the first step is to construct the mesh. The material properties and boundary conditions are then assigned directly to selected nodes and elements. If it becomes necessary to recreate the mesh in order to change the location of a boundary or to refine around a new well, all of the data defined at nodes and elements must be re-entered. With the conceptual model approach, the critical features that define the model, i.e., the material boundaries, sources, sinks, and boundary conditions, etc. are

defined independently of the mesh. If it becomes necessary to recreate the mesh, the model parameters can be automatically reassigned to the appropriate nodes and elements.

The conceptual model approach to ground water model pre-processing has been successfully applied to finite difference models [1][5]. To date, very little has been done in applying this approach to 3D finite element models. In this paper we describe an approach for building GIS based conceptual models that satisfy the unique requirements and challenges inherent in the 3D finite element approach.

Our implementation of the conceptual model approach for 3D finite element models was designed to support construction of FEMWATER models. FEMWATER is a coupled flow and transport model that can be used for simulations involving both saturated and unsaturated domains. FEMWATER was originally developed by G.T. Yeh and is currently maintained by the US Army Engineer Waterways Experiment Station (WES) [2]. The conceptual modeling tools are incorporated into the Department of Defense Groundwater Modeling System (GMS). GMS is a comprehensive groundwater modeling pre- and post-processor developed by the Brigham Young University Environmental Modeling Research Laboratory in partnership with WES [4].

THE CONCEPTUAL MODEL

When applying the conceptual model approach to finite element modeling, the first challenge is to define the data types to be used in the conceptual model. The conceptual model we use for this problem consists of two primary data types. We use GIS objects to define model boundaries, wells, recharge zones, and boundary conditions. Stratigraphic boundaries are modeled with TINs.

GIS Objects. The GIS objects include points, arcs, and polygons. The GIS objects are organized into layers or "coverages." A sample FEMWATER coverage is illustrated in Fig. 1a. Wells are represented using point objects. The arcs are used to delineate the outer model boundary and the interior boundaries of the recharge zones. The polygons are used to define the recharge zones.

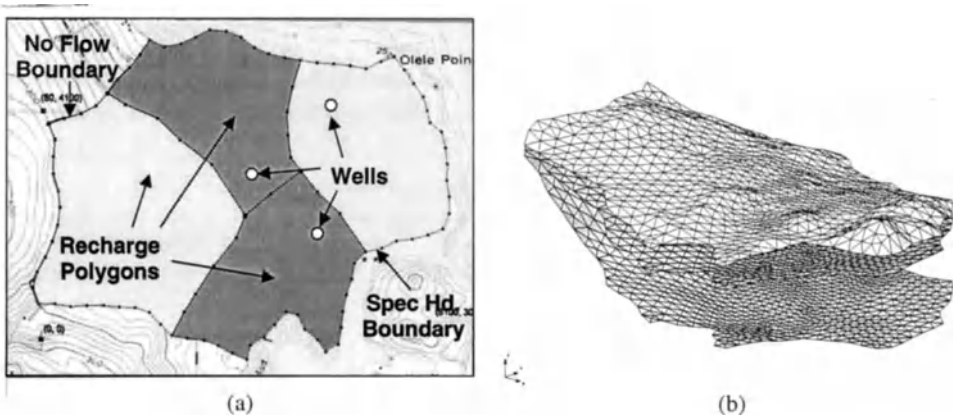

Fig. 1. (a) GIS Objects Defining Wells, Boundaries, and Recharge Zones. (b) Stratigraphic Boundaries Modeled as TINs

TINs. The stratigraphy of the site to be modeled is represented with TINs. A TIN is created at the top and bottom of each stratigraphic unit as illustrated in Fig. 1b. The distribution of the points within the interior of each TIN is accomplished using an automated meshing algorithm originally developed for 2D finite element meshes [3]. The elevations of the TIN vertices are interpolated from a set of scatter points with elevations extracted from borehole logs.

MESH GENERATION

Once the conceptual model is defined, the conceptual model can be used to automatically build a 3D mesh and assign boundary conditions and model parameters. The first step in this conversion process is to create a 3D mesh. The 3D mesh is created in a two step process. First, a 2D projection mesh is created (Fig. 2a). The projection mesh is a plan view representation of the dominant topology of the 3D mesh. The GIS objects in the conceptual model are used as input to a 2D meshing algorithm that constructs the projection mesh. The mesh conforms to both the interior and exterior boundaries defined by the arcs. The spacing of the elements is controlled by the vertex density along the arcs.

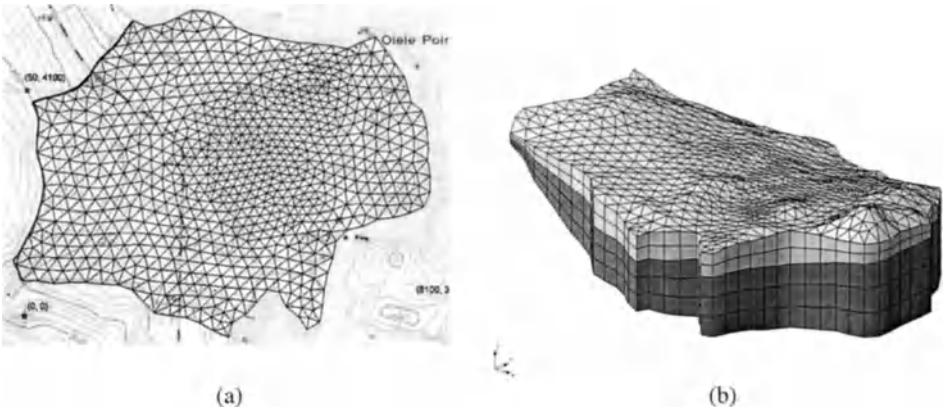

Fig. 2. (a) Plan View of 2D Projection Mesh. (b) 3D Mesh After Extrusion Process.

Once the projection mesh is created, it is used in combination with the TINs to create a 3D mesh. The mesh is created one zone at a time. The TINs defining the top and bottom of the zone are selected and the number of mesh layers to be created between the two TINs is specified. Each of the elements in the 2D mesh is then "projected" through the two TINs to create a vertical column of 3D elements as shown in Fig. 2b. For example, if N layers are specified, N 3D wedge elements are created from each of the triangular elements in the 2D mesh, and N 3D hexahedral elements are created from each of the quadrilateral elements in the 2D mesh. The Z coordinates of the nodes created for the 3D elements are distributed uniformly between the top and the bottom TINs.

The mesh shown in Fig. 2b has relatively simple stratigraphy. Sites with complex features such as pinchouts and embedded seams can be modeled by first creating a mesh using the projection method that models the predominant zones. Discontinuous features are then modeled by selecting elements within the mesh zones and changing the material id assigned to the elements.

BOUNDARY CONDITIONS

Once the mesh is constructed, the next step is to utilize the GIS objects to automatically assign boundary conditions to the mesh. The arcs on the outer boundary of the conceptual model are each marked as either a no-flow, a specified head, or a specified flux arc. For no-flow arcs, no attributes are required. For specified head arcs, a separate head value is assigned to each end of the arc. When the model conversion takes place, each node on the outer (vertical) boundary of the 3D mesh is checked to see if the xy coordinates of the node are coincident with one of the specified head arcs. If so, the node is marked as a specified head node and a head value is linearly interpolated from the head values assigned to the ends of the arc and the interpolated head value is assigned to the node.

For specified flux arcs, a single flux value is assigned to the arc. During the model conversion process, all vertical element faces on the outer boundary of the mesh are checked to see if they are coincident with one of the specified flux arcs. If so, the flux value assigned to the arc is assigned to the element face. In this fashion, all boundary conditions can be automatically assigned to the mesh nodes and elements, saving the modeler substantial time and effort.

RECHARGE ZONES

During the model conversion process, recharge zones on the top surface of the mesh are also automatically assigned. Recharge values are assigned to polygons in the conceptual model. Each face on the top of the 3D mesh is checked and the polygon containing the face is found. The recharge rate assigned to the polygon is then assigned to the element face.

WELLS

For each well, a pumping or injection/extraction rate is assigned to the point. In addition, a ground surface elevation and top and bottom elevation for the screened interval is entered. These values are used to generate a 3D display of the wells as shown in Fig. 3a. The screened interval is also used to partition the well flow rate to the nodes as shown in Fig. 3b. When the model conversion takes place, each of the nodes intercepted by the well screen is found and marked as a well node (point source/sink). A set of mesh nodes are coincident with the xy location of the well because the well points are preserved in the 2D projection mesh which is then used to generate the 3D mesh.

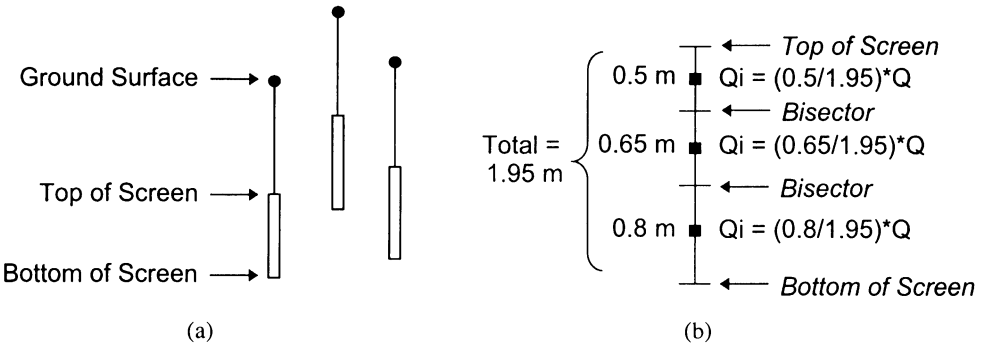

Fig. 3. (a) Wells in Oblique View. (b) Method for Partitioning Flow to Individual Nodes Overlapped by the Well Screen.

Once the well nodes are identified, the total flow rate (Q) assigned to the well must then be distributed among the well nodes. To do this, the length of the well screen adjacent to each node that is closer to the node than the other well nodes is determined. This adjacent length is divided by the total length of the well screen to determine the flow rate (Qi) to be assigned to the node.

RUNNING THE MODEL

Once the boundary conditions have been automatically applied to the nodes and elements of the mesh, the model is almost ready to run. Typically, material properties (K, porosity, etc.) must be entered and analysis and output options must be selected before the model simulation is launched. Nevertheless, the vast majority of the work required in setting up the model is completed automatically using the conceptual model.

MODEL CALIBRATION

Model calibration is also enhanced using GIS objects. Point observations of head and concentration can be easily managed using a GIS layer of point objects. Furthermore, arcs and polygons in the original conceptual model are used to efficiently manage flux observations and automated flow budgeting. FEMWATER outputs a flux file that includes the total flux at each node on the boundary of the mesh. The recharge polygons on the top of the mesh are used to automatically sum the total flux of all nodes in the polygon. Furthermore, the specified head arcs on the boundary of the problem domain are used to identify all nodes associated with the specified head boundary condition and sum the flux of those nodes. As a result, the modeler simply clicks on a polygon or arc and the total flux for that object is displayed. This type of instantaneous flow budgeting greatly aids the model calibration process.

SAMPLE APPLICATION

The Jacksonville District of the US Army Corps of Engineers is studying restoration and mitigation alternatives in an effort to return the Florida Everglades National Park (ENP) to pristine conditions. As part of this effort, the US Army Engineering Research and Development Center's Waterways Experiment Station has been tasked to build a numerical model that accurately simulates the complex interaction between overland and groundwater flow in and around the ENP. In order to accomplish this objective, a specialized version of FEMWATER that couples 1D canal, 2D overland and 3D groundwater flow was developed. This code is known as FEMWATER123.

The finite element mesh used for the ENP model is shown in Fig. 4. The maximum horizontal extent of the model is nearly 100 km east to west, covering a total area of over 4400 km^2. It is comprised of 58140 nodes and 103796 elements. There are ten different material zones that vary in hydraulic properties ranging from peat (0.03 meters/day) to very porous limestone formations (6100 meters/day). Detailed surface topology and subsurface stratigraphic information from boreholes was used to construct the 3D mesh elements.

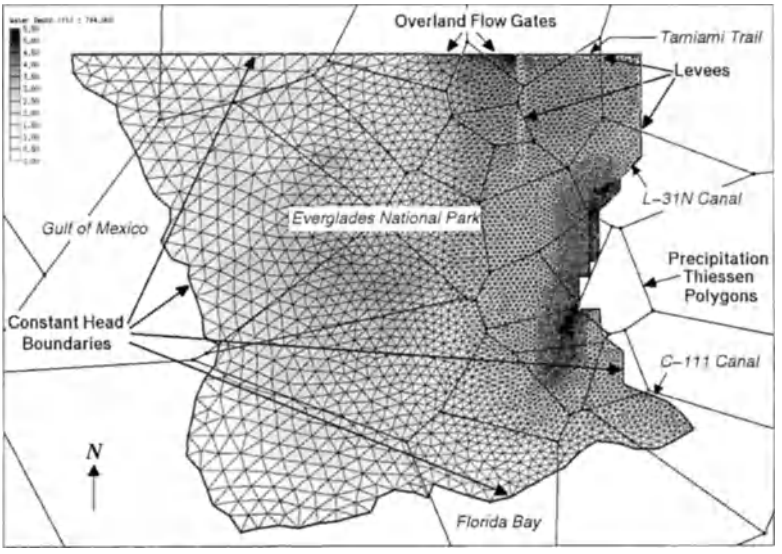

Fig. 4 Everglades National Park FEMWATER Mesh with Conceptual Model Elements Highlighted.

A coupled surface and groundwater model of this magnitude requires the incorporation of many data types, including borehole and stratigraphic data, soil hydrogeologic properties, rainfall and evapotranspiration data, pumping well locations and rates, groundwater gage and canal stages, as well as detailed surface topology. These data types occur in various temporal and spatial domains that often do not coincide with one another. The GIS object-based conceptual modeling approach provides not only an efficient means of storing the disparate data but also provide the means of automatically transferring the data to the model as appropriate boundary condition assignments.

Precipitation and evapotranspiration input values were taken from daily rain gage readings and distributed over the domain of the study area via a network of Thiessen polygons. Boundary conditions were input to the model via time-varying specified head and stage values assigned to arcs. These values were gathered from daily stage readings on canals, groundwater gages and coastal tides that comprise the boundaries of the model. Temporal as well as spatial gaps exist in both data sets but the conceptual model approach seamlessly integrates these data, linearly interpolating both in space and time as needed to ensure assigned flux and head boundary conditions are complete and consistent.

CONCLUSIONS

We have described a "conceptual modeling" approach for building 3D finite element ground water models using GIS objects and TINs. The conceptual model approach has numerous advantages over traditional approaches where model parameters are assigned directly to nodes and elements. The conceptual model approach greatly simplifies the level of effort required to build and maintain the model. Furthermore, the model is defined independently of the computational mesh. If it becomes necessary to refine the mesh or change the mesh topology in any way, the model input can be regenerated in seconds from the conceptual model. This efficiency enhances the model calibration process and gives the modeler more freedom to explore alternate conceptual models. This ultimately leads to more accurate models. This modeling approach has successfully been applied to several large-scale modeling projects.

ACKNOWLEDGMENT

The research in this paper was partially supported by the U.S. Army Engineer Waterways Experiment Station. Permission has been granted by the Office, Chief of Engineers, USACE to publish this paper.

REFERENCES

1. Jones, N.L., and D.R. Richards, (1996) A conceptual model approach to hydroinformatics, Proc. of the 2nd Int. Conf. on HYDROINFORMATICS, Zurich, Switz., Sept. 9-13, 285-291
2. Lin, H.C., D.R. Richards, C.A. Talbot, G.T. Yeh, J.R. Cheng, H.P. Cheng, and N.L. Jones, (1997) FEMWATER : A Three-Dimensional Finite Element Computer Model for Simulating Density-Dependent Flow and Transport in Variably Saturated Media, US Army Engineer Waterways Experiment Station, Technical Report CHL-97-12, pp 143
3. Nelson, E.J., N.L. Jones, and R.J. Berrett, (1999) Adaptive tessellation method for creating TINs from GIS data, ASCE Journal of Hydrologic Engineering, 4:2-9
4. Owen, S.J., N.L. Jones, and J.P. Holland, (1996) A comprehensive modeling environment for the simulation of groundwater flow and transport, Engineering With Computers, 12:235-242
5. Yan J., K.R. Smith, R.M. Greenwald, P. Srivivasan, and D.S. Ward (1995), A modular ground water modeling system (GWZOOM): 1. concept and system, Advances in the Development and Use of Models in Water Resources, 161-168

Numerical Simulation and Homogenization of Two-Phase Flow in Heterogeneous Porous Media

B. Ataie-Ashtiani[1*], S.M. Hassanizadeh[1], M. Oostrom[2] and M.D. White[2]

[1]Delft University of Technology, Department of Water Management, Environmental and Sanitary Engineering, P.O. Box 5048, 2600 GA Delft, The Netherlands (*Permanent address: Department of Civil Engineering, Sharif University of Technology, Tehran, Iran.)
[2]Pacific Northwest National Laboratory, Richland, Washington, USA.

ABSTRACT. This is a theoretical study on the feasibility of replacing a medium containing microheterogeneities with an equivalent homogeneous medium. The infiltration of dense nonaqueous phase liquids (DNAPL) in a water saturated heterogeneous porous medium is investigated numerically. The numerical model STOMP (Subsurface Transport Over Multiple Phases) is used and its suitability is proven by comparison of results with the experimental work of Kueper et al [3]. The proper boundary condition for this problem is identified and it is shown that the commonly used boundary condition is not physically correct. For a porous medium with a periodic heterogeneity, the existence of a representative elementary volume (REV), related to the spatial scale of heterogeneities is investigated. The upscaled permeabilities and constitutive relationships for the REV are numerically calculated and the effects of heterogeneities are discussed

KEY WORDS: two-phase flow, heterogeneous porous media, homogenization, numerical simulation, STOMP.

INTRODUCTION

Contamination of groundwater by DNAPL is one of the major environmental concerns. Heterogeneity can exert an influence on transport processes of DNAPL over a wide range of scales. Many soils and geological formations contain small-scale heterogeneities which have distinctly different multiphase flow properties than the main medium. These micro heterogeneities considerably affect the spreading behaviour of non-aqueous liquids. They are often sources of localized pools of pollutants such as DNAPL.

Commonly, one is not interested in the details of fluid distribution in such a medium. Moreover, it is often computationally not feasible to discretize a compositional multiphase model at such small scales. In this work, upscaling methods are developed for estimating the effective parameters at a larger scale. The proper scale at which effective parameters are defined, is determined based on the basic concept of REV. Here, we will try to define a REV for DNAPL movement in a hypothetical heterogeneous medium and examine the suitability of that REV. The defined REV will be used to determine constitutive relationships at the higher scale.

MODEL COMPARISON

The numerical model STOMP [5] is employed in this study. First, we demostrate the applicability of the model to heteorgeneous media and test its ability to simulate real

systems by modelling a two-dimensional sand pack experiment. The experiment is described fully by Kueper et al. [3]. The configuration of the assembled sand lenses is illustrated in Fig. 1. Table 1 gives sand properties including permeability and parameters of the tetrachloroethylene-water drainage capillary pressure curve. These are best-fit parameters that were obtained by matching the Brooks-Corey model [1].

Table 1. Sand properties

		Sand 1	Sand 2	Sand 3	Sand 4
Permeability k	[m^2]	5.041×10^{-10}	2.051×10^{-10}	5.621×10^{-11}	8.191×10^{-12}
Porosity n	[-]	0.4	0.39	0.39	0.41
Entry pressure p_d	[m]	0.0377	0.0377	0.0377	0.1350
Pore size distribution index λ	[-]	3.86	3.51	2.49	3.30
Residual saturation S_{wr}	[-]	0.078	0.069	0.098	0.189

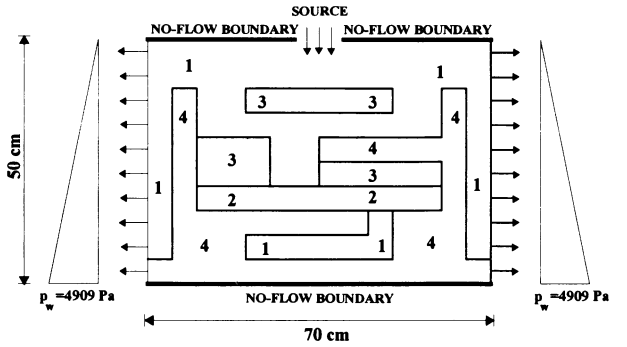

Fig. 1. Configuration and boundary conditions for simulation of DNAPL infiltration in a flow tank (after Kueper et al. [3]).

At the beginning of the experiment, tetrachloroethylene containing a non-volatile dye was released into the initially water-saturated sand. The source area at the center of the top of the flume was subjected to a constant head of 4 cm of tetrachloroethylene, equal to a pressure of 639.35 Pa. The tetrachloroethylene has a density of 1630 $Kg/m^3$and a viscosity of 0.90×10^{-3} Pa s. The DNAPL propagation in time was recorded only visually. Because actual fluid saturation was not measured during the course of the experiment, the saturation of tetrachloroethylene was evaluated by Kueper and Frind [4] by means of numerical simulation so as to obtain a visual match between numerical and experimental results. This match was obtained with a constant tetrachloroethylene saturation of 38% at the source boundary. Helmig [2] also simulated this experiment with a DNAPL saturation of 0.4 at the source points.

In our simulations, the domain was discretized using a constant nodal spacing of 1.25 cm in both horizontal and vertical directions. A time step of 10 s was used throughout the simulation. Two different sets of boundary conditions were employed. One of them is similar to what Kueper and Frind [4] and Helmig [2] applied, based on a constant source saturation. In this case, a constant head of PCE equal to 639.35 Pa (4 cm) for non-wetting phase and a constant pressure of 212.7 Pa for water are applied at the source points. This amounts to a capillary pressure, Pc, of 426.65 Pa which corresponds to a PCE saturation of 39%. In the other case, the same boundary condition for NAPL is employed (a constant head of 639.35 Pa) but a zero-flux boundary condition is employed for water.

Fig. 2 illustrates the distribution of fluids in the flume at different times based on experimental and numerical results. As is evident, the agreement between experimental and numerical sets is reasonably good. The second boundary condition set shows a better match with experimental results. The PCE saturation at one of the nodes below the source and the aqueous and DNAPL fluxes at source points are plotted in Fig. 3 for different sets of boundary condition. As seen, the assumption of constant PCE saturation at the source points leads to a flux of water through the DNAPL source boundary. Such a flux was not reported for the experimental results, and we assume this result is physically unreasonable. In conclusion, although the numerical results based on both types of boundary conditions show good agreement with experimental results, the second set of boundary conditions is physically more realistic and appears to give somewhat better results.

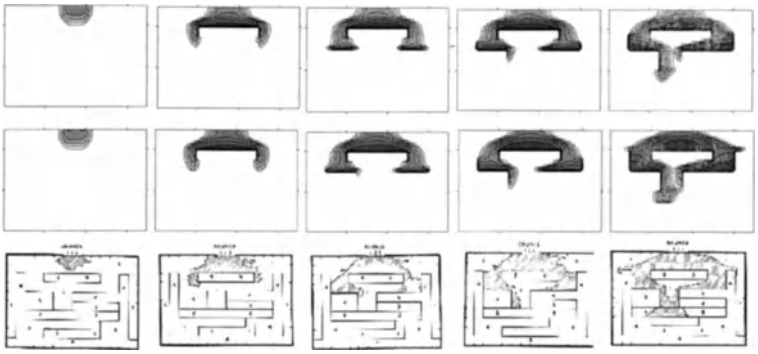

Fig. 2. a) Observed distributions of PCE after 34, 126, 184, **220**, 313 s, b) Simulated distribution of TCE after 30, 130, 180, 220, 310 s with Dirichlet B.C. for DNAPL and for water at source nodes**, c**) Simulated distribution of TCE after 30, 130, 180, 220, 310 s with Dirichlet B.C. for DNAPL and zero-flux B.C. for water at source nodes.

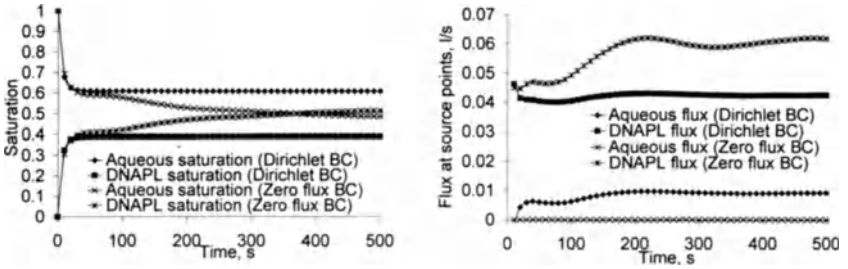

Fig. 3. (a) Aqueous and DNAPL saturation in the node below the source points (b) the fluxes of aqueous and DNAPL at source points.

HETEROGENEOUS MEDIA

For the purpose of study of upscaling heterogeneities, a hypothetical porous medium with dimensions comparable to the sand tank in Kueper et al. Experiment is considered. As the simplest case, we assume that a periodic distribution of find sand blocks is persent within a sandy medium (Fig. 4). Properties of the two sands are chosen to be similar to sands 1

and 3 of Kueper et al. [3]. Other physical and modeling parameters are also similar except for the boundary condition at the source points where a constant flux of 3.15×10^{-4} m/s for DNAPL infiltration is specified.

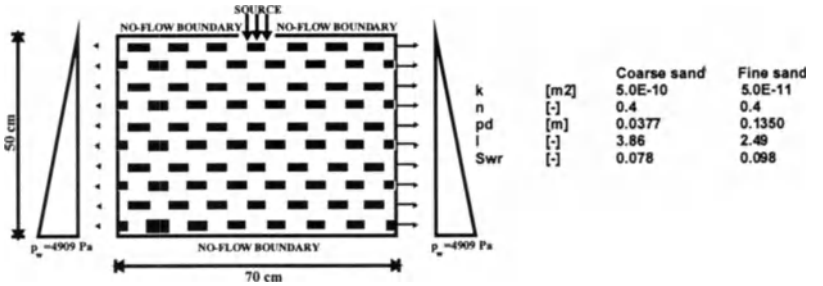

Fig. 4. Configuration and boundary conditions for simulation of vertical DNAPL infiltration in heterogeneous porous media.

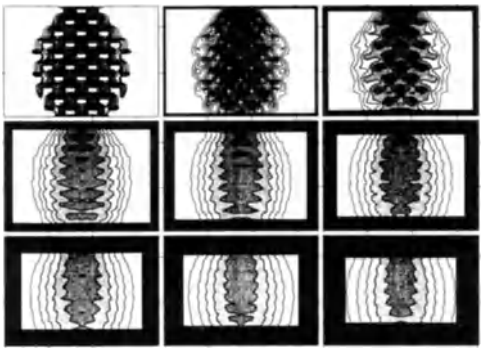

Fig. 5. Contours of average DNAPL saturation at t=500s obtained with averaging domain sizes of 1x1, 3x3, 5x5, 7x7, 9x9, 11x11, 13x13, 15x15 and 17x17 elements, respectively.

Fig. 5-a shows simulation results and the distribution of DNAPL plume at 500 s. To replace the heterogeneous medium with an equivalent homogeneous medium, average properties have to be defined. Thus, we need to identify a representative elementary volume (REV) such that meaningful average properties can be obtained. For an ideal REV, average values are independent of the averaging volume size within an interval.

Here, this concept is used to find the appropriate REV size. At different points, the DNAPL saturation is averaged over various sizes of representative elements. Contours of averaged DNAPL saturation obtained with seven different averaging domain sizes are plotted in Fig.s 5b-5i. Fig. 6 shows the variation of average saturation versus the area of averaging domain at three different points after 500 s. As seen, the fluctuation in DNAPL saturation would not be fully damped even for an averaging domain as large half of the whole solution domain. This is because the scale of heterogeneities is large. However, the amplitude of this fluctuation is reduced very fast at the beginning. Here a block of 10 cm x 10 cm is considered a reasonable averaging domain size. This is in fact the periodicity size of heterogeneities. Although this can not be considered as **a** REV in the strict sense, but it

is a reasonably representative averaging domain as the average saturation fluctuations are quite small beyond this size.

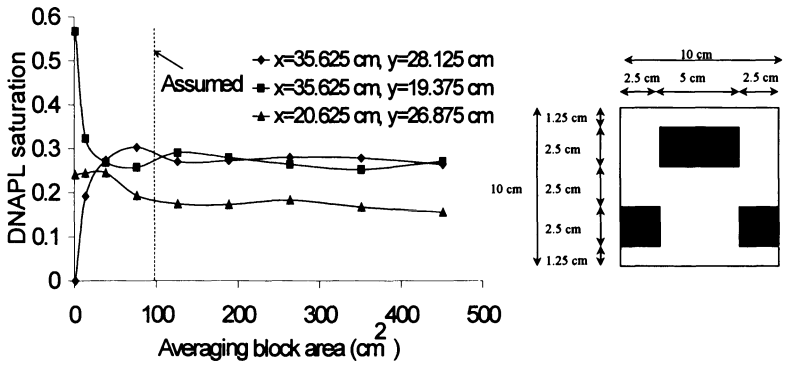

Fig. 6. a) Variation of DNAPL saturation at t=500s versus the area of averaging block, b) Assumed representative elementary block.

Obviously when a homogenized one replaces a heterogeneous media, local details of considered property are lost. This is evident in Fig. 5 where local effects are less distinguished when the averaging domain size is increased. For example, for the averaging domain of 9x9 elements and larger, local pools are not quite recognizable, although they have not fully vanished.

To calculate upscaled permeabilities and constitutive relationships for our representative block, a unidirectional flow of both water and DNAPL is established by applying constant pressure boundary conditions for the DNAPL, Pnw, and the aqueous phase, Pw, at both boundaries perpendicular to the flow direction. The difference Pnw-Pw is chosen to be the same at both ends which means that the same capillary pressure (Pc) exits at the boundaries. The pressure differences across the block, ΔPw and ΔPnw, are kept at a value of 100 Pa for both fluids in all simulations. This corresponds to a pressure gradient comparable to that observed in the main medium (Fig. 5a). Meanwhile, a no-flow boundary condition is imposed on the block faces parallel to the flow. Simulations for a given Pc are performed until (apparent) equilibrium is reached. Average saturation and kr are calculated for the block. Then Pc is increased (up to 10,000 Pa) and the procedure is repeated. In this fashion, constitutive relationships are obtained for the block in two different directions.

Fig. 7 gives Pc-S-kr curves for the two sands (fine and coarse) and the homogenized curves for the block. As seen, the constitutive relationships at higher scale are different from the fine and coarse sands and a simple volumetric averaging of properties of sands can not represent the real situation. The residual saturation is significantly larger at higher scale. The directional dependency of Pc-S curves is probably due to the interplay of the fine material with Dirichlet boundary conditions. When flow is in horizontal direction, the fine material can be fully saturated with NAPL as soon as the Pc exceeds its entry pressure. But when 1-D flow is established in vertical direction, the course sand may reach

its residual water saturation (thus no permeability to water) and cause the entrapment of water inside the fine material. Also, relative permeability curves of REV block are significantly different from those of fine and coarse sands. They are directional dependent. This dependency is not because of boundary condition effects, as it is observed even before NAPL enters the fine media; this is probably characteristic of heterogeneous media.

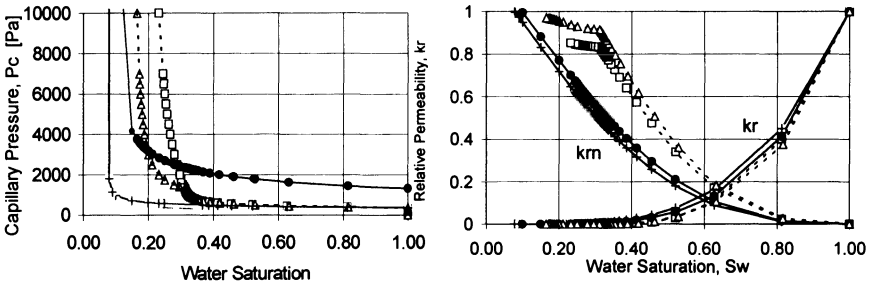

Fig. 7. Pc-Sw-kr relations for the elementary block. Triangular and square symbols indicate curves for horizontal and vertical directions. Circles and plus symbols indicate curves for fine and coarse medium, respectively.

CONCLUSIONS

Upscaling of multiphase properties of a heterogeneous medium is studied. The STOMP model used in this study is tested through simulating experiments of Kueper et al. [3]. A proper boundary condition at the DNAPL source in this experiment is suggested and it is shown that the commonly-used boundary condition is not physically correct. For a porous medium with periodic heterogeneity the concept of REV is studied and a REV block is identified. For that block, upscaled (or effective) relationships for saturation, capillary pressure and relative permeability are calculated. We have found that heterogeneities have a significant impact on effective relationships. It is shown that kr-S relation is directional dependent for heterogeneous porous media.

REFERENCES

1. Brooks, RH, Corey, AT (1964) Hydraulic properties of porous media. Hydrol. Pap. 3, Civ. Eng. Dep., Colo. State Univ., Fort Collins.
2. Helmig, R (1997) Multiphase flow and transport processes in the subsurface. Springer-Verlag, Berlin.
3. Kueper, BH, Abbot, W, Farquhar (1989) Experimental observations of multiphase flow in heterogeneous porous media. J. Contam. Hydrol.,5, 83-95.
4. Kueper, BH, Frind EO (1991) Two-phase flow in heterogeneous porous media 1. Model development. Water Resour. Res., 27(6), 1049-1057.
5. White MD, Oostrom M (1997) STOMP subsurface transport over multiple phases, user's guide. Pacific Northwest National Laboratory, Richland, Washington.

Automatic Grid Adaptation for Multidimensional Coupled Processes in Subsurface Hydrosystems

R. Kaiser, O. Kolditz and W. Zielke

Institut für Strömungsmechanik und Elektronisches Rechnen im Bauwesen
Universität Hannover
Appelstrasse 9A, 30167 Hannover, Germany
email: kaiser@hydromech.uni-hannover.de

Abstract. The finite element program Rockflow-3 has been developed to simulate complex flow and transport processes of one and more fluid phases in subsurface hydrosystems, combining coupled modules with the method of automatic grid adaptation [1].
On the one hand the 3d-start meshes can be constructed by conformly coupled 1d,2d,3d-elements, where the porous rock matrix is discretized by 3d-volumes, fractures by 2d-planes and main pathways within the fractures by 1d-line-elements. On the other hand networks of fractures (2d-planes in the 3d-space) can be used in which the rock matrix can be ignored because of a very low permeability.
The unstructured start mesh needs to contain only the basic structural information on the reservoir geology. During the simulation, the mesh is automatically adjusted only where necessary. The aim of the proposed automatic grid adaptation method for coupled processes is to achieve a more effective simulation of heterogeneous reservoirs.

Key words: Fracture Network Model, Conformly Coupled Elements, Automatic Grid Adaptation

INTRODUCTION

A numerical model has been developed to compute coupled fluid flow and tracer transport processes [1]. If transport processes are dominated by advective mechanisms the velocity field is an important parameter of the transport equation. In a first step, fluid flow processes are computed using automatic grid adaptation. The surroundings of injection or extraction wells, the interaction area between fracture and rock matrix and the area between zones of different material parameters can be discretized for 3d-problems by an automatically adapted grid. After that the method of automatic grid adaptation can be used for the ensuing transport simulation by combining the refined grids.

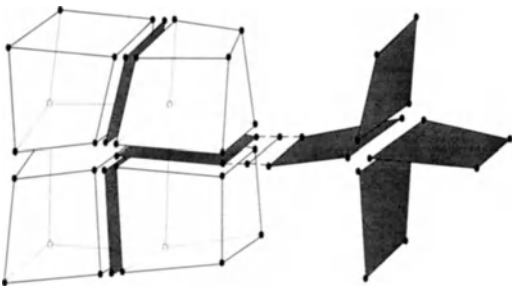

Fig. 1. Conformly coupled elements and a system of intersecting fractures (2d-elements)

The unstructured start mesh, that needs to contain only the basic structural information on the reservoir geology, can be constructed by conformly coupled 1d,2d,3d-elements, where the 3d-elements represent the rock matrix (Fig. 1, left). In the case of a low permeable rock matrix the fractures are represented by a 2.5d-fracture network, i.e. intersecting planes in the 3d-space (Fig. 1, right). Conformly coupled 1d,2d,3d-elements and 2.5d-fracture networks can be coupled with each other. The generation of the start mesh is non-trivial, especially for 3d-problems.

MATHEMATICAL MODEL

With the assumption of an incompressible flow the flow equation becomes linear. The partial differential equation of groundwater flow is then given by

$$S \frac{\partial p}{\partial t} + div\, \mathbf{v_f} - q = 0$$

including Darcy's law

$$\mathbf{v_f} = -\frac{\mathbf{k}}{\mu} \mathbf{grad}\,(p + z\rho g)$$

with S: storage coefficient, t: time, q: flow rate, ρ: density, p: pressure, $\mathbf{v_f}$: seepage velocity tensor, μ: viscosity and $\mathbf{k}$: permeability tensor.

The parabolic flow equation is treated with the Bubnov-Galerkin method in space and the implicit Euler method in time.

The flow equation and the conservative transport equation which reads as

$$n\rho \frac{\partial c}{\partial t} + \rho\, \mathbf{v_f}\, \mathbf{grad} c - div(n\rho\, \mathbf{D}\, \mathbf{grad} c) + \rho q\,(c - c_{in}) = 0$$

(with n: porosity, c: concentration, c_{in}: concentration at inflow node and $\mathbf{D}$: dispersion-diffusion tensor)

are connected by the velocity field and the flux term. A stationary velocity field will normally be required for the computation of long-time transport processes, so that a storage coefficient equal to zero can be selected. In the case of the mixed parabolic/hyperbolic transport equation a Streamline-Upwind/Petrov-Galerkin method is used in space and a Crank-Nicolson method in time.

AUTOMATIC GRID ADAPTATION

Automatic grid adaptation controled by heuristic (differences, gradients, curvatures) or analytical (Babuška, Johnson) indicators is suitable for problem-related discretization [2,3,4]. Refinement is limited to zones where the finite element solution, based on a coarse grid,

cannot approximate the exact solution satisfactorily. If the refined elements are not needed any longer they can be coarsened until the initial grid level is obtained.

Refinement Indicators. Refinement indicators play an important role in order to mark areas, where a mesh refinement or coarsening is necessary.
There exist a great number of mathematically proved error indicators and estimators for elliptic and parabolic problems. But these error indicators often are only proved for 1d- and 2d-elements and depend on the differential equation and the numerical method of the computed problem.
Therefore, in the case of multidimensional (coupled 1d/2d/3d-elements) coupled processes, analytical error indicators have a great disadvantage to heuristic refinement indicators. Since heuristic indicators are problem independent they can be used for different problems, e.g. parabolic (hydraulic simulation) and parabolic/hyperbolic (tracer transport simulation).

For each element type, different indicators can be applied. The gradient of the numerical solution scaled by the element size is an often used refinement indicator.
Such a gradient indicator can be given by

$$\eta_E = h\,|\nabla U(S_E)| \quad on \quad E \in Q$$

with U numerical solution, S_E centre of the element E and h the diameter of the element (longest edge).
In the following application the curvature (jump) indicator

$$\eta_E = h \max_{\tau \in \partial E \cap \Omega} \left| \left[\frac{\partial U}{\partial n_\tau} \right] \right| \quad on \quad E \in Q$$

is used either for the hydraulic or the ensuing tracer transport simulation. In the case of 2d-elements, h can be given by $\sqrt{a}$ (a area of the element E). This indicator calculates (because of the linear shape functions) the maximum of the jumps across the element sides τ in the normal component of the gradient of U. In addition, different refinement indicators can be combined with each other.

Refinement Strategy. After the refinement indicators have determined refinement values for each element it must be decided which elements will be refined and/or coarsened. For this, the refinement values devided by the averaged value can be used. The elements are refined or coarsened if the computed values of the elements are higher or lower than given tolerances.

The implemented h-adaptive algorithm [5] for mixed element types requires irregular nodes in order to establish new elements with a shape identical to that of the original elements (Fig. 2). These irregular nodes are eliminated on the element level. The advantage of this procedure lies in its strongly hierarchical character. In this way, it is possible to reverse the refinement of any element if necessary [2].

If coupled processes (e.g. hydraulic simulation / tracer transport simulation) are considered the method of automatic grid adaptation can be used for each process by combining the refined grids. The elements can only be coarsened if the coarsement is allowed by all processes that have caused the refinement of these elements. Since the coarsement strategy causes a more or less error in the solution of the problem a correction algorithm is implemented.

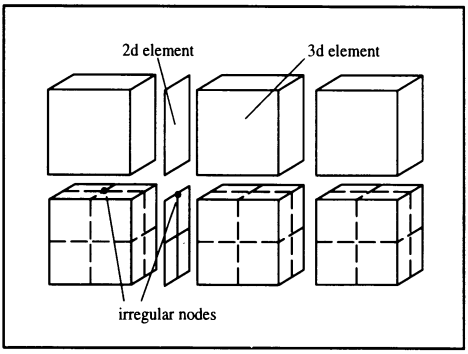

Fig. 2. Refinement strategy

Timestep Control. After the grid adaptation the timestep must be controled in order to adapt the timestep to the varying mesh size. In the case of transport processes the Courant criterion

$$Cr = \frac{|v|\,\Delta t_{Cr}}{\Delta s} <= 1$$

and/or the Neumann criterion

$$Ne = \frac{D\Delta t_{Ne}}{\Delta s^2} <= \frac{1}{2}$$

is used [2]. The new timestep is computed by

$$\Delta t = min(\Delta t_{Cr}, \Delta t_{Ne}).$$

APPLICATION: FRACTURE NETWORK MODEL

The geometry of the reservoir model is based on observations at the geothermal research site in Soultz-sous-Forêts (France) [6]. After successive intersection of single fractures, the resulting triangular mesh was refined, smoothed and converted into a quadrilateral start mesh (Fig. 3, top) [4,7].
The fractures are penetrated by two boreholes (sink and source) with constant discharge and recharge rates and were assumed to be of constant thickness. The position of the boreholes can be seen in Fig. 3 (middle) where the automatic grid adaptation (hydraulic simulation) has caused a mesh refinement.

First of all, fluid flow processes were considered. Especially in the area of the sink and the source the start mesh was refined because of large changes of the pressure gradients (Fig. 3, middle). The jump indicator was used either for the hydraulic simulation or for the coupled hydraulic/tracer transport simulation (Fig. 3).

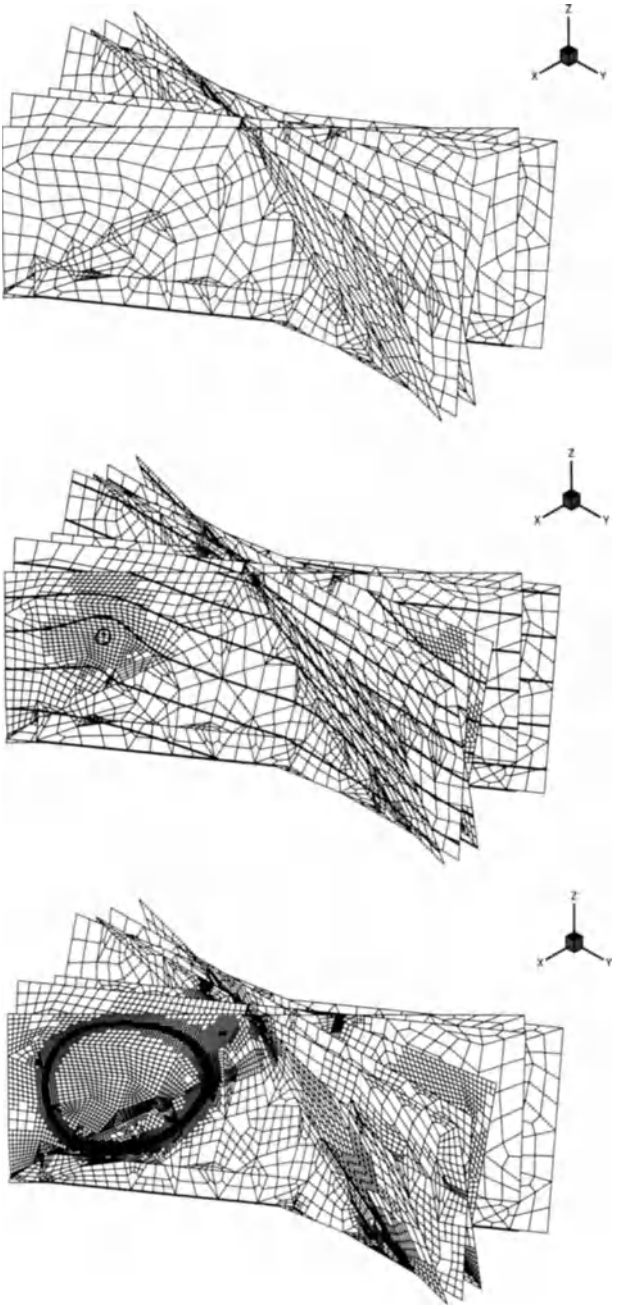

Fig. 3. Initial grid and automatically refined grids after hydraulic simulation and after coupled hydraulic/tracer transport simulation

The adaptively refined grids of the hydraulic simulation and the ensuing tracer transport simulation were automatically combined with each other (Fig. 3, bottom). In the case of the fluid flow process two refinement levels were allowed, whereas in the case of the tracer transport process each element could be refined up to three times.

ACKNOWLEDGEMENT

This work was partly supported by Geowissenschaftliche Gemeinschaftsaufgaben (GGA). The authors appreciate the support of D. Pribnow and C. Clauser, in particular their help in data acquisition.

REFERENCES

1. Kolditz O, Habbar A, Kaiser R, Kasper H, Schulze-Ruhfus M, Rother T, Thorenz C, Zielke W (1998) Software Concept of Simulating Coupled Processes in Subsurface Hydrosystems. In: Proc. Hydroinformatics 98, Copenhagen, pp 613-618

2. Barlag C, Zielke W (1996) Dynamic Adaptive Transport Simulation in Fractured Subsurface. In: Proc. XI Int. Conf. on Computational Methods in Water Resources, Cancun, Mexico

3. Kaiser R, Kolditz O, Zielke W (1998) Automatic grid adaptation for subsurface fluid flow problems - Application to fractured-porous reservoirs. In: Proc. XII Int. Conf. on Computational Methods in Water Resources, Crete, Greece, pp 125-132

4. Kaiser R, Rother T, Kolditz O (1999) Modelling of Flow in Fractured Aquifers Using Automatic Grid Adaptation. In: Proc. XXVIII IAHR Congress, Graz, Austria, page 30 (CD-ROM)

5. Schulze–Ruhfus M (1996) Adaptive Verfeinerung und Vergröberung gekoppelter 1D/2D/3D–Elemente. Diplomarbeit, Institut für Strömungsmechanik und Elektronisches Rechnen im Bauwesen, Universität Hannover

6. Pribnow D, Clauser C.(1998) Heat- and Fluid-Flow in the Rhine Graben: Regional and Local Models for a Hot-Dry-Rock System. 4th HDR Forum, Strasbourg, France

7. Kasper H, Kosakowski G, Rother T, Thorenz C, Kolditz O, Taniguchi T (1998) Development of a 3-D CAD System for Numerical Analysis of Subsurface Flow & Transport. In: Proc. 6th Int. Conf. on Numerical Grid Generation in Computational Field Simulation, Greenwich, UK, pp 683-694

Efficient Computational Algorithm in Groundwater Management

Tanehiro FUTAGAMI[1], Hiroshi YAMAJI[2], Yoshihiro ISHII[1] and Keichiro OKIYAMA[1] and Kazuhito KAIBARA[1]

[1] Department of Civil and Architectural Engineering, Hiroshima Institute of Technology, 1-1, 2-chome, Miyake, Saeki, Hiroshima 731-5193, Japan
[2] Yachiyo Engineering Company, 5-13, 1-chome, Nakameguro, Meguro, Tokyo 153-8369, Japan

ABSTRACT: In this paper an efficient computational algorithm of the finite element and dynamic linear programming method (the FE&DLP method) for transient groundwater management in confined aquifers is studied in order to save computer time and memory due to its special structures. The FE&DLP method has been developed by the combined use of the finite element method with dynamic linear programming to optimize transient distributed parameter systems with both equality or inequality constraints and an objective function. Such systems are frequently encountered in various engineering and scientific problems of control and optimization and, especially are of interest in groundwater management. The finite element method is powerful numerical method for the solution of differential equation systems because of its generality with respect to geometry and material properties. Dynamic linear programming is the extension of linear programming to the time domain. The proposed efficient computational algorithm (the simplified simplex algorithm) makes it possible to obtain an initial basic feasible solution of the simplex method for linear programming without the introduction of artificial variables and to omit the troublesome Phase I of the simplex method. Therefore, the proposed algorithm allows us to solve large-scale optimal control problems in transient groundwater management.

KEY WORDS: groundwater management, optimization, distributed parameter systems, finite element method, dynamic linear programming

INTRODUCTION

In recent years a great deal of research work of distributed parameter systems governed by partial differential equation systems has been carried out by scientists and engineers [1]. By combining the finite element method with linear programming, the finite element and linear programming method (the FE&LP method) has been developed in order to optimize distributed parameter systems [2,3,4,5]. By extending the FE&LP method to the time domain, the finite element and dynamic linear programming method (the FE&DLP method) has been developed in order to solve transient distributed parameter control systems [6]. Dynamic problems of linear programming arise when a program or plan of optimal development of dynamics systems is required [7,8]. Aguado and Remson have suggested a combined use of the finite element method with linear programming in the study of groundwater management, in which the finite difference method has been used instead of the finite element method [9]. In order to save computer time and memory, in this paper an efficient computational algorithm of the FE&DLP method in transient groundwater management is studied due to its special structures.

THE FE&DLP METHOD IN GROUNDWATER MANAGEMENT

Basic Differential Equation Systems. The basic differential equation systems describing transient confined aquifer management with constraints and an objective function are as follows:

1) Objective Function

$$Z = Opt.\int_T\int_\Omega f(h,\theta)\,d\Omega dT \approx Max.\int_T\int_\Omega \theta\, d\Omega dT \quad (1)$$

subject to:

2) Governing Differential Equations

(1) Groundwater Flow Equation

$$S\frac{\partial h}{\partial t} = T_x\frac{\partial^2 h}{\partial x^2} + T_y\frac{\partial^2 h}{\partial y^2} - \theta - Q \quad (in\ \Omega) \quad (2)$$

(2) Initial Condition

$$h = H^0 \qquad (at\ t = 0) \quad (3)$$

(3) Boundary Conditions

$$T_n\frac{\partial h}{\partial n} = -q_n \qquad (on\ \Gamma_1) \quad (4)$$

$$h = H_b \qquad (on\ \Gamma_2) \quad (5)$$

3) Constraints

$$h \geq \underline{H} \qquad (in\ \Omega^g) \quad (6)$$

$$\theta \leq \overline{\Theta} \qquad (at\ point\ fitted\ for\ controllable\ sink) \quad (7)$$

4) Nonnegative Conditions

$$h \geq 0 \quad (8), \qquad \theta \geq 0 \quad (9)$$

in which h = the state variable (groundwater head); θ = the decision variable (controllable sink); Q = known sink; S = the storage coefficient; T_x, T_y = the transmissivity; q_n = groundwater flux; $\underline{H}$ = the lower limit of state variable and $\overline{\Theta}$ = the upper limit of decision variables.

Although the objective function may be composed with the state variables $\{h\}$ and the decision variables $\{\theta\}$ in general, maximization of the total of the decision variables is sought in this research.

Formation of the FE&DLP method. In the discretization of the basic differential equation systems (Eq. 1-9), the Galerkin finite element method based on weighted residual process is used because of its independency of variational principle [10]. Although several time stepping schemes in the finite element method have been presented, the backward differencing is used in this research. Then, the formulation of the FE&DLP method is obtained as follows:

1) Objective Function

$$Z = Opt.\sum_{\tau=1}^{T}\left(\sum_{n=1}^{N} c_n^\tau h_n^\tau + \sum_{i=1}^{I} e_i^\tau \theta_i^\tau\right) \approx Max.\sum_{\tau=1}^{T}\sum_{i=1}^{I} \Delta t\,\theta_i^\tau \quad (10)$$

subject to:

2) State Transformation Equation

$$-[A]\{h_n^{\tau-1}\} + \{h_n^\tau\} + [D]\{\theta_i^\tau\} = \{f_n^\tau\} \quad (\tau = 1\sim T) \quad (11)$$

3) Constraints

$$[G]\{h_n^\tau\} \geq \{\underline{H_l^\tau}\} \quad (\tau = 1\sim T) \quad (12)$$

$$\{\theta_i^\tau\} \leq \{\overline{\Theta_i^\tau}\} \quad (\tau = 1\sim T) \quad (13)$$

4) Nonnegative Conditions

$$\{h_n^\tau\} \geq 0 \ (\tau = 1\sim T) \quad (14), \qquad \{\theta_i^\tau\} \geq 0 \ (\tau = 1\sim T) \quad (15)$$

in which c_n^τ, e_i^τ = cost coefficients; Δt = time step; τ = time step number; n = node number; and i = controllable sink (well) number.

EFFICIENT COMPUTATIONAL ALGORITHM

Conversion of Inequality Systems to Equality Systems. The obtained equation systems (Eqs. 10-15) include inequality constraints (Eqs. 12 and 13). In developing of the solution procedures of the FE&DLP method, we shall find much easier to work with equality constraints. By converting the inequalities to the equalities through the use of slack variables $\{\chi_l^\tau\}$ and $\{\gamma_i^\tau\}$, we obtain the following equality systems (standard systems).

1) Objective Function

$$Z = Opt.\sum_{\tau=1}^{T}\left(\sum_{n=1}^{N} c_n^\tau h_n^\tau + \sum_{i=1}^{I} e_i^\tau \theta_i^\tau\right) \approx Max.\sum_{\tau=1}^{T}\sum_{i=1}^{I} \Delta t\,\theta_i^\tau \tag{16}$$

subject to:

2) State Transformation Equation

$$-[A]\{h_n^{\tau-1}\}+\{h_n^\tau\}+[D]\{\theta_i^\tau\}=\{f_n^\tau\} \quad (\tau=1\sim T) \tag{17}$$

3) Constraints

$$[G]\{h_n^\tau\}-\{\chi_l^\tau\}=\{H_l^\tau\} \quad (\tau=1\sim T) \tag{18}$$

$$\{\theta_i^\tau\}+\{\gamma_i^\tau\}=\{\Theta_i^\tau\} \quad (\tau=1\sim T) \tag{19}$$

4) Nonnegative Conditions

$$\{h_n^\tau\}\ge 0 \ (20), \quad \{\theta_i^\tau\}\ge 0 \ (21), \quad \{\chi_l^\tau\}\ge 0 \ (22), \quad \{\gamma_i^\tau\}\ge 0 \ (23)$$

Finding of Initial Basic Feasible Solution with Introduction of Artificial Variables -- Usual Two Phases Simplex Algorithm. Usually, the obtained standard systems (Eqs. 16-23) of linear programming are solved by using the simplex method. Before the use of the simplex method, however, it is necessary to find a solution which satisfies Eqs. 17-23. Such a solution which satisfies the given conditions (Eqs. 17-23) is called a basic feasible solution. The simplex method is always initiated with a program whose equations are in canonical systems which apparently show a basic feasible solution. In the case where a canonical form, or an initial basic feasible solution, can not be found, we have to use the two phases (Phase I and Phase II) of the simplex method. Phase I is to find to an initial basic feasible solution and Phase II is to find an optimal feasible solution, if one exists. And Phase I of the simplex method augments the systems to include a basic set of artificial variables $\{\lambda_n^\tau\}$, $\{\xi_l^\tau\}$ and $\{\zeta_i^\tau\}$ as follows:

1) Objective Function

$$Z = Opt-\left(\sum_{\tau=1}^{T}\sum_{n=1}^{N}\lambda_n^\tau+\sum_{\tau=1}^{T}\sum_{l=1}^{L}\xi_l^\tau+\sum_{\tau=1}^{T}\sum_{i=1}^{I}\zeta_i^\tau\right) \tag{24}$$

subject to:

2) State Transformation Equation

$$-[A]\{h_n^{\tau-1}\}+\{h_n^\tau\}+[D]\{\theta_i^\tau\}+\{\lambda_n^\tau\}=\{f_n^\tau\} \quad (\tau=1\sim T) \tag{25}$$

3) Constraints

$$[G]\{h_n^\tau\}-\{\chi_l^\tau\}+\{\xi_l^\tau\}=\{H_l^\tau\} \quad (\tau=1\sim T) \tag{26}$$

$$\{\theta_i^\tau\}+\{\gamma_i^\tau\}+\{\zeta_i^\tau\}=\{\Theta_i^\tau\} \quad (\tau=1\sim T) \tag{27}$$

4) Nonnegative Conditions

$\{h_n^\tau\} \geq 0$ (28), $\{\theta_i^\tau\} \geq 0$ (29), $\{\chi_l^\tau\} \geq 0$ (30), $\{\gamma_i^\tau\} \geq 0$ (31), $\{\lambda_n^\tau\} \geq 0$ (32), $\{\xi_l^\tau\} \geq 0$ (33), $\{\varsigma_i^\tau\} \geq 0$ (34)

Finding of Initial Basic Feasible Solution without Introduction of Artificial Variables -- Simplified Simplex Algorithm. In this research, by use of the special structures of the FE&DLP method in transient groundwater management, the following efficient computational algorithm (the simplified simplex algorithm) to find an initial basic feasible solution is developed without introduction of artificial variables. Therefore, the troublesome Phase I of the simplex method becomes unnecessary. The algorithm is based on the following repeated procedure to the state transformation equation (Eq. 17).

$$\{h_n^\tau\} + \sum_{k=1}^{\tau} [D_k^\tau]\{\theta_i^k\} = \{F_n^\tau\} \quad (\tau = 1 \sim T) \tag{35}$$

in which

$[D_\tau^k] = [D] (k = \tau)$ (36), $[D_\tau^k] = [D_{k+1}^\tau] (k = \tau - 1 \sim 1)$ (37), $\{F_n^\tau\} = \{f_n^\tau\} + [A]\{F_n^{\tau-1}\}$ (38), $\{F_n^0\} = [A]\{H_n^0\}$ (39)

Eq 35 means a solution of the state variables $\{h_n^\tau\}$ expressed in the decision variables $\{\theta_i^\tau\}$.
Substituting Eq. 35 into the constraint (Eq. 18) yields the following equation.

$$\sum_{k=1}^{\tau} [E_k^\tau]\{\theta_i^k\} - \{\chi_l^\tau\} = \{P_l^\tau\} \quad (\tau = 1 \sim T) \tag{40}$$

in which

$$[E_k^\tau] = -[G][D_k^\tau] \quad (41), \qquad \{P_l^\tau\} = \{H_l^\tau\} - [G]\{F_n^\tau\} \quad (42)$$

Rewriting Eqs. 17 and 18 in the standard systems (Eqs. 16-23) by Eqs. 35 and 40 yields the following canonical systems.

1) Objective Function

$$Z = Opt. \sum_{\tau=1}^{T} \left(\sum_{n=1}^{N} c_n^\tau h_n^\tau + \sum_{i=1}^{I} e_i^\tau \theta_i^\tau \right) \approx Max. \sum_{\tau=1}^{T} \sum_{i=1}^{I} \Delta t \theta_i^\tau \tag{43}$$

subject to:

2) State Transformation Equation

$$\{h_n^\tau\} + \sum_{k=1}^{\tau} [D_k^\tau]\{\theta_i^k\} = \{F_n^\tau\} \quad (\tau = 1 \sim T) \tag{44}$$

3) Constraints

$$\sum_{k=1}^{\tau} [E_k^\tau]\{\theta_i^k\} - \{\chi_l^\tau\} = \{P_l^\tau\} \quad (\tau = 1 \sim T) \tag{45}$$

$$\{\theta_i^\tau\} + \{\gamma_i^\tau\} = \{\overline{\Theta_i^\tau}\} \quad (\tau = 1 \sim T) \tag{46}$$

4) Nonnegative Conditions

$\{h_n^\tau\} \geq 0$ (47), $\{\theta_i^\tau\} \geq 0$ (48), $\{\chi_l^\tau\} \geq 0$ (49), $\{\gamma_i^\tau\} \geq 0$ (50)

By choosing $\{\theta_i^\tau\}$ to be equal to $\{0\}$ in the above canonical systems, we can easily find an initial basic feasible solution which satisfies the given conditions (Eqs. 44-50) as follows

$\{h_n^\tau\} = \{F_n^\tau\}$ (51), $\{\theta_i^\tau\} = \{0\}$ (52), $\{\chi_l^\tau\} = \{P_l^\tau\}$ (53), $\{\gamma_i^\tau\} = \{\overline{\Theta_i^\tau}\}$ (54)

In the initial basic feasible solution the basic variables are $\{h_n^\tau\}$, $\{\chi_l^\tau\}$ and $\{\gamma_i^\tau\}$, and the non-basic variables are $\{\theta_i^\tau\}$.
Since maximization of total of the decision variables is considered in this research, the FE&DLP

method has the following specialities.

1) All of the cost coefficients associated with the state variables and the slack variables are equal to 0.

2) Since all of the state variables $\{h_n^\tau\}$ always have positive values, they always become basic variables. Then we can exclude the state variables in the pivot operation.

Then the initial simplex tableau of the simplified simplex algorithm is obtained as shown in Table 1. The optimal solution for the state variables $\{h_n^\tau\}$ is given by substitution of the obtained optimal values of decision variables $\{\theta_i^\tau\}$ into Eq. 44.

Table1. Initial Simplex Tableau in Efficient Computational Algorithm of the FE&DLP Method

Basic Variables	① Cost Coefficients	② Constants	Cost Coefficients								
			Δt	Δt	Δt	0	0	0	0	0	0
			Decision Variables			Slack Variables					
			$\{\theta_i^1\}$	$\{\theta_i^2\}$	$\{\theta_i^3\}$	$\{\chi_l^1\}$	$\{\chi_l^2\}$	$\{\chi_l^3\}$	$\{\gamma_l^1\}$	$\{\gamma_l^2\}$	$\{\gamma_l^3\}$
$\{\chi_l^1\}$	0	$\{P_l^1\}$	E_1^1			-I					
$\{\chi_l^2\}$	0	$\{P_l^2\}$	E_1^2	E_2^2			-I			0	
$\{\chi_l^3\}$	0	$\{P_l^3\}$	E_1^3	E_2^3	E_3^3			-I			
$\{\gamma_l^1\}$	0	$\{\Theta_i^1\}$				I			I		
$\{\gamma_l^2\}$	0	$\{\Theta_i^2\}$		0			I			I	
$\{\gamma_l^3\}$	0	$\{\Theta_i^3\}$						I			I
Objective Function		(①·②)	-Δt	-Δt	-Δt	0	0	0	0	0	0
			Optimal Criteria								

NUMERICAL EXAMPLE

A numerical example is conducted in a rectangular model confined aquifer as shown in Fig. 1. The model aquifer is discretized into 192 triangle elements and 117 nodal points. Consider the case in which there will further increase of unsteady controllable (unknown) sinks $\{\theta_1^\tau\}$, $\{\theta_2^\tau\}$ over the existing uncontrollable (known) sink $\{Q_3^\tau\} = \{5\times10^{-2}\} cm^3/s$. Two nodal points A and B are regulated in the same groundwater head requirement, i.e., $\{H_A^\tau\} = \{H_B^\tau\} = \{18.0\} cm$.

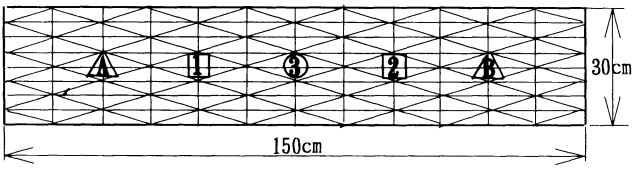

$$\frac{\partial h}{\partial n} = 0 \text{ (on the Four Boundaries)}$$

$$\Delta t = 180s;\ \tau = 1,2,3;\ i = 1,2;\ l = A,B;\ \{H_n^0\} = \{20.0\} cm$$

$$S = 5\times10^{-3},\quad T_x = T_y = 0.05 cm^2/s$$

□: **Nodal Point for Controllable (Unknown) Sink**

$$(\{\theta_{1,2}^\tau\} \le \{\bar{\Theta}_{1,2}^\tau\} = \{2.5\times10^{-2}\} cm^3/s)$$

○: **Nodal Point for Unkontrollable (Known) Sink**

$$(\{Q_3^\tau\} = \{5.0\times10^{-2}\} cm^3/s)$$

△: **Regulated Nodal Point in Groundwater Head**

$$(\{h_{A,B}^\tau\} \ge \{\underline{H}_{A,B}^\tau\} = \{18.0\} cm)$$

Computed results are shown in Fig. 2. Note that the distribution

Fig. 1. Input Data on the FE&DLP Method in Rectangular Model Confined Aquifer

pattens ofthe groundwater head in Fig. 2 arise from the resultant sinks composed of the obtained controllable sinks $\{\theta_1^\tau\}$, $\{\theta_2^\tau\}$ and the given uncontrollable sink $\{Q_3^\tau\}$.

CONCLUSIONS

The paper presents an computational aspect of aquifer management. By use of the special structures of the FE&DLP method in confined aquifer management, an efficient computational algorithm (simplified simplex algorithm) is developed in order to save computer time and memory. The proposed algorithm makes it possible to obtain the initial basic feasible solution without the introduction of the artificial variables and to omit the troublesome Phase I of the general simplex method. Therefore, the proposed algorithm allows us to solve large-scale optimization problems of distributed parameter systems in confined aquifer management. The tractability in the initial conditions, boundary conditions and the equality or inequality constraints makes sure that the FE&DLP method becomes an useful technique in aquifer management.

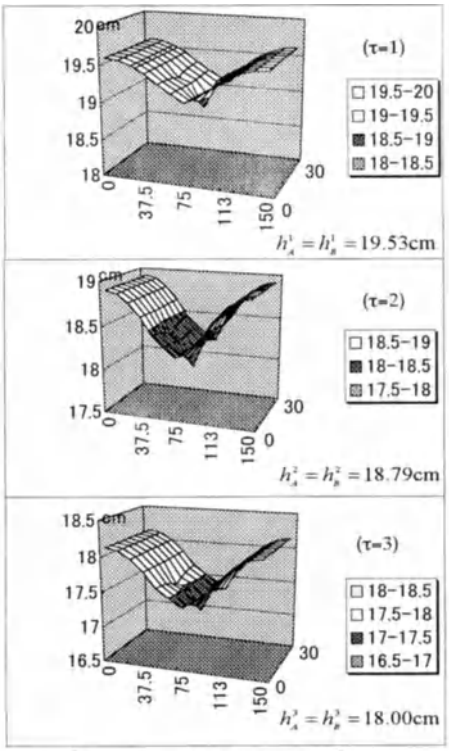

$$Z = \Delta t \times \left(\theta_1^1 + \theta_2^1 + \theta_1^2 + \theta_2^2 + \theta_1^3 + \theta_2^3\right)$$
$$= 180 \times (1.03 + 2.50 + 2.50 + 2.50 + 2.50) \times 10^{-2}$$
$$= 21.7 cm^3$$

Fig.2. Distribution Patterns of Groundwater Heads and Objective Function

REFERENCES

1. Futagami T, Tzafestas SG, Sunahara Y (editors) (1989) Distributed Parameter Systems: Modelling and Simulation. North-Holland .
2. Futagami T (1975) Finite Element & Linear Programming Method and Water Pollution Control. Proc 16th Congress IAHR: c7, 54-61.
3. Futagami T, Tamai N, Yatsuzuka M (1976) FEM Coupled with LP for Water Pollution Control. J Hyd Div ASCE:881-897.
4. Elango K and Rouv G (1980) Aquifers: Finite Element Linear Programming Model. J Hyd Div ASCE HY10:1641-1658.
5. Ueda T, Jinno K, Chyono Y (1979) On the Optimal Well Discharge in Ground Water Area.. Proc JSCE Vol 283: 33-43.
6. Futagmi T, Fukuhara T, Tomita M (1977) Transient Finite Element & Linear Programming Method in Environmental Systems Control The Efficient Computational Algorithm. Proc IFAC Environmental Sympo: 143-150.
7. Dantzig BJ (1963) Linear Programming and Extensions. Princeton Univ Press.
8. Propoi A (1977) Dual Systems of Dynamic Linear Programming. IIASA, Austlia, PR-77-9.
9. Aguado E and Remson I.(1974) Ground-Water Hydraulics in Aquifer Management. J Hyd Div ASCE Vol 100 HY1: 103-118.
10. Zienkiewicz OC (1977) The Finite Element Method: 3rd ed , McGraw-Hill.

Groundwater Modeling by Layer Based Three-Dimensional Concept

Tung-Lin Tsai[1], Liang-Hsiung Huang[2] and Jinn-Chuang Yang[3]

[1]Graduate Student, Department of Civil Engineering, National Chiao-Tung Unversity, Hsinchu, Taiwan 30010, R.O.C.
[2]Professor, Department of Civil Engineering, National Taiwan University, Taipei, Taiwan 10617, R.O.C.
[3]Professor, Department of Civil Engineering, National Chiao- Tung Unversity, Hsinchu,Taiwan 30010, R.O.C.

Abstract. Due to its simplicity and efficiency, the conventional quasi three-dimensional concept has been widely applied in analyzing groundwater flow in multiaquifer system, especially for regional problem. But the conventional quasi three-dimensional concept is not able to deal with the discontinuous and interconnected strata and fully three-dimensional flow. Therefore, in order not only to overcome these shortcomings but also to maintain efficiency, we propose a new layer based three-dimensional concept to develop a groundwater simulation model. This new concept assumes that the pore pressure of every aquifer and aquitard in the vertical direction can be depicted by the quadratic polynomial interpolation function, then the vertical integration is performed on each layer to ensure the continuity of pore pressure and flux at the interfaces between any two layers. The finite analytical numerical method is adopted to develop the present groundwater simulation model. The results show that the present model is capable of simulating fully three-dimensional flow pattern.

Key words. Layer based three-dimensional concept, Quadratic polynomial interpolation function, Vertical integration, Continuity of pore pressure and flux

INTRODUCTION

Due to natural sedimentary reaction, the groundwater basins are usually composed of a series of aquifers separated by aquitards of relatively low permeability. This is called a multiaquifer system. Generally speaking, the movement of groundwater in multiaquifer is three-dimensional. Although in the past 20 years or so, a number of three dimensional groundwater flow models were developed, they are found to be expensive even for modern-day computers. Furthermore, the groundwater basin has much greater horizontal than vertical extent and the permeability contrasts between the adjacent layers are large, hence it's not wise to deal with the groundwater problem from a complete three-dimensional viewpoint. So a popular conventional quasi three-dimensional concept is widely applied, especially for regional problem.

described as quadratic polynomial function

$$\Phi^e(x,y,z,t) = a(x,y,t) + b(x,y,t)z + c(x,y,t)z^2, \tag{2}$$

and apply vertical integration to every layer, we then obtain the flow governing equations of every aquifer or aquitard shown as below:

$$\frac{\partial^2 \overline{\Phi^e}}{\partial x^2} + \frac{\partial^2 \overline{\Phi^e}}{\partial y^2} = \frac{Ss}{K}\frac{\partial \overline{\Phi^e}}{\partial t} + \frac{1}{B}(-6\Phi^e\big|_{bi+1} - 6\Phi^e\big|_{bi} + 12\overline{\Phi^e}) + Q_L^e(x_w, y_w). \tag{3}$$

Note that the flux of top and bottom boundaries at the interface of every layer can be expressed as

$$\frac{K}{B}(4\Phi^e\big|_{bi+1} + 2\Phi^e\big|_{bi} - 6\overline{\Phi^e}) = q_l\big|_{bi+1}, \tag{4}$$

$$\frac{K}{B}(-2\Phi^e\big|_{bi+1} - 4\Phi^e\big|_{bi} + 6\overline{\Phi^e}) = q_l\big|_{bi}, \tag{5}$$

where $\overline{\Phi^e} = \int_{bi}^{bi+1}\Phi^e dz$, $\Phi^e\big|_{bi}$ = hydraulic head increment of bottom boundary in every layer and $\Phi^e\big|_{bi+1}$ = hydraulic head increment of top boundary in every layer.

Note that the initial condition of increment value, $\overline{\Phi^e}$, which can be written as

$$\overline{\Phi^e}(x,y,t=0) = 0\ , \qquad x,y \in \Omega\ , \tag{6}$$

where Ω = computation domain. The boundary condition at the natural boundary is

$$\Phi^e\big|_{boundary} = \Phi^*\ , \tag{7}$$

if it is applied to Dirichlet type boundary, while it is

$$\left.\frac{\partial \Phi^e}{\partial n}\right|_{boundary} = -q_n \tag{8}$$

if it is applied to Neuman type boundary. Φ^* and q_n are known values. In addition, the pore pressure and flux at the interface of any two layers must be continuous, and they can be expressed as

$$K^{(1)}\frac{\partial \Phi^{e(1)}}{\partial n} = K^{(2)}\frac{\partial \Phi^{e(2)}}{\partial n}, \tag{9}$$

and

$$\Phi^{e(1)} = \Phi^{e(2)}, \tag{10}$$

where the superscript (1), and (2) represent media of the neighboring two layers

NUMERICAL METHOD

The finite analytical numerical method (FA method) has been applied not only to computation of fluid dynamics but also to solution transport in groundwater flow for many years and obtained correspondent recognition (see Chen and Chen [5], Hwnag et al. [6]). The finite analytical method includes both implicit and explicit schemes. Because the implicit scheme is unconditional stable and it has the important trait of local analytical solution, we use the implicit finite analytical

The conventional quasi three-dimensional concept assumes that the flow is predominantly horizontal in the aquifers and vertical in the intervening aquitard, so the three dimensional governing equation is simplified to be horizontal two-dimensional for aquifer and vertical one-dimensional for aquitard. Then the aquifers and aquitards are coupled by leakage flux between them. In comparison with fully three-dimensional concept, the reduction of the computational cost and the significant increment of the efficiency make the conventional quasi three-dimensional concept very attractive for analysis of groundwater flow in multiaquifer system. For example, Berdehoft and Pinder [1], Choreley and Frind [2], Neuman et al. [3] and the popular commercial software, MODFLOW, all use this simple and efficient concept to simulate the multiaquifer system.

The error introduced in the conventional quasi three-dimensional concept has been investigated by Neuman and Witherspoon [4] for the particular case of flow within a single well in a two-aquifer system. They conclude that the error is less than 5% when the permeability contrast between neighboring aquifers and aquitards surpasses two orders of magnitude. However, the conventional quasi three-dimensional formulation was designed for layers of continuous and regularly alternating aquifer and aquitard units, and its generality will be restricted and misleading results can be produced since most real flow systems rarely contain such geologic simplicity. In addition, due to the over simplification of horizontal flow in aquifers, the conventional quasi three-dimensional concept can not simulate the three-dimensional flow pattern. Furthermore, because the vertical flow component is disregarded, the pollutant to be traced cannot travel through the aquitards to the underlying or overlying layers in this approach.

In order not only to overcome these shortcomings and difficulties but also to maintain efficiency in the study, we propose a new layer based three-dimensional concept to develop a groundwater simulation model. In this new layer based three-dimensional concept we assume that the interpolation function of pore pressure (hydraulic head) of every aquifer and aquitard in the vertical direction can be described by the quadratic polynomial, then the vertical integration technique is performed on each aquifer and aquitard to ensure the continuity of pore pressure and flux at the interfaces between any two layers. The finite analytical numerical method is adopted to develop the present groundwater simulation model.

GOVERNING EQUATIONS

The governing equation for general three-dimensional groundwater flow can be derived by applying the principle of conservation of mass and Darcy's law and written as

$$\frac{\partial}{\partial x_j}(k\frac{\partial \Phi^e}{\partial x_j}) = Ss\frac{\partial \Phi^e}{\partial t} + Q(x_w, y_w, z_w), \quad j = 1,2,3, \tag{1}$$

where k = hydraulic conductivity; Φ^e = increment hydraulic head; Q = point source rate. If we assume that the pore pressure of every aquifer and aquitard in the vertical direction can be method to develop groundwater model in this study.

MODEL VERIFICATION

a confined aquifer with partially penetrated well

The main purpose of this case is to demonstrate that the present model has the ability to simulate the fully three-dimensional groundwater flow pattern. A partially penetrated pumping well with a constant discharge rate $Q=3.01593*10^{-2}$ m^3/sec is located at the middle of a square simulation region of 180 m × 180 m. The aquifer has depth of 24 m. The partially penetrated well is shown in Fig. 1. The analytical solution of the problem is derived by Hantush [7]. According to Hantush [7], when the total time of simulation is larger than $B^2S_s/2k$, the exact solution can be expressed as the sum of well function and the zero-order modified Bessel function of the second kind. The B, S_s and k are aquifer depth, specific storage coefficient and hydraulic conductivity, respectively.

When we simulate this problem, the aquifer shown in Fig. 1 is considered as a whole layer or two or four virtual sublayers, respectively. The horizontal grid size is 6 m × 6 m. The top and bottom boundaries are all impervious. The initial state is steady and the analytical solutions are applied to horizontal boundary conditions of computation. In addition, the exact solutions are also applied to the grid points around the well. The simulation results of five times of $B^2S_s/2k$ are shown from Fig. 2 to Fig. 5. Fig. 2 to Fig. 4 show the distribution of the average drawdowns of every sublayers at different horizontal position from the well when the aquifer is considered as a whole layer or two or four virtual sublayers respectively. The distribution of drawdowns in vertical direction at the position 12 m and 24 m from the well are shown in Fig. 5. From the Fig. 4, we can find that at 12 m from the well the results are coincident with the analytical solution in the case of four sublayers but there are some deviations from exact solution for the case of two sublayers. Also notice that because the drawdown is nearly uniform in the vertical direction at 24 m from the well, the results are all coincident with exact solution in both cases of two and four sublayers .

From above discussions, we can clearly find that the present layer based three dimensional concept is capable of simulating the fully three dimensional flow pattern. We also find an interesting result that in the case of two sublayers at 12 m form the well, the vertical drawdown has some deviations from exact solution but the vertical average drawdown of every sublayer is nearly the same as the analytical solution.

CONCLUSIONS

In this study we apply the new layer based three-dimensional concept and adopt finite analytical numerical method to develop a groundwater simulation model. The results show that it can simulate the fully three-dimensional flow pattern near pumping well. The present model surmounts

the limitations of the conventional quasi three-dimensional formulation and maintains its efficiency.

ACKNOWLEDGEMENT

The authors thank the National Science Council of R.O.C. for supporting this research under the grant NSC87-2211-E002-051.

REFERENCES

1.Bredhoft, J.D., Pinder, G.F. (1970) Water Resource Research 6: 883-888
2.Choreley, D.W., Frind, E.O. (1978) Water Resource Research 14: 943-952
3.Neuman, S.P., Preller, C., Narasimhan, T.N. (1982) Water Resource Research 18: 1551-1561
4.Neuman, S.P., Witherspoon, P.A. (1969) Water Resource Research 5: 803-816
5.Chen, C.J., Chen, H.C. (1984) Journal of Computation Physics 53: 209-226
6.Hwang, J.C., Chen, C.J., Sheikhoslami, M., Panigrahi, B.K. (1985) Water Resource Research 21: 1354-1366
7. Hantush, M.S. (1961) Journal of Hydraulic Division, ASCE, 5: 171-195

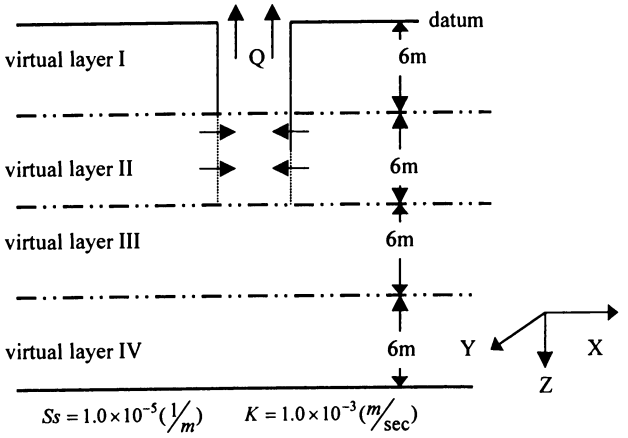

Fig. 1. Confined aquifer with a partially penetrated well

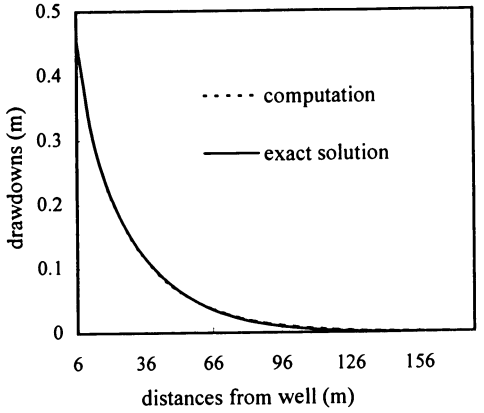

Fig. 2. Comparision of numerical and analytical solutions of average drawdowns (one layer case)

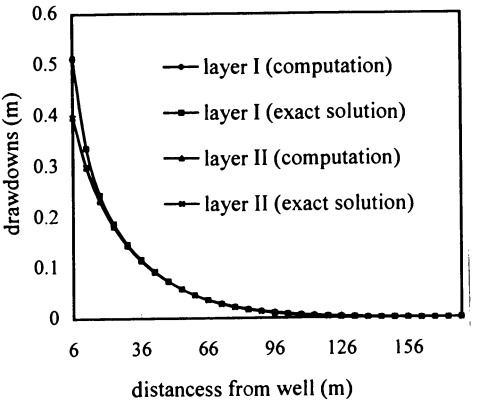

Fig. 3. Comparision of numerical and analytical solutions of average drawdowns (two layers case)

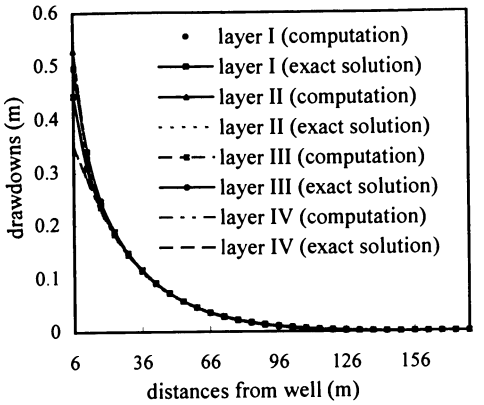

Fig. 4. Comparision of numerical and analaytical solutions of average drawdowns (four layers case)

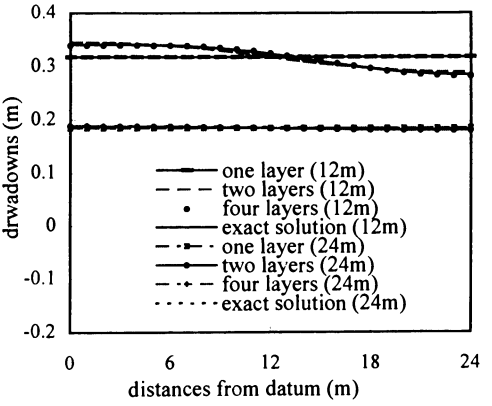

Fig. 5. Comparsion of numerical and analytical solutions of drawdowns in the vertical direction

Numerical modeling of volatile and slightly soluble contaminant flow in unsaturated and saturated zone

Kazumasa Itoh[1], Hiroyuki Tosaka[2], Osamu Matsubara[3]and Yoshio Hirota[4]

[1]Rock EngineeringDepartment, OYO Corporation 2-61-5 Toro, Omiya, Saitama, 330 8632, Japan
[2]Department of Geosystem Engoneering, The University of Tokyo, 7-3-1 Hongo Bunkyo-ku, Tokyo 113 7656 Japan.
[3]Department of Geosystem Engineering, The University of Tokyo, 7-3-1 Hongo Bunkyo-ku, Tokyo 113 7656 Japan. (Present Affiliation : Japan National Oil Corporation)
[4]DOWA ENGINEERING CO., LTD.

ABSTRACT. In order to predict contamination of the soil and groudwater by several chemical contaminant, the authors developed the multi-phase type numerical simulation technique considering the dissolution and volatilization of contaminant to air, in which they are modeled as the transient diffusion between different phases. Laboratory experiment was carried out to check the behaviour of volatile material in unsaturated zone. According to the result of comparison between laboratory experiment and numerical simulation, we could reproduce the measured transient concentration, and the transient volatilization model was verified.

Key words: Groundwater contamination, Volatilization, Dissolution, Numerical simulation

INTRODUCTION

In recent years, there are many problems of soil and groundwater contamination by VOCs (volatile organic chrolides). Advection-diffusion type numerical simulators become useful tools in investigating the contaminated area and designing remediation. However, because of the low solubility of VOCs to groundwater and high capacity of volatilization, conventional numerical simulation technique based upon solute transport equation can not realize the complicated movement of chemical component directly.
In order to predict the movement of VOCs in saturated and unsaturated zone, the author developed multi-phase type fluid flow simulator which can treat transient dissolution and volatilization of the chemical component to water/air in the phase transfer term [Tosaka et al. 1996].
In this paper, the authors introduce the simulation technique, and several result of laboratory and numerical experiments .

NUMERICAL MODELING OF VOCs FLOW IN POROUS MEDIA

Basic flow equations. In order to treat the flow of air, slightly soluble and highly volatile liquid and groundwater simulteneously, the authors have applied multi-phase multi-component numerical simulation technique. The basic equations are mass conservation eqations based upon genaralized Darcy's law and continuity equation. The basic equations of fluid flow and mass transport are written as,

$$\nabla\left(\frac{kk_{rcw}}{\mu_{cw}B_{cw}}(\nabla\Psi_{cw})\right)+\nabla\left(\frac{kk_{rcc}}{\mu_{cc}B_{cc}}(\nabla\Psi_{cc})\right)-q_{ws}^{cw}-q_{ws}^{cc}=\frac{\partial}{\partial t}\left(\frac{\partial\phi S_{cw}}{B_{cw}}+\frac{\phi S_{cc}}{B_{cc}}\right) \tag{1}$$

$$\nabla\left(\frac{kk_{rca}}{\mu_{ca}B_{ca}}(\nabla\Psi_{ca})\right)-q_{as}^{ca}=\frac{\partial}{\partial t}\left(\frac{\partial\phi S_{ca}}{B_{ca}}\right) \tag{2}$$

$$\nabla\left(\frac{kk_{rcc}R_{cc}}{\mu_{cc}B_{cc}}(\nabla\Psi_{cc})\right) - f_{cs}^{cc-cw} - f_{cs}^{cc-ca} - f_{cs}^{cc-r} - q_{cs}^{cc} = \frac{\partial}{\partial t}\left(\frac{\partial\phi S_{cc}R_{cc}}{B_{cc}}\right) \tag{3}$$

$$\nabla\left(\frac{kk_{rcw}R_{cw}}{\mu_{cw}B_{cw}}(\nabla\Psi_{cw})\right) + \nabla\left(D_{cw}\left(\frac{R_{cw}}{\alpha_{cw}}\right)\right) + f_{cs}^{cw-cc} + f_{cs}^{cw-ca} - f_{cs}^{cw-r} - q_{cs}^{cw} = \frac{\partial}{\partial t}\left(\frac{\partial\phi S_{cw}R_{cw}}{B_{cw}}\right) \tag{4}$$

$$\nabla\left(\frac{kk_{rca}R_{ca}}{\mu_{ca}B_{ca}}(\nabla\Psi_{ca})\right) + \nabla\left(D_{ca}\left(\frac{R_{ca}}{\alpha_{ca}}\right)\right) + f_{cs}^{ca-cc} + f_{cs}^{ca-cw} - f_{cs}^{ca-r} - q_{cs}^{ca} = \frac{\partial}{\partial t}\left(\frac{\partial\phi S_{ca}R_{ca}}{B_{ca}}\right) \tag{5}$$

where, k:permeability $[m^2]$, k_{rp}:relative permeability of each phase $[-]$, μ_p:viscosity of each phase $[ML^{-1}T^{-1}]$, B_p:formation volume factor of each phase $[-]$, Ψ_p:hydraulic potential of each phase $[MLT^{-2}]$ S_p:saturation of each phase $[-]$ ϕ:porosity $[-]$ R_p, α_p:volumetric concentration $[-]$. D_p:diffusion coefficient$[LT^2]$
Phase indicator p denotes either cw : contaminated water, cc : contaminant chemical, or ca : contaminated air. The equations show the mass balance of water (1), air(2), pure chemical contaminant(3), dissolved chemical contaminant (4), evaporated chemical contaminant(5). The volumetric concentration R and α is defined as shown in Figure 1

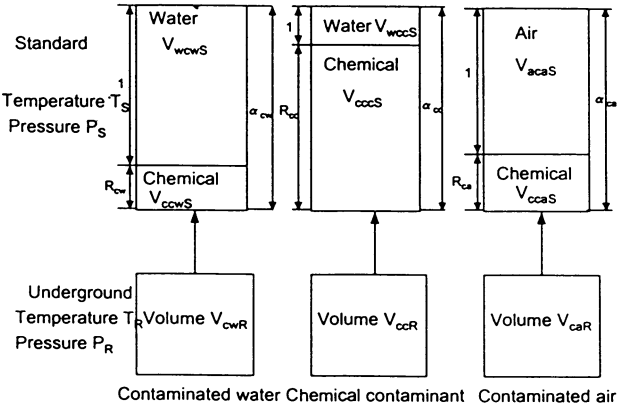

Fig.1 The definition of volumetric concentration

In these equations, the number of unknown parameters are 9 ($\Psi_{cw,cc,ca}, S_{cw,cc,ca}, R_{cw,cc,ca}$). In order to reduce unknowns, supplementary eqauations are introduced as follows,

$$S_{cw} + S_{cc} + S_{ca} = 1.0 \tag{6}$$

$$\Psi_{cw} = P_{cc} - P_{c.cw} - \rho_{cwR}gZ \tag{7}$$

$$\Psi_{cc} = P_{cc} - \rho_{ccR}gZ \tag{8}$$

$$\Psi_{ca} = P_{cc} + P_{c.ca} - \rho_{caR}gZ \tag{9}$$

where, $P_{c.p}$: capillary pressure between each phase and contaminant phase. ρ_{pR}: mass per unit volume of each phase in underground condition. g: gravity accelation. Z: depth.
Capillary pressure is defined as the function of saturation of each phase.

Modeling of phase transfer phemomena. For the dissolution and volatilization modeling, the authors introduced the phase transfer chemical component term f in the basic equations. $f_{cs}^{p1,p2}$ denotes the phase transfer volume of chemical component in standard condition from phase-1 to phase-2. So, f_{cs}^{cc-cw} and f_{cs}^{cw-cc} denote the dissolution term from chemical contaminant phase to contaminated water phase. For the volatilazation, f_{cs}^{cc-ca}, f_{cs}^{ca-cc} denote the volume of chemical component that is evaporated. When the chemical component is evaporated, dissolution of chemical component from air phase to water cannot be negligible. So, f_{cs}^{ca-cw} and f_{cs}^{cw-cs} was introduced as the second dissolution term. The terms f_{cs}^{p-r} denote the sorption term neglected in this paper.
For the dissolution from chemical phase to water phase, the authors adopted the diffusion equation modeling. Considering the evaporation process in one-dimensional diffusion within water phase, diffusion equation can be introduced.

$$\frac{\partial C}{\partial t} = D_{cw}\frac{\partial^2 C}{\partial^2 x} \tag{10}$$

where, C:volumetric concentration.
From this equation, volume of chemical contaminant that transfer between chemical and water phase within time Δt accross the area A_{cc-cw} is,

$$f_{cs}^{cc-cw} = A_{cc-cw}\sqrt{\frac{D_{cw}}{\pi\Delta t}}\left(\frac{R_{sat}}{1+R_{sat}} - \frac{R_{cw}}{1+R_{cw}}\right) \tag{11}$$

where, R_{sat}:concentration in saturated condition.
The contact area A is assumed to be a function of saturation as is shown below.

$$A = (V(1-S_{cw}-S_{ca}))^{2/3}\frac{S_{cw}}{S_{cw}+S_{ca}} \tag{12}$$

For the volatilization, the authors introduced the same assumption. However, the volume of the same mass chemical component in liquid and gas phase is formulated respectively as follows [Itoh, 1997].

$$f_{cs}^{ca-cc} = A_{ca-cc}\sqrt{\frac{D_{ca}}{\pi\Delta t}}\left(\frac{P_{sat}}{P_{cc}+P_{c,ca}} - \frac{R_{ca}}{1+R_{ca}}\right) \tag{13}$$

$$f_{cc}^{cc-ca} = A_{ca-cc}\frac{xP_{sat}}{\rho_{cc}RT}\sqrt{\frac{D_{ca}}{\pi\Delta t}}\left(\frac{P_{sat}}{P_{cc}+P_{c,ca}} - \frac{R_{ca}}{1+R_{ca}}\right) \tag{14}$$

where, P_{sat} : saturation pressure of chemical, R : gas constant, T:temperature ρ_{cc} : mass per unit volume of chemical in liquid, x : molecular weight of chemical component.
Equation (13) denotes the volume of chemical component that transfers in gas chemical phase, and equation (14) shows the volume in liquid phase from conditional equation of gas. And, contact area between liquid chemical phase and air phase (A_{ca-cc} in equation (13) ,(14)) is assumed as,

$$A_{ca-cc} = (V(1-S_{cw}-S_{ca}))^{2/3}\frac{S_{ca}}{S_{cw}+S_{ca}} \tag{15}$$

Secondary dissolution from air phase to water is modeled with similar method, in which Henry's law was introduced as boundary condition. The dissolution rate of chemical in gas phase is formulated as,

$$f_{cs}^{ca-cw} = A_{cw-ca}\sqrt{\frac{D_{cw}}{\pi\Delta t}}\left(\frac{HR_{ca}(P_{cc}+P_{c,ca})}{\rho_{cc}(1+R_{ca})} - \frac{R_{cw}}{1+R_{cw}}\right) \tag{16}$$

where,H:Henry's Constant.
The dissolution rate can be transformed to the volume in liquid phase as,

$$f_{cs}^{cw-ca} = A_{cw-ca}\frac{\rho_{cc}RT}{x}\frac{(1+R_{ca})}{R_{ca}(P_{cc}+P_{c,ca})}\sqrt{\frac{D_{cw}}{\pi\Delta t}}\left(\frac{HR_{ca}(P_{cc}+P_{c,ca})}{\rho_{cc}(1+R_{ca})} - \frac{R_{cw}}{1+R_{cw}}\right) \tag{17}$$

In the case, the contact area A_{cw-ca} can be calculated as follows,

$$A_{cw-ca} = (VS_{ca})^{2/3}\frac{S_{cw}}{1-S_{ca}} \tag{18}$$

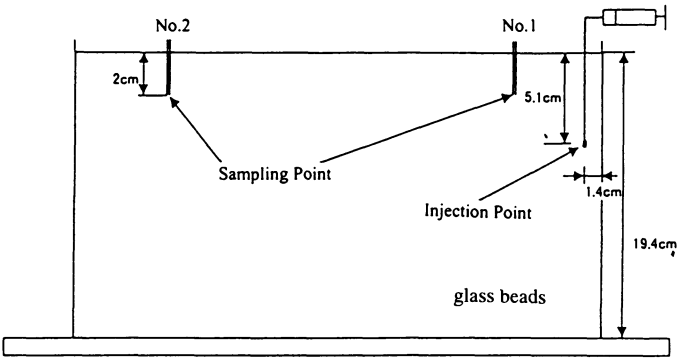

Fig.2 A schematic view of experiment apparatus

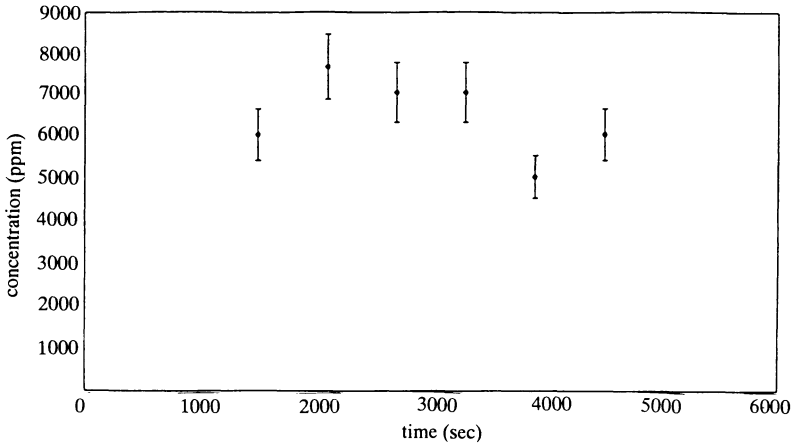

Fig.3 Transient alcohol concentration in gas sample at point 1

LABORATORY EXPERIMENT ON VOLATILIZATION

In order to verify the modeling of phase transfer as diffusion, vertical two-dimensional experiment of volatlization has been carried out. A schematic view of experiment apparatus is shown in Figure 2. In this experiment, grass beads with 1mm in diameter are packed in the two dimensional box, and ethyl-alcohol was injected at the right side. And, air was vacuumed at 2 points. The concentration of alcohol in the sampled air was measured with gas indicator tube. The upper side of was open to an atmosphere.

Examples of result of measured transient change in alcohol concentration at 2 sampling points are shown in Figure 3 and Figure 4.

The measurement error in alcohol concentration with gas indicator tube is supposed about 10% of measured value.

From those results, alcohl concentration at point 1, in the vicinity of the injection point shows high value from an early period, while alcohol concentrations at point 2 increase with considerable delay. The authors supose that, at the point 2, alcohol concentration in gas phase increased after volatilization of liquid alcohol at the basement of the apparatus that dropped from the injection point by gravity.

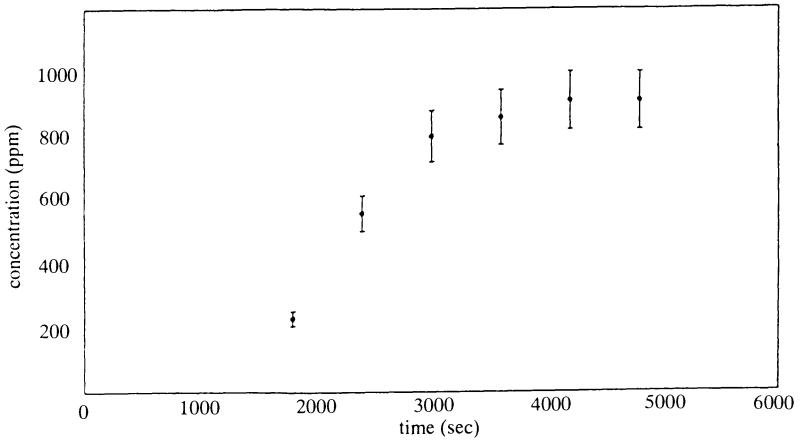

Fig.4 Transient alcohol concentration in gas sample at point 2

REPRODUCIBILITY OF NUMERICAL SIMULATION

Numerical simulation has been made under the condition of the laboratory experiment. Porosity, saturarion pressure. viscosity temperature were measured in advance, and permeability, diffusion coefficient for volatilization. diffusion coefficient of alcohol in gas phase were changed to reproduce measured concentration. As the result, calculated change of the alcohol concentration is shown in Figure 5, compared with the measured.

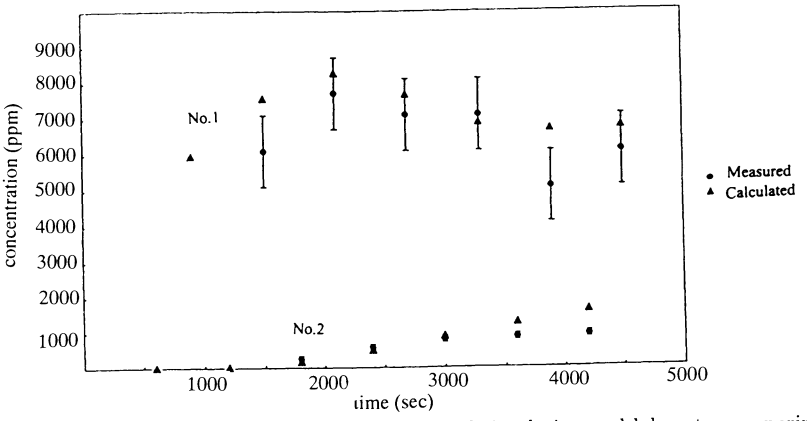

Fig.5 Concentration at sample point by numerical simulation and laboratory experiment

At sample points, measured and calculated concentrations show good accordance with each other. It shows that our numerical simulation method might be advantageous for tracing the flow of volatile chemical contaminant in unsaturated zone.

CONCLUSION

In this study, the authors applied multi-phase flow simulation to groundwater contamination problems, and modeled dissolution and volatilization phenomena as the diffusion between the phases. Laboratory experiment shows that evaporation of the volatile chemical component along the flow as the liquid phase causes the wide spread contamination of soil in unsaturates zone. The application of the developed numerical simulator to the laboratory experiment shows that multi-phase and diffusive phase transfer model can reproduce the laboratory result in acceptable accuracy.
The authors want to provide the general purpose code to the simulation of contamination of wide catchment area for the monitoring of quality in both river and groundwater.

REFERENCES

Tosaka, H., Itoh, K., Ebihara, M., Inaba, K., Itoh, A., and Kojima, K., (1996) 'Comprehensive treatment of groundwater pollution by multi-component, multi-phase convection/diffusion modeling' Groundwater Hydrology vol.38, No,3, pp.167-180 (in Japanese with English abstract)
Itoh, K. (1997) 'Numerical modeling of groundwater contamination -Modeling as a multi-component flow-' Monthly Chikyu vol.19. No.6 pp.387-391 (in Japanese)

Boundary Conditions Effect on the Accuracy of Groundwater Head Evaluation

Yu.A.Medovar and I.O.Yushmanov

Water Problems Institute, Russian Academy of Sciences,
3, Gubkina str., Moscow, 117735 Russia

ABSTRACT. To solve prediction problems involving the quantitative evaluation of groundwater backing and its effect on ecosystems it is primarily necessary to substantiate their computation schemes. Therefore, the seepage schematisation of the hydrogeological structure of the object under study is the immediate stage in the realization of problems of such a type. It is based on the analysis of special geological and hydrogeological work and hydrodynamic subdivision of areas and is reflected on the map of hydrodynamic regions of a river basin. A computational scheme for plan and section is selected to be the main taxonomic regioning unit. The ground surface is accepted to be its upper boundary and sediments having low seepage properties (a boundary conditions of the 2-nd type) are the lower boundary. The flow medium is represented by one-layer or two-layer schemes with different boundary conditions (1-st, 2-nd and 3-d type) on the upper and lower boundaries. The boundaries between areas are traced with allowance for facial horizontal changeability of sediments (boundary conditions of 4-th type) and on the assumption of the groundwater flow direction normal to the river. Thus, the selection of a computation scheme that is as close as possible to real natural conditions allows the minimization of the error in evaluating groundwater backing. For this purpose, a complex of direct and reverse problems is solved for the substantiation of boundary conditions (both external and internal), as well as hydrodynamic parameters for computation.
A right choice of groundwater flow boundary conditions allows the interaction between surface- and ground water in the zone affected by a water reservoir to be assessed more exactly.

KEY WORDS. Mathematical model, backing of groundwater

A change of natural stream-flow regime fundamentally changes a course and a trend of some natural processes, causing their artificial speeding and slowing down. It primarily relates to the process of rising the groundwater level (water logging, underflooding), that is the main reason for changing conditions of biocenosis growing.
Development of groundwater head (backing) in time is described by different analytical and numerical mathematical models. Analytical models [3] are used for relatively simple hydrogeological conditions.
Numerical models make it possible to assess a head in complex hydrogeological conditions, for which correct (exact) analytical solutions have not been found yet [8,9].
As suggested by the authors, numerical variant of a planned model for nonstationary filtration has some advantages in comparison to other models of this category [1,4,5,7]. It relates primarily to setting boundary conditions and form of filtration area outer boundaries that in the model are

determined only in separate nodal points with a further linear interpolation of initial data along the whole boundary. Thus a suggested model makes it possible to describe processes of head (backing) development in both areas with limited volume of initial information and studied in detail [6].

Let a modeling of groundwater head be considered with an example of the Prisykhonsk lowland [2] (Volodga district, Russian Federation).

Prisykhonsk lowland is flat, mainly bogged up lake-accumulative plain where swamping processes are intensively developing now. Side tributary valleys (system boundaries in plan) are slightly cut in and have only a high floodplain. Lacustrine-alluvial deposits are constituted a thickness of interbedding fine – and medium-grain sands (filtration coefficient K=1-3 m/d, coefficient of water yield m=0,1) with rare pebble inclusions. A depth of groundwater level (GWL) varies from 1,5 to 5 m. A maximum raise of groundwater is observed in May-June, minimum – in March and also during summer low water.

A moraine is mainly constituted by loams with small-raised gravel (K=0,3 m/d, m=0,05). The depth of groundwater occurrence depends on the relief and changes from 4-6 m in watershed and to 1 m in the bank slopes. Minimal GWL is observed in March, maximal – in May – June.

A non-linear two-dimensional Boussinesq's equation is assumed to be the initial equation in the model

$$m\frac{\partial H}{\partial T}=\frac{\partial}{\partial X}\left(KH\frac{\partial H}{\partial X}\right)+\frac{\partial}{\partial Y}\left(KH\frac{\partial H}{\partial Y}\right)+E$$

Where H – head, counted from a confined bedroof; E – total intensity of infiltration recharge, inflowing the bed through a flow free surface; X, Y – Cartesian coordinates; T – time. Initial conditions are $H(X,Y,0)=H_0(X,Y)$.

BOUNDARY CONDITIONS. At the first stage of modeling the studied area is approximated by an orthogon (Fig. 1):

a) on the boundary – river

$H(X,L_y,T)=I_bX+B_b+D_b(t)$

where I_b – river gradient, I_bX+B_bb - level in point X during low water, B_b – minimal water level in the river in the place considered, $D_b(T)$ – excess of water level in the river over low-water one;

b) boundaries with conjugated side tributaries –

"left" tributary

$$H(0,Y,T)=\begin{cases} I_lY+B_l, & I_lY+B_l>H(0,L_y) \\ H(0,L_y), & I_lY+B_l<H(0,L_y) \end{cases}$$

"right" tributary

$$H(L_x,Y,T)=\begin{cases} I_pY+B_p, & I_pY+B_p>H(L_x,L_y) \\ H(L_x,L_y), & I_pY+B_p<H(L_x,L_y) \end{cases}$$

Here I_l, I_p – stream gradients, I_lY+B_l, I_pY+B_p – water levels in tributaries with coordinates $X=0$, $X=L_x$; B_l, B_p – water level in the river where side tributaries issue it.

c) on the stream upper boundary $Y=0$ condition of the I-st or II-nd order is given

$H(X,0,T)=F(X,T)$ or $KH\,\partial H/\partial n = Q(X,T)$

where F – water level, Q – groundwater discharge (yield).

A numerical solution of Boussinesq's equation is made by a splitting method by spatial variables using uniterative scheme of "predictor-corrector" type.

In the first stage of investigations the following problems were solved: assessing the character of giving conditions in the flow upper boundary; relieving conditions of acceptable approximation of flow boundary in plan and refining of filtration coefficient experimental values, obtained during test filtration work.

Initial conditions were set by the results of numerical solution of a stationary problem with a future correction of obtained values according to the field data.

There is a swamp that can be related to the upper type, in upper boundary of a considered filtration area. In this case it is possible to set flow boundaries of both the I-st and the II-nd order.

Time dependence of water level in the river was given as a condition in the boundary aquifer-surface stream. Tributaries (accounting for natural gradients) were approximated by straight lines in the initial stage of investigations. The intensity of recharge was assumed to be mean perennial and uniformly distributed over a studied area in calculations.

A map of hydroisohypses was compiled according to the regime observations in natural conditions.

Schemes of hydroisohypses (Fig. 1) with boundary conditions of the I-st and II-nd order for the time moment which an earlier compiled map of isohypses corresponds to were made by realization of the model. When comparing model and natural maps, it appeared that the I-st order conditions should be given at a swamp outline, as a close to natural head distribution, obtained on the model, is characteristic just for this variant.

Modeling made it possible to assess GWL position under different variants of approximation for side boundaries of the filtration area: 1) rectangular; 2) simple stepped area; 3) analogous to the 2-nd variant, but a more complex one with an increased number of fragments, approximating a studied area.

As a result it appeared that calculated GWL rise under a chosen approximation differs that between the 2-nd and 3-rd variants by 5-10 % from a difference of water level position in the river for years of high and low water content. Thus it appeared that a suggested approximation of natural boundaries by a stepped area (Fig. 2) on the whole preserves a real form of the boundary in plan and makes simple a setting of initial data for calculating groundwater backing on the model.

In the initial stage, values K = 0.5-10 m/d, obtained due to test filtration works were put into the model. Filtration area was divided into two parts with different rock permeability. Conditions of the IV-th order were given at the boundary. Running of the model for wide range of filtration coefficient values was continued until a distribution of heads obtained in the model actually coincide with a map of hydroisohypses according to observation data. The accepted schematization of the area considered does not on the whole affect a common picture of head distribution within the area though some hydroisohypses in the near-contact zone are deformed. Corrected values of filtration coefficients were assumed to be initial ones and were used for solving problems.

In the second stage numerical experiments were made for assessing groundwater head (backing). There is a scheme of superposed hydroisohypses for natural and disturbed conditions in Fig. 3. Position of isolines in the studied area, calculated for 5 months, before and after water level rise in the river, coincides qualitatively and their values are given in the Table 1.

Table 1. Absolute values of hydroisohypses 1-10 in natural and disturbed conditions (after 150 days from the beginning of process in the Prisukhonsk lowland

Number of line	1	2	3	4	5	6	7	8	9	10
Natural	105.5	106.3	107.5	108.8	110.0	11.2	112.5	113.7	115.0	116.2
Disturbed	107.5	108.5	109.4	110.0	11.4	112.3	113.3	114.3	115.2	116.2

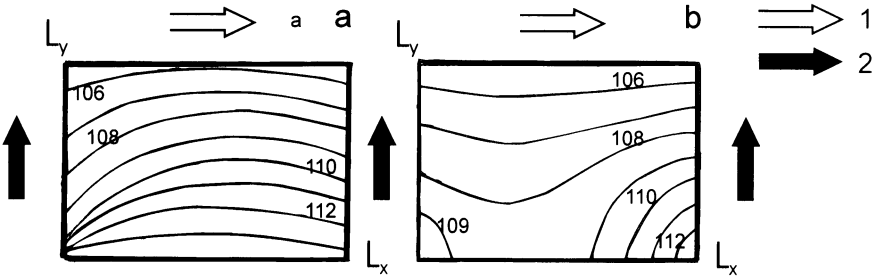

Fig. 1. Distribution of heads in the studied area of filtration with the boundary condition of I-st (a) and II-nd order (b) on the upper boundary; numbers near curves - absolute marks of hydroisohypse, m; 1,2 here and in Fig. 2,3 - flow directions in the river and tributaries.

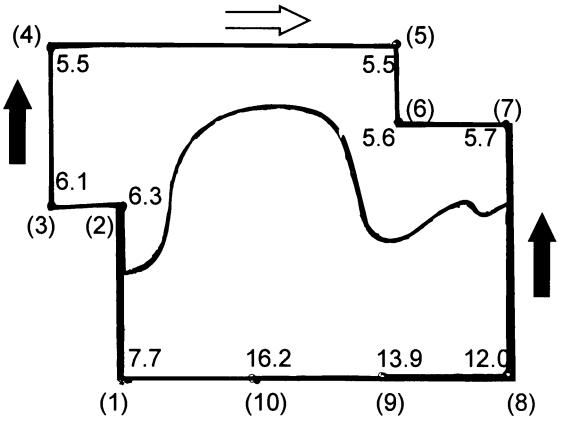

Fig.2. A scheme of studied filtration area. A number at a point – thickness of groundwater flow, m; a number in brackets - number of a point, with information for setting boundary condition; a curve - boundary of filtration heterogeneity.

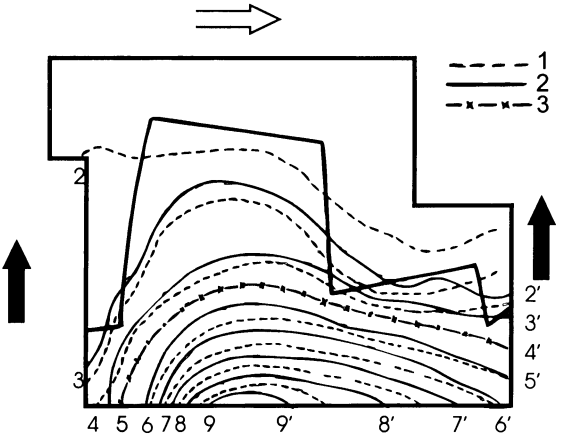

Fig. 3. Position of hydroisohypses before and after backing. 1,2 – hydroisohypses before and after backing; 3- zone of backing distribution H = 0.5 m (absolute values of hydroisohypses are given in Table 1).

It is possible to outline a zone in Fig. 3 where a difference between GWL in natural and disturbed conditions DH=0.5 m. This zone is limited by isohypse 4, that is at a distance of 1500 m from the river in the center of the studied area. Thus, for instance, isohypse 2 with absolute mark 108.5 corresponds to isohypse 3 (107.5) after backing, i.e. in this case GWL rises by 1 m. As removing from river water line, a value of backing decreases and actually becomes zero (according to the scheme) in isohypse 4 position. GWL rise is insignificant in the zone behind isohypse 4 as it is affected by upper boundary (I-st order condition), that restrain groundwater backing (head) development.

Thus use of the model suggested makes it possible to assess the effect of filtration heterogeneity and groundwater flow boundary conditions on the GWL formation, that allows a dynamic of water logging process in the studied area to be described reliably enough.

When comparing schemes both considering their boundary conditions of the IV-th order, and ignoring them, it appeared that this boundary condition affects the accuracy of calculations only in the near-contact zone (100-150 m). Thus it is necessary to consider this boundary condition when solving concrete problems with insignificant area of filtration or under a combined solution of masstransfer and filtration problems. In our case it is possible to omit using the IV-th order boundary condition.

REFERENCES

1. Abutaliev F.B., Baklushin M.B., Erbekov Ya.S. and etc. Analysis of groundwater dynamics by analytical and numerical methods. Tashkent, FAN, 1975, 151 pp.
2. Alifanov V.M., Medovar Yu.A., Yushmanov I.O. Prediction of soil-hydrogeological conditions under antropogenic factor effect.// Problems of predictive soil-melioration mapping and topographic- geodetical prospecting in meliorative and hydroeconomic constructing. Proc. of "Soyuzvodproekt", Moscow, 1989, 35-49.
3. Vasiliev F.V., Verigin N.N., Razumov G.A. and etc. Filtration out of water reservoirs and ponds. Moscow, "Kolos", 1975, 303 pp.
4. Epikhov G.P. Mathematical model of planned filtration in the interconnection with river runoff and its realization. // Water Resources, 19809, N 2, 35-44.
5. Lukner L., Shestakov V.M. Geofiltration modeling. Moscow, "Nedra", 1976, 407 pp.
6. Medovar Yu.A., Yushmanov I.O. Numerical modeling of groundwater backing when assessing coastal ecosystems. Mathematical problems in ecology. Theses of reports, III Training courses, Chita, 1990, 32-33.
7. Pashkovsky I.S. Developing geofiltration models for the aeration zone - groundwater system and their use when studying the interrelation between ground- and surface water. Author's Abstract, PhD Thesis. Moscow, 1985, 38 pp.
8. Khublaryan M.G., Churmaev O.M., Yushmanov I.O. Studying a hydrodynamic problem of filtration and convective diffusion in heterogeneous and anisotrophic porous media. //Water Resources, 1984, N 3, 23-29.
9. Todsen M. Numerical studies of two-dimensional saturated/unsaturated drainage models. // J. Hydrol., 1973, V. 20, N 4, 311-326.

Hysteretic Unsaturated Flow in Porous Media Caused by Periodic Movement of the Phreatic Surface: Model and Experiment

Fritz Stauffer[1]

[1]Institute of Hydromechanics and Water Resources Management, ETH Zurich, CH-8093 Zurich / Switzerland

ABSTRACT. A cyclic rise and decline of the groundwater table results in a subsequent cyclic movement of the water content and pressure profiles. The sequence of periodic wetting and drying processes can be affected by hysteresis effects in the capillary zone. A one-dimensional saturated/unsaturated flow model based on Richards' equation and the Mualem [3] model is formulated which can take into account multi-cycle hysteresis effects in the relation between capillary pressure and water content. The numerical integration of the unsaturated flow equation is based on a Galerkin-type finite element method. The flow domain is discretised by one-dimensional finite elements with linear shape functions. Simulations start with water content and pressure profiles which correspond to either a boundary drying or wetting curve. To facilitate the treatment of the hysteretic case a non-iterative procedure was chosen for the solution of the non-linear differential equation. Laboratory experiments were performed with a vertical sand column by imposing a high frequency periodic pressure head at the lower end of the column. The total water volume in the column, and the steady state cyclic water content profile averaged over time were measured. The boundary drying and wetting curves of the relation between water content and capillary pressure were determined by independent experiments. The simulations show a clear effect of the hysteresis on the water content profile above a fluctuating water table. The simulations with hysteresis agree well with the measurements.

KEY WORDS: Groundwater, unsaturated, phreatic surface, cyclic boundary condition, hysteresis

INTRODUCTION

A cyclic rise and decline of the groundwater table imposes a periodic boundary condition for the capillary zone above the phreatic surface. Such periodic conditions result in a subsequent cyclic movement of the water content and pressure profile in the capillary zone. These processes are influenced by the relation between capillary pressure and water content, which generally is not unique but influenced by hysteresis effects. Therefore, the sequence of periodic wetting and drying processes can be subject to considerable hysteresis effects. The water content profiles depend on the preceding wetting and/or drying processes in the capillary zone. A cyclic movement of the groundwater table represents an idealization of the more irregular temporal behavior in natural systems.

In the present study a one-dimensional model for saturated/unsaturated flow based on Richards' equation and the Mualem model [3] is formulated. It can take into account multi-cycle hysteresis effects in the capillary pressure - water content relation. The model is tested by laboratory experiments using a vertical sand column with a high frequency periodic pressure head boundary

condition. The impact of hysteresis on the water content profile above a fluctuating lower boundary condition is demonstrated by simulations with and without hysteresis.

FLOW EQUATION IN A VERTICAL SOIL COLUMN

The equation for unidirectional saturated/unsaturated flow in porous media is given by the Richards equation:

$$n \frac{\partial S}{\partial h} \frac{\partial h}{\partial t} = \frac{\partial}{\partial z}\left(K_r(S)\, K_s \cdot \left(1 + \frac{\partial h}{\partial z}\right)\right) \tag{1}$$

where n is the porosity, S is the water saturation, h is the pressure head, t is the time, z is the vertical coordinate, K_r is the relative hydraulic conductivity, and K_s is the hydraulic conductivity at S=1.

The parameters S(h) and $K_r(S)$ are represented by using the relationships of Brooks and Corey [2]:

$$\begin{aligned} &\frac{S - S_r}{1 - S_r} = \left(\frac{h_b}{h_c}\right)^{\lambda} && \text{for } h_c > h_b \\ &S = 1 && \text{for } h_c \le h_b \end{aligned} \tag{2}$$

where S_r is the residual saturation, h_b is the air entry pressure head, and λ is a constant exponent. The symbol h_c is the capillary pressure head. Assuming that the relative air pressure is zero everywhere in the capillary zone, h_c=-h. The relative hydraulic conductivity is described as:

$$K_r(S) = \left(\frac{S - S_r}{S_{max} - S_r}\right)^{\varepsilon} \tag{3}$$

where S_{max} is the maximum occurring saturation, and ε is a constant exponent, which is given by ε=3+2/λ according to Brooks and Corey [2].

Boundary conditions are either a prescribed water flux, or a prescribed pressure head at the boundary. Both conditions can be time-dependent or cyclic.

HYSTERETIC CONCEPTS

By using Mualem's concept [3], the boundary drying and wetting curves alone are sufficient to express the hysteretic drying and wetting scanning curves $S(h_c)$. The primary wetting curves are modeled by:

$$S(h_c) = S_d(h_d) + \frac{S_{max} - S_d(h_d)}{S_{max} - S_w(h_d)} \cdot \left[S_w(h_c) - S_w(h_d)\right] \tag{4}$$

where h_d is the maximum capillary pressure head of the preceding drainage process (reversal pressure). S_d represents the boundary drying and S_w the boundary wetting curve. Primary drying curves are modeled by:

$$S(h_c) = S_w(h_w) - P_d(S)\cdot[S_{max} - S_w(h_c)]\cdot[S_w(h_w) - S_w(h_c)] \quad (5)$$

where h_w is the minimum capillary pressure head of the preceding wetting process (reversal point).
The function $P_d(S)$ is given by:

$$P_d(S) = \frac{[S_{max} - S_r]\cdot[S_{max} - S]}{\left[S_{max} - S_w(h_c^*)\right]^2} \quad (6)$$

where h_c^* is given by the condition $S_d(h_c^*)=S(h_c)$. Secondary wetting curves are obtained as:

$$S(h_c) = S_{I,d}(h_d) + P_d(S_{I,d}(h_d))\cdot[S_{max} - S_w(h_d)]\cdot[S_w(h_c) - S_w(h_d)] \quad (7)$$

and secondary drying curves are expressed by:

$$S(h_c) = S_{I,w}(h_w) - P_d(S)\cdot[S_{max} - S_w(h_c)]\cdot[S_w(h_w) - S_w(h_c)] \quad (8)$$

where $S_{I,w}$ and $S_{I,d}$ represent primary wetting and drying curves. Higher order wetting and drying curves of the order J are obtained by replacing I by J-1.

NUMERICAL PROCEDURE

The numerical integration of equation 1 is based on a Galerkin-type finite element method as described by Neuman [4]. The flow domain is discretised by one-dimensional finite elements with linear shape functions. For the integration over time a fully implicit backward difference scheme is applied which leads to a tri-diagonal symmetric system of equations for the unknown nodal values of the pressure head h_i. The functions $h_c(S)$, $K_r(S)$ and the capacity coefficient $\partial\theta/\partial h(h)$ depend on the variable h. Moreover S(h) and $\partial S/\partial h(h)$ are hysteretic, i.e. depend on the history in h at a particular location z. The capacity coefficient approximation according to Abriola and Rathfelder [1] was used in order to reduce mass balance errors.

It was assumed that any simulation starts with water content and pressure profiles h(z) and S(z) corresponding to either a boundary drying or a boundary wetting curve. Multiple hysteretic cycles are allowed with higher order scanning curves using equations 7 and 8. This leads to an additional memory requirement compared to the non-hysteretic case since for every nodal point the reversal pressure head and the water contents have to be stored for all relevant hysteretic cycles. At every step the relevant order of the scanning curve has to be evaluated for every nodal point. Therefore every nodal point has its own history. To facilitate the treatment of the hysteretic case a non-iterative procedure was chosen for the solution of the non-linear differential equation. Numerical accuracy of the integration has to be achieved by an appropriate time increment. For the non-hysteretic case iteration of the variable h is optional. Upper boundary conditions can be either prescribed pressure head, or prescribed flux. The lower boundary

conditions are prescribed pressure head or prescribed flux. All conditions may be time-dependent. A periodic pressure head boundary condition is optional.

SAND COLUMN EXPERIMENTS

Laboratory experiments using a vertical sand column were performed with a periodic lower pressure head boundary condition of high frequency. The sand column had a length of 87.5 cm and a diameter of 5.35 cm. The column was placed on a balance which allowed the recording of the total water volume in the column. The water content in the sand column was measured by two probes using the gamma ray absorption method [5]. The two probes (Z_1 and Z_2) were moved vertically to prescribed locations using a step motor. With this device the water content could be measured at a given location within 100 s with an accuracy of about 3%. The cyclic lower pressure boundary condition was established by a head vessel which was moved vertically by a second step motor according to a preselected program. Four pressure ports were located along the column. All measurement devices were controlled by a PC.

The boundary drying and wetting curves of relation $S(h_c)$ were determined by independent experiments (Fig. 1) for (quasi-) static conditions in the sand column.

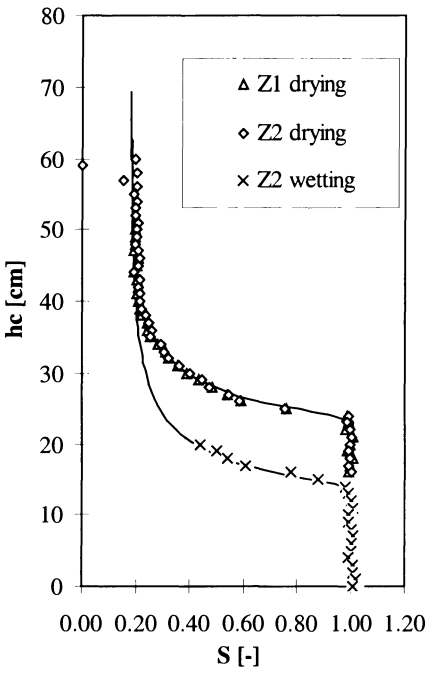

Fig. 1 Measured and fitted boundary drying and wetting curves of the relation between capillary pressure head h_c and saturation S for the sand column.

The total porosity of the sand packing was 0.41. Since the sand packing was slowly flushed with tap water from the bottom, the maximum water content which corresponds to an effective

porosity of 0.37 which corresponded to S_{max}=1 in Fig. 1. The hydraulic conductivity K_s at this water content was 0.0336 cm/s.

The initial condition of pressure and saturation in the column was (quasi-) hydrostatic and was controlled by the initial level of the head vessel at z=20 cm. Measurements of the total water volume in the column and of the steady state cyclic saturation profile were taken. The saturation was measured over the time period T of the cyclic boundary condition. The cyclic boundary condition had an amplitude of 30 cm and a period T of 153 s.

RESULTS

Simulations were performed with and without consideration of hysteresis in $S(h_c)$. The simulations without hysteresis comprise the use of the boundary drying curve and of the boundary wetting curve. After 30 cycles the cyclic saturation conditions were quasi-steady. The saturation profile were averaged over the time period T. The results of the simulations are shown in Fig. 2 and 3 together with the experimental data. The simulation results without hysteresis using the boundary wetting retention curve is situated outside Fig. 3 (starting value for time t=0 of 14.6).

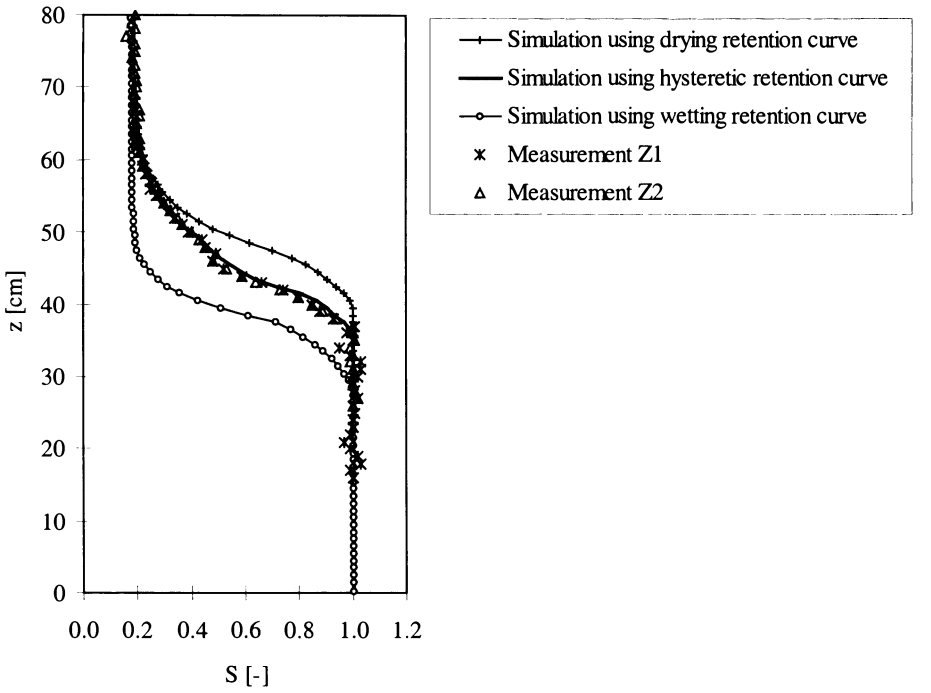

Fig. 2 Mean simulated saturation profiles (with and without hysteresis) averaged over period of the cyclic boundary condition, after 30 cycles, compared with measured profiles.

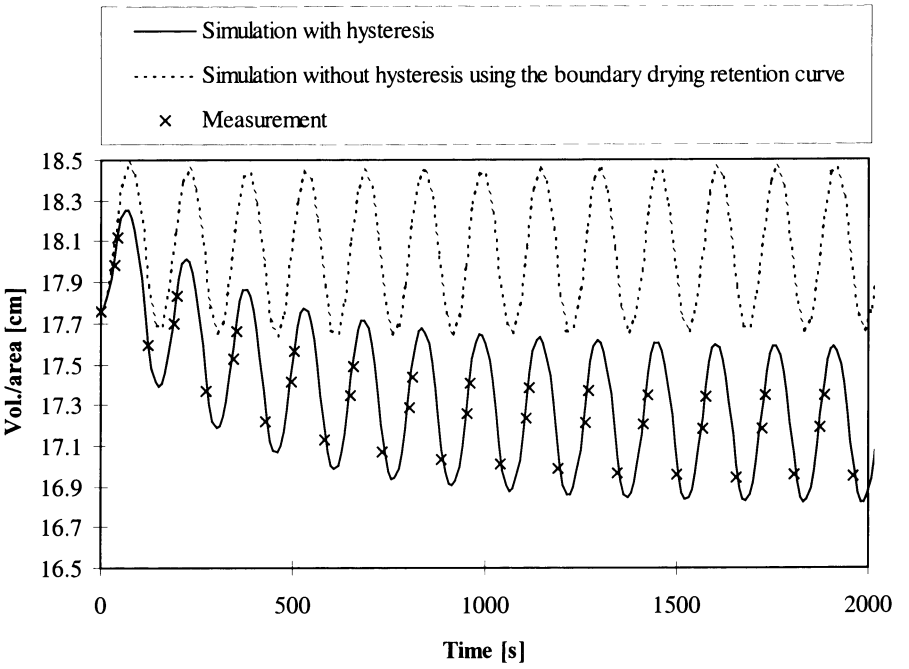

Fig. 3 Simulated integrated water volume per unit cross section of the soil column over time compared with measured data

CONCLUSION

The simulations agree well with the measurements in the sand column when hysteresis in the relation $S(h_c)$ is taken into account. Without hysteresis they differ considerably. The simulations and the experimental data show that the hysteresis can exert a significant influence on the water content profile above a fluctuating water table in sandy porous media.

REFERENCES

1. Abriola L.M., and K. Rathfelder, (1993) Mass balance errors in modeling two-phase immiscible flows: causes and remedies. Advances in Water Resour. 16, 223-239
2. Brooks and Corey, (1966) Properties of porous media affecting fluid flow. J. Irrig. Drain. Div. ASCE, 92, (IR2), 61-88
3. Mualem, (1984). A modified dependent-domain theory of hysteresis. Soil Science 137, (5), 283-291
4. Neuman S.P., (1973) Saturated-unsaturated seepage by finite elements. J. Hydraul. Div. ASCE, 99 (HY12), 2233-2250
5. Stauffer F., and T. Dracos, (1986) Experimental and numerical study of water and solute infiltration in layered porous media. J. Hydrology 84, 9-34

Confidence Intervals of Hydraulic Properties Estimated by Highly Efficient Numerical Inversion with Pressure Change Rate Matching

Kiyoshi MASUMOTO and Mario VALLE

Department of Geoscience, Faculty of Science and Engineering, Shimane University, Matsue 690-8504, Japan

Abstract. An assessment method to quantify and qualify unsteady state collected data was developed through the use of a pressure change rate matching technique. This method allowed us to improve the reliability of the estimation of heterogeneous hydraulic property derived from various crosshole tests, such as hydropulse. Adjoint state method efficiently calculated gradients of a modified objective function, introduced in this paper as the conventional objective function type plus an additional pressure change rate term to reflect information of unsteady state data. A modified bootstrap method, a type of Monte Carlo method, was used to objectively evaluate the difference in reliability of estimation derived from the inversion method. Various types of pumping rate patterns were changed systematically and compared with their reliability indexes, such as confidence intervals of estimation, calculated for a 1-D simple model. The objective function, proposed in this paper for matching rate of pressure change with respect to time, has proved to be effective for estimation of adequately heterogeneous permeability distributions under certain conditions, assuming two cycle pulse tests. Different flow rate patterns cause clearly different reliability of estimations. The optimum pulse test (pumping rate pattern) to characterize hydraulic properties under certain conditions is also estimated for the 1-D hypothetical model.

Key word. Groundwater models, Confidence intervals, Reliability of estimated hydraulic property, Pressure change rate matching, Numerical inversion, Unsteady state pressure.

INTRODUCTION

The inverse solution method is used in groundwater modeling to estimate heterogeneous distribution of hydraulic properties, such as permeability. Nevertheless, it is difficult to make an adequate estimation with limited observation wells, and the reliability of estimates becomes a problem. Unsteady state pressure data allow estimation of heterogeneous properties when only limited numbers of wells exist. Hydropulse Tomography was proposed by Tosaka et al.[12] to obtain sufficient data for inversion of heterogeneous permeability. In practice, the optimum design for the measuring method should be determined; hence, an index to objectively evaluate the measuring design should be defined. Some papers have presented methods to evaluate the reliability of estimation ([4], [9], [10]). However, it seems that an adequate method for evaluation of the value of unsteady state data has not yet been proposed. In oil fields, type-curve matching with derivatives is commonly used for single well testing. However, this can not be applied to multiple well testing data because of the excessive computing effort required.

Masumoto et al. [6] modified the adjoint state method to simultaneously evaluate matching of pressure and its change rate. The results showed clearly that a new objective function which includes pressure change rate is useful for a one dimensional heterogeneous model estimation under certain pulse test. With this method, the new objective function can be used without an increment of computing effort with respect to the original objective function.

The following problems need to be solved to maintain total balance of the system when we evaluate the reliability of estimation:
1.Optimum measuring method is unknown (pumping rate pattern, location of measuring points)
2.Optimum type of objective function is unknown
3.Optimum set of parameters is unknown
4. The previous conditions are dependent on the unknown true model

The Bootstrap Method (BSM) was used as a resampling method to derive an index for objectively evaluating the confidence interval and the reliability of estimation obtained by the pressure change

rate matching method [5]. BSM has some merits: for instance, there is no need to assume a probability distribution function (pdf) for the data. This means that we do not need to assume a region of white noise which is required for other common Monte Carlo methods. BSM can also be applied to nonlinear problems. There are methods such as the perturbation method [7] that do not require many inversions. However, the usual Monte Carlo method needs several thousands of simulation runs; whereas, the BSM needs only about 25 to 200 inversions [1]. The BSM requires some assumptions, for instance that data are independent from each other, and that all data depend on the same pdf. Using the methods described above, numerical case studies using a 1-D heterogeneous model have been carried out to objectively compare the effect of different flow rate pattern under 2 cycle pulse test conditions.

INVERSION METHOD WITH PRESSURE CHANGE RATE MATCHING

A quasi-Newton method with adjoint state method for the modified objective function J shown in Eq.(1) ([6]) was used in this study to solve the nonlinear inverse problem numerically.

$$J = J_1 + J_2 \qquad \cdots\cdots(1)$$

where:

$$J_1 = \sum_{n=1}^{N_t}\sum_{m=1}^{N_w} W_1^{m,n}\left(p_{cal}^{m,n} - p_{obs}^{m,n}\right)^2 \qquad \cdots\cdots(2)$$

$$J_2 = \sum_{n=1}^{N_t}\sum_{m=1}^{N_w} W_2^{m,n}\left(\frac{p_{cal}^{m,n} - p_{cal}^{m,n-1}}{\Delta t^n} - \frac{p_{obs}^{m,n} - p_{obs}^{m,n-1}}{\Delta t^n}\right)^2 \qquad \cdots\cdots(3)$$

where: p_{cal} :calculated pressure, p_{obs} :observed pressure, m :index of observation point, n :index of time step, Δt :time step interval, W :weighting.

Eq.(3) consists of new terms for pressure change rate matching.
When the implicit method is used for forward solution, we can express Eq.(3) as shown in Eq.(4).

$$J_2 = \sum_{n=1}^{N_t}\sum_{m=1}^{N_w} W_2^{m,n}\left(f_{i(m)}^n\left(p^n, u\right) - \frac{p_{obs}^{m,n} - p_{obs}^{m,n-1}}{\Delta t^n}\right)^2 \qquad \cdots\cdots(4)$$

where

$$\frac{p_i^n - p_i^{n-1}}{\Delta t^n} = \left\{\left[\frac{K}{\mu}\right]_{i+1/2}\frac{p_{i+1}^n - p_i^n}{\Delta x_{i+1/2}} - \left[\frac{K}{\mu}\right]_{i-1/2}\frac{p_i^n - p_{i-1}^n}{\Delta x_{i-1/2}} - \Delta x_i Q_i^n\right\}\frac{1}{\Delta x c_B \phi_i}$$
$$\equiv f_i^n\left(p^n, u\right) \qquad \cdots\cdots(5)$$

where μ:viscosity, K :permeability, Δx :grid length, c_B :compressibility, Q :pumping rate ϕ :porosity, u :unknown parameters of inverse solution.

Eq.(5) is the discretized governing equation for 1-D model and slightly compressible fluid flow in a confined aquifer. For simplicity, in this study, only one dimensional model is considered, and penalty functions which are often added to an objective function are not included. This way, we can eliminate p^{n-1}, pressure at the previous time step, in each term of the modified objective function $J= J_1+J_2$, and the adjoint state method can be applied. Calculation efforts for gradients of $J=J_1+J_2$ are almost the same as those required to calculate the gradient for only J_1. This inversion method can also be easily applied to a 3-D problem, and to the case when penalty functions are added to objective functions.

MODIFIED BOOTSTRAP RESAMPLING METHOD

The resampling method used in this paper is a modified BSM [5] which is a Monte Carlo simulation method. The BSM was applied to groundwater inverse modeling to calculate reliability indexes such as confidence intervals of estimation obtained by inversion.

A similar procedure to original BSM was carried out for a finite number of data which were obtained at multiple observation points through discretization over a time region for unsteady state pressure data. With this procedure, we can obtain many estimations which have some deviation from each other. Subsequently, errors or other indexes can be calculated with the estimations computed.

The procedure for our problem is as follows; n* is defined as the number of terms which consist of the square of difference between observed and calculated state variables. The objective function is the weighted sum of these terms. When $J=J_1$, n* equals the number of discretized transient pressure data at multiple observation points; and when $J=J_1+J_2$, n* equals 2 times the number of data for $J=J_1$.

(step1) Repeat for n* times randomly picking up the data, which is a function of time and well points. Replacement is allowed
(step2) For each term, the chosen number is multiplied by original weighting. A new set of weightings will be made. Fig.1 shows an example of the weighting pattern when original weighting is W=1.
(step3) Calculate the inverse solution for the weighting pattern made by step2.
(step4) Repeat step1～step3 for N times, and we can obtain N estimations. For the case study discussed below, N=100.
(step5) Calculate indexes such as 90% confidence interval (CI90) or average of estimations for each unknown parameter with the N estimation sets, where CI90 can be calculated as the difference between the 6th largest estimation and the 6th smallest estimation for N=100.

In fact, the method described above differs from the original bootstrap method because the discretized transient pressure data can be thought not to be independent from each other, and also not to depend on same distribution. Nevertheless, with this method, we can obtain many estimations with some deviation; and we can solve it without using information from the true model. The variance is considered to reflect sensitivity or accuracy, or reliability of the inversion result.

1	1	1	0	1	2	0	2	0	1	1	3	0	1	1	2	0	2	2	1
0	1	5	0	0	3	1	1	2	0	2	0	0	1	0	0	0	1	1	1
1	0	0	0	1	0	0	1	1	1	2	0	3	1	0	1	0	3	0	0
1	2	2	2	2	0	1	0	1	2	0	1	0	1	1	2	0	0	2	0
1	1	2	1	1	1	2	1	1	0	0	2	0	0	0	1	1	1	0	3
1	0	1	1	1	1	0	0	2	0	2	2	1	1	0	0	4	1	0	3
0	0	3	1	1	1	0	2	0	3	0	0	1	3	0	2	2	3	1	0
0	3	3	1	0	0	0	2	0	0	1	0	0	1	2	0	2	0	0	
3	0	1	0	1	1	1	2	0	3	0	0	0	1	0	2	1	0	1	
0	4	2	0	1	0	3	1	1	3	1	1	1	3	0	1	1	1	0	
1	2	0	3	0	3	1	2	0	2	1	0	3	4	0	1	1	1	1	
1	2	2	0	1	1	0	0	1	1	1	1	0	1	0	0	1	0	2	2

Fig.1 An example of the weighting pattern made by bootstrap resampling

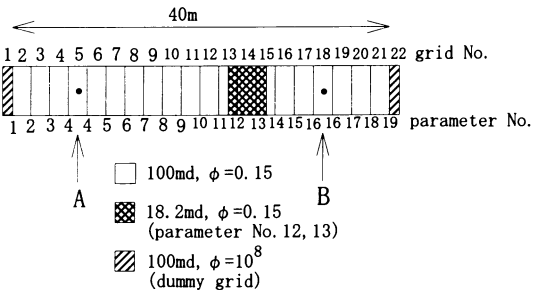

Fig.2 Discretized 1-D model and model permeability distribution

METHODOLOGY OF THE CASE STUDY

1-D model case studies were executed to estimate optimum flow rate pattern for Hydropulse test which is one type of unsteady state flow test. The validity of the method was also examined. Fig.2 shows the one dimensional artificial numerical model with 2 observation points (A,B); these two points are also used as pumping points. A low permeability zone (18.2[md]) exists between the two observation points, as shown in Fig. 2. This model is similar to that used by Masumoto et al. [6]. Numerical inversion was performed to estimate 19 unknown inter-grid permeabilities (as shown in Fig. 2) of the model by using data obtained at A and B.

Twenty cases were calculated by changing pumping rate (Y) and pumping time(X) as shown in Fig. 3 for two objective functions, J_1+J_2 and J_1. Y was varied as follows: 6, 10, 15, and 30 cc/sec; while X was 25, 50, 75, 100, and 125 sec.. Each pumping pattern consists of 2-cycle pulses as shown in Fig. 3. Other conditions are fixed as shown in Table 1. An example of pressure performance at point A, calculated with the true model, is shown in Fig. 4. We calculated 90% confidence interval (CI90) and average for each parameter, and reliability index ($1/\Sigma CI90^2$) for a total of 40 cases.

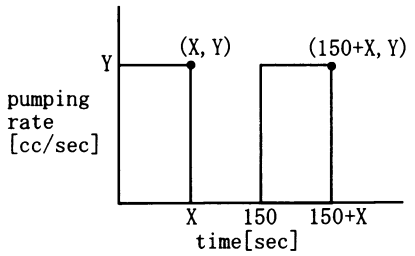

Fig.3 Pumping pattern of two cycle pulse used for case study
Y varies as follows: 6, 10, 15, 30 (cc/sec);
X varies as follows: 25, 50, 75, 100, 125

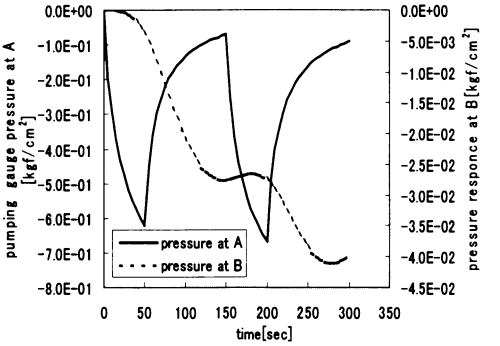

Fig.4 An example of pressure performance for 2 cycle pulse test

Table 1 fixed conditions for numerical case study

Cycle of pulse tests	2 cycles
Timestep interval	5 [sec]
Number of timesteps for one pulse	30 steps
Initial guess for inversion	10 [md] for all unknown inter-grid permeabilities
Porosity	0.15 for all grids except terminal two dummy grids
Boundary condition	Constant pressure (porosity of both terminal dummy grids are set as 1.0e8 to approximate constant pressure)
Initial condition	101325 [Pa] for all grids
Original weighting in J1 and J2	W_1^n=1, W_2^n=1.0e-6 (n=1,..,30)
Number of inversion iterations	200 for all
Number of resampling	N=100

CASE STUDY RESULTS AND DISCUSSION

The best result of estimations occurs when objective function is $J=J_1+J_2$ (Fig. 5). The upper and lower boundary are also shown in Fig.5, as represented by the 90% confidence interval (the difference between the sixth largest estimation and the sixth lowest estimation of 100 estimations for each parameter). Fig. 5 also shows that all 19 parameters could be estimated, not only within the measuring points but also outside them, with the data obtained at 2 points by using a 2 cycle pulse test. Fig. 6 shows the worst result that occurs when $J=J_1+J_2$ is used. It is clear that the results from Fig. 5 are more reliable than those from Fig.6; the previous results proved that different pumping patterns of flow rate produce remarkably different results. Fig. 7 shows the best result that occurs when $J=J_1$ is used; this is not as good as those shown in Fig.5 and 6. This means that the use of pressure change rate matching method with adequate flow rate pattern of Hydropulse test will result in higher quality data.

To judge which result is the best, a new index (R*) was used. R* is defined as the inverse of sum of $CI90^2$ (Eq.(6)), and can be thought to represent some measure of the quality of the data and to reflect reliability of the estimation.

$$R^* = 1/\sum_{s=1}^{S} CI90_s^2 \qquad \cdots\cdots(6)$$

S: Number of parameters (for this case S=19)

Fig.8 shows R* for various flow patterns when $J=J_1+J_2$ is used; and Fig. 9 shows R* when $J=J_1$. The best case is when $J=J_1+J_2$, because R* is the largest. Among all the cases studied, X=50 [sec] and Y=10 [cm^3/sec] with $J=J_1+J_2$ was chosen as the best. These figures show that the new objective function using J_1+J_2 produces more reliable estimation than the original objective function that considers J_1 only. In fact, other objective functions should be coupled with other variable factors, such as flow pattern or number of parameters, to calculate the best flow pattern. In this paper, we tried to change flow patterns for only the two objective functions shown previously.

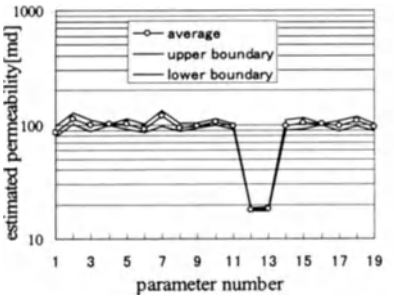

Fig.5 Estimation and its 90% confidence interval (X=50[sec], Y=10[cc/sec], $J=J_1+J_2$)

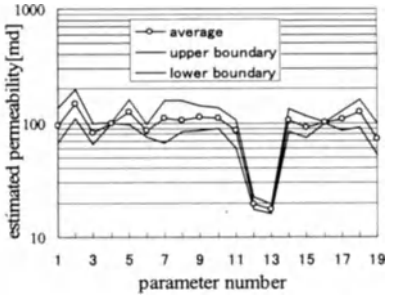

Fig.6 Estimation and its 90% confidence interval (X=25[sec], Y=6[cc/sec], $J=J_1+J_2$)

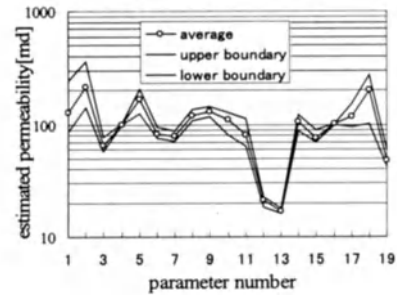

Fig.7 Estimation and its 90% confidence interval (X=50[sec], 6[cc/sec], $J=J_1$)

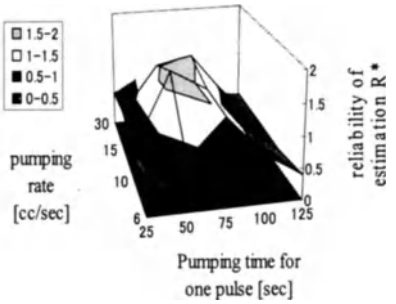

Fig.8 Reliability of estimation R* for various flow patterns ($J=J_1+J_2$)

The best flow pattern was selected by using effective inversion method for the new type of objective function. This method proved to be useful for a 2 cycle pulse test, which is one type of unsteady state testing. Fig.10 shows R* vs. difference between estimated parameters and true (model) parameters. $\Sigma CI90^2$, calculated by the bootstrap resampling method, and the index of deviation between estimated and true parameters show some proportional relationship (Fig. 10).

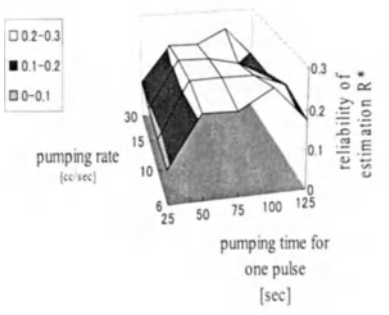

Fig.9 Reliability of estimation R* for various flow patterns ($J=J_1$)

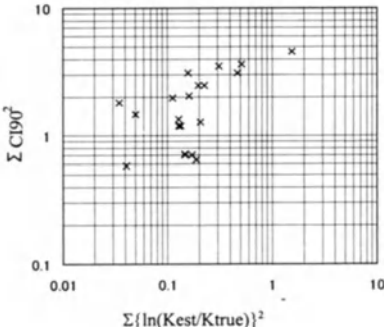

Fig. 10 $\Sigma CI90^2$ vs. $\Sigma\{\ln(K_{est}/K_{true})\}^2$ for $J=J_1+J_2$

We conclude that R* represents some error of inversion, and that this method has proved to be useful to estimate reliability of estimations. With this method, we can evaluate errors of estimation without using Ktrue (set of true values of parameters), which is unknown in practice.

CONCLUSION

The bootstrap method was applied to groundwater inverse modeling with the use of a modified objective function that includes a term for pressure change rate matching. Case studies to check the validity of the method were also carried out. We conclude:

1. Optimum pumping pattern of a 2 cycle pulse test for a 1-D model under certain conditions was estimated systematically, and the best match represents a sufficiently good estimation.
2. An objective function for pressure change rate matching (J_1+J_2) has proved to be useful for the pulse test used for the case studies, without increasing computing effort with respect to the original objective function (J_1).
3. The new index R* introduced here is useful for calculation of the reliability of estimation, and can quantify the unsteady state pressure data in Hydropulse test without using the true model, which is unknown in practice.

Future work should consider other types of objective functions, which should be coupled with other variable factors that were fixed in the case study shown in Table 1. This coupling will help to define the optimum pumping pattern for hydraulic characterization. Further studies on this subject should also evaluate 2-D and 3-D models.

ACKNOWLEDGMENT

The authors thank Dr. Kanta Naito (Shimane Univ.) and Dr. Takashi Amisaki (Assoc. Prof. of Shimane Univ.) for their useful suggestions, to Dr. Hiroyuki Tosaka (Assoc. Prof. of Tokyo Univ.) for his support, and to Dr. Barry Roser (Shimane Univ.) for his assistance with the edition.

REFERENCES

Books.

1. Efron, B. and Tibshirani, R. (1993) An Introduction to the Bootstrap. Chapman & Hall
2. Sun, Ne-Zheng (1994) Inverse Problems in Groundwater Modeling, Kluwer Academic Publishers

Journal paper.

3. d Bourdet, T. M. Whittle, A. A. Douglas and Y. M. Pirard (1983) A new set of type curves simplifies well test analysis, World Oil
4. Cooley, R. L. and Vecchia A. V. (1987) Calculation of nonlinear confidence and prediction intervals for ground-water flow models, Water Resources Bulletin, American Water Resources Association, Vol. 23, No. 4, 581-599
5. Efron, B. (1979) Bootstrap methods: another look at the jackknife, Ann. Statist., 7, 1-26
6. Masumoto, K., Tosaka, H. and Kojima, K. (1998) New Algorithm for Identifying Hydraulic Property Distribution of Rock Mass by Simultaneous Fitting of Pressure and its Change rate at Multi-Points in Multi-Wells, J. Groundwater Hydrology of JAGH, Vol. 40, No. 3, 273-287
7. McLaughlin, D. and Wood, E. F. (1988) A Distributed Parameter Approach for Evaluating the Accuracy of Groundwater Model Predictions 1. Theory, WWR, Vol. 24, No.7, 1037-1047
8. Sun, Ne-Zheng and Yeh, W. W.-G. (1992) A Stochastic Inverse Solution for Transient Groundwater Flow:Parameter Identification and Reliability Analysis, WRR, Vol. 28, No.12, 3269-3280
9. Yeh, W. W.-G. and Sun, Ne-Zheng (1990) Variational Sensitivity Analysis, Data Requirements, and Parameter Identification in Leaky Aquifer System, WRR, Vol. 26, No.9, 1927-1938

Edited works.

10. Masumoto, K., Tosaka, H., Kojima, K., Ito,K. and Otsuka, Y. (1995) New Measuring System and High Speed Three Dimensional Inversion Method for Hydropulse Tomography., Proc. International Congress on Rock Mechanics, ISRM, 847-850
11. Masumoto, K., Matsuda, I., Ito, K., Tosaka, H., MacDonald, O. (1998) Estimate precision of parameters estimated from multi-well interference test data, Proc. of annual meeting of Japan Society of Engineering Geology, 309-312
12. Tosaka, H., Masumoto, K. and Kojima, K. (1993) Hydropulse Tomography for Identifying 3-D Permeability distribution. Proc. Int. High Level Radioactive Waste Management Conf., Las Vegas, Nevada, U.S., 955-959

Characterization of Hydraulic Properties of Fractured Rock Mass with Numerical Model

Akira Kobayashi[1], Kenichi Hosono[1] and Tomoo Fujita[2]

[1]Iwate University, Faculty of Agriculture, 3-18-8, Ueda, Morioka, Iwate, 020-8550, JAPAN
[2]Japan Nuclear Cycle Development Agency, 4-33, Muramatsu, Tokai-mura, Ibaraki, 319-1194, JAPAN

ABSTRACT. The flow aspect in the fractured rocks is examined by using the general theory by Barker. It is found from the examination that the correlation between the flow dimension and hydraulic conductivity is positive. This observed correlation is related to the geometry of the flow network and hydraulic properties of flow paths. To examine the characteristics of hydraulic properties of fractures, the discontinuous fracture network model is used for the parametric study of the statistical properties. The variety in the relation between flow dimension and hydraulic conductivity is examined. The observed relation of flow dimension to hydraulic conductivity cannot be realized when the fracture length is independent of the fracture aperture. It is expected from the examination that the fracture aperture increases exponentially with the fracture length.

KEY WORDS. Hydraulic conductivity, Fractured rocks, Discontinuous model, Statistical properties, In-situ test

INTRODUCTION

Seepage flow in fractured rock mass is influenced by the hydraulic properties of existing fractures. However, it is not so easy to identify the hydraulic characteristics of fracture network from in-situ tests. Many of recent numerical models formulating the flow in the fractured rock mass try to realize directly such a fracture structure, e.g., Dershowitz et al. (1991) [1] or to model an equivalent anisotropic continuum to the fractured rock mass, e.g., Oda(1986)[2]. In such models, the results of joint survey have been used to develop the fracture network for a numerical modeling. Each property is treated independently in many cases. This is probably because the relation between properties is difficult to be cleared from the survey results. The hydraulic conductivity is, however, related to the entire system of fracture structure, i.e., the combination of the hydraulic aperture of each fracture and the geometry of fracture network. If we can understand the relation between the hydraulic conductivity and the flow regime in the ground, the relation is the result of the behavior of the entire system. The model should be made to regenerate the relation.

Although it is impossible to grasp the detail flow pattern in the ground, we can evaluate the flow pattern at the field by using the general flow model proposed by Barker (1988)[3]. This model considers the flow aspect by the dimension of a real number. The flow dimension obtained from this method is the same as the fractal dimension. In the process, the real number dimension is found by fitting the type curves of the real number dimensions with the observed result and then the hydraulic conductivity and specific storage are calculated at the meeting point in the conventional way of the well problem. If high flow dimension close to three is obtained, water may flow homogeneously in the ground. On the other hand, the small dimension close to one shows the biased flow situation. By using this method, the relation between the hydraulic conductivity and the dimension can be obtained. If the model can represent such a relation, it may be concluded that the model is realistic.

In this paper, firstly we try to examine the flow aspect in the real fractured rocks by using the general theory by Barker. The relation between the flow dimension and hydraulic conductivity is obtained. This observed correlation is related to the geometry of the flow network and hydraulic

properties of flow paths. Secondly the characteristics of hydraulic properties of fractures are examined with the discontinuous fracture network model. This model uses the statistical properties of fracture geometry. Through the parametric study for the aperture distribution, the variety in the relation between flow dimension and hydraulic conductivity is tested. The characteristics of the fracture properties to represent the real behavior is examined

DIMENSION EXAMINATION

Theory. The Barker's general flow theory is briefly introduced in this section.
The continuity equation of ground water flow in the rock mass from the injection hole is given as following by Barker:

$$\frac{1}{\alpha_1}\frac{\partial h}{\partial t} = \frac{1}{r^{n-1}}\frac{\partial}{\partial r}\left(r^{n-1}\frac{\partial h}{\partial r}\right) \tag{1}$$

where α_1 is K_f/S_{sf}, in which K_f is the hydraulic conductivity and S_{sf} is the specific storage of the fractured rock mass. n is the real number dimension between 1 and 3, h is the total head in the rock mass and r is the distance from the central point of the injection hole.
The conservation equation in the injection hole is given as

$$S_w\frac{\partial H}{\partial t} = Q + K_f b^{3-n}\alpha_n r_w^{n-1}\left.\frac{\partial h}{\partial r}\right|_{r=r_w} \tag{2}$$

where S_w is the storage capacity of the source which is given as πr_w^2, Q is the injection rate, H is the total head in the injection hole and r_w is the radius of the injection hole. α_n is given as

$$\alpha_n = \frac{2\pi^{n/2}}{\Gamma(n/2)} \tag{3}$$

where Γ is the gamma function. $b^{3-n}\alpha_n r^{n-1}$ implies the area through which the injected water goes in n dimensional way. Fig. 1 shows the schematic view of the area given by this equation with some specific values of n. Eq. (1) is fundamentally the same as the one obtained from the fractal consideration by O'Shaughnessy and Procaccia (1985)[4]. Thus, the meaning of the real number dimension in this equation is similar to the fractal dimension.
Unfortunately, only the type curve for the limited condition of the constant rate test is introduced in the Barker's paper. The constant pressure test like Lugeon test is more popular in Japan than the constant rate test. The type curve has to be derived to analyze a constant head test. Kobayashi, et al(1998)[5] introduced the type curve for the constant pressure test by using Laplace transform. Fig. 2 shows the type curve of the constant pressure test.

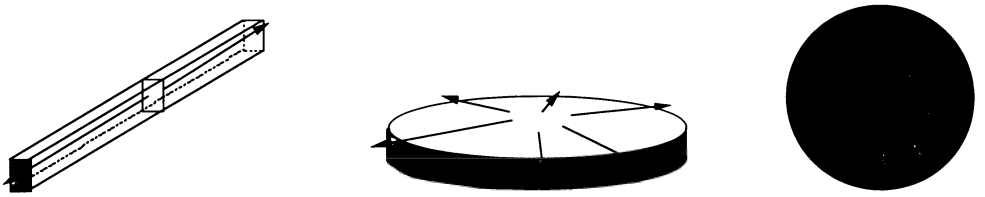

(a) 1 dimension (b) 2 dimension (c) 3 dimension

Fig. 1. Flow patterns of the different dimension

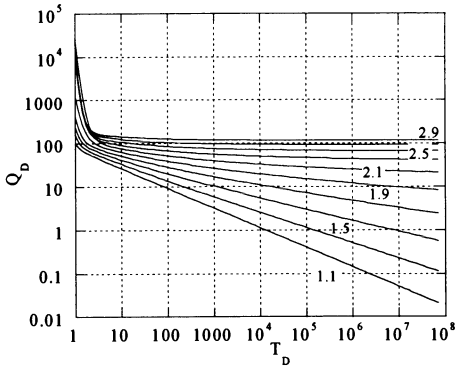

Fig. 2. Type curves for constant pressure test

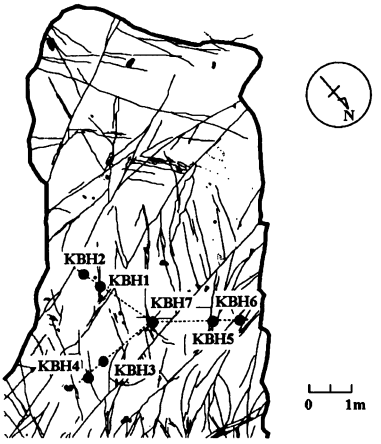

Fig. 3. Fracture map on the floor and boreholes

In-situ test. Japan Nuclear Cycle Development Agency (JNC) has conducted the activities of geoscientific R & D program at Kamaishi mine in order to understand the deep geological condition. The bedrock in the area consists of Paleozoic sedimentary rock, Cretaceous sedimentary rock, and igneous complexes. The test site is located at the drift 550 m above the sea level in the Cretaceous-age Kurihashi granodiorite. The overburden thickness at the test site is about 260 m. Fig. 3 shows the location of seven boreholes at the test site. This figure also shows the fracture map on the floor. The length of each borehole is 8 m. By using the boreholes, the constant pressure test is carried out at the several depths of each borehole. The constant rate test is also carried out for some boreholes.

Examination results. Fig. 4 shows the examination result of the relation between hydraulic conductivity and dimension. It is found from the figure that the flow dimension has the positive correlation to the hydraulic conductivity. The dimension and permeability obtained from the constant rate test are mostly similar to the ones by the constant pressure test [5].

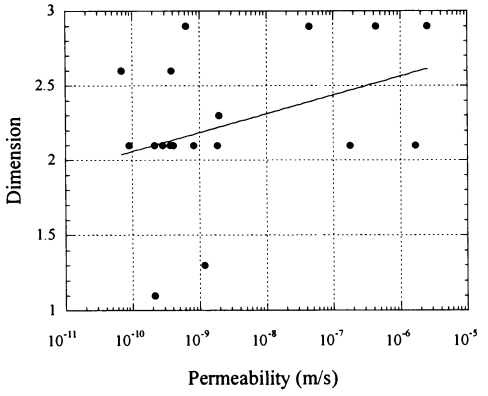

Fig. 4. Relation between measured dimension and hydraulic conducitivity

NUMERICAL EXAMINATION

Method. The discontinuous flow model is used to examine the characteristics of the fracture system. This model is fundamentally the same as the one like FracMan[6]. The statistical information of fracture geometry is used to realize the fracture network. The shape of the fracture plane is assumed to be a circle. The intersecting planes are obtained by geometric calculation, and the points connecting to the other fracture plane are gotten on each fracture plane. The finite element discretization of each fracture plane is carried out by Delaunay triangulation method[7].
While the statistical information on the fracture length and direction can be obtained from the in-situ investigation, the aperture information is inferred from the hydraulic test in many cases. This is because of the difficulty to measure the aperture directly at the in-situ investigation. Thus, the parametric study on the aperture distribution is carried out to find the model realizing the real relation between the dimension and permeability as shown in Fig. 4. In the process, four cases are examined; the constant aperture case (Case1), the lognormal distribution case (Case2), the week exponential relation between aperture and length (Case3) and the strong exponential relation between aperture and length (Case4).
The mean and standard deviation of the aperture are obtained from the permeability distribution by the single hole hydraulic test results. The permeability distribution is according to the lognormal one. The aperture is calculated by the cubic law from the measured permeability. Table 1 shows the statistical information obtained from the in-situ geological survey and hydraulic tests. The center of the fracture plane is located by Poisson's distribution, the fracture length is generated by the lognormal distribution, the direction is according to the normal distribution, and the aperture is according to the lognormal distribution in Case2.
By using the statistical information shown in Table 1, the discontinuous model is produced with different random seeds. For the examination, about 30 realizations are generated. Fig. 5 shows an example of the discontinuous model. The region is 10x10x10m. Water is injected at the constant rate of $10^{-4}m^3/s$ from the node that is located at the center of the region. All boundaries have a fixed total head of 10m, which is mostly the same as the measured in-situ hydraulic pressure. The transient response at the injection node is calculated, and is used to determine the dimension and the permeability. Thus, 30 values of the dimension and permeability are obtained for each case. By ergodicity, the fluctuations of 30 realizations mean the heterogeneous distribution of the region. Therefore, the relation between the dimension and permeability from 30 realizations is corresponding to the measured relation.

Results. Figs. 6 and 7 show the results of Cases 1 and 2. Case1 has the constant aperture for each set. The aperture is the same as the mean values shown in Table 1. On the other hand, Case2 has the lognormal distribution of the aperture. It is found that the dimension of Case1 is smaller than that of Case2, and that the large negative correlation is shown in Case2. The tendencies of both cases are different from the real one because both have negative correlation.
In Case3, the correlation between aperture and length(diameter) is assumed as

Table 1. Statistical data of fracture

No. of set	1	2	3	4	5
Fracture Density (No/m^3)	0.5847	0.2811	0.1455	0.3033	0.2637
Average Fracture Length (m)	1.50	1.65	1.86	2.18	1.81
Standard deviation	0.859	0.868	0.988	0.572	1.010
Average Fracture aperture (m)	0.358E-4	0.358E-4	0.358E-4	0.358E-4	0.358E-4
Standard deviation	0.116E-3	0.116E-3	0.116E-3	0.116E-3	0.116E-3
Dip Direction (°)	335.5	345.3	348.6	346.1	0.6
Standard deviation	57.4	91.9	168.9	129.2	48.3
Dip Angle (°)	68.5	72.6	77.6	29.5	76.7
Standard deviation	11.7	13.6	7.1	18.1	13.4

(*apeture*) = (*mean apercure*) x *exp*[2 {(*diameter*) – (*mean diameter*)}/ (*mean diameter*)] (4)

For Case 4, the factor 2 in the exponent is replaced by factor 4. The maximum aperture is temporaly set at 1mm. Fig. 8 shows the probability of log of the aperture(mm) in Case 4. While the maximum value is truncated at 1mm, the aperture under 1mm is accoding to the lognormal distribution. Figs.9 and 10 show the relation between the aperture and length. The aperture of Case 4 increases dastically with the fracture length.

Fig. 5. Example of discontinuous model

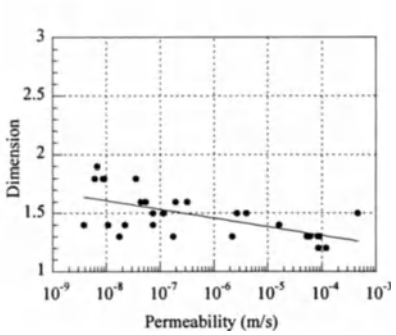

Fig. 6. Result of Case 1

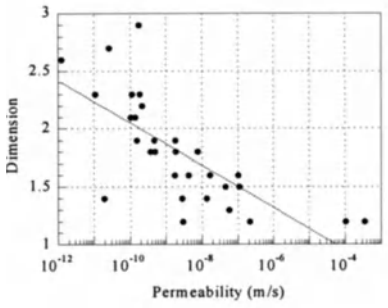

Fig. 7. Result of Case2

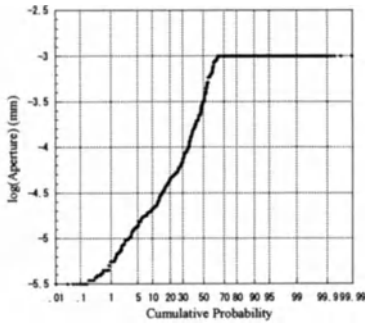

Fig. 8. Probability of log of aperture

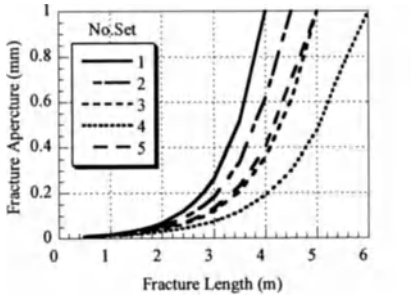

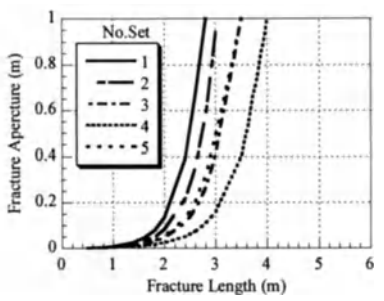

Fig. 9. Relation between apeture and length of Case3 **Fig. 10**. Relation between apeture and length of Case4

Figs. 11 and 12 show the result of Cases 3 and 4, respectively. Both results have a positive correlation between the dimension and permeability. This is the same tendency as the measured one. It is found that the result of Case4 has a larger positive correlation than that of Case3, and the tendency of Case4 is similar to the measured one.

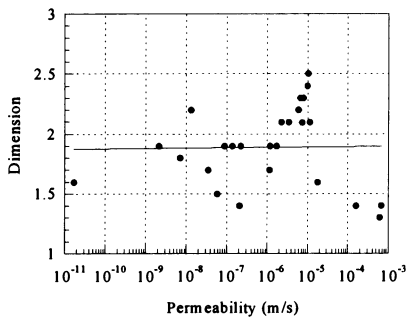

Fig. 11. Result of Case3

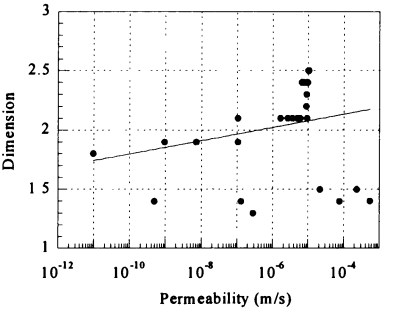

Fig. 12. Result of Case 4

CONCLUSION

The dimension obtained from the general theory by Barker indicates the aspect of fracture network. If the dimension is close to unit, the large high permeable fracture may exist. In the case of the dimension close to three, the fracture network system is connected well. The larger the dimension is, the smaller the flow section is. Thus, the permeability becomes small with the increase in the dimension in general. In the case that the properties of fracture geometry have no correlation each other (Cases 1 and 2), the result has a negative correlation between dimension and permeability. This is the generally expected result. However, the measured relation shows the positive correlation. This indicates the possibility that the properties of fracture geometry have correlation each other. In the examination, the case that the aperture has a correlation with the fracture length is tested. This is because the other properties than the aperture can be measured at the in-situ survey, but the aperture is difficult to measure directly. The result shows that the correlation between dimension and permeability becomes realistic in the case that the aperture becomes large drastically with the increase in the length. Although the other factors to produce the positive relation between dimension and permeability may exist, it can be concluded that the properties of fracture geometry have a correlation each other in some way.

REFERENCES

1. Dershowitz W., Wallmann P., Kindred S. (1991) Stripa Project Technical Report 91-16, SKB.
2. Oda M. (1986) Water Resources Research, Vol. 22, No. 13:1845-1856
3. Barker J.A. (1988) Water Resources Research, Vol. 24, No.10:1796-1804
4. O'Shaughnessy B. and Procaccia I. (1985) Physical Review Letters, Vol. 54, No. 5:455-458
5. Kobayashi A., Fujita T., Chijimatsu M. (1998) Soils and Foundations, Vol. 38, No. 4:57-70
6. Dershowitz, W., Lee G., Geier J., Hitchcock S., LaPointe P. (1994) FRACMAN, User documentation, Golder Associates Inc., Redmond, WA.
7. Sloan S.W. (1987) Adv. Eng. Software, Vol.9, No.1:34-55

Evaluation of the Heterogeneous Hydrogeological Structure

Kei Nakagawa[1] and Kenji Jinno[2]

[1]Graduate School of Kyushu University, Division of Bioresources and Environmental sciences, 6-10-1, Hakozaki, Higashi-Ku, Fukuoka, 812-8581, Japan
[2]Institute of Environmental Systems, Kyushu University, 6-10-1, Hakozaki, Higashi-Ku, Fukuoka, 812-8581, Japan

ABSTRACT. In general, a natural aquifer has a heterogeneous hydrogeological structure. The movement of pollutants in groundwater flow is influenced by this heterogeneity when transported through local advection and microscopic dispersion. Macroscopic dispersivity, which is correlated with the characteristics of the random hydraulic conductivity field has been theoretically studied for the sufficiently converged stage by many researchers up to now. On the other hand, the transient development of dispersion before reaching the converged stage becomes important when the remediation of groundwater pollution is planned immediately downstream of the pollution source. However, this transient stage has not yet been sufficiently analyzed. In the present paper, a random field of logarithms of hydraulic conductivity is synthetically generated using a two-dimensional stochastic regression model in order to directly identify the transient pollutant growth. The autoregressive parameters used in the generation model are calibrated by comparing the observed and calculated average pollutant concentrations in a tracer observation bore hole. Subsequently, the two-dimensional groundwater flow and mass transport equations are adapted. An application of the present scheme is made for the field test which was carried out by Ptak and Teutsch in Horkheimer Insel, Germany [1]. The proposed scheme can identify the autoregressive parameters and predict the hydrogeological structure. The numerical solution of the two-dimensional flow and transport equations can also evaluate the converged macroscopic dispersivity with almost as good agreement as Ptak and Teutsch obtained by the field test.

KEY WORDS: Heterogeneous field, Tracer test, Numerical simulation, Chi-square test

INTRODUCTION

In general, a natural aquifer has a hydrogeologically heterogeneous structure. In order to evaluate the convective and dispersive characteristics of the groundwater, it is important to estimate the structure of the aquifer. Aiming at identifying the distribution of the hydraulic conductivity, many approaches have been made (e.g., [2]). In the present method, the borehole data are used for the boundary condition, which is required to obtain the distribution of log-hydraulic conductivity. A chi-square test is used to evaluate the fitting between the observed and calculated breakthrough curves.

THE METHOD TO EVALUATE THE DISTRIBUTION OF HYDRAULIC CONDUCTIVITY

Autoregressive model.

For the generation of the heterogeneous field, an autoregressive model is employed as follows.

$$a_{xx}\frac{\partial^2 Y_k}{\partial x^2} + a_{yy}\frac{\partial^2 Y_k}{\partial y^2} - a_0 Y_k + \varepsilon(x,y) = 0 \tag{1}$$

where Y_k is the log-transformed hydraulic conductivity, $\varepsilon(x, y)$ is the noise term, and a_{xx}, a_{yy}, a_0 are the autoregressive parameters. Random numbers of normal distribution (μ =0.0, σ^2=1.0) are used for the noise term ε (x, y) and the boundary conditions, where no available data are found. The hydraulic conductivity k is obtained from Y_k.

Numerical model.

For the numerical tracer test, the equations of groundwater flow and non-reactive tracer transport are applied.

$$S_s\frac{\partial h}{\partial t} = \frac{\partial}{\partial x}\left[k\frac{\partial h}{\partial x}\right] + \frac{\partial}{\partial y}\left[k\left(\frac{\partial h}{\partial y} + 1\right)\right] \tag{2}$$

$$\frac{\partial C}{\partial t} + \frac{\partial (u'C)}{\partial x} + \frac{\partial (v'C)}{\partial y} = \frac{\partial}{\partial x}\left(D_{xx}\frac{\partial C}{\partial x} + D_{xy}\frac{\partial C}{\partial y}\right) + \frac{\partial}{\partial y}\left(D_{yy}\frac{\partial C}{\partial y} + D_{yx}\frac{\partial C}{\partial x}\right) \tag{3}$$

where S_s is the specific storage coefficient (L^{-1}), k is the hydraulic conductivity (LT^{-1}), h is the pressure head (L), u' and v' are pore velocities (LT^{-1}), C is the tracer concentration (%), and D is the dispersion coefficient tensor (L^2T^{-1}). For more information about the autoregressive model and numerical models, see [3].

The procedure to evaluate the heterogeneous field.

The procedure to evaluate the heterogeneous field is shown in Fig. 1. For the conversion from k to longitudinal microscopic dispersivity α_L, equation (4) is employed. This equation is obtained from Hagen, Seelheim equation [4] with the relationship between the longitudinal microscopic dispersivity and the material diameter.

$$\alpha_L = 0.3688\sqrt{\frac{k}{A}} \tag{4}$$

where, A is the dimensionless coefficient which depends on various parameters of the porous medium such as grain shape, structure, etc. Practically, the value of A should be determined from borehole core samples. In this study, A=55.0 is used, which is obtained for the glass bead. And the

transverse microscopic dispersivity α_T is set to $\alpha_L/10$.

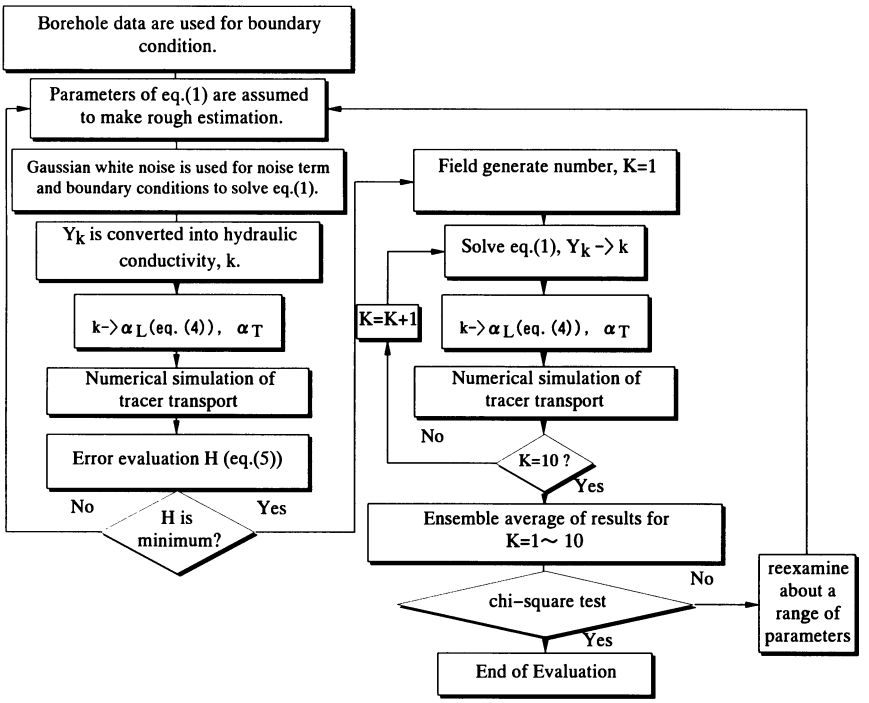

Fig. 1. The procedure to evaluate autoregressive parameters.

At first, the ε (x, y) is fixed and the best fit parameters are determined using equation (5), which evaluates the error between measurement and numerical result.

$$H = \sqrt{\frac{1}{N}\sum_{i=1}^{N}\left(C_{obs}(t_i) - C_{cal.}(t_i : a_{xx}, a_{yy}, a_0)\right)^2} \tag{5}$$

where $C_{cal}(t_i : a_{xx}, a_{yy}, a_0)$ is the calculated vertically averaged concentration at time t_i, $C_{obs}(t_i)$ is the measured vertically averaged concentration at time t_i, subscript i is the observation step number, and N is the total number of observation steps. Then, autoregressive parameters are fixed and for agreement between the ensemble averaged calculated breakthrough curves and observed curves is evaluated by chi-square test.

APPLICATION FOR THE TRACER TEST IN HORKHEIMER

The tracer test data by Ptak and Teutsch [1] are used for examining the validity of the present procedure. The tracer test was done at Horkheimer Insel field, Germany. Ptak and Teutsh evaluated 0.0364 cm/s for the velocity and 138 cm for the dispersivity. Fluorescent was used as the tracer [1]. In this study, the vertical distribution of hydraulic conductivity and the breakthrough curve of the tracer at the observation well are assumed to be given. The numerical simulation area is set to 4.0 m depth × 11.12 m length. The grid intervals are Δx=8.28 cm and Δy=5.33 cm. Fig.2 shows the boundary conditions; AB and CD are the hydrostatic pressure boundaries, BC and AD are the impermeable boundaries.

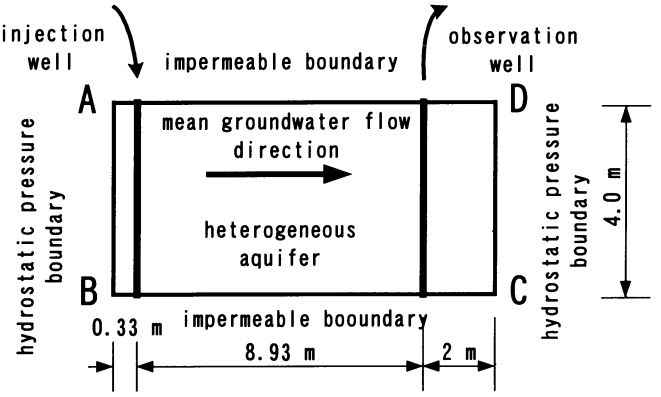

Fig. 2. The numerical simulation area with boundary conditions.

By the procedure to evaluate the heterogeneous field explained above, autoregressive parameters for the Horkheimer Insel were found to be a_{xx}=200 cm^2, a_{yy}=100 cm^2, a_0=0.03 at a significance level of 5 %. In the chi-square test, the time and concentration axes were divided into 30 intervals, and the breakthrough curves are shown in Fig.3.

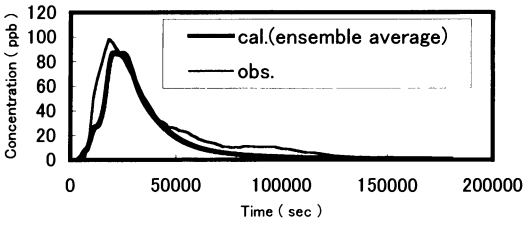

Fig. 3. Calculated and observed time series of the vertically averaged concentration curves.

The calculated curve agrees well with the depth averaged measurements, which reveals that the applied procedure is valid for the evaluation of heterogeneous aquifer properties. Fig.4 shows an example of a calculated field. The integral scales of this field are Lx=74.52 cm and Ly=58.63 cm. Fig.5 shows the plume for the field of the best parameters which are obtained by the numerical simulation of an instantaneous line injection of tracer. The central part of the plume (Y=100～300 cm) flows faster than the upper and lower regions where the plumes remain longer. This property agrees with the field observation. It also shows that the present procedure is applicable method for evaluation of the heterogeneous aquifer.

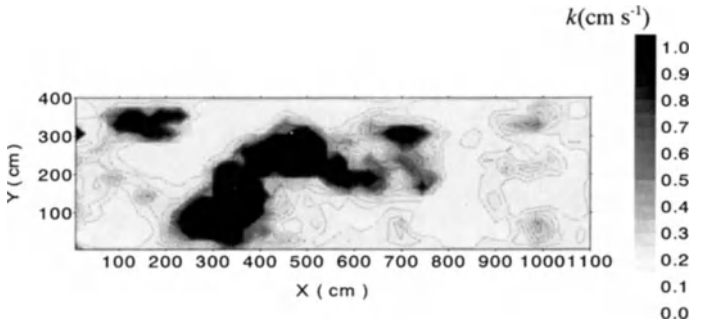

Fig. 4. Example of a calculated field (a_{xx}=200 cm^2, a_{yy}=100 cm^2, a_0=0.03). The fluctuation of k is tolerant and integral scale of log k distribution is relatively large.

The macroscopic dispersion coefficient in the longitudinal direction can be calculated from the time series of the tracer concentration at the observation well. At first, in order to calculate the variance α_T^2 as a function of time, the following equation is applied.

$$\sigma_T^2 = \frac{\sum C(t)(t-\bar{t})^2 \Delta t}{\sum C(t) \Delta t} \tag{6}$$

where $C(t)$ is the concentration at time t, t is the central time of the concentration distribution. Then, α_T^2 can be converted to α_L^2 by,

$$\sigma_L^2 = \frac{\sigma_T^2}{\bar{t}^2} x^2 \tag{7}$$

where x is the distance from the injection well to the observation well. Finally, D_L can be calculated by,

$$D_L = \frac{\sigma_L^2}{2\bar{t}} \tag{8}$$

For the ensemble averaged calculated breakthrough curves, D_L=5.36 $cm^2 s^{-1}$ was obtained, whereas, D_L=5.12 $cm^2 s^{-1}$ is obtained for the measurements by Ptak and Teutsch [1].

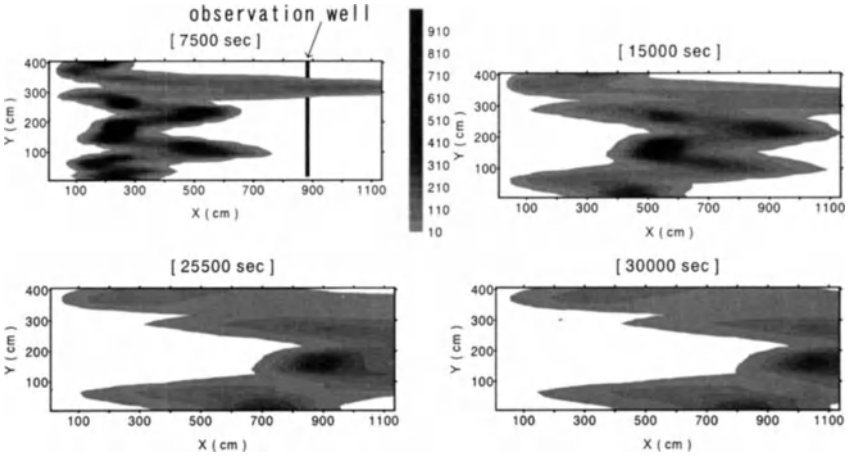

Fig. 5. Tracer movement in the calculated field shown in Fig. 4. The central part of the plume flows faster than the upper and lower regions when the plume remain longer.

CONCLUSIONS

In order to evaluate the convection and dispersive characteristics of the groundwater, it is important to know the distribution hydraulic conductivity. The procedure to evaluate autoregressive parameters developed here gives reasonable results. The following conclusions can be deduced from the present study. (1) The center part of the plume flows faster than upper and lower boundary plume, as can be seen in the tracer movement in the calculated field. (2) The integral scales of the calculated field are Lx=74.52 cm and Ly=58.63 cm. (3) The computed D_L shows good agreement with the analytically derived D_L from observation.

ACKNOWLEDGMENT

My special thanks are due to Dr. Thomas Ptak for permission to use the tracer test data in his paper.

REFERENCES

1. Ptak T, Teutsch G (1994) J of Hydrology 159: 79-104
2. Woodbury AD, Smith L, Durbar WS (1987) Water Resources Research 23(8): 1586-1606
3. Nakagawa K, Jinno K, Hosokawa T, Hatanaka K, Ijiri Y, Watari S (1998) In: Herbert M, Kovar K (eds) Groundwater Quality: Remediation and Protection. IAHS Publ. no. 250, pp.567-574
4.Sasaki H (1954) J of the Waterworks and Sewerage Association 237: 7-10 (in Japanese)

Evaluation of In-situ Air Permeability Test for Designing of Soil Vapor Extraction.

Keisaku Yasumoto and Junichi Kawabata

Kajima Technical Research Institute

ABSTRACT. Soil vapor extraction is a commonly used method for removing volatile organic compounds(VOC) from the vadoze zone. Rational designing method is, however, not established due to the difficulty in evaluating in-situ characteristics of air permeability and of volatility quantitatively. The authors conducted in-situ air permeability tests in a unsaturated ground to develop a practical method of in-situ air permeability test for designing and to obtain knowledge on air permeability in unsaturated ground. The negative pressure distribution was investigated in the ground surrounding of an extraction well. Non-Darcy's high pressure range is clearly observed in the vicinity of the extraction well even under commonly used conditions, which shows that the efficient area by soil vapor extraction strongly depends on the size and negative pressure values in this area. Radius of influence(the area which negative pressure is observed) and air permeability are rationally evaluated through theoretical analyses based on Darcy's law. The drop of Carbon dioxide(CO_2) in the ground with time is clearly observed, which is considered to be a valid index for evaluating vapor extraction effect. Those new evaluation methods for in-situ air permeability test should be effective and useful for rational designing of soil vapor extraction method.

key words : In-situ test, Soil vapor extraction, Air permeability, Radius of Influence, Unsaturated ground

INTRODUCTION

Volatile organic compounds such as trichloroethylene(TCE) and tetrachloroethylene (PCE) is one of the main contaminants in the ground. Those contaminants have been found at factory areas of chemical and electrical industries, laundry facilities etc. It now comes to be a serious social problem. Soil vapor extraction method is one of the effective remediation methods for the volatile organic compounds in vadoze zone(Fig.1). Rational designing method is, however, not established due to the difficulty in evaluating in-situ characteristics of air permeability and volatility quantitatively. It was attempted to evaluate air permeability of unsaturated soil [1]. But the number of studies based on in-situ air permeability test is very limited. The authors, therefore, attempted to evaluate air permeability of unsaturated ground through in-situ air permeability tests in an unsaturated ground which consists mainly of loam. Negative pressure and CO_2 concentration distribution in the ground were measured with time during extraction air by vacuue pump from a extraction well.

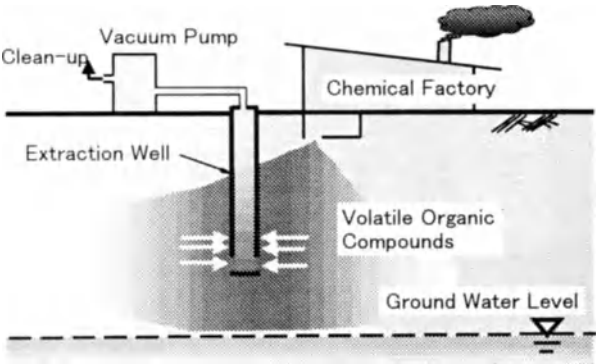

Fig.1 Soil Vapor Extraction Method

IN-SITU AIR PERMEABILITY TEST (PART 1)

Fig.2 shows outline of in-situ air permeability test and soil profile of the ground. In general, CO_2 concentration in the ground tends to be higher than that in the air (about 400 ppm) due to activities of microbes in the ground [2] . In this ground, CO_2 concentration measured in the monitoring wells were between 9,000 and 21,000 ppm, which were higher than that in the air by about two digits. In the test, negative pressure occurred in the unsaturated zone by an air extraction through vacuum pump installed in the extraction well G-1 (at an initial vacuum pressure P_0 of approximately 75 kPa and vacuum air volume Q of approximately 1.4 m^3/min.). Then, negative pressures and CO_2 concentration were measured with time in monitoring wells G-2 through 6 (F=50 mm) located at distances r of 1.25, 2.5, 5.0, 7.5, and 10.0 m from the extraction well.

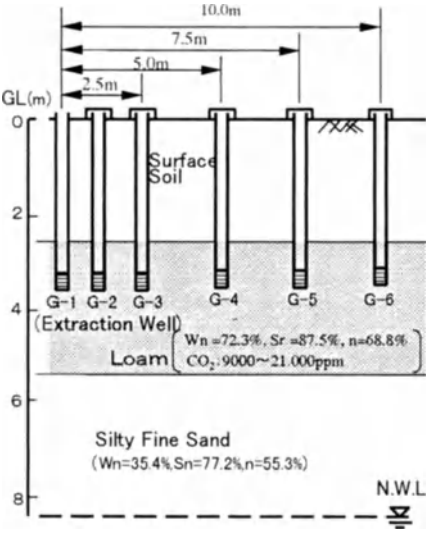

Fig.2 Outline of In-situ Air Permeability Test and Soil Profile

Fig.2 shows change of the vacuum air volume Q and vacuum pressure P_0 with time, as measured in the extraction well. It is shown that the vacuum air volume Q increases with time, while P_0decreases. Fig.4 shows change of the induced negative pressure Pi with time measured at each monitoring well. Similar to the values of vacuum air volume Q shown in Fig.3, the induced negative pressure Pi also increases with time. Furthermore, measurement data for time t of 0.5 hours, 4 hours, and 17 hours were rearranged based on Fig.4 to derive the relationship between the distance r from the extraction well and the induced negative pressure Pi, as shown in Fig.5. It can be seen that the radius of influence R of induced negative pressure P in the ground expand as the vacuum air volume Q increases. Furthermore, the radius of influence R deviates from the theoretical straight line drawn based on Darcy's law for larger values of the vacuum air volume Q in a vicinity of the extraction well, and the values falling non-Darcy range increases with time. On the other hand, the radius of influence R obtained by extrapolating the theoretical straight line drawn based on Darcy's law was approximately 15 m.

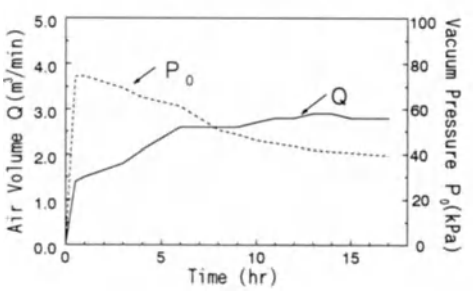

Fig.3 Q and P_0 with Time

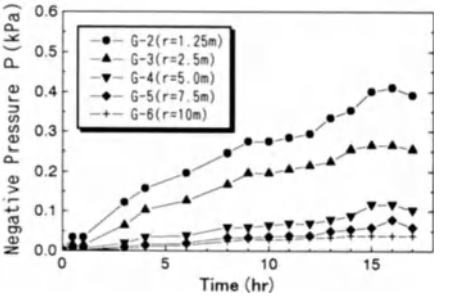

Fig.4 P_i with Time

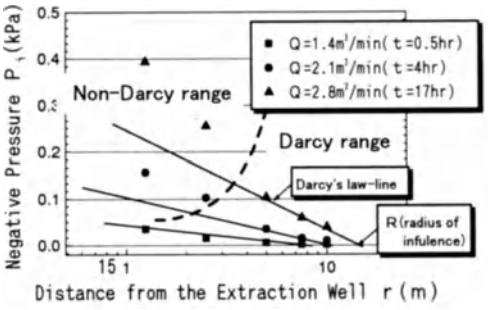

Fig.5 Relationship r and P_i

Table 1 Intrinsic Permeability (cm^2)

	Model A	Model B
Q=1.4m³/min	2.13×10^{-7}	1.35×10^{-7}
Q=2.1m³/min	2.20×10^{-7}	1.57×10^{-7}
Q=2.8m³/min	1.21×10^{-7}	9.08×10^{-8}

Table 1 shows results of calculation for the degree of air permeability k of the test ground based on Darcy's law shown in Fig. 4 based on the following equation (1) and (2) [3,4],

$$Q = \left(\frac{4\pi k}{\nu}\right)\frac{(P_{atm}-P_w)\{1+(P_{atm}/P_0)\}}{(1/r_0-1/R)} \quad (1)$$

$$Q = \left(\frac{2\pi k}{\nu}\right)\frac{H(P_{atm}-P_w)\{1+(P_{atm}/P_0)\}}{\ln(R/r_0)}\sqrt{\frac{L}{H}}\sqrt[4]{\frac{2H-L}{H}} \quad (2)$$

where Q is vacuum air volume (m^3/ min.), k is intrinsic permeability (m^2), ν is viscosity coefficient, H is thickness of the unsaturated layer (m), P_0 is vacuum pressure at the extraction well (kpa), P_{atm} is atmospheric pressure (kpa), R is radius of influence (m), r_0 is radius of the extraction well, L: length of a screen in the extraction well (m). Equation(1) is based on the three-dimensional radial-flow theory applied to a point in the ground, which takes into consideration viscosity and compressibility of the air(see Model A of Fig.6). Equation(2) is based on the theory of a partial-penetration well which takes into consideration viscosity and compressibility of the air. (See Model B of Fig.6).

All calculated air intrinsic permeability k of the unsaturated test ground consisting mainly of loam were around 10^{-7} cm^2, regardless of the increase in Q. Therefore, it can be surmised that the increase in vapor extraction effect(Q, R) was due to enlargement of the non-Darcy range. The enlargement of the non-Darcy range, on the other hand, is believed to be caused by pass ways formed in the porous medium which produces high-negative-pressure zone in a vicinity of the extraction well.

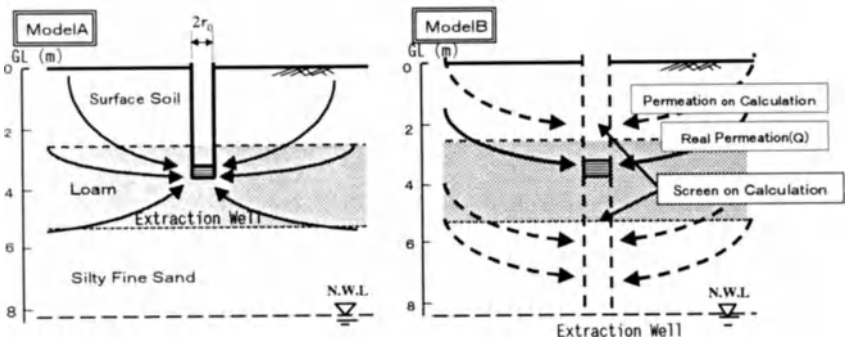

Fig.6 Calculation Model of Intrinsic Permeability (k)

Fig.7 shows change of ground CO_2 concentration with time, measured at each monitoring well. It can be seen that ground CO_2 concentration in the monitoring wells in a vicinity of the extraction well drops rapidly after vapor extraction starts. Ground CO_2 concentration in the monitoring wells away from the extraction well drops gradually after the extraction starts. Therefore, it was confirmed from ground CO_2 concentration change with time that values of vacuum air volume Q and radius of influence R increases with time. The results indicate that ground CO_2 concentration can be used for evaluation of the extraction effect of the soil vapor extraction method.

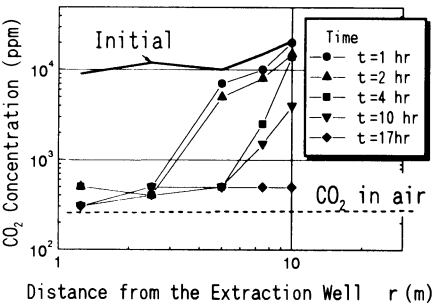

Fig.7 CO_2 Concentration with Time

IN-SITU AIR PERMEABILITY TEST (PART 2: Confirmation of the Radius of Influence)

For confirmation of the radius of influence R, which obtained by extrapolating the theoretical straight line drawn based on Darcy's law, additional monitoring wells G-7 and 8 were located at distances r of 12.5 and 15 m from the extraction well G-1.

Fig.8 shows change of the vacuum air volume Q and vacuum pressure P_0 with time as measured at the extraction well. Vacuum air volume Q increases immediately after the extraction starts, thereafter, keeps the nearly same value at the end of the first test (PART1). The vacuum pressure P_0 also decreases rapidly, thereafter, keeps the nearly same value at the end of the first test (PART1).

Fig.9 shows change of the induced negative pressure Pi with time, as measured in each monitoring well. The induced negative pressure Pi increases immediately, similar to the vacuum air volume Q and vacuum pressure P_0 in Fig.8, after the extraction stars, and keeps the nearly same value at the end of the first test (PART1) thereafter. This cause is surmised that pass ways formed in the porous medium produced in the first test (PART1) are not easily recovered.

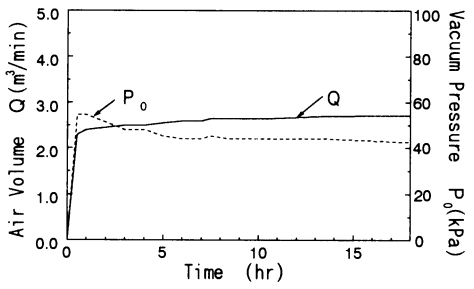

Fig.8 Q and P_0 with Time

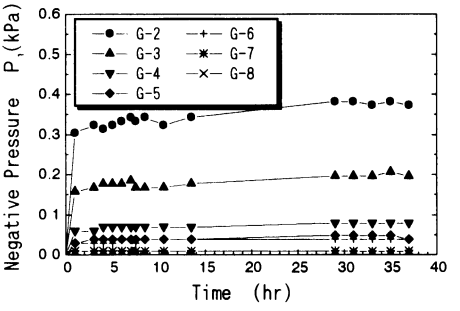

Fig.9 P_i with Time

Based on Fig.9, measured data for time t of 1hour, 4houres, and 37 hours were rearranged to derive the relationship between the distance r from extraction well and the induced negative pressure Pi, as shown in Fig.10. The data measured in the monitoring well G-7 and 8 located at a distance of 12.5 and 15m from the extraction well G-1 was on the theoretical straight line drawn based on Darcy's law. Therefore, it was confirmed the validity about the radius of influence R obtained based on Darcy's law.

Fig. 11 shows change of ground CO_2 concentration with time, measured in each monitoring well. Similar to the first test (PART1), ground CO_2 concentration in the monitoring wells in a vicinity of the extraction well drops rapidly after the extraction starts. Ground CO_2 concentration in the monitoring wells away from the

extraction well drops gradually after the extraction starts, specially, the drop speed of Ground CO_2 concentration in the monitoring well G-7 and 8, which, located at a distance of 12.5 and 15m from the extraction well G-1 was very slow. Therefore, it was also confirmed the validity about the radius of influence R obtained based on Darcy's law, through Ground CO_2 concentration in the monitoring wells with time

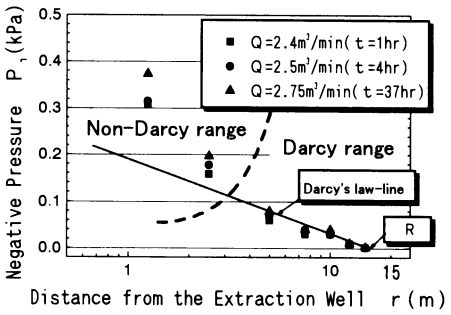

Fig.10 Relationship r and P_i

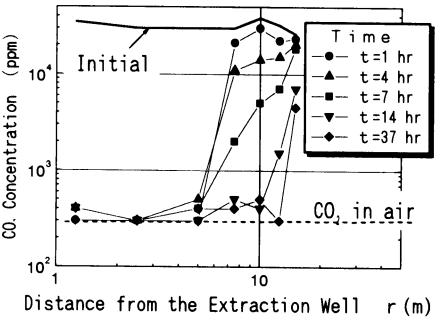

Fig.11 CO_2 Concentration with Time

CONCLUSION

The following conclusions are obtained through a series of in-situ air permeability tests performed in an unsaturated ground, which mainly consists of loam.

When negative pressure is induced in an unsaturated ground by a vacuum extraction under well used conditions in actual remediation, two ranges are observed within the radius of influence R. The pressure distribution in the range that's relatively far from an extraction well, indicates that the air flow in that range seems to be the Darcy's flow. On the other hand, the air flow in the vicinity of an extraction well seems to be the Non-Darcy's flow. The area of Non-Darcy's range is relatively large if we compare it to that of groundwater flow.

The extraction effect (pressure lowering area) corresponds to area sizes of the non-Darcy range and to its enlargement with time. This enlargement with time is to be caused by pass ways automatically formed in the porous medium, which produces high permeability zone and then high-negative-pressure zone in this range.

It is possible to apply the theory of Darcy's Law to evaluating the radius of influence R if negative pressure distribution in the ground of Darcy's range is actually measured.

Ground CO_2 concentration decreases in the area that the air is removed and replaced by flesh air outside of ground. The lowering area of CO_2concentration is useful as an index to evaluate the effect of the soil vapor extraction method.

REFERENCE

1. Tetsuo Nagafuji, Satoshi Imamura, Omamu Kusakabe, Kazumasa Hirata (1999) The pollution form of volatile organic compounds and The estimation method of pollution deposits. Journal of Environmental Systems and Engineering. Japan Society of Civil Engineering. No.615. Ⅶ-10 : 33-40.
2. Hamada, Tanaka(1997) The distribution of Carbon dioxide in the ground at the forest. Japanese. Journal of the Japan Society of Hydrological Engineering : 3-16.
3. Kiichiro Kono (1990) Ground water engineering : 104-105.
4. Л.Л.Климентовл (1961) Ground water mechanics : 268-273.

Parameter identification in discontinuous rock mass aquifers using thermal fluid logging method

Martin Schreck[1], Akira Omata[2], Makoto Nishigaki[3]

[1]Central Research Institute of Electric Power Industry, 1646 Abiko, Abiko-shi, 270-1194 Japan

[2]DIA Consultant Co. LTD, 2-272-3, Yoshino, Omiya-shi, Saitama, 330-8660, Japan

[3]Department of Environmental Engineering & Civil Design Okayama University, Japan 701-01

ABSTRACT: A tool for determining the hydraulic conductivity, flow direction and flow rate in discontinuous rock mass is presented using heat for tracing these processes. A borehole was heated by warm water injection and the cooling process was afterwards monitored using a 3D fibre-optic temperature monitoring device. The applied temperature measurement device shows an accuracy of $0.05K$. Using an heat-exchanger-model the monitored temperature effects are linked to hydraulical parameters of the discontinuous rock mass. The results obtained are further compared to results of RQD and pressure head measurements.

key words: Fluid logging, Hydraulic conductivity, Flow rate, Discontinuous rock mass

INTRODUCTION

During the past years geotechnical engineering engaged more and more in projects related to energy production. The Hot-Dry-Rock method (HDR), Compressed Air Energy Storage projects (CAES) or nuclear waste deposit projects necessary the joint work with geotechnical engineers for solving these tasks. Within these projects the following tasks may occur [1]:

- temperature monitoring of structures;
- determination of heating processes;
- monitoring of the temporal development of temperature fields;
- determination of qualitative and quantitative parameters in discontinuous rock mass; and
- monitoring of mechanical and thermal stress.

Information of the spatial distribution and temporal development of heat migration in the subsurface enables determination of performance parameters and possible hazard caused by such structures.

The subsurface in Japan consists mainly of either continuous or discontinuous rock mass. Therefore the determination of subsurface parameters is sometimes very complicated. Information of direction and connectivity of water conducting zones in discontinuous rock mass is expensive and sometimes unsatisfying. Within this presentation we will show an enhancement of the classical fluid logging method introduced by Chang [2].

The presented method uses heat for tracing flow-processes inside and around a borehole. A numerical tool is used for computing geohydraulical parameters from the temperature measurement. The data is compared to data obtained by standard measurement.

DESCRIPTION OF THE CLASSICAL FLUID LOGGING METHOD

Chang introduced the fluid logging method for quantification of fluid flow in discontinuous rock mass in 1990 [2]. Here the temporal development of electric conductivity of a borehole fluid is used for determining flow into the borehole. According to the natural/initial conditions the electric conductivity profile of a borehole is changed. This is facilitated by installing an injection tube inside the borehole. Then a fluid with a higher, respectively lower, electric conductivity than the natural electric conductivity of the borehole is injected. Afterwards the reclamation process of the natural electric

conductivity profile is monitored. A quantification of inflow by separate depth levels is possible, if the total inflow into the borehole is known. The spatial amount of measurement data versus depth as well as versus the horizontal profile section is limited by the size of the applied sensors. Therefore it is not possible to determine the inflow direction. The obtained information profile is sampled with a vertical resolution of $1 - 2m$.

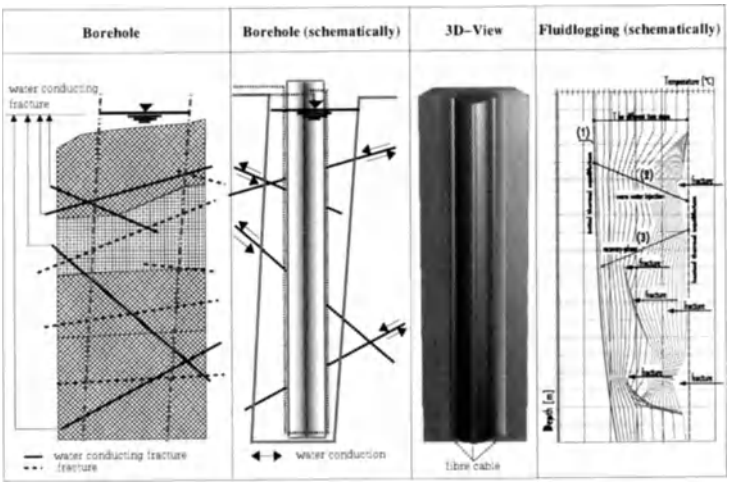

FIG. 1. Experimental Setup.

DESCRIPTION OF THERMAL FLUID-LOGGING

Thermal Fluid Logging is carried out using basically the same experimental steps, but heat instead of electric conductivity is monitored for tracing flow processes inside and around a borehole. The temperature is measured by distributed intrinsic fibre-optic temperature measurement technique. Therefore a fibre cable is attached to the outside surface of the injection tube. The fibre-cable is installed in two loops, whereas each half loop side is attached strictly vertical along the injection tubing. Each full loop lies in one plane which are intersecting each other at an angle of 90° (see also Figure 1). Thus the vertical temperature profile inside the borehole is measured four times, one time on each side of the injection tube. This enables a $3D$-measurement of temperature processes inside a borehole. This setup could be applied to boreholes with a maximum depth of $1km$ and a spatial distribution of up to $0.25m$. The accuracy of temperature measurement is $\theta = \pm 0.05K$.

NUMERICAL TOOL

The numerical tool for computing flow direction, flow rate and hydraulic fracture conductivity is described in detail in [1].

Determination of flow direction. For a water filled borehole in a rock formation the temperature (T) is given by:

$$T = f(x, y, z) \tag{1}$$

Here heat transfer is governed by three separate mechanisms: (1) heat conduction ($\ddot{Q}_{Formation}$) in the formation matrix, (2) heat migration by the fluid phase $\ddot{Q}_{FluidPhase}$), and (3) heat exchange between the two phases, which is depending on the temperature difference. For very short heating periods (1) and (3) become very small. Thus we can write:

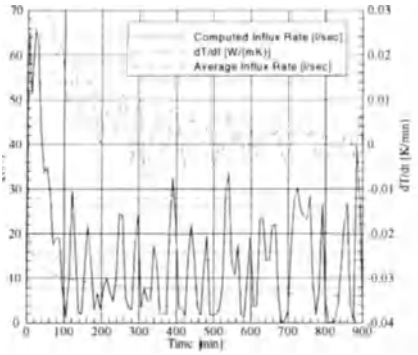

FIG. 2. Recovery phase: Computed influx rate.

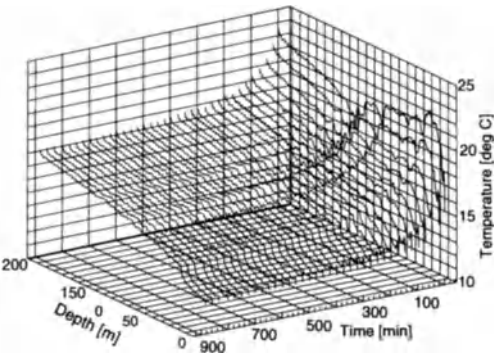

FIG. 3. Temperature profile versus time.

$$\frac{\dot{Q}_x}{\ddot{Q}_x} + \frac{\dot{Q}_y}{\ddot{Q}_y} + \frac{\dot{Q}_z}{\ddot{Q}_z} = 0 \tag{2}$$

According to *Bernoulli's law* and $\ddot{Q} = \lambda \frac{\partial T}{\partial x,y,z}$ the balance of heat migration due to fluid flow at the section of the borehole for short periods of time can be written as:

$$\dot{Q}\frac{\partial h}{\partial x} + \dot{Q}\frac{\partial h}{\partial y} + \dot{Q}\frac{\partial h}{\partial z} = \lambda\frac{\partial T}{\partial x} + \lambda\frac{\partial T}{\partial y} + \lambda\frac{\partial T}{\partial z} = 0 \tag{3}$$

With lack of vertical flow ($\frac{\partial T}{\partial z} = 0$) and for $\partial x = \partial y = \partial d_a$ we can write Eq. 2 as:

$$\frac{Q_x}{Q_y} = \frac{\Delta T_x}{\Delta T_y} \tag{4}$$

Determination of influx. The temperature variation along a borehole profile during fluid logging arises because of:

(1) heat transfer due to inflow into the borehole,
(2) time dependent convection within the borehole,
(3) heat transfer between the formation and the annulus of the borehole, and
(4) heat transfer between the injection tubing and the annulus of the borehole.

$$0 = \rho_w C_w Q\frac{\partial T}{\partial z} + \pi({r_B}^2 - {r_I}^2)\rho_w C_w \frac{\partial T}{\partial t} - H_f(T_B - T_F) - C_I(T_B - T_I)\ . \tag{5}$$

The heat transport inside the borehole takes place in either direction between formation and borehole fluid as well as between the fluid in the injection line and the fluid in the annulus. This results in a heat exchanger [3], [4]. The heat losses are given by the heat exchange between annulus and formation and are equal to the heat efficiency. As the heat efficiency is expected to be constant, the considered case corresponds to a quasi-stationary case [5]. The function $H_f(t)$ is defining the heat transfer coefficient from formation to annulus [5]:

$$H_f(t) = \frac{\lambda_F}{G_0(t)} \tag{6}$$

EXPERIMENTAL SETUP

The experimental setup is shown in Figure 1. A $201.3m$ deep borehole with an inner diameter of $7.6cm$ was drilled in crystalline rock. The subsurface consisted mainly of Gneiss. The borehole was drilled with a vertical inclination of $1deg$.

A PVC-injection tube with an outside diameter of $4.3cm$ was installed inside the borehole for the experiment. The injected water flows down this tubing to the bottom of the borehole. Using this system, a constant flow of hot or cold water from the bottom of the borehole can be created as shown in Figure 1. The injected water flows downwards in the injection tubing, out the tubing bottom and subsequently moves upwards through the annulus between the tube and the well.

The experiment was carried out in the following steps (see Figure 1):

(1) The injection tubing is installed and the initial thermal equilibrium is monitored.
(2) Warm water is injected into the borehole until a new thermal equilibrium is reached.
(3) The change in temperature after cessation of injection (here-ford the recovery phase) is monitored. Here the "influx-fractures" show as crater like decreases in the graph of the temperature distribution versus time and depth.

The experiment is finished when the initial thermal equilibrium is re-established.

Temperature data. The measurement data is sown in Figure 3. The temperature measurement was carried out with a spatial resolution of $0.5m$. The temperature resolution of the fibre optic measurement system is $\theta = 0.05K$. The temperature was continuously monitored with a time interval of $260sec$.

RESULTS

Influx. The mathematical routine and computation algorithm of the influx rate is described in [1]. The computed data is shown in Figure 2. The plot of the computed influx rate can be divided into two sections. The duration of section one is $200min$ minutes. It starts immediately after the warm water injection is turned off. During this time the well was pumped to enable the hydraulic gradient for the influx into the borehole. Within the first $200min$ during the recovery phase the influx into the borehole decreases from $65\frac{l}{s}$ to $9\frac{l}{s}$. Section 2 represents the final state in which the influx decreases to $8\frac{l}{s}$ which is shown in Figure 2.

Hydraulic conductivity. An average (over the whole profile) hydraulic conductivity estimate of $1.7 \times 10^{-5}\frac{cm}{s}$ was obtained from the thermal fluid logging experiment.

The conductivity was also determined applying constant-head injection tests [7] (see also Figure 4). The average hydraulic conductivity was determined to be $1.8 \times 10^{-5}\frac{cm}{s}$ with this method. The finest vertical resolution for this measurement method was $3m$.

Due to the very high spatial distribution of the temperature measurements, the spatial resolution of the computed hydraulic conductivity was also very high. Influx zones can be located within $1m$. When these results are compared to the results of standard measurement systems, the data correspond to the RQD measurement, as well as to the conductivity. The same zones of higher conductivity have been determined within both standard and thermal approaches.

From the temperature data, the influx direction was determined as shown in Figure 5.

In Table 1, a summary of the results shown in Figure 4 and Figure 5 is shown. In total, 17 levels with an influx of $Q \gtrapprox 0.03l/s$ have been found. These levels supply 17.5% of the total influx of $8\frac{l}{s}$. The remaining 82.5% result from influx zones with an $\dot{Q}$ smaller than $Q = 0.03\frac{l}{s}$ and therefore not considered for localisation of influx zones and determination of influx direction. Four different direction zones can be differentiated (A,B,C,D). Zone A, (8 times, $0.67\frac{l}{s}$); Zone B (4 times, $0.36\frac{l}{s}$); Zone C (1 time, $0.13\frac{l}{s}$); Zone D (3 times; $0.24\frac{l}{s}$). A more generalised interpretation over main influx depth zones using Figure 5 delivers a main influx direction corresponding to *Zone A* from SSE-NNW. In the lower levels, mainly from a depth of $150m$, the influx direction changes to East-West direction.

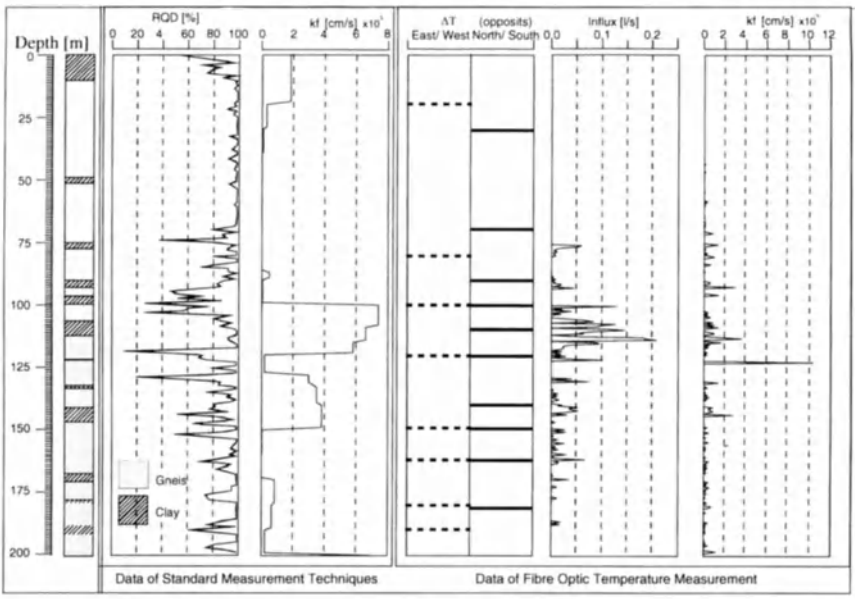

FIG. 4. RQD, k_f, flow direction and influx rate.

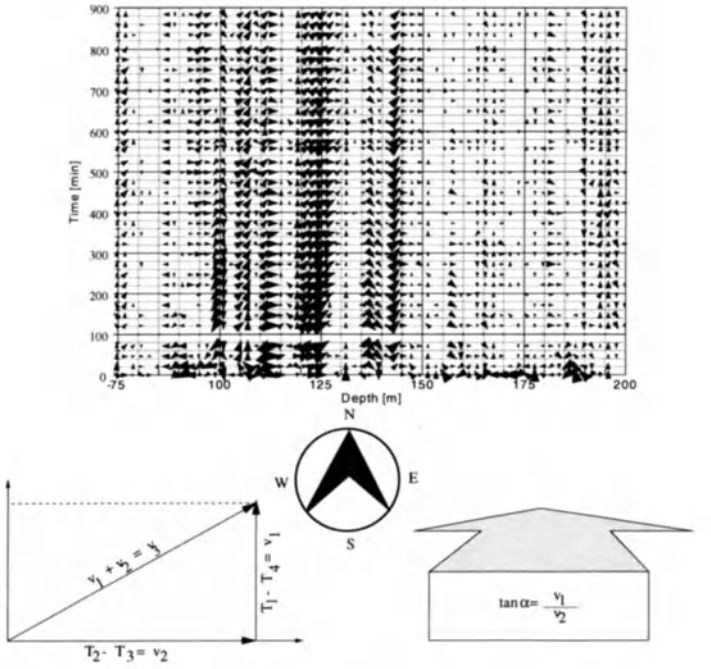

FIG. 5. Computed influx direction versus depth and time.

TABLE 1. Influx Direction of the Influx Zones with 17.5% Share of the Total Influx Rate.

No.	Z [m]	$\dot{Q}$ $[\frac{l}{s}]$	Direct.	Direct. Zone
1	76	0.06	SSE-NNW	A
2	93	0.05	S-N	B
3	101	0.13	W-E	C
4	103	0.04	SSE-NNW	A
5	107	0.09	SSE-NNW	A
6	109	0.13	E-W	D
7	110	0.15	SSE-NNW	A
8	116	0.21	S-N	B
9	117	0.10	SSE-NNW	A
10	123	0.10	SSE-NNW	A
11	130	0.04	E-W	D
12	131	0.07	E-W	D
13	142	0.05	SSE-NNW	A
14	143	0.05	SSE-NNW	A
15	145	0.03	SSE-NNW	A
16	163	0.07	S-N	B
17	172	0.03	S-N	B
Total: 1.40 (17.5%)				

CONCLUSION

The presented experimental setup has the advantage, that a thermal condition inside a borehole is measured at once over the whole borehole profile without any thermal or hydraulical disturbance of the condition inside the borehole by the measurement technique. This enables a new procedure for investigation of geohydraulic parameters of discontinuous rock mass aquifers.

The application of one fibre cable in twos loops attached to an injection tube enables a temperature measurement which shows good data accuracy and good time discretisation in order to determine the longitudinal and radial temperature processes inside a borehole during Thermal Fluid Logging experiment.

Temperature effects can be linked to hydraulic parameters if this experimental setup is applied in conjunction with a numerical tool. Flow direction, flow rate and hydraulic conductivity can be determined with respect to depth. The obtained data delivers a better information than standard measurement.

By use of a heat tracer the quality of ground water is not effected. The heat impact on the subsurface is subsided within $48 hours$ in maximum. This makes this type of setup specially suitable for the investigation of wells used for drinking water production.

REFERENCES

[1] M. Schreck. *Applied Distributed Intrinsic Fibre Optic Sensing Technique: Research on Measurement Strategies on Distributed Intrinsic Fibre Optic Sensing Technique for Geohydraulic & Environmental Engineering.* PhD thesis, Okayama University, 1999.

[2] C.-F. Chang; P. Hufschmied; F. Hale. Determination of fracture parameters with borehole fluid conductivity logging method. *Water Resources Research*, pages 519–524, 1990.

[3] J. Dornstädter. Das Temperaturangleichverfahren (TAV) - Ein Verfahren zur in-situ Bestimmung Thermischer Gesteinseigenschaften. Master's thesis, Karlsruhe University, 1987.

[4] J. H. Blackwell. A Transient-Flow Method for Determining of Thermal Constants of Insulting Materials in Bulk. *Journal of Applied Physics*, pages 137–144, 1954.

[5] H. S. Carslaw; J.C. Jaeger. *Conduction of Heat in Solids.* University Press Oxford, 1946, 1956.

[6] Ian Farmer Cheng-HawLee. *Fluid Flow in Discontinuous Rocks.* CHAPMANN & HALL, 1993.

[7] K. Nakagawa; T. Shidahara; Y. Edo; A. Nozaki. Field studies on geohydrological aspects of deep sedimentary rock for compressed air storage. Technical report, Central Research Institute of Electric Power Industry, 1998.

Estimation of Hydrogeological Parameters in Groundwater Modeling by Genetic Algorithm

K. Lakshmi Prasad[1] and A. K. Rastogi[2]

[1]Research Scholar, Department of Civil Engineering, Indian Institute of Technology, Bombay, Mumbai- 400 076, INDIA
[2]Associate Professor in Water Resources Engineering, Department of Civil Engineering, Indian Institute of Technology, Bombay, Mumbai- 400 076, INDIA

ABSTRACT: Efficient management of groundwater systems depends primarily on adequate knowledge of its hydrogeologic parameters. Estimation of these spatially distributed hydrogeologic parameters in large aquifer systems often involves considerable amount of time and financial resources. These parameters are required for the groundwater system simulation to predict head behavior in the flow domain. Inverse modeling of the system helps us in the adequate assessment of these parameters for getting a meaningful system simulation. A new approach for parameter estimation of groundwater systems based upon genetic algorithm (GA) global optimization technique coupled with Galerkin's finite element (FEM) flow simulation model is presented. The developed inverse GA model is applied for Mahi Right Bank Canal (MRBC) command area aquifer to estimate optimal aquifer parameters hydraulic conductivity and net recharge in the flow domain. The results show that the computed head distribution using the estimated parameters from inverse modeling is closer to the observed head contours. The estimated parameters are in acceptable agreement with the results obtained from another inverse model developed from conventional optimization technique of Gauss-Newton-Marquardt method. The study concludes that the developed algorithm is useful for successful estimation of aquifer parameters in the case of large aquifer systems.

KEY WORDS: Inverse modeling, parameter estimation, genetic algorithm, Gauss-Newton-Marquardt method, hydraulic conductivity

INTRODUCTION

The problem of estimating aquifer parameters with the aid of a numerical model using limited geologic and hydrogeologic data is often referred to as inverse modeling. The fundamental benefit of inverse modeling is its ability to automatically calculate parameter distribution that produce the best fit between observed and simulated hydraulic heads and flows. Inverse modeling involves system simulation and optimization. Optimization algorithms of gradient, conjugate gradient, quasi Newton, Gauss-Newton, or modified Gauss-Newton methods are widely used for computing optimum parameters. Yeh (1986) and Sun (1994) have discussed relevant aspects of these inverse modeling techniques in greater detail. The solutions of these methods however, give local optimum due to the inherent non-convexity in many field problems. Consequently, there may be more than one optimal points in the solution domain and the obtained parameters may not be considered as the best solution. More importantly, the solution convergence of these methods depends on the initial guess values for the parameters.

In this paper, we present application of genetic algorithm (GA) global optimization tool for estimating aquifer parameters. A particular advantage of the GA approach is its insensitivity for the initial guess of the parameters. It also doesn't require the calculation of derivative with respect to the estimated parameters, which is the primary source of numerical instability. The estimated parameters are used to simulate a flow domain by Galerkin's finite element formulation. The aquifer

domain is parameterized by zonation technique and weighted least squares function is used as objective function. In brief, genetic algorithm (GA) is a stochastic global search procedure based upon the concepts of natural selection and reproduction. It relies on the principles of "survival of the fittest" and "inheritance of the characteristics of the parent populations" and is able to search complex multimodal decision spaces. It can efficiently solve for non-convex functions which are difficult to tackle by many optimization methods (Goldberg, 1989). The optimal parameter estimates for the problem presented can be derived, by the following steps involved in GA evolutionary computation process. (1) Producing an initial population, (2) describing a coding scheme for all the variables, (3) running the flow simulation finite element model for all the sets of variables, (4) computing the fitness function based upon the objective function, and (5) performing the computation with genetic operators.

In the present study an initial population of parameters of specified values proportional to total string length is generated using random generator. Binary coding method is adopted to transform the parameters to a binary string of specific length. Each variable has its own length corresponding to the allowed minimum and maximum value of that parameter. The length of sub-string is determined according to the desired solution accuracy. By decoding the individuals in the population, the solution for each instance is determined. From this population the next generation is evolved by performing three distinct operations, namely reproduction (selection), crossover and mutation. Based upon the statistics of this population the next generation is reproduced following the stochastic roulette wheel method (Deb, 1998), which follows a bias law that assigns probabilities to the members of the population analogous to the statistics of the generation. This means that the weak solutions will be assigned small probabilities and the strong solutions (fittest) will be assigned high probabilities of existence in the next generation. In this way the next generation evolves where stronger solutions have survived and increased their presence. In the process of reproduction of new generation, the operations of crossover and mutation are performed. Single point crossover scheme is followed in our study, which states that with a specified probability of crossover, two members of population are randomly selected and are modified by exchanging the right part of their string at a randomly selected position. The probability of crossover determines whether or not crossover to be applied to a selected pair of parents. Finally, depending upon the probability of mutation zero and one of binary string are altered. After crossover and mutation the population takes its final form in the current generation. The values of objective function are determined by decoding the strings. These values express the fitness of the solutions of the current generation. The new population is used to generate another one and so on, yielding solutions that are more and more concentrated in the vicinity of global optimal.

THE STUDY AREA

The present study of MRBC command area situated in Kheda and Anand districts in Gujarat State, India (Fig. 1) covers an area of 2997 sq. km and is bounded by Shedi river in the north, Mahi river in the east and south and Alang drain in west direction. The MRBC command area lies between north latitudes 22^0 26′- $22^0$55′ and east longitudes 72^0 49′- 73^0 23′ and climate of the area is arid to semi arid with an average rainfall of 823 mm. About 96% of rainfall occur in the monsoon season (June-Sept) and there is substantial variation in the monthly and annual rainfall. Detailed field investigations of the region were carried out by Gujarat Water Resources Development Corporation (GWRDC). Lithological cross sections of selected regions of the area have indicated the presence of a main water table aquifer consisting mostly of a mixture of gravel and sand which exhibits a large variation in the conductance properties. The applicable value of specific yield within the aquifer region is 0.15. Analysis of water table maps of the past few years suggested that the recharge to the aquifer from rainfall, canal seepage, and irrigation return flows exceeds the groundwater withdrawals from the region resulting in a steady rise of water table. For simulation purposes net annual recharge values over the area were considered. It is also assumed that in the present model

the average annual inflow is almost negligible compared to average annual outflow across the boundaries, which is computed by subtracting pumping withdrawals and aquifer storage from the net annual recharge. The no inflow assumption is justified for a continuously rising trend in the water level suggesting aquifer storage and outflows.

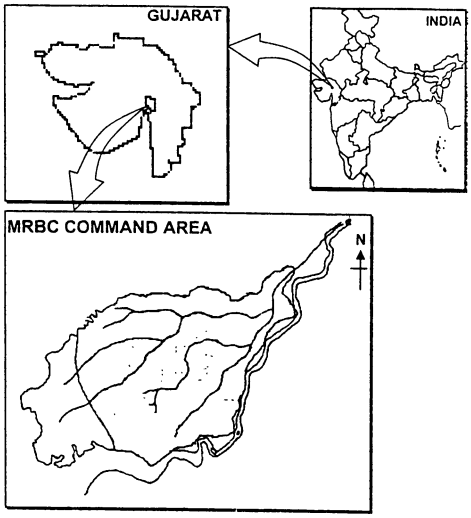

Fig. 1. Location map of the study area

INVERSE MODELING

The governing equation for the groundwater flow in the MRBC command area can be given as

$$\frac{\partial}{\partial x}\left\{k_x(h-\eta)\frac{\partial h}{\partial x}\right\}+\frac{\partial}{\partial y}\left\{k_y(h-\eta)\frac{\partial h}{\partial y}\right\}+R=S_y\frac{\partial h}{\partial t} \tag{1}$$

where h (x, y, t) is the hydraulic head (m), s_y is the specific yield, $\eta(x,y)$ is the elevation of aquifer bottom (m), k_x and k_y are the hydraulic conductivity values (m/d) in the principal axes direction and R (x,y,t) is the net nodal recharge (m/d).

The initial and boundary conditions for the problem are given as,

$$h(x,y,0) = H(x,y) \text{ for all } x,y \in \Omega \tag{2}$$

$$h(x,y,t) = H_R(x,y,t) \text{ for all } x,y \in \Omega_1 \tag{3}$$

where, H is the initial groundwater head (m) in the aquifer domain Ω and H_R is the known head (m) along the Alang drain and the river boundaries Ω_1.

The solution of the above governing equation (Eq. 1) is obtained by Galerkin's finite element approach. The study area is discretized into 171 nodes and 294 triangular elements (Fig. 2). Aquifer properties and applicable net recharge are assigned to each element of the domain. The resulting system of linear equations can be finally written in the matrix form as,

$$\left([G]+\frac{1}{\Delta t}[P]\right)\left\{h_L^{t+\Delta t}\right\}=\frac{1}{\Delta t}[P]\left\{h_L^{t}\right\}+\left\{F_L\right\} \tag{4}$$

where [G] is the conductance matrix containing hydraulic conductivity terms, [P] is the storage matrix with specific yield terms, Δt is the size of timestep, vector $\{F_L\}$ is the net flux at node L, $\{h^{t+\Delta t}\}$ is the unknown head vector and $\{h^t\}$ is the known head vector at time t. The solution is then carried out iteratively and during each timestep the right hand side known vector and the conductance matrix is updated with the latest head values to take care of the transient nature of the problem. The objective function is weighted least squares function where the functional to be minimized is

$$\underset{T_1,\ldots,T_M}{\text{Min}}\ J = \sum_{L=1}^{L}\sum_{t=t_0}^{t=t_f} W_{L,t}\left[h_{L,t}^{C} - h_{L,t}^{OB}\right]^2 \tag{5}$$

subject to the lower and upper bounds of the parameters

$$T_i^l \le T_i \le T_i^u \tag{6}$$

where, $h_{L,t}$ and $h_{L,t}$ are computed and observed heads at observation well L and at time t, T_i is transmissivity at homogeneous zone I, M are number of transmissivity zones, L are number of observation wells, t_0 and t_f are beginning and ending times of observations, l and u are superscripts used to denote lower and upper bounds of parameters and $W_{L,t}$ is weighting factor. Presently all head observations are given equal weight ($W_{L,t} = 1$).

Estimation of Hydraulic Conductivity

The field data of 1984 and 1985 is used for inverse modeling. The observation heads at 57 observation wells in the aquifer domain are used in the present study. The net annual recharge (Table 1) during 1984-85 (June 1st to May 31st) is estimated considering the rainfall, seepage from the main canals and distributaries, return flow from the canal irrigated areas and area irrigated by wells, groundwater draft and groundwater outflow. The net annual recharge is estimated using the norms provided by Groundwater Resources Estimation Committee, Ministry of Irrigation (1984, 1997).

TABLE 1. Net annual groundwater recharge (1984– 85) in MCM

Year	Rainfall	Seepage from main canal and branches	Seepage from distributaries	Return flow from canal irrigation	Return flow from well irrigation	Ground Water extraction	Ground water outflow	Aquifer storage or Net recharge (1)+(2)+(3)+(4)+(5) -(6)-(7)
	(1)	(2)	(3)	(4)	(5)	(6)	(7)	(8)
1984-85	299.89	48.69	127.67	722.24	32.22	214.79	401.60	614.32

The MRBC aquifer domain is parameterized into 10 zones (Fig. 3) based upon the geological mapping, topography and prior information on parameters. The hydraulic conductivity of various zones is estimated using developed inverse model. The range for the parameters is chosen as 20 to 200 m/d. String length for each parameter is taken as 8 bits resulting in a total string length 80 bits. The initial population and maximum number of generations are considered as 75 and 600 respectively after a number of trial runs. The crossover and mutation probabilities are varied from 0.65 to 0.75 and 0.01 to 0.015, respectively. Largely, the parameters estimated for various zones agree with the weighted average hydraulic conductivity (WAHC) values from practical considerations (Table 2). Disagreement in hydraulic conductivity values estimated for zone 4 and 8

can be attributed to the following reasons: (1) Lack of adequate and reliable quantity of observation head data in the region zone 8. (2) Head at the observation well in these zones may be more sensitive to the aquifer recharge as compared to zonal hydraulic conductivity. It is observed that heads computed by using the parameters (Fig. 4) estimated by inverse modeling are closer to observed heads except in the eastern region of Zone 8.

TABLE 2. Estimated hydraulic conductivity (m/d)

Zone No.	1	2	3	4	5
WAHC	77.130	33.289	27.381	61.222	98.195
GA	84.941	29.882	23.529	87.765	81.412
GNM	98.186	46.476	23.888	77.883	71.117
Zone No.	6	7	8	9	10
WAHC	38.713	55.122	69.304	137.692	62.844
GA	37.647	57.412	20.706	148.471	55.294
GNM	31.455	40.631	21.946	131.151	47.452

WAHC = Σ {(Hydraulic conductivity of element) (element area)}/ (Zone area)

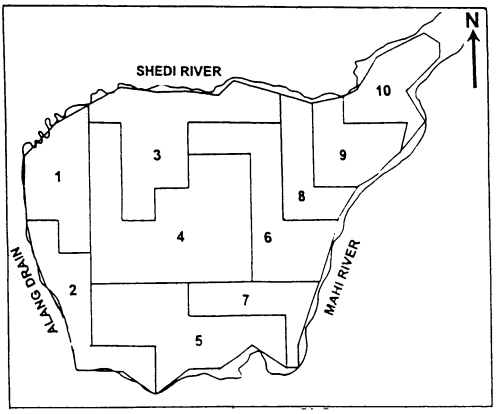

Fig. 2. Zonation pattern

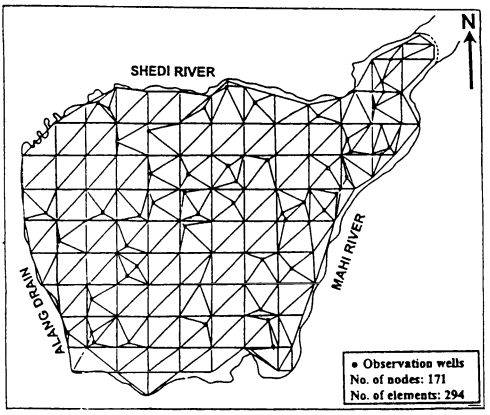

Fig. 3. Finite element discretization of the study area

Estimation of Zonal Recharge

The zonal recharges (Table 3) are also estimated by inverse modeling. It is observed that the estimated net annual recharge by inverse modeling is closer to the estimated annual recharge from the field data considering the inflows and outflows of the aquifer region. From the estimated zonal recharges, the net annual recharge in the aquifer domain is computed as

$$\sum_{i=1}^{\text{No.of zones}} \{(\text{Zonal recharge})\,(\text{Zonal area}) \times 365\}$$

Thus, the estimated net annual recharge by inverse modeling is 685.93 MCM (GA approach) and 688.45 MCM (GNM method). These values are in close agreement with the estimated net annual recharge (614.32 MCM) based upon the mass balance approach considering the various inflow and outflow data collected from the field. Further, the computed head distributions using the zonal recharges estimated by inverse modeling are in acceptable agreement with the observed head contours (Fig.5).

TABLE 3. Estimated zonal recharge (10^{-5} m/d)

Zone No.	1	2	3	4	5
GA	25.490	62.373	69.824	97.765	35.922
GNM	29.486	64.901	71.619	96.073	33.773
Zone No.	6	7	8	9	10
GA	77.275	68.706	96.275	15.804	5.373
GNM	81.752	65.895	89.727	17.835	5.000

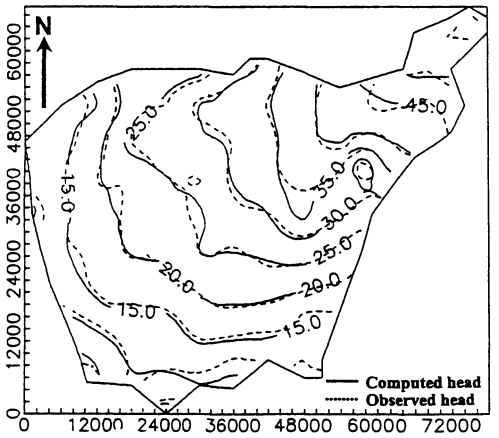

Fig. 4. Comparison of computed head using estimated hydraulic conductivity and observed head

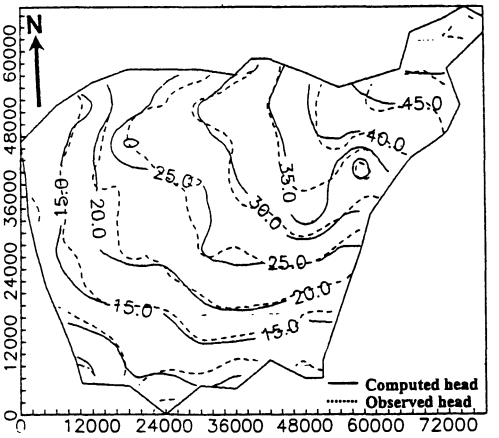

Fig. 5. Comparison of computed head using estimated zonal recharge and observed head

CONCLUSION

The study concludes the utility of genetic algorithm global optimization model for aquifer parameter estimation. The developed algorithm is useful for inverse modeling of regional aquifers, which is an important step towards real system simulation and effective management of groundwater resources.

ACKNOWLEDGEMENT

The authors wish to acknowledge the assistance of GWRDC of Gujarat State and GERI (Vadodara) for providing the necessary data for the present study.

REFERENCES:

1) Deb K. (1998) *Optimization for engineering design.* PHI Pvt Ltd., New Delhi, India.
2) Goldberg DE. (1989) *Genetic algorithms in search, optimization, and machine learning.* Addison-wesley Publishing Co., Reading, Mass.
3) IARI Research Bulletin- 42. (1983) Resource analysis and plan for efficient water management- A case study of Mahi Right Bank Canal Command area, Gujarat. Water Technology Centre, Indian Agricultural Research Institute, New Delhi.
4) Ministry of Water Resources. Reports of the groundwater resource estimation committee- Groundwater resource estimation methodology, Govt. of India, New Delhi (1984, 1997).
5) Sun Ne-Zheng (1994) *Inverse problems in Groundwater modeling.* Kluwer academic publishers, Netherlands.
6) Yeh WW-G (1986) Review of parameter identification procedure in groundwater hydrology: The inverse problem. *Water Resour. Res*, 19: 225-233.

Mathematical Modeling of Groundwater Flow and Radionuclide Transport in Heterogeneous Aquifer

Masahiro Munakata and Hideo Kimura
Waste Disposal Safety Assessment Laboratory, Department of Fuel Cycle Safety Research,
Japan Atomic Energy Research Institute, Tokai, Ibaraki, 319-1195 Japan

ABSTRACT. Atomic Energy of Canada Limited carried out a series of tracer tests in the Twin Lake site, to study geologic heterogeneity on the aquifer dispersion properties. Moltyaner et al. [6] analyzed the heterogeneity in statistical terms as variability in the hydraulic conductivity. Their statistical results were used here to develop a geostatistical approach based on the correlation between observed hydraulic conductivity values. The geostatistical model assumes that the correlation strength of the values of hydraulic conductivities between any two locations depends on the distances between these locations, and is expressed as an exponential function. Numerically, a matrix decomposition method is used. The groundwater flow field is calculated by three-dimensional finite element method using the realized spatial distribution of hydraulic conductivity that is calculated by the geostatistical model. The flow simulation results are used as input into the transport computer code, which in turn is used to simulate the tracer breakthrough curves at different observation wells. A random walk method is used for the radionuclide transport simulation. The simulated tracer plumes of tracer tests explain favorably the experimental tracer plumes. The simulations showed that the correlation length of the geostatistical model is a key parameter that characterizes the heterogeneous flow field, and the value of 5m in the flow direction and 0.5m in the direction perpendicular to the flow is obtained through the geostatistical analysis. The heterogeneous flow field in this aquifer is adequately characterized by the statistical spatial distribution of hydraulic conductivity based on the geostatistical model.

KEY WORDS: geostatistical model, spatial variability, correlation length, radionuclide transport

INTRODUCTION

Safety assessment of a radioactive waste disposal use models to predict a long-term performance of the disposal system. It is important that assessing models are applied with a satisfactory level of confidence. Therefore, an energetic effort is directed towards the validation of safety assessment models. As a part of this effort, Atomic Energy of Canada Limited carried out a series of tracer tests in the Twin Lake site, to investigate experimentally the geologic heterogeneity and field-scale dispersion, and to collect data for developing and evaluating groundwater flow and transport models. The tests showed that the complicated movements of tracer plume were due to the heterogeneity of the aquifer. The movements were attributed to the spatial variability of groundwater flow velocity caused by the spatial variability of the hydraulic conductivity. The main objective of the reported study is to describe the spatial variability of the hydraulic conductivity and, subsequently, the tracer plume motion by means of geostatistical modeling. The procedure used here and the geostatistical modeling is discussed in this paper.

TWIN LAKE TRACER TEST

The detailed description of the natural gradient tracer tests in the Twin Lake aquifer can be found in Killey et al. [1]. Let us use here some of the reported experimental results including the position coordinates of boreholes, the hydraulic heads, tracer concentrations and hydraulic conductivities,

estimated from gravimetric analyses of continuous cores, extracted at 86 borehole locations. The tracer tests have revealed that the Twin Lake aquifer has a heterogeneous structure in itself. The statistical analysis of the heterogeneous structure gives the mean of log hydraulic conductivity of -1.68 and the variance of 0.014. The Twin Lake aquifer is illustrated in Fig.1 along a vertical cross section drawn through the tracer injection well. The longitudinal extent of the modeled domain is 130m starting from the edge of the Twin Lake. The horizontal width is 14m with this vertical section as symmetrical plane. The Twin Lake aquifer are consists of the lower fluvial sand deposits and the upper less silty sand deposits. This gives main reason for dividing the Twin Lake aquifer into two zones; the upper zone of a low permeability near the water table and the lower zone of a high permeability through which active transport took place. The replenishment in the aquifer is recharged through precipitation and seepage from the Twin Lake. The groundwater flow in the lower zone of the aquifer is almost horizontal.

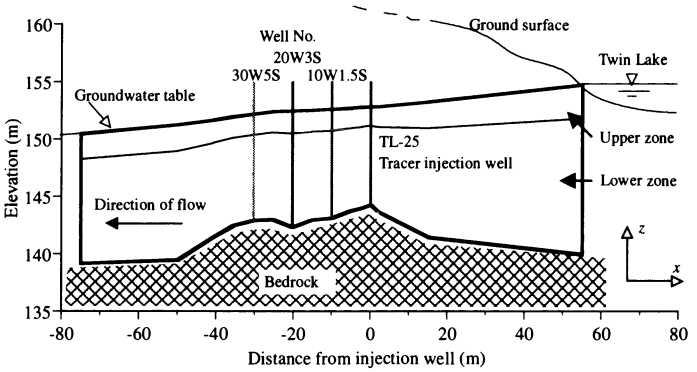

Fig.1 Vertical cross-section of Twin Lake aquifer. Thick lines show model boundaries. 10WS1.5S, 20W3S and 30W5S indicate the name of observation wells.

MATHEMATICAL MODEL

It seems that the complicated movement of tracer plume in the experimental results depends on a spatial variability of the hydraulic conductivity. Therefore, in order to characterize the spatial variability of the hydraulic conductivity, we assume that the correlation strength of the values of hydraulic conductivities between any two locations depends on the distances between these locations, and is expressed as an exponential function. And we also assume that the spatial distribution of the hydraulic conductivity can be approximated by using a lognormal distribution and a correlation length scale, which obtained from a geostatistical analysis of measured data of hydraulic conductivities. The field of correlated conductivities is generated numerically with conditioning upon the measured data of the hydraulic conductivities at 86 points. For the generated field of the hydraulic conductivities, the groundwater flow equation is solved numerically by the finite element method. The same discretized elements are also used in the random walk method to estimate the tracer concentration. The matrix decomposition method [2] is used for generating the lognormally distributed values of hydraulic conductivity k. The k can be transformed to the normal distribution Y, i.e. $Y = \log_{10} k$. The values of Y are estimated from

$$Y = L \cdot \varepsilon + v \tag{1}$$

in which v is the averaged values of Y, ε is a vector N [0,1] (i.e., normally distributed around zero with a standard deviation of 1), and L is defined in terms of the covariant matrix A.

$$A = LL^T \tag{2}$$

Equation (1) represents the generated process because the mean is given by

$$E[Y] = LE[\varepsilon] + v = v \tag{3}$$

and the covariance is given by following equation using the expected value E.

$$E[(Y-\nu)(Y-\nu)^T] = LE[\varepsilon\varepsilon^T]L^T = LL^T = A \tag{4}$$

The exponential form of the covariance matrix A

$$A = \sigma^2 \exp(-2\Delta x_{ij}/\lambda_x - 2\Delta y_{ij}/\lambda_y - 2\Delta z_{ij}/\lambda_z) \tag{5}$$

is assumed in which σ^2 is the variance of Y, λ_x, λ_x and λ_z indicate the components of the directional correlation length, Δx_{ij}, Δy_{ij} and Δz_{ij}, the components of the distance between element i and j, x, y and z direction denote the flow direction and the horizontal and vertical direction perpendicular to the flow, respectively. Thus, the spatial variations of hydraulic conductivity can be obtained from Eq. (1) by decomposing the matrix A. If the value Y_i of element i is known, we can obtain ε_i by following equation;

$$\varepsilon_i = (Y_i - \nu - \sum_{j=1}^{i-1} L_{ij}\varepsilon_j)/L_{ii} \tag{6}$$

And then, by replacement between original ε_i and new ε_i obtained by Eq. (6), the value Y_i of element i is restricted to the measured value.

To simulate the groundwater flow, the basic equations are derived from the Darcy's low and the mass conservation of fluid. The groundwater flow in the Twin Lake aquifer will be analyzed by using numerical code, 3D-SEEP [3], which is a three-dimensional finite element code simulating the saturated-unsaturated groundwater flow. The tracer transport will be analyzed by the advection-dispersion equation with the random walk method. Uffink [4] give the principles of the random walk model.

SIMULATING PROCEDURE

The about 108000 elements are used in the simulation. The smallest element in the center part of the area has dimensions of 0.2m in the flow direction (x) and horizontal direction perpendicular to the flow (y) and 0.1m in vertical direction (z). The process of simulation consists of four steps. In the first step, we generate the spatial distribution of hydraulic conductivity by using the random field generator. In the second step, the groundwater flow velocity field is calculated for the generated hydraulic conductivity field and the simulated hydraulic head is compared with the observed one. At this stage, we verify that the error of hydraulic head in comparison with the observed one is well within 5%. In the third step, the tracer transport simulation is performed for the calculated velocities. We simulate 30 cases for different realizations of the random field and summed up each result of transport calculation in order to avoid the singularity of random number. In the last step, the simulated tracer breakthrough curves are compared with the experimental ones and the error between observed and simulated values is estimated at 86 monitoring wells.

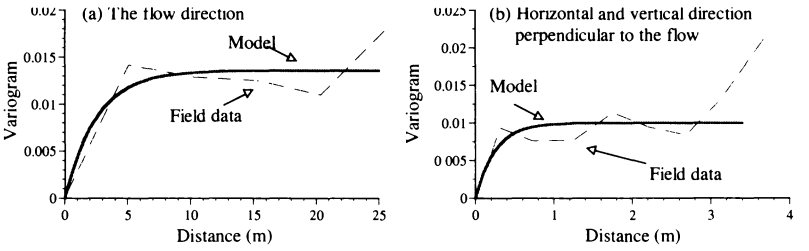

Fig. 2 Variogram of the flow direction (a) and horizontal and vertical direction perpendicular to the flow (b) based on Killey et al. [1] by dashed lines and calculated by the model by solid lines (λ_x =5.0m, λ_z =0.5m, σ_x^2 =0.014, σ_z^2 =0.01).

To generate the spatial distribution of hydraulic conductivity, the geostatistical model requires the correlation length, mean value and variance. These parameters (except for the correlation length) were obtained by statistical analysis based on the data from Killey et al. [1]. The correlation length is found by fitting the theoretical variogram of the hydraulic conductivity to the experimental variogram. The directional variograms of log value of hydraulic conductivity are shown in Fig. 2 by dashed lines. The solid lines in this figure show the calculated values obtained from the model, which uses Eq. (5) and a relation between the covariance $C(\mathbf{h})$ and variogram $\gamma(\mathbf{h})$, i.e. $\gamma(\mathbf{h}) = C(0) - C(\mathbf{h})$ where $\mathbf{h}$ is a vector of distance and $C(0)$ means the variance. The correlation length for each direction can be estimated from curve fitting. The estimated values, λ_x=5.0m, λ_z=0.5m, σ_x^2=0.014, σ_z^2=0.01, suggests the correlation in the horizontal direction is stronger than that in the vertical one. Based on the estimated correlation length, calibration was performed by changing the correlation length. For the upper zone, there were few data to use for a statistical analysis of hydraulic conductivity from the investigations. Therefore, the values of the statistical parameter were determined by fitting to a simulated head distribution in the upper zone.

For the groundwater flow calculation, upstream and downstream boundaries were restricted to the measured pressure head, and for the top and the bottom of boundaries the flow was set to zero. For the transport calculation, the accuracy of the random walk model is influenced by the maximum fraction of the element dimension in which particles are allowed to move within a time step and also by the number of particles. Appropriate values for the fraction of the grid dimension are 1/5 to 1/10 [5]. Thus, a time step of 0.01 day was used. The transport simulation with the random walk model by using 68,000 particles was applied to one case of generation of the spatial distribution of hydraulic conductivity. The dispersivities of longitudinal and transverse direction were determined to be 0.02m, 0.001m, respectively, from Moltyaner et al. [6,7].

RESULTS

The best-fitted parameters of log hydraulic conductivity are summarized in Table 1. The vertical correlation length is in general agreement with the one obtained by Moltyaner et al. [8] and Dagan et al. [9]. Also, other parameters are almost same as the ones obtained by Killey et al. [1]. The difference among the three directional correlation lengths indicates the anisotropy of this aquifer. The statistical property of the parameters in the horizontal and vertical direction perpendicular to the flow is assumed same in this simulation.

Figure 3 shows one example of three-dimensional realization of the spatial distribution of hydraulic conductivity (x component) calculated by the geostatistical model in the Twin Lake aquifer. Main transport area (lower zone) is only displayed in this figure. Also, Fig. 4 shows the results of the numerical analysis on (a) the observed concentration distribution, (b) the concentration distribution simulated at 4.44, 13.39 and 25.16 days after tracer injection. The illustrations of tracer movements are given for the relative tracer concentration. The different shading represent the variation of the tracer concentration, i.e. the darker the shading, the larger the value of concentration. A good agreement of the observations and calculation is obtained, although some differences appear with elapsed time. The differences seem to arise from the non-uniform injection of the tracer. The initial

Table 1 Input parameters for generation of the spatial distribution of log hydraulic conductivity k in cm/sec. The x, y and z direction denotes the flow direction, horizontal and vertical direction perpendicular to the flow, respectively.

Parameter	Upper zone	Lower zone
Mean of log$k$ in x direction m_x	-2.000	-1.680
Variance of log$k$ in x direction σ_x^2	0.014	0.014
Mean of log$k$ in y, z direction m_y, m_z	-3.400	-1.990
Variance of log$k$ in y, z direction σ_y^2, σ_z^2	0.010	0.010
Correlation length in x direction λ_x (m)	5.0	5.0
Correlation length in y, z direction λ_y, λ_z (m)	0.5	0.5

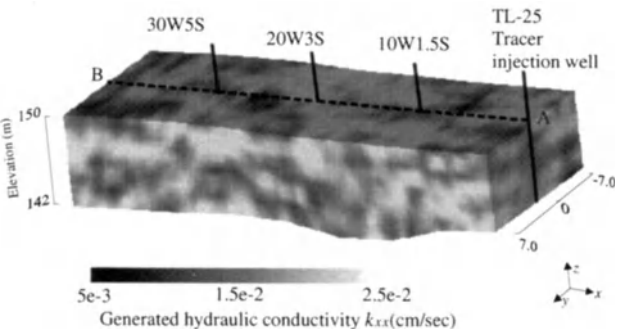

Fig. 3 One example of 3D realization of the spatial distribution of hydraulic conductivity k_{xx}(x component). The correlation length λ_y = 5.0m is assumed. Main transport area (lower zone) is only displayed.

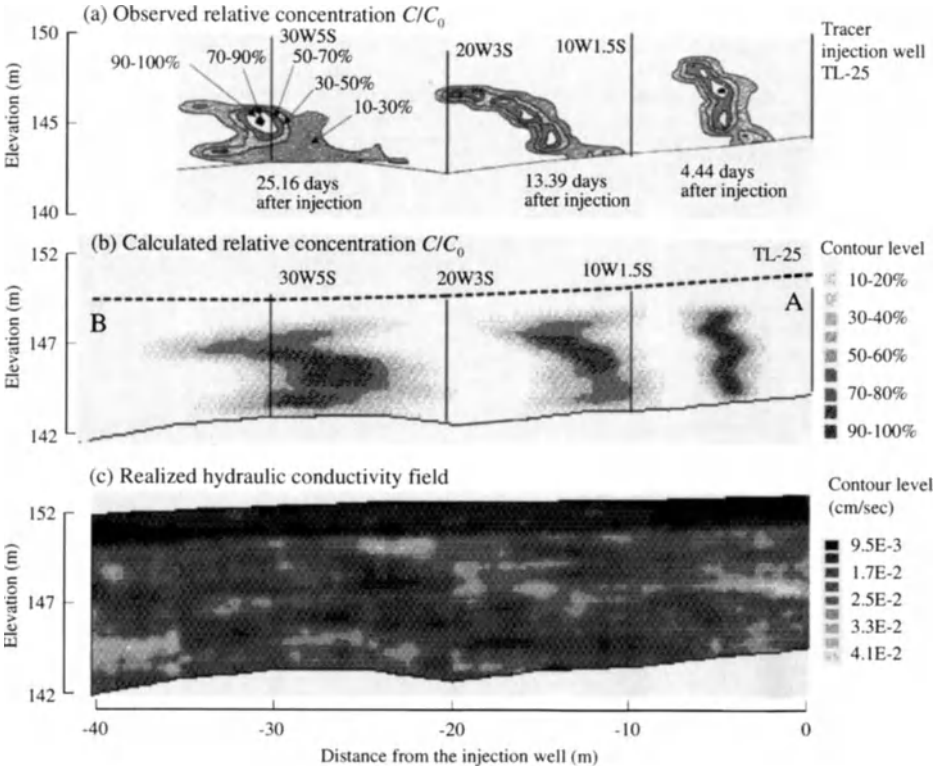

Fig. 4 Concentration distribution of tracer plume obtained from (a) observation, (b) calculation at 4.44, 13.39 and 25.16 days after injection and (c) one example of realized hydraulic conductivity (x component) used for calculation of (b). Illustrations of plumes of (a) and (b) are drawn by contours representing 10-20%, ..., and 90-100% of the relative maximum concentration.

dimension of injected tracer plume was estimated from the breakthrough curves measured at a well located 2 m downstream from the injection point. Figure 4(c) is the vertical cross section of three-dimensional realization of the hydraulic conductivity field shown in Fig. 3 along center plane. Highly permeable parts in the aquifer are described by the white color. Anisotropy of the correlation length is clear from the spatial distribution of hydraulic conductivity illustrated, i.e. there is a strong correlation between flow parameter values in the horizontal direction and a weak correlation in the vertical direction.

The simulated results reproduce not only the microscopic heterogeneity of flow parameter caused by that of sandy materials, but also the macroscopic one caused by layered heterogeneity. Thus, the geostatistical model conditioned by observed data is a useful tool for describing the layered structure. From the realized hydraulic conductivity field, one can expect that the tracer move in the permeable layers selectively, showing a fingering, due to the complicated spatial variation of hydraulic conductivity. These results indicate that the geostatistical model used here adequately characterizes the aquifer heterogeneity.

CONCLUSION

For realizing numerical simulation of the radionuclide transport in a heterogeneous aquifer, the spatial distribution of the hydraulic conductivity has important task for groundwater engineer. In this work, a model based on the geostatistical analysis was developed and applied to the Twin Lake aquifer, and then the usefulness of the model is evaluated. It is concluded that the simulated tracer plumes of the Twin Lake tracer test explain favorably with the experimental tracer plumes. The simulated results may put to endorse the experimental results at the Twin Lake tracer test, and the geostatistical model adequately describes the heterogeneity of aquifer. The correlation length between the values of hydraulic conductivities is suggested an important parameter for characterizing heterogeneity. The correlation length of 5m in flow direction follows a tendency of observed results in the spatial concentration of the tracer plume. The anisotropy of the correlation length is manifested in validity of the variogram analysis; the correlation in the horizontal direction is found to be stronger than that in the vertical one. The anisotropy was realized in the simulated distribution of the hydraulic conductivity.

REFERENCES

1. Killey, R. W. D. and Moltyaner, G. L. (1988) Twin Lake tracer tests: setting, methodology and hydraulic conductivity distribution. Water Resources Research, 24(10), 1585-1612
2 Williams, S. A. and El-Kadi, A. I. (1986) COVAR - a computer program for generating two-dimensional fields of autocorrelated parameters by matrix decomposition, Int. Groundwater Model. Cent., Holcomb Res. Inst., Butler Univ., Indianapolis, Ind..
3 Kimura, H. and Muraoka, S. (1992) The 3D-SEEP computer code user's manual, JAERI-M, 86-091, JAERI
4 Uffink, G. J. M. (1985) A random walk method for the simulation of macrodispersion in a stratified aquifer, In Relation of Ground-water Quantity and Quality, IAHS-Publication Nr. 146, 103-114
5 Prickett, T. A., Nayamik, T. G. and Lonnquist, C. G., (1981) A "random walk" solute transport model for selected groundwater quality evaluations, Illinois State Water Survey, Bulletin 65, 103p
6 Moltyaner, G. L. and Killey, R. W. D. (1988) Twin Lake tracer tests : longitudinal dispersion, Water Resources Research, 24(10), 1613-1627
7 Moltyaner, G. L. and Killey, R. W. D. (1988) Twin Lake tracer tests : transverse dispersion, Water Resources Research, 24(10), 1628-1637
8 Moltyaner, G. L., and Wills, C. A. (1993) Characterization of aquifer heterogeneity by in situ sensing, Water Resources Research, 29(10), 3417-3431
9 Dagan, G., P. Indelman and G. Moltyaner (1997) Stochastic analysis of concentration measurements in the transport experiment at Twin Lake site, Water Resources Research, 33(4), 559-567

Investigation of the Accuracy of Numerical Modelling of Seepage through Variably Saturated Soils

M. Mavroulidou and R.I. Woods

Dept. of Civil Engineering, University of Surrey, Guildford, Surrey, GU2 5XH, UK

Abstract. A numerical model is presented for the solution of flow in variably saturated porous media (single-phase, isothermal fluid flow), assuming continuity of flow between unsaturated and saturated soil zones. It allows for continuous variation of the hydraulic properties as a function of the pressure head using real soil data taken from relevant literature [12] and takes into account hydraulic property hysteresis. Numerical results compared with experimental results found in the literature [12], show the significant impact of ignoring hysteresis in numerical analyses of seepage. Moreover, a linear type model for hysteresis is shown to produce satisfactory results, despite its simplicity.

Key words: Variably saturated soil, Numerical modelling, Hysteresis of the hydraulic properties, Transient analyses

INTRODUCTION

Unsaturated soil zone in isothermal state affects significantly the movement of water in the hydrologic cycle. Mathematically, flow in an unsaturated-saturated soil system is described by non-linear differential equations. Thus, for many interesting problems, including cyclic wetting and drying of a soil due to seasonal variations, numerical methods may offer the only possible solution. The assessment of the performance of these numerical models is, therefore, of primary importance for reliable numerical predictions.

The non-linearity of the equations is due to the strong non-linearity of the coefficients representing the hydraulic properties of the soil. These can vary within several orders of magnitude for the same soil, often non-monotonically (storage capacity coefficient). Moreover, their variation with suction in the unsaturated zone is hysteretic, depending on the drying and wetting history to which the soil was subjected. There is therefore, one curve for a drying process and another one for a wetting process for both the soil water characteristic curve and the unsaturated hydraulic conductivity curve. The forms of the functions for wetting and drying are similar and can therefore be fitted by the same form of mathematical equation. For several cycles of wetting and drying, scanning curves between the two main wetting and drying curves also need to be calculated.

The amount of experimental work needed for the knowledge of the re-wetting re-drying scanning curves when two or more wetting-drying circles are involved, is rather prohibitive. For this reason, several empirical/mathematical models for the scanning curve description have been proposed in the literature. They are often classified into two categories, namely the independent domain models and dependent domain models, based on the assumptions that they involve. Thus, the

independent domain method (e.g. [1] and [2]) is based on the assumptions that the draining or filling of each pore of the domain is produced independently of the surrounding pores state and that the water volume difference between the empty and the filled state of each pore is independent of the pressure head. Only the pore geometry determines the drying and wetting characteristics of each pore. Conversely, the dependent domain models (e.g. [3] and [4]) include a domain dependence factor, such that the draining and wetting of each pore be dependent on the state of the neighbouring pores.

Extensive research has been carried out by soil scientists, agricultural engineers and hydrologists, in order to provide hysteresis models. Conversely, geotechnical engineers tend to neglect such phenomena. They normally use single-valued functions in numerical simulations, on the ground that this is supposed to be sufficient for engineering purposes. Nevertheless, recent research has shown that hydraulic property hysteresis may also be of relevance for geotechnical applications (e.g. hysteresis was observed for compacted clay-liner soils [5]; the impact of hydraulic property hysteresis on the mechanical behaviour of unsaturated soils was also reported [6] etc.).

The writers have developed finite element seepage software in which several proposed models for soil water characteristic curve hysteresis were implemented. The present paper attempts to point at the importance of considering hydraulic property hysteresis in seepage analyses. This is shown through comparisons between experimental results found in the literature and those obtained by the writers' program when a simple linear hysteresis model was used.

DESCRIPTION OF THE NUMERICAL MODEL

Governing equation. The basic equation governing flow of water through the soil is:

$$\frac{\partial}{\partial x}\left(K_x(\psi)\frac{\partial h}{\partial x}\right)+\frac{\partial}{\partial y}\left(K_y(\psi)\frac{\partial h}{\partial y}\right)+\frac{\partial}{\partial z}\left(K_z(\psi)\frac{\partial h}{\partial z}\right)=\left(\beta S_s+C(\psi)\right)\frac{\partial h}{\partial t} \qquad (1)$$

where h is the total head, ψ is the pressure head and $K_x(\psi)$, $K_y(\psi)$ and $K_z(\psi)$ the hydraulic conductivities in the x, y and z directions respectively. S_s is the elastic storage coefficient; β is equal to 1 for fully saturated conditions and 0 for unsaturated conditions and $C(\psi)$ is the moisture capacity coefficient. For the derivation of Eqn (1) flow was assumed to obey Darcy's law in both saturated and unsaturated zones.

To describe the form of the moisture retention (i.e. soil water characteristic) and hydraulic conductivity curves versus pressure head, the following expressions have been adopted:

$$\theta(\psi) = (\theta_s - \theta_r)\frac{A_1}{A_1+|\psi|^{n_1}} + \theta_r \qquad (2)$$

$$K=K_S\Theta^{\delta} \qquad (3)$$

In Eqn (2) θ is the volumetric water content and θ_s and θ_r stand for the saturated and residual volumetric content respectively; A_1 and n_1 are fitting parameters. In Eqn (3) K_s is the saturated hydraulic conductivity coefficient, δ is an empirical constant estimated as 3 by Averjanov [7] and 3.5 by Irmay [8] and Θ the *normalised volumetric water content*, defined as $\Theta=(\theta-\theta_r)/(1-\theta_r)$.

The specific moisture capacity term $C(\psi)=\frac{\partial\theta(\psi)}{\partial\psi}$ is obtained by differentiation of (2).

The method used herein to model soil water characteristic curve hysteresis (i.e. hysteresis of the volumetric water content versus suction curve) is the so called *linear method.* According to this method, the scanning curves are modelled as straight lines spanning between the main drying and wetting curves (see e.g. [9]). For this method the knowledge of the main wetting and the main drying curves is necessary. Where no experimental scanning curves are provided at all, the scanning curve slope may be chosen arbitrarily, with the only constraint that it is less than the slope of the main curves at intersection [10]. Note that hysteresis of the hydraulic conductivity curve is not considered here, since the hysteresis of the $K(\theta)$ curve (Eqn. (3)) is usually supposed to be negligible [11].

NUMERICAL ANALYSES

Geometry, material properties and boundary conditions. To check the importance of hysteresis, we used experimental results found in [12] for one-dimensional flow in a soil column with variable boundary conditions (causing alternating drying and wetting of the porous medium). The material used in [12] was a medium sand of density equal to 1.64 gr/cm^3, θ_s = 0.359, θ_r=0.02 and K_s= 0.106 cm/s. In Eqn. (2), $A_1=12\times10^6$ and n_1=5.82 for the drying curve and A_1=780 and n_1=3 for the wetting curve. The height of the column was 34cm. The initial and boundary conditions were the following:

$$t=0,\ 0\text{cm}\le z\le 34\text{cm},\ h=17.6\text{cm};\ t\ge 0,\ z=34\text{cm},\ \frac{\partial h}{\partial z}=0$$

$$t=1\text{min},\ z=0\text{cm},\ h=11.8\text{cm};\ t=2\text{min},\ z=0\text{cm},\ h=5\text{cm};\ t=2.5\text{min}\le t\le 14\text{min},\ z=0\text{cm},\ h=0\text{cm};$$
$$t=15\text{min},\ z=0\text{cm},\ h=12\text{cm};\ t=15.5\text{min}\le t\le 24\text{min},\ z=0\text{cm},\ h=17.6\text{cm};$$
$$t=25\text{min},\ z=0\text{cm},\ h=8.5\text{cm};\ t\ge 26\text{min},\ z=0\text{cm},\ h=0\text{cm} \qquad (4)$$

To find the slope of the scanning lines spanning between the main curves, scanning curves obtained experimentally by Abrishami [12] were used.

Results and discussion. Due to space limitations and for the sake of clarity, only some indicative numerical results will be presented here. The numerical results for the first drainage (using the drying curve of the medium) show satisfactory agreement with the experimental results (Fig.1(a)). This is not the case when the main drying curve is used to simulate the subsequent re-wetting of the soil and then the first re-drying that follows it (i.e. when no hysteresis is accounted for and a single-valued $\theta(\psi)$ function is assumed), where the results tend to show faster rates of evolution than those found from the experimental results. Conversely, when hysteresis is considered the results are in better agreement with the experimental results (Fig. 1(b)-(c)). It should be noted that the available experimental results were relevant to shallow water tables. The relative effect of hysteresis when modelling deep water table movement is yet to be assessed. One could also point out that this hysteresis model ignores deformation of the soil. Moreover, it could be argued that the representation of the scanning curves by straight lines is not the most faithful one. Concerning the latter point it was, nevertheless, shown [10] that more sophisticated hysteresis models (e.g. [13]) did not necessary provide a good representation of the scanning lines either, and that, additionally, some of them (e.g. [14]), presented a 'pumping effect' (i.e. a decrease in the predicted soil-water contents

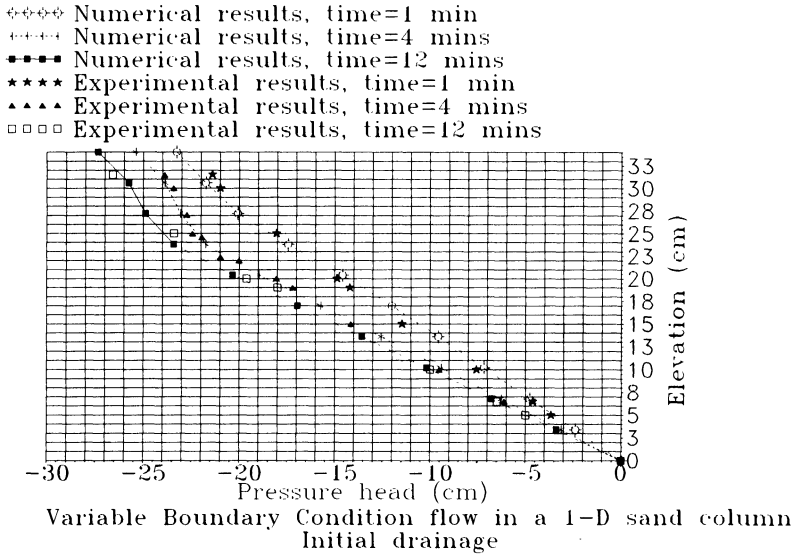

(a) First (initial) drying

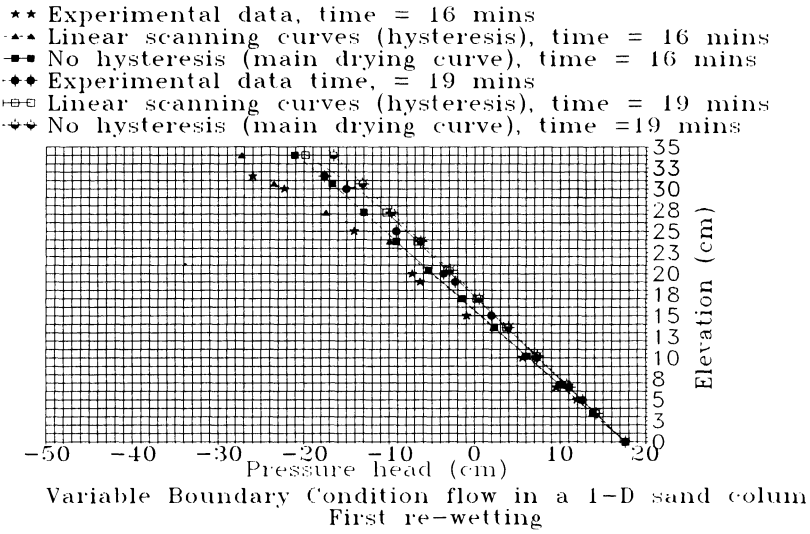

(b) First wetting

Fig. 3 Flow in sand column

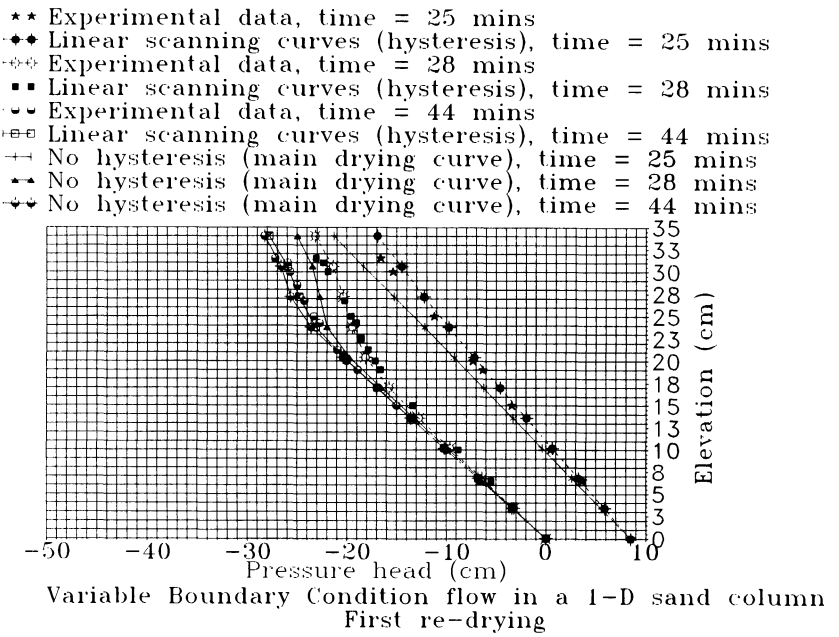

(c) First re-drying

Fig. 3 (continued) Flow in sand column

during the initial pressure fluctuations until some stable water content configuration is reached) which is an aberration of the numerical algorithm, rather than a real property of the soils. Conversely, the linear model was found to be free of pumping effects [10].

CONCLUSION

The results have shown the inability of a model based on single-valued functions (e.g. use of one of the main curves throughout the cyclic soil re-wetting and re-drying process) to simulate reversible boundary condition problems. This finding points at the importance of including hysteretic behaviour of the medium in models of flow through variably saturated soils. The linear hysteresis model used in this paper to simulate soil water characteristic curve hysteresis, was shown to reproduce satisfactorily experimental results of seepage, despite the fact that it is very crude (such that it might not represent the shape of the curves very faithfully). Its use in numerical models of seepage could therefore be advantageous, due to its simplicity, the reduced computer memory requirements and especially, due to the fact that it requires minimal experimental data to be formulated.

Study on Breakwater Stability under Waves Induced Seepage Flow

Mao Chang-xi[1] , Duan Xiangbao[1] Mao Peiyu[2]

[1]Department of Hydraulic Engineering, Nanjing Hydraulic Research Institute, Nanjing 210029, P. R. China
[2] Department of River and Harbour, Nanjing Hydraulic Research Institute, Nanjing 210029, P. R. China

ABSTRACT. Based on the damage effect of waves induced seepage flow, the stability of protective blocks on sloping breakwater is investigated through calculation and analysis by finite element method (FEM). Combining types of breakwaters and high tide level with waves in the southeast coastal area of China, the calculating flow field data were obtained and analyzed to give a formula depicting the size of blocks for local stability on sloping breakwater. The formula was verified by experimental data in wind-wave flume and compared with the usual formula of Hudson.

KEY WORDS: sea dike; structural type; seepage flow; stability analysis; wave attack

INTRODUCTION

The sea dikes and breakwaters were destroyed mainly by waves attack. So the earlier and most studies were carried out experimentally with wave flumes to obtain empirical formulas for the local stability of rubble or concrete blocks of revetment is only considering the wave forces outside the dike [1,2]. In this paper the instantaneous varying external wave attack and the induced seepage flow field inside the dike are considered.

STABILITY ANALYSIS OF RUBBLE MOUND OR BLOCKS UNDER SEEPAGE ACTION

If the induced seepage field by wave action is known, the stability of individual block can be analyzed as shown in Fig.1. The direction of seepage flow acting on a certain rubble makes an angle α with the horizontal line and the seepage gradient J. For a unit volume of block on the slope, its buoyant unit weight is γ'_1, and the seepage force acting on the unit volume is γJ. Thereby two cases of damage, i.e. rubble sliding downward along slope and tipping out normal to slope can be analyzed by writing the equilibrium equation of forces as shown in Fig.1. The derived equations for critical seepage gradient of damage referred to [(3) p.465] can be cited here as follows.

For sliding down $$J = \frac{\gamma'_1(\tan\varphi - \tan\beta)\cos\beta}{\gamma[\cos(\beta-\alpha) + \sin(\beta-\alpha)\tan\varphi]} \quad (1)$$

For tipping out $$J = \frac{\gamma'_1(1 + \tan\varphi\tan\beta)\cos\beta}{\gamma[\sin(\beta-\alpha) - \cos(\beta-\alpha)\tan\varphi]} \quad (2)$$

From the instantaneous seepage flow induced by wave, it can be seen that the direction of seepage flow in a mild slope is approximately along the slope, $\alpha = \beta$,then Eq.(1) can be simplified to

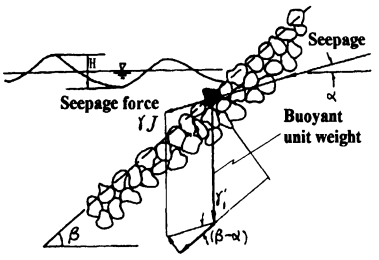

Fig. 1 Sketch for the stability of rubble mound breakwater

$$J = \frac{\gamma_1'}{\gamma}(\tan\varphi - \tan\beta)\cos\beta \tag{3}$$

The steeper the slope, the flatter the instantaneous seepage flow direction nearby the slope. that is, approximately $\alpha=0$. Thus, Eq. (1) is simplified to

$$J = \frac{\gamma_1'}{\gamma}\cdot\frac{\tan\varphi - \tan\beta}{1+\tan\varphi\tan\beta} \tag{4}$$

Because the permissible gradient calculated by this equation is slightly smaller than that from Eq. (3), it can be taken as the basis for discussion and calculation of the size of stable rubble.

For a steep or vertical sea dike, the possibility of the rubble tipping out by seepage flow should be checked. Supposing that the direction of seepage is horizontal, i.e., $\alpha=0$, Eq.(2) can be simplified to

$$J = \frac{\gamma_1'}{\gamma}\cdot\frac{1+\tan\varphi\tan\beta}{\tan\beta - \tan\varphi} \tag{5}$$

The above mentioned equations are suitable for all kinds of individual rubble, concrete block, gabion, and soil mass. But there are differences in unit weight and friction coefficient of materials.

Now by use of seepage flow field the calculation for the stability of individual rubble can be performed. Assuming the water head loss of the seepage flow passing through a distance of rubble thickness or its size d is h, then $J=h/d$. Expressing it by the specific weight of rubble $s=\gamma_s/\gamma$, since the submerged unit weight $\gamma'_1=(\gamma'_s-\gamma)=(s-1)\gamma$, then stable size of individual rubble against sliding and tipping out from Eq. (1) and Eq. (5), can be obtained respectively.

For sliding down
$$d \geq \frac{h(1+\tan\varphi\tan\beta)}{(s-1)(\tan\varphi - \tan\beta)} \tag{6}$$

For tipping out
$$d \geq \frac{h(\tan\beta - \tan\varphi)}{(s-1)(1+\tan\varphi\tan\beta)} \tag{7}$$

CALCULATION OF SEEPAGE FIELD AND DETERMINING WATER HEAD h

Now, the key problem is how to determine the acting water head h induced by wave action in each of the equations mentioned above. According to the wave parameters of southeast of China and using computer program UNSST2 of FEM [4], the seepage field distributions induced by wave action these types of sea dike were computed and the results at wave run up to crest and down to trough were analyzed. Shown in Fig.3 is one set of computing result for sloping sea dike. The wave pressure distribution on the slope is the experimental data from model test in wave flume under wave parameters of wave height H=2.3m, wave period T=6s, wave run up from high tidal stage 6.9m to crest elevation 10.0m and down to wave trough elevation 5.8m after 3s. The total drop is 4.2m, and the total head over downstream level is 10.0-4.0=6.0m. In Fig. 3(b), it may be seen that there is a local stroke zone with the maximum intensity nearly and below the static water level in a range of 1/3 wave height, wherein the maximum difference between these two sets of equi-potential lines (up to wave crest and down to wave trough) is 75%-48%=27% of the total head, i.e. head difference 1.62m. This seepage head variation acts with impact and suction alternately just in slope. Supposing this seepage head dissipates gradually in the same linear manner as the wave drop down from crest to trough along the slope. Then taking the wave stroke center at elevation of 6.5m as the check point for damage, which accounts a proportion to the total drop 4.2m by a fraction (10.0-6.5)/4.2=0.83, its residual seepage head should be 0.17×1.62=0.275m. Which equals to 0.12 times

of the wave height H=2.3m. By comparison of several sets of computing seepage field for sloping, vertical and composite types of dikes, the results are listed in Table 1. Thereby we may take h=0.12H and substitute into above equations. For instance, Eq. (6) for sliding down becomes

$$d \geq \frac{0.12H(1+\tan\varphi\tan\beta)}{(s-1)(\tan\varphi-\tan\beta)} \tag{8}$$

Table 1 Residual seepage head induced by wave for different dikes

Structural type	Wave height H(m)	Run up R_u	Total head H_1-H_2	Difference of total head %	Residual seepage head h	h/H
Sloping type	2.3	3.10	6.0	27	0.275	0.120
	1.04	2.17	7.54	10	0.128	0.123
The berm type	2.04	2.30	5.2	28	0.240	0.117
Vertical wall type	2.37	3.11	6.0	30	0.290	0.122

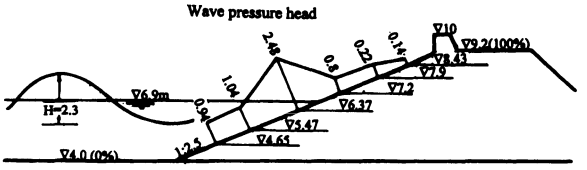

Fig. 3(a) Wave pressure distribution over slope sea dike

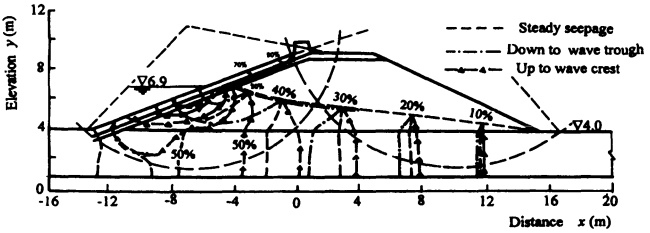

Fig. 3(b) Seepage field distribution and slid circle of slope sea dike under wave action

FORMULA COMPARISON AND VERIFICATION BY MODEL TEST DATA

The Hudson formula is used and expressed in rubble weight W or diameter d as follows

$$W \geq \frac{\gamma_s H^3}{K(s-1)^3 c\tan\beta} \quad \text{or} \quad d \geq \frac{K'H}{(s-1)(c\tan\beta)^{1/3}} \tag{9}$$

Here K is a stability factor, for round and smooth rubble K=2.1~2.6, for angular and rough rubble K=2.8~3.5, for rubble set in row K = 4.8~5.5 and for special artificial blocks K=7~13. K' is a coefficient, and for round and smooth rubble K'= l, for angular rubble K'=0.9, for rubble set in row K'= 0.75, and for concrete block K'=0.5. Since the variation of volume from sphere to cube is $\pi/6$ ~1, the relation of the rubble weight and its size may be taken as W=(0.75d^3)γ_s.

A practical breakwater design may be discussed here, i.e. the breakwater of the Sines Harbor in Japan. Its slope is 1:2, and the Dolos artificial special block with a weight of 42 t is adopted, whose specific weight s = 2.5, and stability factor K = 8.73, the wave height $H_{1/3}$ =9.5m. According to the calculation by the Hudson formula the breakwater should be stable, but it collapsed under the wind wave action on Feb. 26. 1978 [5]. Using Eq. (8), we have d = 3.18m, weight W= 0.75$d^3\gamma_s$=0.75 × (3.18)^3 × 2.5=60 t for φ=40°, showing that the original block weight of 42 t adopted for the Sines

Harbor is unsafe. If φ=42°, then, d = 2.76m, W=39 t, the adopted weight 42 t is safe. Thereby the value of φ selected is important which depends on shape, size and arrangement of blocks on slope.

Now some wave test data of special block revetments are used to seek reversely the friction coefficient tanφ or the angle of repose φ of the special blocks under critical stable state so that Eq. (8) can be used to check the block size d or weight W in design. The test data are from model tests of the breakwater of the Zhenhai harbor in Zhejiang Province. The breakwater has a wide platform, both its upper and lower slopes being 1:2. Comparative test for stability was carried out with three kinds of blocks. Tests were conducted in a wind wave flume with a model on a scale of 1: 20, the specific weight of block $s=\gamma_s/\gamma$=2.35. These test data are analyzed. First the block weights (tons) affirmed as the critical stable state in tests are listed in Table 2. Through inverse calculation the angle φ in the present formula and the stability factor K in the Hudson formula are obtained.

Table 2 Angle of repose φ and stability factor K of the special block under critical stable state

Wave height	4-leg square hollow block		I-block		Nut-shaped block	
H_s(m)	2.2(t)	3.0(t)	1.84(t)	2.3(t)	1.85~2.2(t)	2.5~3.0(t)
3.48	φ=42.6° K=9.15		φ=43.5° K=10.94	3.48	φ=43.5° ~42.6° K=10.88~9.15	
3.86		φ=42.6° K=9.16		φ=44° K=11.94		φ=43.6° ~42.6° K=10.99~9.16

From the analysis of the experimental data for stability of different revetment blocks the values of friction angle φ a lot of are given in Table 3 for reference in design.

A comparison of Eq.(8) in this paper with the Hudson formula Eq.(9) shows that the angle of repose of revetment material corresponds to the stability factor K, however, the meaning of angle $\overline{\varphi}$ is very clear but that of K is rather ambiguous. The K value determined by experiments varies greatly, e.g., the Technical Specifications for Harbor Engineering established by the Ministry of Communications of P. R. China gives K=24 for I-block and K=14 for 4-leg square hollow block; Yu (1987) suggested that K=22~25 for I-block; Iwagaki (1987) proposed K=13.6 for the 4-leg square hollow block; indicating that some questions exist in the application of the Hudson formula and further comparative study is needed.

Table 3 Angle of repose ϕ -values in formula (8) for blocks on breakwater

Wave pattern	Internal friction angleϕ of						
	Stone block (size>10cm)	4-leg squarehollow blocks		I-blocks		Nut-shaped blocks	
	$\overline{\phi}$	$\overline{\phi}$	K	$\overline{\phi}$	K	$\overline{\phi}$	K
Irregular waves	38° ~40°	41° ~43°	7~10	42° ~44°	8~12	42° ~44°	8~12
Regular waves	39° ~42°	42° ~44°	8~12	43° ~45°	10~15	44° ~45°	12~15

REFERENCES

1 Hudson, R. Y., 1959. Laboratory Investigation of Rubble Mound Breakwater, J. Waterways and Harbors Division, ASCE.

2 Hanzawa, M. et al.,1996. New Stability Formula for Wave Dissipating Concrete Blocks Covering Horizontally Composite Breakwaters, 25th Coastal Eng. Conf. Vol.2, 1665~1678.

3 Mao Changxi, 1990. Computational Analysis and Control of Seepage Flow, Beijing, Water Resources and Electric Power Press. (in Chinese)

4 Mao changxi et al., 1999 Numerical Computation in Seepage Flow and Programs Application, Hohai university Press.

5 Iwagaki, Y., 1987. Newest Coastal Engineering, Morikita Co. Ltd. (in Japanese)

Short Papers

Optimization of Groundwater Resources in Basins

Investigation of Groundwater Flow by Using Fiber-Optic Temperature Sensor

Kenzo Hiroki[1], Motoi Nasu[1], Kouji Nukina[1], Shuji Unno[2], Tomonori Sato[2], Osamu Watanabe[3], Kazuki Fukasawa[4], Hiromichi Ishibashi[3], and Seiji Horiuchi[5]

[1]Fukushima Public Works Office, Tohoku Regional Construction Bureau, Ministry of Construction, 36 Enokidaira Kuroiwa Fukushima-shi Fkushima-ken 960-8153, Japan.
[2]Foundation of River and Basin Integrated Communications, 1-3 Kouji-machi Japan.
[3]Suimon Research Inc., 3-11-19 Matsunami Chuo-ku Chiba-shi 260-0044, Japan.
[4]Takasago Works, Hitachi Cable, Ltd., 880 Isagozawa-cho Hitachi-shi Ibaraki-ken 319-1418, Japan.
[5]Department of Geo-system Sciences, Nihon University, 3-25-40 Sakura-Jyousui Setagaya-ku Tokyo 156-8550, Japan.

ABSTRACT. In-situ measurement of subsurface temperature (temperature prospecting) has been developed as a method of groundwater-vein surveying. However, the usual method is labour intensive and the temporal resolution is poor, so we could never obtain sequential data of the temperature distribution. Continuous observation of the temperature distribution (i.e. distribution of the preferential flow-path) using fiber-optic temperature sensor is reported in this paper. High temperature regions indicate the groundwater pathway. And the intensity of its signature was found to show slight fluctuations. These signatures may be associated with the fluctuations of the preferential flow-path of groundwater, indicate the dynamic state of groundwater flow, and provide new parameters for the temperature prospecting method.

KEY WORDS: preferential flow-paths, groundwater flow, fiber-optic temperature sensor, subsurface temperature

EXPERIMENTAL FACILITIES

At first, we looked for a test site which satisfied following conditions; easy installation and maintenance, existing boreholes for peripheral groundwater monitoring, and presence of at least one preferential flow-path. Basing on the classification of landform and results of pilot field investigations, the region between the 18.2 km post (length = 200 m) of the left bank of Abukuma River, Fukushima Prefecture was selected for the test site.
A fiber-Optic Temperature Sensor (hereafter, it will be referred as FTR) was used in order to obtain temporal variation of subsurface temperature distribution.
A fiber-optic temperature sensor was placed underground (GL. minus 1.0 m and 0.5 m) near the foot of riverbank slope. Additional temperature observations were made with a thermistor sensor. A borehole for groundwater monitoring was also available in the test site. The configuration of experimental facilities is illustrated in Fig.1.

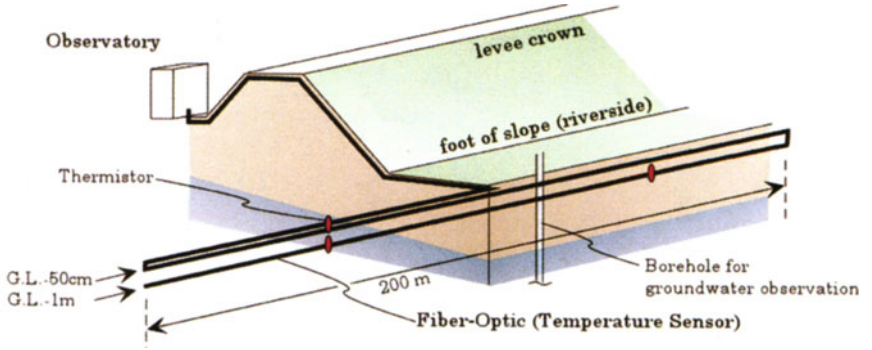

Fig. 1. Configuration of experimental facilities.

OBSERVATIONAL RESULTS

As the first term of test observation, the temperature distribution at the test site was monitored between 13 February to 17 March 1999. Measurements were taken every 10 minutes on a 1.0 m grid. The data are shown in Fig.2 as Position-Time display in order to grasp both temporal variation and spatial distribution easily. Based on the theory for the temperature prospecting, relatively high temperature in winter indicates a preferential flow-path for groundwater (groundwater-vein).

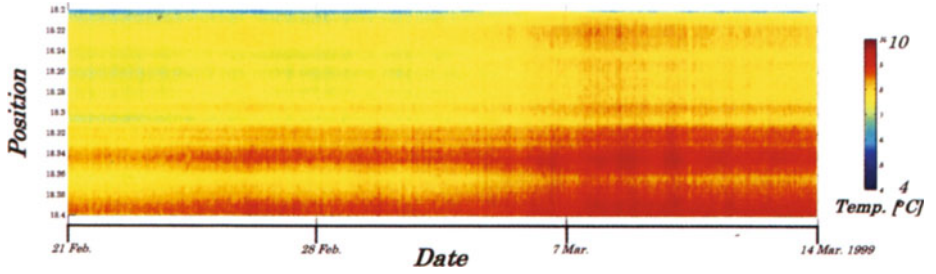

Fig. 2. Position-Time display of corrected FTR temperature data observed at GL. -1.0m. The spatial distribution of temperature (color corded) is shown on the vertical axis, and temporal variation is shown on the horizontal axis.

To emphasize high temperature region at GL.- 1.0 m, and the fine structure of the temperature distribution in it, this region has been replotted in Fig.3. The average temperature was calculated for every sampling time, and temperature difference between the average temperature and FTR data ($=\Delta T$) are shown in Fig.3 by color code. So the colored regions in Fig.3 indicate relatively high temperature (at GL.- 1.0 m) in comparison with the spatial average temperature. Two high temperature regions are seen at the test site. They probably represent the preferential flow–path along the abandoned channel of Surigami River. Although the positions of these high temperature regions are almost steady in this period, intensity of the signatures, namely temperature difference: ΔT, were found to be fluctuated in temporally. ΔT slightly increased around 28 February, decreased around at 7 March, and increased again around 13 March.

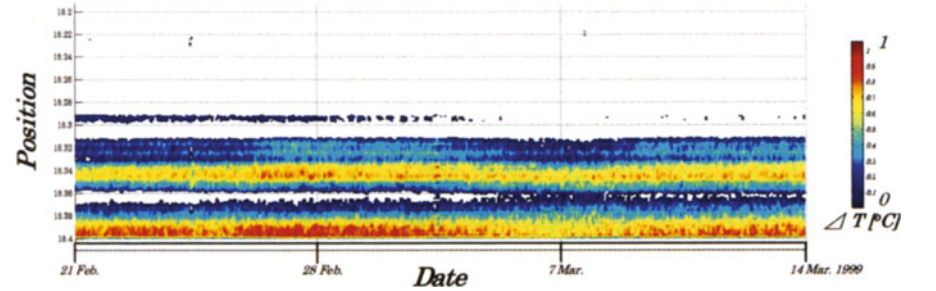

Fig. 3. Same as Fig.2, but for emphasized FTR data.

CONCLUSION

Data from fiber-optic temperature sensor (FTR) indicate preferential flow-paths for groundwater as regions of relatively high temperature. The intensity of this signature showed slight fluctuations. These fluctuations may reflect fluctuations of the preferential flow-path for groundwater, and further research may link these with the dynamic state of groundwater flow.

After this, comparative study of temporal variation of temperature obtained at different depth (G.L. - 0.5m, - 1.0m) will be carried out. Results of the study will arrow us to know vertical distribution of temperature, and characteristics of temperature disturbance propagation in shallow subsurface region. They are expected to be new parameters for groundwater-vein surveying.

Subsidence in the Noubi plains

Fumihiro Hara[1], Shin Sasaki[1] , Jyun Hijikata[2] ,Osamu Matsuo[3] and Yasuhiro Itoh[3]

[1]CTI Engineering Co., Ltd. Tokyo Branch Office, Coastal Engineering & Development Division, 4-9-11 Nihombashi-honchou, Chuou-ku, Tokyo 103-8430, Japan
[2]CTI Engineering Co., Ltd. Nagoya Branch Office, River Engineering Division, 1-3-18 Nisiki, Naka-ku, Nagoya 460-0003, Japan
[3]Ministry of Construction , Chubu Regional Construction Bureau , River Planning Division, 2-5-1 Sannomaru, Naka-ku, Nagoya 460-8514, Japan

ABSTRACT. This paper discusses a history of ground subsidence in the Noubi plains, which is one of the largest zero-meter areas in Japan, based on the past data on groundwater level and ground subsidence. Noubi plains span across the three Prefectures in the central Japan, namely Aichi, Gifu and Mie; they are alluvial plains located in downstream of the Kiso, Nagara, Ibi, and Syounai Rivers, with an area totalling about 1,485 km^2. Results of analyses on correlation between the groundwater level and ground compaction revealed that after the groundwater levels turned for the rise, a decrease of 0.6 mm was observed in the monthly ground compaction for every 1.0 m of rise in the monthly average groundwater level. Thus, it is important to keep seasonal changes in groundwater level at a minimum in order to prevent ground subsidence, at the same time promoting the recovery of groundwater level.

KEY WORDS: Noubi plains, observation well, ground subsidence, ground compaction , groundwater levels, the results of leveling survey

CORRELATION BETWEEN THE GROUNDWATER LEVELS AND GROUND COMPACTION

Figs. 1 and 2 show the correlation between the monthly averages of groundwater level and monthly ground compaction measured at the 50-m and 150-m wells, respectively. The positive values of monthly ground compaction shown along the Y-axis indicate contraction, and vice versa the negative values indicate expansion.

The monthly average groundwater level of the 50-m well was above Tokyo Peil (standard mean sea level of Tokyo Bay; T. P.) -20 m, and monthly ground compactions were less than 5 mm. When the monthly average groundwater level rose above T. P. -15 m, monthly ground compaction began to diminish.

In the 150-m well, monthly ground compaction was 17 mm when the monthly average groundwater level was the lowest (at T. P. -33 m). In the range of monthly groundwater levels between T. P. -33 m and T. P. -15 m, ground compaction decreased along with the rise in groundwater level. Ground compaction diminished when the monthly average groundwater level rose above T. P. -15 m, as in the case of the 50-m well.

For clarification of correlations for the 150-m well, scatter diagrams were prepared separately based on measurement data taken in 1979 or earlier and in 1980 or later, since the correlations differ for the monthly groundwater levels below and above about T. P. -15 m. Relationship between the monthly average groundwater level and monthly ground compaction was approximated for each case by linear regression.

The linear regression line for the years before 1979 has a slant of -0.6 mm/m, which indicates that for every rise of 1.0 m in the monthly average groundwater level, the monthly ground compaction could be reduced for 0.6 mm. Correlation factor (R^2) decreased after 1980, when the relationship between the groundwater level and ground compaction became dispersive. In other words, monthly ground compaction was below 2 mm but dispersive for monthly groundwater levels above T. P. -15 m, which indicates that the groundwater level is no longer a decisive factor that induces ground compaction.

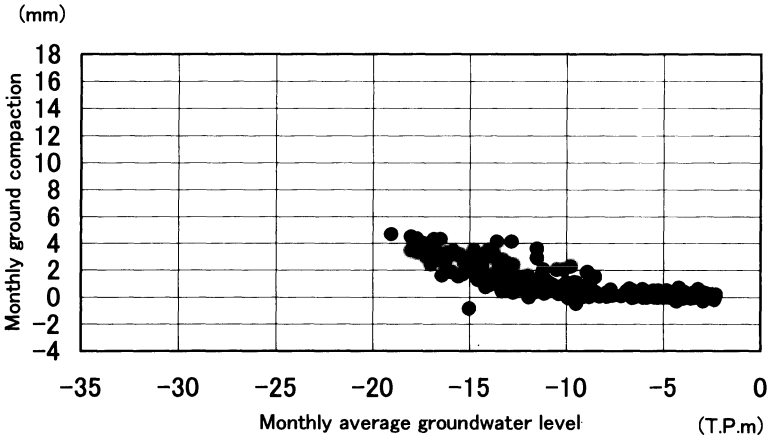

Fig. 1. Correlation between the Monthly Average Groundwater Level and Monthly Ground Compaction Measured at the 50-m Well of Matsunaka Observation well

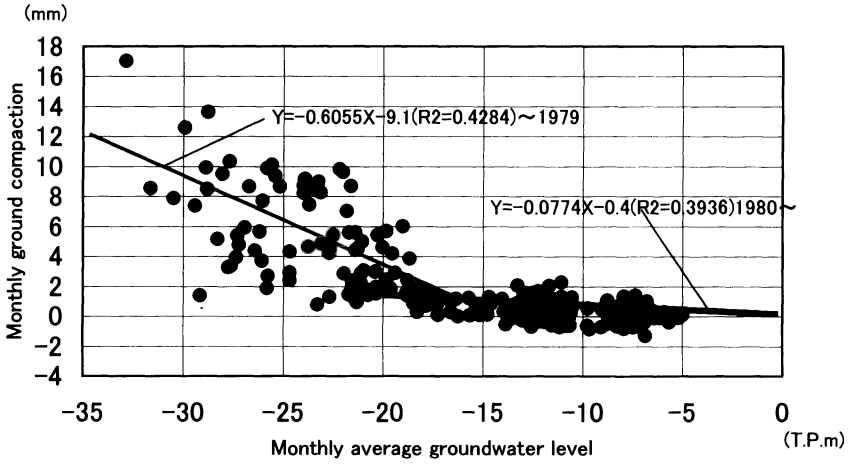

Fig. 2. Correlation between the Monthly Average Groundwater Level and Monthly Ground Compaction Measured at the 150-m Well of Matsunaka Observation well

ACKNOWLEDGMENT

The author is grateful toward relevant personnels of the Toukai-Sanken-Jibanchinka- Chousakai for their generous cooperation and offering of measurement data.

Analysis on Influence Factors of Sustainable Groundwater Development in Jining City, Shandong Province, CHINA

Shu Longcang[1], Sun Qingyi[2], Peng Xuming[2], and Wen Zhonghui[1]

[1]Department of Hydrology and Water Resources, Hohai University, Nanjing, Jiangsu 210098 P. R. China
[2]Commission of Water Resources Management of Jining City, Jining , Shandong 272119 P. R. China

Abstract. Prior to 1970, groundwater was pumped from shallow aquifers, and in 1958, the pumping rate was only $1\times10^4m^3/d$ in Jining City. At present, water quantity and quality of shallow aquifers can not meet the water demands, so groundwater is being pumped from a deep aquifer and the rate is about $21.06\times10^4m^3/d$ in 1996. The groundwater level is dropping, the shallow groundwater is seriously polluted and land subsidence is developing. So it is very important to analyze the influence factors pertinent to sustainable groundwater development in Jining City. There are many relevant factors, but they can be divided into two kinds: natural factors and artificial factors. This paper elucidates the main factors relevant to Jining City and suggests some fundamental actions to remedy the situation that has arisen.

Key words. influence factors, sustainable groundwater pumping, Jining City, the natural factors, the artificial factors

INTRODUCTION

Jining City is located in the southwest of Shandong Province, China. The long-term average precipitation is 700mm. There are two aquifers, one shallow and unconfined, the other deep and confined, and there is a relatively steady aquitard between these two aquifers. At present, groundwater is pumped from deep confined aquifer and supplied for industrial users and domestic users. In Jining City, groundwater overdraft has influenced present day sustainable social and economic development. There are many factors affecting sustainable groundwater development in Jining City. But, in general term, these can be classed as either natural, or artificial. The natural factors mainly include groundwater quantity and quality and load-bearing capacity of the environment. The artificial factors mainly include development of science and technology, over-population and groundwater pumping rate, and the water management system.

ANALYSIS OF MAIN INFLUENCE FACTORS

Groundwater quantity and quality. For sustainable groundwater development, the principle that "actual rate of pumping of groundwater should be less than allowable withdrawal of groundwater" should be followed. In any given certain place, the allowable groundwater withdrawal rate is relatively steady. If the allowable withdrawal is greater than demand, sustainable groundwater development will be easily implemented.

Load-bearing capacity of environment. The load-bearing capacity of the environment directly affects groundwater sustainable development and utilization. For some water source fields, where the environment is fragile, groundwater withdrawal must be strictly controlled, or

measures such as artificial recharge must be adopted. At the beginning of the groundwater exploitation in this area roughly the 1950s and 1960s, the level of the groundwater in the deep confined aquifer was higher than that in the shallow unconfined aquifer, and the confined water quality was very good. With the development of industry and agriculture in Jining city, however, the withdrawal of groundwater was increased, especially of deep confined water, which caused the groundwater level of the deep confined aquifer to became much lower than that of the shallow unconfined aquifer. Furthermore, wastewater was directly discharged to surface water, and this polluted the shallow unconfined aquifer. There is leakage between the shallow unconfined aquifer and the deep confined aquifer. So the environment of deep confined water is fragile and its quality is becoming worse. The hardness and content of total dissolved solids (TDS) are increasing. So pumping of the confined aquifer must be strictly controlled. Otherwise the groundwater will be further polluted.

Population and groundwater pumping. The population of Jining City is increasing rapidly. It was less then 4×10^4 in 1949, but it was 29.59×10^4 in 1992. The rate of increase is about 7755 per year, which means, if the trend continuous, that it will be 65×10^4 in 2000. So the domestic use of groundwater will also increase. In Jining City, domestic use of groundwater accounts for 15% of total groundwater pumping. The quantity of groundwater used for domestic was about $3.44\times10^4 m^3/d$ in 1995. The influences of population on groundwater resources and environment concern both population quantity and population "quality".

SUGGESTIONS AND CONCLUSIONS

According to the analysis of main influence factors of sustainable groundwater development in Jining City, all influence factors are important. While the natural factors are not easily controlled, the artificial factors, especially population, groundwater pumping rates can be easier controlled. In order to implement sustainable groundwater development in Jining City, Shandong Province, we should bring every positive factor into play and control every negative factor in the process of groundwater development. The concrete measurements, possible include engineering measures and management measures. The engineering measures, such as artificial recharge of groundwater in north of Jining City, establishment of a wastewater treatment plant and joint use of surface water and groundwater, should be adopted as soon as possible. At the same time, management measures, such as optimal allocation of groundwater resources, analysis of influence factors of sustainable groundwater development, management of water utilization and water demand, should be emphasized in the process of groundwater development.

REFERENCES

1. A. K. Biswas (1991) Water for sustainable Development in the 21st century: a global perspective. Water International. 16: 219-224
2. A.K. Biswas (1994) Sustainable water resources development: Some personal thoughts. Water Resources Development. 2: 109-116
3. S. P. Simonovic (1996) Decision support systems for sustainable management of water resources: 1. General Principles. Water International. 21: 223-232
4. S. P. Simonovic (1996) Decision support systems for sustainable management of water resources: 2. Case Studies. Water International. 21: 233-244

Groundwater Pollution and Remediation Technologies

Construction of an Integral Monitoring System for Contaminated Groundwater Resources in the Municipal Area of Glauchau Using a Ground Water Model

Carsten Leibenath, Peggy Zinke, Michaela Palm

Umweltbuero GmbH Vogtland, Dieselstr. 47, D-01257 Dresden

ABSTRACT: The city of Glauchau was a traditional centre of textile and chemical industry. Most of the enterprises are closed down. Nowadays ground water investigations indicate a chlorinated organic hydrocarbon aquifer contamination. The contamination treatment is very complicated due to the difficult interaction between soft rock and hard rock aquifers. For an integral assessment of contamination sites and for investigation of the geohydraulic interactions between the soft rock and hard rock aquifer, a 3D ground water model was generated. Using this model the contaminant migration between the soft rock aquifer was identified. A performance analysation for different de-contamination treatments was compiled and the migration paths of the contaminats were identified.

KEYWORDS: ground water contamination, modelling, municipal area

INTRODUCTION

The city Glauchau is located in the western Saxony and was a traditional centre of textile and chemical industry. The most industrial enterprises have been closed down during the past years. For the further development of these territories the investors urgently need safety for planning. So it is necessary to predict the migration of industrial contaminants (especially clorinated organic hydrocarbons) into aquifers and to treat contaminated water and/or soil. The protection of groundwater against degradation is also of great importance for Glauchau because the local drinking water supply bases on these resources. For this reason the following tasks need to be solved:

- Treatment of contaminated sites by optimal use of the financial ressources;
- Establishment of an economically balanced relationship between local water supply and supplying water resources from outside.

The previous investigations showed: the identification of point source contaminations, the derivation of an effective aquifer restoration and the definition of priorities are quit difficult and did therefore not lead to success. Interactions between soft and hard rock aquifer as far as very different pumping rates during the last fourty years entail a complicated groundwater flow and quality dynamics. Therefore an integral assessment of contaminated sites according to the Saxon method catalogue was tackled including the application of a ground water model.

AREA OF INVESTIGATIONS

From the regional geological point of view the research area is located in the north and north-west edge of the surrounding of the Ore Mountains not far from the transition zone to the Saxon Granulit Mountains. The most important factor of the hydrogeolical situation is the interaction of the deep hard rock aquifer of the Permian Mülsen layers with the Quaternary soft rock auqifers in the valleys of the rivers Mulde and Lungwitzbach. Quite impermeable Leukersdorf layers are located below the permeable Mülsen layers. The Mülsen layers are represented by brittle and fractured conglomerates, sandstones and claystones. The upper zones of the Mülsen layers are weathered to clays. This horizon is an aquitard to the soft rock aquifer of the river valleys. The aquifer of the river valleys, represented by sands and gravels, has a thickness between 1 and 7*m* and is covered by alluvial loam.

The geological history is coined by numerous tectonic and volcanic events. The permeability of the Mülsen layers depends on location of this tectonical fractures.

MODELLING

The model was built using PCGEOFIM® [1]. For the construction of the model the following steps were executed:

- Systematical recording of all informations about ground water quality and the hydrogeological situation, given by previous investigations to the treatment of contaminated sites in Glauchau and its surroundings;
- Recording and evaluation of geological and hydrological data in public and privat archives (Geological Survey of Saxony, WISMUT uranium mining company etc.);
- Development of an advanced geolocical model based on the increased knowledge especially about tectonical situation.

The construction of a ground water model allows a three-dimensional simulation of ground water flow and a first assessment of mass transfer in the saturated zone. For this a commonly used numerical model for porous medium was adapted to the conditions of the hard rock aquifer. Using special pre-processing routines, the tectonical influenced zones were integrated into the model as *channels* of high water conductivity. Special pre-processing routines were designed in order to transfer the primary data into the data used for the ground water model.

The following model scenarios were calculated:

1. Simulation of the present ground water flow with the present pumping rate of the water works Niederlungwitz and permanent impact of chlorinated hydrocarbons from contaminated sites,
2. Simulation of the ground water flow for the same boundary conditions and the case, that the water production wells and aquifer de-contamination wells are switched-off.

RESULTS

The following results were obtained:

- Due to the hydraulic gradient pollutants from the deep aquifer are shifted to the soft rock aquifer,
- The drinking water production wells can be effectively protected by aquifer de-contamination wells,
- In case drinking water production wells and aquifer decontamination wells are switched-off, high pollution migrates toward the rivers.

The model proved himself as an effective instrument for the decision making and designing of water management elements.

REFERENCES

1. IBGW. Programmbeschreibung PCGEOFIM®, Leipzig, 1997.
2 Leibenath, Daffner, Palm, Zinke, Jung. Aufbau und Betrieb eines Altlastenmonitorings und hydrogeologischen Modells für den Raum Glauchau. *non published, in german, Res. rep. Nr. GLA14195*, Dresden, 1996.
3 Daffner, Leibenath, Scholz. Hydrogeologisches Rahmengutachten Dresden-Innenstadt. *non published, in german, Res. rep. Nr. GWMD8995*, Dresden, 1996.

Application of A Simple Method for the Convection Direction Estimation to the Groundwater Polluted by Volatile Chlorinated Hydrocarbons

Yasushi Sakamoto, Yasuhiro Yamanaka, Fumi Minai and Kei Nishida

Dept. of Civil and Environmental Engineering, Faculty of Engineering, Yamanashi University, 4-3-11 Takeda, Kofu, 400-8511, Japan

ABSTRACT. A simple method for estimating the convection direction of volatile chlorinated hydrocarbons in groundwater was applied to an actual polluted site. This method consisted of : (1) identification of a polluted aquifer by a principal component analysis and a cluster analysis of water quality and (2) estimation of the convection direction by the polluted-well location and concentration distributions. This method is based on the water quality data without the water level data and can be applied to the geologically homogeneous area of several hundred meters. The estimated migration directions were compared with the results of simulations using computer models, MODFLOW and MODPATH. The results showed that the estimated flow line passed through the area of the pollution source factory and this method was promising.

KEY WORDS: Volatile chlorinated hydrocarbon, Convection direction, Cluster analysis

INTRODUCTION

In Japan, there are many sites of the groundwater pollution by volatile chlorinated hydrocarbons. These sites have been left unremedied because it is difficult and expensive to specify the location of their pollution sources. In this paper, a simple method [1] for estimating the convection direction was applied to one of the polluted sites in Japan.

METHODS

Study Area, Sampling and Chemical Analysis. Our study area is located on the southern foot of the Mt. Yatsugatake, Central Japan. Fig.1 shows the topography of our study area, the sampling points and the potential sources of pollutants. The factory shown in Fig.1 reported its soil

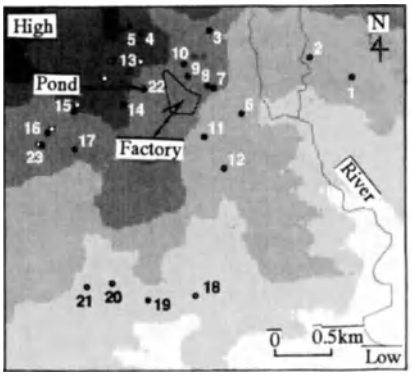

Fig. 1. Study area and sampling locations

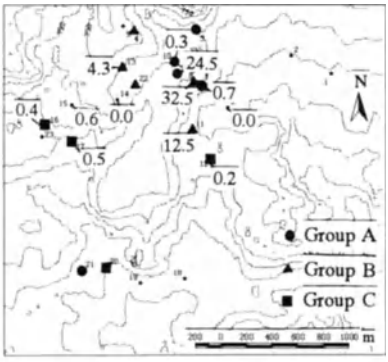

Fig. 2. 1,1,1-trichloroethane conc. (μg/l) and well groups

pollution by volatile chlorinated hydrocarbons to the prefecture government. Waters were sampled at 21 (Nos.1-21) wells and 1 pond (No.22) on Dec. 22 in 1998. All sampled waters were analyzed for the major anions (Cl^-, NO_3^- and SO_4^{2-}) and cations (K^+, Na^+, Ca^{2+} and Mg^{2+}). The concentrations of 1,1,1-trichloroethane, trichloroethylene and tetrachloroethylene were also analyzed for 12 wells (Nos.6-17) near the factory.

Grouping of Wells based on Principal Component Scores for Water Quality. The observation wells are grouped by a cluster analysis. Clustering is based on the scores of the principal components of groundwater qualities. The scores are computed on the basis of the major anion and cation concentrations. The clustering procedure is the Ward's method using Euclidean distance. The group involving the most polluted well is considered as the polluted group.

Estimation of Convection Direction. We assume that the convection direction roughly coincides with the direction of the long axis of the oval area enclosing the wells of the polluted group and that the variances of location coordinates (X and Y) and concentration coordinates (Z) of the wells are maximum along the axis. Therefore, the projection of the first principal component axis for x, y and z to X-Y plane is estimated as the convection direction. The results of the estimation were compared with the results of simulations using computer models of MODFLOW and MODPATH.

RESULTS AND DISCUSSION

Fig.2 shows the 1,1,1-trichloroethane concentrations and the polluted and unpolluted well groups (A, B, and C). Fig.3 shows the water levels and the flow directions estimated by MODFLOW. Fig.4 shows the convection direction estimated by our method along with the results of MODPATH. Fig.4 shows that the estimated flow line passed through the area of the pollution source factory.

CONCLUSIONS

Our method was effective for the estimation of the convection direction of volatile chlorinated hydrocarbons without the water level data.

REFERENCES

1. Sakamoto Y and Nishida K(1999) Estimation of Convection Direction of Groundwater Pollutants on the Basis of Polluted Well Location and Concentration Distribution, JHHE, 17, 1: 29-36.

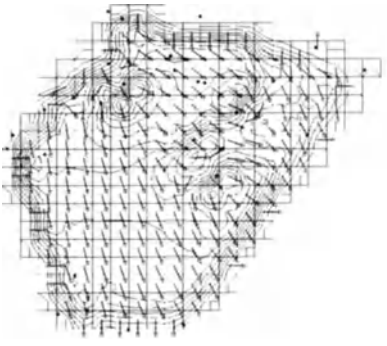

Fig.3. Simulated water levels and flow directions

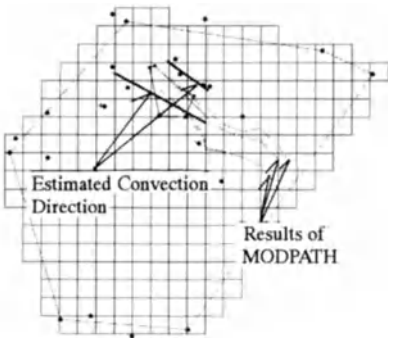

Fig.4. Estimated convection direction

Effect of injection mode on the spatial moments of a non-reactive solute plume

Sten Berglund[1] and George Demmy[2]

[1]Department of Civil and Environmental Engineering, Royal Institute of Technology (KTH), SE-100 44 Stockholm, Sweden
[2]Department of Agricultural and Biological Engineering, University of Florida, Gainesville, Florida 32611, U.S.A.

ABSTRACT: The effects of solute injection mode on the spatial moments of instantaneously injected, non-reactive solute plume are examined in the stochastic-advective framework. Two different modes for the introduction of a solute in a heterogeneous aquifer are considered, namely injection of solute in the resident fluid and in fluid flux. The first and second spatial moments for the two injection modes are quantified using closed-form expressions.

Key words. Solute transport, Groundwater quality, Stochastic processes

INTRODUCTION

Two different "modes" for the introduction and subsequent detection (observation) of a solute in a physical transport system are common in the literature, namely injection and detection of solute in the resident fluid and in fluid flux. The two modes of injection and detection have been recognized and discussed in the context of deterministic advective systems [1], and for systems where solute transport is described by means of the advective-dispersive equation [2]. In a recent study [3], we used the stochastic-advective framework to investigate the injection mode effects on the temporal moments associated with field-scale breakthrough curves. The present work comprises a similar analysis of the plume spatial moments [4,5], focusing on the first and second, longitudinal moments obtained for the two injection modes.

THEORY

We consider a three-dimensional aquifer with spatially variable hydraulic conductivity, K, where the groundwater flow is steady with the uniform mean velocity in the x_1 direction of a Cartesian coordinate system $\mathbf{x}(x_1, x_2, x_3)$, and the plane $x_1 = 0$ is referred to as the injection plane (IP). In the stochastic-advective approach, the flow field is viewed as a collection of streamtubes along which solute parcels are transported. We define the streamtubes such that they all have a cross sectional area in the IP equal to ΔA and that the total water discharge in a streamtube is $\Delta Q = \theta V_0 \Delta A$, where V_0 is the x_1 component of the advective velocity at $x_1 = 0$.

As discussed in [3], placing a constant mass $\Delta M = \theta C_0 \Delta A \Delta x_1$ at $x_1 = 0$ into each streamtube, where θ is the porosity, C_0 is the concentration and Δx_1 is the length of the solute parcel (assumed small), corresponds to the uniform [1] or resident [2] injection mode, whereas injection in flux is obtained by using a velocity-proportional mass $\Delta M = \theta C_0 V_0 \Delta A \Delta t$, where Δt is a brief injection interval. Neglecting pore-scale dispersion, the concentration resulting from instantaneous injection of the mass ΔM at $x_1 = 0$ can be written as $C(\tau, t) = (\Delta M / \Delta Q)\delta(t - \tau)$, where δ is the

Dirac delta function and τ is the solute travel time (e.g., [5]). The travel time is the time required for a solute parcel to be advected from the IP to the plane x_1. In order to evaluate spatial moments associated with all streamtubes, we consider uniform (resident) or flux injection of the mass M within a source area of size A in the IP. The mass elements can be written as $\Delta M = M\Delta A / A$ and $\Delta M = MV_0\Delta A / (UA)$ for uniform and flux injection, respectively, where U is the mean velocity.

We consider normalized, longitudinal spatial moments which, by invoking the ergodic hypothesis [4] and following the steps in [5], can be expressed as:

$$m_p(t) = \frac{\theta}{M}\int x_1^p C(\mathbf{x},t)d\mathbf{x} = \frac{\theta A}{M}\left\langle \int [X_1(\tau)]^p V_0 C(\tau,t)d\tau \right\rangle$$

where $\langle\cdot\rangle$ denotes ensemble mean, and X_1 is the longitudinal trajectory component. By using the solution for C with the mass elements for the two injection modes, and writing the random injection velocity and trajectory as $V_0 = U + V'$ and $X_1 = Ut + X'$ (primes denote fluctuations), we obtain the following results for m_1 and the second, centered moment, $m_2^* = m_2 - m_1^2$:

$m_1(t) = Ut$; $m_2^*(t) = X_{11}(t)$ for uniform (resident) injection

$m_1(t) = Ut + U^{-1}\sigma_{VX}(t)$; $m_2^*(t) = X_{11}(t) + U^{-1}\langle V'[X'(t)]^2\rangle - [U^{-1}\sigma_{VX}(t)]^2$ for injection in flux

where $X_{11} = \langle X'X'\rangle$ is the longitudinal trajectory covariance and $\sigma_{VX} = \langle V'X'\rangle = (1/2)dX_{11}/dt$.

RESULTS

For illustrative purposes, we assume $\langle V'(X')^2\rangle = 0$ and use Dagan's closed-form expression for X_{11} in an aquifer of three-dimensional, isotropic heterogeneity [4]. It is found that the first moment for flux injection is nonlinear and larger than that for uniform injection. The difference increases with increasing degree of heterogeneity in K. For example, at $tU / I = 2$, where I is the integral scale of $\ln K$, and a variance of $\ln K$ of 0.5, the first moment for flux injection is 16% larger than the one for uniform injection (difference normalized by the result for uniform injection), whereas the injection mode effect increases to 31% for a variance of 1.0. Furthermore, the effect decreases with time; e.g., it is 10% at $tU / I = 10$ for the variance 1.0. It may also be noted that the opposite results were obtained for the first temporal moments [3], i.e., a larger and nonlinear moment for uniform injection.

The analysis of the second moments shows that the moment for uniform injection is larger than that for flux injection, and that both moments are nonlinear functions of t. These results are in qualitative agreement with the results for the temporal moments [3]. The injection mode effects are found to be of the same order as for the first moments, with the exception that the effect on the second moment decreases more rapidly. The extent to which the present results are affected by the approximations in the analytical expressions should be investigated by numerical simulations.

REFERENCES

1. Levenspiel O, Turner JCR (1970) Chemical Engineering Science 25: 1605-1609
2. Kreft A, Zuber A (1978) Chemical Engineering Science 33: 1471-1480
3. Demmy G, Berglund S, Graham W (1999) Water Resources Research 35: 1965-1973
4. Dagan G (1989) Flow and transport in porous formations. Springer-Verlag, New York
5. Cvetkovic V, Dagan G (1994) J Fluid Mechanics 265: 189-215

Flow path and material cycle for groundwater of floodplain in the Nagata district of the Tama River

Kouji Tsushima[1], Hiroyuki Ohno[2], Shingo Ueda[3] and Norio Ogura[1]

[1] The United Graduate School of Agriculture, Tokyo University of Agriculture and Technology. 3-5-8 Saiwaicho, Fuchu, Tokyo, Japan, zip code 183-8509
[2] River Engineering Department of Oyo Technical Center, OYO Corporation. 2-61-5 Torocho, Ohmiya, Saitama, Japan, zip code 330-8632
[3] College of Bioresource Sciences, Nihon University. 1866 Kameino, Fujisawa, Kanagawa, Japan, zip code 252-8510

ABSTRACT

Possible role of floodplains in nitrogen dynamics in the middle reach of the Tama River, Tokyo is discussed based on analyses of groundwater flow and water chemistry.
On flow path from G-5 toward G-11, residence time of groundwater was over fivefold longer than that in the rest area. Finer grain sediment and small gradient of groundwater level of 1/1500 in part of 「G-10 to G-11」 was suggested to cause longer residence time of groundwater. Exceeding denitrification and NO_3^- exhaustions were notable characteristics of the longer residence time groundwater, whereas groundwater in the rest area had shorter residence time, relative coarse size sediment and aerobic water chemistry.
Groundwater research was not carried out at this site before 1980, however the cause of longer residence time of groundwater and anaerobic groundwater formation seemed to be finer grain in sediment near the G-10 and G-11 by flood in the early 1980's. Area of sediment before the 1980's is considered to be in contrast to area of sediment during the early 1980's. Groundwater level gradient in sediment before the 1980's was large at 1/150, and groundwater residence time was shorter. It is suggested that difference of sedimentation affected groundwater chemistry. Thus, river-bed water plays an important role in floodplain nitrogen dynamics.

KEY WORDS : the Tama River, floodplain, channel transition, $\delta^{15}N$, denitrification

INTRODUCTION

River water comprises not only 'stream water' as water in the channel but also 'river-bed water' as groundwater in unconfined aquifers around rivers. River-bed water contains much organic carbon which is available for microorganisms and has much longer residence time in comparison with the stream water. Therefore, there is large biogeochemical change, leading to differences in water chemistry between stream water and river-bed water [1,2,3]. Moreover, river-bed water may contribute to river material cycles due to its flowing under floodplains.
This study aimed to identify groundwater flow in floodplains and sedimentologic situations, and to investigate dynamics of NO_3^- in floodplain groundwater.

SITE AND METHODS

The study site is locate in the right bank, middle reach of the Tama River. Sample waters were collected from wells (G-1 to 12), river (TR), spring points (SP-1 to 7) and streamlet points (SW, F-3,5,9, and EF) on a monthly basis from April 1997 to July 1998. In the field, measurements

included water temperature, pH, electric conductivity, and water level for groundwater. In the laboratory, analyses included concentrations of dissolved organic carbon, dissolved inorganic carbon, dissolved oxygen (DO), N_2O, major ions, and nitrogen stable isotope ratio ($\delta^{15}N$) of NO_3^-. Topographic maps (1882 and 1940) and aerial photographs (1947, 1972, 1974, 1984 and 1998) were used to determine channel transition.

RESULTS AND DISCUSSION

Groundwater level tended to decrease downstream along the present river course in spite of temporal fluctuation. Gradient of groundwater level was 1/150 for the most part, however, it was 1/1500 in the area from G-10 to G-12.

The topographic maps and aerial photographs from 1882 to 1998 suggested that the channel changed its course with relative ease until a 1974 flood in the Nagata district. As a result, most of the area was covered with coarse size sediment.

Before floods in 1981-1983, vegetation grew into the floodplain of the study site, causing part of 「G-10 to G-11」 to be sedimented mainly by fine grain, due to vegetation-induced slowing of flood water flow. It differed from the sediment until 1970's, which was composed mainly of coarse grain. This fine grain sediment seemed to cause low groundwater permeability. It is inferred from Cl^- concentration fluctuation that the residence time of groundwater of 「G-5→G-10」 (0.4km/50～100 days) was about five-tenfold longer than that of 「G-2→G-8」 (0.4km/～10 days). The longer residence time of groundwater of 「G-5→G-10」 was probably caused by fine grain in 「G-10 to G-11」 located downstream of groundwater flow of 「G-5→G-10」. This result is consistent with difference in groundwater level gradient (1/1500 and 1/150).

In longer residence time groundwater (G-5, 7,10,11), DO reduced to 1-2mg/l (saturation of 10-30%) for most of the year during our research. However, relatively high concentrations of DO were observed from March to April. While NO_3^- was exhausted in the middle of summer, DO was detected. Denitrification is usually inhibited by the presence of oxygen. It seemed that denitrification occured after oxygen began disappearing in pore parts, in spite of the presence of dissolved oxygen in groundwater.

NO_3^- is the predominant inorganic nitrogen species in aerobic groundwater. In some sites, NO_3^- concentration decreased overperiods of 5 to 11 months when groundwater temperature was relatively high. The $\delta^{15}N$ of NO_3^- increased when the concentration decreased, which was attributed to nitrogen isotopic fractionation during denitrification [2]. In this study, N_2O decreased to below the atmospheric equilibrium concentration (～10nM) paralleling NO_3^- decreases. These facts strongly suggest that denitrification occurs in floodplain sediments where residence times of groundwater are long.

REFERENCES

1. Bourg ACM, Bertin C (1993) Biogeochemical processes during the infiltration of river into an alluvial aquifer. Environ Sci Technol 27:661-666
2. Grischek T, Hiscock KM, Metschies T, Dennis PF (1998) Factors affecting Denitrification during infiltration of river water into a sand and gravel aquifer in Saxony, Germany. Wat Res 32:450-460
3. Pinay G, Ruffinon C, Wondzel S, Gazelle F (1998) Change in groundwater nitrate concentration in a large river floodplain : Denitrification, uptake, or mixing? J N Am Benthol Soc 17:179-189

Pollution Problems of the Groundwater Regimes in Calicut City, Kerala, due to Cannoly Canal

Jalaja. T.K[1], Nirmala. E[2], Nirmala Stephen[3] and Nair. S.R[4]

[1,2,3,4] Environmental Studies Division, Centre for Water Resources Development and Management, Kunnamangalam, Calicut 673 571, Kerala, India

Kerala state occupies the south-west part of India, between 8° 17' 30'' and 12° 47' 40" north latitude and 74° 51' to 77°24' 47" east longitude. The majestic western ghats and the Arabian sea on the west have given Kerala distinctive physical and cultural features. Kerala enjoys a tropical monsoon climate and receives good monsoon rains i.e., south-west monsoon [June -September] and north-east monsoon [October-December]. The average rainfall is about 3000 Mm. The state, with a total area of 38,863 sq.km, has a groundwater potential of 5000 Mm^3. Even though it receives fairly good average rainfall, bulk of our rural population depend on groundwater for multipurpose activities.

Cannoly canal is a manmade water course running across the heart of Calicut city in Kerala state. This canal receives pollutants from small scale industries like log setting, coir retting, food processing units, domestic sewage, hospital wastes, hotel wastes and city garbage. Downward movement of these pollutants through subsurface seepage, finally reaches the groundwater sources. Dug wells are the main drinking water sources for the public living in the suburbs of Cannoly canal. But due to the input of pollutants from the canal, the wells have lost their potability.

To study the pollution load carried by the canal and the nearby groundwater sources, a survey was conducted and sampling points were fixed along the course of the canal. Dug wells for studies were selected which were located about 0.5 km and 1 km away from the canal. Water chemistry and biological aspects were studied at seasonal interval from 1991 to 1993 as per Standard Methods for the Examination of Water and Wastewater [APHA, 1986]. Very low oxygen concentration of 0.53 mg/l was encountered in Cannoly canal during premonsoon period. The same trend was observed in the canal and wells situated within 0.5 km during the other two seasons also. Neither acidic nor alkaline condition prevailed in the canal and wells. High conductivity values were observed in the canal round the year showing 33,500µs/m. Correspondingly, conductivity values of the wells in the vicinity of the canal were above the permissible drinking water standards. Pronounced seasonal variation in hardness was observed in the canal and wells, maximum being 5630 mg/l, during postmonsoon period.

INDUSTRIAL POLLUTION

Small scale industries like coir retting and log setting are practised in the canal, which creates a lot of pollution problems. Pollutants like.polyphenols, mercaptans, lignin, tannin etc. are leached out into the canal, which in turn pollutes the nearby groundwater sources. Slightly low pH observed can be attributed to the leaching of acidic pollutants into the nearby wells.

SALINITY INTRUSION

Cannoly canal has free influx of saline water through Korapuzha in the north and Kallaipuzha in the south, which in turn merges with the Arabian sea. Salinity fluctuated from 0.81 ppt to 20.8 ppt during the different seasons. This variation may be attributed to the diurnal tidal effect. Sub surface seepage of the saline water was manifested in the wells located within 0.5 km from the canal [S.R Nair, et al,'94]. Studies show that salinity did not extend to a distance of 1km. Wells having high salinity values showed high conductivity values also.

MICROBIOLOGICAL QUALITY

Sanitary quality of the canal and the potability of the wells were assessed. The canals and wells within 0.5 km were fecally contaminated. E.coli was absent in the wells located 1 km away from the canal during monsoons and postmonsoon seasons. Total bacterial count was maximum during premonsoon. MPN index was maximum throughout the year in the canal and wells within 0.5 km.

STATISTICAL ANALYSIS

Using ANCOVA (Analysis of co-variance software package) the results showed that the canal has significant effect on wells with respect to the parameters pH and calcium. Seasonal variation was highly significant at 5% level of significance with respect to the variables pH and temperature. But distances (0.5 km and 1 km) were not significantly different with respect to pH.

CONCLUSION

The study of the quality of the canal water and the nearby wells has revealed the polluted condition of the canal which has indirectly led to groundwater pollution. The canal is used as a sink for disposal of sewage from residential areas, hospitals, hotels and slaughter houses. Pollutants released from small scale industries like retting of coconut husk and log setting, aggravates the condition. Low pH, low Dissolved Oxygen, greyish black colour and foul smell of hydrogen sulphide, prevailed in the areas where log setting and coir retting were practised. Correspondingly low Dissolved Oxygen and pH content was observed in the wells situated within 0.5 km of the canal. Offensive odour and decolourisation was noticed in the canal and nearby wells where hospital wastes were discharged. Preliminary bacteriological studies revealed the poor sanitary quality of these wells. Wells situated within 0.5 km of the canal were saline prone. The silt and debris from the adjacent elevated areas get collected in the canal during the South -West and North - East monsoons. This reduces the depth of the canal and also obstructs the flow of water, making the water body stagnant in some areas . This stagnant polluted water has created the site for breeding of mosquitoes, which spreads Filariasis, a water related disease. Statistical analysis showed that the canal has significant effect on wells with respect to the parameters pH and calcium. Seasonal variation was highly significant at 5% level of significance with respect to the variables pH and temperature. But distances (0.5 km and 1 km) were not significantly different with respect to pH. People living in Calicut city suffer much from lack of safe drinking water. Hence, they are forced to depend upon public water supply for their domestic uses. The above study has revealed the pollution load carried by the wells, as a result of subsurface seepage of the pollutants from the canal.

Relations between Behavior of Gaseous VOCs in Unsaturated Zone and Gas Adsorption to Soil

Yoshihiro ISHII[1], Kohji MURAOKA[2] and LEE Changsoo[3]

[1] Department of Civil and Architectural Engineering, Faculty of Engineering, Hiroshima Institute of Technology, 2-1-1 Miyake, Saeki-ku, Hiroshima 731-5193, JAPAN
[2]Department of Civil Engineering, Graduate School of Engineering, Osaka University, 2-1 Suita, Osaka 565-0871, JAPAN
[3]Department of Civil and Environmental Engineering, Hanyang University, Ansan, Kyunggi-do, 425-791, KOREA

ABSTRACT. The soil vapor extraction (SVE) is one of in situ remediation techniques, and the behavior of gaseous volatile organic compounds (VOCs) plays an important role of the purification of underground pollution and groundwater contamination. Numerical simulations, including the delay of a gas transport, will allow evaluating the gas behavior in unsaturated zone. The factors related with the delay depend on mainly the dissolution from a gas to moisture, the adsorption from moisture to a soil, and the adsorption from a gas to a soil directly. The retardation coefficient is formulated by including these three factors, and some laboratory experiments are performed about the adsorption from a gas to a soil and the retardation coefficient. The result of these experiments is that kind, diameter and specific surface area of soils relate with the adsorption coefficient, within the limit of this investigation. Two-dimensional numerical simulations under some boundary conditions make clear the velocity profile, the concentration distribution of gaseous VOCs in unsaturated zone at the extraction, and the relation between the condition of the ground surface and the mass of removed contaminants.

KEY WORDS: Soil Vapor Extraction, Numerical simulations, Retardation coefficient, Adsorption coefficient, VOCs

INTRODUCTION

SVE is one of effective purification techniques. The effectiveness of this method is clarified in Takatsuki City and Kumamoto City and, etc. The efficient method of extracting the gas and the judgement of the purification are still not clear, because the behavior of the contaminant and the pollution gas in the soil is complex, and it is difficult to estimate the amount of the contaminant existing in an underground space. So, the numerical simulation including the delay of gaseous VOCs in unsaturated zone estimates the gas profile and the distribution of the contamination.

GAS BEHAVIOR AND RETARDATION COEFFICIENT

Gaseous VOCs such as trichloroethylene and tetrachloroethylene are heavier than air. Sleep and Sykes [1], Mendoza and Frind et al.[2] research the effect of the advection in the behavior of high-density gas. The behavior of contaminant in unsaturated zone is assumed to be able to handle by the fluid continuity equation for the density dependent flow of the gas and the material transport equation for the vapor. And the retardation coefficient is defined as Eq.1 including the dissolution from a gas to moisture, the adsorption from moisture to a soil, and the adsorption from a gas to a soil directly, and details are written in Lee et al.[3].

$$R = 1 + \rho_W \frac{(\theta_T - \theta_D)}{\theta_D} K_W + \frac{(\theta_T - \theta_D)}{\theta_D} K_W K_d + \rho_S \frac{(1 - \theta_T - \theta_W)}{\theta_D} K_d' \qquad (1)$$

Several kinds of the gas behavior are calculated by using these equations under the some kinds of the boundary condition at the extraction. The results of calculation are displaying in *the poster presentation.* The velocity profile, the concentration distribution of gaseous VOCs in unsaturated zone is made clear.

ADSORPTION TO SOIL AND RETARDATION COEFFICIENT

The state of oven-dried soil is assumed, in order to examine only the effect of directly adsorption from the gas to the soil. The adsorption coefficient Kd' is obtained by using *the batch experiments* and the Henry type's isothermal, and the retardation coefficient R is calculated by Eq.1. The gaseous trichloroethylene and six kinds of soils as which the specific gravity is almost the same; the glass bead (ϕ = 0.6 and 1mm), silica sand (ϕ = 1mm), the ground soil (at the campus of Osaka Univ. : ϕ = 1mm), the field soils (in Mino City : ϕ = 1mm), *akadama* soil (ϕ = 0.7, 1, and 3mm), and *kanuma* soil (ϕ = 0.7, 1, and 3mm) , are used for the experiment. All soils are dried for 24 hours with a dry furnace, and soil moisture is 0%.

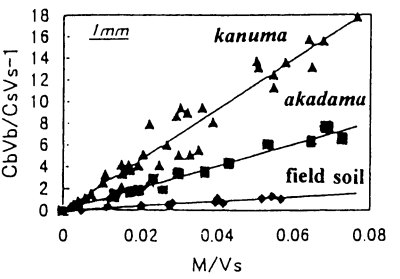

Fig.1 Comparison by the kind of soil

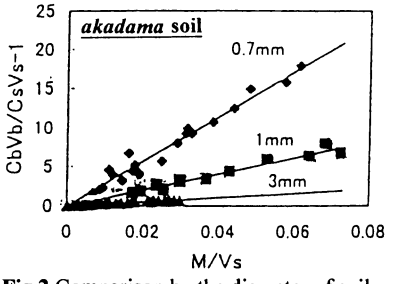

Fig.2 Comparison by the diameter of soil

Fig.1 shows the comparison by the kind of soil. Six kinds of soils as same diameter(ϕ =1mm) are analyzed. *Kd'* is about 100 and about *R*=80 in *akadama* soil, and *Kd'* of *kanuma* soil is about 200 and about *R*=70. The glass bead (*Kd'*=3.59×10^{-2} and *R*=1.13), silica sand (*Kd'*=5. ×10^{-1} and *R*=2.7) and the ground soil (*Kd'*=2 and *R*=5) is not display in the Fig.1. The adsorption coefficient is greatly different depending on the kind of the soil. Fig.2 shows the comparison by the diameter of *akadama* soil. *Akadama* soil (ϕ = 0.7, 1, and 3 mm) is selected for this experiment. The case of the 0.7 mm is the largest *Kd'*, and is about ten times as the case of the 3 mm. The adsorption coefficient shows the tendency to grow when the diameter increases. Fig.3 shows the relation to specific surface area. The specific surface area of five kinds of the soil is analyzed for only 1mm diameter. The value of the specific surface is sequentially indicated from the small one; glass bead (0.0061 m^2/g), silica sand (0.229), the ground soil (2.39), *akadama* soil (105), and *kanuma* soil (145). *Kd'* increases as the specific surface becomes bigger. It is clarified that the kind, the diameter and the specific surface area of the soil have an effect on the delay of the gas diffusion in the oven-dry soil. It is necessary to consider the adsorption of the gas to the soil particle in order to understand the gas movement.

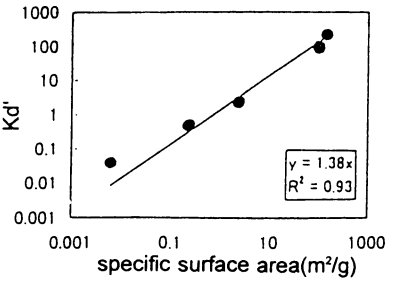

Fig.3 specific surface area and Kd'

REFERENCES

1. Sleep, B.E. and J.F. Sykes (1989) Water Resource Research 25(1): 81-92
2. Mendoza, C. and Frind, E.O. (1990) Water Resource Research 26: 379-387
3. Lee C.S., Muraoka K.and Ishii Y. (1997): Proc. Asian Waterqual'97, 1088-1095

Study on Remediation of Oil Contaminated Soil

Kenji NISHIDA, Takayuki UENO, Toshihiko MIURA, Hiroshi KUBO, and Takeshi KAWACHI

Obayashi Corporation Technical Research Institute, 640, Shimokiyoto 4-chome, Kiyose-shi, Tokyo 204-8558, Japan

Abstract: The effect of heating on remedial efficiency has been investigated by carrying out a column test under fixed heat and suction conditions. The results show that the volume of ventilation needed to remove kerosene decreased by approximately one-tenth as the temperature rose from 20℃ to 50℃. Based on the relationship between temperature and vapor pressure, we propose a remedial model equation for volatile organic compounds under heat and suction conditions. We verified the equation using experimental results for kerosene.

Key Words: Laboratory test, Numerical analysis, Temperature effect, Contaminated soil

INTRODUCTION

Soil vapor extraction may be the in situ technology that comes closest to being a universal solution for remediation of soils contaminated with volatile organic compounds. However, it takes a lot of time to complete remediation with this technology. To shorten the time, soil vapor extraction combined with heating has been designed. However, this technology has not put to practical use because there have been insufficient studies on an effective heating method and evaluation of the heating effect [1]. To investigate the effect of heating on remedial efficiency, a small-size column test was carried out under fixed heat and suction conditions. We propose a remedial model equation for a volatile organic compound under heat and suction conditions, based on the relation of temperature and vapor pressure.

EXPERIMENTS

The experimental conditions are shown in Table 1. Fig.1 shows the experimental apparatus. The soil sample was dry sand with a uniform grain diameter. Oil of 3% of the weights of the dry soil was added to the sand, and the sample of contaminated soil was placed in a column. The column was 10cm in diameter and 10cm high, and the density of the soil was 1.30g/cm^3. In the thermostatic chamber, the soil was exposed to 3 temperatures: 20, 35, and 50℃. The contaminated soil in the column was sucked, and the ventilation speed in the column was adjusted to a constant 1.0NL/min. After extracting the soil, the oil content was measured by extracting kerosene from the soil. The relationship between the unit volume of ventilation and the kerosene removal rate is shown in Fig.2. As the soil temperature increased, it became obvious that the oil was removed faster and with a smaller ventilation volume.

NUMERICAL ANALYSES

Based on the following assumption, the evaporation speed for volatile organic compounds can be expressed by Eq.(1). 1) Evaporation speed is proportional to the pressure difference between the saturation steam pressure and the actual steam pressure. 2) As the remaining quantity decreases, the evaporation speed decreases. 3) The evaporation speed is proportional to the air speed.

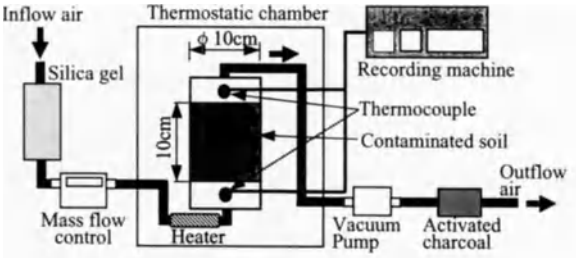

Fig.1. Apparatus of a small-size columm Test

Table 1. Experimental conditions

No.	Temperature of inflow air (℃)	Remediation time (hr)
D-20	18～20	18, 72 ,84
D-35	35～37	4, 12, 24, 42
D-50	50～52	1, 4, 12, 24

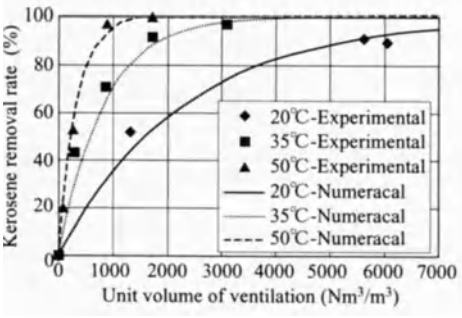

Fig.2 The change of kerosene removal rate

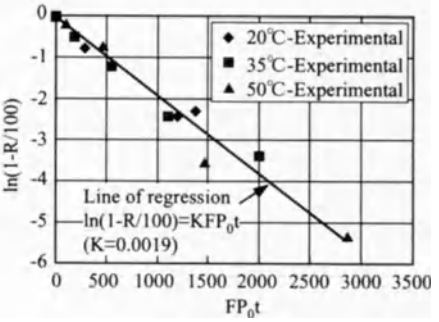

Fig.3 The Relation between ln(1-R/100) and FP_0t

$$\frac{dW(t)}{dt} = -KF\{P_0 - P(t)\}W(t) \quad (1)$$

Where W(t): remaining quantity of volatile organic compounds, P_0: a saturation steam pressure of volatile organic compounds, P(t): actual steam pressure, t: time, F: air speed, and K: experimental coefficient. Now, suppose that is $P(t) \ll P_0$, removal rate R for kerosene, can be written as Eq.(2).

$$\ln\left(\frac{1-R}{100}\right) = -KFP_0t \quad (2)$$

The experimental relationship between ln(1-R/100) and FP_0t is shown in Fig.3, where P_0 is calculated from the expression Clausius-Clapeyron [2]. The relationship of ln(1-R/100) and FP_0t fitted a proportional plot at all temperatures. Therefore, it is judged that Eq.(2) and the aforementioned assumption are correct. From Fig.3, the experimental coefficient is calculated as 0.0019, so the kerosene removal rate can be calculated using Eq.(2). Numerical results are shown Fig.2, and the experimental results were good agreements. From the proposed Eq.(2), the removal rate of all volatile organic compounds except kerosene can be estimated too.

CONCLUDING REMARKS

As the soil temperature increased, it became obvious that the oil was removed faster and with a smaller ventilation volume. And an estimation equation for removal rate of all volatile organic compounds can be proposed.

REFERENCES

1. Walter W.Kovalick (1998) Remediation Technologies in the US, IWGER'98 : 77-86
2.A.W.Adamson (1973) A Textbook of Physical Chemistry, Academic Press, 286-292

The Strategy and Development of Solid Waste Disposal in China

Qiu Hanxue, Liu Guanqun, Zheng Xilai

Dept of Environmental Engineering, Ocean University of Qingdao, 5 Yushan Road, Qingdao, 266003, China

Abstract. The safe solid waste disposal in China started much later. Before 1990, most solid wastes disposed as compost and simple landfilling and the pollution on environment shows seriously. Now some large comprehensive disposal projects are under construction or under running. No matter in the present or in the future, from (In viewing the economic condition (investment and running cost), the composition of solid wastes and the land sources for landfill, the sanitary landfill or comprehensive disposal will be the main methods for solid waste disposal. However, to realize the sanitary operation of the landfill still have a long way to go in the aspects of the technology, equipment and management that dealing with solid waste collection and transportation system, separating and pre-disposal system, the optimal designing and operation of the landfill, the leachate treatment etc.

Key words: Solid waste disposal, Safety landfill, Groundwater pollution

INTRODUCTION

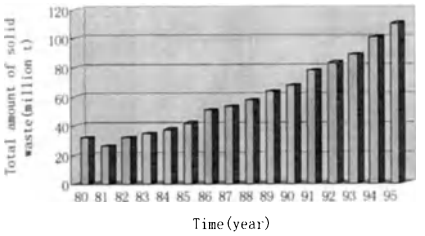

Fig 1 The yield of solid waste in China

The urbanization and growth of city scale cause solid waste increase necessarily with a high living standard of people. As one of the largest developing countries China has 300 million urban population living in 600 cities and the annually increasing amount of waste leads to the environment risk boosting. So, the safe disposal of solid waste is regarded urgently for China.The yield and composition of solid waste strongly depends on such factors as population, living level, habit and custom, fuel composition, industrial level, food composition, stage of social development as well as climate. In developed countries, the yield of solid waste is 3.5kg/day per person in average [1]. While in China, the increasing rate was 13.31% during 1983 to 1990 and the amount of solid waste has increased greatly with the urbanization (Fig.1). Comparing with developed countries, the urban solid waste in China contends much more inorganic component (Tab.1) [1,2]

THE DISPOSAL OF SOLID WASTE IN CHINA

The disposal of solid waste in China started much later than the developed countries. Before 1985, some large cities like Beijing, Shanghai and Guangzhou were seriously surrounded by landfills surveyed by remote sensing. In that period, compost was prevalent for the demand of fertilizer from farmer. The landfills usually dump simply in the valley, natural depressions or rock-mining pit. The overall solid waste disposal level is much lower (Tab.2)[3].

The leachate prevention measures include lateral prevention and bottom prevention technologies. The lateral prevention is done by high pressure-cement injection in the downstream of valley or aquifer to block the leaking of leachate, for example, Tianziling

sanitary landfill in Hongzhou [3]. Bottom prevention usually realized though artificial anti-leakage material like PVC being spreaded on the bottom of the sanitary landfill.

Table 1 The comparing of urban solid waste composition between China and developed countries

Country or cities		Organic					inorganic				
		Animal & plant from kitchen	paper	Plastic	Fiber cloth	Total	Coal cinder & sand	Glass & China	metal	other	Total
Developed Countries	America	22	47	4.5	--	73.5	5	9	8	4	26
	UK	28	33	1.5	3.55	66.0	19	5	10	--	34
	Japan	18.6	46	18.3	--	82.9	6.1	--	--	10.7	16.8
	Germany	16	31	4	2	53.0	22	13	5.2	7	47.2
	Holland	50	22	6.2	2.2	80.0	4.3	11.9	3.2	--	19.4
Chinese Cities	Fuzhou	21.8	0.53	0.48	--	22.8	62.22	1.1	0.5	3.4	67.2
	Shanghai	42.7	1.63	0.40	0.47	45.2	53.79	0.43	0.53	--	54.7
	Beijing	50.29	4.17	0.61	1.16	56.2	42.27	0.92	0.80	--	43.9
	Wuhan	26.53	2.36	0.31	0.74	29.9	68.00	0.85	0.17	1.04	70.1
	Haerbin	16.62	3.6	1.46	0.5	22.2	74.71	2.22	0.88	--	77.8
	Leshan	16.45	1.04	0.23	0.54	18.3	80.27	0.36	0.53	0.58	81.7
	Qingdao	59.2	3.12	4.54	1.52	68.4	30.48	0.82	0.32	--	31.6

Table 2 The evaluation and spreading of technologies to domestic solid waste disposal project in 1990

Technology	Total projects	Spreading technologies	Tentative spreading	Disused projects
Landfill	13	4	1	8
Compose	20	4	7	9
Incineration	13	3	1	9
Comprehensive utilization	16	1	1	14
Total	62	12	10	40

SOLID WASTE DISPOSAL SCHEME OF CHINA

The relatively low flammable material in the waste of China and the high running cost constrains the development of incineration. Compost is also restricted for the reason of the waste being inorganic-rich and the fertilizer marketing problem with the low benefit policy to agriculture of China. The method of using safe landfill shows great advantages for its low cost and easily running. During 1996~2000, 69 sanitary landfills or comprehensive disposal sites will be constructed (Tab.3). These sites cover only parts of cities among more than 600 cities in China. In the first 10 years of the 21st century, China needs more investment and work for the solid waste sites choosing towards the middle and small cities.

Table.3 The construction project of solid waste disposal during 1996-2000 in China

Type	Sanitary landfill	incineration	compost	Comprehensive	Excrement	others
Sites	20	7	6	32	8	5

REFERENCES

1. Liu G. Q, Qiu H. X, et al, (1996), The disposal scheme of municipal solid waste of Qingdao city, Journal of Ocean University of Qingdao, vol. 26(3):369-374
2. Yang D. H., Song L. P., 1996, The present situation of solid waste disposal in Shanghai, Environment Bulletin, No. 2, 7-9
3. Qiu H. X, et al, 1997, Sanitary landfill site choosing for municipal solid waste disposal of Qingdao city, Journal of Ocean University of Qingdao, Vol. 27(4): 533-538.

Survey of Soil and Groundwater Contamination due to Waste Disposal - A Study of 'Contaminant Diagnosis Remediation System'-

Tohru Furuichi[1], Kazuei Ishii[1], Tsugiya Fukumoto[2], and Takuya Wada[2]

[1]Division of Environment Resource Engineering, Graduate School of Engineering, Hokkaido University , W8, N13, Sapporo, 060-8628, Japan.
[2]Geotechnial Division, Osaka Branch Office, CTI Engineering Co.,Ltd, 1-2-15, Otemae, Chuo-ku, Osaka, 540-0008, Japan.

ABSTRACT. When surveying and diagnosing the contamination of soil and groundwater caused by waste disposal, a number of typical waste-related problems will tend to occur in the initial period. These result from 1) lack of feasibility study (topography, geological conditions, contaminants), 2) diversity of contaminants (chemical and physical properties, subsurface water, and behavior in the environment), and 3) lack of a sense of responsibility in remediation. To solve those problems, it is important to implement a policy, making a purification plan in an early stage of the remediation project, examine the surveying goals in line with an efficient purification plan, and establish the items and index regarding the quantity and quality of required data.
With a view to standardizing the survey of soil and groundwater contamination, the authors have proposed a "Contaminant Diagnosis Remediation System[1] [2]." By creating a survey chart and a management and operation system of the survey data, based on GIS (Geographic Information System), they suggested efficient survey plan to deal with soil and groundwater contamination by waste, which involves various complex problems.

KEY WORDS: contamination, soil, groundwater, diagnosis, remediation, waste

INTRODUCTION

"Contaminant Diagnosis" is like that a doctor makes comprehensive judgement about the disease by inquiring, diagnosing and examining his patient, and then prescribes medicine. It also means that the doctor accurately understands the conditions of various complex contaminated sites, selects the optimal remediation method, and helps with the actual remediation measures [1]. The contaminant diagnosis remediation system consists of the contamination chart, the contamination analysis/countermeasure evaluation, the "design of the remediation method," and depending on GIS which one-dimensionally processes the data. The system makes it possible to display on the computer monitor not only a set of measured data and simulated data, but also on-site photographs, descriptive data on the contaminated conditions, and map information. Fig. 1 shows the elements and processes of the system.

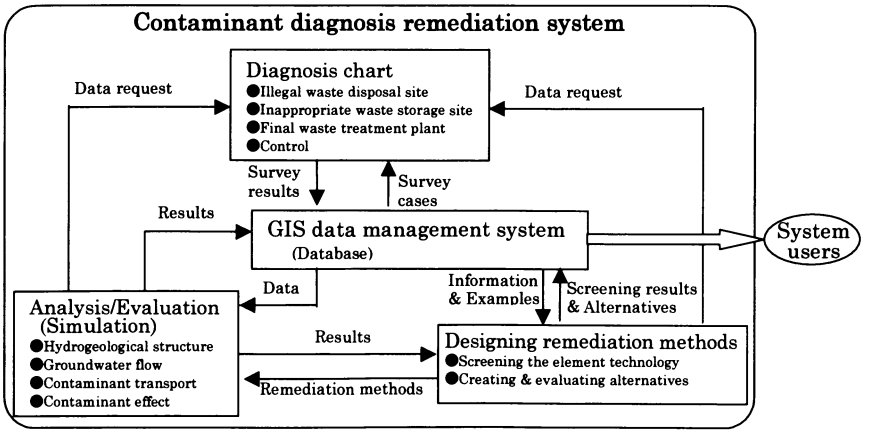

Fig. 1 Elements of the Contaminant Diagnosis Remediation System

OUTLINE OF THE CONTAMINANT DIAGNOSIS REMEDIATION SYSTEM

1. Diagnosis Chart

The diagnosis-chart is a standardized form to filling in the survey purpose, survey items, evaluation items, and survey plans to be carried out in the next phases. The chart serves as a check sheet for the survey, and it makes easier to extract the un-surveyed areas during the drafting stage of the survey plan. Furthermore, by filling in the conditions and characteristics of individual sites, it becomes easier to share information between the people concerned, in the case of a selective survey or a special survey method.

2. GIS Data Management System

The contaminant diagnostic system must handle the multiple information varied with a spatial and time-oriented range. Therefore, the GIS (Geographic Information System) is very effective in managing this kind of information. At the actual contaminated site that is applying the GIS, the preparation process of the pollution data is shown in Fig. 2.

3. Evaluation System

The roles of the evaluation system are to report the current state of contamination, to make predictions from the data accumulated by the GIS data management system, and to analyze and evaluate the effect, cost, and period of remediation in the case of adopting alternative ideas. At the actual contamination site, the following will be carried out: (1) an analysis of the hydrogeological structure, (2) an analysis of the groundwater flow, (3) a prediction of the contaminant transport, and (4) a prediction of the remediation effect.

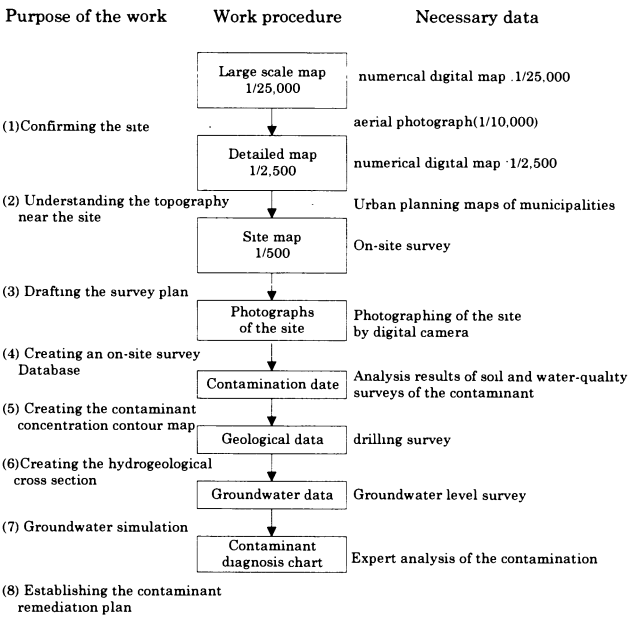

Fig. 2 Procedure of Creating the GIS Data

4. Designing the Remediation Method

To design the remediation method, various technology information and a countermeasure case are extracted with the contamination diagnosis system from the data that is accumulated by the GIS data management system, and suggest a number of combinations (alternatives) of remediation method. Those alternatives are individually evaluated by the simulation of the remediation effect, and provide beneficial information in selecting remediation techniques.

CONCLUDING REMARKS

In this study, the authors reported the outline of the "soil and groundwater contamination diagnosis - a remediation support system." In the future, we plan to aim at the standardization of the system through further improvement.

REFERENCES

1. Furuichi, Tohru, et al. (1997) Proceedings of The 8th Waste Research Conference. pp.941~943.
2. Furuichi, Tohru, et al. (1998) Proceedings of The 6th Sanitary Engineering Symposium.
3. Morishita, Kanetoshi, et al. (1999) Proceedings of The 10th Waste Society Conference.

Interaction Between Surface and Subsurface Water

Temporal Changes of Fluid Balance for Lake Stechlin and its Subsurface Watershed

Ekkehard Holzbecher[1], Gerhard Ginzel[1], Gunnar Nützmann[1]

[1]Inst. of Freshwater Ecology and Inland Fisheries (IGB), Rudower Chaussee 30, 12489 Berlin, Germany

Abstract: Based on observations of long-time series of groundwater and surface water levels in the Lake Stechlin region (Germany) the movement of water divides can be recognized. The watershed of Lake Stechlin changes in response to water table fluctuations in neighboring lakes, revealing the interaction between adjacent watersheds with different sensitivity to climatic variations.

Key Words: Fluid mass balance, Watershed, Groundwater, Water divide, Long timeseries

Lake Stechlin is one of the main research areas of the Institute of Freshwater Ecology and Inland Fisheries, Germany. It is located in north-east Germany, 130 km north of the city of Berlin. Lake Stechlin has no inflow from streams or rivers; it is a groundwater lake, typical for the north-east German landscape. Lake Stechlin and it's watershed is included in UNESCO's IVP-V program in the framework of ecohydrology [1]. More information about the lake can be found at internet address *http://www-3.igb-berlin.de/abt3*.

Lake Stechlin covers an area of 4.25 km^2, has a mean depth of 22 m, a maximum depth of 68.5 m and a volume of $96.88 \cdot 10^6$ m^3 [2]. Lake Stechlin and its surrounding are part of the Northern (Baltic) Land Ridge which was formed in the latest glacial period - the Weichselian. The lakes are fed by groundwater from the unconfined aquifer with a depth of 20 to 40 m [3]. The extent of the groundwater catchment of Lake Stechlin is relatively well known from measurements of the ground- and surface water levels at 50 groundwater observation wells and 16 surface-water observation points. The catchment of Lake Stechlin encompasses a land surface of 12.57 km^2.

Meteorological data have been sampled regularly since 1901. Long-term time series are available from lakes and from various observation wells in the region since 1908. A detailed study on meteorological conditions and its relationship to the water budget for Lake Stechlin and the neigboring Lake Nehmitz was published recently by Richter [4].

Mean annual precipitation in the period from 1958 to 1995 on land and water surfaces in the Stechlin/Nehmitz watershed is 654.3 mm/a. Evaporation and evapotranspiration amount to 549.2 mm/a. The difference of 104.1 mm/a almost equals losses through surface water and to the subsurface; leaving a marginal amount for storage only. The ratio of subsurface drainage to surface drainage is approximately 1 to 4 (calculated from data in [4]).

Mean groundwater discharge into surface water is 594.1 mm/a. Based on the assumption that groundwater storage is negligible a steady-state groundwater model for Lake Stechlin was set up [5,6].

Fig. 1 depicts time series of measured water tables in Lake Stechlin, Lake Glietzen and in groundwater observation wells between the two lakes. Both wells 9 are located not far from the sea-shore of Lake Stechlin, well 8 lies near to Lake Glietzen. Most time of the studied period the highest water level can be observed in Lake Stechlin, lowest in Lake Glietzen with groundwater tables in between. There are few instances in which water in Lake Glietzen rises above the level in the neighbour lake. In some periods the highest level is found in the aquifer.

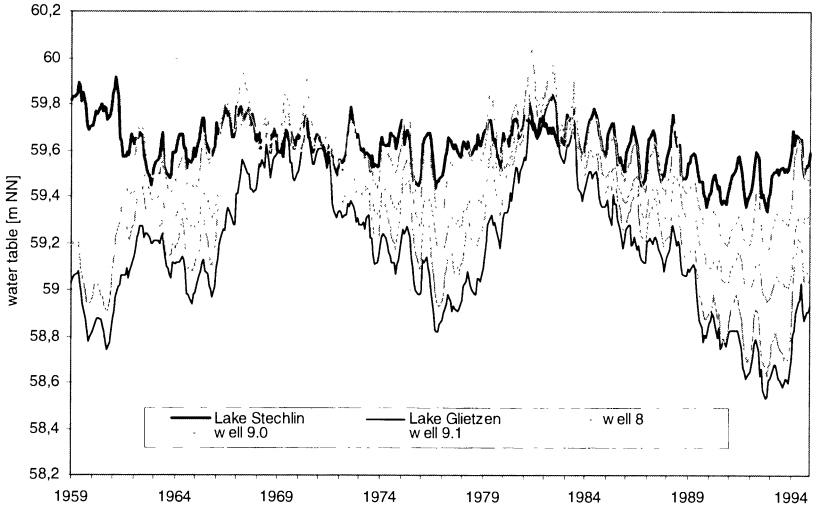

Fig. 1: Time series of water levels in Lakes Stechlin and Glietzen and in wells between both lakes

The time-period from 1959 to 1994 is characterized by two relatively wet periods which alternate with relatively dry periods. The first period is in the late 60s, the second in the early 80s. At the northern shore of Lake Stechlin temporary groundwater discharge can be observed. During the dry periods, which dominate in the observated time range, there is flow from Lake Stechlin into the aquifer and of groundwater into Lake Glietzen. That means that in the fluid balance of Lake Stechlin subsurface losses become more important. During the two wet periods, in the late 60s and early 80s, a water divide built up. Then Lake Stechlin becomes influent along it's entire shore line.

REFERENCES

1. Zalewski M, McClain M (eds) (1998) Ecohydrology - A List of Scientific Activities of IHP-V Projects 2.3/2.4. IHP-V, Techn. Doc. in Hydrology, No.21, UNESCO, Paris: 31

2. Krey L (1985) The lakes of the Lake Stechlin area: aspects of their morphometry. in: Lake Stechlin - a temperate oligotrophic lake (ed. by Casper SJ), Dr W. Junk Publishers, Dordrecht/Boston/Lancaster: 29-40

3. Ginzel G, Handke H (1995) Hydrogeologische Studie zur Abgrenzung des unterirdischen Einzugsgebietes des Stechlin- und Nehmitzsees. IGB, Berlin, (internal paper)

4. Richter D (1997) Das Langzeitverhalten von Niederschlag und Verdunstung und dessen Auswirkungen auf den Wasserhaushalt des Stechlinseegebiets. Berichte des Deutschen Wetterdienstes, Nr. 201, Offenbach am Main

5. Holzbecher E, Ginzel G.(1998) Modeling the Subsurface Watershed of Lake Stechlin. in: 3rd Intern. Conf. on Hydroscience and -Engineering (ed. by Holz KP, Bechteler W, Wang SSY, Kawahara M), Proc., Cottbus:150

6. Holzbecher E, Nützmann G, Ginzel G, Water and Component Mass Balances in the Catchment of Lake Stechlin. in: Integrated Methods in Catchment Hydrology—Tracer, Remote Sensing and New Hydrometric Techniques (ed. by Leibundgut C, McDonell J, Schultz G),. Symp. IUGG 99 (XXII Ass. Int. Union of Geodesy and Geophysics), IAHS Publ. No. 258

The Effect of Soil Excavation on the Water Balance of a Small Lake in Northern Finland

Titta Anttila[1] and Jussi Hooli[2]

[1]PSV-Soil and Water Ltd. P.O. Box, FI-90571 Oulu, Finland
[2]University of Oulu, Water Resources and Environmental Engineering Laboratory, P.O. Box 4300, FI-90401 Oulu, Finland

Abstract. Sand excavation underneath the groundwater table has been planned near the shore of Lake Hämeenjärvi, a small lake located in Northern Finland. In this paper, a well-known groundwater model is applied to assess the effects of the excavation on the water balance and water level of the lake. The model is based on a common mathematical two-dimensional finite element method.

Key words. groundwater, modelling, soil excavation, water balance

INTRODUCTION

Description of the study area. Lake Hämeenjärvi is a small lake about 1 km^2 in area, situated in Northern Finland. Water comes to the lake by direct precipitation and by groundwater seepage from a 1 km^2 large catchment area located on the eastern and south-eastern side of the lake. Outflow from the lake occurs through sandbanks on the northern and western shores.
The sand excavation area is located about 800 m from the eastern shore of the lake. The soil profile at the modelled eastern shore consists of a layer of medium-coarse sand stratified on top of a tight till layer. A sharp till ridge formation runs along the eastern shore of the lake. The sand layer on the peak of the till ridge is about 0.5-1.0 m thick and it grows thicker towards the east where the till layer declines. There is a short depression on the till ridge formation where the water level of the lake lies about 0.8 m higher than the peak of the ridge formation and only the sand layer reaches above the lake's water level.
According to the groundwater observations done in the area, the water divide is located along the peak of the till ridge, which runs about 10 to 30 m from the shoreline. From this narrow strip, groundwater seeps to the lake so that, at present, there is no groundwater flow from the lake eastward towards the excavation area.

Effects of soil excavation. Underwater soil excavation increases the groundwater drainage from the lake towards the excavation area through the depression on the till ridge where only the sand layer reaches above the lake's water level. At the same time, the soil excavation decreases the groundwater flow from the narrow catchment area towards the lake. Both of these factors affect the water balance of the lake by causing the water level to drop.
The water balance of the lake, which is based on flow calculations done by the groundwater model, was used to estimate the largest possible lowering of the lake's water level. To begin with, the groundwater flow conditions on other shore areas were considered to be unaffected by a small drop in the water level. After that, the drawdown of the lake's water level was specified by also taking into consideration the decrease of the outflow through the western bank of the lake.

GROUNDWATER MODEL

Modelling was done using a groundwater model based on a two-dimensional finite element method (ABCFEM, Adrian Brown Consultant Finite Element Method Ground Water Flow and Transport Model, 1994). For the flow calculations the model uses a modified iterative Gauss-Seidel solution technique.

The model was constructed at the eastern shore of the lake on the basis of the soil and groundwater investigations carried out in the area during the period 1970-90. The western border of the model was limited to the shoreline of the lake and to the till ridge formation, which can be considered to be a water divide. The eastern border of the model was extended to a ditch and to another till formation rising above the groundwater table. Southern and western borders were extended sufficiently far from the excavation area so that the effects of the excavation could be assumed to be negligible.

Parameters describing the soil and aquifer were the conductivity of the sand, infiltration caused by rain, storage coefficient and the thickness of the aquifer (sand layer). Either the known water level or non-flow boundary conditions were specified on the borders of the model.

The model was calibrated for both steady state and transient flow. The steady state flow was calibrated by using average groundwater table observations from the years 1986 to 1996 and the transient flow conditions were calibrated by using groundwater table observations from the period of March 30, 1986 to January 20, 1987. The necessary sensitivity analyses were performed on the calibrated model to prove the accuracy.

The final stage of the soil excavation was modelled by defining the conductivity of the soil at the excavation site as being extremely large so that it would not cause any resistance to the groundwater flow. The effects of soil excavation on the lake's water level, as well as the development of these effects, were estimated for steady state and transient flow.

RESULTS AND CONCLUSIONS

When applying the model to the eastern shore of the lake, the largest estimated drawdown of the lake's water level was 13 cm. The greatest effects would occur during the first hundred years after the excavation, although it would take four hundred years until the drop of the water level would come to a standstill. When the decrease of the groundwater flow westwards from the lake was also taken into account, the total lowering of the water level was predicted to be 5 to 6 cm and it would be reached within 30 to 40 years.

The mathematical model applied in this paper was successful in assessing the hydrological effects of soil excavation in a real life situation. As has been proven, reliable boundary conditions were found to solve this difficult practical problem.

REFERENCES

1. Anttila, T. (1998) *The Effect of Soil Excavation on the Water Balance of Lake Hämeenjärvi.* University of Oulu, Faculty of Technology. Master's Thesis. 122 p. English abstract.
2. Vehkaperä, H. (1988) *The Effect of Soil Geological Factors on the Land Management. Example case: The Area of the Lakes Hämeenjärvi and Jäälinjärvi in the Municipalities of Haukipudas and Kiiminki.* University of Oulu, Institute of Geoscience. Philosophy Licentiate Thesis. 90 + 25 p. Finnish original.
3. Hertzman, R. and Brown, A. (1994) *ABCFEM. Adrian Brown Consultants Finite Element Method.* IGWMC. 129 p.

Estimation of Vertical Recharge of Karst Aquifer by Surface Water in Tropical Monsoon Climate

Sahid Susanto
Department of Agricultural Engineering, Faculty of Agricultural Technology, Gadjah Mada University, Yogyakarta, Indonesia

THE MODEL

The vertical recharge was estimated by modified simple monthly water balance model developed by Van Der Beken and Byloos. [1] The model assumes that groundwater quantity balance for a cell of horizontal area bounded by impervious recharge from underflow another basin because that flow is affected by geological formation of the basin. Therefore, this variable is neglected (**Fig.1**). The rest of the catchment is considered to be non-contributory with respect to base flow. This area can be checked by comparing base flow of a given basin with the estimated recharge.

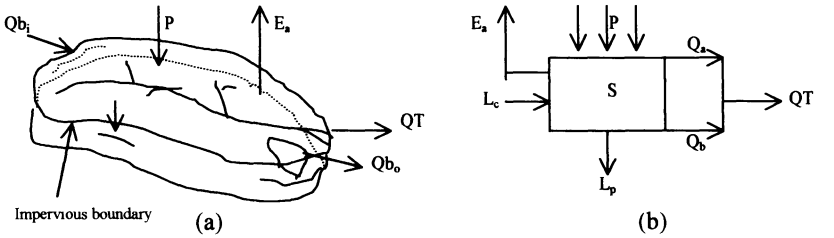

Fig. 1. Structure of the model

P is natural rainfall, E_a is actual evapotranspiration, Q_T is total run-off, Q_o is surface run-off, Q_b is base flow, L_c is seepage from natural canals, L_p is deep percolation, Qb_i and Qb_o is underflow input and output from another basin, respectively, and S is storage.

The governing model equation can be expressed as:

$$\Delta S = N - V_Q - R \quad \ldots\ldots\ldots\ldots\ldots\ldots\ldots\ldots\ldots\ldots\ldots\ldots\ldots\ldots\ldots\ldots\ldots\ldots \quad (1)$$

Δ S is the change in storage S, N is effective rainfall, V_Q is streamflow, R is the net loss as vertical recharge resulting from deep percolation (loss) and seepage (gain), and the time period is 1 month. The effective rainfall is the rainfall minus evapotranspiration.

[1] Singh, V. P., 1989. Hydrologic System, Volume I & II. Prentice Hall. Englewood Cliffs, New Jersey 07632, India, pp. 193-195.

RESULTS

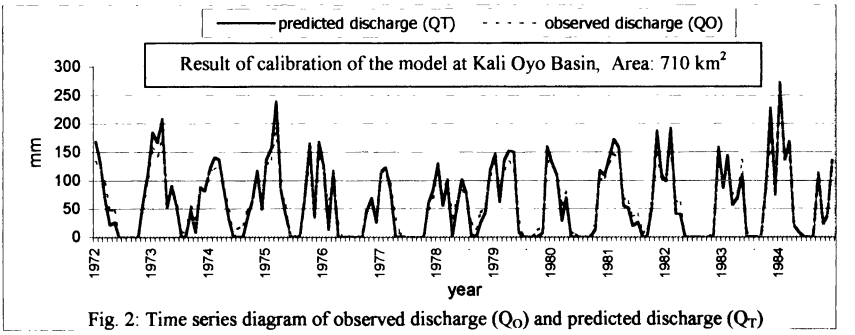

Fig. 2: Time series diagram of observed discharge (Q_O) and predicted discharge (Q_T)

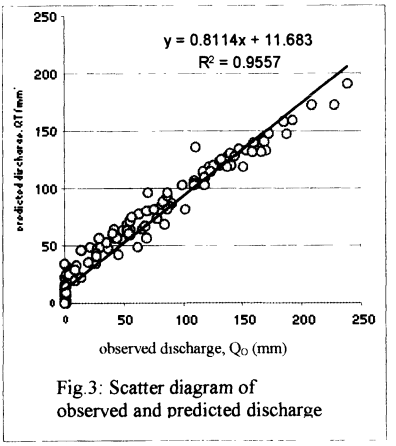

Fig.3: Scatter diagram of observed and predicted discharge

Table 1. Optimal parameter achieved in calibration process

Parameter	Value
Evapotranspiration, a_1	0.01
Storage, a_2	0.0008
Immediate run-off, a_3	0.55
Deep percolation, a_4	0.10
Natural canals, a_5	2.0

Statistical indicators were found from coefficient determination (CD) and standard error (SE), that is 0.906 and 15.971,

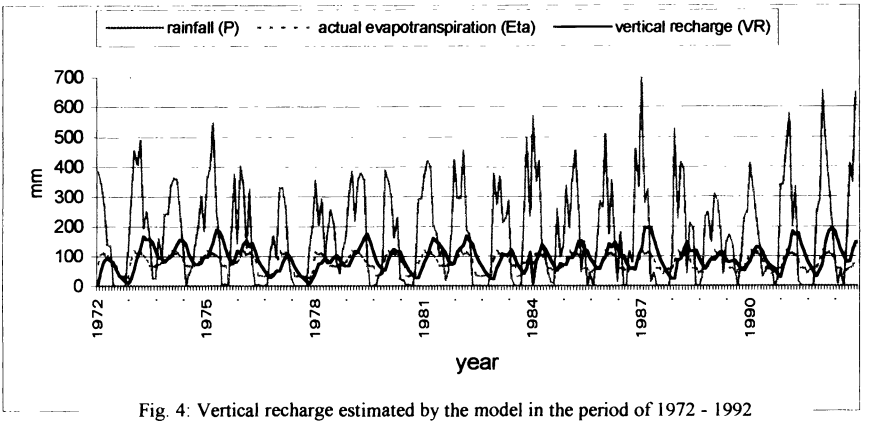

Fig. 4: Vertical recharge estimated by the model in the period of 1972 - 1992

Application of Multi-layer Dewatering and Vertical Recharge System in Dewatering for Underground Works

Nobuaki Kohsaka and Noriharu Miyake

Civil Engineering Research and Development Division
Technical Research Institute, Shimizu Corporation
3-4-17 Etchujima, Koto-Ku, Tokyo 135-8530 Japan

ABSTRACT. When planning dewatering for underground works, it is necessary to adopt the method with a little of economy and impact on the environment. From this point of view, a new dewatering method, which reduces the pumping rate during excavation using special wells, was developed. This multi-layer dewatering method is made up of three technologies, which are as follows:
(1) A multi-layer pumping test to determine the three-dimensional permeability of the ground.
(2) A multi-layer dewatering method, which uses wells of special structure having multiple well screens, reduces the pumping rate required.
(3) A vertical recharge method for injecting groundwater pumped up back into aquifers deeper underground.
These technologies were applied on a construction site where the depth of excavation at the deepest point was 28m. At first, multi-layer pumping tests were performed to evaluate the permeability of the ground. Next, cutoff wall length and a dewatering system were designed applying seepage flow analysis by the finite element method. During the execution of the work, an automatic measuring system was adopted to observe the groundwater head, and control was provided so that drawdown of head would be held to the necessary minimum. Consequently, pumping rate and external discharge rate were greatly reduced, and effective results were obtained from the point of view of economics and reduction of impacts on the environment.

KEY WORDS: underground work, dewatering, pumping test, recharging, deep well

Large-scale underground work shown in Fig.1 with depth of 28m was planned. A thick sand layer having a head of GL -11m was deposited below the excavation bottom. In order to be able to safely proceed with the underground work, the groundwater level of this aquifer should be lowered by 19m.

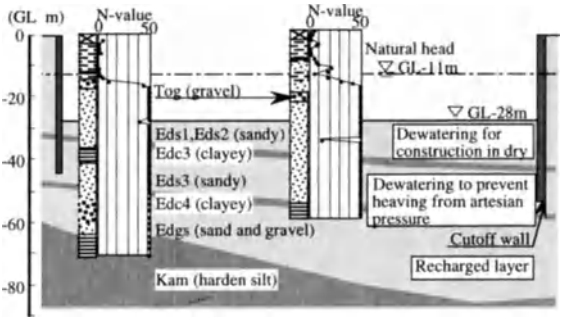

Fig. 1 Outline of the Ground and Underground Works

To determine the three-dimensional permeability of the ground, a multi-layer pumping test was planed. An outline of the testing facilities is shown in Fig. 2. The pumping well had four well screens, and it was possible to pump up from each of the screens independently. The observation holes had several piezometers installed at aquifers corresponding respectively to the well screens of the pumping well.

The structure of the well employed for dewatering of this project is shown in Fig. 3. This well possesses the functions of both a deep well of multi-layer pumping type and a recharging deep well. There are two well screens for pumping, and it is possible to pump water from these screens in the quantity and for the period needed. Further, there is one well screen for recharging water, and groundwater pumped up can be recharged into the ground from this screen.

Fig. 4 (a) shows the results of measuring head variation at observation holes in the excavation area during the period of underground works. At the upper pumping layer, the groundwater level was lowered below the excavation bottom and a dry condition was maintained inside the excavation area. At the lower pumping layer, the artesian head was lowered below the limit value of head set against heaving due to artesian pressure.

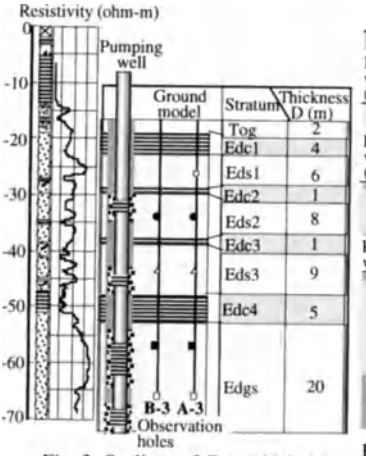

Fig. 2 Outlines of Ground Model and Pumping Test Facility

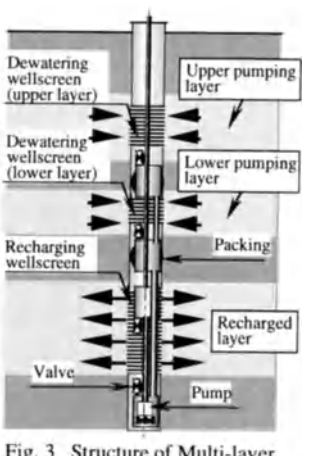

Fig. 3 Structure of Multi-layer Dewatering Type Recharging Deep Well

The operating performance of the recharging deep well is shown in Fig. 4 (b). The head in the upper pumping layer has fallen gradually with the stage of excavation. Since collected groundwater at the upper pumping layer was returned to the recharged layer, the head in the recharged layer has risen higher than the natural head. The head in the recharged layer gradually increased as operation continues. This is because clogging of the recharging well screen due to collection of minute particles. Backwashing was performed whenever clogging had progressed to some extent. The length of time for one backwashing was about 30 minutes. The head in the recharged layer was lowered by backwashing and recharging capacity was recovered.

Consequently, it was succeeded in realizing a dewatering operation, which was ideal from the point of view of economics and, further, impacts on the environment.

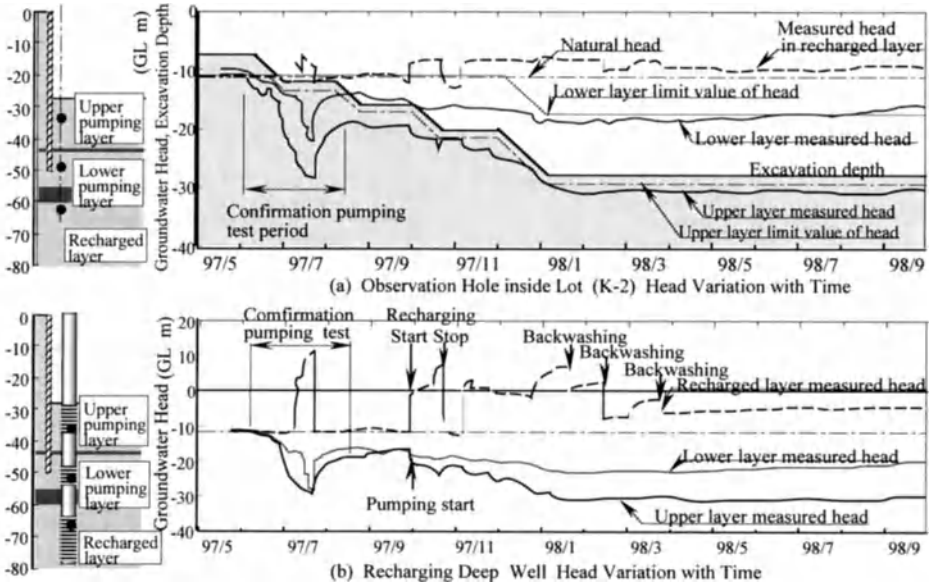

Fig. 4 Variation with Time in Head during Construction

Reliability of Numerical Methods and Scaling in Geohydraulics

Parameter estimation methods to determine hydraulic properties of aquifers using genetic algorithms

Yuji Takeshita[1], Katsutoyo Yasui[2], Hideyasu Uekuma[3] and Akira Nishimura[4]

[1]Faculty of Environmental Science and Technology, Okayama University,Okayama,700-8530,Japan
[2]Shimizu Corporation, Tokyo branch, Minato-ku, Tokyo, 105-0023, Japan
[3]OYO Corporation, Cyugoku branch, Saeki-ku, Hiroshima,731-5124, Japan
[4]OYO Corporation, Tokyo branch, Bunkyo-ku,Tokyo,112-0012, Japan

ABSTRACT. Numerical seepage flow analysis often requires characterization of hydraulic parameters of aquifers. The exact determination of the hydraulic properties of aquifer systems is very important for the correct groundwater flow prediction. A new approach to determination of these properties from pumping test data with the aid of Genetic algorithms (GA) incorporating finite element seepage flow analysis is presented. GA are search algorithms based on the mechanics of natural selection and natural genetics, which combine an artificial survival of the fittest with genetic operators abstracted from nature. The advantages of our method are identifying of the optimal hydraulic properties and geological formations of aquifers. Pumping test data measured actually under the multi-layered conditions are used to verify our proposed method.

KEY WORDS: hydraulic properties, inverse analysis, genetic algorithms, pumping tests

INTRODUCTION

Pumping tests are widely performed to evaluate the hydraulic properties of aquifers. They are usually carried out under the multi-layered aquifer systems. It is, however, difficult to analyze the data obtained from pumping tests under these conditions "analytically". In this study, a numerical code of Genetic algorithms (GA)[1]-based parameter estimation procedure for determining hydraulic parameters of multi-layered aquifer systems is developed. The possible hydraulic conductivity, specific storage and the thickness of each aquifer layer can be found out from immensity parameters by GA. Pumping test data observed in the two layered confined diluvial aquifer system are used to evaluate the efficiency of the proposed method.

STUDY SITE

The study was conducted in the confined diluvial aquifer at Okayama city in Japan. Fig. 1 illustrates the diagram of well construction and geological conditions of the test site. The diluvial sand-gravel (Dg) layers are revealed as a confined aquifer existing in this region. With the vertical profiles of hydraulic conductivity in Dg layer, this aquifer is divided into two layers, Dg1 and Dg2 at the depth of about 17 m from the ground surface. This considered system consists of two aquifers. Each of these layer has its own hydraulic properties, and they are separated by an interface that allows unrestricted crossflow.

PARAMETER ESTIMATION USING GENETIC ALGORITHMS

Five unknown parameters, hydraulic conductivity k_1, k_2, specific storage Ss_1, Ss_2 and the thickness of Dg2 layer are estimated using GA. Drawdown data obtained from our pumping test are simulated by the axisymmetric transient flow through the rigid porous medium. The sums of weighted differences between observed and computed drawdown data are evaluated as the objective function in our method.

By using GA, five unknown parameters are encoded as binary strings. The range of k_1 and k_2 is from 5.0×10^{-4} to 3.4×10^{-1} cm/s respectively. It is divided into 128 possibilities, which can be represented by a 7-bit binary code. The range of Ss_1 and Ss_2 is from 9.0×10^{-8} to 4.5×10^{-4} cm^{-1} respec-

tively. It is divided into 64 possibilities, which can be represented by a 6-bit binary code. The range of thickness of Dg2 layer is from 18.8 to 20.3 m. It is divided into 8 possibilities, which can be represented by a 3-bit binary code. There are about 2^{29} ($=2^7 \times 2^6 \times 2^7 \times 2^6 \times 2^3$) different combinations of unknown parameters. The possible solutions can be searched from the immensity parameters by using GA.

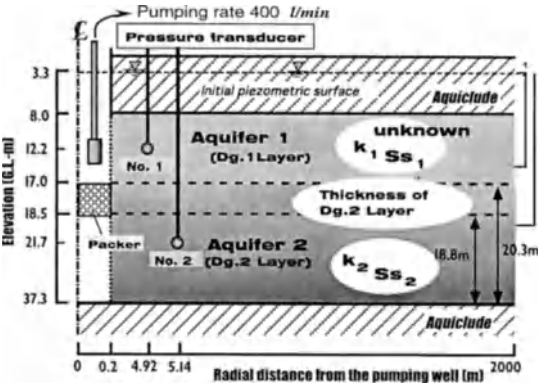

Fig. 1. Schematic diagram of well construction and geological conditions of pumping test.

RESULTS AND DISCUSSION

Transient drawdown data measured in Dg1 and Dg2 layer are used to perform the GA-based parameter estimation procedure. In our GA operations the number of population of 60, crossover probability of 0.6 and mutation probability of 0.1 are defined as the empirical parameters. These parameters may need frequent adjustment to ensure successful and efficient application of the GA. Estimated hydraulic conductivity, specific storage in each aquifer and thickness of Dg.2 are listed in Table 1. Fig. 2 shows the estimated and measured drawdown of our pumping test. As can be seen in this figure, the behavior of computed drawdown was in good agreement with the measured data.

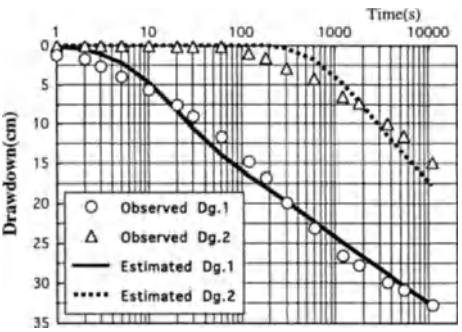

Fig. 2. Estimated and measured drawdown with time.

The results presented in this study confirm the ability of the proposed GA-based parameter estimation method. Hydraulic conductivity, specific storage and thickness of aquifer were estimated simultaneously. Estimated parameters are accurate enough for practical use. The Genetic algorithms is more stable compared to traditional gradient-based methods. This advantage will become more obvious when dealing with a lot of unknown parameters or a highly nonlinear problem such as inverse problems of estimating unsaturated soil hydraulic properties.

Table 1. Estimated aquifer parameters by GA

GA Run	*RMSE* (cm)	k_1 (cm/s)	k_2 (cm/s)	Ss_1 (cm^{-1})	Ss_2 (cm^{-1})	Thickness of Dg.2 (m)
trial 1	1.39	6.6×10^{-2}	7.6×10^{-3}	2.5×10^{-7}	9.5×10^{-5}	20.3
trial 2	1.38	6.6×10^{-2}	7.6×10^{-3}	8.5×10^{-7}	1.0×10^{-4}	20.3
trial 3	1.37	8.2×10^{-2}	8.2×10^{-3}	7.0×10^{-7}	1.0×10^{-4}	20.3

$$RMSE = \left\{ \sum_{j=1}^{N} \left(y_j - Y(b)_j \right)^2 / N \right\}^{1/2}$$

y : observed drawdown data,
$Y(b)$: estimated drawdown data,
N:number of measurements

REFERENCES

1. Goldberg, D. E. (1989) Genetic Algorithms in Search, Optimization, and Machine Learning, Addison-Wesley Pub. Co., 412p.

Integration of well hydraulics formulae considering several conditions of pumping test and/or hydraulic boundaries

Yoshihide SHINSHI[1], Katsusi Nakano[2], Sin-ichiro Mikake[2], Ryuji Takeuchi[2]
[1]Civil Engineering Department, Konoike Construction CO., Ltd., 3-6-1, Kitakyuhoji-machi,Chuo-ku, Osaka, 541-0057, Japan
[2]Geoscience Research Execution Group, Tono Geoscience Center, Japan Nuclear Cycle Development Institute, 959-31, Jorinji, Izumi, Toki, Gifu, 509-5102, Japan

ABSTRACT. Formulae of well hydraulics considering conditions of pumping tests and/or hydraulic boundaries are integrated. The numerical inversion of Laplace transformation is used in order to avoid introducing highly complicated mathematical techniques. Moreover, the classified factors of pumping tests and aquifer conditions can be combined when the formulae are used. The factors are Pumping Style and Well, Influence Radius and Leakage from an adjacent layer. In the first category, Pumping Style and Well, its factors are of constant discharge rate in a pumping well with infinitesimal and finite radius, and constant drawdown in a pumping well with finite radius. In the second category, Influence Radius, its factors are of finite and infinite radius, and constant head and impermeable boundaries on the radius. In the third category, Leakage from an adjacent layer, its factors are of non leakage, non-storage and storage leakage. The calculated variables with the formulae can be selected among drawdown, hydraulic gradient, and also time-derivative of them at an arbitrary observation point. Consequently, there are two main advantages over the integration. One is that the variables for which any model has not been developed can be estimated. The other is that its effortless calculation is handy and useful for automatic analysis of test data.

KEY WORDS: well hydraulics, numeric Laplace inversion, type curves

INTRODUCTION

Data of a pumping test are commonly analyzed with schemes based on classical well hydraulics theories. Although several formulae have been developed for different models, these formulae must be understood by each model and need much effort to calculate their type curves or to read a lot of values on their own tables. Moreover, as for undeveloped mathematical models, the other calculation, that is, an FEM analysis must be performed even for a case under relatively simple conditions. These disadvantages should be improved for analyses of pumping test data because one of the most important objects of the analyses is to identify the investigating aquifer to the mathematical model by means of a trial and error procedure.

In order to resolve these problems, the integration of several formulae of well hydraulics is proposed. The authors focused on the fact that formulae of well hydraulics were developed on the basis of a few governing equations and boundary conditions. The equations and boundary conditions are easily combined on the Laplace transformed field and their solutions on the field are well-known. Conventionally it is extremely difficult to inversely transform the solutions to ones on real time field. The theory of numeric Laplace inversion, however, made the work easy. The scheme based on the theory expects several advantages of calculating formulae. The first advantage is to improve speed of the calculation. The second is to systematically combine conditions of pumping well, aquifer and aquitard.

MATHEMATICAL MODELS of WELL HYDRAULICS

A schematic illustration of a mathematical model is given on Fig. 1. Pumping well is fully penetrated into a confined aquifer. The thickness of the aquifer is the same at arbitrary location. An aquitard is overlaid the aquifer. The governing equations are referred to Hantush's work [1]. The set of the equations expresses the hydraulics of a fully penetrated well in non-leaky and/or leaky aquifer.

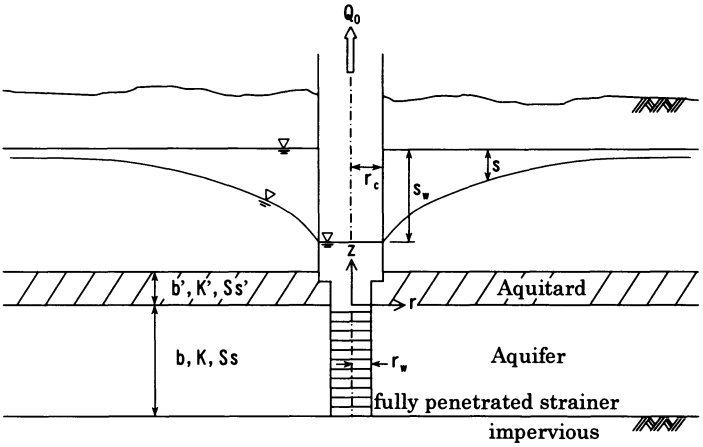

Fig. 1 Schematic model of Well and Formations

In order to solve the set of equations, boundary conditions are introduced. The conditions is classified into the following categories.

Category 1: Pumping Style and Well
- (1) Constant discharge rate in pumping well with finitesimal radius.
- (2) Constant discharge rate in pumping well with finite radius.
- (3) Constant drawdown in pumping well with finite radius.

Category 2: Influence Radius
- (1) Constant head at infinite radius.
- (2) No-flow at infinite radius.
- (3) Constant head at finite radius, R.
- (4) No-flow at finite radius, R.

Category 3: Leakage from an adjacent aquitard
- (1) non leakage
- (2) leakage without storage with constant head at the upper of the aquitard
- (3) leakage with storage with constant head at the upper of the aquitard
- (4) leakage with storage with no-flow at the upper of the aquitard

The term of time is reduced from the governing equations and boundary conditions with Laplace transformation[2]. The general solution of the governing equations is specified by introducing boundary conditions. After that, the specified solutions are changed to a real time field with a numerical inversion scheme of Laplace transformation[3,4].

REFERENCES

1. Hantush, M.S.(1964), Hydrailics of Wells, Advances in Hydroscience, edited by V.T.Chow, Academic Press, Vol.1, 281-432.
2. Churchill, R.V.(1958), Operational Mathematics, McGraw-Hill Publishing Company.
3. Crump, K.S.(1976), Numerical Inversion of Laplace Transforms Using a Fourier Series Approximation, J of the Association for Computing Machinery, 23(1), 89-96.
4. de Hoog, F.R., J.H.Knight, A.N.Stokes(1982), An improved method for numerical inversion of Laplace transform, J.Sci.Stat.Comput., 3(3), Sept.. 357-366.

Arsenic Problem in Groundwater, a Growing Threat to Public Health in Bangladesh : An Overall Perspective and Management Modelling Approach

Afzal Hossain, M Fazle Rabbi, Abdur Rahman Abid, Sabina Sadek

Surface Water Modelling Centre (SWMC), House # 476, Road # 32, New DOHS, Mohakhali, Dhaka – 1206, Bangladesh

INTRODUCTION: The groundwater in Bangladesh is contaminated with high Arsenic concentrations. SWMC has undertaken a pilot research study to (1) understand the occurrences of Arsenic in groundwater through data collection and analysis (2) develop mathematical model for groundwater flow movement, solute transport, and geo chemical model with specific reference to Arsenic and (3) establish a strategy for proper watershed management as long-term mitigation measures. An area of 570 sq km in the districts of Narayanganj-Narsingdi has been selected as a pilot study area (Figure 1)

METHODOLOGY: For the present study a physically based mathematical model has been developed to simulate flow movement processes, interaction between surface and groundwater, pollutant transport and geochemical processes.

Data collection and processing: A huge amount of data and information are collected from several organizations in Bangladesh and processed. This data with due quality control procedure fulfil the data requirement of MIKE SHE [1] model. The Arsenic data were collected in three phases: reconnaissance; detailed survey of one administrative union; and systematic sampling constructing a gridded network.

Detailed Survey in Aminpur Union: Efforts were made to cover all the Hand Tube Wells (HTW) in Aminpur union, the most affected area. A total of 227 water samples were collected and analysed using field kit. The result confirms that the occurrence of Arsenic is isolated in nature. Two tubewells having similar depth and located within a distance of 20 meters shows one affected and the other unaffected. No correlation exists between the Arsenic concentrations and the depth. However, depth of the affected tubewells varies from 20 to 60 meters from the ground surface.

Survey under Gridded Network: A 4 kmX4 km gridded network was established. In total 29 water samples were collected in November 1997 from each grid-corner and analysed for Arsenic from the BUET laboratory. The coordinate was recorded by GPS for each of the tubewells.

Continued Field Monitoring: Two HTWs have been selected for creating a time series database. One is very near to Meghna river and other is in the Aminpur Union. Table 1shows the results.

Table 1. Time Series Data of Arsenic Concentration for Two Locations

	Oct' 97		Nov' 97		Jan' 98		Mar' 98		Jun' 98		Oct' 98		June'99	
Parameter	P43	67	P43	67	P43	67	P43	67	P43	67	P43	67	P43	67
Arsenic, mg/1	0.171	0.092	0.225	0.098	0.167	0.041	0.043	0.10	0.019	0.04	0.041	0.084	*No Trace*	.0215
PH							6.70	6.50	6.76	7.02	6.0	6.1	6.7	6.8
Iron, mg/1							7.19	3.96	20.0	8.0	18.0	4.0	30.0	8.0
$CO_{2,\ mg/1}$							50.0	95.0	68.0	61.0	94.0	56.0	115	59
$SO_{4,\ mg/1}$							36.8	16.9	18.0	28.0	0.6	24.3	1.5	22.0

MODEL DEVELOPMENT

Groundwater Management Modelling : A MIKE SHE based groundwater model has been developed to describe all the important flow processes in the hydrological system.

Fig. 1. Base Map Showing Borelog Location

Calibration of the Model: The model was calibrated against the potential head data for the six locations. The calibration plot of two locations is shown in Figure 2.

Solute Transport Modelling : As the release and migration mechanisms of Arsenic are unknown sorption-degradation module has not been applied in the current set-up. A simple conservative solute transport modelling was set-up for the current study. Three locations where the measured concentrations of Arsenic found high were assumed as point sources. The sources were placed in the upper calculation layer

A 20-year simulation result indicated faster migration of Arsenic in the downward direction compared to horizontal direction. This might be due to uniform distribution of the abstraction wells within each thana in the dry season, while the infiltration imposes during monsoon. Figure 3 shows long-term Arsenic migration across the depth of the aquifer.

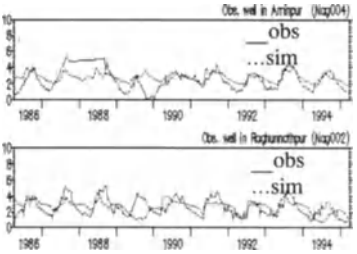

Fig. 2. Model calibration with

CONCLUSIONS: It is too early to make any conclusions on the overall objectives of the study. However, based on the findings so far received the following comments can be made[2]: (1) surface water is free from high Arsenic concentrations, (2) occurrence of high Arsenic concentrations in groundwater is a local phenomenon, (3) high concentrations are found in clay and fine sand, (4) no definite correlation exists between the water sample depth and Arsenic concentration, (5) high Arsenic may have some relation with high iron and low pH value and (6) migration process seems very slow,

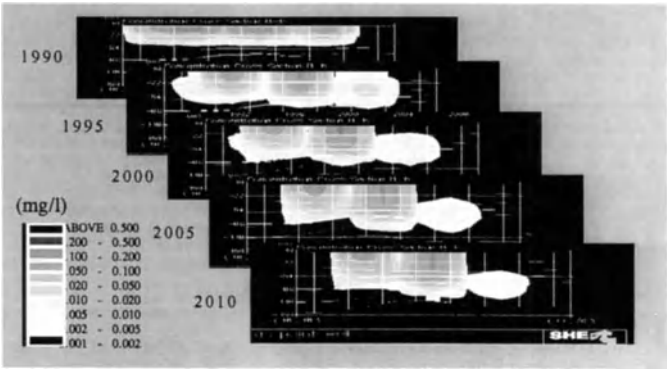

Fig. 3. Long Term Migration of Arsenic

REFERENCE

1. DHI, (1993): MIKE SHE WM Technical Reference Manual.
2. SWMC, DHI, VKI, BUET, (April, 1998): Arsenic management Modelling (A Pilot Study in Narayanganj-Narsingdi Area)

Special Topics

Modeling of Flow and Transport Processes in the Subsurface

Convener: R. Helmig [1]
Speakers: R.E. Ewing[2], S. Finsterle[3], R. Hinkelmann[1]

[1]Institut für ComputerAnwendungen im Bauingenieurwesen, Technische Universität Braunschweig, Pockelsstr. 3, 38106 Braunschweig, Germany, email: (r.helmig, r.hinkelmann)@tu-bs.de
[2] Texas A & M University, College of Science, 517 John R. Blocker Building, College Station, Texas 77843-3257, email: richard-ewing@tamu.edu
[3] Lawrence Berkeley National Laboratory, Earth Sciences Division, One Cyclotron Road, Mail Stop 90–1116, Berkeley, California 94720, email: SAFinsterle@lbl.gov

R. Helmig: Comprehensive Methods and Modeling Techniques for Subsurface Systems

During the last years, the development of numerical methods and modeling techniques for the simulation of flow and transport processes in subsurface hydrosystems has emerged to a powerfull tool in the prediction of human impacts on nature regarding the changes in flow conditions, water budget, as well as water quality. But it is important to note that the state of the art as well as the spatial and temporal application ranges significantly vary for different processes. Single–phase flow and transport processes are comparatively well–understood, and a number of different suitable numerical simulators are available. As a consequence, such applications are carried out up to the regional scale and have belonged to the engineering practice for years. With a number of restrictions, this is also the case for density–driven flows which are caused by e.g. salt–water.

Multiphase flow processes as well as isothermal or non–isothermal multiphase / multicomponent flow and transport processes are only partially well–understood. One major problem is the effect that the fluid properties, e.g. density or viscosity, vary in interaction with porous media properties. Another difficulty results from the limited validity of certain model assumptions for determining constitutive relationships, e.g. for the relative permeability and the capillary pressure as a function of the saturation. As better information is lacking, such models are used for problem fields where their validity is not ensured. Moreover, special effects, like hystereses, which require additional model concepts, may occur. The problems described above lead to possibly highly non–linear partial differential equations which require special problem–dependent methods and modeling techniques for their solution. As the computational effort can be huge, highly–developed solvers based on parallel adaptive multigrid methods should be applied. Due to the very complex processes in multiphase flow, only a few numerical simulators exist. Generally, the application field ranges from the small to the technical scale. There are only very few large / regional scale simulations.

As an example, methods and modeling techniques which were developed to optimize remediation measures, especially thermal enhanced NAPL recovery, are discussed. The processes are described by a non–isothermal three–phase / three–component model concept. Special attention is given to an algorithm for substituting variables in order to adapt to the disappearance and appearance of phases.

Scaling effects, multiphase inverse modeling, and recent application fields of gas–water flow point out some challenging research topics and show evolving areas in modeling flow and transport processes in the subsurface. Consequently, they are addressed in this technical workshop.

R.E. Ewing: Scaling Effects in the Subsurface

The processes of both single and multiphase flow involve convection, or physical transport, of the fluids through a heterogeneous porous medium. The equations used to simulate this flow at a macroscopic level are variations of Darcy's law. Darcy's law has been derived for both single and multiphase regimes via a volume averaging of the Navier-Stokes equations, which govern flow through the porous medium at a microscopic or pore-volume level. The length scale for Navier-Stokes flow ($10^{-4} - 10^{-3}$ meters) is quite different from the scale required by field-scale simulations ($10 - 10^3$ meters). Reservoirs themselves have scales of heterogeneity ranging from pore-level to field scale. In the standard averaging process for Darcy's law, many important physical phenomena which may eventually govern the macroscopic flow may be lost. The continued averaging of reservoir and fluid properties necessary to use grid blocks of the size of $10–10^2$ meters in field-scale simulators further complicates the modeling process. We consider techniques to address these scaling problems.

The understanding and prediction of the behavior of the flow of multiphase or multicomponent fluids through porous media are often strongly influenced by the heterogeneities in the media, either large-scale lithological discontinuities or quite localized phenomena. Considerable information can be gained about the physics of multiphase flow of fluids through porous media via laboratory experiments and pore-scale models; however, the length scales of these data are quite different from those required from field-scale simulations. The coupled fluid-fluid interactions are highly nonlinear and quite complex. The presence of heterogeneities in the medium greatly complicates this flow. We must use the simulators as "experimental tools" in the laboratory of high performance computing to simulate the process on increasingly larger length scales to develop intuition on how to model the effects of heterogeneities at various levels.

Diffusion and dispersion are often critical to the flow processes and must be understood and modeled. Molecular diffusion is typically fairly small. However, dispersion, or the mechanical mixing caused by velocity variations and flow through heterogeneous rock, can be extremely important and should be incorporated in some way in our models. Macrodisperson concepts try to incorporate the effects of heterogeneities at various length scales.

Numerical results have illustrated the success of dispersion models for many of these problems. However, in reservoirs where there is a higher degree of correlation in the permeability fields, there is a type of channeling of flow that is non-Fickian and may have important history effects in the flow. Several authors have developed a theory of anomalous diffusion and macrodispersion that has enormous potential in understanding the scale-up problem. They found a non-Fickian behavior. In order to try to use existing simulators – that model diffusion as Fickian, we have tried to address the channeling effects of correlated heterogeneities via an effective permeability developed by a multi-level scaling process where at each step the information that is correlated at that scale is homogenized to obtain an effective permeability and the uncorrelated information is modeled with a diffusion/dispersion term. By upscaling in many steps of increasingly larger length scales,

we hope to incorpoarate the channeling effects via the permeability tensor. Alternately, we are developing models that incorporate a temporal history of the flow via integral terms.

The simulation of processes such as bioremediation and chemically reacting flows involves the use of nonlinear reaction terms. The form of the reaction kinetics must be determined from laboratory tests at laboratory length scales. Scaling these nonlinear reaction terms is very different and may require a new form of reaction kinetics to model the process at the field scale.

S: Finsterle: Multiphase Inverse Modeling – Possibilities and Limitations

Multiphase flow and transport simulators are continually being improved in terms of their physical process description, computational speed, accuracy, and robustness of the numerical solution. Despite these advances, model calculations frequently fail to predict the actual system behavior. One source of prediction error is the use of inappropriate input parameters, which include hydrologic and geochemical properties as well as initial and boundary conditions. While some of these input parameters can be determined in the laboratory or inferred from the analysis of field tests, most of the many parameter values required for a simulation of multiphase flow processes are difficult to measure or estimate. Moreover, these measured parameters may represent a local property in a heterogeneous system and are thus conceptually different from the values required by a numerical model, which often requires effective large-scale parameters.

We developed inverse modeling capabilities for a general-purpose multiphase flow simulator to be able to determine input parameters by automatically calibrating the model against laboratory and field data. The parameters estimated by inverse modeling are related to the scale, physical process, and parameterization of the numerical model. This is an important advantage of inverse modeling over other parameter estimation techniques. On the other hand, this strong connection to a specific model is sometimes regarded as a disadvantage because parameters cannot be simply transferred to other models.

Automatic model calibration has been applied to a variety of unsaturated and multiphase flow problems. We present illustrative examples, in which we highlight the power and usefulness of a formalized inverse modeling approach. We demonstrate that prediction reliability increases when using parameters that are determined from process-related data rather than apparently independent information. We also examine the benefits from performing detailed residual and error analyses, which enable detection of flaws in either the model or the data, thus pointing toward aspects of the conceptual model or the experimental setup that need to be refined. At the same time, we discuss potential caveats and limitations, specifically the fact that errors in the model structure lead to a bias in the estimated parameters.

Inverse modeling relates the numerical model to the real hydrogeologic system and, as such, is an undertaking of great theoretical importance and practical relevance. For more information on multiphase inverse modeling, visit http://www-esd.lbl.gov/iTOUGH2.

This work was supported, in part, by the U.S. Department of Energy under Contract No. DE-AC03-76SF00098.

R. Hinkelmann:
Recent Application Fields of Gas–Water Flow in the Subsurface

In recent years, several new application fields for the numerical simulation of gas–water flow processes in the subsurface systems have emerged. Three of them are addressed in this lecture. First, the problem fields are explained, and thus the research work is motivated.

- In coal mining areas, methane is degasing out of coal and migrating through the saturated and the unsaturated zone of the subsurface to the surface of the earth. At several locations, the methane fluxes are so high that they cause danger for human life as well as restrictions for the use of buildings.
- In coastal areas, most of the dikes which serve as flood defense structures are made of layered material, especially soils. As a consequence of increasing height and frequency of storm surge levels, the probability of overtopping dikes increases, too. Overtopping evokes complex gas-water flow processes inside the flood defense structure, enhances the stress, and thus has a significant influence on the stability of such systems.
- At several locations in coastal zones of the Baltic and North Sea, field measurements have detected submarine groundwater and methane fluxes into the surface water. This phenomenon together with the transport of contaminants involved has a considerably larger influence on the surface water quality than it has been expected up to now.

The flow and transport processes described above require different model concepts for the numerical simulation in heterogeneous porous media. If dissolution processes can be neglected, a two–phase flow model concept, consisting of a water phase and gas phase (e.g. methane, air) is applied. If additional component transport processes must be considered, a two–phase / multicomponent model concept (phases: water, gas; components: water, methane, air, salt, contaminants ...) is used. Both model concepts are part of the modular program system MUFTE_UG which allows for the simulation of multiphase / multicomponent flow and transport (including energy) processes in heterogeneous porous media. Different numerical schemes, e.g. finite–element and finite–volume based methods, are available for the discretization of the governing equations. The arising linear and non–linear algebraic equations are solved with multigrid methods including parallel and adaptive techniques.

Finally, the applications are presented together with an outlook on future work:

- A two–phase (water, methane) flow model was chosen for the degasing methane problem. As the geological structures have considerable influence, sensitivity analyses have been carried out using simple systems to identify dominant parameters and processes depending on the geological structures. For this, the influence of heterogeneities and fault zones on vertical methane flows has been investigated. A model calibration for a real field case is envisaged.
- For the overtopping dikes, a two–phase (water, air) flow model was used. The complex forms of the gas–water interface caused by infiltrating water, entrapped air, and the water table have been analysed and will be compared with experiments in the near future.
- For the submarine groundwater and methane fluxes, a two–phase / three–component (phases: water, gas; components: water, salt, methane) was applied. Density–driven flow caused by salinity was taken into account. The phase switch of methane from dissolution into the gas phase is of special interest in the simulations which are partially compared with small scale measurements. Future work will deal with larger scales or reaction processes of methane.

INTERACTION BETWEEN THE GROUNDWATER AND GEOMECHANICS

Convener : Ichiro KOHNO[1]
Speakers : Frans B J BARENDS[2], Ashim Das GUPTA[3], Makoto NISHIGAKI[4]

[1]The President of Okayama University, Tsushimanaka 3-1-1 Okayama 700-8530, JAPAN, e-mail: gel94@cc.okayama-u.ac.jp
[2]GeoDelft, PO Box 69, 2600 AB Delft, the NETHERLANDS, e-mail: f.b.j.barends@geodelft.nl
[3]Water Engineering and Management Program, School of Civil Engineering, Asian Institute of Technology, PO [3]Box 4, Klong Luang, Phathumthani 12120, THAILAND, e-mail: adg@ait.ac.th
[4]Department of Environmental Design and Civil Engineering, Okayama University, Tsushimanaka 3-1-1 Okayama 700-8530, JAPAN, e-mail: n_makoto@cc.okayama-u.ac.jp

I. KOHNO:
Interaction between Groundwater and Geomechanics

Water is one of important sources of life for mankind and other living creatures on earth. The life on earth depends upon both quantity and quality of groundwater. According to figures recently issued by the World Health Organization, one people die about every two seconds from diseases associated with bad water. In every minute, three people will die because they do not have ready access to a safe and reliable supply of drinking water. The figures are a grim reminder of how much we need water and how important the quality of water for human life.

The present of groundwater can also introduce a geomechanical problem on earth structures. The groundwater can affect the strength and stability of the ground. In the country like the Netherlands, most of areas are under water level and the earth structures like embankments have been built to protect the areas against flooding. However, the problem with the instability of embankment has been very often encountered due to the rising water level. The country with high rainfall intensity and steep slopes also often faces a problem with failure of natural slopes during rainy season. The occurrence of slope failures has claimed untold number of human lives and million dollars of property losses.

The extent to which the groundwater causes instability is dependent on the pore-water pressure. In soil mechanics, pore-water pressure affects effective stress on soil framework. If pore-water pressures are increased in response to the rise in water level, then effective stress will be reduced. This means soil particles will lose grain-to-grain contact. If pore-water pressures were increased to a point beyond which there would no longer be any grain-to-grain contact, the soil would be cause to liquefy. Even if the effective stress is not reduced to zero, the reduction of soil shear strength caused by the increase in pore-water pressure can also results in the occurrence of slope failures.

The rapid growth of population in many countries around the world has been accompanied by increase in water usage. In order to meet the demand for water, pumping is a very common method for extracting water from the aquifer. However, excessive pumping from a confined aquifer at the rate much greater than natural replenishment can lead to contraction of the aquifer and corresponding subsidence of the land surface. In soil mechanics point of view, lowering water level will reduce pore-water pressures, or increase effective stresses of soil particles, which can cause the aquifer to be compacted, leading to land subsidence. The occurrence of land subsidence can cause a considerable damage to building. Notable examples of such subsidence have occurred in around Mexico City and Bangkok Metropolitan areas.

The above discussion has shown briefly the interaction between groundwater and geomechanics, and the geomechanical problems due to the action of groundwater require remedial measures. This technical workshop will present some challenging research topics related to interaction between groundwater and geomechanics. A probabilistic approach to assess groundwater effect on defense structures on coast and low land, integrated management approach for water supply in metropolitan areas and environmental preservation towards subsurface construction will be addressed and discussed thoroughly.

F. B. J. BARENDS:

Geohydrodynamic Engineering in Sustainable Protection of Coast and Low Land; Dutch Experience

The last millennium the Netherlands was created by cultivation of the land, by protection against floods from sea and rivers and permanent water drainage from low land and polder areas. Large cities developed, including an intricate infrastructure of roads, waterways and pipelines for sewerage, gas, water and underground transport. The main ports for shipping in Rotterdam and air transport in Amsterdam are a cradle for industry and commerce. The protections of commercial and social values in the low land demand a continuous engineering effort.

Kilometers of sea dikes, river dikes and canal embankments, numerous sluices, bridges, harbors, tunnels, dams and closures and sophisticated monitoring and control systems from the backbone of the low land protection. Engineering skill developed during centuries within a special legislative, social and political frame. The expertise has settled in a vast range of laws, guidelines, handbooks and codes.

At present, new developments are required meeting the demands of the society of today. Demands related to multiple functioning and integral values. Moreover, the expectation of climate changes in terms of sea level rise and profound river discharges rings the bell for risk engineering in design and maintenance of water defense structures.

The lecture will focus on this development with the emphasis on white spot in our knowledge and related research topics, particularly the probabilistic approach and the way to involve time through groundwater effects, which happens to play a dominant role.

A. Das GUPTA:

Ground Settlement due to Pumping

Settlement of the land surface, also known as land subsidence, is an important environmental consequence of groundwater overdraft. It is caused by the consolidation of the soil deposits due to the lowering of the groundwater level or the potentiometric pressure. For confined aquifers, the increase in effective stress is due to the reductions in upward hydraulic pressure against the bottom of the upper confining layer caused by the drop in the potentiometric head. In a multi-layer system, this drop in potentiometric head induces release of water from the confining layers whereby confining layers get compressed. For unconfined aquifers, the increase in inter-granular pressure is due to the loss of buoyancy of solid particles in the zone de-watered by the falling water table. In addition, initiation or acceleration of lateral flow of groundwater can cause lateral compression of the aquifer and hence, lateral movement of the land surface, due to an increase in the seepage force or frictional drag exerted by the flowing water on the solid particles. Most of the major subsidence areas around the world have developed in the past 50 years or so and many of them are still experiencing continual settlement due to increasing use of groundwater. As an example of recent time, large-scale groundwater utilization in the city of Bangkok, Thailand resulted in adverse economic-cum-environmental problems such as continual decline of potentiometric levels, land subsidence and groundwater quality deterioration by salt-water encroachment. Many associated and potential problems like flooding, loss of property and human lives, severe deterioration of infrastructure facilities, groundwater pollution, and health hazards have been attributed to the effect of excessive groundwater withdrawal and land subsidence.

An assessment of the geologic and the hydrogeologic settings; yield, storage and the transmissive characteristics of the water bearing strata; consolidation characteristics of formation materials, and the recharge and pumping pattern of the system is necessary for the evaluation and prediction of land subsidence resulting from the abstraction of groundwater through pumping wells. The alleviation of environmental consequences of land settlement would require curtailment of groundwater pumping which implies a subsequent need of supplemental water supply from surface source. As well as a built up of the potentiometric pressure level could be initiated through artificial recharge for which a proper source of additional water of required quality is necessary. A successful implementation of these remedial measures requires societal realizations of the consequences of continual groundwater overdraft and their coordination and cooperation, and the most importantly, the institutional commitment towards required actions.

In the light of the above discussion, the intention of this paper is to present the outcome of several studies and investigations conducted over the last two decades addressing the issues of groundwater development and land subsidence in the Bangkok Metropolitan area. Possibility of artificially recharging the aquifer has been investigated through a small-scale recharge experiment and its applicability for a large-scale recharging of the deep aquifer system in the Bangkok area has been considered. A discussion on the effectiveness of the mitigation measures on groundwater pumping through litigation and water charging system is provided.

Since groundwater utilization will continue in the future, there is an urgent need to identify some critical gaps in our past efforts towards groundwater management if we want to avoid or significantly reduce the serious consequences, while continuing to bear the fruits of the resource use on a sustained basis over a long period of time. The Paper, therefore, concludes identifying some important planning and management issues, and emphasizing on an integrated management approach for the water supply of the City of Bangkok and its vicinity.

M. NISHIGAKI:

Subterranean and Subsurface Environmental Conservation

Recently, rapid development in the Metropolitan City or densely populated area has not been supported by the availability of land. This problem has motivated engineers and decision-makers to utilize the underground space for meeting the demand for engineering constructions, such as nuclear disposal refractory, natural gas storage, underground highway/ railway, etc.

The use of underground space had given some significant consequences to mankind. However, many potential and associated environmental consequences of the underground construction had not been thoroughly examined prior to the construction.

This Paper will discuss the methods of preservation of the subsurface environmental conditions under the subterranean utilization. The method for maintaining the original movement of groundwater, which is disturbed/ altered by the constructions, is especially explained in practical point of view. A discussion on the field and laboratory methods to investigate the characteristics of the underground formations and multi-layered aquifers and the methods to design the preservation facilities of the groundwater flow are provided. The methods to maintain the faculty of the facilities and to prevent the screen, the filter as well as the fine sandy aquifer from clogging are also emphasized. Finally, the more active utilization in the subsurface region is proposed by considering the artificial system for controlling the groundwater level using the underground structures. This control system can prevent the liquefaction disaster during earthquake and remediate the contaminated aquifers in long term.

Groundwater flow and subsurface thermal regime

Yasuo Sakura[1], Makoto Taniguchi[2], Cristoph Clauser[3] and Wang Ji-yang[4]

[1]Department of Earth Sciences, Chiba University, Chiba 263-8522, Japan
[2]Department of Earth Sciences, Nara University of Education, Nara 630-8528, Japan
[3]Geothermics and Groundwater Dynamics Joint Research Institute (GGA) Stilleweg 2, D-30655 Hannover, Germany
[4]Institute of Geology and Geophysics, Chinese Academy of Science, Beijing 100029, China

Abstract. It is generally recognized that the temperature profile in a borehole is influenced by both groundwater flow and past climatic change. Geophysicists seek to remove such effects from a temperature profile for the corrections of heat flow values. It is also well known by hydrogeologists that the distribution of subsurface temperature is affected by groundwater flow and that temperature data can be used to estimate the direction and velocity of groundwater flow. Until present, there are few studies dealing simultaneously with both effects. This workshop provides a review of the literature dealing with the effects of groundwater flow and past climatic change on the subsurface thermal regime. Then, temperature profiles and the distribution of temperature inversions in Japan, Germany and China are analyzed and presented as examples showing both effects as well as the effects of surface warming owing to urbanization.

Key words: borehole temperature, groundwater flow, climate change, heat transfer

INTRODUCTION

Generally, the normal geothermal gradient of the subsurface thermal regime is affected by groundwater flow and changes in surface temperature. A theoretical analysis of temperature field distortion by topographically driven groundwater flow was presented by [1] as shown in Fig. 1. Their results show that groundwater temperature increases with depth under the influence of both heat conduction and advection. At the same altitude, subsurface temperature in the recharge area is lower when groundwater flow is included than under no flow conditions. In the discharge area, temperature is higher with groundwater flow than under no flow conditions. Thereafter, Fig. 1c and 1d provide a conceptual and theoretical framework for an analyzing subsurface temperature distribution in a groundwater basin.

The effects of past climatic changes on subsurface temperatures have been recognized for a long time. The effect of the Pleistocene ice-age, which lasted for several hundred thousand years, is usually assumed to extend to a few thousand meters below land surface, while the effect of climatic changes in the last thousand years extend to 500 m. The effects of seasonal fluctuations extend to a few tens of meters and the effect of

daily changes extend to a few meters. The most recent major climatic change, i.e., the rapid warming for the last 100 years, has caused a temperature inversion in many parts of North America, Europe and Australia at a depth of 50 to 100 m, depending on the thermal properties of the rock [2,3]. In this paper, the depth below which the effects of seasonal temperature change are negligible is called the isothermal layer.

In analyzing temperature profiles to depths of a few hundred meters, it is necessary to take account of two effects, namely topographically driven groundwater flow and surface warming. Furthermore, transient effects caused by pumping and natural hydrologic events also should be considered. In this workshop, we present a summary of recent work and field observations on the effects of groundwater flow and surface warming in the subsurface thermal regime

EFFECTS OF GROUNDWATER FLOW

A numerical model of heat transfer combined with groundwater flow was introduced and simulated the groundwater flow and thermal regime in northern Ontario, Canada [4]. The theoretical relationship between heat transfer and regional groundwater flow using analytical techniques assuming steady-state two-dimensional flow was presented by [1]. These early studies documented the importance of groundwater flow on the thermal regime. The International Union of Geodesy and Geophysics Symposium " Hydrogeological Regimes and Their Subsurface Thermal Effects" was held in August 1987 at General Assembly in Vancouver, British Columbia [5]. Papers from this symposium showed that subsurface temperatures within a depth of several thousand meters were affected by deep groundwater circulation. Moreover, temperature and surface heat flow are relatively high in the structural center of basins, grabens and plains, e.g. in the Unita Basin, Colorado, USA [6], in the Rheingraben, Germany [7,8], in crystalline basement, northern part of Switzerland [9], in the sedimentary basin, Czechoslovakia[10], in the Panonian basin, Hungary[11], and in the Liaohe and Longyan basins, Zhangzhou and Beijing geothermal fields, North China [12]. It became also clear that the existence of regional groundwater flow caused a significant disturbance of thermal regimes produced a zone of high temperature in the central part of the Yonezawa Basin, Northeast Japan [13].

CLIMATE CHANGE AND SUBSURFACE TEMPERATURE

From meteorological data, global temperature changes which show recent warming trends of about 0.5℃ globally over the last century were evaluated by [14]. The methods for detecting climatic change from observational data including air temperature, sea surface temperature, tropospheric temperature, tree ring thickness, temperature from isotopic fractionation, temperature profiles in a borehole and snow and ice cover data were reviewed by [15]. These data suggested significant cooling in the late 1700's with recovery to natural early levels rather than global warming. Problems in interpreting temperature records are caused by the effects of significant urban warming, station change and changes in measurements [15,16,17].

The most recent major climatic change, the rapid warming during the last 100 years, has caused a temperature inversion that is manifested as a low or inverse temperature gradient in the subsurface shallow layer in many parts of the world. This phenomenon is shown in Fig. 1e schematically. Hence, a temperature profile in a borehole is influenced both by surface warming and by groundwater flow.

CONCLUSIONS

There are some studies dealing individually with the effect of groundwater flow and surface temperature change to the subsurface thermal regime, but there are few studies including both effects. Temperature profiles and the distribution of temperature inversions in Japan, Germany and China were presented as examples of profiles showing both effects. The conclusions are summarized as follows:

(1) It is generally recognized that the subsurface thermal field within several thousand meters of the surface is affected by deep groundwater circulation; temperatures and thermal gradients in the shallow layers are relatively high in the structural center of basins, grabens and coastal plains, and are low in the peripheral area.
(2) Inversions appear in the temperature profile as a near surface minimum temperature below the isothermal layer. Inversions are observed where subsurface temperature is influenced more by the warmed surface temperature than by regional groundwater flow. Hence, inversions are rarely observed in the discharge areas.
(3) The subsurface thermal regime is influenced not only by groundwater flow, but also by surface climatic change. Surface warming is enhanced in urban areas owing to the effects of urbanization.

REFERENCES

1.DOMENICO, P. A. and V. V. PALCIAUSKAS(1973) Geol. Soc. Amer. Bull., 84: 3803-3814.
2.CERMAK, V.(1971) Palaeogeography, Palaeoclimatology, Palaeoecology, 10: 1-19.
3.JESSOP, A. M.(1990) Thermal Geophysics. Developments in Solid Earth Geophysics, 17, Elsevier.
4.PARSONS, M. L.(1970) Water Resour. Res., 6: 1701-1720.
5.BECK, A. E., G. GARVEN, and L. STEGENA(1987) Hydrogeological Regimes and Their Subsurface Thermal Effects. Geophysical Monograph 47, IUGG 2, AGU.
6.WILLETT, S. D., and D. S. CHAPMAN(1987) In: B. HITCHON, S. BACHU and C. SAUVEPLANE (eds) Proceedings of the Third annual Canadian/American Conference on Hydrogeology, Hydrology of Sedimentary Basin: Application to Exploration and Exploitation, pp 159-168.
7.PERSON, M. A. and G. GARVEN(1987) In: Beck et al. (eds) Hydrogeological Regimes and Their Subsurface Thermal Effects, Geophysical Monograph 47, IUGG 2, AGU, pp 35-58.
8.CLAUSER, C.(1987) In: Beck et al. (eds) Hydrogeological Regimes and Their Subsurface Thermal Effects, Geophysical Monograph 47, IUGG 2, AGU, pp 59-64.

9.Griesrser, J. C. and L. RYBACH(1987) In: Beck et al. (eds) Hydrogeological Regimes and Their Subsurface Thermal Effects, Geophysical Monograph 47, IUGG 2, AGU, pp 65-74.

10.CERAMAK, V.(1987) In: Beck et al. (eds) Hydrogeological Regimes and Their Subsurface Thermal Effects, Geophysical Monograph 47, IUGG 2, AGU, pp 75-80.

11.STEGENA, L.(1987) In: Beck et al. (eds)Hydrogeological Regimes and Their Subsurface Thermal Effects, Geophysical Monograph 47, IUGG 2, AGU, pp 81-86.

12.WANG, J. and L. XIONG(1987) In: Beck et al. (eds) Hydrogeological Regimes and Their Subsurface Thermal Effects, Geophysical Monograph 47, IUGG 2, AGU, pp 87-99.

13.SAKURA, Y.(1993) Int. Assoc. Hydrol. Publ. 215: 161-170.

14.HANSEN, J., and S. LEBEDEFF(1987) J. Geophys. Res., 92: 13345-13372.

15.ELLSAESSER, H. W., M. C. MACCRACKEN, J. J. WALTON, and S. L. GROTCH(1986) Reviews of Geophysics, 24: 745-792.

16.WOOD, F. B.(1988 Climatic Change, 12: 297-312.

17.KARL, T. R., J. D. TARPLEY, R. G. QUAYLE, H. F. DIAZ, D. A. ROBINSON, and R. S. BRADLEY(1989) Reviews of Geophysics, 27: 405-430.

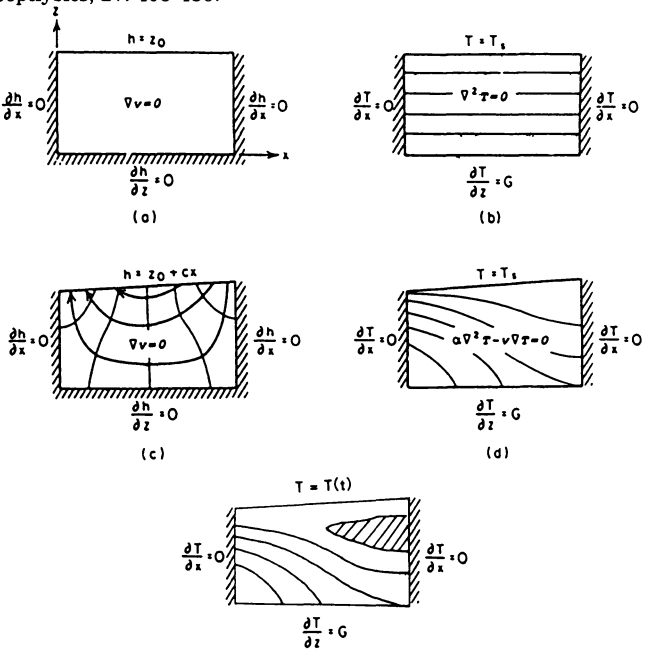

Fig.1. Subsurface thermal regime influenced by a simple regional groundwater flow system and surface warming in a vertical section (modified from [1]). (a) static groundwater flow condition, (b) thermal regime under the condition of (a), (c) simple regional groundwater flow system, (d) thermal regime under the condition of (c) and (e) thermal regime caused by the effects of groundwater flow and surface temperature warming (Hatching shows the zone of temperature inversion which shows anomalous low temperature). Where, h, v, T, T_s, G, x, y and t are groundwater hydraulic head, groundwater flow velocity, subsurface temperature, constant surface temperature, constant temperature gradient, x-y coordinate and time, respectively.

Keyword Index

G

H

I

K

L

M

N

O

P

Q

R

S

T

U

V

W